Development and validation of kinase activity reporters for the dynamical study of cell response modalities by microscopy

~

“Role of the kinase MAPK/ERK in necroptosis”

François Sipieter

December, 3rd 2015

Thesis submitted in partial fulfillment of the requirements for the degree of
DOCTOR IN SCIENCES: Biotechnology
&
DOCTOR IN BIOLOGY: Cellular and Molecular Aspects of Biology

Promotors:
Prof. Dr. Franck Riquet
Prof. Dr. Peter Vandenabeele
Dr. Katia Cailliau-Maggio
Dr. Laurent Héliot

Joint Ph.D. Fellowship
Ghent University & Lille 1 University
Academic year: 2015-2016

Development and validation of kinase activity reporters for the dynamical study of cell response modalities by microscopy

By François Sipieter

Death Dynamics Team
Unit for Molecular Signaling and Cell Death
Inflammation Research center, a VIB-UGent Department
Ghent University and Flanders Institute for Biotechnology
Technologiepark 927
B-9052 Gent-Zwijnaarde / Belgium

Team *Régulation des Signaux de Division*
Structural and Functional Glycobiology Unit
Centre National de la Recherche Scientifique (UMR 8576)
Lille 1 University
Cité Scientifique
59658 Villeneuve d'Ascq / France

Team *Biophotonique Cellulaire Fonctionnelle*
Laboratoire de Physique des Lasers, Atomes et Molécules
Centre National de la Recherche Scientifique (UMR 8523)
Lille 1 University
Cité Scientifique
59658 Villeneuve d'Ascq / France

Academic year 2015-2016

Promotors
Prof. Dr. Franck Riquet
Prof. Dr. Peter Vandenabeele
Dr. Katia Cailliau-Maggio
Dr. Laurent Héliot

Examination committee

Chair:	Prof. Dr. Xuefen Le Bourhis[1]
Co-Chair:	Prof. Dr. Kris Vleminckx[2,3]
Reading Committee:	Prof. Dr. Patrizia Agostinis[4]
	Prof. Dr. Georges Baffet[5]
	Prof. Dr. Olivier Gavet[6]
	Dr. Saskia Lippens[3]
Other members:	Prof. Dr. Franck Riquet[2,3,7]
	Prof. Dr. Peter Vandenabeele[2,3]
	Dr. Laurent Héliot[8]
	Dr. Katia Cailliau-Maggio[7]

[1]INSERM U908, Lille 1 University, F-59658 Villeneuve d'Ascq, France

[2]Department of Biomedical Molecular Research, Ghent University, B-9052 Ghent, Belgium

[3]Inflammation Research Center, a VIB-UGent Department, B-9052 Ghent, Belgium

[4]Department of Cellular and Molecular Medicine, Katholieke Universiteit Leuven, B-3000 Leuven, Belgium

[5]*Institut de Recherche sur la Santé l'Environnement et le Travail* (IRSET), INSERM U1085, Rennes 1 University, F-35043 Rennes, France

[6]*Institut Gustave Roussy* (IGR), CNRS-UMR 8200, Paris-Sud University, F-94805 Villejuif, France

[7]Structural and Functional Glycobiology Unit (UGSF), CNRS-UMR 8576, Lille 1 University, F-59658 Villeneuve d'Ascq, France

[8]*Laboratoire de Physique des Lasers, Atomes et Molécules* (PhLAM), CNRS-UMR 8523, Lille 1 University, F-59658 Villeneuve d'Ascq, France

The Joint Ph.D. Fellowship was conducted between Lille 1 University (Lille, France) and Ghent University (Ghent, Belgium).

The research described in this thesis was performed at:

- the Interdisciplinary Research Institute (IRI CNRS-USR 3078), Lille 1 University
- the Inflammation Research Center (IRC), Flanders Institute for Biotechnology (VIB) and the Department of Biomedical Molecular Research, Faculty of Sciences, Ghent University.

This research has been supported by Lille 1 University, the *Centre National de la Recherche Scientifique* (CNRS), the *Agence Nationale pour la Recherche* (ANR): G2Progress program (ANR-13-BSV2-0016-02) and Vandenabeele's group research funding: *Fonds Wetenschappelijk Onderzoek* (FWO G.0875.11) and Methusalem grant (*Bijzonder Onderzoeksfonds*, BOF09/01M00709).

Research in the Vandenabeele group is further supported by Belgian grants (Interuniversity Attraction Poles, IAP 7/32), Flemish grants (FWO G.0973.11, FWO G.0A45.12N, FWO G.0172.12, FWO G.0787.13N, FWO G.0C31.14N), Ghent University grants (Multidisciplinary Research Platforms (MRP), Ghent Researchers On Unfolded Proteins in Inflammatory Disease (GROUP-ID) consortium), grant from the Foundation against Cancer (2012-188) and grants from Flanders Institute for Biotechnology (VIB).

This thesis contains, at time of printing:

- three published peer-reviewed scientific articles:
    - Riquet F, Vandame P, **Sipieter F**, Cailliau-Maggio K, Spriet C, Héliot L, et al. Reporting Kinase Activities Paradigms, Tools and Perspectives. J Biol Med. 2011;1: 10–18.
    - **Sipieter F**, Vandame P, Spriet C, Leray A, Vincent P, Trinel D, et al. From FRET imaging to practical methodology for kinase activity sensing in living cells. Prog Mol Biol Transl Sci. 2013;113: 145–216. doi:10.1016/B978-0-12-386932-6.00005-3
    - **Sipieter F**, Ladik M, Vandenabeele P, Riquet F. Shining light on cell death processes - a novel biosensor for necroptosis, a newly described cell death program. Biotechnol J. 2014;9: 224–40. doi:10.1002/biot.201300200

- one research article in press:
    - **Sipieter F**, Cappe B, Gonzales-Pisfil M, Spriet C, Bodart J-F, Cailliau-Maggio K, et al. Novel reporter for faithful monitoring of ERK2 dynamics in living cells and model organisms. PLoS One. 2015

- one research article close to submission:
    - Déméautis C, **Sipieter F**, Roul J, Chapuis C, Padilla-Parra S, Riquet FB, et al. Single wavelength excitation dual color FLIM for multiplexing genetically encoded FRET biosensors. Biophys J. 2015

- two research articles in preparation:
    - **Sipieter F**, Cappe B, Gavet O, Héliot L, Vincent P, Riquet FB. A novel approach for rapid development of optimized FRET-based biosensors for signaling network interrogation in living cells. 2016
    - **Sipieter F**, Cappe B, Vincent P, Vandenabeele P, Riquet FB. Spatio-temporal characterization of ERK activity in survival, apoptosis and necroptosis. 2016

Table of contents

Table of contents ..... **xi**
List of illustrations ..... **xv**
List of abbreviations ..... **xvii**
General Summary ..... **xxi**
Algemeen overzicht ..... **xxiii**
Résumé général ..... **xxv**

Part 1:Introduction **1**

1.1. The Programmed Cell Death (PCD) 3

1.1.1. Review – Shining light on cell death processes - a novel biosensor for necroptosis, a newly described cell death program *3*
1.1.2. MLKL as a new executioner in necroptosis progression *39*
1.1.3. Other cell death processes *41*

1.2. The MAPK signaling pathways 47

1.2.1. JNK pathway *48*
1.2.2. p38/SAPK pathway *50*
1.2.3. ERK1/2 pathway *53*

1.3. Involvement of ERK1/2 in cell death processes 68

1.3.1. ERK1/2 in apoptosis *68*
1.3.2. ERK1/2 in autophagy *71*
1.3.3. ERK1/2 in paraptosis *72*
1.3.4. ERK1/2 in ferroptosis *73*
1.3.5. ERK1/2 in parthanatos *73*
1.3.6. Hallmarks of ERK1/2 in cell death *74*

1.4. Why use dynamic approaches to elucidate ERK1/2 functions? 78
1.5. Review – Reporting kinase activities: paradigms, tools and perspectives 83

Abstract *85*
Background *86*
1.5.1. Spatiotemporal dynamics of kinase drives cellular functions: case review of MAPK/Erk, PKA and Akt *87*
1.5.2. Getting into more dynamism: FRET-Based Kinase Activity Reporters *90*
1.5.3. Bioluminescence-based reporters for protein kinase activity *94*
1.5.4. Concluding remarks *97*
Acknowledgements *97*
References *97*

Part 2:Aims and objectives **101**

2.1. Scientific Objectives 103
2.2. Biotechnological Objectives 107

Part 3:Experimental strategies **109**

3.1. 2A-mediated eGFP-ERK2 and MEK1 coexpression system to monitor ERK2 in living cell 110
3.2. Review – From FRET imaging to practical methodology for kinase activity sensing in living cell 113

Abbreviations *116*
Foreword *117*
3.2.1. Introduction *118*
3.2.2. Fluorescence generalities *121*
3.2.3. FRET measurement *126*
3.2.4. FRET measurements: methods and instrumentation. *135*

3.2.5. Data analysis ... *142*
3.2.6. Design and optimization of genetically encoded Kinase activity reporters (KARs) ... *153*
3.2.7. Considerations for KAR measurements ... *164*
3.2.8. Towards quantitative approaches in biological processes ... *172*
3.2.9. Outlook and perspective ... *173*
Acknowledgments ... *176*
References ... *176*

Part 4:Results ... **183**

4.1. Research article – Novel reporter for faithful monitoring of ERK2 dynamics in living cells and model organisms ... 185

Abstract ... *188*
4.1.1. Introduction ... *188*
4.1.2. Materials and Methods ... *191*
4.1.3. Results ... *199*
4.1.4. Discussion ... *215*
4.1.5. Conclusion ... *221*
Acknowledgements ... *222*
Fundings ... *222*
References ... *222*
Supporting Information ... *226*

4.2. Research article – A novel approach for rapid development of optimized FRET-based biosensors for signaling network interrogation in living cells ... 231

4.2.1. Introduction ... *234*
4.2.2. Material and Methods ... *236*
4.2.3. Results ... *238*
4.2.4. Conclusion ... *243*
References ... *243*

4.3. Research article – Spatio-temporal characterization of ERK activity in survival, apoptosis and necroptosis ... 245

4.3.1. Introduction ... *248*
4.3.2. Materials and methods ... *249*
4.3.3. Results and discussion ... *253*
4.3.4. Conclusion ... *260*
Acknowledgements ... *261*
References ... *261*

4.4. Research Article – Single wavelength excitation dual color FLIM for multiplexing genetically encoded FRET biosensors ... 263

Abstract ... *266*
4.4.1. Introduction ... *267*
4.4.2. Materials and methods ... *269*
4.4.3. Results and discussion ... *273*
4.4.4. sREACh is a good non-fluorescent FRET acceptor for mTFP1 to avoid spectral bleed-through in LSSmOrange channel when using dual color FLIM ... *274*
4.4.5. Single wavelength excitation dual color FLIM methodology can be used to simultaneously monitor ERK and PKA kinase activities in a single cell ... *277*
4.4.6. Conclusion ... *282*
Acknowledgment ... *283*
Fundings ... *284*
References ... *284*
Supplementary Material ... *287*

Part 5:Summary and discussion 291
Résumé de la thèse 301

1. Introduction 301

1.1. Les morts cellulaires programmées 301
1.2. Les voies de signalisation ERK1/2 302
1.3. Implication de ERK1/2 dans les processus de mort cellulaire 303
1.4. Pourquoi utiliser des approches dynamiques pour la compréhension des fonctions de ERK1/2 ? 303
1.5. Article de revue – Reporting kinase activities: paradigms, tools and perspectives 304

2. Buts et objectifs 305

2.1 Objectifs scientifiques 305
2.2. Objectifs biotechnologiques: 309

3. Approches Expérimentales 311

3.1. Co-expression équimolaire des kinases GFP-ERK2 et MEK1 pour le suivi dynamique de GFP-ERK2 en cellules vivantes 311
3.2. Chapitre d'ouvrage – From FRET imaging to practical methodology for kinase activity sensing in living cell. 311

4. Résultats 312

4.1. Article de recherche – Novel reporter for faithful monitoring of ERK2 dynamics in living cells and model organisms 312
4.2. Article de recherche en préparation – A novel approach for rapid development of optimized FRET-based biosensors for signaling network interrogation in living cells 313
4.3. Article de recherche en préparation – Spatio-temporal characterization of ERK activity in survival, apoptosis and necroptosis. 314
4.4. Article de recherche en préparation – Single wavelength excitation dual color FLIM for multiplexing genetically encoded FRET biosensors. 315

5. Discussion générale et conclusion 317

References 319
Curriculum Vitae 339
Acknowledgements 343

List of illustrations

Figure 1: Cascade of molecular events leading to necroptosis 39
Figure 2: Molecular characterization of autophagy, apoptosis, and necrosis 43
Figure 3: Schematic representation of MAPKs signaling pathways 48
Figure 4: Crosstalk between JNK and p38/SAPK signaling pathways 51
Figure 5: ERK1/2 MAPK signaling pathway 54
Figure 6: Feedback mechanisms in the regulation of ERK1/2 cascade 60
Figure 7: Subcellular distribution of ERK1/2 62
Figure 8: Molecular mechanisms of ERK1/2 translocation into the nucleus 64
Figure 9: ERK1/2-mediated apoptosis 69
Figure 10: Hallmarks of ERK1/2-mediated cell death 75
Figure 11: A new model for signals-induced ERK1/2 activation 78
Figure 12: Time scale for dynamical studies of signaling pathways 79
Figure 13: “Vocabulary” for the characterization of oscillatory kinase activation 80
Figure 14: General scheme of regulatory mechanisms for ERK1/2 activation 82
Figure 15: Scheme of the ribosome skipping 111
Figure 16: Schematic overview summarizing the strategy established for this research project 300

Table 1: ERK1/2-mediated cell death in different cellular models 99

List of abbreviations

4-HBD ..... 4 Helical Bundle Domain
AC ..... Adenylyl cyclases
ADP ..... Adenosine Diphosphate
AFM..... Atomic Force Microscopy
AIF ..... Apoptosis-Inducing Factor
AKAP..... A Kinase Anchoring Proteins
AKT ..... Protein Kinase B (PKB)
ALA ..... ?-Aminolevulinic Acid
AMC 7-Amino-4-Methylcoumarin
AMP ..... Adenosine Monophosphate
AMPK ..... AMP-activated protein Kinase
ANT..... Adenine Nucleotide Translocase
Apaf-1..... Apoptotic Protease-Activating Factor 1
ASK1..... Apoptotic Signal Kinase 1
ATF ..... Activating Transcription Factor
ATM..... Ataxia Telangiectasia Mutated
ATP ..... Adenosine Triphosphate
Bad..... Bcl-2-Associated Death Promoter
Bak..... Bcl-2 Homologous Antagonist/Killer
Bax..... Bcl-2-Associated X Protein
Bcl-2 ..... B-Cell Lymphoma-2
Bcl-XL..... B-Cell Lymphoma-Extra Large
BCR-ABL..... Breakpoint Cluster Region-Abelson
BFP ..... Blue Fluorescent Protein
BH domain..... Bcl-2 Homology Domain
BHK-21..... Baby Hamster Kidney Cells
Bid..... Bh3 Interacting Domain Death Agonist
Bok..... Bcl-2 Related Ovarian Killer
BrdUTP..... 5-Bromo-2'-Deoxyuridine 5'-Triphosphate
CA-GFP..... Caspase-Activatable GFP
Caspase ..... Cysteine-Dependent Aspartate-Directed Protease
CB-NP ..... Cathepsin B Nanoprobe
CD..... Common docking
CD95 ..... Cluster Of Differentiation 95
CDK..... Cyclin-Dependent Kinases
CDKi..... CDK inhibitors
CdS-QDs ..... Cadmium Sulfide Quantum Dots
c-FLIP..... cellular FLICE-like inhibitory protein
CFP ..... Cyan Fluorescent Protein
CHYSEL ..... *cis*-acting hydrolase elements
cIAP1/2..... Cellular Inhibitor Of Apoptosis Protein 1/2
CL ..... Cardiolipins
CML..... Chronic Myeloid Leukemia Cells
c-Mos ..... Cellular Moloney murine sarcoma
cPLA2..... Cytosolic Phospholipase A2
CR..... Conserved regions
CRD ..... Cysteine Rich Domain
CRISPR..... Clustered Regularly Interspaced Short Repeats
CrkL..... V-Crk Avian Sarcoma Virus Ct10 Oncogene Homolog-Like
Cyt c..... Cytochrome C
DAPK ..... Death-Associated Protein Kinase
DD..... Death Domain
DED..... Death Effector Domain
DEJL ..... Docking site for ERK and JNL, LXL
DISC..... Death Inducing Signaling Complex
DLK ..... Dual Leucine zipper Kinase
DNA..... Deoxyribonucleic Acid
DR..... Death Receptor
DUSP ..... DUal-Specificity Phosphatases
ECL ..... Electrochemiluminescence
EGF..... Epidermal Growth Factor
eGFP..... Enhanced GFP
EGFR ..... EGF Receptor

EKAR ..... Erk Kinase Activity Reporter
EKAR-EV..... EKAR with Eevee linker
ELK ..... ETS domain-containing protein
ER..... Endoplasmic Reticulum
ERK..... Extracellular-signal Regulated Kinases
ERK1/2-ACT..... ERK1/2 Activity - Optimized version of EKAR-EV
ERK2-LOC..... ERK2 Localization - reporter of ERK2 localization
ESA..... Eleostearic Acid
ETO..... Etoposide
ETS ..... E26 transformation-specific or E-twenty-six
FADD ..... Fas Associated Protein With Death Domain
FBL ..... Feedback Loops
FFL..... Feedforward Loops
FGF..... Fibroblast Growth Factor
FLIM..... Fluorescent Lifetime Imaging
FP ..... Fluorescent Protein
FRDA ..... Friedrich's ataxia disease
FRET..... Förster Resonance Energy Transfer
FRS..... F-site recruitment site
GBM..... Glioblastoma-Multiform Cells
GEF..... Guanine nucleotide Exchange Factor
GFP..... Green Fluorescent Protein
GPCR..... G Protein-Coupled Receptors
GPX4..... GSH peroxidase 4
GSH ..... Glutathione
GSK3b..... Glycogen Synthase Kinase 3b
GTP..... Guanosine Triphosphate
H2O2..... Hydrogen Peroxide
HeLa..... Henrietta Lacks Cells
HMEC..... Human mammary epithelial cells
HMG..... High Mobility Group
HMGB1..... High-Mobility Group Protein B1
HSPB1..... Heat Shock Protein Beta-1
HT-29 ..... Human colorectal adenocarcinoma cell line
ID ..... Intermediary Domain
IFNγ..... Interferon Gamma
IGFIR..... Insulin-like Growth Factor I Receptor
IGFR1..... Insulin-like Growth Factor 1 Receptor
IL..... Interleukin
IMS..... Intermembrane Space
IMS-RP..... Intermembrane Space Reporter Protein
IR ..... Ischemia-reperfusion
IRES..... Internal Ribosomal Entry Site
JNK ..... Jun-NH2 terminal Kinases
KAR..... Kinase Activity Reporter
KD ..... Kinase Domain
kDA ..... Kilo Dalton
KSR..... Kinase Suppressor of Ras
LC3 ..... Light Chain 3
L929 ..... Fibroblastic mouse cell line
LMP..... Lysosomal Membrane Permeabilization
MAP ..... Mitogen-Activated Protein
MAP2K ..... Mitogen-Activated Protein Kinase Kinases (MAPKK)
MAP3K ..... Mitogen-Activated Protein Kinase Kinase Kinases (MAPKKK)
MAPK ..... Mitogen-Activated Protein Kinase
MAPKAPK ..... MAP Kinase Activated Protein Kinase
MAPKK..... Mitogen-Activated Protein Kinase Kinases
MAPKKK..... Mitogen-Activated Protein Kinase Kinase Kinases
MCF-7 ..... Michigan Cancer Foundation-7 Cells
Mcl-1 ..... Induced Myeloid Leukemia Cell Differentiation Protein
MEF..... Mouse Embryonic Fibroblasts
MEK ..... MAPK/ERK Kinase
MK..... MAPK-activated protein kinase
MKK ..... Mitogen-Activated Protein Kinase Kinase
MKP ..... MAP Kinases Phosphatases
MLCK ..... Myosin Light Chain Kinase
MLKL..... Mixed Lineage Kinase-Like Domain

MMP ..... Mitochondrial Membrane Permeabilization
MNK ..... MAPK iNteracting Kinases
MNNG ..... N-methyl-N´-nitro-N-nitrosoguanidine
MOMP ..... Mitochondrial Outer Membrane Permeabilization
MPF ..... M-phase-promoting factor
MRE ..... Molecular Recognition Element
mRNA ..... Messenger Ribonucleotidic Acid
MSK ..... Mitogen- and Stress-activated protein Kinase
mTOR ..... mammalian Target Of Rapamycin
MTP ..... Mitochondrial Transmembrane Potential
NAD ..... Nicotinamide Adenine Dinucleotide
Nec-1 ..... Necrostatin-1
NES ..... Nuclear Export Signal
NGF ..... Nerve Growth Factor
NGFR ..... Nerve Growth Factor Receptor
NIRF ..... Near-Infrared Fluorescence
NK ..... Natural Killer
NLS ..... Nuclear Localization Sequence
NO ..... Nitric Oxide
NSA ..... Necrosulfonamide
NTS ..... Nuclear Translocation Signal
OXPHOX ..... Oxidative Phosphorylation
PAR ..... Poly(Adp)-Ribose
PARP ..... Poly(Adp)-Ribose Polymerase
PC-12 ..... Pheochromocytoma-12 Cells
PCD ..... Programmed Cell Death
PDGF ..... Platelet-Derived Growth Factor
PDT ..... Photodynamic Therapy
PI ..... Propidium Iodide
PI3K ..... Phosphoinositide 3-Kinase
PIP ..... Phosphatidyl-Inositol Phosphates
PKC ..... Protein Kinase C
PS ..... Phosphatidylserine
PTM ..... Post-Translational Modifications
PTP ..... Permeability Transition Pore
Puma ..... P53 Upregulated Modulator Of Apoptosis
RBD ..... Ras Binding Domains
RFP ..... Red Fluorescent Protein
RHIM ..... RIP Homology Interaction Motif
RIP3i ..... RIPK3 inhibitor
RIPK ..... Receptor Interacting Protein Kinase
RIP-KARs ..... RIP Kinase Activity Reporters
RKIP ..... Raf Kinase Inhibitor Protein
ROS ..... Reactive Oxygen Species
RTK ..... Receptor Tyrosine Kinases
SAPK ..... Stress-Activated Protein Kinases
Ser ..... Serine
SGK ..... Serum and Glucocorticoid-inducible Kinase
siRNA ..... Small Interfering Rna
Smac ..... Second Mitochondria-Derived Activator Of Caspases
SOS ..... Son Of Sevenless
SPS ..... Ser-Pro-Ser
STAT ..... Signal Transducer and Activator of Transcription
sYFP2 ..... Super Yellow Fluorescent Protein ver.2
TAJ ..... Toxicity and JNK inducer, also known as TROY or TNFRSF19
TAK1 ..... TGF Activated Kinase 1
tBid ..... Truncated Bid
TC ..... Tetra Cysteine motif
TGF ..... Transforming Growth Factor
Thr ..... Threonine
TMRE ..... Tetramethylrhodamine Ethyl Ester
TMRM ..... Tetramethylrhodamine Methyl Ester
TNF ..... Tumor Necrosis Factor
TNFR1 ..... Tumor Necrosis Factor Receptor 1
Tpl2 ..... Tumor progression locus 2 protein kinase
TRADD ..... TNF-α Receptor Associated Death Domain
TRAF ..... TNF-α Receptor Associated Factor

TRAIL ..... TNF-α Related Apoptosis-Inducing Ligand
TROY ..... Tumor Necrosis Factor Receptor Superfamily, also know as TNFRSF19 or TAJ
TS ..... TNF-α + Smac-Mimetic - Apoptosis Trigger
TSC ..... Tuberous Sclerosis Complex
TSZ ..... TNF-α + Smac-Mimetic + z-VAD-Fmk - Necroptosis Trigger
TUNEL ..... Terminal Deoxynucleotidyl Transferase (Tdt) Dutp Nick End Labelling
Tyr ..... Tyrosine
U2OS ..... Human osteosarcoma cell line
UV ..... Ultra Violet
VDAC ..... Voltage Dependent Anion Channel
VEGF ..... Vascular Endothelial Growth Factor
YFP ..... Yellow Fluorescent Protein

General Summary

Necroptosis was recently defined as a caspase-independent programmed cell death. Necroptosis plays an important role in physio-pathological processes. It was shown to act as a prominent antiviral mechanism and is often associated with neurodegenerative diseases and ischemia–reperfusion injuries. Yet our understanding of the underlying mechanisms is only beginning to emerge. Tumor Necrosis Factor alpha (TNFα)-induced necroptosis relies on a signaling pathway involving mainly two serine-threonine kinases: Receptor-Interacting Protein Kinase 1 and 3 (**RIPK1** and **RIPK3**). In 2012, the pseudo-kinase Mixed-Lineage Kinase Like (**MLKL**) was identified as the crucial executioner of necroptosis downstream of RIPK3.

One of the best-studied models of receptor-induced necroptotic cell death is the L929 mouse fibrosarcoma cell line stimulated by the pleiotropic cytokine TNFα. Although the activation of different types of Mitogen-Activated Protein Kinases (MAPKs) has been studied in cell death, molecular mechanisms underlying MAPKs activation are poorly understood in the context of necroptosis. Interestingly, activation of Extracellular signal-Regulated Kinases 1 and 2 (ERK1/2) was reported to be involved in different modes of programmed cell death such as apoptosis, autophagy and ferroptosis in various cellular models. It is now accepted that the regulation of the duration, magnitude and subcellular compartmentalization of ERK1/2 activity by specific **spatio-temporal regulators** is interpreted by the cell towards **cell fate determination**.

To investigate the involvement of ERK1/2 in TNFα-induced necroptosis in L929 cells, the effects of chemical inhibitions of the ERK1/2 cascade were monitored. Inhibition delayed necroptosis considerably in a dose dependent manner but did not block it. Our results are in agreement with previous studies and provide arguments for **a pro-necrotic function of ERK1/2** in this context. Phosphorylation patterns of ERK1/2 revealed a compartmentalized biphasic phosphorylation of ERK1/2 when L929 cells were exposed to a necrotic trigger. In addition, combined treatment of L929 with TNFα and necrostatin-1, a specific inhibitor of RIPK1 activity, altered the phosphorylation patterns of ERK1/2, corroborating previous findings indicating that RIPK1 activity is required for TNFα-mediated ERK1/2 activation.

Owing to the importance of ERK1/2 spatio-temporal dynamics in determining cellular responses, we investigated the **ERK1/2 temporal code** in necroptosis using fluorescence-based reporters of both ERK1/2 activity and localization in single living cells. To faithfully monitor ERK2 subcellular distribution in living cells throughout necroptosis, we developed a new genetically encoded reporter of ERK2 localization named **ERK2-LOC**. This reporter was fully characterized and validated in order to provide an accurate and reliable read-out of ERK2 localization during cell survival and cell death processes. We observed a transient translocation of ERK2 when necroptosis was triggered, followed by progressive ERK2 accumulation in the nucleus, which is a **hallmark of ERK1/2-mediated cell death**.

To investigate ERK1/2 activity profiles in living cells, we first used a genetically encoded FRET biosensor for ERK1/2 (EKAR-EV). However, this reporter failed to reveal any changes in ERK1/2 activity upon TNFα-induced necroptosis in L929 cells, which was inconsistent with our biochemical data. Using a newly developed approach, we optimized EKAR-EV to generate a new ERK1/2 biosensor with a substantially improved dynamic range (**ERK1/2-ACT**). Using ERK1/2-ACT, a dedicated spatio-temporal signature of ERK1/2 activity was recorded for the first time during necroptosis.

Finally, to correlate the necroptosis ERK1/2 code with necroptosis occurrence, we also engineered a first generation of FRET-based kinase biosensors to report on both RIPK1 and RIPK3 activities during necroptosis.

Algemeen overzicht

Necroptose werd recent geïdentificeerd als een vorm van caspase-onafhankelijke geprogrammeerde celdood die een belangrijke rol speelt in fysio-pathologische processen. Er werd aangetoond dat necroptose een prominente rol speelt als antiviraal mechanisme en dat het in een aantal gevallen geassocieerd is met neurodegeneratieve ziekten en ischemie-reperfusie orgaanbeschadiging. De moleculaire mechanismen die necroptose induceren zijn echter nog weinig begrepen. Tumor Necrosis Factor alpha (TNFα)-geïnduceerde necroptose is afhankelijk van een signaaltransductieweg die gebruik maakt van twee serine-threonine kinasen: 'Receptor-Interacting Protein Kinase' 1 en 3 (**RIPK1** and **RIPK3**). In 2012 werd het pseudo-kinase 'Mixed-Lineage Kinase Like' (**MLKL**) geïdentificeerd als RIPK3 substraat en cruciale molecule tijdens membraanpermeabilisatie bij necroptose.

TNFα-geïnduceerde necroptose in de muis L929 fibrosarcoma cellijn is één van de best bestudeerde receptor-geïnduceerde necroptose modelsystemen. Alhoewel de activering van verschillende types Mitogen-geactiveerde Proteïne Kinasen (MAPKs) reeds bestudeerd werden celdood inductie, zijn de moleculaire mechanismen van MAPKs activering tijdens necroptose weinig gekend. Activering van 'Extracellular signal-Regulated Kinases 1 en 2' (ERK1/2) werd reeds gerapporteerd tijdens verschillende vormen van geprogrammeerde celdood, zoals apoptose, autofagie en ferroptose. Het is nu geaccepteerd dat de regulatie, duratie, magnitude en subcellulaire compartimentalizatie van de ERK1/2 activiteit door **spatio-temporale regulatoren** vertaald wordt door de cel **tot passend antwoord** van die cel op de initiële stimulus.

Om de betrokkenheid van ERK1/2 in TNFα-geïnduceerde necroptose in L929 cellen te onderzoeken werden de cellen met chemische ERK1/2 inhibitoren behandeld. ERK1/2 inhibitie resulteerde in een aanzienlijke vertraging van, maar geen bescherming tegen, TNF-geïnduceerde necroptose. Onze resultaten zijn in overeenstemming met voorafgaande studies en suggereren een **pro-necrotische functie van ERK1/2**. De ERK1/2 fosforylatiepatronen vertonen een gecompartimentalizeerde bi-fasische fosforylatie wanneer L929 cellen behandeld werden met TNF. Gecombineerde behandeling van L929 cellen met TNFα en

necrostatine-1, een RIPK1-specifieke inhibitor, resulteerde in een gewijzigd ERK1/2 fosforylatiepatroon. Deze observatie is in overeenstemming met het feit dat RIPK1 activiteit nodig is voor TNFα-geïnduceerde ERK1/2 activering.

Omwille van het belang van de ERK1/2 spatio-temporale dynamiek bij het bepalen van cellulaire responsen onderzochten wij de **ERK1/2 temporale code** tijdens necroptose gebruik makend van fluorescente ERK1/2-activiteit rapporteermoleculen. Deze rapporteermoleculen geven zowel de activiteit als de localizatie van geactiveerd ERK1/2 aan in levende cellen. Om de ERK2 subcellulaire distributie betrouwbaar weer te geven in levende of necroptotische cellen werden genetisch gecodeerde rapporteerconstructen, **ERK2-LOC** genaamd, in de cellen gebracht. Deze rapporteerconstructen werden volledig gekarakteriseerd en gevalideerd. We namen een transiënte ERK2 translocatie waar bij TNF-geïnduceerde necroptose, gevolgd door ERK2 accumulatie in de nucleus, **wat een kenmerk is van ERK1/2-afhankelijke celdood.**

Om de ERK1/2 activiteitsprofielen in levende cellen te onderzoeken, gebruikten we eerst een genetisch gecodeerde ERK1/2 FRET biosensor (EKAR-EV). Dit rapporteerconstruct kon echter geen veranderingen in ERK1/2 activiteit detecteren, wat in tegenspraak is met onze biochemische data. Daarom ontwikkelden we een geoptimaliseerde ERK1/2 biosensor met een substantieel verbeterde dynamisch bereik (**ERK1/2-ACT**). Gebruik makend van ERK1/2-ACT konden we wel een spatio-temporaal verschil in ERK1/2 activiteit waarnemen tijdens TNF-geïnduceerde necroptose.

Tenslotte ontwikkelden we eveneens een eerste generatie van FRET-gebaseerde RIPK1 en RIPK3 kinase biosensors.

Résumé général

La nécroptose a récemment été définie comme une mort programmée caspase indépendante. Elle présente un rôle physiopathologique et montre une implication dans certains mécanismes antiviraux, des maladies neuro-dégénératives ou encore les phénomènes d'ischémie–reperfusion. Cependant, notre compréhension des mécanismes moléculaires de la nécroptose commence tout juste à voir le jour. La nécroptose induite par le *Tumor Necrosis Factor alpha* (TNFα) fait intervenir une voie de signalisation spécifique impliquant deux kinases, les *Receptor-Interacting Protein Kinases* 1 et 3 (**RIPK1** et **RIPK3**) et la pseudo-kinase *Mixed Lineage Kinase domain-Like protein* (**MLKL**), identifiée en 2012 comme l'exécuteur crucial de la nécroptose en aval de RIPK3.

Un des modèles cellulaire les plus étudiés de la nécroptose est la lignée de fibrosarcome de souris L929 stimulée par le TNFα. Bien que l'activation de différents types de *Mitogen Activated Protein Kinases* (MAPKs) ait été impliquée dans ce processus, les mécanismes moléculaires mis en œuvre dans le cadre de la nécroptose demeurent mal compris. De manière intéressante, l'activation des kinases *Extracellular signal-Regulated Kinase 1 et 2* (ERK1/2) a été rapportée dans plusieurs types de morts cellulaires programmées telles que l'apoptose, l'autophagie ou encore la ferroptose. Par ailleurs, la régulation de l'activité de ERK1/2 en termes d'amplitude, de durée et de localisation *via* des **régulateurs spatio-temporels** spécifiques est interprétée par la cellule pour la **détermination du destin cellulaire**.

Afin d'étudier l'implication de ERK1/2 dans la nécroptose induite par le TNFα dans les L929, nous avons testé l'effet d'inhibiteurs chimiques sur la cascade de signalisation ERK1/2. Nos résultats mettent en évidence un retard significatif de la nécroptose de manière dose-dépendante, sans pour autant la bloquer. Nos données sont en accord avec les études antérieures suggérant ainsi **un rôle pro-nécrotique de ERK1/2** dans ce contexte cellulaire. Les profils de phosphorylation de ERK1/2 révèlent une activité biphasique et compartimentée dans ces conditions expérimentales. Par ailleurs, l'inhibition de l'activité de RIPK1 par la nécrostatine-1 dans des L929 traitées par le TNFα perturbe les profils de phosphorylations de ERK1/2, indiquant que RIPK1 est impliquée dans l'activation de ERK1/2 induite par le TNFα.

La régulation spatio-temporelle de l'activité de ERK1/2 étant déterminante dans l'engagement du processus cellulaire, nous avons étudié le **code d'activation temporel** de ERK1/2 au cours de la nécroptose *via* l'utilisation en cellules vivantes de rapporteurs fluorescents de l'activité et de la localisation de ERK1/2. Afin d'assurer un suivi fidèle de la distribution subcellulaire de ERK2, nous avons développé un nouveau rapporteur génétiquement codé, appelé **ERK2-LOC**. Cet outil nous a permis d'observer une translocation transitoire de ERK2 suite à la stimulation des L929 par le TNFα, suivi d'une accumulation nucléaire progressive de ERK2. Cette signature est considérée comme **caractéristique de l'implication de ERK1/2 dans les processus de mort cellulaire**.

L'examen des profils d'activité de ERK1/2 au cours de la nécroptose a été initialement réalisé grâce à l'utilisation d'un rapporteur basé sur le *Förster Resonance Energy Transfer* (FRET) d'activité kinase (EKAR-EV). Ce biosenseur n'a pas permis l'enregistrement de variations d'activité, contrairement aux résultats obtenus par biochimie. L'optimisation de EKAR-EV, par une approche nouvellement développée, a amélioré substantiellement sa gamme dynamique (**ERK1/2-ACT**). L'utilisation de ERK1/2-ACT a permis de mettre en évidence pour la première fois une signature spatio-temporelle spécifique de l'activité de ERK1/2 au cours de la nécroptose.

Dans la perspective de corréler les signatures d'activité de ERK1/2 avec celles des kinases RIPK1 et RIPK3, nous avons également développé une première génération de biosenseurs FRET pour ces kinases initiatrices de la nécroptose.

Part 1: Introduction

1.1. The Programmed Cell Death (PCD)

1.1.1. Review – Shining light on cell death processes - a novel biosensor for necroptosis, a newly described cell death program

Sipieter François*[1,2,3,4,5], Ladik Maria*[2,3], Vandenabeele Peter¶[2,3] and Riquet Franck¶[1,2,4,5]

* These authors contributed equally to this work

¶ These authors share senior authorship

[1]Laboratoire de Régulation des Signaux de Division, EA4479, University Lille1, Villeneuve d'Ascq, France

[2]Molecular Signaling and Cell Death Unit, Department of Biomedical Molecular Biology, Ghent University, B-9052 Ghent, Belgium.

[3]Molecular Signaling and Cell Death Unit, Inflammation Research Center, VIB, B-9052 Ghent, Belgium

[4]IRI CNRS USR 3078, University Lille1–University Lille2, Villeneuve d'Ascq, France

[5]Groupement de Recherche Microscopie Imagerie du vivant, GDR2588 MIV-CNRS, Villeneuve d'Ascq, France

Published in Biotechnology Journal, 2014, Volume 9, 224-240, doi: 10.1002/biot.201300200

Review

Shining light on cell death processes - a novel biosensor for necroptosis, a newly described cell death program

Sipieter François*[1,2,3,4,5], Ladik Maria*[2,3], Vandenabeele Peter¶[2,3†] and Riquet Franck¶[1,2,4,5]

*These authors contributed equally to this work

¶These authors share senior authorship

1: Laboratoire de Régulation des Signaux de Division, EA4479, University Lille1, Villeneuve d'Ascq, France

2: Molecular Signaling and Cell Death Unit, Department of Biomedical Molecular Biology, Ghent University, B-9052 Ghent, Belgium.

3: Molecular Signaling and Cell Death Unit, Inflammation Research Center, VIB, B-9052 Ghent, Belgium

4: IRI CNRS USR 3078, University Lille1–University Lille2, Villeneuve d'Ascq, France

5: Groupement de Recherche Microscopie Imagerie du vivant, GDR2588 MIV-CNRS, Villeneuve d'Ascq, France

† Corresponding author
Prof. Peter Vandenabeele
Molecular Signaling and Cell Death Unit, Department for Molecular Biomedical Research, VIB, 9052 Ghent, Belgium
Department of Biomedical Molecular Biology, Ghent University, 9052 Ghent, Belgium
Address: Technologiepark 927, B-9052 Ghent, Zwijnaarde, Belgium.
Fax: +32 9 3313609.
E-mail address: Peter.Vandenabeele@irc.ugent.be

Additional corresponding author
Prof. Franck Riquet
Department of Biomedical Molecular Biology, Ghent University, 9052 Ghent, Belgium
Address: Technologiepark 927, B-9052 Ghent, Zwijnaarde, Belgium.
Fax: +32 9 3313609.
E-mail address: Franck.Riquet@irc.ugent.be

1.1.1.1. Abstract

Cell death contributes to the maintenance of homeostasis, but mounting evidence has confirmed the involvement of programmed cell death in some diseases. The concept of “programmed cell death,” which was coined several decades ago to refer to apoptosis, now also encompasses necroptosis, a newly characterized cell death program. Research on programmed cell death has become essential for the development of some new therapies. To study cell death signaling and its molecular mechanisms, new biochemical and fluorogenic approaches have been devised. We first provide an overview of programmed cell death modes and the importance of dynamic cell death studies. Next, we focus on both apoptotic and necroptotic signaling and their mechanisms by providing a systematic review of all the methods and approaches that have been used. We emphasize the contribution of advanced approaches based on fluorescent probes, reporters, and FRET-based biosensors for studying programmed cell death. Because apoptosis and necroptosis signaling pathways share some effectors molecules, we discuss how these new tools could be used to discriminate between apoptosis and necroptosis. We also describe how we developed specific FRET-based biosensors for detecting necroptosis. Finally, we touch on how dynamic measurement of biomolecules in living models will play a role in personalized prognosis and therapy.

Keywords

Cell Death, Biosensors, Cytochrome C, RIPK, Caspase

1.1.1.2. Abreviations

ADP .....adenosine diphosphate
AFM.....atomic force microscopy
AIF.....apoptosis inducing factor
ALA .....δ-aminolevulinic acid
AMC 7-amino-4-methylcoumarin
ANT .....adenine nucleotide translocase
Apaf-1.....apoptotic protease-activating factor 1
ATP .....adenosine triphosphate
Bad.....Bcl-2-associated death promoter
Bak.....Bcl-2 homologous antagonist/killer
Bax.....Bcl-2-associated X protein
Bcl-2 .....B-cell lymphoma-2
Bcl-X_L .....B-cell lymphoma-extra large
BCR-ABL.....breakpoint cluster region-abelson
BFP .....blue fluorescent protein
BH domain.....Bcl-2 homology domain
BHK-21.....baby hamster kidney cells
Bid.....BH3 interacting domain death agonist
Bok.....Bcl-2 related ovarian killer
BrdUTP.....5-Bromo-2'-deoxyuridine 5'-triphosphate
CA-GFP.....caspase-activatable GFP
Caspase .....cystein-dependent aspartate-directed protease
CB-NP .....cathepsin B nanoprobe
CD95 .....cluster of differentiation 95
CdS-QDs .....cadmium sulfide quantum dots
CFP.....cyan fluorescent protein
cIAP1/2.....cellular inhibitor of apoptosis protein 1/2
CML.....chronic myeloid leukemia cells
CrkL.....v-Crk avian sarcoma virus CT10 oncogene homolog-like
Cyt c.....cytochrome c
DD.....death domain
DISC.....death inducing signaling complex
DNA.....deoxyribonucleic acid
DR.....death receptor
ECL .....electrochemiluminescence
eGFP.....enhanced GFP
ER .....Endoplasmic reticulum
ETO.....etoposide
FADD.....Fas associated protein with death domain
FRET.....förster resonance energy transfer
GBM.....glioblastoma-multiforme cells
GFP.....green fluorescent protein
GSK3b.....glycogen synthase kinase 3b
HeLa.....Henrietta Lacks cells
HMGB1.....high-mobility group protein B1
ID .....intermediary domain
IMS.....intermembrane space
IMS-RP.....intermembrane space reporter protein
KAR.....kinase activity reporter
KD .....kinase domain
MAPK/ERK.....mitogen-activated protein kinase / extracellular signal-regulated kinase
MCF-7 .....Michigan Cancer Foundation-7 cells
Mcl-1 .....induced myeloid leukemia cell differentiation protein
mESCs .....mouse embryonic stem cells
MLKL.....mixed lineage kinase-like domain protein
MOMP .....mitochondrial outer membrane permeabilization
MRE .....molecular recognition element

MTP.....mitochondrial transmembrane potential
NIRF.....near-infrared fluorescence
OXPHOX.....oxidative phosphorylation
PARP.....poly(ADP)-ribose polymerase
PC-12.....pheochromocytoma-12 cells
PCD.....programmed cell death
PDT.....photodynamic therapy
PI.....propidium iodide
PS.....phosphatidylserine
PTP.....permeability transition pore
Puma.....p53 upregulated modulator of apoptosis
RFP.....red fluorescent protein
RHIM.....RIP homology interaction motif
RIP-KARs.....RIPK kinase activity reporters
RIPK1/3.....receptor interacting protein kinase 1/3
ROS.....reactive oxygen species
siRNA.....small interfering RNA
Smac.....second mitochondria-derived activator of caspases
tBid.....truncated Bid
TC.....tetracysteine motif
TMRE.....tetramethylrhodamine ethyl ester
TMRM.....tetramethylrhodamine methyl ester
TNF.....tumor necrosis factor
TNFR1.....tumor necrosis factor receptor 1
TRADD.....TNF-α receptor associated deat domain
TRAF2/5.....TNF-α receptor associated factor 2/5
TRAIL.....TNF-α related apoptosis-inducing ligand
TUNEL.....terminal deoxynucleotidyl transferase (TdT) dUTP nick end labeling
YFP.....yellow fluorescent protein

1.1.1.3. Introduction

In adult humans, several million cells die per minute to balance the number of newly formed cells. Every cell in an organism is programmed to respond specifically to extracellular signals. The delivery of this information to subcellular levels, which requires the mobilization of intracellular signaling pathways, modulates the functions of subcellular compartments such as mitochondria, ER, and nucleus, to generate the appropriate response. Pre- and post-translational modifications of molecules regulate cellular processes quickly and reversibly. At the organism level, cellular homeostasis is essential and relies on three processes: proliferation, differentiation and cell death. In the past, much attention was given to the study of cell proliferation and differentiation while cell death was relatively neglected.

The concept of programmed cell death (PCD) was first introduced, in 1923, to describe the response of a plant cell infected by an incompatible fungus [1]. In plants, PCD is involved in xylogenesis, loss of foliage in autumn, cellular responses to counter pathogens and the preservation of the organism under environmental stress [2-5]. While plant scientists allowed physiologists to generalize this concept to other contexts in animal cells, it was not until the seventies that attention was given to cell death. The term “programmed cell death” was then used to define particular cellular events that occur during embryonic development [6-8]. In animals, PCD has been characterized in the cells of interdigital spaces, disappearance of certain embryonic structures, remodeling of early neural structures to establish functional synaptic connections, and death of certain cells of the immune system to prevent autoimmune diseases (for review [8]).

PCD is fundamental in both plant and animal physiology, playing a prominent role in the regulation and maintenance of cellular homeostasis. Programmed cell death is genetically regulated, relies on specific signaling pathways, and has been strongly conserved throughout evolution [9-15]. So it has become essential to gain a deep understanding of this process and to elucidate its mechanisms at the molecular level.

Mutations in cell death genes contribute to the development of many diseases such as cancer [16, 17] and immunologic [18-20], neurodegenerative [21, 22] and cardiovascular diseases [23-25]. The involvement of PCD malfunction in

pathogenesis has raised interest and contributed to the emergence of a new biomedical research field.

Indeed, cardiovascular diseases, including heart failure, myocardial infarction and ischemia/reperfusion, are the leading cause of death worldwide. Cell death mechanisms are involved in the development of these disorders, and pharmacological inhibition of PCD decreases the severity and progression of cardiac injuries (for review [26]).

Alzheimer's disease is characterized by progressive neuronal cell death, mainly in the neocortex and limbic system structures. Accumulation and aggregation of amyloid β peptides promote cell cytotoxicity and alter the activation state of several kinases, which provoke subsequent activation of cell death signaling pathways [27, 28].

Viruses can counteract the defense mechanisms of infected cells by controlling both extrinsic and intrinsic apoptotic machinery that lead to cell suicide. Some viruses can hijack the cell’s defense mechanisms, to the detriment of the cell. However, depending on the cellular context, certain cells can escape viral attacks by triggering necrotic cell death [19, 20, 29].

In cancer, depending on the severity and accumulation of mutations, cells either repair the defects or, to preserve genetic integrity, they activate signaling pathways leading to cell death. However, evasion of cell death is a hallmark of cancer (for review [30, 31]), as some cells can escape PCD and engage in tumorigenesis [31, 32].

Based on morphological and biochemical criteria, three distinct major types of cell death have been identified: apoptotic cell death (type I), autophagic cell death (type II) and necrotic cell death (type III) [33]. While autophagy has been considered more as a cell survival mechanism, it has also been shown to promote cell death in a cell context-specific manner [34]. Autophagic cell death is a type of cell death that lacks chromatin condensation but involves massive autophagic vacuolization of the cytoplasm. Unlike apoptotic cells which are efficiently cleared by macrophages, autophagic cells are not engulfed by phagocytes [33].

Recently, two new types of cell death have been described. The first, charontosis, is a type of PCD occurring in mouse embryonic stem cells (mESCs)

upon etoposide (ETO) treatment [35]. Another type of cell death, ferroptosis, is a unique iron-dependent form of non-apoptotic cell death that is induced by erastin [36].

In this review, we focus on apoptotic and necroptotic cell death. We review the biochemical and live-cell imaging approaches developed to track specific markers and discriminate between these two types of PCD. Because cellular processes are dynamic, we emphasize approaches that capture this dynamic feature in living cells.

1.1.1.4. Importance of dynamic studies of signaling pathways

Recently, many papers have shown that the biological response is dictated by the duration, magnitude and subcellular compartmentalization of enzymatic activity [37-39]. Specifically, the response of the cell is based on the modulation of the spatiotemporal dynamics of kinase activity. One of the most striking examples is the kinase MAPK/ERK. A central question about the MAPK/ERK signal transduction cascade is how the same protein kinase can elicit different cellular responses [38, 40, 41]?

In cell death processes, cell fate is the result of a dynamic balance between extracellular signals promoting survival or cell death. In the absence of trophic factors, cells initiate programmed cell death. Depending on cell type and stimulus, ERK dynamics can mediate different programmed cell death modes, such as apoptosis, autophagy, or senescence in various cellular models (for review [42]). The involvement of ERK in various cell death forms requires its sustained and sequestered activity. These two characteristics are recognized as hallmarks of ERK-mediated cell death. Sustained cytoplasmic ERK activity triggers senescence or autophagy by activating pro-death proteins in the cytoplasm [43, 44]. By contrast, sustained nuclear compartmentalization of ERK activity can promote apoptosis [45]. It has been suggested that signals provoking sustained activation of ERK in different subcellular compartments trigger cell death.

It is essential to determine the spatiotemporal patterns of initiator and executioner molecules that lead progressively and irreversibly to a particular type of cell death. The specific enzyme activity profiles required for cell death initiation and execution should be identified *in living cells*. Biosensors and reporters are suitable for

such approaches [46]. It is important, though, to distinguish between biosensors and bioprobes. A bioprobe provides only a snapshot of the cellular state at a given time, and is often discarded after its use. A biosensor can follow modifications of biomolecules in living cells with improved spatiotemporal resolution, while a reporter will indicate the occurrence of a specific event.

There are two main types of genetically encoded biosensors: environment-sensitive fluorophores and biosensors based on Förster resonance energy transfer (FRET).

Environment-sensitive fluorophores are the result of fluorescent protein engineering. In this situation, biomolecules binding to specifically engineered fluorophores modulate the fluorescence intensity of the fluorophore, which provides information about the concentration changes of the biomolecule inside the cell. Environment-sensitive biosensors include those reporting on the concentration of several ionic and reactive oxygen species (for review [47-50]).

By contrast, FRET biosensors consist of two parts: the "bioreceptor" part allows specific recognition of the biomolecule of interest, whereas the "transducer" part converts biochemical information into a photo-physical signal that is then recorded by a microscope (for review [51]).

It is important to distinguish intermolecular from intramolecular FRET biosensors [41]. Intermolecular FRET biosensors consist of two distinct proteins of interest, each of which is fused to a fluorescent protein [52, 53], and are well suited for protein–protein interaction studies.

Intramolecular FRET biosensors useful for the study of PCD include cleavage reporters and conformational change biosensors, which sense post-translational modifications such as proteolysis and phosphorylation in living cells (for review [54, 55]). FRET biosensors are based on the arrangement of several components, and in particular two fluorescent proteins flanking a molecular recognition element (MRE). Many types of FRET biosensors are now available, and in particular Kinase Activity Reporters (KAR) (for review [46]). While KAR show an increase in FRET between the two fluorophores upon phosphorylation, protease biosensors, such as caspase reporters, are based on FRET decrease after protease cleavage at a specific site between two FRET compatible fluorophores.

Many caspase reporters have been developed in attempts to identify the type of PCD and monitor the activity of initiator and executioner caspases in cells undergoing cell death [56-58]. They are reviewed below.

1.1.1.5. Apoptosis

Apoptosis is essential for cell homeostasis and during embryonic development [59, 60]. An excellent example of apoptosis playing a central role in morphogenesis is the development of the vertebrate limb [60].

Morphologically, apoptosis is characterized by membrane blebbing, cell shrinkage, chromatin aggregation, and appearance of apoptotic bodies [59]. Depending on the initial signal, two major signaling pathways can be distinguished: the intrinsic and the extrinsic signaling pathway. Intrinsic signaling involves the mitochondrial pathway and is usually induced by internal stimuli, such as DNA damage, inhibition of cell survival factors, defective cell cycle, hypoxia, or other forms of cellular stress. The signaling cascade induced in the mitochondrial pathway depends on the release of proapoptotic proteins from the mitochondrial intermembrane space (IMS), such as cytochrome c (cyt c). This protein binds apoptotic protease-activating factor 1 (Apaf-1), inducing a conformational change and oligomerization that leads to the formation of a caspase activation platform called the apoptosome. The formed complex recruits, dimerizes, and activates initiator caspase-9, which in turn cleaves and activates caspase-3 [61]. On the other hand, extrinsic signaling is induced by activation of transmembrane receptors of the death receptor family, including Fas/CD95, tumor necrosis factor-alpha (TNF-α) receptor 1 (TNFR1), and two death receptors (DR4 and DR5), which bind to TNF-α related apoptosis-inducing ligand (TRAIL) [62]. As the signaling of the extrinsic pathway is shared by apoptosis and necroptosis (the regulated form of necrosis) we will emphasize its molecular mechanism.

Molecular pathways of apoptosis

- **The intrinsic pathway of apoptosis**

This pathway is engaged at the mitochondrial level by mitochondrial outer membrane permeabilization (MOMP), which is tightly regulated by members of the Bcl-2 family. Coordinated function of Bcl-2 family proteins is critical during apoptosis. The Bcl-2 family members have some homologous regions known as Bcl-2 homology

(BH) domains. These molecules can be divided in two groups: anti-apoptotic proteins such as Bcl-2, Bcl-X_L, Bcl-w and Mcl-1, which contain BH domains 1 – 4 and pro-apoptotic proteins, including the multi-domain effectors (comprising BH domains 1–3) Bax, Bak, Bok and BH3-only proteins such as Bid, Bim and Bad (For review see [63]). The induction of MOMP is promoted by pro-apoptotic proteins Bax and Bak, which oligomerize to form pores in the outer mitochondrial membrane (OMM) [64]. BH-3 only proteins function as either direct activators of Bax and Bak, or as de-repressors of anti-apoptotic Bcl-2 and Bcl-X_L [65, 66]. Currently, there are two opposite models describing the activity of BH-3 only proteins (see review [67]). According to one model, Bax and Bak are constantly repressed by the anti-apoptotic activity of Bcl-2 like proteins. Activated BH3-only proteins associate with Bcl-2 like proteins, thereby releasing Bax and Bak to promote MOMP. The other model indicates that some BH3-only proteins, such as Bid, Bim and Puma, directly bind to and activate Bax and Bak. But in normal conditions, their exposed BH3-domains interact with and are sequestered by anti-apoptotic Bcl-2 proteins. Binding of other BH3-only proteins, such as Bad, to the anti-apoptotic proteins results in the release of Bid, Bim and Puma, allowing them to activate Bax (for review [63]). Figure 1A shows a representation of the mitochondrial pathway.

- **The extrinsic pathway of apoptosis**

As mentioned above, several stimuli, such as Fas ligand and TRAIL, can lead to apoptosis. However, the most extensively studied mechanism is the one induced by TNF. Binding of TNF to the extracellular domain of TNFR1 [68] results in the formation of complex I, which contains TNF-α receptor associated death domain (TRADD), the E3-ubiquitin ligases TNF-α receptor associated factor 2/5 (TRAF2/5), and the cellular inhibitor of apoptosis proteins (cIAP1/2), which promote K63-linked ubiquitination of receptor interacting protein kinase 1 (RIPK1) [69, 70].

RIPK1 is a serine/threonine kinase of the RIPK family and is considered as a molecular switch between RIPK1 kinase-dependent apoptosis and necroptosis [71]. The RIPK1 ubiquitination state is crucial because it determines whether RIPK1 functions as a molecular platform for the recruitment of molecular adapters that can elicit a pro-survival response, or as a kinase that promotes cell death.

In apoptosis, K63-linked ubiquitination of RIPK1 finally leads to the induction of the nuclear factor-kappa B signaling pathway, which generates a pro-survival response. When the ubiquitination of RIPK1 is inhibited [72-74], it dissociates from complex I and forms, together with Fas associated protein with death domain (FADD) and initiator caspase-8, the cytoplasmic death inducing signaling complex (DISC) [75]. Recruitment and oligomerization of caspase-8 monomers in the DISC result in its autocatalytic activation [76]. Functional caspase-8 subsequently activates executioner caspase-3 and -7 by limited proteolysis within their interdomain linker. By contrast to caspase-8, the executioner caspase zymogens exist in the cytosol as inactive dimers [77]. The activated executioner caspases finally mediate apoptosis by proteolytically processing their substrates, such as poly(ADP)-ribose polymerase (PARP) [78, 79]. Figure 1B shows a representation of the apoptosis and necroptosis signaling pathways and key molecular effectors.

Approaches for apoptosis assessment

As apoptosis plays an essential role in cell homeostasis, it has to be fully characterized in order to define specific molecular targets to modulate it therapeutically. Multiple analytical procedures have been developed to determine apoptosis presence and its extent. These approaches can be divided into two groups: biochemical assays and fluorogenic assays.

- **Biochemical assays**

Apoptosis is characterized by the cleavage of DNA at internucleosomal (linker) sections by an activated endonuclease [80], and by membrane blebbing [81]. In electrophoretic gels the fragmented DNA shows a typical ladder pattern [80]. The morphological changes in the plasma membrane can be detected by atomic force microscopy (AFM), which has been successfully applied in studies on K562, HeLa and Ishikawa cell lines [81, 82].

An alternative approach for identifying apoptotic cells is based on the detection of DNA strand breaks by labeling their 3'OH termini by using exogenous terminal deoxynucleotidyl transferase (TdT) dUTP nick end labeling (TUNEL) assay [83]. The labeling substrates include biotin- or digoxigenin-conjugated nucleotides [84, 85] and BrdUTP [86]. The TUNEL assay has been successfully used to detect, at earlier stages of apoptosis, the activation of a serine protease that hydrolyzes protein(s)

associated with the internucleosomal linker DNA. In this way, the serine protease, increases the accessibility of DNA to the apoptosis-associated endonuclease [84]. Moreover, by performing TUNEL staining on organ sections, cell death can be precisely localized *in situ* [87].

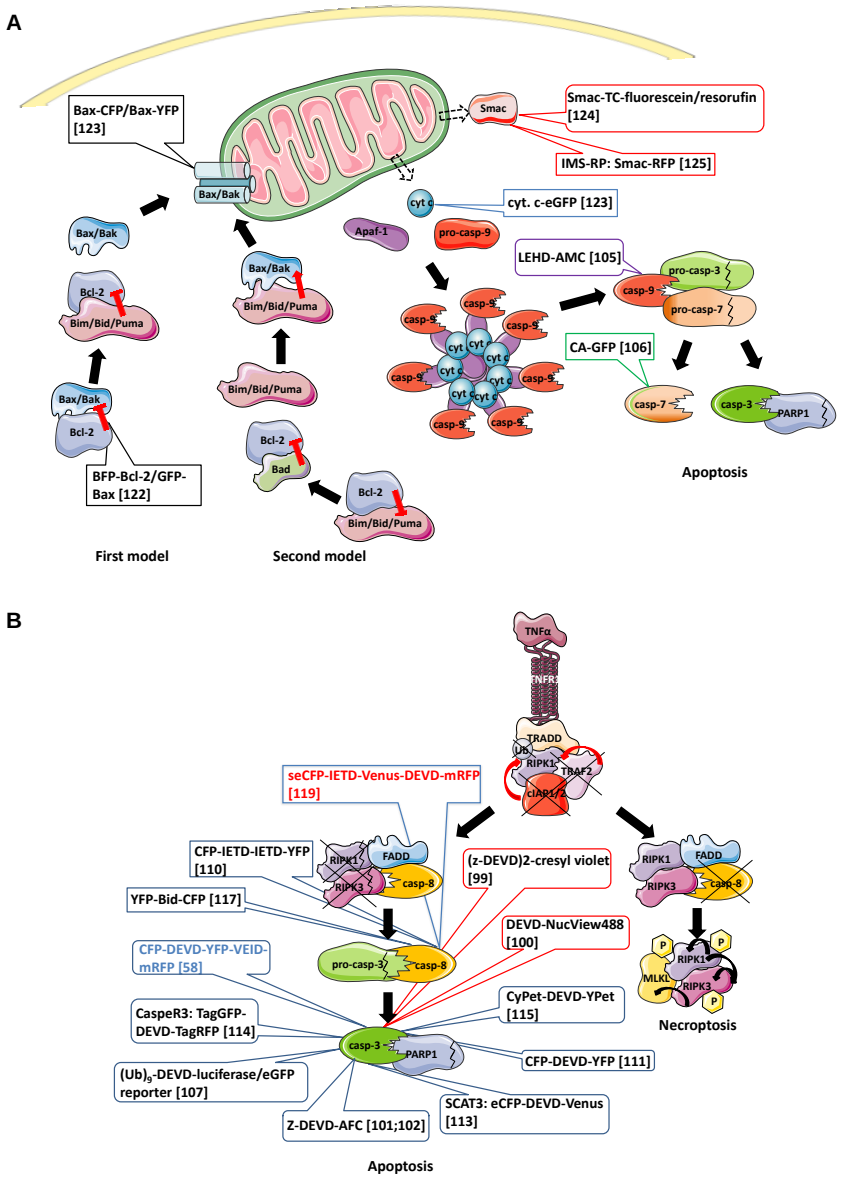

Figure 1: Programmed cell death signaling pathways and dedicated fluorescent probes and FRET based biosensors. (A) The intrinsic pathway. Signaling pathways are indicated by solid-line arrows. Release of cytochrome c and Smac from mitochondria is indicated by a dashed-line arrow. Red T signs indicate protein inhibition. Red arrows indicate protein activation. Cleavage of the protein is denoted by zigzag lines. Fluorescent probes and biosensors are indicated by callouts (rectangles: biosensors; rounded rectangles: bioprobes; black: conditional biosensors; blue: for cyt c; red: for Smac, green: for caspase-7; purple for caspase-9). Names and domain compositions of fluorescent indicators are indicated and are followed by the references in parentheses. Domain names are linked with hyphens from the N- to the C-terminus. casp, caspase; cyt c, cytochrome c. **(B)** The extrinsic pathway. Signaling pathways are indicated by solid-line arrows. Curved arrows indicate post-translational modifications (red: ubiquitination; black: phosphorylation). Crossovers denote the absence of the functional protein or post-translational modification. Zigzag lines designate the cleavage of the protein. Fluorescent probes and biosensors are indicated by callouts (rectangular: for caspase-8; rounded rectangular: for caspase-3; oval: for caspase-9; red callout: fluorescent probe; blue callout: biosensor). Names and domain compositions of fluorescent indicators are designated and are followed by the references in parentheses (black

font: single caspase indicators; red font: biosensor designed for caspase-8 and -3; blue font: biosensor designed for caspase-3 and -6). Domain names are linked with hyphens from the N- to the C-terminus. Ub, ubiquitin; casp, caspase; P, phosphate. (Figure designed using references [58, 99–102, 105–107, 110, 111, 113–115, 117, 119, 122–125].)

Another characteristic of apoptosis widely used to detect it is the external exposure of phosphatidylserine (PS), which is normally located on the inner surface of the lipid bilayer [88]. The anticoagulant protein annexin V binds phosphatidylserine with high affinity. Upon induction of apoptosis, cells surface-exposing phosphatidylserine are available to annexin V. During the early stages of apoptosis, cells can still exclude cationic dyes such as propidium iodide (PI). Therefore, during the early stages of apoptosis cells bind annexin V and exclude PI, becoming PS^+/PI^-. At later stages of apoptosis, cells can no longer exclude PI and become double fluorescent, PS^+/PI^+. The use of fluorochrome-conjugated annexin V in flow cytometry is now widespread [89, 90]. In 2000, Belloc *et al*. used flow cytometric analysis with annexin V and anti-active caspase-3 antibodies to show that a partial caspase-3 activation precedes external exposure of PS [91]. Recently, a new technique called eletrochemiluminescence (ECL) cytosensing has been introduced. This technique uses annexin V immobilized on L-cysteine-capped cadmium sulfide quantum dots (CdS-QDs)/Polyaniline nanofibers. Interaction between PS on the surface of apoptotic cells and annexin V can be probed by ECL. This method is highly sensitive, selective, reproducible and simple [92].

An alternative approach frequently used to detect apoptosis is the measurement of cyt. c release. This analysis can be performed using various fractionation techniques whereby cells are either permeabilized with digitonin or mechanically ruptured followed by separation of the cytosolic fraction from the heavy membrane fraction containing mitochondria. Both fractions are analyzed by western blotting to determine cyt. c distribution and amount [93]. This method has been successfully applied to demonstrate that cell death stimuli such as Bax- or Bax/Bak-dependent pro-apoptotic drugs induce hierarchical release of the mitochondrial factors involved in the induction of cell death [94].

As mentioned above, the relatively early caspase activation is a major event and a hallmark of apoptosis [78]. One way to determine caspase activation is by detection of the cleavage products of caspase substrates such as PARP1 [78, 79] by western blotting [78] or flow cytometry [95]. The latter technique has been used to show the difference in kinetics between apoptosis induced by camptothecin and that

caused by TNFα together with cycloheximide [95]. Another way to assess activation of caspases is by detecting the epitope of the activated (cleaved) caspases with specific antibodies using western blotting analysis or flow cytometry [91]. Like TUNEL staining, immunohistochemistry can be used to detect apoptotic cell death, and an antibody directed against activated caspase-3 can be used on organ sections to identify the localization of cell death *in situ* [87]. The use of specific substrates for caspase-3 has been successfully applied *in vivo*. By performing positron emission tomography in mice, apoptosis could be traced using caspase-3 substrates labeled with CP18 or ICMT-11 [^{18}F] [96-98]. Table 1 summarizes the biochemical approaches used to assess apoptosis.

Cellular structure/biomolecule	Approach/ technique	Reference
DNA cleavage at internucleosomal sections	Gel electrophoresis	[80]
Membrane blebbing	Atomic force microscopy (AFM)	[81, 82]
DNA strand break	Tunnel	[83-87]
External exposure of phosphatidylserine (PS)	Flow cytometry	[89-91]
	Electrochemiluminescence cytosensing	[92]
Cytoplasmic cyt. c release	Fractionation techniques followed by western blotting	[93, 94]
Caspase activation	Western blotting against caspase substrates (PARP1) or activated caspases	[78, 91]
	Flow cytometry against caspase substrates (PARP1) or activated caspases	[91, 95]
	Immunohistochemistry against activated caspases	[87]
	Positron emission tomography	[96-98]

Table 1: Biochemical approaches for assessing apoptosis

- **Fluorogenic assays**

The techniques mentioned above are useful for detecting cells undergoing apoptosis. However, most of these techniques have one major disadvantage: the analysis requires lysis or fixation of the cells, which hampers spatiotemporal resolution. Besides, these methods cannot characterize the dynamics of key biomolecules involved in apoptosis. So, approaches that can monitor apoptosis in living cells have been developed. One example of such a system is the use of fluorogenic caspase substrates [99-103]. These are peptides that are not fluorescent but emit strong fluorescence upon caspase-induced cleavage. As they are highly

permeant and not cytotoxic, these reporters can be used effectively in living cells even during long-term incubations [100]. A high content screening with the cell death siRNA pool and using NucView488™ as a caspase-3 fluorogenic substrate demonstrated the reliability of fluorescent signal production [104].

Kasili *et al*., 2004 described the use of a fluorogenic probe containing a cleavage site for caspase-9 linked to 7-amino-4-methylcoumarin (AMC). This probe was used to reveal caspase-9 involvement in apoptotic MCF-7 cells after photodynamic therapy (PDT) with δ-aminolevulinic acid (ALA) [105].

Recently, several caspase activity reporters that use GFP as a fluorescent label have been described. One of them, Caspase Activatable-GFP (CA-GFP), is specific for caspase-7 and contains a version of GFP that does not show any fluorescence due to the presence of a hydrophobic quenching peptide that tetramerizes GFP, thus preventing its maturation. The fluorescence can be completely restored by catalytic removal of the quenching peptide following caspase activation. The reporter appeared to be more sensitive than other apoptosis reporters: in mammalian cells it provides a three-fold increase in fluorescence upon induction of apoptosis and activation of caspases. The system is effective for time-resolved observation of apoptosis [106]. Another recently described reporter contains an enhanced green fluorescent protein (eGFP) and a luciferase encompassing a caspase cleavage sequence flanked by a proteasome recognition site. In the absence of active caspases, the proteasome recognition site gets ubiquitinated and is degraded by the proteasome. But when caspases are activated, the caspase recognition sequence is cleaved, releasing luciferase and GFP. The presence of both luciferase and GFP makes this versatile reporter suitable for both *in situ* and *in vivo* use. Using this reporter Huang *et al*. demonstrated caspase-3 activation in solid tumors during radiotherapy [107].

Another approach that is gaining much attention is the use of FRET-based biosensors and probes to assess the initiation and execution of apoptosis. This method makes use of two GFP derivatives encompassing a peptide substrate specific for a certain caspase [108]. In the absence of active caspase, the two proteins are brought together and non-radiative energy is transferred from the donor to the acceptor fluorophore. But when caspase activity is present, the peptide is cleaved, separating the two fluorophores and eliminating FRET [108]. The two most

commonly used fluorophores are cyan fluorescent protein (CFP) and yellow fluorescent protein (YFP) [109-112] or its improved version Venus [113]. Another combination is TagGFP (an enhanced bright mutant of the GFP-like protein) and TagRFP (a monomeric red fluorescent protein) generated from the wild-type RFP [114]. This biosensor (TagGFP-DEVD-TagRFP sensor) has a wide dynamic range, bright fluorescence, and enhanced pH and photo-stability [114]. Nguyen and Daugherty described an improved FRET pair, CyPet-YPet that has a 20-fold ratiometric FRET signal change, which is much greater than the 3-fold change of the parental pair CFP-YFP [115].

Currently used apoptotic biosensors are specific for the activation of caspase-3 [111, 113, 114, 116] or caspase-8 [110, 117]. They enable visualization of the dynamics of caspase activity with high spatial resolution [110, 113]. For instance, the use of a caspase-8 biosensor that contains the Bid protein, a known caspase-8 substrate [118], fused to YFP and CFP at the N- and C-terminus, respectively, showed a difference in caspase-8 activation in SK-N-SH cells by anti-Fas antibody and Aβ or tunicamycin. Moreover, this biosensor has been used for real-time detection of cytoplasmic caspase-8-mediated cleavage of Bid, which is followed by translocation of truncated Bid [118] (tBid)-CFP to mitochondria [117]. In 2006, Wu *et al*. developed a dual FRET biosensor for caspase-3 and caspase-6 [58]. The study highlighted a difference in activity kinetics between caspase-3 and -6. The analysis revealed that following apoptosis induction, caspase-3 activation preceded caspase-6 by ~30 min [58]. Another apoptotic biosensor recently developed by Kominami *et al*. monitors the activities of both caspase-8 and caspase-3. This biosensors detected distinct activation patterns of caspase-8 and -3 in response to different apoptotic stimuli in mammalian cells. This study emphasizes the necessity for positive feedback amplification of caspase-8 activation [119].

Cell death can be characterized by monitoring not only caspase activity but also the activation of the intrinsic apoptotic pathway, which includes the assessment of mitochondrial transmembrane potential (MTP) modulation. MTP modulation can be recorded by tetramethylrhodamine-based fluorescent probes, such as tetramethylrhodamine ethyl ester (TMRE) and tetramethylrhodamine methyl ester (TMRM). These probes are cell permeant, positively-charged dyes that readily accumulate in active mitochondria due to their relative negative charge. Depolarized

or inactive mitochondria fail to sequester the probes due to their decreased membrane potential. Using TMRE and in HeLa cells stimulated with staurosporine, actinomycin D or TNF together with cycloheximide Goldstein *et al.* showed that a decrease of MTP is an early event in apoptosis [120]. By contrast, Vanden Berghe *et al*. showed that mitochondria membrane is hyperpolarized in L929sAhFas cells (L929 cells stably expressing human Fas receptor). This study demonstrated that the hyperpolarization kinetic is stimulus-dependent. Upon TNF stimulation, mitochondria were hyperpolarized with biphasic kinetics, whereas H_2O_2 stimulation caused immediate hyperpolarization that rapidly returned to baseline [121].

Activation of the intrinsic apoptotic pathway can be monitored using FRET based approaches that can be used for biosensing as well as for protein–protein interaction studies. By performing FRET measurements on NIH3T3, BHK-21 and porcine aortic endothelial cells co-expressing BFP-Bcl-2 and GFP-Bax, Mahajan *et al.* not only showed their cellular localization but also demonstrated interaction between the two proteins during apoptosis [122]. A similar approach showed multimerization of Bax at the mitochondria following mitochondrial permeability transition pore (PTP) using COS-7 cells expressing either CFP-Bax or YFP-Bax. In the same study, use of cyt c coupled to eGFP also indicated that the release of cyt c following PTP opening takes place within minutes but occurs only several hours after the PTP has been locked in the open conformation [123].

Researchers also investigated the cytosolic release kinetics during apoptosis of other mitochondrial intermembrane space proteins, such as Smac, Omi and adenylate kinase-2. Recombinant proteins were fused to a short tag 10 – 15 amino acids containing a tetracysteine motif (TC). This motif is specifically recognized by a cell-permeant fluorescein- or resorufin-based fluorescent dye that binds covalently to the tag. A confocal microscopy-based, real-time approach using fluorescently labeled proteins revealed that cyt c, adenylate kinase-2, Smac, and Omi are released rapidly and simultaneously and that their release does not depend on caspase activity [124]. More recently, Albeck *et al.* described a fluorescent reporter for MOMP based on a fusion of mitochondrial import sequence of Smac and RFP. Inter-membrane space reporter protein (IMS-RP) differs from the Smac fusion protein described above, by the absence of an IAP-binding motif and is consequently biochemically inactive. Using IMS-RP in combination with specific initiator caspase reporters revealed that

MOMP occurs at a later stage during apoptosis in HeLa cells and is preceded by the activity of initiator caspases [125].

1.1.1.6. Necrosis and necroptosis

For a long time necrosis was considered as an accidental cell death. In 1988 it was discovered that TNF stimulation triggers distinct responses in different cell lines. It was then observed that some cell lines show 'classical' features of apoptosis in response to TNF while others exhibit a rounded up morphology without nuclear disintegration [126]. Two decades later, in 2005, a new term 'necroptosis' was introduced to describe a new regulated form of necrotic cell death [127]. Necroptosis is an important mechanism of virus-induced inflammation and innate immune control of viral infections [128, 129]. In animal models deficient in caspase-8 or FADD, necroptosis appears to play an important role during development [130, 131]. In addition, necroptosis is involved in pathologies in animal models of acute pancreatitis [132], hypoxic/ischemic injury [127], and septic shock [133]. Inhibition of necroptosis reduces tissue damage in models of cardiac infarction [134] and ischemic brain injury [127]. These findings demonstrate the biological importance of necroptosis, but the molecular components regulating this newly reported cell death program are not well defined.

Molecular pathway of necroptosis

As mentioned above, the molecular pathway triggered by TNF is shared by apoptosis and necroptosis. Functional caspase-8 proteolytically inactivates RIPK1 and RIPK3, which are important in necroptosis, thus promoting the initiation of apoptosis [135]. However, when the proteolytic activity of caspase-8 is pharmacologically or genetically inhibited, the cell undergoes a shift from apoptosis to necroptosis. In such a cellular context, RIPK1 and RIPK3 are not proteolytically inactivated, and they form a complex called the necrosome, which regulates various downstream effectors of signaling cascades [129, 135, 136]. A new component of the necrosome was recently identified: mixed lineage kinase-like domain protein (MLKL). This protein is phosphorylated by RIPK3 and then recruited to the necrosome, triggering necroptosis [137, 138]. Figure 1B shows a representation of the signaling pathway of necroptosis and highlights the cross-talk with the apoptosis pathway.

The serine/threonine kinases, RIPK1 and RIPK3, of the RIPK family have similar modular structures consisting of an N-terminal kinase domain (KD) and an intermediary domain (ID). Both domains play a significant role in necrosome formation. The intermediary domain is important for RIPK1−RIPK3 interaction because it contains the RIP homology interaction motif (RHIM). Mutation of RHIM disturbs the RIPK1–RIPK3 interaction and therefore necrosome formation. The kinase activity of the kinase domains is necessary for the phosphorylation of RIPK1 and RIPK3, because it promotes necrosome formation and complex stabilization [129, 135]. Unlike RIPK3, RIPK1 contains an additional C-terminal death domain (DD). The DD belongs to the 'death-fold'-superfamily of homotypic interaction motifs [139] and is necessary for the interaction of RIPK1 with other DD-proteins, such as TNFR1 and FADD [140].

Although the molecular mechanisms of necroptosis initiation are well characterized, less is known about the downstream signaling cascades responsible for the disruption of specific cellular functions. Cellular functions associated with necroptotic cell death include increased mitochondrial production of reactive oxygen species (ROS) [141], reduction of the cellular energy by unregulated ATP-consuming processes and disturbed ATP synthesis [142], lysosomal membrane permeabilization [121], and plasma membrane permeabilization [121] at the final stage of necroptosis. Some of these perturbations have been linked to the formation of the necrosome complex. The kinase activity of RIPK3 is central in necroptosis, as it plays a role in the overactivation of various metabolic cascades. The resulting increased concentration of breakdown products enhances the activity of Krebs cycle, which results in increased ROS production by mitochondria [136]. A sudden decrease in cellular ATP during necroptosis can be partially explained by the RIPK1-mediated inhibition of the adenine nucleotide translocase (ANT). This ATP/ADP antiporter is located at the inner mitochondrial membrane and is necessary for keeping the mitochondrial ADP concentration in balance for efficient ATP production and transport to the cytoplasm. Temkin *et al*. showed that RIPK1 inhibits ANT following TNFR1 stimulation. This leads to inhibition of ADP/ATP exchange and decrease of cellular ATP, and subsequently to necrotic cell death [142].

Approaches for necroptosis assessment

The methods for detecting necroptosis can be divided into two groups: biochemical and fluorogenic assays.

- **Biochemical assays**

Necroptotic cell can be analyzed morphologically by time-lapse microscopy or electron microscopy [87]. During necroptosis the cellular morphology is characterized by cellular swelling and formation of a balloon-like structure, known as oncosis [87]. Necroptosis is characterized by the absence of caspase activity. In the absence of caspase activity one can assess the involvement of necroptosis by using a novel necroptotic marker, RIPK1-dependent RIPK1/RIPK3 phosphorylation [129, 135, 136]. Normally, RIPK1 and -3 are phosphorylated in a biphasic way: an early wave (5–15 min after TNF stimulation) and a late wave (90–120 min after TNF stimulation). Only the late phosphorylation peak of RIPK1/3, which is dependent on RIPK1, is linked to necroptosis induction [143]. Therefore, the second RIPK1/3 phosphorylation has to be blocked by adding the RIPK1 kinase inhibitor, Necrostatin-1 [87].

Necroptosis can be assessed by using the RIPK1 specific inhibitor Necrostatin-1 [127], or by knocking down RIPK3 [144] or MLKL [137] expression, and then determining the phosphorylation profiles of necroptotic kinases by western blot analysis.

Calpains, ubiquitous cysteine proteases activated by calcium signaling, have important roles in cell death programs. Although this molecular effector is not described here, the interconnection with caspases is crucial and approaches to determine caspases and calpain activities simultaneously have been considered in neurosciences [145]. AlphaII-spectrin, a substrate of both caspases and calpain, was used in a biochemical approach to determine necroptosis and to distinguish it from apoptosis. The study performed by Zhang *et al.* in pheochromocytoma-12 (PC-12) cells after various treatments triggering either apoptosis or necroptosis aimed at assessing caspase versus calpain activity relied on multiple alphaII-spectrin breakdown products using specific antibodies. Table 2 summarizes the biochemical approaches to assess necroptosis.

- **Fluorogenic assays**

To distinguish necroptotic cells from apoptotic cells undergoing secondary necrosis, the nucleus is stained with PI. As secondary necrotic cells have already passed through an apoptotic stage, their nuclei are condensed and/or fragmented. The internucleosomal fragmentation of the DNA in apoptotic cells produces a homogenous DNA staining with PI. As necrotic cells retain their chromatin structure, their nucleoli show prominent staining [87].

A calpain FRET biosensor designed to follow synaptic activity in dendritic spines [146] was characterized in cell lines and dissociated hippocampal neurons. This biosensor composed of the micro-calpain cleavage site from alpha-spectrin flanked by eCFP and eYFP fluorescence proteins and should be used in combination with caspases activity reporters in a different cell death context.

Cellular structure / Biomolecule	Approach / technique	Reference
Cellular swelling and formation of balloon-like structure	Time-lapse microscopy or electron microscopy	[87]
RIPK1-dependent RIPK1/RIPK3 phosphorylation	*In vitro* kinase assay	[129, 135, 136]
Formation of the necrosome complex	Inhibition by RIPK-1 specific inhibitor Necrostatin-1, knockdown of RIPK3 or MLKL followed by western blotting	[127, 137, 144]
AlphaII-spectrin breakdown by calpains	Western blotting or immunocytochemistry against breakdown products of alphaII-spectrin	[136]

Table 2: Biochemical approaches for assessing necroptosis

To date, only caspase FRET biosensors can be used negatively. Because caspase biosensors function on the basis of FRET decrease upon caspase activation, and caspase activity is inhibited during necroptosis, it might be possible to monitor non-FRET change in living cells. However, if the cells are in secondary necrosis, this approach is not valid because caspases are activated during apoptosis and the protease biosensor is intrinsically irreversible.

Although RIPK1 and RIPK3 kinases are involved in initiating necroptosis, no FRET biosensors have been developed for these molecules so far. Thus, development and optimization of FRET biosensors for “positive” detection of this particular PCD should be considered. In line with this idea, we are using a genetically encoded FRET-biosensor of the sandwich design to develop RIPK kinase activity reporters (RIP-KARs). Specific RIK1 and RIPK3 substrates were identified by

proteomic approaches in cells undergoing necroptosis. RIP-KARs are currently being tested and optimized (personal communication).

Finally, cathepsins, which are proteases involved in final protein degradation by lysosomes, have been used to monitor apoptosis. Lysosomes are tightly linked with cell death. Several studies reported that release of cathepsins mediated by lysosome rupture leads to mitochondrial membrane permeabilization and a subsequent cyt c leakage into the cytoplasm, resulting in further caspase 9 activation (for review [147, 148]. A relationship between the amount of lysosomal proteins released following lysosomal rupture and the type of cell death has been established. It was reported that a small leakage of lysosomal proteins into the cytoplasm triggers apoptosis whereas extensive lysosomal rupture leads to rapid necrosis [149]. Thus, cathepsin activity should be monitored during necrosis. Cathepsin activity has been assessed mainly with chemical activity-based probes both *in vitro* and *in vivo* (for review, [150]). To investigate cathepsin B activity, Yhee *et al.* developed a cathepsin B nanoprobe (CB-NP) consisting of a near-infrared fluorescence (NIRF) dye, a dark quencher, and highly specific cathepsin-sensitive substrate [151]. CB-NP was delivered in mouse tumor tissues to monitor the fluorescent signal in the cytosol in response to cathepsin B activity [152]. Cathepsin probes are often used to monitor the effects of various pharmacological inhibitors of several cathepsins at different stages of tumor progression [153].

1.1.1.7. Perspectives

In this review, we also focus on the recent contribution of fluorogenic approaches using biosensors and reporters for cancer therapy design and treatment.

Necroptosis: the new player in cancer therapy

Most anti-cancer therapeutic strategies cause death of tumor cells by inducing damage that is recognized as an apoptosis signal. However, cancer cells undergo mutations of key effector proteins of the apoptotic machinery, such as p53, and thereby acquire resistance to therapeutic agents [154]. Before 2004, apoptosis was the only cell death program considered for the blocking of tumor growth. In most solid tumors, cancer cells metabolism is completely reorganized and consist of a complex metabolic reprogramming [155]. Generally, cancer cells present oxidative phosphorylation (OXPHOX) defects and an increase in aerobic glycolysis pathway

("Warburg phenomenon"). Although OXPHOX is more effective than glycolysis in terms of energetic yield, cancer cells prefer using this metabolic shunting to generate intermediates for anabolic reactions [156]. Cancer-specific metabolic molecules production may therefore favor cell death evasion, angiogenesis, tissue invasion, metastasis and immunosuppressive effects. Interestingly, mutations of oncogenes and/or tumor suppressor genes contribute to the control of cancer cells metabolic reprogramming [157].

In 2004, Zong *et al*. showed for the first time that alkylating agents provoke necroptosis in tumor cells [158, 159]. Indeed, alkylating agents activate the DNA repair PARP, which catalyzes the synthesis of poly(ADP-ribose) chains on specific nuclear proteins. In these experimental conditions, cells using aerobic glycolysis undergo rapid depletion of ATP and cell death while cells maintaining OXPHOS are resistant to ATP depletion and cell death. Based on the fact that most cancer cell relies on aerobic glycolysis for ATP production, the authors propose this mechanism for tumor cell death induction following alkylating agents treatment.

The mitochondrial intermembrane space protein, apoptosis inducing factor (AIF), also mediates necroptosis. Indeed, in response to DNA alkylation and subsequent PARP activation, AIF is released in the cytosol and rapidly relocalizes to the nucleus, where it promotes DNA degradation, leading to apoptosis or necroptosis [160, 161]. In this AIF-dependent necroptosis, RIPK1 participates in AIF release from mitochondria [162]. Emerging anticancer therapeutic strategies targeting AIF-mediated PCD have been developed for patients with metastatic breast and pancreatic cancers. These compounds can induce high levels of ROS, leading to AIF release from mitochondria and necroptosis of cancer cells without affecting neighboring normal cells (for review, [163]).

By contrast to apoptosis, necroptotic cancer cells drive a local inflammatory reaction by releasing pro-inflammatory molecules into the extracellular space, such as the nuclear factor high-mobility group protein B1 (HMGB1) [164], which promotes tumor cell death. Cancer cells can become resistant to current chemotherapeutic agents, targeting necroptosis has become a potential alternative approach for fighting cancer (for review [165]). Recent studies have confirmed the sensitivity of cancer cells to necroptosis [166, 167].

The main objective of therapeutic strategies used to be the targeting of caspases in cancer cells to trigger apoptosis. Nowadays, induction of necroptosis is recognized as an effective means for killing cancer cells, especially when they are apoptosis-resistant. It is important to keep in mind that apoptosis and necroptosis are not mutually exclusive processes that are entirely separated [168-170]. Apoptosis and necroptosis share many common molecular effectors. Depending on cell context and specifically on the caspase activation state, a cell can die by apoptosis or necroptosis [136, 171, 172]. In line with this view, detailed analysis of the enzyme activation state of a tumor cell line is thought to be crucial for establishing a prognosis before treatment (Figure 2). Applying this approach might help predict effective treatment in order to kill tumor cells. Genetically encoded FRET biosensors are particularly relevant for this purpose because several parameters could be measured dynamically, including activation state and concentration of specific biomolecules. The monitoring of biochemical events in real time in living cells can yield qualitative and quantitative information on signal integration mechanisms and kinetics of signal transduction. Very recently, Earley *et al.* [173] used MOMP probes [125] to visualize drug-induced apoptosis of single cells in live mice. Breast and pancreatic cancer cell lines stably expressing an intermembrane space reporter (IMS-RP) were established to detect IMS-RP release into the cytoplasm upon induction of apoptosis. Comparison of apoptotic rates between *in cellulo* and *in vivo* models showed that cancer cells outside the tumor are more sensitive to drugs. This study highlights not only the importance of improving high-resolution intra-vital microscopy [174] for *in vivo* biosensing, but also the necessity of taking into account the pathophysiological context of tumors for the development of adapted therapy. Recently, Bagci-Onder *et al.* [175] elegantly used both bioluminescence and fluorogenic reporters to overcome TRAIL resistance in glioblastoma- multiforme (GBM) cells *in cellulo* and *in vivo*. Dual bioluminescence imaging of the death receptors DR4/DR5 identified chemical modulators of DR4/DR5 expression to sensitize GBM cells to apoptosis. Live-cell imaging of GBM cells expressing FRET caspase biosensors allowed the monitoring of the effects of TRAIL stimulation on GBM cells. This study also evaluated GBM cell responses to engineered neural stem cells delivering secreted TRAIL [176] *in cellulo* and *in vivo*. This innovative and original approach provided an effective method using live-cell imaging technology, relevant biosensors, and pertinent use of stem cells properties.

FRET biosensors for prognosis and therapy design

A combination of several FRET biosensors and/or ionic species probes such as ROS can be used for multiparameter assays in living cells with high spatiotemporal resolution ([56, 177]; (for review) [178]). This “lab-on-chip” approach based on biosensors and reporters might increase our understanding of the molecular mechanisms of tumorigenesis and tumor resistance to therapeutic agents. This approach could detect cellular abnormalities and identify kinetic changes in enzyme activation and/or aberrant enzymatic activities in order to develop more effective strategies for cancer therapy. For example, if tumor cells are resistant to apoptosis, the treatment can be aimed to induce necroptosis. In addition, biosensors can also be used to monitor cellular responses to therapeutic agents [179].

A very recent study has identified a specific targeted molecule that could bypass apoptosis resistance of p53-/- colon carcinomas cells. Analysis of carcinoma cells by tissue microarray revealed overactivation of glycogen synthase kinase 3b (GSK3b) compared to normal cells from the same patient. Downregulation of the kinase in combination with chemotherapy promotes AIF-mediated necroptosis of drug-resistant colon carcinoma cells [180]. A “lab-on-chip” approach using a specific GSK3b FRET biosensor could have helped identifying GSK3b as overactivated in the cellular context, adapting treatment to the phenotype of tumor cells and finally monitoring the necroptotic process. Now there is only an atypical half-life biosensor for measuring the activity of GSK3 kinase [181].

The concept of personalized prognosis and therapy design relying on FRET-based biosensors was illustrated in a study by Mizutani *et al*. [182]. They developed a reliable genetically encoded FRET-based biosensor to measure breakpoint cluster region-abelson (BCR-ABL) activity directly in living chronic myeloid leukemia cells (CML) obtained from a patient. Since chimeric BCR-ABL kinase exists only in tumor cells, Imatinib (US) and Gleevec (EU) work specifically in tumor cells without affecting neighboring normal cells. This biosensor approach is radically different from conventional techniques trying to capture a snapshot of BCR-ABL activity by assessing the phosphorylation level of its substrate v-Crk avian sarcoma virus CT10 oncogene homolog-like (CrkL) *in vitro*. This novel dynamic approach has enabled the identification of a small population of CML cells resistant to Gleevec. The biosensor approach was then applied to optimize therapy design for targeting both drug-

sensitive and drug-resistant CML cells according to the patient's tumor stage [183, 184]. Interestingly, this biosensor approach was also used to evaluate and compare BCR-ABL mutation effects on cell sensitivity to several inhibitors in order to predict the most appropriate treatment, thus providing a new method for prognosis.

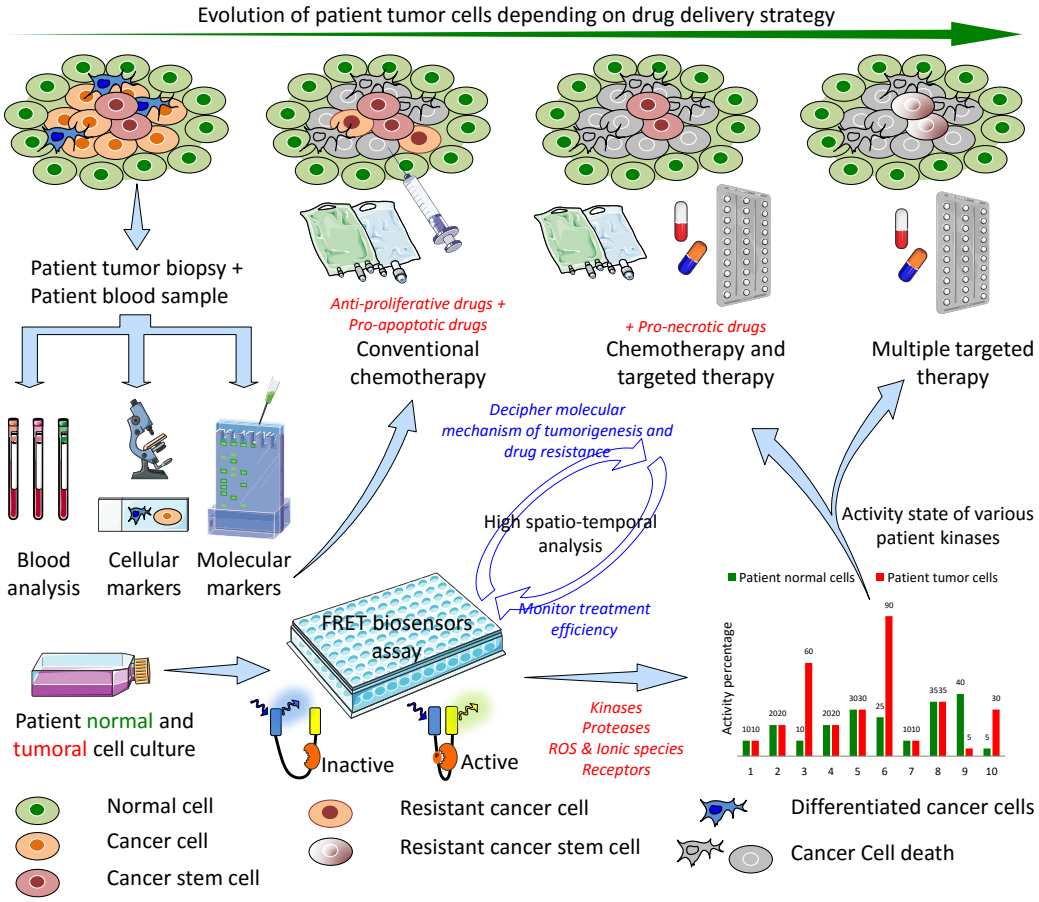

Figure 2: The evolution of therapeutic strategies and biotechnologies for cancer therapy and the use of FRET biosensor strategies for evaluating cancer drug combinations. A few years ago, treatments were mainly based on cellular and molecular markers and limited to chemotherapy with both anti-proliferative and pro-apoptotic drugs. These treatments remained ineffective against various resistances developed by cancer cells. Nowadays, new strategies tend to analyze the activation state of the enzymes within patient tumor cells to tailor treatment, including both chemotherapeutics and agents that target specific enzymes responsible for the aggressiveness of the tumor. FRET biosensors provide powerful tools for accurate determination of the activation state profiles of key regulators in a patient's tumor cells. Live-cell, biosensor-based dynamic approaches can be used to refine therapy design and to monitor treatment efficacy. Biosensors and reporters can also be used for *in cellulo* screening of new drug candidates. In the near future, therapeutic strategies relying on biosensors will surely contribute to personalized medicine.

In conclusion, to overcome the drawback of biochemical approaches, biosensors and reporters with greater spatiotemporal resolution have been developed by molecular engineering to cope with new challenges in biology, namely, the measurement of activity and interaction of biomolecules in living cells in real time. These new powerful and optimized tools are slowly but surely joining the biologist's toolbox to determine the dynamics of biomolecules in their physiological context

[185-187]. These dynamic approaches will surely help us deepen our understanding of the molecular mechanisms of PCD, and will allow us to develop new therapeutic strategies to improve the efficacy of personalized treatment.

Acknowledgements

PV is senior full professor at Ghent University and holder of a Methusalem grant (BOF09/01M00709). FR is a visiting research professor at Ghent University and full associate professor at Lille1 University. ML is paid by the FWO G.0875.11 project in the Vandenabeele lab. FS is a joint PhD. student between Lille1 University and Ghent University, and is funded by Lille 1 University, the Centre National de la Recherche Scientifique (CNRS), and Vandenabeele's group research funding (FWO G.0875.11). Research in the Vandenabeele group is supported by Belgian grants (Interuniversity Attraction Poles, IAP 7/32), Flemish grants (Research Foundation Flanders: FWO G.0875.11, FWO G.0973.11, FWO G.0A45.12N, FWO G.0787.13N Methusalem grant - BOF09/01M00709), Ghent University grants (MRP, GROUP-ID consortium), grant from the 'Foundation against Cancer, F94) and grants from VIB. This work was encouraged by the CNRS Groupement de recherche (GDR) 2588 "Microscopie et Imagerie du Vivant" via its French Biosensor Workgroup.

We thank Dr. Sandrine Jouan-Lanhouet and Dr. Brigitta Brinkman for helpful discussions, and Dr. Amin Bredan for advices and editing of this manuscript.

Figures were generated using the image bank from Servier Medical Art.

No conflict of interest to declare.

References

[1] Allen, P. J., *Journal of Agricultural Research* 1923, *23*, 131-152.
[2] Greenberg, J. T., Programmed cell death: a way of life for plants. *Proc Natl Acad Sci U S A* 1996, *93*, 12094-12097.
[3] Jones, A. M., Programmed cell death in development and defense. *Plant Physiol* 2001, *125*, 94-97.
[4] Reape, T. J., McCabe, P. F., Apoptotic-like regulation of programmed cell death in plants. *Apoptosis* 2010, *15*, 249-256.
[5] Bozhkov, P. V., Lam, E., Green death: revealing programmed cell death in plants. *Cell Death Differ* 2011, *18*, 1239-1240.
[6] Lindsten, T., Ross, A. J., King, A., Zong, W. X.*, et al.*, The combined functions of proapoptotic Bcl-2 family members bak and bax are essential for normal development of multiple tissues. *Mol Cell* 2000, *6*, 1389-1399.
[7] Henson, P. M., Hume, D. A., Apoptotic cell removal in development and tissue homeostasis. *Trends Immunol* 2006, *27*, 244-250.
[8] Fuchs, Y., Steller, H., Programmed cell death in animal development and disease. *Cell* 2011, *147*, 742-758.
[9] Declercq, W., Vanden Berghe, T., Vandenabeele, P., RIP kinases at the crossroads of cell death and survival. *Cell* 2009, *138*, 229-232.
[10] Galluzzi, L., Kroemer, G., Necroptosis: a specialized pathway of programmed necrosis. *Cell* 2008, *135*, 1161-1163.
[11] Galluzzi, L., Vanden Berghe, T., Vanlangenakker, N., Buettner, S.*, et al.*, Programmed necrosis from molecules to health and disease. *Int Rev Cell Mol Biol* 2011, *289*, 1-35.
[12] Ouyang, L., Shi, Z., Zhao, S., Wang, F. T.*, et al.*, Programmed cell death pathways in cancer: a review of apoptosis, autophagy and programmed necrosis. *Cell Prolif* 2012, *45*, 487-498.
[13] Vandenabeele, P., Declercq, W., Van Herreweghe, F., Vanden Berghe, T., The role of the kinases RIP1 and RIP3 in TNF-induced necrosis. *Sci Signal* 2010, *3*, re4.
[14] Vandenabeele, P., Galluzzi, L., Vanden Berghe, T., Kroemer, G., Molecular mechanisms of necroptosis: an ordered cellular explosion. *Nat Rev Mol Cell Biol* 2010, *11*, 700-714.
[15] Vanlangenakker, N., Vanden Berghe, T., Vandenabeele, P., Many stimuli pull the necrotic trigger, an overview. *Cell Death Differ* 2012, *19*, 75-86.
[16] Ghavami, S., Hashemi, M., Ande, S. R., Yeganeh, B.*, et al.*, Apoptosis and cancer: mutations within caspase genes. *J Med Genet* 2009, *46*, 497-510.
[17] Wong, R. S., Apoptosis in cancer: from pathogenesis to treatment. *J Exp Clin Cancer Res* 2011, *30*, 87.
[18] Golstein, P., Controlling cell death. *Science* 1997, *275*, 1081-1082.
[19] Kaiser, W. J., Upton, J. W., Mocarski, E. S., Viral modulation of programmed necrosis. *Curr Opin Virol* 2013.
[20] Upton, J. W., Kaiser, W. J., Mocarski, E. S., Virus inhibition of RIP3-dependent necrosis. *Cell Host Microbe* 2010, *7*, 302-313.
[21] Mattson, M. P., Apoptosis in neurodegenerative disorders. *Nat Rev Mol Cell Biol* 2000, *1*, 120-129.

[22] Murphy, A. C., Weyhenmeyer, B., Schmid, J., Kilbride, S. M., *et al.*, Activation of executioner caspases is a predictor of progression-free survival in glioblastoma patients: a systems medicine approach. *Cell Death Dis* 2013, *4*, e629.
[23] Konstantinidis, K., Whelan, R. S., Kitsis, R. N., Mechanisms of cell death in heart disease. *Arterioscler Thromb Vasc Biol* 2012, *32*, 1552-1562.
[24] Kung, G., Konstantinidis, K., Kitsis, R. N., Programmed necrosis, not apoptosis, in the heart. *Circ Res* 2011, *108*, 1017-1036.
[25] Whelan, R. S., Kaplinskiy, V., Kitsis, R. N., Cell death in the pathogenesis of heart disease: mechanisms and significance. *Annu Rev Physiol* 2010, *72*, 19-44.
[26] Chiong, M., Wang, Z. V., Pedrozo, Z., Cao, D. J., *et al.*, Cardiomyocyte death: mechanisms and translational implications. *Cell Death Dis* 2011, *2*, e244.
[27] Carter, J., Lippa, C. F., Beta-amyloid, neuronal death and Alzheimer's disease. *Curr Mol Med* 2001, *1*, 733-737.
[28] Castro, R. E., Santos, M. M., Gloria, P. M., Ribeiro, C. J., *et al.*, Cell death targets and potential modulators in Alzheimer's disease. *Curr Pharm Des* 2010, *16*, 2851-2864.
[29] Benedict, C. A., Norris, P. S., Ware, C. F., To kill or be killed: viral evasion of apoptosis. *Nat Immunol* 2002, *3*, 1013-1018.
[30] Hanahan, D., Weinberg, R. A., The hallmarks of cancer. *Cell* 2000, *100*, 57-70.
[31] Hanahan, D., Weinberg, R. A., Hallmarks of cancer: the next generation. *Cell* 2011, *144*, 646-674.
[32] Igney, F. H., Krammer, P. H., Immune escape of tumors: apoptosis resistance and tumor counterattack. *J Leukoc Biol* 2002, *71*, 907-920.
[33] Kroemer, G., Galluzzi, L., Vandenabeele, P., Abrams, J., *et al.*, Classification of cell death: recommendations of the Nomenclature Committee on Cell Death 2009. *Cell Death Differ* 2009, *16*, 3-11.
[34] Das, G., Shravage, B. V., Baehrecke, E. H., Regulation and function of autophagy during cell survival and cell death. *Cold Spring Harb Perspect Biol* 2012, *4*.
[35] Tichy, E. D., Stephan, Z. A., Osterburg, A., Noel, G., Stambrook, P. J., Mouse embryonic stem cells undergo charontosis, a novel programmed cell death pathway dependent upon cathepsins, p53, and EndoG, in response to etoposide treatment. *Stem Cell Res* 2013, *10*, 428-441.
[36] Dixon, S. J., Lemberg, K. M., Lamprecht, M. R., Skouta, R., *et al.*, Ferroptosis: an iron-dependent form of nonapoptotic cell death. *Cell* 2012, *149*, 1060-1072.
[37] Caunt, C. J., Finch, A. R., Sedgley, K. R., McArdle, C. A., GnRH receptor signalling to ERK: kinetics and compartmentalization. *Trends Endocrinol Metab* 2006, *17*, 308-313.
[38] Ebisuya, M., Kondoh, K., Nishida, E., The duration, magnitude and compartmentalization of ERK MAP kinase activity: mechanisms for providing signaling specificity. *J Cell Sci* 2005, *118*, 2997-3002.
[39] Herbst, K. J., Allen, M. D., Zhang, J., Spatiotemporally regulated protein kinase A activity is a critical regulator of growth factor-stimulated extracellular signal-regulated kinase signaling in PC12 cells. *Mol Cell Biol* 2011, *31*, 4063-4075.
[40] Mebratu, Y., Tesfaigzi, Y., How ERK1/2 activation controls cell proliferation and cell death: Is subcellular localization the answer? *Cell Cycle* 2009, *8*, 1168-1175.
[41] Riquet, F. B., Vandame, P., Sipieter, F., Cailliau-Maggio, K., *et al.*, Reporting Kinase Activities: Paradigms, Tools and Perspectives. *Journal of Biological Medicine* 2011, *1*, 10-18.
[42] Cagnol, S., Chambard, J. C., ERK and cell death: mechanisms of ERK-induced cell death--apoptosis, autophagy and senescence. *FEBS J* 2010, *277*, 2-21.
[43] Bartholomeusz, C., Rosen, D., Wei, C., Kazansky, A., *et al.*, PEA-15 induces autophagy in human ovarian cancer cells and is associated with prolonged overall survival. *Cancer Res* 2008, *68*, 9302-9310.
[44] Tresini, M., Lorenzini, A., Torres, C., Cristofalo, V. J., Modulation of replicative senescence of diploid human cells by nuclear ERK signaling. *J Biol Chem* 2007, *282*, 4136-4151.
[45] Kohda, Y., Matsunaga, Y., Shiota, R., Satoh, T., *et al.*, Involvement of Raf-1/MEK/ERK1/2 signaling pathway in zinc-induced injury in rat renal cortical slices. *J Toxicol Sci* 2006, *31*, 207-217.
[46] Sipieter, F., Vandame, P., Spriet, C., Leray, A., *et al.*, From FRET Imaging to Practical Methodology for Kinase Activity Sensing in Living Cells. *Prog Mol Biol Transl Sci* 2013, *113*, 145-216.
[47] Arosio, D., Ricci, F., Marchetti, L., Gualdani, R., *et al.*, Simultaneous intracellular chloride and pH measurements using a GFP-based sensor. *Nat Methods* 2010, *7*, 516-518.
[48] Belousov, V. V., Fradkov, A. F., Lukyanov, K. A., Staroverov, D. B., *et al.*, Genetically encoded fluorescent indicator for intracellular hydrogen peroxide. *Nat Methods* 2006, *3*, 281-286.
[49] Tantama, M., Hung, Y. P., Yellen, G., Imaging intracellular pH in live cells with a genetically encoded red fluorescent protein sensor. *J Am Chem Soc* 2011, *133*, 10034-10037.
[50] Zhang, Y., Xie, Q., Robertson, J. B., Johnson, C. H., pHlash: a new genetically encoded and ratiometric luminescence sensor of intracellular pH. *PLoS One* 2012, *7*, e43072.
[51] Ibraheem, A., Campbell, R. E., Designs and applications of fluorescent protein-based biosensors. *Curr Opin Chem Biol* 2010, *14*, 30-36.
[52] Kerppola, T. K., Bimolecular fluorescence complementation (BiFC) analysis as a probe of protein interactions in living cells. *Annu Rev Biophys* 2008, *37*, 465-487.
[53] Lukasiewicz, S., Faron-Gorecka, A., Dobrucki, J., Polit, A., Dziedzicka-Wasylewska, M., Studies on the role of the receptor protein motifs possibly involved in electrostatic interactions on the dopamine D1 and D2 receptor oligomerization. *FEBS J* 2009, *276*, 760-775.

[54] Aye-Han, N. N., Ni, Q., Zhang, J., Fluorescent biosensors for real-time tracking of post-translational modification dynamics. *Curr Opin Chem Biol* 2009, *13*, 392-397.
[55] Kunkel, M. T., Newton, A. C., Spatiotemporal Dynamics of Kinase Signaling Visualized by Targeted Reporters. *Curr Protoc Chem Biol* 2009, *1*, 17-18.
[56] Ai, H. W., Hazelwood, K. L., Davidson, M. W., Campbell, R. E., Fluorescent protein FRET pairs for ratiometric imaging of dual biosensors. *Nat Methods* 2008, *5*, 401-403.
[57] Shekhawat, S. S., Campbell, S. T., Ghosh, I., A comprehensive panel of turn-on caspase biosensors for investigating caspase specificity and caspase activation pathways. *Chembiochem* 2011, *12*, 2353-2364.
[58] Wu, X., Simone, J., Hewgill, D., Siegel, R.*, et al.*, Measurement of two caspase activities simultaneously in living cells by a novel dual FRET fluorescent indicator probe. *Cytometry A* 2006, *69*, 477-486.
[59] Herold, C., Rennekampff, H. O., Engeli, S., Apoptotic pathways in adipose tissue. *Apoptosis* 2013.
[60] Montero, J. A., Hurle, J. M., Sculpturing digit shape by cell death. *Apoptosis* 2010, *15*, 365-375.
[61] Li, P., Nijhawan, D., Budihardjo, I., Srinivasula, S. M.*, et al.*, Cytochrome c and dATP-dependent formation of Apaf-1/caspase-9 complex initiates an apoptotic protease cascade. *Cell* 1997, *91*, 479-489.
[62] Elmore, S., Apoptosis: a review of programmed cell death. *Toxicol Pathol* 2007, *35*, 495-516.
[63] Lindsay, J., Esposti, M. D., Gilmore, A. P., Bcl-2 proteins and mitochondria--specificity in membrane targeting for death. *Biochim Biophys Acta* 2011, *1813*, 532-539.
[64] Mikhailov, V., Mikhailova, M., Degenhardt, K., Venkatachalam, M. A.*, et al.*, Association of Bax and Bak homo-oligomers in mitochondria. Bax requirement for Bak reorganization and cytochrome c release. *J Biol Chem* 2003, *278*, 5367-5376.
[65] Letai, A., Bassik, M. C., Walensky, L. D., Sorcinelli, M. D.*, et al.*, Distinct BH3 domains either sensitize or activate mitochondrial apoptosis, serving as prototype cancer therapeutics. *Cancer Cell* 2002, *2*, 183-192.
[66] Willis, S. N., Chen, L., Dewson, G., Wei, A.*, et al.*, Proapoptotic Bak is sequestered by Mcl-1 and Bcl-xL, but not Bcl-2, until displaced by BH3-only proteins. *Genes Dev* 2005, *19*, 1294-1305.
[67] Chipuk, J. E., Green, D. R., How do BCL-2 proteins induce mitochondrial outer membrane permeabilization? *Trends Cell Biol* 2008, *18*, 157-164.
[68] Andera, L., Signaling activated by the death receptors of the TNFR family. *Biomed Pap Med Fac Univ Palacky Olomouc Czech Repub* 2009, *153*, 173-180.
[69] Mahoney, D. J., Cheung, H. H., Mrad, R. L., Plenchette, S.*, et al.*, Both cIAP1 and cIAP2 regulate TNFalpha-mediated NF-kappaB activation. *Proc Natl Acad Sci U S A* 2008, *105*, 11778-11783.
[70] Varfolomeev, E., Goncharov, T., Fedorova, A. V., Dynek, J. N.*, et al.*, c-IAP1 and c-IAP2 are critical mediators of tumor necrosis factor alpha (TNFalpha)-induced NF-kappaB activation. *J Biol Chem* 2008, *283*, 24295-24299.
[71] Duprez, L., Bertrand, M. J., Vanden Berghe, T., Dondelinger, Y.*, et al.*, Intermediate domain of receptor-interacting protein kinase 1 (RIPK1) determines switch between necroptosis and RIPK1 kinase-dependent apoptosis. *J Biol Chem* 2012, *287*, 14863-14872.
[72] Shembade, N., Ma, A., Harhaj, E. W., Inhibition of NF-kappaB signaling by A20 through disruption of ubiquitin enzyme complexes. *Science* 2010, *327*, 1135-1139.
[73] Kovalenko, A., Kim, J. C., Kang, T. B., Rajput, A.*, et al.*, Caspase-8 deficiency in epidermal keratinocytes triggers an inflammatory skin disease. *J Exp Med* 2009, *206*, 2161-2177.
[74] Wertz, I. E., O'Rourke, K. M., Zhou, H., Eby, M.*, et al.*, De-ubiquitination and ubiquitin ligase domains of A20 downregulate NF-kappaB signalling. *Nature* 2004, *430*, 694-699.
[75] Wu, W., Liu, P., Li, J., Necroptosis: an emerging form of programmed cell death. *Crit Rev Oncol Hematol* 2012, *82*, 249-258.
[76] Park, H. H., Structural features of caspase-activating complexes. *Int J Mol Sci* 2012, *13*, 4807-4818.
[77] Boatright, K. M., Renatus, M., Scott, F. L., Sperandio, S.*, et al.*, A unified model for apical caspase activation. *Mol Cell* 2003, *11*, 529-541.
[78] Kaufmann, S. H., Desnoyers, S., Ottaviano, Y., Davidson, N. E., Poirier, G. G., Specific proteolytic cleavage of poly(ADP-ribose) polymerase: an early marker of chemotherapy-induced apoptosis. *Cancer Res* 1993, *53*, 3976-3985.
[79] Nicholson, D. W., Ali, A., Thornberry, N. A., Vaillancourt, J. P.*, et al.*, Identification and inhibition of the ICE/CED-3 protease necessary for mammalian apoptosis. *Nature* 1995, *376*, 37-43.
[80] Arends, M. J., Morris, R. G., Wyllie, A. H., Apoptosis. The role of the endonuclease. *Am J Pathol* 1990, *136*, 593-608.
[81] Jin, H., Zhao, H., Liu, L., Jiang, J.*, et al.*, Apoptosis induction of K562 cells by lymphocytes: an AFM study. *Scanning* 2013, *35*, 7-11.
[82] Kim, Y. S., Kim, K. S., Cho, C. H., Yoon, K. S.*, et al.*, Quantitative analysis with atomic force microscopy of cisplatin-induced morphological changes in HeLa and Ishikawa cells. *J Nippon Med Sch* 2012, *79*, 320-326.
[83] Gavrieli, Y., Sherman, Y., Ben-Sasson, S. A., Identification of programmed cell death in situ via specific labeling of nuclear DNA fragmentation. *J Cell Biol* 1992, *119*, 493-501.
[84] Gorczyca, W., Bruno, S., Darzynkiewicz, R., Gong, J., Darzynkiewicz, Z., DNA strand breaks occurring during apoptosis - their early insitu detection by the terminal deoxynucleotidyl transferase and nick translation assays and prevention by serine protease inhibitors. *Int J Oncol* 1992, *1*, 639-648.
[85] Gorczyca, W., Gong, J., Darzynkiewicz, Z., Detection of DNA strand breaks in individual apoptotic cells by the in situ terminal deoxynucleotidyl transferase and nick translation assays. *Cancer Res* 1993, *53*, 1945-1951.

[86] Li, X., Darzynkiewicz, Z., Labelling DNA strand breaks with BrdUTP. Detection of apoptosis and cell proliferation. *Cell Prolif* 1995, *28*, 571-579.
[87] Vanden Berghe, T., Grootjans, S., Goossens, V., Dondelinger, Y.*, et al.*, Determination of apoptotic and necrotic cell death in vitro and in vivo. *Methods* 2013, *61*, 117-129.
[88] Fadok, V. A., Voelker, D. R., Campbell, P. A., Cohen, J. J.*, et al.*, Exposure of phosphatidylserine on the surface of apoptotic lymphocytes triggers specific recognition and removal by macrophages. *J Immunol* 1992, *148*, 2207-2216.
[89] Koopman, G., Reutelingsperger, C. P., Kuijten, G. A., Keehnen, R. M.*, et al.*, Annexin V for flow cytometric detection of phosphatidylserine expression on B cells undergoing apoptosis. *Blood* 1994, *84*, 1415-1420.
[90] van Engeland, M., Nieland, L. J., Ramaekers, F. C., Schutte, B., Reutelingsperger, C. P., Annexin V-affinity assay: a review on an apoptosis detection system based on phosphatidylserine exposure. *Cytometry* 1998, *31*, 1-9.
[91] Belloc, F., Belaud-Rotureau, M. A., Lavignolle, V., Bascans, E.*, et al.*, Flow cytometry detection of caspase 3 activation in preapoptotic leukemic cells. *Cytometry* 2000, *40*, 151-160.
[92] Zhang, L., Jiang, J. H., Luo, J. J., Cai, J. Y.*, et al.*, A label-free electrochemiluminescence cytosensors for specific detection of early apoptosis. *Biosens Bioelectron* 2013, *49C*, 46-52.
[93] Arnoult, D., Apoptosis-associated mitochondrial outer membrane permeabilization assays. *Methods* 2008, *44*, 229-234.
[94] Arnoult, D., Gaume, B., Karbowski, M., Sharpe, J. C.*, et al.*, Mitochondrial release of AIF and EndoG requires caspase activation downstream of Bax/Bak-mediated permeabilization. *EMBO J* 2003, *22*, 4385-4399.
[95] Li, X., Darzynkiewicz, Z., Cleavage of Poly(ADP-ribose) polymerase measured in situ in individual cells: relationship to DNA fragmentation and cell cycle position during apoptosis. *Exp Cell Res* 2000, *255*, 125-132.
[96] Nguyen, Q. D., Lavdas, I., Gubbins, J., Smith, G.*, et al.*, Temporal and Spatial Evolution of Therapy-Induced Tumor Apoptosis Detected by Caspase-3-Selective Molecular Imaging. *Clin Cancer Res* 2013.
[97] Xia, C. F., Chen, G., Gangadharmath, U., Gomez, L. F.*, et al.*, In Vitro and In Vivo Evaluation of the Caspase-3 Substrate-Based Radiotracer [F]-CP18 for PET Imaging of Apoptosis in Tumors. *Mol Imaging Biol* 2013.
[98] Su, H., Chen, G., Gangadharmath, U., Gomez, L. F.*, et al.*, Evaluation of [F]-CP18 as a PET Imaging Tracer for Apoptosis. *Mol Imaging Biol* 2013.
[99] Lee, B. W., Johnson, G. L., Hed, S. A., Darzynkiewicz, Z.*, et al.*, DEVDase detection in intact apoptotic cells using the cell permeant fluorogenic substrate, (z-DEVD)2-cresyl violet. *Biotechniques* 2003, *35*, 1080-1085.
[100] Cen, H., Mao, F., Aronchik, I., Fuentes, R. J., Firestone, G. L., DEVD-NucView488: a novel class of enzyme substrates for real-time detection of caspase-3 activity in live cells. *FASEB J* 2008, *22*, 2243-2252.
[101] Keppler-Hafkemeyer, A., Brinkmann, U., Pastan, I., Role of caspases in immunotoxin-induced apoptosis of cancer cells. *Biochemistry* 1998, *37*, 16934-16942.
[102] Stennicke, H. R., Salvesen, G. S., Biochemical characteristics of caspases-3, -6, -7, and -8. *J Biol Chem* 1997, *272*, 25719-25723.
[103] Liu, J., Bhalgat, M., Zhang, C., Diwu, Z.*, et al.*, Fluorescent molecular probes V: a sensitive caspase-3 substrate for fluorometric assays. *Bioorg Med Chem Lett* 1999, *9*, 3231-3236.
[104] Antczak, C., Takagi, T., Ramirez, C. N., Radu, C., Djaballah, H., Live-cell imaging of caspase activation for high-content screening. *J Biomol Screen* 2009, *14*, 956-969.
[105] Kasili, P. M., Song, J. M., Vo-Dinh, T., Optical sensor for the detection of caspase-9 activity in a single cell. *J Am Chem Soc* 2004, *126*, 2799-2806.
[106] Nicholls, S. B., Chu, J., Abbruzzese, G., Tremblay, K. D., Hardy, J. A., Mechanism of a genetically encoded dark-to-bright reporter for caspase activity. *J Biol Chem* 2011, *286*, 24977-24986.
[107] Huang, Q., Li, F., Liu, X., Li, W.*, et al.*, Caspase 3-mediated stimulation of tumor cell repopulation during cancer radiotherapy. *Nat Med* 2011, *17*, 860-866.
[108] Chudakov, D. M., Matz, M. V., Lukyanov, S., Lukyanov, K. A., Fluorescent proteins and their applications in imaging living cells and tissues. *Physiol Rev* 2010, *90*, 1103-1163.
[109] Luo, K. Q., Yu, V. C., Pu, Y., Chang, D. C., Application of the fluorescence resonance energy transfer method for studying the dynamics of caspase-3 activation during UV-induced apoptosis in living HeLa cells. *Biochem Biophys Res Commun* 2001, *283*, 1054-1060.
[110] Luo, K. Q., Yu, V. C., Pu, Y., Chang, D. C., Measuring dynamics of caspase-8 activation in a single living HeLa cell during TNFalpha-induced apoptosis. *Biochem Biophys Res Commun* 2003, *304*, 217-222.
[111] Zhu, X., Fu, A., Luo, K. Q., A high-throughput fluorescence resonance energy transfer (FRET)-based endothelial cell apoptosis assay and its application for screening vascular disrupting agents. *Biochem Biophys Res Commun* 2012, *418*, 641-646.
[112] Delgado, M. E., Olsson, M., Lincoln, F. A., Zhivotovsky, B., Rehm, M., Determining the contributions of caspase-2, caspase-8 and effector caspases to intracellular VDVADase activities during apoptosis initiation and execution. *Biochim Biophys Acta* 2013.
[113] Nagai, T., Miyawaki, A., A high-throughput method for development of FRET-based indicators for proteolysis. *Biochem Biophys Res Commun* 2004, *319*, 72-77.
[114] Shcherbo, D., Souslova, E. A., Goedhart, J., Chepurnykh, T. V.*, et al.*, Practical and reliable FRET/FLIM pair of fluorescent proteins. *BMC Biotechnol* 2009, *9*, 24.

[115] Nguyen, A. W., Daugherty, P. S., Evolutionary optimization of fluorescent proteins for intracellular FRET. *Nat Biotechnol* 2005, *23*, 355-360.
[116] Tawa, P., Tam, J., Cassady, R., Nicholson, D. W., Xanthoudakis, S., Quantitative analysis of fluorescent caspase substrate cleavage in intact cells and identification of novel inhibitors of apoptosis. *Cell Death Differ* 2001, *8*, 30-37.
[117] Onuki, R., Nagasaki, A., Kawasaki, H., Baba, T.*, et al.*, Confirmation by FRET in individual living cells of the absence of significant amyloid beta -mediated caspase 8 activation. *Proc Natl Acad Sci U S A* 2002, *99*, 14716-14721.
[118] Li, H., Zhu, H., Xu, C. J., Yuan, J., Cleavage of BID by caspase 8 mediates the mitochondrial damage in the Fas pathway of apoptosis. *Cell* 1998, *94*, 491-501.
[119] Kominami, K., Nagai, T., Sawasaki, T., Tsujimura, Y.*, et al.*, In vivo imaging of hierarchical spatiotemporal activation of caspase-8 during apoptosis. *PLoS One* 2012, *7*, e50218.
[120] Goldstein, J. C., Waterhouse, N. J., Juin, P., Evan, G. I., Green, D. R., The coordinate release of cytochrome c during apoptosis is rapid, complete and kinetically invariant. *Nat Cell Biol* 2000, *2*, 156-162.
[121] Vanden Berghe, T., Vanlangenakker, N., Parthoens, E., Deckers, W.*, et al.*, Necroptosis, necrosis and secondary necrosis converge on similar cellular disintegration features. *Cell Death Differ* 2010, *17*, 922-930.
[122] Mahajan, N. P., Linder, K., Berry, G., Gordon, G. W.*, et al.*, Bcl-2 and Bax interactions in mitochondria probed with green fluorescent protein and fluorescence resonance energy transfer. *Nat Biotechnol* 1998, *16*, 547-552.
[123] De Giorgi, F., Lartigue, L., Bauer, M. K., Schubert, A.*, et al.*, The permeability transition pore signals apoptosis by directing Bax translocation and multimerization. *FASEB J* 2002, *16*, 607-609.
[124] Munoz-Pinedo, C., Guio-Carrion, A., Goldstein, J. C., Fitzgerald, P.*, et al.*, Different mitochondrial intermembrane space proteins are released during apoptosis in a manner that is coordinately initiated but can vary in duration. *Proc Natl Acad Sci U S A* 2006, *103*, 11573-11578.
[125] Albeck, J. G., Burke, J. M., Aldridge, B. B., Zhang, M.*, et al.*, Quantitative analysis of pathways controlling extrinsic apoptosis in single cells. *Mol Cell* 2008, *30*, 11-25.
[126] Laster, S. M., Wood, J. G., Gooding, L. R., Tumor necrosis factor can induce both apoptic and necrotic forms of cell lysis. *J Immunol* 1988, *141*, 2629-2634.
[127] Degterev, A., Huang, Z., Boyce, M., Li, Y.*, et al.*, Chemical inhibitor of nonapoptotic cell death with therapeutic potential for ischemic brain injury. *Nat Chem Biol* 2005, *1*, 112-119.
[128] Chan, F. K., Shisler, J., Bixby, J. G., Felices, M.*, et al.*, A role for tumor necrosis factor receptor-2 and receptor-interacting protein in programmed necrosis and antiviral responses. *J Biol Chem* 2003, *278*, 51613-51621.
[129] Cho, Y. S., Challa, S., Moquin, D., Genga, R.*, et al.*, Phosphorylation-driven assembly of the RIP1-RIP3 complex regulates programmed necrosis and virus-induced inflammation. *Cell* 2009, *137*, 1112-1123.
[130] Kaiser, W. J., Upton, J. W., Long, A. B., Livingston-Rosanoff, D.*, et al.*, RIP3 mediates the embryonic lethality of caspase-8-deficient mice. *Nature* 2011, *471*, 368-372.
[131] Oberst, A., Dillon, C. P., Weinlich, R., McCormick, L. L.*, et al.*, Catalytic activity of the caspase-8-FLIP(L) complex inhibits RIPK3-dependent necrosis. *Nature* 2011, *471*, 363-367.
[132] Mareninova, O. A., Sung, K. F., Hong, P., Lugea, A.*, et al.*, Cell death in pancreatitis: caspases protect from necrotizing pancreatitis. *J Biol Chem* 2006, *281*, 3370-3381.
[133] Duprez, L., Takahashi, N., Van Hauwermeiren, F., Vandendriessche, B.*, et al.*, RIP kinase-dependent necrosis drives lethal systemic inflammatory response syndrome. *Immunity* 2011, *35*, 908-918.
[134] Smith, C. C., Davidson, S. M., Lim, S. Y., Simpkin, J. C.*, et al.*, Necrostatin: a potentially novel cardioprotective agent? *Cardiovasc Drugs Ther* 2007, *21*, 227-233.
[135] He, S., Wang, L., Miao, L., Wang, T.*, et al.*, Receptor interacting protein kinase-3 determines cellular necrotic response to TNF-alpha. *Cell* 2009, *137*, 1100-1111.
[136] Zhang, D. W., Shao, J., Lin, J., Zhang, N.*, et al.*, RIP3, an energy metabolism regulator that switches TNF-induced cell death from apoptosis to necrosis. *Science* 2009, *325*, 332-336.
[137] Sun, L., Wang, H., Wang, Z., He, S.*, et al.*, Mixed lineage kinase domain-like protein mediates necrosis signaling downstream of RIP3 kinase. *Cell* 2012, *148*, 213-227.
[138] Zhao, J., Jitkaew, S., Cai, Z., Choksi, S.*, et al.*, Mixed lineage kinase domain-like is a key receptor interacting protein 3 downstream component of TNF-induced necrosis. *Proc Natl Acad Sci U S A* 2012, *109*, 5322-5327.
[139] Kersse, K., Verspurten, J., Vanden Berghe, T., Vandenabeele, P., The death-fold superfamily of homotypic interaction motifs. *Trends Biochem Sci* 2011, *36*, 541-552.
[140] Stanger, B. Z., Leder, P., Lee, T. H., Kim, E., Seed, B., RIP: a novel protein containing a death domain that interacts with Fas/APO-1 (CD95) in yeast and causes cell death. *Cell* 1995, *81*, 513-523.
[141] Sakon, S., Xue, X., Takekawa, M., Sasazuki, T.*, et al.*, NF-kappaB inhibits TNF-induced accumulation of ROS that mediate prolonged MAPK activation and necrotic cell death. *EMBO J* 2003, *22*, 3898-3909.
[142] Temkin, V., Huang, Q., Liu, H., Osada, H., Pope, R. M., Inhibition of ADP/ATP exchange in receptor-interacting protein-mediated necrosis. *Mol Cell Biol* 2006, *26*, 2215-2225.
[143] Vanlangenakker, N., Vanden Berghe, T., Bogaert, P., Laukens, B.*, et al.*, cIAP1 and TAK1 protect cells from TNF-induced necrosis by preventing RIP1/RIP3-dependent reactive oxygen species production. *Cell Death Differ* 2011, *18*, 656-665.

[144] Vanlangenakker, N., Bertrand, M. J., Bogaert, P., Vandenabeele, P., Vanden Berghe, T., TNF-induced necroptosis in L929 cells is tightly regulated by multiple TNFR1 complex I and II members. *Cell Death Dis* 2011, *2*, e230.
[145] Zhang, Z., Larner, S. F., Liu, M. C., Zheng, W*., et al.*, Multiple alphaII-spectrin breakdown products distinguish calpain and caspase dominated necrotic and apoptotic cell death pathways. *Apoptosis* 2009, *14*, 1289-1298.
[146] Vanderklish, P. W., Krushel, L. A., Holst, B. H., Gally, J. A*., et al.*, Marking synaptic activity in dendritic spines with a calpain substrate exhibiting fluorescence resonance energy transfer. *Proc Natl Acad Sci U S A* 2000, *97*, 2253-2258.
[147] Boya, P., Kroemer, G., Lysosomal membrane permeabilization in cell death. *Oncogene* 2008, *27*, 6434-6451.
[148] Repnik, U., Stoka, V., Turk, V., Turk, B., Lysosomes and lysosomal cathepsins in cell death. *Biochim Biophys Acta* 2012, *1824*, 22-33.
[149] Kagedal, K., Johansson, U., Ollinger, K., The lysosomal protease cathepsin D mediates apoptosis induced by oxidative stress. *FASEB J* 2001, *15*, 1592-1594.
[150] Drake, C. R., Miller, D. C., Jones, E. F., Activatable Optical Probes for the Detection of Enzymes. *Curr Org Synth* 2011, *8*, 498-520.
[151] Yhee, J. Y., Kim, S. A., Koo, H., Son, S*., et al.*, Optical imaging of cancer-related proteases using near-infrared fluorescence matrix metalloproteinase-sensitive and cathepsin B-sensitive probes. *Theranostics* 2012, *2*, 179-189.
[152] Ryu, J. H., Kim, S. A., Koo, H., Yhee, J. Y*., et al.*, Cathepsin B-sensitive nanoprobe for in vivo tumor diagnosis. *Journal of Materials Chemistry* 2011, *21*, 17631-17634.
[153] Joyce, J. A., Baruch, A., Chehade, K., Meyer-Morse, N*., et al.*, Cathepsin cysteine proteases are effectors of invasive growth and angiogenesis during multistage tumorigenesis. *Cancer Cell* 2004, *5*, 443-453.
[154] Lane, D. P., Cheok, C. F., Lain, S., p53-based cancer therapy. *Cold Spring Harb Perspect Biol* 2010, *2*, a001222.
[155] Kroemer, G., Pouyssegur, J., Tumor cell metabolism: cancer's Achilles' heel. *Cancer Cell* 2008, *13*, 472-482.
[156] Zhao, Y., Butler, E. B., Tan, M., Targeting cellular metabolism to improve cancer therapeutics. *Cell Death Dis* 2013, *4*, e532.
[157] Jones, R. G., Thompson, C. B., Tumor suppressors and cell metabolism: a recipe for cancer growth. *Genes Dev* 2009, *23*, 537-548.
[158] Borst, P., Rottenberg, S., Cancer cell death by programmed necrosis? *Drug Resist Updat* 2004, *7*, 321-324.
[159] Zong, W. X., Ditsworth, D., Bauer, D. E., Wang, Z. Q., Thompson, C. B., Alkylating DNA damage stimulates a regulated form of necrotic cell death. *Genes Dev* 2004, *18*, 1272-1282.
[160] Cande, C., Vahsen, N., Garrido, C., Kroemer, G., Apoptosis-inducing factor (AIF): caspase-independent after all. *Cell Death Differ* 2004, *11*, 591-595.
[161] Moubarak, R. S., Yuste, V. J., Artus, C., Bouharrour, A*., et al.*, Sequential activation of poly(ADP-ribose) polymerase 1, calpains, and Bax is essential in apoptosis-inducing factor-mediated programmed necrosis. *Mol Cell Biol* 2007, *27*, 4844-4862.
[162] Baritaud, M., Cabon, L., Delavallee, L., Galan-Malo, P*., et al.*, AIF-mediated caspase-independent necroptosis requires ATM and DNA-PK-induced histone H2AX Ser139 phosphorylation. *Cell Death Dis* 2012, *3*, e390.
[163] Delavallee, L., Cabon, L., Galan-Malo, P., Lorenzo, H. K., Susin, S. A., AIF-mediated caspase-independent necroptosis: a new chance for targeted therapeutics. *IUBMB Life* 2011, *63*, 221-232.
[164] Scaffidi, P., Misteli, T., Bianchi, M. E., Release of chromatin protein HMGB1 by necrotic cells triggers inflammation. *Nature* 2002, *418*, 191-195.
[165] Hu, X., Han, W., Li, L., Targeting the weak point of cancer by induction of necroptosis. *Autophagy* 2007, *3*, 490-492.
[166] Han, W., Li, L., Qiu, S., Lu, Q*., et al.*, Shikonin circumvents cancer drug resistance by induction of a necroptotic death. *Mol Cancer Ther* 2007, *6*, 1641-1649.
[167] Tenev, T., Bianchi, K., Darding, M., Broemer, M*., et al.*, The Ripoptosome, a signaling platform that assembles in response to genotoxic stress and loss of IAPs. *Mol Cell* 2011, *43*, 432-448.
[168] Jain, M. V., Paczulla, A. M., Klonisch, T., Dimgba, F. N*., et al.*, Interconnections between apoptotic, autophagic and necrotic pathways: implications for cancer therapy development. *J Cell Mol Med* 2013, *17*, 12-29.
[169] Nikoletopoulou, V., Markaki, M., Palikaras, K., Tavernarakis, N., Crosstalk between apoptosis, necrosis and autophagy. *Biochim Biophys Acta* 2013.
[170] Walsh, C. M., Edinger, A. L., The complex interplay between autophagy, apoptosis, and necrotic signals promotes T-cell homeostasis. *Immunol Rev* 2010, *236*, 95-109.
[171] Lim, S. C., Choi, J. E., Kang, H. S., Han, S. I., Ursodeoxycholic acid switches oxaliplatin-induced necrosis to apoptosis by inhibiting reactive oxygen species production and activating p53-caspase 8 pathway in HepG2 hepatocellular carcinoma. *Int J Cancer* 2010, *126*, 1582-1595.
[172] Prabhakaran, K., Li, L., Borowitz, J. L., Isom, G. E., Caspase inhibition switches the mode of cell death induced by cyanide by enhancing reactive oxygen species generation and PARP-1 activation. *Toxicol Appl Pharmacol* 2004, *195*, 194-202.
[173] Earley, S., Vinegoni, C., Dunham, J., Gorbatov, R*., et al.*, In vivo imaging of drug-induced mitochondrial outer membrane permeabilization at single-cell resolution. *Cancer Res* 2012, *72*, 2949-2956.

[174] Andresen, V., Pollok, K., Rinnenthal, J. L., Oehme, L.*, et al.*, High-resolution intravital microscopy. *PLoS One* 2012, *7*, e50915.
[175] Bagci-Onder, T., Agarwal, A., Flusberg, D., Wanningen, S.*, et al.*, Real-time imaging of the dynamics of death receptors and therapeutics that overcome TRAIL resistance in tumors. *Oncogene* 2013, *32*, 2818-2827.
[176] Nesterenko, I., Wanninge, S., Bagci-Onder, T., Anderegg, M., Shah, K., Evaluating the effect of therapeutic stem cells on TRAIL resistant and sensitive medulloblastomas. *PLoS One* 2012, *7*, e49219.
[177] Piljic, A., Schultz, C., Simultaneous recording of multiple cellular events by FRET. *ACS Chem Biol* 2008, *3*, 156-160.
[178] Welch, C. M., Elliott, H., Danuser, G., Hahn, K. M., Imaging the coordination of multiple signalling activities in living cells. *Nat Rev Mol Cell Biol* 2011, *12*, 749-756.
[179] Yu, J. Q., Liu, X. F., Chin, L. K., Liu, A. Q., Luo, K. Q., Study of endothelial cell apoptosis using fluorescence resonance energy transfer (FRET) biosensor cell line with hemodynamic microfluidic chip system. *Lab Chip* 2013, *13*, 2693-2700.
[180] Grassilli, E., Narloch, R., Federzoni, E., Ianzano, L.*, et al.*, Inhibition of GSK3B Bypass Drug Resistance of p53-null Colon Carcinomas by Enabling Necroptosis in Response to Chemotherapy. *Clin Cancer Res* 2013.
[181] Taelman, V. F., Dobrowolski, R., Plouhinec, J. L., Fuentealba, L. C.*, et al.*, Wnt signaling requires sequestration of glycogen synthase kinase 3 inside multivesicular endosomes. *Cell* 2010, *143*, 1136-1148.
[182] Mizutani, T., Kondo, T., Darmanin, S., Tsuda, M.*, et al.*, A novel FRET-based biosensor for the measurement of BCR-ABL activity and its response to drugs in living cells. *Clin Cancer Res* 2010, *16*, 3964-3975.
[183] Shi, S., Yao, W., Xu, J., Long, J.*, et al.*, Combinational therapy: new hope for pancreatic cancer? *Cancer Lett* 2012, *317*, 127-135.
[184] Weisberg, E., Manley, P. W., Cowan-Jacob, S. W., Hochhaus, A., Griffin, J. D., Second generation inhibitors of BCR-ABL for the treatment of imatinib-resistant chronic myeloid leukaemia. *Nat Rev Cancer* 2007, *7*, 345-356.
[185] Al-Lazikani, B., Banerji, U., Workman, P., Combinatorial drug therapy for cancer in the post-genomic era. *Nat Biotechnol* 2012, *30*, 679-692.
[186] Kohnke, M., Schmitt, S., Ariotti, N., Piggott, A. M.*, et al.*, Design and application of in vivo FRET biosensors to identify protein prenylation and nanoclustering inhibitors. *Chem Biol* 2012, *19*, 866-874.
[187] Komatsu, N., Aoki, K., Yamada, M., Yukinaga, H.*, et al.*, Development of an optimized backbone of FRET biosensors for kinases and GTPases. *Mol Biol Cell* 2011, *22*, 4647-4656.

1.1.2. MLKL as a new executioner in necroptosis progression

In 2012, a new necroptosis effector was characterized: the pseudo-kinase Mixed-Lineage Kinase Like (MLKL) that is catalytically inactive due to a lack two of the three conserved catalytic domain crucial for phosphoryl transfer activity [1–3]. MLKL is composed of an N-terminal coiled-coil domain and a kinase-like domain located at its C-terminus. MLKL is considered as the crucial executioner of necroptosis signaling downstream of Receptor Interacting Protein Kinase (RIPK) 3 [4,5]. Indeed, MLKL deletion impairs necroptosis accomplishment in several cellular models (e.g. HT-29, Jurkat, MEF, L929) [1–3,5–7].

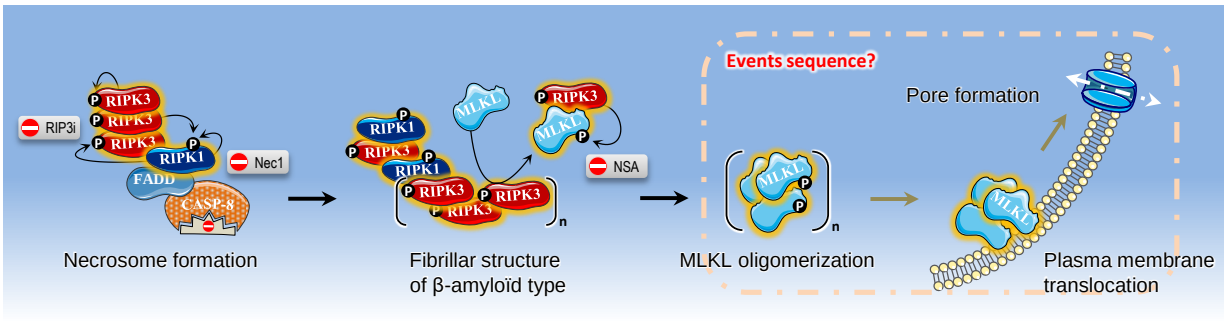

Figure 1: **Cascade of molecular events leading to necroptosis**. The different steps and molecular effectors involved in necroptosis initiation and execution are indicated. The “no entry sign” represents action of chemical inhibitors (Nec-1, Necrostatin 1; RIP3i, RIP3 inhibitor; NSA, necrosulfonamide). NSA inhibits necroptosis by targeting the cysteine 86 of human MLKL [1]. Highlighted molecules indicate their “active” forms.

RIPK1 and RIPK3 interact via their homotypic RIP Homology Interaction Motif (RHIM) domain to form the core of the necrosome which also includes Fas Associated Protein With Death Domain (FADD) and Caspase-8 [8,9]. RIPK1/RIPK3 interaction was shown to lead to the formation of amyloid-like filamentous structures *in vitro* [10]. RIPK3/MLKL complexes were detected in living cells (HeLa, HT-29) but the amount of these complexes increased drastically upon necroptosis induction [1]. The RIPK3/MLKL interaction occurs through the kinase domain of RIPK3 and the kinase-like domain of MLKL [1]. RIPK3 kinase activity is necessary for RIPK3/MLKL interaction and the subsequent autophosphorylation of RIPK3 on serine 227 was shown to reinforce the stability of RIPK3/MLKL complexes [1]. In response to TNF, MLKL is phosphorylated by RIPK3 on the threonine 357 and the serine 358 residues located within its activation loop [1] leading to a conformational change of MLKL from

an inactive to an active state [3,11,12]. This major event appears to be essential for MLKL translocation to the plasma membrane, as it allows the exposure of a positively charged amino-acid patch located on the 4 helical bundle domain (4-HBD) at its N-terminus [13–15]. In line with this, it was demonstrated that the N-terminus domain that contained the 4-HBD interacts with phosphatidylinositol phosphates (PIPs) or cardiolipins (CL) in lipid rafts at the plasma membrane [13,14,16]. Additionally, translocation of the 4-HBD domain was necessary and sufficient to trigger necroptosis [6,7,13].

Several research groups have proposed that MLKL oligomerization is also a key step for necroptosis to proceed [6,7,13,14,16]. The phosphorylated MLKL molecules appears to form oligomers that localize at the plasma membrane but the precise stoichiometry of phosphorylated MLKL oligomers remains controversial ranging from trimers [6], tetramers [7] to hexamers [14] and even more [13]. The sequence of events concerning the oligomerization of phosphorylated MLKL and MLKL plasma membrane translocation is still under investigation and might actually be dependent on the cellular context (Figure 1).

Upon necroptosis induction, phosphorylated MLKL oligomers were shown to compromise plasma membrane integrity leading to cellular swelling and ultimately to cell membrane rupture [13,14,16]. Several studies support this hypothesis, where MLKL would possibly contribute to ionic flux modifications across the plasma membrane, yielding to plasma membrane permeabilization and rupture [6,7]. There are some apparent discrepancies on the types of ion channels affected by MLKL [17]. Han and colleagues described a rapid influx of sodium during necroptosis in L929 cells [7], while Liu and colleagues reported a TRPM7-mediated calcium intake in HT29 cells [6]. *In silico* studies based on structure prediction analysis revealed that MLKL shares structural similarities with bacterial α-pore-forming toxins, which do oligomerize and form a pore in plasma membrane [13]. *In vitro* experiment performed with recombinant MLKL reported its capacity to permeabilize PIPs-containing liposomes, hence revealing an important role of PIPs in its plasma membrane recruitment and thus, supporting a direct pore-forming capacity of MLKL in plasma membrane [13,14,16]. Recently, several observations reported that phosphorylated MLKL as well as RIPK1 and RIPK3 translocate to the nucleus of cells exposed to a necroptotic trigger before MLKL relocalization at plasma membrane [18]. MLKL

nuclear translocation occurs through a bipartite Nuclear Localization Sequence (NLS) motif found at its C-terminus in the kinase-like domain that is exposed following MLKL phosphorylation [18]. Phosphorylated MLKL translocation seems to contribute to its cytotoxic function as mutations in the NLS region decreased cell death [18].

Altogether, it remains important to elucidate the function of MLKL and to illuminate its dynamic after RIPK3-mediated activation.

1.1.3. Other cell death processes

1.1.3.1. Autophagy

Autophagy is evolutionary conserved, highly regulated and genetically controlled. This process was initially described as a physiological “self-eating” catabolic program to protect the cell from nutrient or growth factor deprivation [19]. Autophagy was thus considered as a pro-survival mechanism in cell homeostasis in response to metabolic cellular stress. The term “autophagy” generally referred to “macro-autophagy”. Beside this non-selective autophagy, it exists other types of autophagy including selective autophagy targeting the mitochondria (mitophagy), the peroxisomes (pexophagie), the nucleus (nucleophagy), the ribosomes (ribophagy) and the endoplasmic reticulum (ER-phagy or reticulophagy) [20,21]. Micro-autophagy also known as a chaperone-mediated autophagy is described as chaperone-dependent degradation of cytosolic proteins directly targeted to lysosomes [22,23].

Autophagy is mainly characterized by the formation of double-layered membrane vesicles termed autophagosomes that encircled cytoplasmic material including soluble macromolecules and organelles [19]. These sequestered cytoplasmic components are then directed to the lysosomes for recycling. Autophagy occurs through a multiple step process including the initiation, elongation, formation and maturation of the autophagosome before the fusion and degradation by lysosomes (Figure 2) [24]. Numerous studies conducted in yeast identified a specific group of molecules highly conserved in the evolution known as autophagy-related (ATG) proteins in different steps of autophagosome formation [25,26].

However, although autophagy is a cellular response to maintain survival and to preserve cellular integrity when faced with cellular stress [27], autophagic cells were often observed in dying cell populations [28]. Therefore it has been questioned

whether autophagy is a specific cell death program or a consequence due to an extensive autophagy in an attempt to rescue stressed cells from death. There is now compiling evidences that autophagy may be specifically triggered in response to intensive stress signals leading to cell death, now classified as type II programmed cell death [29]. Hence, autophagy activation could elicit both a pro-survival or pro-death mechanism depending on the cellular context [21,23,30]. Emerging studies reveal that autophagy is a highly regulated process by several signaling pathways including PI3K-I/AKT/mTOR pathway (mTOR for mammalian Target Of Rapamycin), MAPK (JNK, p38, ERK) pathways, AMP-activated protein Kinase (AMPK) pathway, calcium or endoplasmic reticulum stress pathway [23,31]. These pathways are thus acting as sensors of energetic reserves to modulate autophagy activation and expression level and/or activities of autophagy-related proteins. In line with this view, autophagy outcome appears to be modulated through the crosstalk with other programmed cell death pathways including apoptosis and necroptosis [28,30,32]. Several studies highlight the prominent role of autophagy in the development of pathology including heart and liver diseases and cancer [20]. Indeed, the dysfunction/deletion of numerous autophagy-related genes or autophagy-regulated factors has been associated with the emergence of several cancers [33]. While autophagy can operate as a tumor suppressor in oncogenesis, pro-tumor functions of autophagy have been reported in tumorigenesis [34], emphasizing the ambiguous role of autophagy during cancer progression.

1.1.3.2. Paraptosis

Paraptosis is a form of caspase-independent cell death characterized by cytoplasmic vacuolization and organelles swelling, including mitochondria and endoplasmic reticulum [35]. This particular cell death does not exhibit morphological and molecular hallmarks of apoptosis since caspases inhibitors as well as anti-apoptotic Bcl-2 family proteins overexpression do not prevent paraptosis accomplishment. Paraptosis appears to be triggered both by the receptor Toxicity and JNK inducer (TAJ, also known as TROY), an orphan TNF receptor superfamily member, and by the insulin-like growth factor receptor I [36,37]. Additionally, few studies revealed that several members of the mitogen-activated protein kinase family could be involved in IGFR1-mediated paraptosis, including MEK-2 and Jun-NH2 terminal Kinase-1 (JNK-1) [36]. While paraptosis is fundamentally different from

apoptosis, it is still unclear whether paraptosis presents similarities or cross-talk with autophagy or other PCDs.

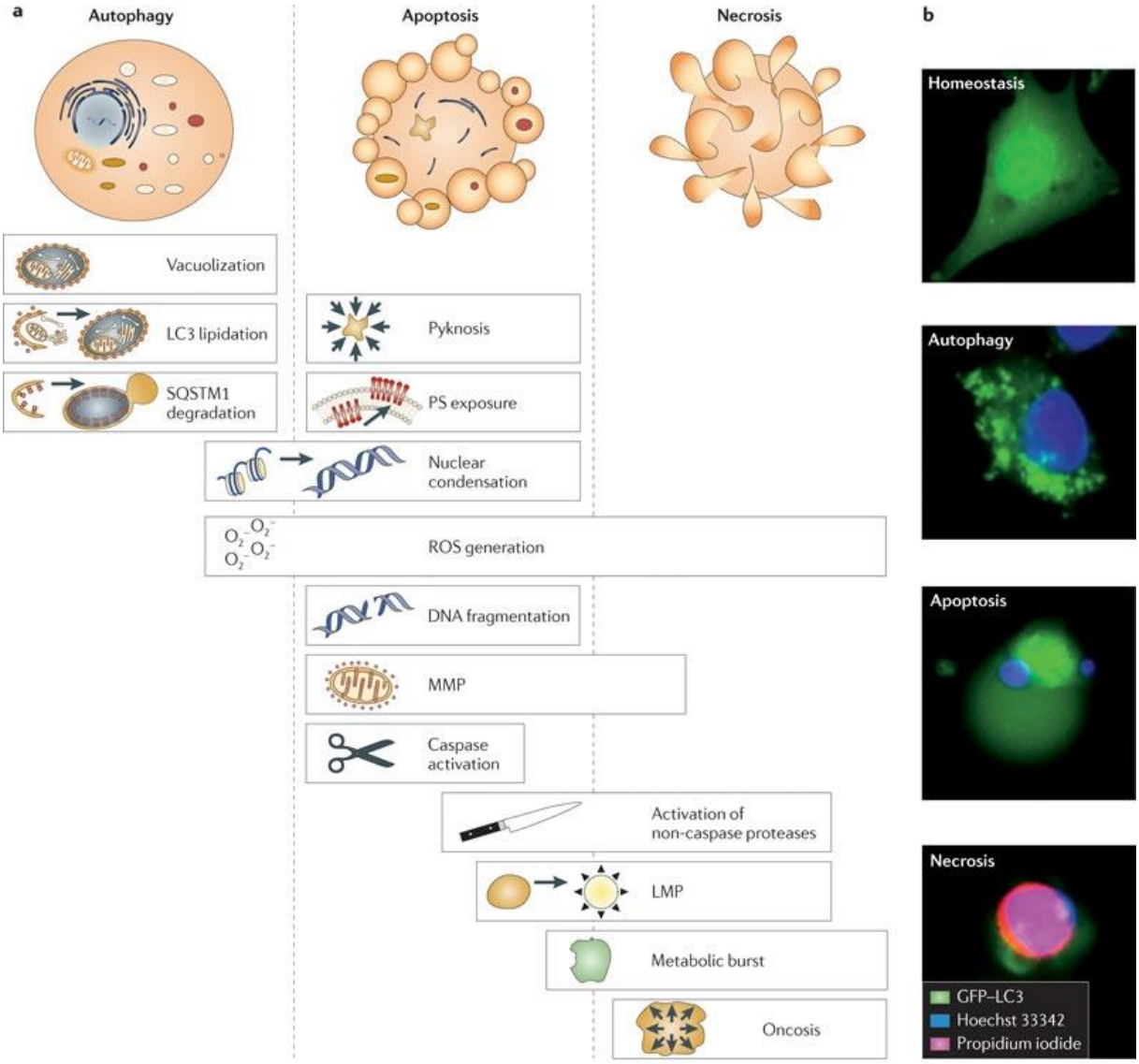

Figure 2: **Molecular characterization of autophagy, apoptosis, and necrosis**. (**a**) The scheme describes molecular and phenotypic features of autophagy, apoptosis and programmed necrosis and illustrates that these cell death share several common characteristics. LC3-I, microtubule-associated protein 1A/1B-Light Chain 3-I; SQSTM1, sequestosome 1 protein also called p62; MMP, Mitochondrial Membrane Permeabilization; LMP, Lysosomal Membrane Permeabilization, PS, Phospatidylserine; ROS, Reactive Oxygen Species (**b**) Human osteosarcoma U2-OS cells expressing a green fluorescent protein tagged-LC3-I correspond to the basal state without stimulation (homeostasis). Cells were then stimulated for 12 hours either by rapamycin (autophagic trigger) or staurosporine (apoptotic trigger) or a combined treatment of stautosporine and benzyloxycarbonyl-Val-Ala-Asp-fluoromethylketone (zVAD-fmk) (necrotic trigger). Cells were stained both with Hoechst and propidium iodide (PI). Autophagy exhibits aggregation of GFP-LC3-I, whereas apoptosis shows nuclear condensation. Programmed necrosis displays PI uptake (adapted from [38]).

1.1.3.3. Ferroptosis

A new form of regulated necrosis was recently described and defined as ferroptosis [39]. It is a RIP3-independent programmed necrosis sharing common morphological features with necrosis. This is an iron-dependent form of non-apoptotic cell death, induced by erastin, an oncogenic toxic small molecule. Erastin functions as an inhibitor of the System X_c^- Cys/Glu antiporter resulting in an inhibition of extracellular cystine uptake and in a charge of intracellular glutamate transport across the plasma membrane. The reduction of cystine to cysteine is then blocked which provokes a progressive depletion of glutathione (GSH) causing a cascade of events including a loss-of-function of GSH peroxidase 4 (GPX4) [40,41], increasing levels of intracellular hydrogen peroxide (H_2O_2), reactive oxygen species (ROS)-mediated lipid peroxidation, and ultimately cell death (for review, [42]). Ferroptosis critically depends on intracellular iron metabolism and is inhibited by iron chelators, lipophilic anti-oxidants and ferrostatin-1 (Fer-1) [39,43].

Upon full amino acid deprivation, it was shown that serum could induce and potentiate necrosis in MEF cells in a RIP3-independent manner. Serum-components including L-glutamine as well as transferrin (an iron carrier protein) have been identified in serum-induced necrosis, which was further determined to be ferroptosis.Ferrostatin-1 was reported to block this serum-induced necrosis upon deprivation of full amino acids or of cysteine alone. Conversely, L-glutamine, transferrin as well as glutaminolysis metabolic pathway are essential for erastin-induced ferroptosis (for review, [44]). However, the precise molecular regulatory mechanisms and the interplay between cellular metabolism and iron/redox homeostasis still need to be clarified.

Amounting evidences indicated that ferroptosis is involved in the pathogenesis of several human diseases such as neurodegenerative diseases, ischemia/reperfusion-induced organ injury (e.g. kidney, hepatic, heart injury) and cancers [45,46]. Abnormalities in iron metabolism characterized by aberrant accumulation of iron and/or ROS production are implicated in the pathogenesis of degenerative diseases (e.g. Friedrich’s ataxia (FRDA) disease) [45]. GPX4 deficiency in neurons results in neurodegeneration. A pronounced decrease of cystine in blood in ischemic conditions could increase the susceptibility to ferroptosis. Patients with deficiency in cystine uptake, cystine maturation, or glutaminolysis-related enzymes

are at higher risk for ferroptosis initiation [44]. Recent studies highlighted the modulation of ferroptosis by the Protein kinase C (PKC) and MAPK signaling pathways. PKC-mediated phosphorylation of the heat shock protein beta-1 (HSPB1) results in a protection against erastin-induced ferroptosis [47]. Finally, cancer cells with oncogenic *Ras* are more susceptible to ferroptosis induction [40]. These findings shed new light on the potential pharmacological targeting of ferroptosis in cancer therapy.

1.1.3.4. Parthanathos

Parthanathos is a form of caspase-independent and RIPK1/RIPK3-independent regulated necrosis, since caspases or RIPK1 and RIPK3 inhibitors cannot rescue it. Parthanatos shares necrotic but not apoptotic-like morphological features such as loss of plasma membrane integrity (but not swelling) and can be specifically distinguished from apoptosis by large-scale DNA fragmentation (for review, [42]).

Parthanatos has been described as the result of the rapid overactivation of PARP1, a member of poly(ADP-ribose) polymerase (PARP) family that is involved in DNA repair. PARP1, also called poly(ADP-ribose) transferase, catalyzes the transfer of ADP-ribose groups from NAD+ (Nicotinamide Adenine Dinucleotide) to its protein targets (also referred as poly(ADP-ribosyl)ation or PARylation) at the site of DNA damage [42]. As observed in several cellular models, PARP1-mediated parthanathos is induced by severe DNA damages in response to numerous chemical agents and toxic conditions including alkylating agents such as N-methyl-N-nitro-N-nitrosoguanidine (MNNG), Ultra-Violet (UV) radiation, ROS production such as H_2O_2, NO generation or even oxygen-glucose deprivation (ischemia conditions) in a time and dose-dependent manner [48–50]. The rapid activation of PARP1 is crucial to favor parthanatos over other regulated necrosis. It causes a cascade of events including accumulation of Poly(ADP)-Ribose (PAR) polymer in the cytosol and mitochondria, calpains activation, cleavage of Apoptosis-Inducing Factor (AIF), translocation of active truncated form of AIF in the nucleus and subsequent PARP1 activation due to enhanced DNA damages [50–52]. Once this positive feedback loop is active, NAD+ and Adenosine Triphosphate (ATP) intracellular reserves are progressively depleted, ultimately leading to cell death.

Parthanatos shares biochemical features with other forms of cell death, such as PARP1 activation, mitochondrial depolarization or caspase activation at the very late stage [50]. The sequence of event leading to parthanatos depends on the duration and/or intensity of the stimulation, distinguishing thereby parthanatos from other cell death [42,50]. In addition, specific inhibitors of PARP1 do not protect from TNF-induced cell death in several cell lines. But these inhibitors were reported to completely prevent parthanatos. PARP1 inhibitors are of great interest in cancer therapy in combination with other chemotherapeutic, in order to induce cell death of cancerous cells and to impair the recruitment of DNA repair machinery [53]. This approach could be adapted and applied to treat vascular and neurodegenerative disorders [50].

1.2. The MAPK signaling pathways

The MAPK signaling pathways are highly conserved through evolution of eukaryotic cells, bridging cell surface receptors to specific effector molecules for signal integration. Consisting of interconnected signaling nodes, MAPKs signaling pathways share characteristic three-tiered signaling core architecture, ensuring not only signal transduction but also amplification of signals from different membrane-stimulated receptors, such as Receptor Tyrosine Kinases (RTK) and G Protein-Coupled Receptors (GPCRs) [54,55] (Figure 3). Typically each level of the cascade is composed of a kinase. At the top of the cascade, the Mitogen-Activated Protein Kinase Kinase Kinases (MAPKKKs or MAP3K) – Ser/Thr kinases activated by interaction with a member of the Ras/Rho family – initiate a series of sequential phosphorylation [54]. MAPKKKs activation leads to the phosphorylation and the subsequent activation of the downstream Mitogen-Activated Protein Kinase Kinases (MAPKKs or MAP2K), which in turn provoke the phosphorylation and the activation of the MAPKs. Finally, in response to extracellular stimuli, activated MAPKs phosphorylate a myriad of substrates in different subcellular compartments to execute specific gene expression programs required to generate the appropriate biological response such as cell survival, proliferation, differentiation, migration as well as cell death [56,57] (Figure 3). The specificity of the biological outcome is mainly dictated by scaffolding proteins [58,59] and docking sites-mediated high-affinity protein-protein interactions [60,61]. MAPKs are grouped into three main families or modules including ERKs, JNKs and p38/SAPKs (Stress-Activated Protein Kinases) (for review, [62]) which are known to play a prominent role in the control or modulation of cell death.

In the following paragraphs, the three main members of MAPK family will be briefly defined and presented as follows: (1) definition and stimulation conditions, (2) molecular mechanisms of activation, and (3) substrates and biological functions.

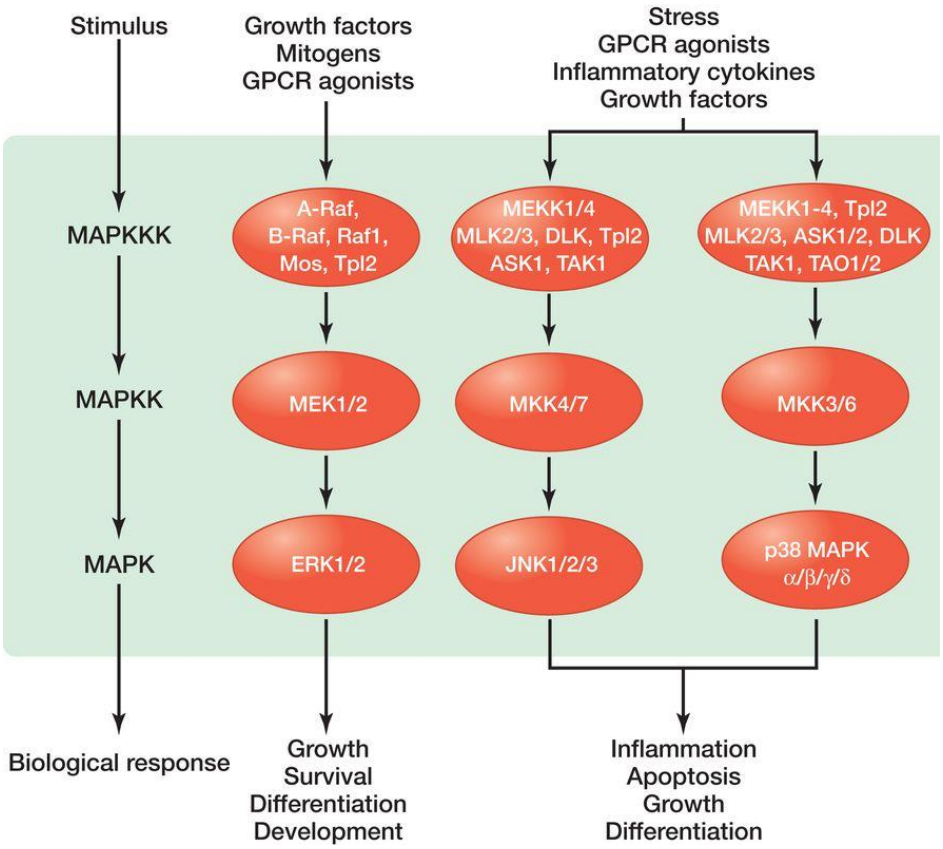

Figure 3: **Schematic representation of MAPKs signaling pathways**. The three main groups of MAPKs are represented (ERKs – JNKs – p38/SAPK) (adapted from [55]).

1.2.1. JNK pathway

The first member of JNK family also named Stress Activated Protein Kinase is activated by stress stimuli [63]. There are three isoforms of JNK: JNK1 (SAPKγ or MAPK8), JNK2 (SAPKα or MAPK9) and JNK3 (SAPKβ or MAPK10) [55,64,65], expressed from three distinct genes known to produce spliced isoforms ranging from 46 to 55 kDa [66]. JNK1 and JNK2 are ubiquitously expressed in a wide range of tissues, whereas JNK3 expression seems mainly restricted to a few organs and tissues including testis, neuronal and heart tissues [67].

JNK signaling pathway is mainly activated by various environmental stress stimuli including heat and osmotic shock, ionizing radiation, UV radiation, oxidative stress, alkylating agents-induced DNA damages as well as inflammatory cytokines such as members of TNF family, protein synthesis inhibitors, severe growth factor starvation and growth factor stimulation (for review, [68]) The stimulation of the JNK signaling pathway involves Ras/Rho family members, RTKs, and GPCRs and leads to the dual phosphorylation of JNKs kinases on Thr and Tyr residues occurring within

a highly conserved TPY motif located in the activation loop. These phosphorylations on JNKs kinases are conducted in a cooperative manner both by the Mitogen-Activated Protein Kinase Kinase 4 and 7 (MKK4 and MKK7) [69], which are themselves phosphorylated and activated by several upstream MAPKKKs including: Mitogen-activated protein kinase kinase kinase 1, 2, 3, and 4 (MEKK1/2/3/4), Mixed Lineage Kinase 2 and 3 (MLK2/3), mixed lineage kinase Dual Leucine zipper Kinase (DLK), Tumor progression locus 2 protein kinase (Tpl2), regulated Apoptotic Signal Kinase 1 (ASK1), and Transforming Growth Factor (TGF) Activated Kinase 1 (TAK1) (for review [70]) (Figure 4).

Upon stimulation of the pathway, it was reported that a pool of activated JNK kinases translocates to the nucleus to modulate the activity of wide array of transcription factors regulating specific genes expression [71–73]. Many transcription factors have been identified as being phosphorylated by JNK kinases such as c-Jun, Activating transcription factor 2 (ATF-2), Signal Transducer and Activator of Transcription 3 factor (STAT3) or E26 transformation-specific (also know as E-twenty-six, ETS) domain-containing protein Elk-1 (Elk1) [57,64,68]. The precise contribution of each JNK kinase to the transcription factors regulation is not clear and remains to be determined. The same holds true concerning the nature of the cytoplasmic targets of JNK kinases. JNK kinases play a prominent role in the control of cell cycle progression, inflammation, metabolism and cell death [74–77]. JNK1/2-dependent c-Jun transactivation contributes to AP-1 complex formation leading to the regulation of cell cycle-related genes expression including Cyclin D1 and Cyclin-Dependent Kinases (CDKs) [57,74,78,79]. It has been shown a JNK-dependent modulation of mRNA stability of several cytokines (e.g. IL-2, IL-3 and VEGF) [80–82]. Cumulative evidences highlighted the involvement of JNK kinases in apoptosis signaling [83,84]. Indeed, MEF generated from JNK1$^{-/-}$ and JNK2 $^{-/-}$ mice exhibited a marked resistance to apoptosis in response to genotoxic or environmental stresses [85]. Similar resistance to UV-induced apoptosis was also reported with a non-phosphorylatable form of c-Jun [86]. Moreover, hippocampal neurons isolated from JNK3$^{-/-}$ but not from JNK1$^{-/-}$ and JNK2$^{-/-}$ mice exhibited resistance to glutamate-induced apoptosis [87], which reflects a differential activation of JNK isoforms depending on the cell type and the stimulus. Additionally, other studies reported the role of JNK kinases in growth factors- (e.g. TNFα), Fas-ligand-, and other cellular

stresses-induced apoptosis [88–90]. JNK kinases can promote c-Jun-AP-1-mediated expression of pro-apoptotic genes (e.g. TNFα, Fas-L, Bak), concomitant with the repression of pro-survival genes [91]. Besides JNK-mediated c-Jun-AP-1 complexes formation, JNK kinases can stabilize p53 expression level resulting in an increase of p53-mediated expression of pro-apoptotic genes including Bcl2-associated X protein (Bax) and p53-upregulated modulator of apoptosis (PUMA) [92,93]. JNK kinases are also reported to directly activate and inhibit mitochondrial pro-apoptotic (BH3-only family, [94]) and anti-apoptotic (Bcl2, [95,96]) proteins, respectively. Finally, it is now accepted that the duration and the strength of JNK activation often determined cell fate. Indeed, several studies suggest that a sustained activation of JNK may preferentially lead to apoptosis, whereas cell proliferation or a survival response may be more associated with a transient JNK activation [97,98].

1.2.2. p38/SAPK pathway

The first member of p38 family, p38α, also known as SAPK2, is the best characterized member and is much more activated by stress stimuli by comparison to JNK kinases [99]. In addition to p38α, there are three other isoforms: p38β, p38γ (or SAPK3) and p38δ (or SAPK4) (for review, [100]). p38α and p38β are ubiquitously expressed in a wide range of tissues and cell lines, whereas p38γ and p38δ expression is more restricted to specific tissues and may therefore exert particular functions [101]. Indeed, the expression of p38γ is particularly high in skeletal muscle [102]. Additionally, p38α is highly expressed in comparison to p38β in cell lines, so that p38/SAPK refers more often to p38α isoform in the literature.

p38/SAPK signaling pathway is mainly activated by environmental stresses (e.g. heat stress, hyperosmolarity, UV irradiation, oxidative stress), inflammatory cytokines such as Interleukin 1 (IL-1) and TNFα, quite similarly to what has been reported to stimulate JNK kinases (for review, [100,103]). The stimulation of the p38/SAPK signaling pathway relies on the stimulation of Ras/Rho family members and GPCRs, as well as TNF Receptor 1 (TNFR1) and IL-1 receptors [104,105]. TNFR1 and IL-1 receptors initiate the signaling cascade through the recruitment of TNF Receptor Associated Factor (TRAF) adaptors that bind to specific MAPKKKs and thereby facilitate their subsequent activation [106]. Most MAPKKKs involved in p38/SAPK signaling pathway including MEKK1/2/3/4, MLK2/3, DLK, Tpl2, ASK1 and

TAK1 [100,107], also contribute to the stimulation of JNK signaling pathway (Figure 4). MKK3 and MKK6 are the main downstream MAPKKs responsible for p38/SAPK activation [108] even if MKK4 (a MAPKK also shared by JNK signaling) has been reported to be preferentially involved in response to UV-irradiation [69,109]. While MKK6 does not exhibit selectivity over p38/SAPK isoforms, MKK3 seems to preferentially activate p38α, p38γ as well as p38δ isoforms. The specificity of p38/SAPK activation could be due to the formation of multiple complexes between various MKK3/4/6 and p38/SAPK isoforms depending on the stimulus, the cell type and expression level of both MKKs and p38/SAPK isoforms [62]. Indeed, MKK3 and MKK6 have been identified as the main activators of p38/SAPK kinases in murine mesangial cells and in thymocytes, respectively [110,111]. Finally, p38/SAPK kinases are in turn activated by a MAPKK by dual phosphorylation on Thr and Tyr residues occurring within a highly conserved TGY motif located in their activation loop [109,112,113].

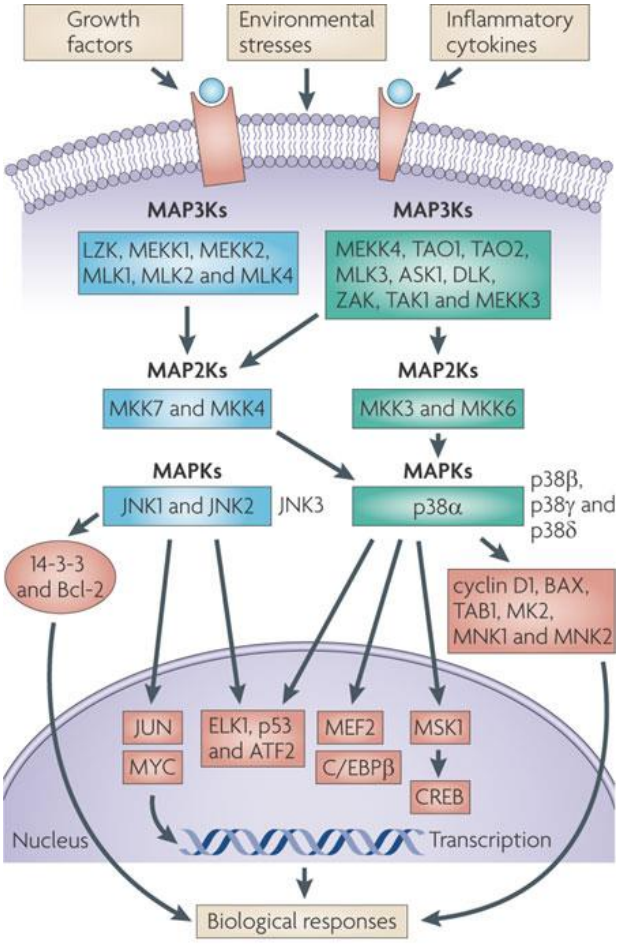

Figure 4: **Crosstalk between JNK and p38/SAPK signaling pathways**. These pathways display the characteristic three-tier core cascade MAPK architecture and share several upstream effectors (from [114]).

In quiescent cells, p38/SAPKs are homogeneously distributed between the cytoplasm and the nucleus but translocate from the cytoplasm to the nucleus when expose to cellular stresses [103,115]. Like other members of MAPK family, p38/SAPKs subcellular localization relies on interaction with scaffold proteins depending on specific docking domains [116,117]. Once p38/SAPK becomes activated, it can phosphorylate a large number of cytoplasmic and nuclear substrates on Ser or Thr residues, depending on the stimulus and p38/SAPK isoform [100,118,119]. Cytoplasmic substrates include the cytosolic phospholipase A2 (cPLA2), MAPK iNteracting Kinases (MNK) 1/2, MAPK-activated protein kinase (MK) 2/3 and Bax. Nuclear substrates include many transcription factors such as ATF1/2, Elk-1, p53 and Mitogen- and Stress-activated protein Kinase (MSK) 1/2 (for review, [100]). p38α isoform plays a prominent role in inflammatory responses [100,120] by inducing pro-inflammatory genes (e.g. IL-1 or TNFα, [121]). Besides its role in inflammation, p38 pathway plays a role in the regulation of metabolism as p38α and p38β isoforms have been shown to phosphorylate cPLA2 and the glycogen synthase [70,122,123]. Unlike other p38 isoforms, p38α knockout mice are not viable [124], but a tissue-specific knockout strategy for p38α revealed the involvement of this isoform in cell proliferation and survival of cardiomyocytes [125,126]. p38α is also implicated in the control of cell cycle checkpoints through the differential regulation of cyclins and cyclin-dependent kinase inhibitors (CDKI) gene expression [127–129]. Several studies demonstrated the crucial role of p38α and p38γ isoforms in the differentiation of myoblasts into myotubes [102,130,131]. Indeed, it was shown that myoblasts from knockout mice for p38α isoform do not differentiate, hence suggesting the role of p38α at the early phase of myogenesis [132]. At the opposite, p38γ isoform level increase gradually throughout the differentiation and accumulate in the skeletal muscle [102]. Other studies reported a preponderant role for p38δ isoform in the differentiation of keratinocytes [133]. However, compelling evidences indicated that p38α activation leads to apoptosis during ischemia-reperfusion [131,134,135] and that p38α inhibition prevents cardiomyocytes apoptosis and necrosis after myocardial ischemia-reperfusion [136]. Additionally, inhibition of p38α completely impairs Bax translocation to the mitochondria [137] thereby reinforcing p38α involvement in cellular stress-induced cell death through regulation of death receptors and pro- or anti-apoptotic Bcl-2 family genes expression [138]. In contrast, p38α isoform was also associated with cardioprotection by activating the extended p38/SAPK signaling

(also named p38α – Mitogen-Activated Protein (MAP) Kinase Activated Protein Kinase (MAPKAPK)) cascade, following cardiac failure [139–141]. MAPKAPK family contains several members including MSK1/2, MNK1 and MK2/3/5 [62]. Finally, p38/SAPK and JNK signaling pathways have been suggested to play a synergistic role in Nerve Growth Factor (NGF)-withdrawal-induced PC-12 apoptosis [142].

1.2.3. ERK1/2 pathway

1.2.3.1. Components of the ERK1/2 pathway

ERK1/2 signaling pathway displays the characteristic three-tier core cascade MAPK architecture [143] (Figure 3) and is composed of the three main MAPKKKs A-Raf, B-Raf and C-Raf, also known as Raf-1, at the first cascade level. Rafs are dual specificity Ser/Thr kinases composed of three conserved regions (CRs). The CR1 contains two Ras Binding Domains (RBD) and a cysteine-rich domain (CRD). The CR2 domain harbors numerous positive and negative regulatory Ser/Thr phosphorylation sites required to activate the catalytic kinase domain (CR3) (for review, [144]). While Raf-1 isoform is highly expressed in all tissues, A-Raf isoform shows restricted expression in intestine, cartilage, spleen, heart, urogenital tissues, thymus and muscles. B-Raf isoform is predominately expressed in neuronal tissues, testes and hematopoietic cells (for review, [145–148]). Depending on cell type and cellular stimulation, other MAPKKKs are involved to stimulate the pathway including c-Mos in reproductive tissues [149], Tpl2 in transformed cells [150], and MEKK1 activated under stress conditions [151] (for review, [57,58]) (Figure 5)

The second level of the cascade is formed by the MAPKKs named MAPK/ERK Kinase (MEK) 1 and 2 with a molecular weight of 45 kDa and 46 kDa, respectively. These dual threonine and tyrosine kinases display high sequence homology and contain a Nuclear Export Signal (NES), a D-domain (also known as Docking site for ERK and JNL, LXL (DEJL)) with basic residues, a proline-rich domain and a kinase domain [152,153]. While MEK2 isoform is highly expressed in mouse embryonic tissues, MEK1 isoform appears to be mainly expressed in adult tissues [154].

The evolutionary conserved MAPKs ERK1 (MAPK3) and ERK2 (MAPK1) form the last level of the cascade. ERK1 (44 kDa) and ERK2 (42 kDa) are dual specificity Ser/Thr kinases and share more than 80% identical amino acids. ERKs consist of a catalytic kinase domain and a CD domain (also known as common docking (CD)

domain) containing acidic and hydrophobic residues required for high-affinity protein interaction with their substrates [155]. ERK1 and ERK2 are ubiquitously expressed in a wide range of tissues and cell lines, with higher levels found in certain tissues such as the brain, the heart, the thymus and skeletal muscle [62]. Alternative splicing has been described for components of each level of the cascade. These additional variants contribute to determine the signaling specificity of the cascade, though they are expressed at lower levels than the mains isoforms [58].

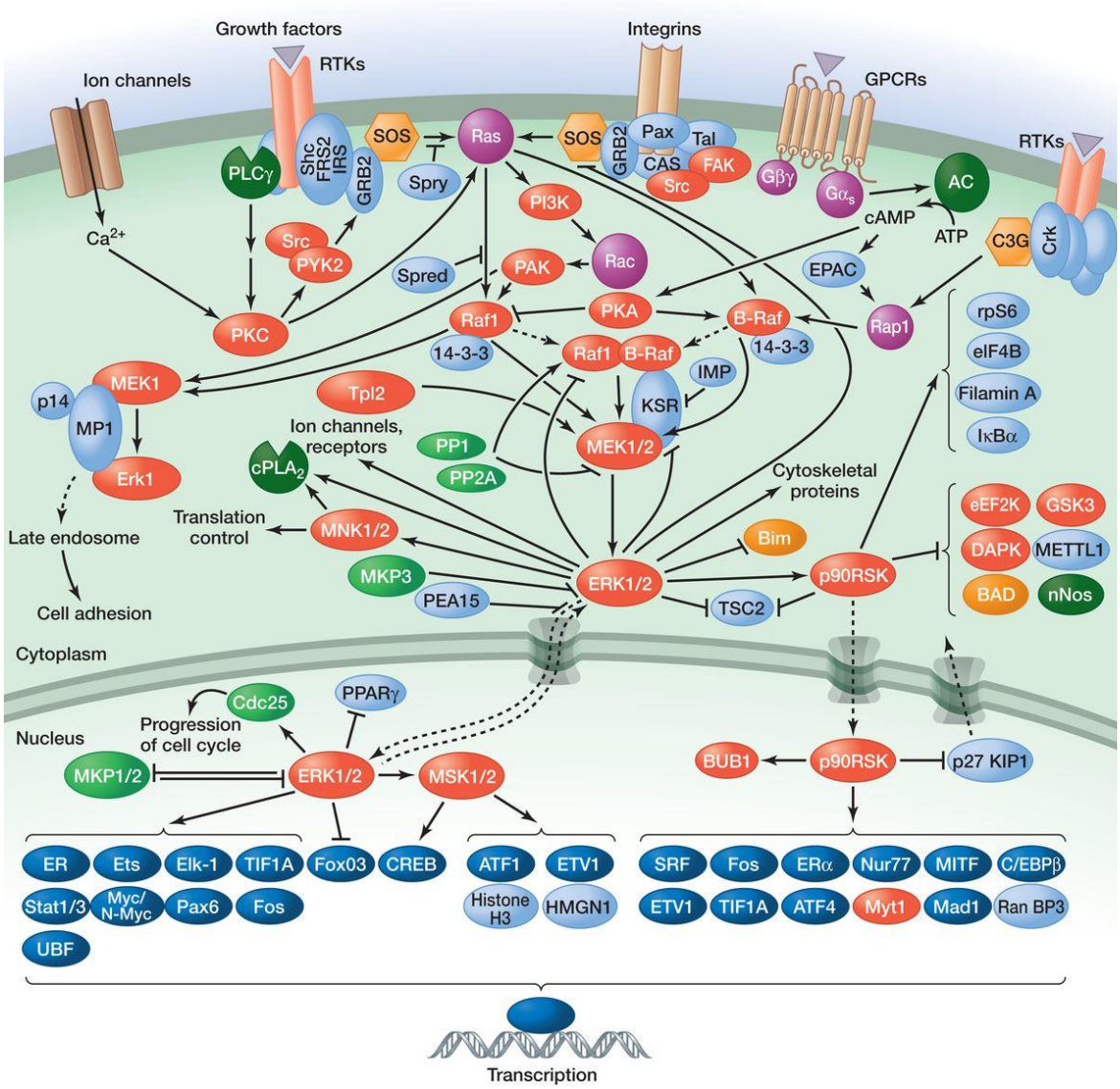

Figure 5: **ERK1/2 MAPK signaling pathway** (from [55]).

The alternative splicing of B-Raf isoform results in the expression of ten variant isoforms with a variable basal B-Raf activity [156]. The presence of exon 10a insertion located before the kinase domain increases the basal activity of MEK1/2 whereas the exon 8a insertion has an opposite effect [157]. On the other hand, the

alternative spliced isoform MEK1b lacking a portion in the kinase domain was previously considered as an inactive kinase [152,158]. It has later been shown that not only MEK1b exhibited kinase activity but also that it specifically phosphorylated and activated an alternative spliced isoform of ERK1 (ERK1c) [159]. Alternative splicing could modify the substrate specificity of each variant isoform leading to the phosphorylation of different downstream substrates; thereby contributing to form an independent signaling pathways and therefore increase the signaling diversity and specificity of the cascade. Finally, at the last tier of the cascade, other alternative spliced isoforms have been identified for ERK1 (ERK1b [160], ERK1c [161] and ERK1d [162]) and ERK2 (ERK2b [162]). These variant isoforms exert distinct functions depending on tissue-specific expression and subcellular distribution, extending again the diversity and specificity of the signaling cascade [58,146].

1.2.3.2. Activation of ERK1/2 pathway and substrates

A wide range of extracellular triggers stimulates the pathway, including numerous growth factors such as Epidermal Growth Factor (EGF), Fibroblast Growth Factor (FGF), Platelet-Derived Growth Factor (PDGF), Nerve Growth Factor (NGF) and insulin, but also cytokines, agonists targeting GPCR, osmotic stress as well as certain cell adhesion proteins [57,62]. Extracellular stimulation and subsequent activation of cell surface receptors such as Receptor Tyrosine Kinases (RTK), G Protein-Coupled Receptors (GPCRs) and ion channels [163–166] trigger sequential phosphorylation of Rafs, MEK1/2 and ERK1/2 that constitute a conserved signaling module [55]. In the case of EGF Receptor (EGFR), stimulated-membrane receptors harbor numerous tyrosine phosphorylation sites serving as binding sites for specific proteins such as Growth-factor-Receptor-Bound protein 2 (GRB2) that contain corresponding phosphotyrosine docking domains such as Src Homology 2 (SH2). Upon stimulation of EGFR, Son Of Sevenless (SOS) proteins relocalize from the cytoplasm to the plasma membrane due its interaction with GRB2. Acting as a Guanine nucleotide Exchange Factor (GEF), SOS binds to GDP-Ras and induces exchange with Guanosine Triphosphate (GTP) leading to the conformational change of Ras thereby eliciting Ras activation [167]. In humans, there are four isoforms for Ras including H-Ras, N-Ras and two alternatives spliced isoforms of K-Ras referred to as K-Ras-4A and K-Ras-4B. Although these isoforms are able to bind to Raf proteins, K-Ras is more effective in the activation of Raf proteins than H-Ras or N-

Ras. Several studies have shown different localization of Ras isoforms at plasma membrane and membrane of organelles, due to the differential prenylation and palmitoylation states of Ras proteins [168–170] leads to distinct Ras isoform-mediated signaling cascades [171,172].

Before stimulation of the pathway, cytoplasmic Raf proteins are phosphorylated (inhibitory phosphorylations) and blocked in a 14-3-3-mediated inactive conformation. This inhibition occurs through the phosphorylation of Ser residues located in the CR2 domain (Ser 259 and Ser 621 in the case of Raf-1) that involves Protein Kinase A (PKA), Protein Kinase B (PKB or AKT), Serum and Glucocorticoid-inducible Kinase (SGK) and Phosphoinositide-Dependent protein Kinase 2 (PDK1) depending on the Raf isoform [173]. Upon Ras activation, Raf kinases are recruited to the plasma membrane due to interaction of GTP-bound Ras with the RBD domain of Raf proteins [174]. GTP-bound Ras promotes Raf proteins activation by removing 14-3-3 from Rafs and allowing the recruitment of the Protein Phosphatase 1 (PP1) and the Protein Phosphatase 2A (PP2A) to the CR2 domain [175]. The full activation occurs through the phosphorylation of multiple Ser/Tyr residues located both in the CR2 and in the kinase domain CR3 and involves P21 protein (Cdc42/Rac)-Activated Kinase (PAK) 1 and 3, the Phospho-Inositide 3-Kinase (PI3K) pathway [176,177] and the kinase Src [178].

In order to transmit the signal to downstream components, activated Raf binds and catalyzes the dual phosphorylation of MEK1/2 on two Ser residues occurring within a highly conserved typical Ser-X-Ala-X-Ser/Thr motif located in the activation loop (Ser 218 and Ser 222 for human MEK1; Ser 222 and Ser 226 for human MEK2) [179,180]. As mentioned above, Rafs isoforms activate MEK1/2 differentially. A-Raf is considered as a weak activator of MEK1/2, B-Raf displays a better affinity and activates preferentially MEK1 and Raf-1 efficiently activates both MEK1 and MEK2 [147]. MEK1/2 activity is also positively or negatively regulated by non-canonical phosphorylations outside their activation loop [181,182] that involves PAK1 (Ser 298 of MEK1).

Finally, activated MEK1/2 bind and activate their downstream kinases, ERK1 and ERK2, by phosphorylation on Thr and Tyr residues within a conserved Thr-Glu-Tyr (TEY) motif located in the activation loop [123]. MEK1/2 are crucial effectors for the activation of the ERK1/2 cascade (Thr 185 and Tyr 187 for ERK1 and Thr 202

and Tyr 204 for ERK2) [183,184]. Following extracellular stimulations and activating phosphorylations, MEK1/2 and ERK1/2 are released from cytoplasmic anchors and this event is mainly characterized by their rapid translocation into the nucleus where ERK1/2 regulates positively or negatively the expression of multiple target genes under the control of specific associated-transcription factors including Elk-1, c-Fos, c-Jun and Erf-1 [185–188]. Several hundreds of substrates of ERK1/2 have been identified and contain the common consensus sequence Pro-X-Ser/Thr-Pro (or Ser/Thr-Pro) in the immediate vicinity of the phosphorylation sites [185,189,190]. By the phosphorylation of their substrates, ERK1/2 control their activity and/or their stability by preventing or accelerating their degradation by the proteasome [191,192]. Cytoplasmic substrates of ERK1/2 include the Death-Associated Protein Kinase (DAPK), the cPLA2, the tuberous sclerosis complex (TSC) 2, the p90 Ribosomal S6 Kinase (RSK) and the MNK. The kinases RSK, MNK and MSK are identified as MAPKAPKs that extend the ERK1/2 signaling [62,123]. Other members of the MAPK family also target these MAPKAPKs, thereby highlighting the increased complexity of these MAPK signaling pathways. Finally, other substrates are located in cellular membranes such as the EGFR, the Spleen tyrosine kinase (Syk) and the calnexin. Cytoskeletal components such as the neurofilament proteins and paxillin are also targeted by activated ERK1/2 [62]. But, the majority of ERK1/2 substrates are nuclear proteins and regulate mainly nuclear functions such as transcription, chromatin condensation and nuclear translocation that appear to be an essential feature of the ERK1/2 signaling pathway [185,193].

1.2.3.3. The regulation of ERK1/2 activity

Kinase-mediated ERK1/2 regulation

The ERK1/2 activity is controlled by a fine-tuned balance between kinases and phosphatases activities targeting the Thr/Tyr residues required for ERK1/2 activity [194,195]. ERK1/2 activity is heavily regulated by multiple phosphorylations occurring outside the activation loop to modulate ERK1/2 activity. Theses MEK1/2 independent phosphorylations are not directly involved in ERK1/2 full activity but rather play a regulatory role in both ERK1/2 activity and localization [196,197].

Phosphatase-mediated ERK1/2 regulation

The timing of ERK1/2 activation depends on the cell type and the stimuli. Upon EGF stimulation, ERK1/2 activity can last 20 minutes with an activation peak between 10-15 minutes (referred as transient activation) or remains elevated for several hours after the stimulus in the case of NGF stimulation in PC12 cells (referred as sustained activation) [198]. Because the duration of ERK1/2 is also very important for cell fate determination [98] (developed in the following paragraphs), inactivation of ERK1/2 requires the removal of phosphate(s) from Thr and/or Tyr residues in the activation loop by phosphatases. While dual phosphorylation is crucial for full activation of ERK1/2, a single dephosphorylation is sufficient to provoke the full inactivation. Three phosphatases families enable the dephosphorylation of ERK1/2: Ser/Thr phosphatases such as PP2A [199], specific Tyr phosphatases such as STriatal-Enriched protein tyrosine Phosphatase (STEP), STEP-Like Protein Tyrosine Phosphatase (PTP-SL) [200] or Hematopoietic Protein Tyrosine Phosphatase (HePTP) [201,202], and the DUal-Specificity Phosphatases (DUSP) also known as MAP Kinases Phosphatases (MKP) [203]. MKPs include nuclear phosphatases MKP1 (or DUSP1) and MKP2 (or DUSP4) and the cytosolic phosphatase MKP3 (or DUSP6). The distinct distribution of MKPs in the different subcellular compartments contributes to the spatio-temporal control of ERK1/2 activity [204,205]. Moreover, MKPs are identified as immediate-early gene products which expression is directly induced [206], stabilized [207] or repressed [191] by ERK1/2 signaling. Upon the stimulation, the initial pool of MKP could inactivate phosphorylated-ERK1/2 resulting in a transient activation pattern of ERK1/2, while new synthetized MKPs could definitively inactivate ERK1/2 for signal termination [208]. MKPs also serve as anchors for ERK1/2 and become active after an ERK1/2-mediated conformational change [58].

Crosstalk between PKA and ERK1/2

In addition to numerous regulations and extensive crosstalk previously described for the activation of the ERK1/2 cascade, compelling evidences demonstrated that the ERK1/2 cascade is regulated by cAMP/PKA pathway (for review, [209,210]). This crosstalk was reported to modulate the duration and the strength of ERK1/2 activity [211]. In the cellular model PC12, it is now well established that EGF stimulation is responsible for a transient activation of ERK1/2,

whereas NGF stimulation provokes a sustained activation leading to the proliferation or the differentiation of PC12 cells [212,213]. Differences in ERK1/2 activity mainly rely on both Ras/C-Raf-1/MEK/ERK and Rap1/B-Raf/MEK/ERK differential activation, respectively, and involved the Ras-like small G-proteins (Rap1) coupled with the Nerve Growth Factor Receptor (NGFR). Upon EGF stimulation, elevated levels of cAMP, by activating adenylyl cyclases (AC) or inhibiting phospodiesterases (PDE), leads to a sustained activation of ERK1/2 resulting in the differentiation of PC12 cells. Activation of the Exchange protein directly activated by cAMP (Epac) by increasing cAMP concentration triggers the activation of Rap1 and sustained activation of B-Raf/MEK/ERK pathway [210,214]. But PKA activation is generally known to directly inhibit C-Raf-1 mediated by A Kinase Anchoring Proteins (AKAP) preserving overactivation of MEK/ERK pathway from high cAMP levels [215]. This controversial role of cAMP in the regulation of ERK1/2 pathway is cell-type specific and is explained by the expression level of the different isoforms of Raf [210,211]. cAMP was reported to either inhibit C-Raf-1 or activate B-Raf. Therefore, cells expressing low level of B-Raf will preferentially impair mitogenic signals in response to cAMP release.

Feedback and feedforward loops

In a biological context, signaling pathways can be considered as specific “modules” contributing to generate a complex cellular “system”. The “cellular module” can be therefore conceptualized as a set of compartmentalized biochemical reactions thereby integrating extracellular signals and finally leading to the modulation of the biological response. Each module is not disconnected but rather interconnected with other modules. Moreover, “modularity” is the main characteristic of an efficient “system” providing therefore flexibility and adaptability (for reviews, [216,217]). As mentioned above, differential ERK1/2 activation in PC12 cells involves two interconnected “modules” in response to EGF or NGF to engage cell proliferation and differentiation respectively. Depending on cell type and cell stimulation, ERK1/2 cascade can activate several control mechanisms involving positive and/or negative feedback loops (FBL) as well as feedforward loops (FFL) to regulate its own activity and elicit a specific biological response [218,219]. Indeed, in PC12 cells, EGF-mediated cell proliferation requires a negative feedback loop from ERK1/2 to SOS

and Raf-1, whereas NGF-mediated cell differentiation in PC12 cells relies on a Rap1-mediated positive feedback loop [213,220].

Briefly, a feedback loop is defined as a loop in which a protein A induces expression or activation of a protein B that in turn regulates positively or negatively the protein A. A feedforward loop corresponds to a regulatory mechanism in which a protein A regulates a protein B via other intermediate proteins, and can be considered as coherent or incoherent depending on the action mechanism of each participating protein [221]. These feedback mechanisms precisely control the spatio-temporal profile of ERK1/2 activation and adjust activity of the network upon extracellular or intracellular perturbations by soliciting other redundant modules and thereby ensure the specificity and the reproducibility of the outcome in any circumstances [219,222]. Additionally, these control mechanisms operate over a different time scale upon stimulation and include positive or negative phosphorylations, endocytosis of plasma membrane receptors, and transcriptional regulation of moderators of the cascade such as phosphatases [222].

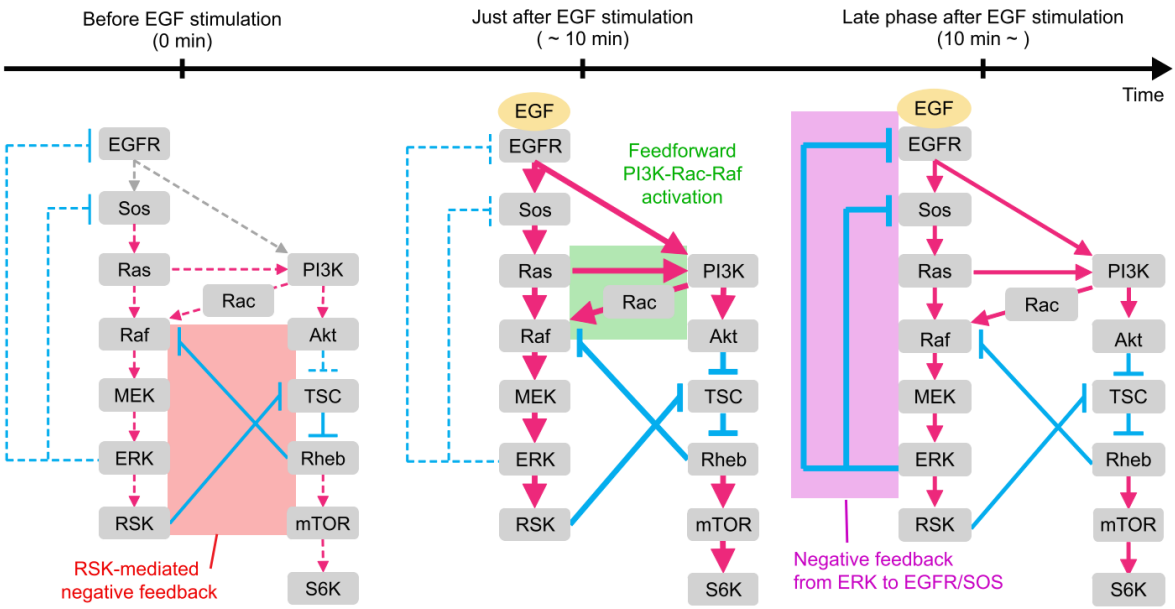

Figure 6: **Feedback mechanisms in the regulation of ERK1/2 cascade**. *"Before EGF stimulation"*: the use of a RSK inhibitor BI-D1870 increases the basal level of ERK1/2 activation and decrease S6K activity, reflecting the negative regulation of RSK on ERK1/2, as previously described [223]. RSK is known to phosphorylate and inactivate TSC1/2 complex leading to the activation of Rheb [224] and inhibition of Raf-1 [225]. A decrease of Rheb expression reveals a significantly increased ERK1/2 activity. "*In the early phase of EGF stimulation"*: inhibitions of PI3K by PI-103 and expression of Ras and Rac-1 dominant negative mutants block EGF-induced ERK1/2 activity as previously reported in the literature [226,227]. "*In the late phase of EGF stimulation"*: inhibition of MEK1 by PD184352 decreases EGFR activity suggesting a negative regulation of EGFR by ERK1/2 [228] (from [219]).

As a negative FBL, ERK1/2 enable to negatively regulate Raf-1 by phosphorylation of specific residues located in the CR2 domain such as Ser43 (for review, [229]). In the same line, ERK1/2 could also phosphorylate and inhibit the upstream kinase MEK1 [230]. Recently, Matsuda's research unit revealed several FBL and FFL between the ERK1/2 and PI3K/Akt pathways by using a kinase-inhibiting strategy associated with a Förster Resonance Energy Transfer- (FRET) biosensor imaging [219] (Figure 6). Here is a compilation of feedback mechanisms identified:

- a negative FBL from RSK to Raf-1 mediated by TSC2 and the Ras homolog enriched in brain (Rheb) (Figure 6)
- a coherent FFL from Ras to Raf-1 mediated by PI3K and Ras-related C3 botulinum toxin substrate 1 (Rac1) (Figure 6)
- a negative FBL from ERK1/2 to SOS and EGFR (Figure 6)
- a negative FBL from ERK1/2 to Raf-1 mediated by TSC2 and Rheb [231]
- a positive FBL from activated GTP-bound Ras to SOS [232]
- a positive FBL from ERK1/2 to Raf-1 mediated by Raf Kinase Inhibitor Protein (RKIP) inhibition [218]

1.2.3.4. ERK1/2 subcellular distribution

In resting cells, due to interaction with cytoplasmic scaffold/anchoring proteins, components of ERK1/2 signaling are localized in the cytoplasm [58]. One of the positive regulators of ERK cascade is the evolutionary conserved Kinase Suppressor of Ras (KSR) that acts by bringing components of ERK signaling into close proximity with Ras at the plasma membrane to facilitate activation of the pathway [117,233]. MEK1/2 is sequestered in the cytoplasm of resting cells also via its N-terminal NES and functions as a cytoplasmic anchor for inactive ERK [234,235]. Besides its apparent cytoplasmic localization, 5% of MEK1/2 can be found in the nucleus at the peak of activation of the pathway [236]. MEK1/2 can rapidly transit between the cytoplasm and the nucleus much faster than ERK1/2 and acts therefore as a nuclear export shuttle for ERK1/2 and other nuclear proteins [237]. Mitogenic stimulation is followed by a rapid entry of ERK1/2 in the nucleus, being detectable only a few minutes after pathway stimulation, and then a massive nuclear accumulation of

ERK1/2 after several hours following the stimulation can be observed. At the opposite, non-mitogenic stimulation provokes only a rapid nuclear translocation of ERK1/2 and does not cause any accumulation in the nucleus [208,238]. It has been reported that nuclear ERK1/2 accumulation occurring several hours after the stimulation required nuclear anchors such as MKP1 and MKP2 phosphatases which expression is induced by ERK1/2 signaling for signal termination [206,208]. Calculation of MEK/ERK ratios in several cellular models revealed strong differences. In HeLa cells, the concentration of MEK exceeds that of ERK (1,4µM and 0,96µM respectively) whereas a ratio of 0,7:9 were estimated in NIH-3T3 cells [239,240]. But, because ERK1/2 is sequestered in the cytoplasm in most cellular models before stimulation, other scaffold proteins than MEK1/2 exist to maintain ERK1/2 in the cytoplasm (Figure 7).

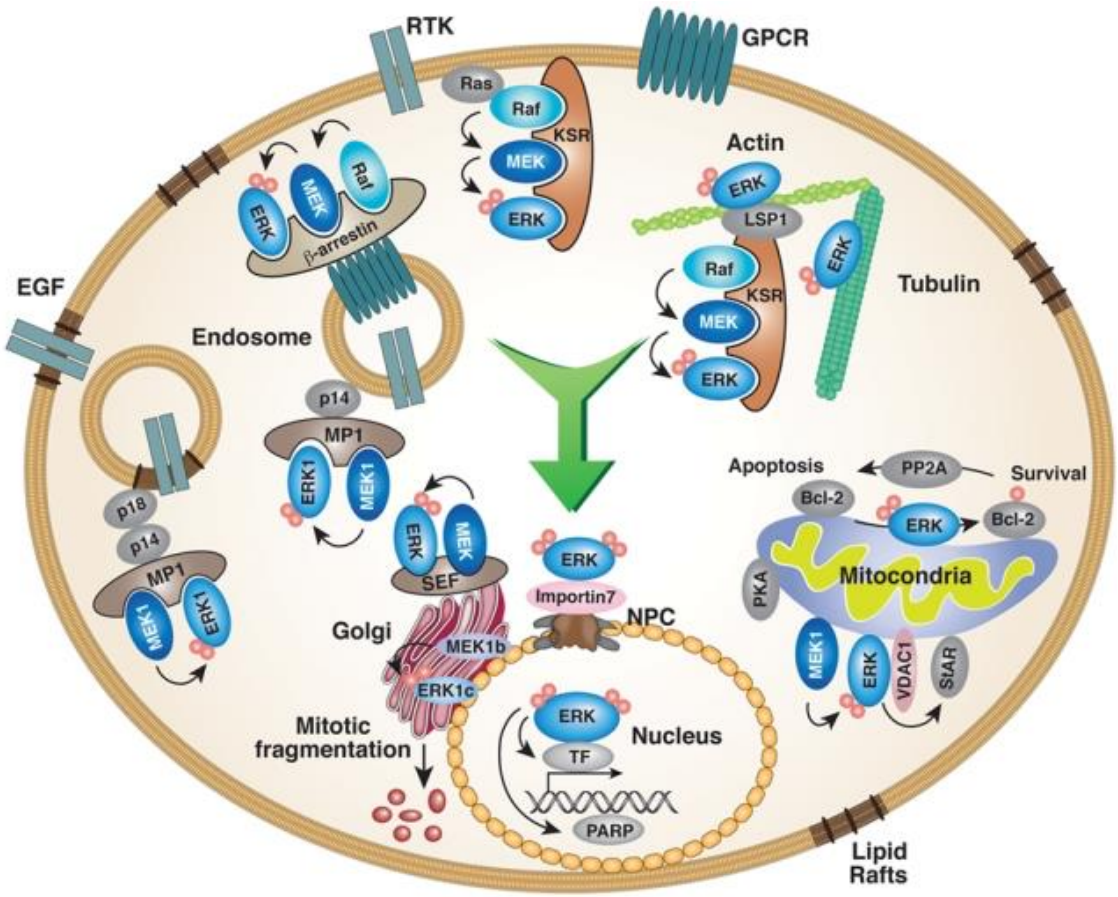

Figure 7: **Subcellular distribution of ERK1/2** mediated by specific ERK1/2 scaffold proteins thereby ensuring the transmission of the signal into the nucleus and multiple organelles to facilitate ERK1/2 substrates phosphorylation (from [58]).

Remarkably, depending on the cell type and MEK1/2 and ERK1/2 cellular relative concentrations, a large portion of ERK1/2 (between 30-70%) translocates to

the nucleus after stimulation of the pathway [187,238]. A large number of cytoplasmic anchors including Phosphoprotein Enriched in Astrocytes 15 kDa (PEA-15), MEK Partner 1 (MP-1), Similar expression to *fgf* genes (Sef-1) and Voltage Dependent Anion Channel (VDAC) guide and retain a significant portion of activated ERK1/2 in the cytoplasm, the endosomes, the Golgi apparatus and the mitochondria respectively. Compartmentalized ERK1/2 exert their specific cytoplasmic functions such as regulating intrinsic activities of organelles and prevent therefore an excessive accumulation in the nucleus after stimulation of the pathway [241–245]. Moreover, specific docking domains mediate the specificity of the interaction of ERK1/2 with its partners and may explain distinct their spatio-temporal subcellular localization. Several studies revealed the interaction between proteins containing a D-domain and/or F-site (also known as Docking site for ERK, F*X*F (DEF) motif) with the CD domain and FRS (also known F-site recruitment site) of an ERK1/2 protein, respectively [246–250]. Importantly, ERK1/2 binding affinity with a specific substrate is governed by conformational changes of ERK1/2 proteins in the docking domains upon Thr-Glu-Tyr (TEY) phosphorylation [251]. Interaction of ERK1/2 with DEJL motif is non-reversible even upon TEY phosphorylation and therefore prevents mobility of ERK1/2 proteins in particular subcellular regions such as cytoskeletal filaments [252].

1.2.3.5. ERK1/2 nuclear translocation

ERK1/2 translocation was initially thought to be a mechanism based on both passive diffusion and active transport involving dimerization of ERK1/2 [253,254]. While ERK1/2 proteins do not contain a dedicated NLS, a particular domain named MAPK Insert Domain (KID) was shown to be involved in ERK1/2 nuclear import [255]. In 2008, Seger's laboratory clearly identified a Ser-Pro-Ser motif (SPS motif) within the KID domain. Upon stimulation, phosphorylation patterns of the SPS motif were correlated with the rate of ERK1/2 translocation. This SPS motif acts as a Nuclear Translocation Signal (NTS) (Figure 8). The phosphorylated SPS motif then binds to the nuclear translocating protein Importin 7 (Imp7) that mediates the transport of activated ERK1/2 into the nucleus through the interaction with Nuclear Pore proteins (NUPs) [196]. Plotnikov *et al.,* proposed the Casein Kinase 2 (CK2) as the major kinase responsible for SPS phosphorylation. Point mutations on the two serine residues contained in the SPS motif as well as depletion or inhibition of CK2 systematically prevent ERK1/2 translocation without altering ERK1/2 activity in the

cytoplasm reflecting that ERK1/2 activation by MEK1/2 and CK2-mediated ERK1/2 translocation are independent events [256,257]. Moreover, similar NTS sequences were identified in other NLS-lacking proteins such as MEK1/2 and can therefore be considered as generic sequences mediating protein nuclear translocation upon stimulation [258].

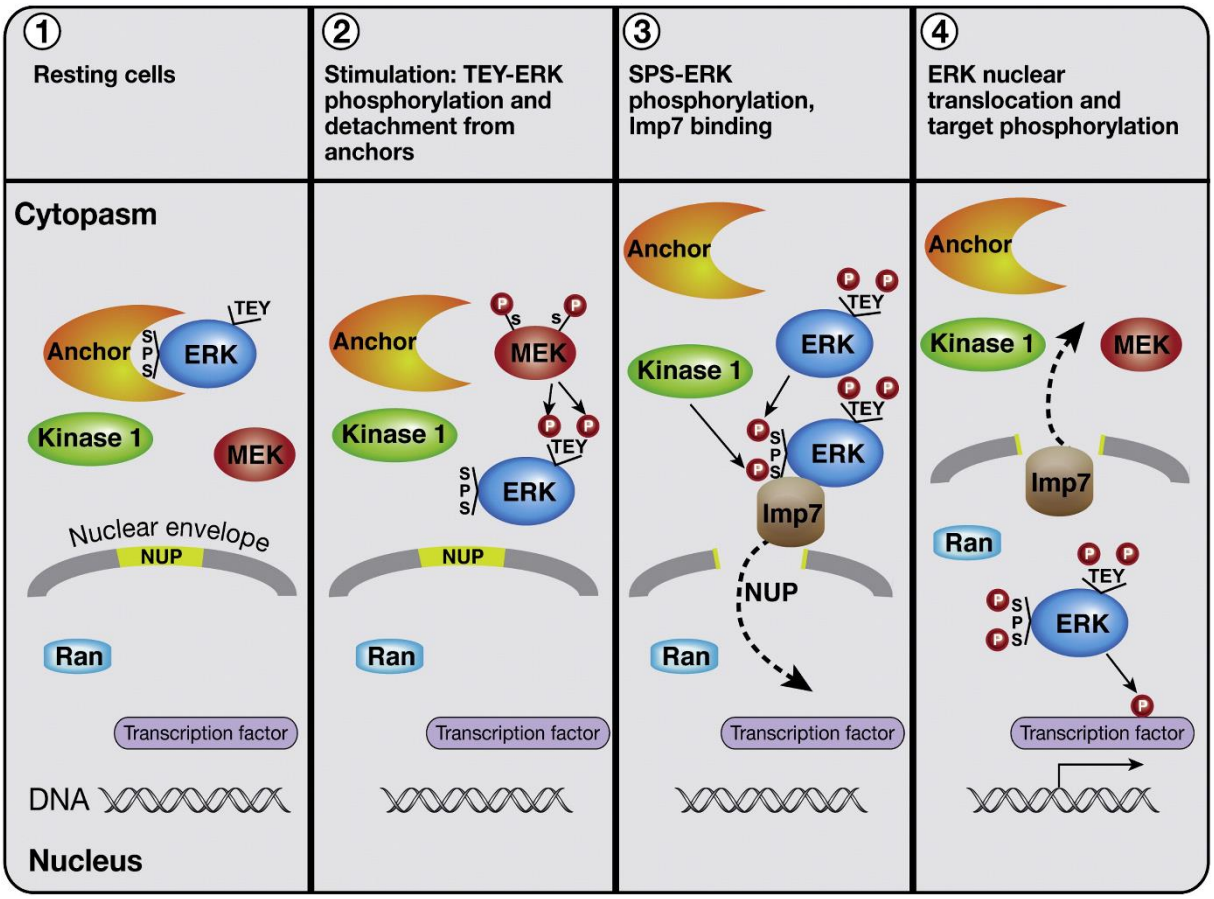

Figure 8: **Molecular mechanisms of ERK1/2 translocation into the nucleus** involving first the TEY-ERK phosphorylation by MEK1 and then the CK2-mediated ERK1/2 phosphorylation on SPS motif leading to its nuclear translocation mediated by Imp7. This translocation enables activated ERK1/2 to phosphorylate numerous substrates and activate specific gene expression programs. Ran: RAs-related Nuclear protein; NUP: NUcleoPorins; Kinase1: unknown kinase but now identified as CK2; Imp7: Importin 7 (from [193]).

1.2.3.6. Uncoupling mechanisms

As described in previous studies, mitogenic stimulation is followed by a rapid entry of ERK2 in the nucleus and then a massive nuclear accumulation of ERK2 several hours after the stimulation for signal termination. At the opposite, non-mitogenic signals trigger solely the initial translocation of ERK2 [208,238]. ERK2-mediated phosphorylation of MKPs triggers inactivation and nuclear retention of ERK2 through high-affinity interactions, limiting access to cytoplasmic activated MEK1. Consistent with previous studies, this late accumulation of ERK2 in the

nucleus is uncoupled from MEK1-dependent TEY-phosphorylation of ERK2. In addition, recent findings identified a similar uncoupling mechanism of TEY-phosphorylation from ERK2 nuclear localization at the early phase of the stimulation [259,260]. This uncoupling mechanism is not explainable by the sole expression of specific nuclear anchors and relies on a Casein Kinase 2-dependent SPS-phosphorylation in the kinase insert domain of ERK2 that is independent of ERK2 activation [196,257,258]. These findings shed light the importance to closely correlate ERK1/2 activation to its subcellular localization to determine cell fate and assess involvement of specific spatio-temporal regulators of ERK1/2 pathway. This has become particularly relevant when considering the kinase-independent functions of ERK1/2 that has been reported both in the cytoplasm and in the nucleus [261]. In combination with ERK1/2 subcellular distribution, monitoring of compartmentalized ERK1/2 activity would address the complete spatio-temporal signature of ERK1/2 and reveal potential uncoupling mechanisms depending on the cellular context [262,263].

1.2.3.7. Biological functions and physiopathology of ERK1/2 module

ERK1/2 signaling pathway plays an important role in cellular signaling network by regulating several cellular processes including survival, proliferation, differentiation, cell migration, neuronal plasticity and cell death depending on cellular context and the type of stimulation [57,59,264].

ERK1/2 is involved in cell proliferation at different levels (for review, [265]). ERK1/2 is known to regulate the pyrimidine nucleotides biosynthesis through the phosphorylation of Carbamoyl Phosphate Synthetase for II (CPSII) on Thr 456 residue [266]. ERK1/2-mediated MSK1 and MSK2 activation is also involved in the chromatin remodeling through the phosphorylation of Histone 3 (H3) and High Mobility Group (HMG) proteins [267]. Moreover, ERK1/2-mediated MNK1 activation induces phosphorylation and activation of the translation initial factor 4E (eIF4E) leading to increased protein translation [268]. Protein translation is also up-regulated both by PI3K/AKT (for review, [269]) and ERK1/2 interconnected pathways through inhibition of the tuberous sclerosis (TSC) proteins 1 and 2 complex [231,224].

During the cell cycle, ERK1/2 activity is essential for the G1/S transition through the induction of Cyclin D1 expression and therefore the activation of

CDK4/Cyclin D1 complex. ERK1/2 regulates Cyclin D1 expression through the activation of Elk-1 [270], the Fos family of transcription factors including c-Fos and Fra-1 [271], but also via the Myc transcription factor [272]. At the opposite, ERK1/2 negatively regulates the transcription of anti-proliferative genes such as JunD [273], providing another strategy for ERK1/2 to control cell cycle progression (for review, [265]).

ERK1/2 activity was also reported to regulate the G2/M transition. In the *Xenopus laevis* oocyte model, M-phase-promoting factor (MPF) and ERK2 pathways are interconnected, and MPF may control the magnitude and duration of ERK2 activation [274,275]. By contrast, in mammalian cells, the role of ERK1/2 is more controverted. While inhibition of ERK1/2 expression or activity was reported to provoke an accumulation of cells in G2/M [276–278], other studies showed no particular effect on the kinetics of entry into mitosis or the duration of the mitosis [279]. However, the study of the role of ERK1/2 in the proliferation and homeostasis of human epidermis provided new insights. ERK1/2 depletions in skin fibroblast cells resulted in a G1 arrest due to a decrease of Cyclin D1 expression level, whereas its loss in epithelial cells resulted in a G2/M arrest [280]. Upon ERK1/2 overactivation in immortalized mammary epithelial cells, increased levels of mRNAs encoding mitotic proteins have been detected such as Cyclin B1, CDK1, CENtrosome-associated Protein E (CENP-E), Budding uninhibited by benzimidazoles 1 (Bub1), Mitotic arrest deficient 2 (Mad2) and Aurora A during early to mid-G2 phase [281], suggesting thereby a role of ERK1/2 in the regulation of G2/M progression of epithelial but not fibroblast cells.

While amino acid sequences of ERK1 and ERK2 as well as their activation and regulation are highly similar, ERK1 and ERK2 exert some specific functions. Recently the role of ERK2 has been emphasized. In a murine system, $ERK2^{-/-}$ embryonic lethality was attributed to failure of placenta and trophoblastic development [282], while $ERK1^{-/-}$ embryos are viable and fertile [283–285] but have problems in thymic development [286]. In the same line, knockdown of ERK2 in *zebrafish* model prevents epiboly and the blastula to gastrula transition, while ERK1 knockdown provokes subtle defects in the embryogenesis [287]. In addition, it has been reported recently that spatiotemporal subcellular localization of ERK1/2 controls either myogenic proliferation (nuclear) or differentiation (cytoplasmic) fates of mouse

embryonic muscle progenitors [288]. These findings underline that ERK1/2 have a prominent role in embryonic development and in cell differentiation.

Briefly, inhibition of ERK1/2 signaling by chemical inhibitors or dominant negative forms of MEK1 causes abnormalities in the assembly/disassembly of focal adhesions. ERK1/2 signaling was reported to be a target of the Focal Adhesion Kinase (FAK)/Src signaling involved in the adhesion turnover [289]. In addition, a decrease in ERK1/2 activation level was described in $FAK^{-/-}$ MEF cells. Activated ERK1/2 are localized to focal adhesions and may promote the phosphorylation of the Myosin Light Chain Kinase (MLCK) involved in cell contractility [290].

Proteins responsible for ERK1/2 signaling cascade are derived from the expression of proto-oncogenes. If cells fail to receive or integrate external signals into the molecular jungle of cell signaling network, it may lead to cellular homeostasis dysfunctions and diseases. Indeed, there is considerable evidences for the involvement of ERK1/2 cascade in pathogenesis, progression and oncogenic behavior of several human cancers including lung cancer, breast cancer, colorectal cancer as well as pancreatic cancer, glioblastoma and melanoma [291–295]. For example, 10% of colorectal cancer patients and 60% of melanoma patients exhibit a substitution of valine with glutamate at position 600 (V600E) in the B-Raf proto-oncogene resulting in a constitutively active form of B-Raf [293,296,297]. This leads to consider this molecular pathway as a potential target in antiproliferative therapeutic strategies [13]. Deregulation of the pathway is also associated with the development of other human diseases including neurodegenerative and cardio-vascular diseases [298,299]. For example, overexpression of EGFR, that is frequently found in brain tumors, alters the duration of ERK1/2 signaling *via* diverse mechanisms [300,301], thereby pushing the cells into (uncontrolled) cell proliferation.

1.3. Involvement of ERK1/2 in cell death processes

In tumors, ERK1/2 was shown to promote the expression and the activity of anti-apoptotic proteins and to repress pro-apoptotic proteins hence contributing to cell survival and tumorigenesis [302]*. At the opposite, an increasing number of studies report the pro-death function of ERK1/2 activity in various programmed cell death depending on cell type and the intensity of cell stimulation.*

1.3.1. ERK1/2 in apoptosis

The first evidence of pro-apoptotic function of ERK1/2 was described in 1996 where depletion of Raf rescues MCF-7 cells from taxol-induced apoptosis [303]. MEK1 depletion was also shown to block bufalin-induced apoptosis in leukemic cells [304]. Chemical inhibitions (U0126 [305] and PD 098059 [306]) as well as dominant negative [307] or constitutively active forms [308] of MEK1 clearly emphasized a significant role for ERK1/2 in mediating apoptosis. ERK1/2-mediated apoptosis was observed upon stimulation with antitumor compounds such as taxol [303,309] or shikonin [310] and DNA-damage agents such as etoposide [311–313] or UV irradiation [312]. Several of these pro-apoptotic drugs that induced ERK1/2-mediated apoptosis are defined in Table 1. These drugs can activate the intrinsic apoptotic pathway but ERK1/2 activity has also been involved in the activation of the extrinsic apoptotic pathway by specific death receptors in response to TNFα [314–316], Fas [307,317] or TNFα-Related Apoptosis-Inducing Ligand (TRAIL) [318–322]. Numerous other stimuli including oxidative stress such as ROS [323–326], toxic heavy metals such as cadmium [327–329], survival growth factors withdrawal [330] and pro-death signals such as interferon-α (IFNα) [331], can induce ERK1/2-related cell death signaling pathways and be counteracted by premature ERK1/2 inhibition. In addition, it was demonstrated that ERK1/2 sustained activation associated with p53 activation [332] or c-Myc overexpression [333] could activate apoptosis, emphasizing the undeniable role of ERK1/2 in promoting cell death. Moreover, Cagnol and colleagues demonstrated that a sustained activation of ERK1/2 pathway using an inducible form of Raf-1 in HEK293T cells (Table 1) was sufficient to induce the extrinsic pathway through caspase-8 activation independently of the intrinsic pathway [334]. Depending

on cell type and under certain cellular insults, ERK1/2-induces apoptosis through either intrinsic or extrinsic apoptotic pathway.

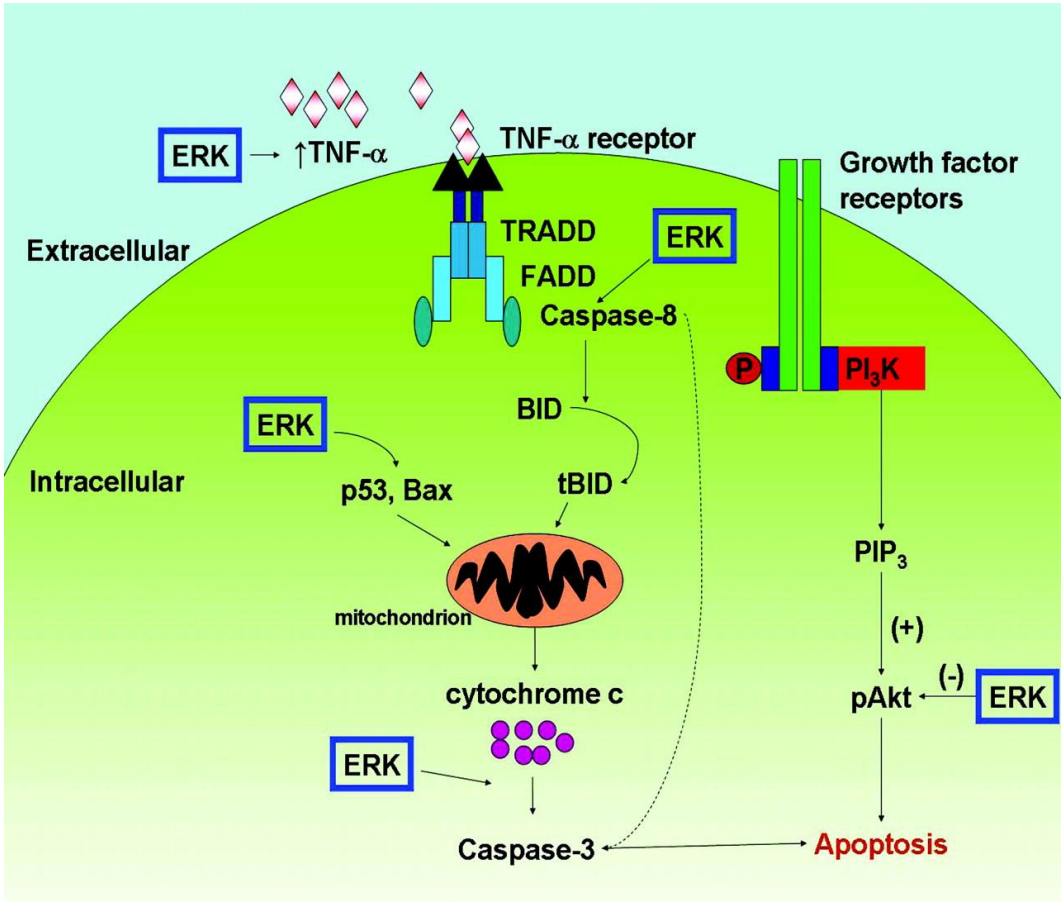

Figure 9: **ERK1/2-mediated apoptosis**. ERK1/2 is involved at different levels to regulate apoptosis and cell survival. The blue box corresponds to the position of ERK1/2 to promote apoptosis (from [335]).

1.3.1.1. ERK1/2 regulation of extrinsic pathway

ERK1/2 may induce apoptosis through regulation of the extrinsic pathway by increasing production of pro-inflammatory cytokines such as TNFα [336] and IL-1β [337] or by increasing the level of death receptors such as Fas [338] and other members of TNFR family [321]. Transcription factors of the ERK1/2 signaling pathway such as c-Fos has been involved in the up-regulation of death receptors [321]. ERK1/2 activity was reported to induce FADD expression [334,338]. Cagnol and colleagues elegantly showed that prolonged ERK1/2 activation promotes activation of caspase-8 and hence triggers apoptosis independently of death receptors and FADD [334]. In addition, overexpression of an anti-apoptotic factor, Bcl-X_L, did not prevent ERK1/2-induced apoptosis, reflecting a direct regulation of the apoptotic pathway at the level of caspase-8 [334]. However, the protein PEA-15

contains an N-terminal Death Effector Domain (DED) and binds to ERK1/2 to control its subcellular distribution [241,339]. PEA-15 was shown to prevent death receptor-activated apoptosis by binding to the DED of FADD [340]. Because FADD binds to the DED of caspase-8 to activate apoptosis, PEA-15 could regulate the extrinsic apoptotic pathway independently of the death receptors (Figure 9).

1.3.1.2. ERK1/2 regulation of intrinsic pathway

ERK1/2 activity was associated with the features of apoptosis. Several studies revealed that activated ERK1/2 is localized in mitochondria and more precisely in mitochondrial membranes [341,342]. ERK1/2 activation was associated with the loss of mitochondrial functions and mitochondrial membrane depolarization in cisplatin-induced apoptosis [308,336,341–343] leading to mitochondrial membranes disruption, cytochrome c release and subsequent caspase-3 activation [343–345]. Moreover, ERK1/2 activation could act on cytochrome c release by regulating the expression of Bcl2 family members. Indeed, upon apoptotic stimulation, ERK1/2 activation was shown to up-regulate pro-apoptotic proteins such as Bax [308,346,347] and Bak [331] and down-regulate anti-apoptotic proteins such as Bcl2 [309,312,348] and Bcl-X_L [349]. Bax is known to promote the release of pro-apoptotic proteins from the mitochondria [350]. Inhibition of the ERK1/2 pathway reverts these effects on Bcl2 family members expression [308,347]. The pro-apoptotic protein Bid is cleaved after ERK1/2 induced capsase-8 activation, leading to the activation of the intrinsic apoptotic pathway [349]. However, targeting p53 using genetic or chemical approaches revealed that p53 is a prominent actor in ERK1/2-mediated apoptosis. In apoptotic conditions, ERK1/2 activation was found to increase p53 expression *via* phosphorylation on its Ser 15 residue, leading to p53 stabilization and subsequent accumulation [312,332,348,351,352]. ERK1/2-mediated p53 phosphorylation on the Thr 55 residue was also found to activate pro-apoptotic functions of p53 by up-regulating pro-apoptotic genes expression [348]. Activated p53 is also localized in the mitochondria to counteract Bcl- X_L action [353] and to promote Bax/Bak activation finally leading to cytochrome c release [354,355]. Although p53 is an important regulator in ERK1/2-mediated apoptosis, several studies report, in certain circumstances, a p53-independent ERK1/2-mediated apoptosis [309,356] (Figure 9).

1.3.1.3. Other actors in ERK1/2-mediated apoptosis

cPLA2 is involved in unsaturated fatty acids production. ERK1/2-mediated cPLA2 phosphorylation [357] is associated with cytochrome c release and subsequent caspase-3 activation [358].

DAPK is a pro-apoptotic protein located in the cytoplasm, which is involved in IFNγ-mediated apoptosis [359,360]. DAPK was found to interact with the D-Domain of ERK1/2 through its death-domain leading to cytoplasmic sequestration of ERK1/2 and subsequent blockage of ERK1/2-mediated pro-survival functions [361]. Upon IFNγ stimulation, ERK1/2 phosphorylates DAPK on Ser 735 resulting in the increase of DAPK activity and finally leads to apoptosis [361]. Similarly, Bik, a member of Bcl2 family, enables sequestration of activated ERK1/2 in IFNγ-mediated apoptosis [362].

Upon etoposide exposure, DNA-damages induced Ataxia Telangiectasia Mutated (**ATM**) activation enables the sustained ERK1/2 activation independently of p53, which promotes apoptosis [312,363,364].

Survival growth factors deprivation is known to elicit apoptosis through a sustained activation of ERK1/2, which in turn down-regulates **PI3K/Akt** and suppresses survival signaling pathways [330,365]. Chemical inhibition of ERK1/2 cascade prevents the decrease of Akt activity and rescues cells from apoptosis [330]. Conversely, Akt is also known to act downstream of ERK1/2 by phosphorylating **PEA-15** [366], which in turn retains activated ERK1/2 in the cytoplasm and thereby suppresses once more the survival functions of ERK1/2 [367,368].

Finally, **ROS production** is involved in ERK1/2-mediated apoptosis [369]. ROS can induce oxidative DNA damages such as DNA strand breaks [370] leading to ATM activation and subsequent p53 phosphorylation, which in turn promotes cell cycle arrest and apoptosis. ERK1/2 inhibition was reported to rescue several cell types from ROS-induced apoptosis [344,371].

1.3.2. ERK1/2 in autophagy

Several studies reported ERK1/2 activation with cytoplasmic vacuolization and cell rounding independently of caspases activation (for review, [372]). Prolonged ERK1/2 activation induced by Raf [334], serum deprivation [373], cadmium exposure in MES-13 cells [328,374], TNFα stimulation in MCF-7 [316] and L929 cells [315]

were associated with autophagic cell death. Prolonged ERK1/2 activation is sufficient to promote autophagic cell death in response to carcinogens exposure [375]. It was also reported that sustained ERK1/2 activation perturbes the maturation of autophagosomes [375]. In addition, depending on the cell type, PEA-15-mediated cytoplasmic sequestration of activated ERK1/2 was associated with autophagy activation [376]. ERK1/2-mediated autophagy is implicated in the regulation of autophagy-related markers including coiled-coil moesin-like Bcl2-interacting protein 1 (Beclin-1) induction and microtubule-associated protein 1A/1B-Light Chain 3-I (LC3-I) conversion to LC3-II [315] that are considered as sensitive molecular markers of autophagy. In TNFα-induced autophagy in L929 cells, ERK1/2 activation leads to phosphorylation of p53 on Ser 392 [315], suggesting a role of p53 in autophagic cell death. In certain neurodegenerative diseases, ERK1/2 activity was involved in neuronal autophagic cell death [377,378]. However, ERK1/2 was found in cytoplasmic vacuoles [379] but also in membranes of these vacuoles [380]. Recently, upon growth factors stimulation, components of ERK1/2 cascade were located at the luminal face of autophagosomes where they interact with membranes-associated Atg or LC3-II proteins acting as scaffolding proteins to regulate ERK1/2 phosphorylation [380]. It was also shown that AMPK-MEK1/ERK2-TSC-mTOR pathway is implicated in the regulation of autophagy through a non-canonical activation of ERK1/2 cascade implicating directly MEK1 [381]. These findings indicate that ERK1/2 activation can either promote or regulate autophagic cell death.

1.3.3. ERK1/2 in paraptosis

Only few articles have described the potential role of ERK1/2 in paraptosis. In 2004, Sperandio and colleagues revealed that the Insulin-like Growth Factor I Receptor (IGFIR) signaling triggers paroptosis. Both Insulin-like Growth Factor I (IGF-I) and active truncated IGFIR result in a significant decrease of cell survival by inducing paroptosis. The molecular mechanisms underlying paraptosis are not clear and remain to be investigated. But, it was shown that IGFIR-induced paraptosis is mediated by MAPKs including MEK-2 and JNK-1 as both chemical inhibition and genetic approaches completely prevented paraptosis [36]. Recently, hesperidin, which exhibits anti-oxidant and anti-cancer properties, was involved in ERK1/2-mediated paraptosis in HepG2 cells. The features of apoptotic and autophagic cell death are lacking and the inhibition of ERK1/2 was shown to block hesperidin-

induced paraptosis [382]. Finally, oligomeric procyanidins (F2) exposure resulted in ERK1/2 and p38 activation leading to the paraptosis of human glioblastoma U87 cells [383].

1.3.4. ERK1/2 in ferroptosis

Similarly, very few articles highlighted a link between ERK1/2 activation and ferroptosis. Yagoda and colleagues described the first evidence of ERK1/2-mediated ferroptosis in 2007 [384]. Erastin is an anti-tumor compound known to induce mitochondrial dysfunctions and generate ROS towards a non-apoptotic and non-autophagic cell death, so-called ferroptosis. Interestingly, H-RasV12-expressing cell lines are more sensitive to erastin. Conversely, RNA interference for K-Ras exhibits resistance to erastin-induced ferroptosis. These findings indicate therefore that activated ERK1/2 signaling pathway could be required for erastin-induced ferroptosis [384]. In 2010, Carr and colleagues highlighted that ERK1/2 activity regulates the glutamine uptake and metabolism in T cells that are particularly sensitive to glutamine variations [385]. GPX4 acts as a scavenger of phospholipid hydroperoxides to avoid membrane lipid peroxidation. Recently, Matsushita and colleagues revealed that inhibition of ERK1/2 signaling pathway impairs GPX4-deficient T cell death by ferroptosis suggesting that ERK1/2 is activated by lipid peroxides in ferroptosis [386].

1.3.5. ERK1/2 in parthanatos

Upon ROS production by ROS-generating myeloid cells or by exogenous ROS such as H_2O_2, phosphorylation of ERK1/2 was detected in Natural Killer (NK) cells and $CD8^+$ lymphocytes. Increasing concentration of ROS promotes PARP1 activation and accumulation of PAR polymer leading to cell death by parthanatos. ROS-induced ERK1/2 phosphorylation was reported to be independent of PARP1 activity. Inhibition of ERK1/2 pathway by chemical inhibitors completely blocks parthanatos, suggesting a prominent role for ERK1/2 in ROS-induced parthanatos [387].

1.3.6. Hallmarks of ERK1/2 in cell death

1.3.6.1. ROS-mediated sustained ERK1/2 activation

ERK1/2-mediated cell death is associated with a prolonged ERK1/2 activation from several hours up to several days (Table 1). ERK1/2 inhibition by chemical agents such as U0126 or PD98059 reduces or prevents this sustained phosphorylation [334]. It was reported that ERK1/2 phosphatases are sensitive to oxidative stress so that ROS could inactivate ERK1/2 phosphatases functions and alter the balance between phosphorylation/dephosphorylation of ERK1/2 leading to a sustained ERK1/2 activation [388,389]. ROS scavengers have been used in combination with cell death stimuli and it appears that ERK1/2-mediated cell death requires ROS production [324,325,390,391]. Cell death stimuli including anti-tumor compounds, DNA-damages agents, pro-inflammatory cytokines and directly oxidative stress contribute to increase ROS production and subsequent ERK1/2 activation [391–394]. ROS-mediated sustained ERK1/2 could be therefore considered as a hallmark of ERK1/2-mediated cell death (for review, [372]). ROS act at different levels to up-regulate the ERK1/2 cascade:

- Activation of plasma membrane receptors such as EGFR [395]
- Activation of adaptor proteins such as Shc [396]
- Oxidation of Cys 118 residue on Ras promoting Raf activation at plasma membrane [397]
- Oxidation of multiple cysteine residues located on the CRD of Raf leading to its auto-activation [398]
- Nitration of MEK1 by the peroxynitrite promoting its auto-activation [325]

Downstream of ERK1/2, ROS-mediated sustained ERK1/2 phosphorylation can occur through inactivation of ERK1/2 phosphatases by oxidation of their redox-sensitive cysteine residues within their active site (for review, [399]):

- Oxidation of tyrosine phosphatase PP1 on Cys 62 residue [400]
- Oxidation of tyrosine phosphatase PP2A on Cys 62 residue [400]
- Oxidation of nuclear MKP1 on Cys 258 residue [401]
- Oxidation of cytosolic MKP3 on Cys 293 residue [401]

The duration of ERK1/2 activation plays a prominent role in determining cell fate [98]. ROS-induced cell death is usually associated with **biphasic activation** of ERK1/2

and corresponds to a **transient** phosphorylation followed by a **sustained** phosphorylation of ERK1/2 finally leading to cell death [327]. ROS-induced activation of molecular effectors upstream of ERK1/2 is responsible for the transient activation of ERK1/2 (first phase of the biphasic activation), whereas ROS-induced inactivation of ERK1/2 phosphatases is associated with the second phase of ERK1/2 activation (for review, [372,402]). However, cell death stimuli can cause either a progressive ERK1/2 phosphorylation [311,344] or a delay of several hours between the stimulation and ERK1/2 phosphorylation [344,403].

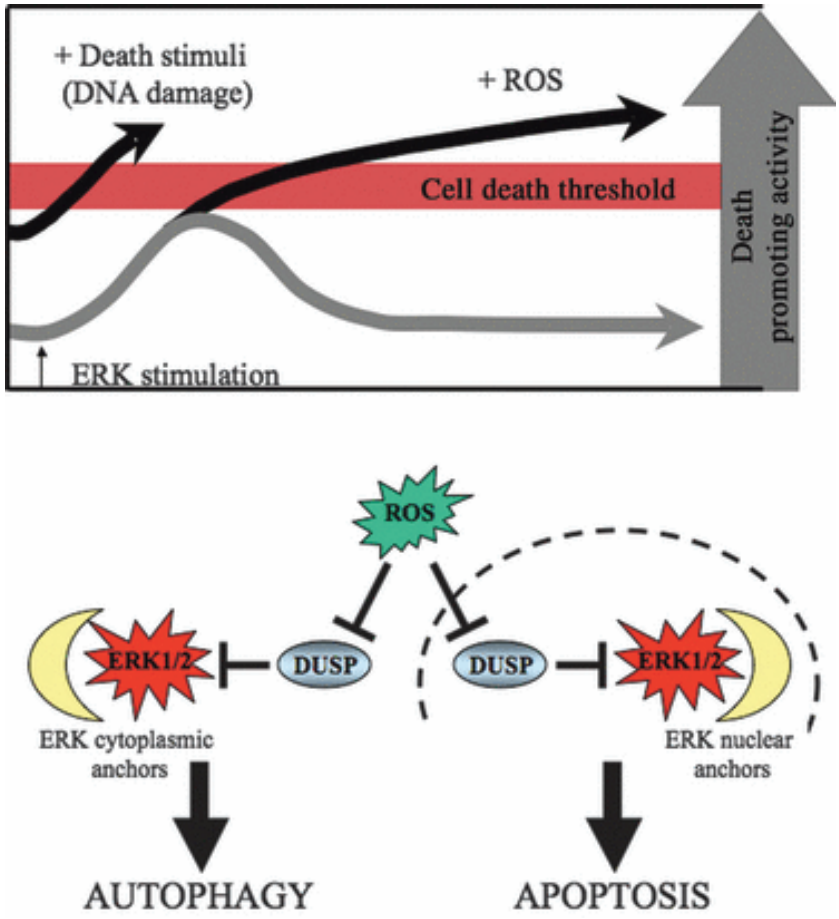

Figure 10: **Hallmarks of ERK1/2-mediated cell death**. Upon mitogenic stimulation (grey arrow), ERK1/2 is activated and translocates into the nucleus to regulate pro-survival gene expression including specific MKPs for its signal termination. The "death promoting activity" remains therefore very low. At the opposite, cell death stimuli result in ROS production, MKP inhibition, and sustained ERK1/2 activation thereby switching "death promoting activity" from low to high levels sufficient to induce cell death (red line). ROS-induced MKP inactivation leads to a compartmentalized ERK1/2 activation required to elicit a specific cell death (from [372]).

1.3.6.2. Sequestration of ERK1/2

Besides the duration of ERK1/2 activation, the compartmentalization of ERK1/2 activity is crucial to elicit a specific cell death [98]. The study of both activity level and subcellular distribution of ERK1/2 could address a specific spatio-temporal

signature of ERK1/2 activity to a specific cell death. ERK1/2 sequestration relies on expression of scaffolding proteins including nuclear and cytoplasmic MKPs [58,222,404]. Upon binding to ERK1/2, phosphatases exhibited an elevated catalytic activity to dephosphorylate ERK1/2 [405]. ROS production inactivates phosphatases so that they cannot dephosphorylate activated ERK1/2 but instead MKPs can interact with activated ERK1/2 leading to an abnormal accumulation of activated ERK1/2 in a specific subcellular compartment depending on the type of docking phosphatases [372]. Nuclear sequestration of ERK1/2 activity is associated with apoptosis, whereas cytoplasmic sequestration of ERK1/2 elicits different cell death depending on ERK1/2 activity. Indeed, cytoplasmic sequestration of ERK1/2 through PEA-15 interaction impairs its translocation to the nucleus for up-regulation of pro-survival gene expression and leads to autophagy [376]. At the opposite, cytoplasmic sequestration of activated ERK1/2 promotes senescence [406] (Figure 10). For example, stimulation of cultured cells with pro-apoptotic stimuli such as doxorubicin or cephaloridine promote accumulation of activated ERK1/2 in the nucleus and subsequent apoptosis [346,392]. In addition, overexpression of active MKP1 prevents taxol-induced apoptosis, reflecting inactivation of endogenous MKP1 by ROS production [407].

Cellular model	Cell death stimuli	Duration of ERK activation	Characteristics	Refs
NIH-3T3	Etoposide, UV, doxorubicin	24h	DNA degradation	[311]
NIH-3T3	γ-irradiation	48h	Membrane integrity, Annexin V	[346]
HeLa	Cisplatin	18h	Caspase-9, PARP cleavage	[308]
HeLa	Shikonin	12h	Caspase-8, Caspase-3	[310]
MCF-7	Taxol	24h	DNA fragmentation	[309]
HT-29	TRAIL	5h	Membrane integrity Nuclear condensation PARP cleavage	[321]
Immortalized L929	H_2O_2	3h	DNA fragmentation Annexin V	[391]
Mouse immortalized osteoblast	H_2O_2	Biphasic (12h)	Cell viability Membrane integrity	[347]
HEK293	Cadmium	Biphasic (96h)	Caspase-8, Caspase-3 PARP cleavage	[327]
MCF-7	Tamoxifen	1h	Membrane integrity	[408]
Primary mouse kidney proximal tubular epithelial cells	EGF deprivation	120h	Cell viability	[330]
U937	Bufalin	12h	DNA fragmentation	[304]
NIH-3T3	DAPK	Constitutive	Cell viability	[361]
HEK293	ΔRaf1:ER	Constitutive	Membrane integrity DNA fragmentation DNA condensation Annexin V Caspase-8, Caspase-3 PARP cleavage Vacuolization	[334]
L929	TNFα	ND	Cell viability LC3-II induction Beclin induction	[315]
MES-13	Cadmium	3h	Cell viability MTT LC3-II induction	[328]
MCF-7	TNFα	10h	Cell viability LC3-II induction	[316]
IMR90	RasV12	Constitutive	LC3-II induction	[379]
42GPA9	Lindane	24h	LC3 relocalization Vacuolization	[375]
HT-22	Glutamate	ND	Cell viability	[409]
Rat retina	Ischemia-reperfusion	12-24h	c-FLIP, RIP3 accumulation	[410]
HepG2	Hesperidin	ND	Vacuolization, mitochondria and ER swelling	[382]
BJ- TERT/LT/ST	H-RasV12 Erastin	ND	ROS production	[384]
NK and $CD8^+$ lymphocytes	ROS	ND	PAR polymer, ROS production	[387]

Table 1: **ERK1/2-mediated cell death in different cellular models**. ERK1/2-mediated apoptosis (yellow), autophagy (green), necroptosis (blue), necrotic-like cell death (cyan) in multiple cellular models. The panel reflects the diversity of cell-death stimuli that induced ERK1/2-mediated cell death and exhibits the most representative evidences that support ERK1/2 involvement in the different programmed cell death. Red selection highlights the low number of publications about the role of ERK1/2 in necroptosis. c-FLIP: cellular FLICE-like inhibitory protein. ND: not determined (adapted from [372]).

1.4. Why use dynamic approaches to elucidate ERK1/2 functions?

While biochemical events of ERK1/2 signaling pathway have been well characterized, a central question remained: **how can this signaling pathway triggers different cellular outcomes?** A simple model would be that a single signaling pathway promotes a specific cell response in response to a specific stimulus (Figure 11) but many studies indicated that this model is not insufficient to explain the complexity of the signaling network and the diversity of cell responses, thereby suggesting numerous crosstalk and regulations mechanisms to deal with the information flow. An increasing number of papers have highlighted that the duration, the magnitude and subcellular compartmentalization of ERK1/2 activity by specific key regulators represent as much as qualitative and quantitative differences in ERK1/2 activity that are interpreted by the cell for determining cell fate [59,98,222,411]. A classic example is the differential activation of ERK1/2 pathway in response to EGF or NGF in a same cellular model. EGF stimulation causes a transient activation of ERK1/2 and hence proliferation, whereas a sustained activation leads to differentiation and neurite outgrowth of PC12 cells.

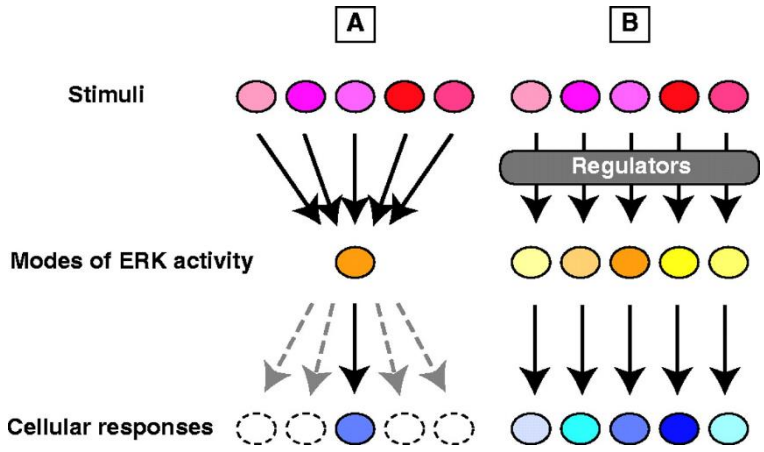

Figure 11: **A new model for signals-induced ERK1/2 activation**. (A) Simple model in which extracellular stimuli activate a single signaling pathway resulting in a single mode of ERK1/2 activity and hence a unique cellular response. (B) Stimulus-specific spatio-temporal patterns of ERK1/2 activity elicit an appropriate cellular response. This contributes to generate a temporal ERK1/2 activation code dependent on the cell type and cell stimulation (from [98]).

In addition, depending on the stimulation, multiple ERK1/2 protein partners are able to change their binding affinity to promote a remodeling of the cascade, indicating that cell fate is also governed by the dynamic ERK1/2 interactome [190]. Adding to the cellular network complexity, chemical inhibition of potential effectors

and computational approaches led to the identification of negative and positive feedback loops to modulate ERK1/2 pathway hence resulting in widespread increase in network connectivity. Spatio-temporal changes in ERK1/2 activity and connectivity generate therefore a particular ERK1/2 code to elicit various cellular responses from cell survival and proliferation to cell death processes [218,219,229,412] (Figure 14).

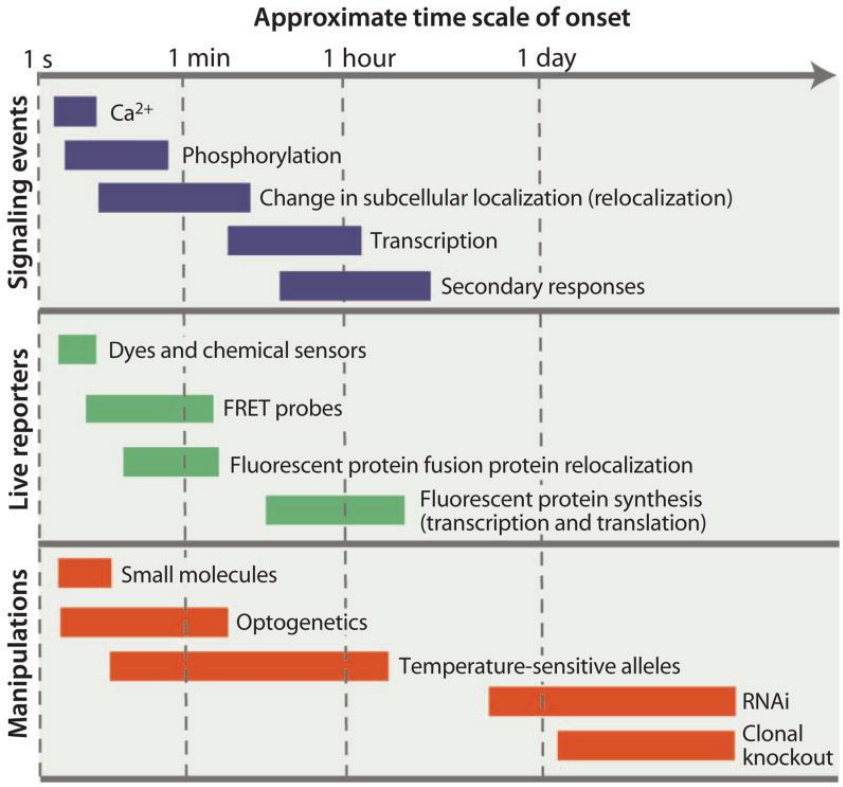

Figure 12: **Time scale for dynamical studies of signaling pathways**. Molecular events for transmitting signals occur within seconds for calcium variations and can take up to several hours for transcriptional gene expression (top). The scheme illustrates also the temporal window for each class of reporter to capture qualitative and quantitative read-outs (middle) with regard to the time scale of several approaches to manipulate signaling pathways (from [413]).

The time scale for the dynamic study of signaling pathways has to be taken into account (Figure 12) (for review, [413]). Indeed, calcium oscillations occur within seconds while phosphorylation and activation of protein kinases can be achieve on a time scale of minutes. In the case of ERK1/2 pathway, ERK1/2 translocate into the nucleus to activate a specific gene expression program within 5 to 10 minutes. But according to several studies, secondary regulatory mechanisms due to crosstalk could affect or modulate the initial outcome at the transcriptional level leading often to data misinterpretations. Although biochemical data, snapshot acquisitions or time-points measurement can provide very valuable information, dissecting and manipulating signaling pathways and crosstalk require high spatio-temporal

resolution that can be achieve by live-cell functional imaging. To this effect, appropriate engineered tools are required to monitor and modulate kinase activities in living cells and in real time at the appropriate time scale. This offers powerful approaches, which can provide new insights in signaling and cell fate regulation.

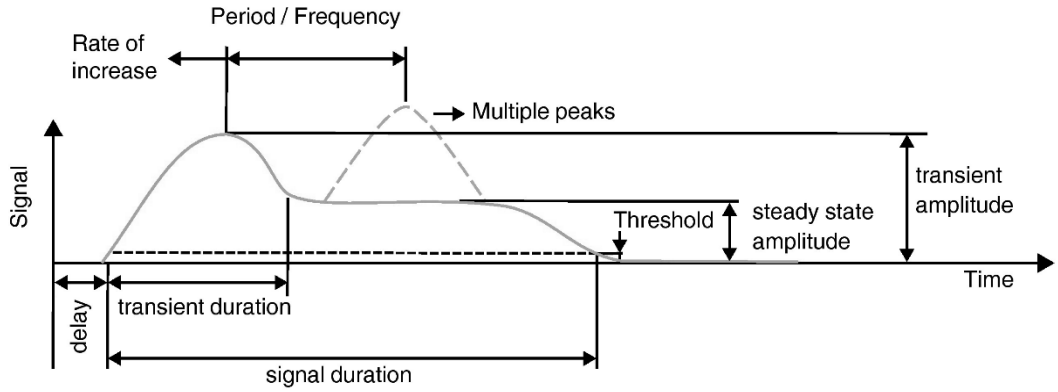

Figure 13: "Vocabulary" for the characterization of oscillatory kinase activation. (adapted from [414]).

Over the last decade, major advances have been made in our fundamental understanding of the regulatory mechanism of ERK1/2 pathway. While immunostaining of ERK1/2 localization and phosphorylation provide a snapshot of compartmentalized ERK1/2 activity at different time points, live cellular imaging of ERK1/2 activities in subcellular compartments have uncovered unexpected dynamics of ERK1/2. Recently, several elegant studies provided new evidences on oscillatory ERK1/2 activation. In the context of circadian rhythms and somitogenesis, FGF-induced Notch effector Hes1 oscillatory expression was associated with an oscillatory activation of ERK1/2 pathway depending on a negative feedback loop from ERK1/2 to SOS [415]. Similarly, Albeck and colleagues showed that ERK1/2 is activated in asynchronous pulses (stochastic ERK1/2 activation) at the basal state and that components at different levels of the pathway can modulate amplitude or frequency of EGF-induced ERK1/2 activity and hence regulate cellular proliferation under certain circumstances [416] (Figure 13). Finally, Aoki and colleagues highlighted another type of oscillatory activations of ERK1/2 using also a FRET-based biosensor approach. They found that Raf induces stochastic ERK1/2 activation pulses under normal cell culture conditions and that different cell densities regulate the frequency but not amplitude of ERK1/2 oscillations and hence cell proliferation. They also nicely demonstrated the propagation of these ERK1/2 oscillations to other adjacent cells.

Besides monitoring kinase activity, certain components of signaling pathways can relocalize to convey specific signals to specific subcellular compartments. This subcellular redistribution may reflect the activation of the pathway and provide qualitative and quantitative read-outs. For example, ERK1/2 [208,238] as well as STAT1/6 [417,418] and NF-κB [419,420] translocate into the nucleus upon activation of their respective signaling pathways. Tagged-version of these proteins led to the characterization of distinct molecular mechanisms required for their translocation but also the identification of specific anchors. For example, Shankaran and colleagues found that EGF-induced ERK1/2 activation in human mammary epithelial cells (HMECs) elicits oscillatory translocation of ERK1/2 between the cytoplasm and the nucleus depending on a negative feedback loop that is now considered as a hallmark of an oscillatory behavior (for review, [421]).

In conclusion, dynamical studies of cellular processes are powerful approaches as they increase spatiotemporal resolution at the single living cell level. Monitoring ERK1/2 activity has already revealed how the spatio-temporal dynamic of ERK1/2 activity affects the cellular responses. Moreover, the concept that emerge from studying spatio-temporal kinase activity is that a specific temporal activation code is required to elicit an appropriate cellular response (for review, [413]). This new trend in cell biology suggests that the information flow may be encoded temporally in frequency, amplitude and duration of the signal but also in space to control cell fate decisions (for review, [221,414]). Therefore, the main challenge nowadays is to decode this spatio-temporal activation code leading to a specific cellular response to finally elucidate regulation mechanisms and crosstalk between pathways.

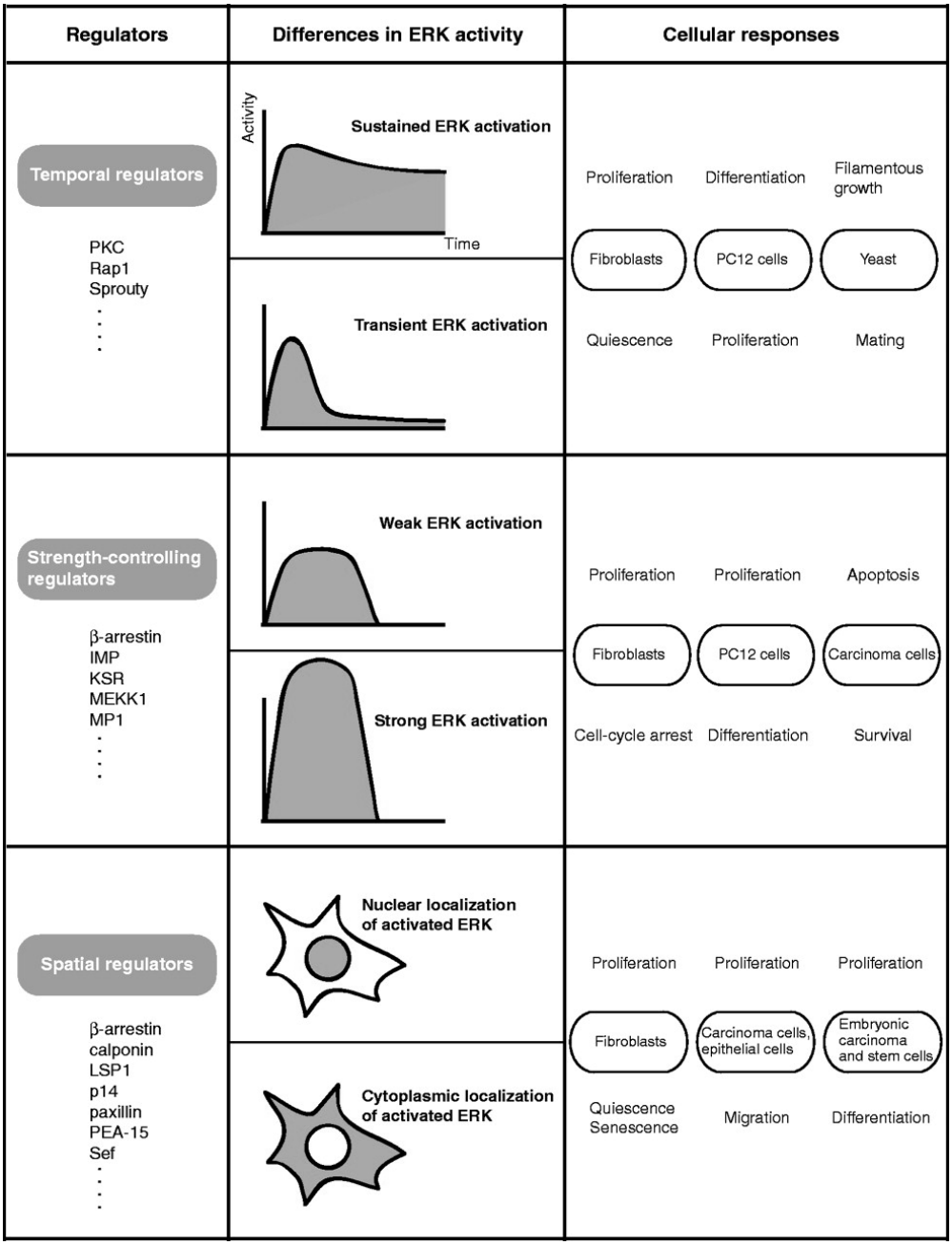

Figure 14: **General scheme of regulatory mechanisms for ERK1/2 activation** to address a specific spatio-temporal signature of ERK1/2 activity to a specific cellular response depending on cell type and cell stimulation (right). Major spatial and temporal modulators of ERK1/2 activity are also indicated (left) (from [98]).

1.5. Review – Reporting kinase activities: paradigms, tools and perspectives

Riquet Franck[1], Vandame Pauline[1], Sipieter François[1,2], Cailliau-Maggio Katia[1], Spriet Corentin[2], Héliot Laurent[2] and Bodart Jean-François[1]

[1] Laboratoire de Régulation des Signaux de Division, EA4479, Lille1 University, F-59655 Villeneuve d'Ascq, France

[2] IRI CNRS USR 3078, Lille1 University / Lille2 University, F-59655 Villeneuve d'Ascq, France

Published in Journal of Biological Medicine, 2011, Volume 1 No.2, 10-18

Review

Reporting kinase activities: paradigms, tools and perspectives

Riquet Franck[1], Vandame Pauline[1], Sipieter François[1], Cailliau-Maggio Katia[1], Spriet Corentin[2], Héliot Laurent[2] and Bodart Jean-François[1,*]

[1] EA4479 Laboratoire de Régulation des Signaux de Division, Science and Technology University of Lille, USR 3078 CNRS, Cell Signalomics Group, Parc de la Haute Borne, 59650 Villeneuve d'Ascq, France.

[2] Interdisciplinary Research Institute, Science and Technology University of Lille, USR 3078 CNRS, Biophotonique Cellulaire Fonctionnelle, Parc de la Haute Borne, 59650 Villeneuve d'Ascq, France.

[*] corresponding author : jean-francois.bodart@univ-lille1.fr

Abstract

Delineating the complexity of the phosphorylation-based signaling network has become imperative for the understanding of cell functions both in physiological and pathological contexts, and for therapeutically perspectives. Protein kinases MAPK, PKA and Akt were here taken as examples of protein kinases whose respective spatiotemporal regulations are crucial for specific cellular functions achievement. To overcome the shortcomings of traditional methods, imaging approaches have been developed, using FRET or bioluminescence, providing high temporal and spatial resolutions for single cell and tissues analysis. Here are discussed properties of kinase activity reporters either based on FRET or bioluminescence.

Keywords

Kinase, MAPK, PKA, Akt, KAR, KiBS, FRET, Bioluminescence

Background

Cellular functions require accurate translation of extracellular stimuli into functional responses via intracellular signaling cascades, many of which are critically regulated by protein kinases. Protein kinases covalently transfer the c-phosphate of ATP to recipient amino acid side chains on target proteins. These processes can be mediated by Serine / Threonine kinases (on Serine or Threonine residues) or by Tyrosine kinases (on Tyrosine residues). Phosphorylation of the target proteins results in changes in activities, interactions, localizations, or stability, thereby propagating a signal, which influences cellular decisions and functions. Signaling cascade propagation through mobilization of protein kinases is tightly controlled by combinations of regulation motifs, including feedforward and feedback mechanisms, which ensure irreversible, sustained or transitory decisions (Novak *et al*, 2007; Tyson and Novak, 2008; Czsikasz-Nagy *et al*, 2009). These mechanisms are tightly controlled to prevent aberrant protein kinases activation or inactivation, and cellular decisions are themselves subjected to regulatory checkpoint like those controlling cell cycle progression throughout replication and division (Nurse, 2000; Morgan, 2007).

In the human genome, 518 protein kinases have been identified, nearly half of which being expressed from loci associated with specific disease or from regions amplified in human cancers (Manning et al., 2002). Deregulations of protein kinases have been involved since then in various pathologies including cancer, neurological disorders, rheumatoid arthritis, immune, cardiac, metabolic and infectious diseases (Blume-Jensen and Hunter, 2001; Kumar et al., 2007; Mueller et al., 2005; Westra and Limburg, 2006; Wirth, 2010). As a result, protein kinases have become one of the major therapeutic targets for the last two decades (Cohen, 2002, Scapin, 2006). With one third of all intracellular proteins being phosphorylated (Johnson and Hunter, 2005), one might consider that virtually all cellular signaling processes involve the transfer of phosphate groups and implies that inhibition of aberrant kinases activity is considered to repair the deregulation of cellular signaling.

Delineating the complexity of the phosphorylation-based signaling network has become imperative for the understanding of cell functioning both in physiological and pathological contexts, and for therapeutically perspectives. Such a task may be

undertaken either (1) by focusing on specific protein kinases, which act as main effectors or contributors in many pathological contexts, that serve as converging hub for oncogenic stimuli, like PKA (Protein Kinase A), Akt or MAPK (Mitogen Activated Protein Kinases), or (2) by considering protein kinases in a global manner through kinome profiling. The latter aims at analyzing all protein kinases in cells or tissues, with respect to their abundance, activity, substrate specificity, phosphorylation pattern and even mutational status (Johnson and Hunter, 2005).

1.5.1. Spatiotemporal dynamics of kinase drives cellular functions: case review of MAPK/Erk, PKA and Akt

Kinase activation profiles are tightly associated to cellular decision. Actually, MAPK/Erk cascade provides a stunning example of how cells division might be driven by MAPK/Erk dynamics. Indeed, the phenotypical outcome of external stimuli might depend on the temporal profile of active, phosphorylated proteins recruited, as it is the case for MAPK/Erk (Murphy et al., 2002; Santos et al., 2007). Typically, the MAPK/Extra-cellular Regulated Kinase (Erk) cascade is a highly conserved signaling pathway throughout eukaryotic cells, bridging cell surface receptors to diverse executor proteins, integrating signals and modulating many aspects of cell life such as cell cycle, survival, differentiation and cell migration. Serving as a node into a network for signal integration, the MAPK cascade consists of three layers, each one being composed of a kinase (MAPKKK or MAP3K, MAP2K or MEK and MAPK). Deregulation of the MAPK/Erk pathway due to alterations affecting the expression or function of a number of pathway components has long been associated with numerous pathologies including cancers, resulting in the constitutive activation of ERK and continual cell proliferation (Bodart et al., 2002; Orton, 2009).

Nevertheless, the MAPK-Erk network exhibits plasticity and different dynamical properties may arise from connections within this network. For instance, rewiring of Erk pathway architecture in the context of NGF and EGF stimulation in PC12 cells (model for neurone differentiation) is believed to built the dynamical response observed for these growth factors; transient or sustained MAPK/Erk cascade activation following EGF or NGF stimulation, respectively. (Santos et al., 2007, Kriegsheim, 2008).

Similar dynamical properties of the MAPK/Erk pathway have been suspected to affect signaling cascade involved in cell death (Mebratu and Tesfaigzi, 2009). In fact, it is now clear that Erk is directly linked to cell death signaling although molecular mechanisms involved in Erk1/2-mediated cell death remain poorly understood. The MAPK/Erk1/2 cascade promotes also cell survival through inactivation of cell death machinery components and increase of pro-survival genes transcription rate. These mechanisms contribute to decrease cell sensitivity to apoptosis and promote cell proliferation since the balance between the intensity and duration of pro- and anti-apoptotic signals transmitted by MAPK/Erk influence the decision of a cell to proliferate or die. In this respect, subcellular localization of MAPK/Erk pathway components and dynamical spatiotemporal changes are believed to determine cell fate between proliferation and death (Ebisuya et al., 2005). Sustained Erk activation observed in cadmium poisoning conditions and in the engineered cellular system Raf-1:ER (Cagnol et al., 2006) can be associated with a cell death signaling, whereas transient activation observed following growth factors stimulation protects cells from death. Sustained ERK activation, which is sufficient to induce cell death, is often associated with cell death mediated by ROS (Dong et al. 2004) because these radicals can suppress protein-phosphatases activities of MKP (MAPK-specific Phosphatases), exerting key roles in the regulation of MAPK/Erk dynamics (Boutros et al., 2008). Inhibition of MAPK/Erk activation using inhibitors against components of the MAPK cascade, has a survival effect on cells induced to die following chemicals or physicals challenges. Forced MAPK/Erk cytosolic localization prevents a survival or a mitogenic response, but potentiates activities of specific pro-apoptotic proteins such as DAPK (Chen et al., 2005), Bik (Mebratu et al., 2008) and PEA-15 (Trencia et al., 2003) via the activation of PI3K/Akt pathway. Compartmentalized MAPK/Erk activity is therefore key to promote a survival or a death signaling. Thus, spatial signatures for the signal propagation of the MAPK/Erk signaling pathway have started to be explored both at experimental and theoretical levels in many different cellular models, from gametes to tissues (Maeder et al., 2007; Kholodenko and Birtwistle, 2010; Blossey et al., 2011). Mechanisms leading to MAPK/Erk signal propagation are challenging issues, especially when considering MAPK/Erk signaling over long distance as in neural tissue or in giant cells like oocytes.

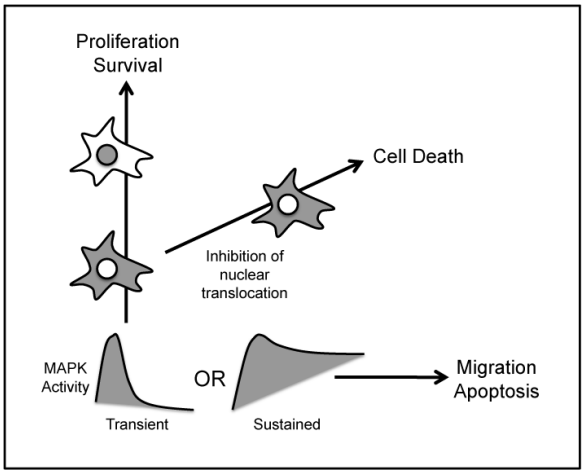

Figure 1. Spatiotemporal signatures of MAPK/Erk signaling drive cell fate between cell death and survival / proliferation. Transient and sustained MAPK activities (in blue) « promote » cell decision while spatial propagation of the signal is crucial to the final integration leading to cellular decision.

MAPK/Erk is not the only protein-kinase exhibiting complex spatial patterns, ranging from gradient to microdomains, tightly associated to cellular functions. Spatio-temporal regulation of PKA, whose activity is involved in many biological processes such as regulation of gene transcription, cell survival, cell cycle progression or cell migration, is known to be crucial for determination of cell response. PKA is a tetramer made up with a regulatory subunit dimmer and two inactive catalytic subunits. When two cyclic Adenosine MonoPhosphate (cAMP) molecules bind with one regulatory dimer, the enzyme dissociates into a regulatory dimer and two active catalytic subunits. The balance between cAMP synthesis by Adenylate cyclase and degradation by phosphodiesterase (PDE), contributes to generate temporal activity profiles, whereas different A Kinase Anchoring-Proteins (AKAPs) restrains PKA to specific subcellular localizations (Taylor *et al.*, 2003) and target PKA to their substrates (Faux and Scott, 1996; Dell'Aqua et al., 2006). As an example, it appeared that a balance of PKA activity- either in extent, space, time, or all three- is necessary for cell movement. In this context, PKA regulates several key events like membrane protrusion or filopodia formation, by controlling the activation states of Rho-GTPases Rac and cdc42 (Howe, 2004). In this context, PKA activity is compartmentalized in protrusive cellular structures formed during chemotaxis. Reorganization of actin cytoskeleton and polarization during cell migration depends also on PKA activity cellular gradients. Those are, at least in part, dependent on the AKAP-Lbc anchoring function that might retain PKA close to its substrates during this migration process (Paulucci-Holthauzen *et al.*, 2009).

Since its identification as an oncogene in 1991 (Bellacosa et al., 1991; Jones et al., 1991), Akt has been targeted by many strategies to unravel its role and mechanisms of activation. Growth factors, cytokines and hormones stimulate the phosphatidylinositol 3-Kinase (PI3K), which generate a secondary messenger phosphatidylinositol (3,4,5)-triphosphate. The latter induces Akt translocation from the cytosol to the plasma membrane, where it is activated by phosphorylation on residue Thr308 and Ser473 (Fayard et al., 2005). Convergent literature had suggested a role of lipid rafts for Akt activation (cholesterol and sphingolipid-enriched detergent resistant compartments) however, proofs have been difficult to gather due to the absence of adequate tools. Genetically encoded fluorescent reporters for kinase activity exhibited amenability to the purpose of dissecting the role of lipid rafts in Akt activation and led to determine that PDGF- (Platelet Derived Growth Factor) or IGF-1- (Insulin Growth Factor-1) mediated Akt activation was differentially controlled between raft and non-raft regions at the plasma membrane (Gao and Zhang, 2008; Gao and Zhang, 2009).

1.5.2. Getting into more dynamism: FRET-Based Kinase Activity Reporters

How a cell integrates multiple signals into a fate remains rahter challenging since cell-specific responses are mainly achieved through common effectors of signaling networks. Answer to this question is commonly addressed through the targeting of downstream effectors substrates (such as cytoplasmic targets, transcription factors and terminal enzymes), which ultimately process cell-specific phenotypes. Specific cell response to stimuli may arise from two possible mechanisms. On one hand, a signaling event may drive different cell phenotypes, but the latter depends only on the cell type that is stimulated because the molecular contributors of signal integration are cell-specific. On another hand, the nature of the activating signal (i.e. being transitory, delayed or sustained) is responsible for the typical or adapted cell response to stimulus. In order to purpose to decipher dynamical properties of signaling networks, integrative approaches have been developed. Indeed, mathematical and computational models have emerged as useful and original tools to address cellular signaling. When working synergistically, experimental and theoretical approaches increase the understanding of information-

processing mechanisms, which mainly involve protein kinases and their regulators (Orton et al., 2009; Kholodenko and Birtwistle, 2009; Gilbert et al., 2010). Nevertheless, traditional methodologies failed to feed synergistically this work, which request quantitative measurements for implementing mechanistic models as well as for verifying generated predictions. Knowledge of how cell regulatory systems are organized to allow signal integration with robust fidelity remains crucial to predicting drug action, understanding pathological deregulation and identifying effective molecular targets for drug discovery.

Suitable tools and methodologies are also requested to enable the dissection of signaling mechanisms at the single cell level up to complex and malignant environment. Thus, acquisition of dynamical parameters is resting upon the development and promises of molecular imaging, through innovations enabling real-time and non-invasive, or at least the less invasive, monitoring of protein kinases as biomarkers in living cells and organisms. These innovations are called to change our view on how disease may be diagnosed, staged, monitored and treated, and how cell decide their fate or drive themselves into such or such phenotypic decision. So far, western blotting, immunostaining and immunohistochemistry for phosphorylated isoforms of kinase, when available, have provided valuable insights into kinases function but these methods only allow obtaining static snapshots of cellular events. For *in vitro* kinase assays, cellular integrity is disrupted (mechanical lysis), and the phosphorylation of an exogenous substrate is classically monitored over time by radioactivity or phosphorylation-specific antibodies. Though these assays can detect kinase activity, the biological context is mainly lost during cell fixation or lysis.

At clinical levels, information are also requested regarding the dynamic changes within malignancy and its environment since biopsies only provide snapshots of biomarkers at the time where the sample is retrieved. These snapshots do not allow adapting rational molecular therapies in real time for clinical oncology purposes, where therapies are called to be adapted at the case-by-case level (bench to bedside approach). Nevertheless, several strategies have been developed for protein kinases profiling such as phosphoproteomic approaches (Opermann et al., 2009; Li et al., 2010), reverse protein arrays (Pawlak et al., 2002; Rubic et al., 2008) and kinase peptide substrate arrays (Tuynman et al., 2008; Schrage et al., 2009; Sikkema et al., 2009; Versele et al., 2009) or peptide reporters (Wu et al., 2010).

Although these techniques cannot overcome the inconvenient of providing snapshots and are demanding in term technology platforms, they are considered as potential clinical diagnostic tool to predict tumor evolution and response to targeted therapies (Piersma et al., 2010). Such techniques will not be further discussed in this article since we aim at focusing on gain from imaging strategies for protein kinases studies.

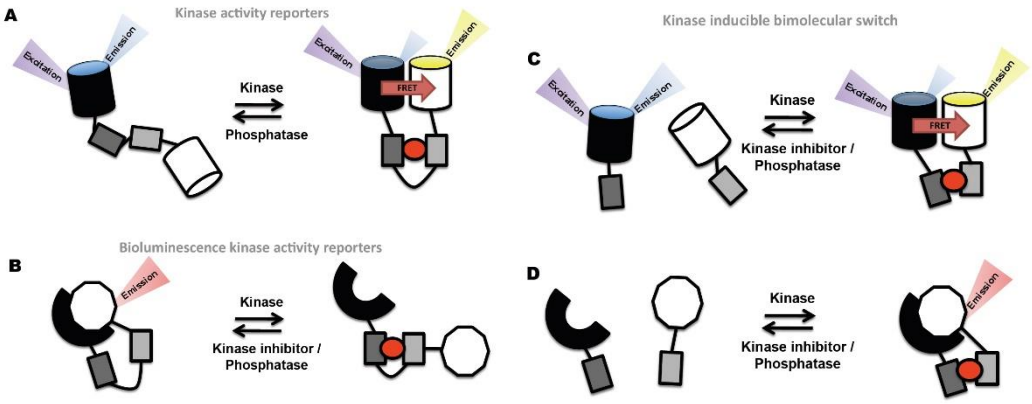

Figure 2. Designs and mechanisms of molecular tools for reporting kinase activity; (**A**) Kinase activity Reporters: a conformational of the molecular switch is induced by phosphorylation (red circle), which results in a subsequent intramolecular binding between the phosphorylated substrates (light grey box) and the phosphoamino acid-binding domain (PAABD, dark grey box). When this switch occurs, it enables a change in FRET for the pair of FRET donor (black cylinder) and acceptor (white cylinder). (**B**) Bioluminescence kinase activity reporters: N-Luc (amino acids 2-416; black cylinder) and C-Luc (amino acids 398-550; white cylinder) are terminals domains of luciferase that are incorporated between phospho-Serine/Threonine binding domain (FAH2 domain; dark grey box), a substrate peptide (light grey box) and flexible linkers; when phosphorylated, the conformation of the construct maintains the two luciferase domains apart, that has minimal bioluminescence while the dephosphorylation of the peptide substrate leads to the association of N-Luc and C-Luc and restoration of bioluminescence. (**C, D**) Kinase inducible bimolecular switch (KIBS): they are made of kinase specific substrate (light grey box), phosphoamino acid-binding domain (PAABD, dark grey box), which will bind to the phosphorylated substrate, in an intermolecular manner contrasting with the intramolecular principle of KAR. Two reporting unit are fused with each domain (reporting unit A, black symbol, reporting unit B, white symbol). These couple might be composed of FRET pairs (C) or Bioluminescent reporting units (D).

Development of imaging approaches overcome the shortcomings of traditional methods, when providing high temporal and spatial resolution for single living cell analysis (Verveer and Bastiaens, 2008) and tissues. To this extent, kinase activity biosensors have been developed. Biological processes are intrinsically dynamics. Although traditional methods provide valuable insights for the understanding of many biological phenomenon, the possibility nowadays to measure, quantify and localize protein activity within a cell, a tissue, an embryo has revolutionized our train of thoughts and has encourage scientists to develop molecular tools for the assessment of protein activity within their physiological context. These ongoing efforts are resting

on the emergence of biophotonics and the everlasting improvement of fluorophores, allowing precise and reliable measurements of cellular functions dynamics. The march of the “in vivo biochemistry” has begun, already yielding breathtaking results, using mostly PKA kinase activity reporter: AKAR (see for review Zhang et al., 2007).

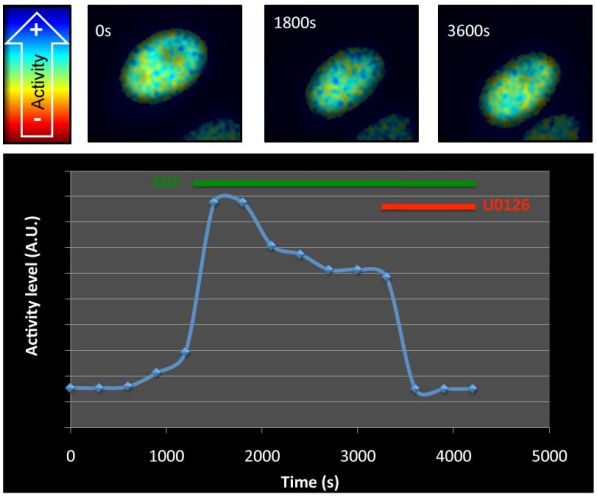

Figure 3. MAPK changes in activity, upon stimulation by Epidermal Growth Factor. HeLA cells were transfected using Nuclear EKAR Cerulean-Venus (genetically encoded fluorescent sensor of ERK activity, Addgene plamid # 18681, Harvey et al., 2008). Cells were deprived in serum, stimulated by EGF (100ng/mL) and treated by MEK inhibitor U0126 (20μM). Phase and modulation lifetime acquisitions were performed in living cells (upper panel) to achieve localized measurements of MAPK activity along time. The mean fluorescence lifetime was measured on the whole cell and normalized to achieve a quantitative view of MAPK/Erk activity as depicted in the graph. For detailed description of the phase and modulation setup and acquisition protocol, see Leray et al., 2009.

As one major class of kinase biosensors, kinase activity reporters (KAR) serve as surrogate substrates for kinases and allow reporting of phosphorylation dynamics by FRET changes. FRET is a quantum mechanical process involving the radiationless transfer of energy from a donor fluorophore to an appropriately positioned acceptor fluorophore. Then, when two fluorescent reporters are close enough due to a conformational change of the KAR, the excitation of the donor induces an energy transfer from the donor to the acceptor resulting in the quenching of the donor and a rise of acceptor fluorescence (Camuzeaux et al., 2005). Such reporters have been developed for various kinases. These reporters utilize, as a molecular switch, a substrate domain highly specific for the kinase of interest, attached to a phosphoamino acid binding domain (PAABD) tailored for maximum recognition of the phosphorylated substrate domain. Upon phosphorylation of the substrate, the PAABD binds the phosphopeptide, altering either the distance and/or the orientation between donor and acceptor fluorophores, resulting in a detectable change in FRET (Figure 2A).

While KAR represent a very attractive option for assessment of kinase activity dynamics in living cells, set-up and optimization of experimental conditions, acquisition technique and data analysis can be time-consuming and at time rather discouraging. After optimizing these conditions, real time kinase activity measurement can be performed every 30sec in living cells. Moreover, depending on the imaging technique utilized for FRET measurements, sub-cellular and even localized kinase activity foyers can be readily identified as well.

An example of what can be performed nowadays using KAR is illustrated in Figure 3. Genetically encoded FRET biosensor of reporting ERK kinase activity (EKAR) has been expressed in living cells. Kinase activity dynamic is readily visible in cell upon stimulation and subsequent inhibition of the MAPK/ERK pathway.

1.5.3. Bioluminescence-based reporters for protein kinase activity

As an alternate to genetically encoded reporters using fluorescence, luciferases derivatives were considered for reporting kinase activity. Similarly to previously mentioned kinase activity reporters (KAR), these tools are called to enable non-invasive, real-time, repetitive imaging for studies of biological processes in intact cells or tissues in whole organisms. Firefly luciferase has appeared an attractive reporter because 30% of the light generated has an emission spectra above 600 nm, at a region where the signal attenuation by the absorbing and scattering properties of living tissues in mammalian, is minimal (Contag and Ross, 2002; Greer and Szalay, 2002). Indeed, the use of GFP or alternate fluorescent reporter systems in animal model is impaired by the high levels of background resulting from the excitation of subject tissue. However, the use of bioluminescence might overcome this disadvantage due to the low level of background autoluminescence in mammalian tissues (Welsh and Kay, 2005).

Nevertheless, one problem remains when using bioluminescence resting on luciferase derivatives, the substrate, luciferin, needs to be provided to the experimental system. As for FRET-based kinase activity measurements, more on more red-shifted fluorophores are being characterized which should enable optimized in-depth imaging in living tissue.

As for KAR, bioluminescence-based reporters are initially monomeric construct, which consists of two separate components, whose close proximity re-constitutes a reporter activity (Figure 2B): each component is inactive when taken individually but when they are brought together by conformational rearrangement, the luciferase enzymatic activity is restored due to the intramolecular complementation. Re-constitution of luciferase was based upon protein complementation assays that were previously used to monitor either protein-protein interaction, or kinase / protease activities (Fields and Song, 1989); the latter was validated upon complementation assays screening truncation libraries of N- and C-terminal fragments of luciferase. The complementation assays was noticeably used to demonstrate the phosphorylation-dependent interaction between hCdc25C and 14-3-3e *in vitro* and the FRB-FKBP12 interaction in real time non-invasively (Luker and Piwnica-Worms, 2004; Piwnica-Worms and Luker, 2005). As previously stated, while these bioluminescence-based reporters, do not need exogenous illumination, they could allow decreased background signals, thus increasing kinase activity reporting sensitivity.

A bioluminescent Akt Reporter (BAR) was built using an Akt consensus substrate peptide and phospho-amino acid binding domain (FHA2), flanked with N- and C-Terminal luciferase domains.When in presence of Akt, phosphorylation of the consensus site on the peptide leads to its interaction with the FHA2 domain. This interaction prevents the restoration of a functional luciferase activity through stearic contraints. Once Akt activity is inhibited, this constraint is released and thus restores vicinity between the N- and C-terminal domains of luciferase, thereby enabling detection of bioluminescence. Thus, Akt inhibition can be easily monitored and quantitative and dynamical characteristics of Akt inhibitors like API2 may be assessed *in vivo* and compared to other inhibitors such as perfosine, an inhibitor of PI-3Kinase, which acts upstream Akt (Nyati et al., 2010). Differential activation of Akt has been reported through the use of BAR, following EGFR (Epidermal Growth Factor Receptor) stimulation in presence of EGFR inhibitor, erlotinib. BAR was able to detect erlotinib-mediated inhibition of EGFR and Akt, in the erlotinib-sensitive HCC287 cell lines while NCI-H1975 cell lines. Contrarily, erlotinib-resistant lung cancer cell lines, did not exhibit changes in Akt activity levels, therefore validating the utility/specificity of this reporter (Zhang et al., 2007). Furthermore, API2 and perfosine

in vivo interactions with substrates were assessed and results were reflective of differences of bioavailability of the drugs at the tumor site, since perfosine induced 12-fold induction of bioluminescence in contrast to API2, which only induced a 4-fold induction (Nyati et al., 2010).

One of the main advantages of these constructions based on bioluminescent is to result in less false positives than other cell-based reporters screen. Kinase reporters in case of bioluminescence are built to result in a gain of function assay, with the inhibition of kinase activity being monitored by an increase in bioluminescence. In standard enzyme-based assays, toxic compounds lead to loss of signal resulting in cell death and show up as false positives. With reporters such as BAR, signals from toxic agents are eliminated and not considered since having no effect on bioluminescence levels. The increase in bioluminescence will only arise from Akt inhibition. Then, bioluminescent kinase reporters may arise as attractive tools for screening validation in case of kinases inhibitors libraries high throughput analysis. In this effort, platforms have been developed (Nyati et al., 2010) and bioluminescent kinase reporters have been developped for Glycogen Synthase Kinase 3-beta (Gsk-3β), Casein Kinase 1-alpha, FADD or Met-tyrosine kinase activities (Khan et al., 2010; Nyati et al., 2010; Zhang et al., 2011).

Kinase activity reporters using fluorescence suffer from limited dynamic range (Kerppola, 2006 ; Hodgson et al., 2010), which is a critical parameter for detection of subtle changes in kinase activity (VanEngelenburg and Palmer, 2008; Ni et al., 2011), since these subtle changes might have non-neglecteable cellular outcomes. In order to overcome these inconvenient, kinase inducible molecular switch (KIBS) were built based on bioluminescence advantages. KIBS consists of a kinase specific substrate and a phosphoamino acid binding domain designed to bind the phosphorylated form of the peptide substrate, but in constrast to KAR these two domains are held by two separate reporting unit (Figure 2C). Thus, recognition of the phosphorylated form of the substrate peptide by the phosphoamino acid domain brings two reporter units in vicinity which enable either a FRET (C) or a bioluminescent (D) signal. Several bimolecular sensors were recently built. In a first step, FRET-based bimolecular sensor were designed to report for PKA and Protein Kinase C, named respectively BimAKAR and C-KIBS and appeared to conserve the advantages of unimolecular KAR regarding subcellular localization while improving

their dynamical range in HEK293T cells (Herbst et al., 2011). Secondly, biomolecular sensors were turn on bioluminescence for readout: a bioluminescent-based reporter for PKA, LumAKAR, was tested and exhibited reversibility, accurate temporal resolution and subcellular localization, enabling for example to detect basal PKA/AMPc states (Herbst et al., 2011).

1.5.4. Concluding remarks

The molecular toolkits for kinases activity reporter are then called to be strengthened by new sensors, whose development will result in the improvement of sensitivity and kinetic properties, the enlargement of dynamic range, the conservation of reversibility and an increased resolution for subcellular localization in living cells. Building other bioluminescent reporters will take also advantages from numerous published resources and methodologies for identification of peptide as specific substrates. From a clinical point of view, the disadvantages for bioluminescence, as for any genetically encoded reporters, is that their use is restricted to the acceptance of a gene therapy protocols in patients. It remain also challenging to determine which protein kinases are “essential” and should be targeted; mostly, the Achilles’heel(s) of specific oncogenic events remain likely to be determined. Nevertheless, kinase activity reporters offer major advantages (1) for fondamental research in the understanding of how protein kinases integrate and achieve cellular functions in physiological and pathological situations, such as in aberrant oncogenic signaling, (2) for drug-target validation, (3) for identification of next drugs generation and (4) for monitoring therapeutic outcomes.

Acknowledgements

FS is supported by the CNRS and the University of Lille 1. PV is supported by the Region Nord-Pas de Calais and the University of Lille 1.

References

Bellacosa A, Testa JR, Staal SP, Tsichlis PN. A retroviral oncogene, akt, encoding a serine-threonine kinase containing an SH2-like region. Science. 1991 Oct 11;254(5029):274-7.

Blume-Jensen P, Hunter T. Oncogenic kinase signalling. Nature. 2001 May 17;411(6835):355-65.

Blossey R, Bodart JF, Devys A, Goudon T, Lafitte P. Signal propagation of the MAPK cascade in Xenopus oocytes: role of bistability and ultrasensitivity for a mixed problem. J Math Biol. 2011 Feb 3.

Bodart JF, Chopra A, Liang X, Duesbery N. Anthrax, MEK and cancer. Cell Cycle. 2002 Jan;1(1):10-5.

Bodart JF. Extracellular-regulated kinase-mitogen-activated protein kinase cascade: unsolved issues. J Cell Biochem. 2010 Apr 1;109(5):850-7

Boutros T, Chevet E and Metrakos P. Mitogen-Activated Protein (MAP) kinase/MAP kinase phosphatase regulation : roles in cell growth, death, and cancer. Pharmacol Rev 2008; 60:261-310.

Cagnol S, Van Obberghen-Schilling E & Chambard J. Prolonged activation of ERK1/2 induces FADD-independent caspase 8 activation and cell death. Apoptosis 2006; 11:337-346.

Camuzeaux B, Spriet C, Héliot L, Coll J, Duterque-Coquillaud M. Imaging Erg and Jun transcription factor interaction in living cells using fluorescence resonance energy transfer analyses. Biochem Biophys Res Commun. 2005 Jul 15;332(4):1107-14.

Chen CH, Wang WJ, Kuo JC, Tsai HC, Lin JR, Chang ZF, Chen RH. Bidirectional signals transduced by DAPK-ERK interaction promote the apoptotic effect of DAPK. Embo Journal 2005; 24:294-304.

Cohen, P. (2002). "Protein kinases--the major drug targets of the twenty-first century?" Nat Rev Drug Discov 1(4): 309-15.

Contag CH, Ross BD. It's not just about anatomy: in vivo bioluminescence imaging as an eyepiece into biology. J Magn Reson Imaging. 2002 Oct;16(4):378-87.

Csikasz-Nagy A, Kapuy O, Toth A, Pál C, Jensen LJ, Uhlmann F, Tyson JJ, Novák B (2009) Cell cycle regulation by feedforward loops coupling transcription and phosphorylation. Mol Syst Biol. 5:236.

Dell'Acqua ML, Smith KE, Gorski JA, Horne EA, Gibson ES, Gomez LL. Regulation of neuronal PKA signaling through AKAP targeting dynamics. Eur J Cell Biol. 2006 Jul;85(7):627-33.

Dong J, Ramachandiran S, Jia Z, Lau SS, Monks TJ. EGFR-independent activation of p38 MAPK and EGFR-dependant activation of ERK1/2 are required for ROS-induced renal cell death. Am J Physiol Renal Physiol 2004; 287:F1049-F1058.

Ebisuya M, Kondoh K, Nishida E. The duration, magnitude and compartmentalization of ERK MAP kinase activity : mechanisms for providing signaling specificity. Journal of Cell Science 2005 ; 118:2997-3002.

Faux MC, Scott JD. More on target with protein phosphorylation: conferring specificity by location. Trends Biochem Sci. 1996 Aug;21(8):312-5.

Fayard E, Tintignac LA, Baudry A, Hemmings BA. Protein kinase B/Akt at a glance. J Cell Sci. 2005 Dec 15;118(Pt 24):5675-8.

Fields S, Song O. A novel genetic system to detect protein-protein interactions. Nature. 1989 Jul 20;340(6230):245-6.

Gao X, Zhang J. Spatiotemporal analysis of differential Akt regulation in plasma membrane microdomains. Mol Biol Cell. 2008 Oct;19(10):4366-73.

Gao X, Zhang J. Akt signaling dynamics in plasma membrane microdomains visualized by FRET-based reporters. Commun Integr Biol. 2009;2(1):32-4.

Gilbert D, Heiner M, Breitling R, Orton R. Computational modelling of kinase signalling cascades. Methods Mol Biol. 2010;661:369-84.

Greer LF 3rd, Szalay AA. Imaging of light emission from the expression of luciferases in living cells and organisms: a review. Luminescence. 2002 Jan-Feb;17(1):43-74.

Harvey CD, Ehrhardt AG, Cellurale C, Zhong H, Yasuda R, Davis RJ, Svoboda K. A genetically encoded fluorescent sensor of ERK activity. Proc Natl Acad Sci U S A. 2008 Dec 9;105(49):19264-9.

Herbst KJ, Allen MD, Zhang J. Luminescent kinase activity biosensors based on a versatile bimolecular switch. J Am Chem Soc. 2011 Apr 20;133(15):5676-9.

Hodgson L, Shen F, Hahn K. Biosensors for characterizing the dynamics of rho family GTPases in living cells. Curr Protoc Cell Biol. 2010 Mar;Chapter 14:Unit 14.11.1-26.

Howe AK. (2004) Regulation of actin-based cell migration by cAMP/PKA. Biochim Biophys Acta. 1692 : 159-74

Howe AK, Baldor LC, Hogan BP.(2005) Spatial regulation of the cAMP-dependent protein kinase during chemotactic cell migration. Proc Natl Acad Sci U S A. 102 :14320-5

Johnson SA, Hunter T. Kinomics: methods for deciphering the kinome. Nat Methods. 2005 Jan;2(1):17-25.

Jones PF, Jakubowicz T, Pitossi FJ, Maurer F, Hemmings BA. Molecular cloning and identification of a serine/threonine protein kinase of the second-messenger subfamily. Proc Natl Acad Sci U S A. 1991 May 15;88(10):4171-5.

Kerppola TK. Complementary methods for studies of protein interactions in living cells. Nat Methods. 2006 Dec;3(12):969-71.

Khan AP, Schinske KA, Nyati S, Bhojani MS, Ross BD, Rehemtulla A. High-throughput molecular imaging for the identification of FADD kinase inhibitors. J Biomol Screen. 2010

Kholodenko BN, Birtwistle MR. Four-dimensional dynamics of MAPK information processing systems. Wiley Interdiscip Rev Syst Biol Med. 2009 Jul Aug;1(1):28-44.

Kriegsheim A, Preisinger C, Kolch W. Mapping of signaling pathways by functional interaction proteomics. Methods Mol Biol. 2008;484:177-92.

Kumar R, Singh VP, Baker KM. Kinase inhibitors for cardiovascular disease. J Mol Cell Cardiol. 2007 Jan;42(1):1-11.

Leray A, Riquet FB, Richard E, Spriet C, Trinel D, Héliot L. Optimized protocol of a frequency domain fluorescence lifetime imaging microscope for FRET measurements. Microsc Res Tech. 2009 May;72(5):371-9.

Li J, Rix U, Fang B, Bai Y, Edwards A, Colinge J, Bennett KL, Gao J, Song L, Eschrich S, Superti-Furga G, Koomen J, Haura EB. A chemical and phosphoproteomic characterization of dasatinib action in lung cancer. Nat Chem Biol. 2010 Apr;6(4):291-9.

Luker KE, Piwnica-Worms D. Optimizing luciferase protein fragment complementation for bioluminescent imaging of protein-protein interactions in live cells and animals. Methods Enzymol. 2004;385:349-60.

Maeder CI, Hink MA, Kinkhabwala A, Mayr R, Bastiaens PI, Knop M. Spatial regulation of Fus3 MAP kinase activity through a reaction-diffusion mechanism in yeast pheromone signalling. Nat Cell Biol. 2007 Nov;9(11):1319-26.

Manning G, Whyte DB, Martinez R, Hunter T, Sudarsanam S. The protein kinase complement of the human genome. Science. 2002 Dec 6;298(5600):1912-34.

Mebratu Y. and Tesfaigzi Y. How ERK1/2 activation controls cell proliferation and cell death. Is Subcellular localization the answer ?. Cell Cycle 2009; 8(8):1168-1175.

Morgan D (2007) The Cell Cycle. Principles of Control. OUP/New Science Press Primers in Biology.

Mueller BK, Mack H, Teusch N. Rho kinase, a promising drug target for neurological disorders. Nat Rev Drug Discov. 2005

Ni Q, Ganesan A, Aye-Han NN, Gao X, Allen MD, Levchenko A, Zhang J. Signaling diversity of PKA achieved via a Ca2+-cAMP-PKA oscillatory circuit. Nat Chem Biol. 2011 Jan;7(1):34-40.

Novak B, Tyson JJ, Gyorffy B, Csikasz-Nagy A (2007) Irreversible cell-cycle transitions are due to systemslevel feedback. Nat Cell Biol. 9:7248.

Nurse P (2000) A long twentieth century of the cell cycle and beyond. Cell 100: 71-78.

Nyati S, Ross BD, Rehemtulla A, Bhojani MS. Novel molecular imaging platform for monitoring oncological kinases. Cancer Cell Int. 2010 Jul 8;10:23.

Nyati S, Ranga R, Ross BD, Rehemtulla A, Bhojani MS. Molecular imaging of glycogen synthase kinase-3beta and casein kinase-1alpha kinases. Anal Biochem. 2010 Oct 15;405(2):246-54.

Oppermann FS, Gnad F, Olsen JV, Hornberger R, Greff Z, Kéri G, Mann M, Daub H. Large-scale proteomics analysis of the human kinome. Mol Cell Proteomics. 2009 Jul;8(7):1751-64.

Orton RJ, Adriaens ME, Gormand A, Sturm OE, Kolch W, Gilbert DR. Computational modelling of cancerous mutations in the EGFR/ERK signalling pathway. BMC Syst Biol. 2009 Oct 5;3:100.

Paulucci-Holthauzen AA, Vergara LA, Bellot LJ, Canton D, Scott JD, O'Connor KL. (2009) Spatial distribution of protein kinase A activity during cell migration is mediated by A-kinase anchoring protein AKAP Lbc. J Biol Chem. 284 : 5956-67

Piersma SR, Labots M, Verheul HM, Jiménez CR. Strategies for kinome profiling in cancer and potential clinical applications: chemical proteomics and array-based methods. Anal Bioanal Chem. 2010 Aug;397(8):3163-71.

Piwnica-Worms D, Luker KE. Imaging protein-protein interactions in whole cells and living animals. Ernst Schering Res Found Workshop. 2005;(49):35-41.

Santos SD, Verveer PJ, Bastiaens PI. Growth factor-induced MAPK network topology shapes Erk response determining PC-12 cell fate. Nat Cell Biol. 2007 Mar;9(3):324-30.

Scapin, G. (2006). "Protein kinase inhibition: different approaches to selective inhibitor design." Curr Drug Targets 7(11): 1443-54.

Schrage YM, Briaire-de Bruijn IH, de Miranda NF, van Oosterwijk J, Taminiau AH, van Wezel T, Hogendoorn PC, Bovée JV. Kinome profiling of chondrosarcoma reveals SRC-pathway activity and dasatinib as option for treatment. Cancer Res. 2009 Aug 1;69(15):6216-22.

Sikkema AH, Diks SH, den Dunnen WF, ter Elst A, Scherpen FJ, Hoving EW, Ruijtenbeek R, Boender PJ, de Wijn R, Kamps WA, Peppelenbosch MP, de Bont ES. Kinome profiling in pediatric brain tumors as a new approach for target discovery. Cancer Res. 2009 Jul 15;69(14):5987-95.

Taylor SS, Yang J, Wu J, Haste NM, Radzio-Andzelm E, Anand G. (2004) PKA: a portrait of protein kinase dynamics. Biochim Biophys Acta.1697 : 259-69

Trencia A, Perfetti A, Cassese A, Vigliotta G, Miele C, Oriente F, Santopietro S, Giacco F, Condorelli G, Formisano P, Beguinot F. Protein kinase B/Akt binds and phosphorylates PED/PEA-15, stabilizing its antiapoptotic action. Mol Cell Biol 2003; 23:4511-4521.

Tuynman JB, Vermeulen L, Boon EM, Kemper K, Zwinderman AH, Peppelenbosch MP, Richel DJ. Cyclooxygenase-2 inhibition inhibits c-Met kinase activity and Wnt activity in colon cancer. Cancer Res. 2008 Feb 15;68(4):1213-20.

Tyson JJ, Novak B (2008) Temporal organization of the cell cycle. Curr Biol. 18:R759-R768.

VanEngelenburg SB, Palmer AE. Fluorescent biosensors of protein function. Curr Opin Chem Biol. 2008 Feb;12(1):60-5.

Verveer, P.J. and Bastiaens, P.I. (2008) Quantitative microscopy and systems biology: seeing the whole picture. *Histochem Cell Biol*, 130, 833-843.

Versele M, Talloen W, Rockx C, Geerts T, Janssen B, Lavrijssen T, King P, Göhlmann HW, Page M, Perera T. Response prediction to a multitargeted kinase inhibitor in cancer cell lines and xenograft tumors using high-content tyrosine peptide arrays with a kinetic readout. Mol Cancer Ther. 2009 Jul;8(7):1846-55.

Welsh DK, Kay SA. Bioluminescence imaging in living organisms. Curr Opin Biotechnol. 2005 Feb;16(1):73-8.

Westra J, Limburg PC. p38 mitogen-activated protein kinase (MAPK) in rheumatoid arthritis. Mini Rev Med Chem. 2006 Aug;6(8):867-74.

Wirth A. Rho kinase and hypertension. Biochim Biophys Acta. 2010 Dec;1802(12):1276-84

Wu D, Sylvester JE, Parker LL, Zhou G, Kron SJ. Peptide reporters of kinase activity in whole cell lysates. Biopolymers. 2010;94(4):475-86.

Zhang L, Lee KC, Bhojani MS, Khan AP, Shilman A, Holland EC, Ross BD, Rehemtulla A. Molecular imaging of Akt kinase activity. Nat Med. 2007 Sep;13(9):1114-9.

Zhang L, Virani S, Zhang Y, Bhojani MS, Burgess TL, Coxon A, Galban CJ, Ross BD, Rehemtulla A. Molecular imaging of c-Met tyrosine kinase activity. Anal Biochem. 2011 May 1;412(1):1-8.

Part 2: Aims and objectives

2.1. Scientific Objectives

TNFR1 signaling occurs through a complex multi-step pathway based on cell death checkpoints directing the cell to a specific cellular response [422]. The first checkpoint is organized by the kinase RIPK1 that is positioned at the crossroads of cell death and survival [423]. The second checkpoint decides on cell death type depending on the pro-death complex that binds RIPK1. Localized in complex I of the TNFR1 signaling upon TNFα stimulation, RIPK1 contributes to the stimulation of MAPKs, including JNK, p38 and ERK1/2 [424]. However, although several studies have examined MAPKs activation in response to TNFα, the function and molecular mechanisms of RIPK1 in TNFα-induced MAPKs activation is still unclear [424–427]. TRAF2 is an adaptor recruited at the membrane with RIPK1 upon TNFα stimulation, and was implicated in JNK and IκB kinase (IKK) activation [428,429]. Moreover, TRAF2 overexpression was reported to activate p38 and ERK1/2 signaling pathways [424]. Devin and colleagues investigated the molecular mechanism between RIPK1 and MAPKs by using both RIPK1$^{-/-}$ and TRAF2$^{-/-}$ MEF [430]. They provided strong evidences of the implication of both RIPK1 and TRAF2 in TNFα-induced JNK, p38 and ERK1/2 activation as a drop of 70% in ERK1/2 activity was observed in RIPK1$^{-/-}$ cells. Interestingly, by using a kinase-dead form of RIPK1, RIPK1 (K45A), in RIPK1$^{-/-}$ cells, they revealed that the kinase activity of RIPK1 is only required for ERK1/2 but not for p38 and JNK activation [430,431]. However, the identity of downstream substrates of TRAF2/RIPK1 remains to be investigated since MEKK1 and MEKK3 as well as A-Raf and B-Raf seems to be dispensable in TNFα-induced JNK, p38 and ERK1/2 activation [430]. But redundancy mechanism among MAP3 kinases could explained that depletion of specific MAP3K do not alter ERK1/2 phosphorylation in response to TNFα. Therefore, the precise events leading to ERK1/2 cascade activation are still not fully understood. Given that ERK1/2 activation requires RIPK1 kinase activity upon TNFα stimulation and that RIPK1 is essential in TNFα-induced necroptosis [432], **the role of ERK1/2 in necroptosis remains to be elucidated**.

Few studies only suggest that ERK1/2 is involved in TNFα-induced necroptosis depending on the cell type and cell death stimulus. Zhang and colleagues revealed that ERK1/2 might play a prominent role in glutamate-induced necroptosis in HT-22 cells [409]. Glutamate-induced necroptosis in HT-22 cells is

associated with elevated ERK1/2 activation levels [433,434] and ERK1/2 inhibition prevents this cell death. It was reported that RIPK1 inhibition abrogates glutamate-induced necroptosis in HT-22 cells by inhibiting ERK1/2 phosphorylation [409]. While Nec-1 inhibits ERK1/2 phosphorylation, no particular effects on p38 or JNK have been detected further demonstrating the role of ERK1/2 in glutamate-induced necroptosis in HT-22 cells. Conversely, another study reported that shikonin-induced apoptosis in HL60 and K562 leukemia cells is enhanced by RIPK1 inhibition through the inhibition of ERK1/2 activation, suggesting therefore a **pro-survival role of ERK1/2** in this context [435]. However, in the context of ischemia-reperfusion (IR) injury in rat retinas, Gao and colleagues uncovered a link between ERK1/2 activation and RIPK1/3 pathway [410]. They found elevated ERK1/2 phosphorylation levels and accumulation of RIPK3 bot not RIPK1 proteins in retinal ganglion cells (RGC) 12h after IR injury of rat retinas associated with increased levels of FLIP expression. Intravitreal injection of U0126 abrogated ERK1/2 activation and down-regulated RIPK3 expression and subsequent necroptosis [436,437], suggesting a crucial role of ERK1/2 in the execution of necroptosis [410]. Given that RIPK1 and RIPK3 phosphorylations drive necrotic complex formation, and this is generally occuring upstream of ERK1/2, their data actually support a different view: phosphorylation of ERK1/2 upstream of RIPK3. These findings that are not in agreement with the conventional TNFR1-mediated necroptosis pathway, **are increasing our curiosity towards ERK1/2 involvement in the initiation of necroptosis**.

The molecular mechanisms underlying RIPK1-mediated ERK1/2 cascade activation are poorly understood. Recently, a study showed that a novel atypical RIPK1-dependent apoptotic cell death induced by eleostearic acid (ESA) is mediated through ERK1/2 pathway [438]. It was shown that ESA-induced apoptosis was neither caspase-3 dependent nor PARP1 dependent. This study also revealed that **RIPK1 could interact constitutively with ERK1/2** and transiently with MEK2. It was further demonstrated that ESA-mediated apoptosis was associated with RIPK1 dephosphorylation and subsequent MEK2-mediated ERK1/2 phosphorylation and decrease in AIF phosphorylation. Both AIF and ERK1/2 were shown to **translocate to the nucleus** accompanied by ROS production and mitochondria dysfunctions ultimately leading to cell death. However, in the context of RIPK1-dependent necroptosis upon TNFα stimulation, phosphorylations between RIPK1 and RIPK3

contribute to stabilize RIPK1/RIPK3 complex so-called ripoptosome leading to a **progressive ROS production** and subsequently cell death [439,440]. Regarding the well-known inhibition of ERK1/2 phosphatases due to elevated intracellular ROS production levels [372,401], ERK1/2 activation occurring during cell death might be more a consequence rather than a cause of ROS production. In addition, in accordance with previous studies, a RIPK1 kinase-dependent ERK1/2 phosphorylation upon TNFα stimulation was reported in L929 cells [439]. Under cIAP1 inhibition (using BV6), ERK1/2 phosphorylation levels were increased as well as RIPK1 kinase activity, accompanied by augmented ROS production [439], hence emphasizing a protecting role of cIAP1 from TNFα-induced necroptosis but also reflecting the **involvement of cIAP1** in the regulation of RIPK1-dependent ERK1/2 phosphorylation.

In the context of **TNFα-induced MAPK activation**, it was reported that TNFα induces a **biphasic activation of JNK**, which started with a transient activation followed by a sustained activation of JNK for several hours, [441]. Upon TNFα stimulation in L929 cells, transient JNK and p38 activations were detected and followed by a prolonged activation of p38 only. Sustained activation of JNK was further observed following the inhibition of JNK phosphatases by TNFα-induced ROS accumulation [401,442]. Transient MAPKs activation could promote a cell survival and abrogate cell cytotoxicity, whereas sustained MAPKs activation may trigger a cell death response [443,444], stressing once more the importance of monitoring kinase activity dynamics in living cells. More recently, a study described oscillatory activation of JNK and ERK1/2 in living cells upon TNFα or IL-1β stimulation of 3T3 cells using specific translocation reporters for each kinase [445]. In addition, it was reported that other pathways such as p38/SAPK could also modulate the frequency but not amplitude of ERK1/2 oscillations under certain conditions. Regarding the oscillations of ERK1/2 activities, it is crucial to emphasize the importance of **single-cell measurements**, because stochastic and growth factors-induced oscillatory kinase activation as well as heterogeneity in cellular responses will be obscured in **averaged cell population**.

Owing to the importance of MAPKs spatio-temporal dynamics in determining cellular responses and evidences of ERK1/2 involvement in TNFα-induced necroptosis, we investigated the **ERK1/2 temporal code** in necroptosis using

fluorescence-based reporters of both ERK1/2 activity and localization in single living cells. Using this appraoch, combine with chemical inhibition strategy targeting specific effectors of necroptosis, we aim to clearly define the relationship between ERK1/2 and RIPK signaling pathways.

In summary, the scientific objectives of this thesis were:

- *Investigate **involvement of ERK1/2** in TNFα-induced necroptosis in L929 cells and MEF cells,*
- *Monitor **spatio-temporal dynamics of ERK1/2** during necroptosis using genetically encoded constructs,*
- *Determine **molecular effectors** responsible of the TNFα-induced ERK1/2 phosphorylation (eg ROS production, protein-protein interactions) and **crosstalks** between ERK1/2 and RIPK signaling pathways,*
- *Correlate the spatio-temporal dynamics of ERK1/2 with **read-outs** of necroptosis occurrence.*

2.2. Biotechnological Objectives

Various studies used ERK2 tagged with GFP-like fluorescent proteins to monitor the spatiotemporal localization of ERK2 in individual living cells [446–450]. We assessed therefore the subcellular distribution of overexpressed eGFP-ERK2 in L929 and MEF cells in serum-starved and non-stimulated conditions. Surprisingly, cells overexpressing eGFP-ERK2 exhibited a strong nuclear localization independently of ERK2 phosphorylation status. Indeed, eGFP-rERK2 accumulated in the nucleus of brightly fluorescent cells but was homogenously distributed between cytoplasm and nucleus in weakly fluorescent cells. To provide an accurate and faithful read-out of the subcellular distribution of ERK2 regardless of its expression level, and to monitor the spatiotemporal signature of ERK2 in living cells by fluorescence imaging, **we need a genetically encoded reporter of ERK2 localization**. It became obvious that proper quantification of ERK2 dynamics in response to specific stimuli requires a robust system for reliable expression at the single cell level.

Besides the assessment of ERK1/2 spatio-temporal localization, we investigated subcellular ERK1/2 activity following a necrotic signal. We first used a genetically encoded FRET biosensor for ERK1/2 (Erk Kinase Activity Reporter with Eevee linker, EKAR-EV) [451]. However, this reporter failed to reveal any changes in ERK1/2 activity upon TNFα-induced necroptosis in L929 cells, which was inconsistent with previous biochemical data. Questionning whether the non-detection of ERK1/2 variations was: (i) a biological paradigm (phosphorylation is not necessarily correlated with activation, [452,453]), (ii) problems inherent to the experimental design or, (iii) limitated dynamic range of the molecular tools used, **we decided to tackle this issue by developing a method to build and/or optimize genetically encoded FRET biosensor**.

Finally, to evaluate the involvement of specific kinases in necroptosis, there is a need for read-out systems that will allow us to monitor this cell death process. Due to the **lack of molecular read-outs / hallmarks to correlate the spatio-temporal ERK1/2 code with necroptosis occurrence** [38] , we set out to develop new FRET-based kinase biosensors to monitor at subcellular level the kinase activity of RIPK1 and/or RIPK3 that are crucial in the initiation step of necroptosis [454]. FRET

biosensors are powerful tools for monitoring spatio-temporal biochemical activities in living samples. A very exciting challenge would be to **monitor several kinase activities in the same time on the same sample** [455] to correlate several kinase activities and so study crosstalks between each signaling node.

In summary, the biotechnological objectives of this thesis were:

- *Resolve the problem of GFP-ERK2 overexpression hampering dynamical studies of ERK2 subcellular distribution during necroptosis,*
- *Optimize the previous FRET biosensor of ERK (EKAR-EV) to decipher the spatio-temporal signature of ERK1/2 activity upon TNFα-induced necroptosis,*
- *Develop new FRET biosensors for RIPK1 and RIPK3 activity as a read-out of necroptosis initiation,*
- *Development of a methodology to monitor two kinases activities at the same time towards dissecting crosstalks between ERK1/2 and RIPK pathways.*

Part 3: Experimental strategies

3.1. 2A-mediated eGFP-ERK2 and MEK1 coexpression system to monitor ERK2 in living cell

In order to study the multi facet of ERK2 spatio-temporal features with respect to different cellular context and processes, we set out to tackle the issue concerning ERK2 faithful localization dynamics in living cells and tissues. Our strategy was to co-express ERK2 and MEK1 with a strict equimolar stoichiometry to avoid cell-to-cell variability in ERK2 subcellular distribution and especially to ensure a robust and reliable live-cell read-out of ERK2 localization in a variety of cellular processes including cell death programs.

Different approaches exist to co-express multiple heterologous proteins in living cells such as Internal Ribosomal Entry Site (IRES) sequence [456,457] and bidirectional or multiple promoters in a same plasmid [458] but all these strategies pointed out problems linked to co-expression efficiency. In the case of IRES sequence, several limitations have been reported including the length of the IRES element (approximately 500bp), the translation efficiency of the different proteins (upstream protein is expressed as almost 10-fold higher than the downstream protein), and the modulation of IRES activity depending on the position of specific genes [459]. Conversely, as a more promising approach, the “2A peptide” was chosen. 2A peptide was initially identified in *Foot and Mouth Disease Virus* (F2A) (FMDV, member of the genus *Aphthovirus*) belonging to the *Picornaviridae* family [460]. It was also found in other *Picornaviridae* including *Porcine teschovirus-1* (P2A), *Thosea asigna virus* (T2A) and *Equine rhinitis A virus* (E2A) but also in other biological systems as “2A-like” peptides [461]. Depending on the virus origin, it consists of a highly conserved short peptide of only 18-22 amino acids fused in frame between two protein-coding sequences derived from a single Open Reading Frame (ORF). 2A peptide functions as a “ribosomal skipping” mechanism or “stop-go” and “stop carry-on” translation and are now referred to as CHYSELs (*cis*-acting hydrolase elements) [462]. The translation results in co-translational “cleavage” of the polypeptide occurring between the C-terminus glycine of 2A peptide and the proline of the downstream fused protein [463,464]. Expression of 2A-linked proteins was efficiently performed *in vitro*, in a wide range of eukaryotic cultured cells and embryonic stem cells and even *in vivo* especially in embryos and total organism

[461,463,465–467]. While no protein degradation and side effects of premature termination of translation were reported [468], previous work described variability in the 2A peptide-mediated cleavage depending on the choice of 2A peptide and cellular model [461,464]. Further support for the 2A strategy is found in previous studies demonstrating robust equimolar coexpression in studies of the molecular interactions of G-coupled proteins [469] and T-cell development in CD3-deficient mice [470].

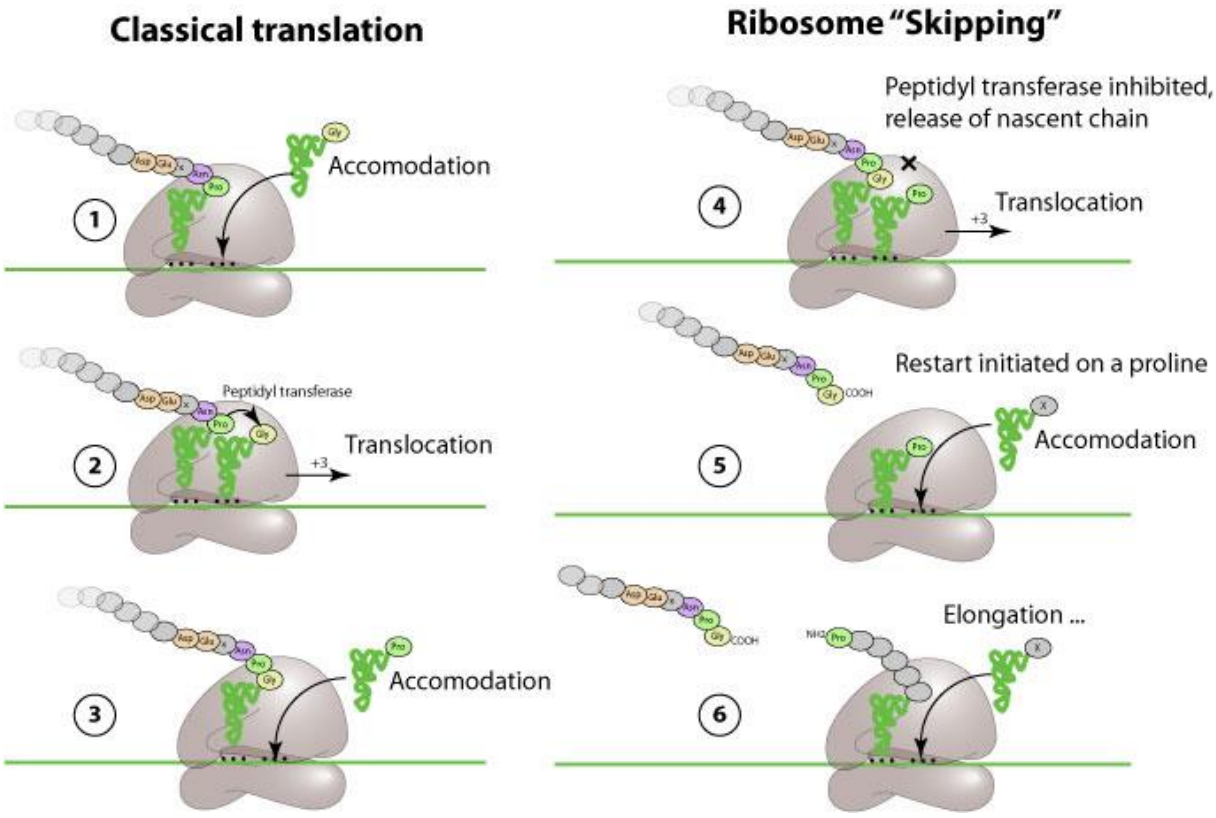

Figure 15: Scheme of the ribosome skipping leading to co-expression of two peptides from one polypeptide. This process is induced by a 2A-like sequence inserted between two distinct peptides. From http://viralzone.expasy.org/.

3.2. Review – From FRET imaging to practical methodology for kinase activity sensing in living cell

François Sipieter[1,2,3], Pauline Vandame[2,3], Corentin Spriet[1,3], Aymeric Leray[1,3], Pierre Vincent[3,4], Dave Trinel[1,3], Jean-François Bodart[2,3], Franck B. Riquet[2,3] and Laurent Héliot[1,3]

[1] Team Biophotonique Cellulaire Fonctionnelle, IRI CNRS USR3078, Lille1 University / Lille2 University, F-59655 Villeneuve d'Ascq, France

[2] Laboratoire de Régulation des Signaux de Division, EA4479, Lille1 University, F-59655 Villeneuve d'Ascq, France

[3] Groupement de Recherche Microscopie Imagerie du vivant, GDR2588-MIV CNRS, F-59655 Villeneuve d'Ascq, France

[4] Neurobiologie des processus adaptatifs (NPA), CNRS UMR 7102, UMPC, F-75005, Paris, France.

Published in Progress in Molecular Biology and Translational Science, 2013, Volume 113, 145-216. doi: 10.1016/B978-0-12-386932-6.00005-3

Review

From FRET imaging to practical methodology for kinase activity sensing in living cells.

François Sipieter[1,2,4] and Pauline Vandame[2,4], Corentin Spriet[1,4], Aymeric Leray[1,4], Pierre Vincent[3,4], Dave Trinel[1,4], Jean-François Bodart[2,4], Franck. B Riquet[2,4*] and Laurent Héliot[1,4*]

1 : Biophotonic Team (BCF), IRI CNRS- University Lille1- University Lille2 USR 3078

2 : Laboratoire de Régulation des Signaux de division EA4479 University Lille1 -

3 : Neurobiologie des processus adaptatifs - UMR 7102, UPMC

4 : Groupement de Recherche Microscopie Fonctionnelle du vivant, GDR2588-CNRS

** Corresponding authors*

Dr Laurent Héliot
Interdisciplinary Research Institute
USR3078 CNRS - Université de Lille 1 - Université de Lille 2
Biophotonique Team (BCF)
And
Groupement de Recherche : Microscopie fonctionnelle du vivant
GDR2588-CNRS
Parc CNRS de la Haute Borne
50 avenue de Halley - BP 70478
F-59658 Villeneuve d'Ascq Cedex
Tel: 33 (+) 3 62 53 17 35
Fax: 33 (+) 3 62 53 17 01
Email: laurent.heliot@iri.univ-lille1.fr

Dr. Franck Riquet
University Lille1 - Cité Scientifique
Bulding SN3, Rm 301
Laboratoire de Régulation des Signaux de Division EA-4479
F-59655 Villeneuve d'Ascq
France
Tel 33 (+)3 62 53 17 34
Fax 33 (+)3 62 53 17 01
Email: franck.riquet@iri.univ-lille1.fr

Running title:

Microscopy for measurement of fluorescence-based reporters in living cells; analysis and methodologies for kinase activity assessment.

Abbreviations

A.....acceptor
AKAR.....A-kinase activity reporter
Akt.....Protein Kinase B
AMDI .....adaptive Monte Carlo data inflation
ATP .....adenosine triphosphate
BFP .....blue fluorescent protein
Bik.....Bcl-2-interacting killer
cAMP.....cyclic adenosine monophosphate
CCD .....charge coupled device
cDNA.....complementary DNA
CFP .....cyan fluorescent protein
CKAR .....C-kinase activity reporter
cp .....circularly permuted
CyPET.....Optimized eCFP for FRET
D .....donor
DAPK.....death associated protein kinase
DC.....direct current
DCR .....dual channel ratio
DNA.....deoxyribonucleic acid
DsRed .....*Discosoma sp.* red fluorescent protein
DVR.....dual view ratio
EGF.....Epidermal Growth Factor
eGFP.....enhanced green fluorescent protein
EKAR.....extracellular regulated kinase activity reporter
Epac.....exchange protein activated by cAMP
ERK.....extra-cellular regulated kinase
FD .....frequency domain
FHA.....forkhead associated
FLIM.....fluorescence lifetime imaging microscopy
FP.....fluorescent protein
FRET.....Förster resonance energy transfer
GFP.....green fluorescent protein
GTPase .....hydrolase enzyme that can bind and hydrolyze guanosine triphosphate (GTP)
IRF .....instrumental response function
JNK .....c-Jun N-terminal kinase
KAR.....kinase activity reporter
LED .....light emitting diode
LSM.....least square method
MAPK .....mitogen-activated protein kinase
MLE.....maximum likelihood estimation
MPK .....mitogen-activated protein kinase phosphatase
MRE .....molecular recognition element
NGF.....Nerve Growth Factor
PAABD .....phosphoamino acid binding domain
PEA.....Astrocytic phosphoprotein
PKA.....protein kinase A
PKC.....protein kinase C
PKG.....protein kinase G
PMT.....photomultiplier tube
PTB .....phosphotyrosine binding
R .....ratio
Rac.....subfamily of the Rho family of GTPases
RFP .....red fluorescent protein
RNA.....ribonucleic acid
ROS .....Reactive oxygen species
siRNA .....small interfering RNA
SR .....sequential ratio
TCSPC .....time correlated single photon counting

TD .....time domain
U2OS.....Osteosarcoma cell line
YPet .....optimized YFP for FRET
YFP .....yellow fluorescent protein

Foreword

Biological processes are intrinsically dynamic. Although traditional methods provide valuable insights for the understanding of many biological phenomenon, the possibility nowadays to measure, quantify and localize proteins within a cell, a tissue and even an embryo has revolutionized our train of thoughts and has encouraged scientists to develop molecular tools for the assessment of protein or protein complex dynamics within their physiological context. These ongoing efforts rest on the emergence of biophotonic techniques and the everlasting improvement of fluorescent probes, allowing precise and reliable measurements of dynamic cellular functions. The march of the “in vivo biochemistry” has begun, already yielding breathtaking results.

3.2.1. Introduction

How cells sense external and internal signals and how these signals are processed to drive specific responses in a multiscale context are major questions for biology.

Protein phosphorylation plays a significant role in a wide range of cellular processes such as cell proliferation, differentiation, and cellular death. In eukaryotes, phosphorylation occurs on serine, threonine, tyrosine and histidine residues. Protein phosphorylation can alter activity of many proteins causing a chain reaction leading to the phosphorylation of many proteins involved in a particular cellular process. Conventional analytical methods have identified and characterized various post-translational modifications but the major drawback is that these methods provide only a snap shot of the cell. In fact, in order to assess activity of protein kinases, immunoblotting and immunocytochemistry with phospho antibodies toward specific residues described to report on kinase activation are global and indirect/static approaches. They are limited to the time resolution and the quality of cell fractionation assay under analysis. In addition, antibodies toward specific phospho-residues do not really reflect activity of the kinase of interest.

To go beyond the snap shot, tools have been developed to answer the new challenges of today's biology quest: protein localization, interaction and activity when applicable. Concerning the latter, fluorescent biosensors are gaining increasingly the biologist's toolbox to visualize especially spatiotemporal dynamics of kinase signaling in living systems. They provide high sensitivity and versatility while minimally perturbing cell physiology.

The word "biosensor" is a rather generic term that is used to define a wide array of systems enabling the sensing of various analytes. Typically, a biosensor is composed of two parts harboring distinct functions. The first one, referred to as the bioreceptor, that recongnize the analyte, is responsible for the selectivity and the sensitivity of the whole biosensor. The second, named transducer is in charge of conveying the signal from the recognition part towards the adapted instrument (Fig 1).

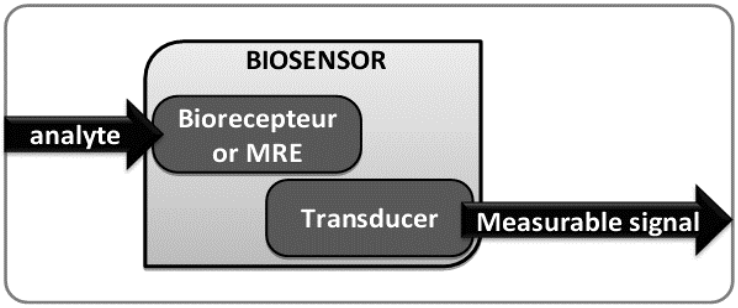

Figure 1: Schematic representation of biosensor basic principle.

This definition is of course applicable to molecular biosensors dedicated to sense biological events in living cells. Indeed, the analyte is represent ted by ions such as Ca^{2+}, second messengers such as, cAMP, an enzymatic activity such as kinase or an active enzyme conformation. The bioreceptor or molecular recognition element (MRE) is materialized by calmodulin/M13 or TroponinC/M13, Epac (Exchange protein activated by cAMP), and substrate /phosphoamino acid binding domain (PAABD), respectively. The transducer element is represented in these cases by fluorescent proteins that when their distance allows it will generate a change in their fluorescent signal or spectral properties. The instrument thus dedicated to signal detection is an optical fluorescent microscope or a spectrofluorimeter.

The first of a long line of such biosensors was developed in R. Tsien‘s lab and published in 1996 [1]. While of simple design, it was then first demonstrated that fluorescent protein variants could be used for biosensing. This first genetically encoded biosensor was composed of a blue fluorescent protein (BFP) and a green fluorescent protein (GFP) encompassing a trypsin cleavable linker. Thereafter, many different types of biosensors have been developed with various molecular structures (Fig 2).

All genetically encoded FP-based biosensors are classified into groups depending on their structure [2, 3]. Kinase Activity Reporters (KARs) are included into the group based on intramolecular FRET. The archetypal structure of such biosensors consists of two FPs flanking an MRE (Fig 3). The interaction of an active kinase with its specific MRE (substrate + phosphor amino-acid binding domain) leads to a change in the molecular conformation of the MRE. This change alters the distance and/or relative orientation between the two FPs and consequently the FRET signal. This chapter will focus on genetically-encoded biosensors, and specifically

those dedicated to kinase activity measurements. Although kinase activity reporters vary in specificity depending on the choice of the substrate, the design strategy of these reporters remains universal [4].

Genetically encoded FRET-biosensors can be used to analyze molecular events in single living cells, tissue and even expressed in animals (e.g. aquatic animals, transgenic mice). They are expressed in the native context of a living cell to report on dynamic events. However, as described by Frommer *et al* [2], these FRET biosensors sense actively ("active reporters") cellular microenvironment and even the subcellular microenvironment and cannot be regarded as "passive reporters" such as simply fluorescent protein (FP) fused-protein.

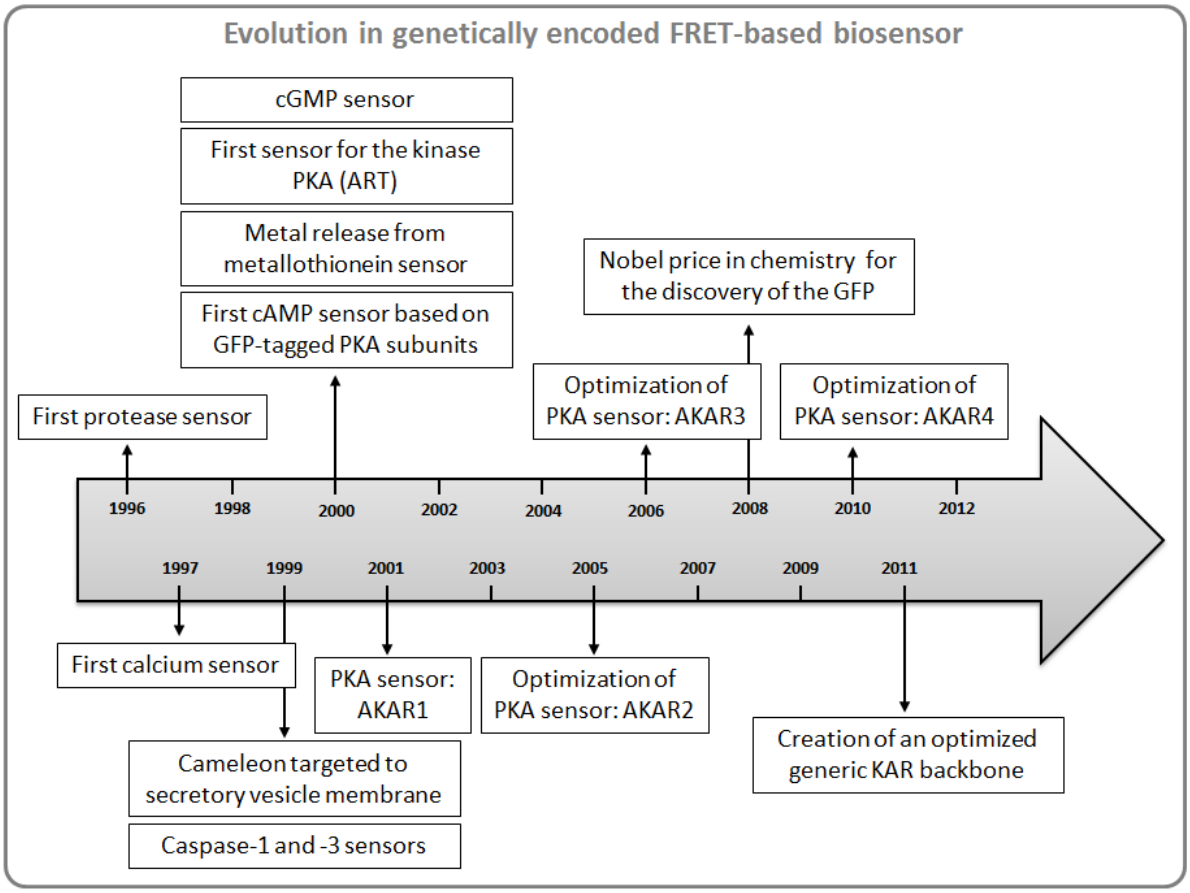

Figure 2: Evolution in genetically encoded FRET-based biosensors.

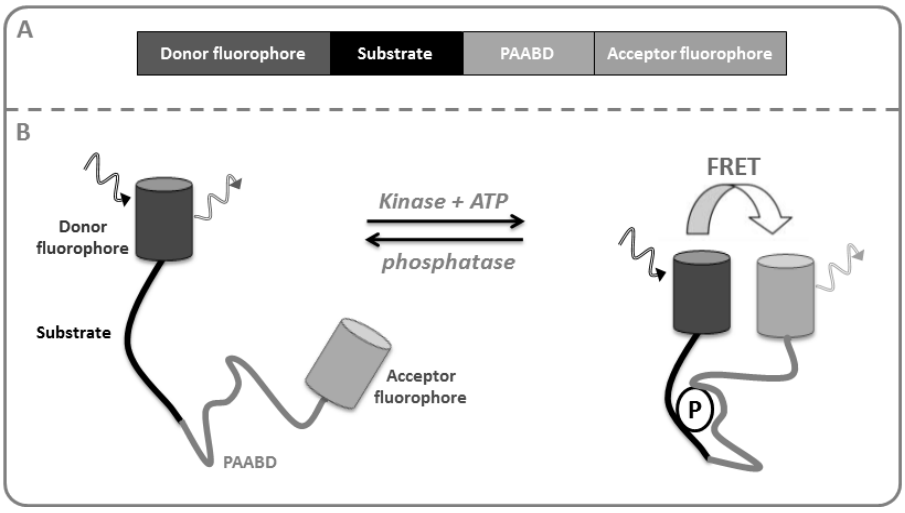

Figure 3: General scheme of the functional domains of FRET-based Kinase Activity Reporter (KAR). Schematic representation of biosensor conformational changes upon phosphorylation by the targeted kinase leading to an increase in FRET between donor and acceptor fluorophores.

3.2.2. Fluorescence generalities

3.2.2.1. Introduction

The relaxation of fluorophore from an excited state to its ground state, after the absorption of an electromagnetic radiation may result in the emission of photons called luminescence. If this transition occurs for an electron in the excited singlet state (with a spin opposite of that of a paired electron in the ground state), this emission is called fluorescence. The fluorescent molecule is often excited to S1 excited states. In most cases a rapid relaxation subsequently occurs to the lowest vibrational level of the first excited state S1; this is the internal conversion process which usually occurs within approximately 10^{-12} s and results in some of the energy loss from the system responsible for the energy difference (Stokes' Shift) between the absorption and emission spectra (See Jablonski diagram in Figure 4.1). The energy of the emitted photon is dependent upon the ground state towards which the transition occurs.

3.2.2.2. The absorption process

The energy of the excited photon must be equal to, or greater than, the energy difference (E_0 and E_1) between the ground state ($S_{0,}$) and the excited state (S_1). The frequency of this photon is $v=(E_1-E_0)/h$, where h is the Plank constant. When a photon is absorbed, its energy is transferred to the valence electron and this electron

is promoted to a higher electronic orbit, thus putting the molecule into the excited state. This absorption is very fast, since it occurs within 10^{-15} s.

A

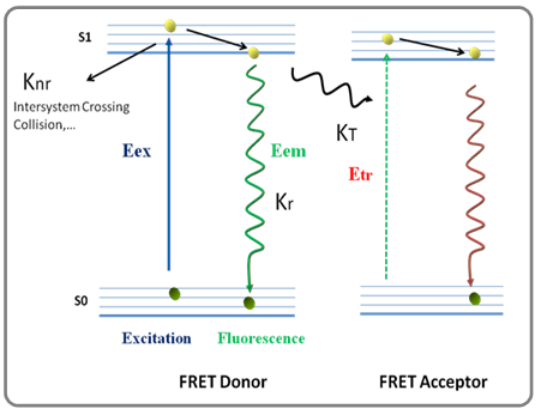

B

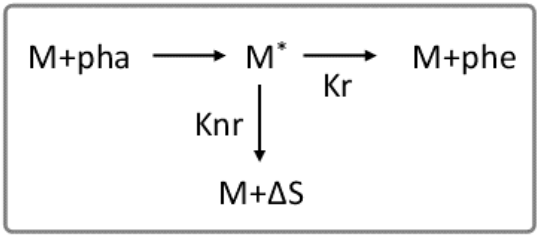

Figure 4.1: (A) Jablonski's diagram. S_0 is the fundamental energy level of the electron and S_1 is the first exited level, the small lines represent the vibrational energy levels. Eex is the energy of excitation, Eem is the energy of fluorescence emission, Kr is the radiative deexcitation rate and Knr is the non radiative deexcitation rate. (**B**) Scheme of the molecular equilibrium occurring between the absorption and emission processes where M is the fluorophore (molecule), M* is the excited state of the molecule, pha is the photon absorbed, phe is the photon emitted, ΔS is the entropy, kr is the radiative deexcitation rate and knr is the non radiative deexcitation rate.

Experimentally, the efficiency of light absorption at a wavelength λ is characterized by the *absorbance* A(λ) related to the *transmittance* T(λ) by

$$A(\lambda) = \log\left(\frac{I_0}{I}\right) = -\log T(\lambda) \qquad \text{eq1}$$

where I_0 is the intensity of a monochromatic incident light of wavelength λ passing through an isotropic sample containing absorbing molecules at a concentration c (mol^{-1}), I is the light intensity leaving the absorbing medium and l (cm) the absorption path length (sample thickness) of the sample (Figure 4.2).

The absorbance follows the Beer-Lambert law

$$A(\lambda) = \varepsilon(\lambda) l c \qquad \text{eq2}$$

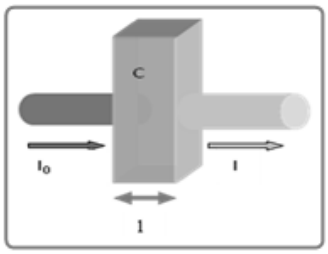

Figure 4.2: Physical parameters implicated in the absorbance measurements.

Where ε(λ) is the molar absorption coefficient (L mol $^{-1}$ cm^{-1}) and l (cm) is the absorption path length (sample thickness) of the sample (Figure 4.2).

The absorbance reflects the probability for a population of fluorophores to jump into an excited state under the effect of an incident photon at the wavelengh (λ).

The *absorption coefficient* α(λ) is the absorbance divided by the optical path length (l) into the medium :

$$\alpha(\lambda) = \frac{A(\lambda)}{l} = \frac{1}{l}\log\left(\frac{I_0}{I}\right) ; I = I_0 e^{-\alpha(\lambda) l} \qquad \text{eq3}$$

3.2.2.3. The emission process

When a molecule has been promoted to an excited state upon the absorption of an electromagnetic radiation, it necessary returns to a ground state through competition between radiative (K_r) and non-radiative (K_{nr}) pathways. The radiative pathways involve photon emission and non-radiative pathways include energy transfer through collisions, resonance energy transfer through near field dipole-dipole interactions (such as FRET detailed in the next section), photochemical decomposition. A change in the vibrational and rotational states of the molecule can also cause a loss of energy via a non-radiative process [5].

The Jablonski diagram shown in Figure 4.1 illustrates the balance of energy through the excitation - relaxation cycle.

The difference in energy (or wavelength) between the absorbed and the emitted photons is known as the Stokes shift shown in Figure 4.3. This phenomenon was first described by Sir G. G. Stokes in 1852. A large Stokes shift is often highly desirable for simplifying the wavelength separation between the fluorescence emission and the excitation [6].

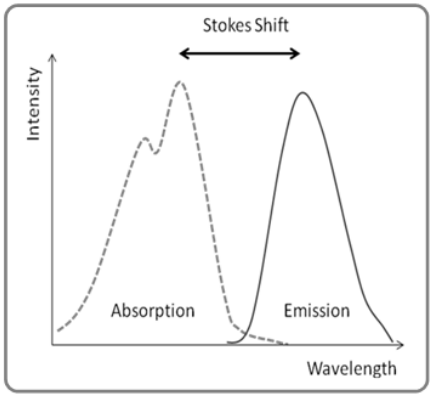

Figure 4.3: Illustration of the Stokes shift between the absorption and emission spectra.

There is a competition between the different de-excitation processes previously discussed (K_r and K_{nr}). The quantum yield (Φ) is the ratio of the number of photons emitted to the number of photons absorbed. It can also be described using the rates of radiative (K_r) and non-radiative (K_{nr}) process of de-excitation.

$$\Phi = \frac{K_r}{K_r + K_{nr}} \qquad \text{eq4}$$

The quantum yield vary from 0 to 1, where 0 corresponds to non- fluorescent materials and 1 corresponds to highly fluorescent materials, where each photon absorbed results in a photon emitted.

The excited molecules (M*) could be desexcited by radiative processes (K_r) or non-radiative (K_{nr}) processes whose intersystem transfer as FRET (K_T). In classical kinetics, the rate of disappearance of excited molecules is expressed by the differential equation:

$$-\frac{\boldsymbol{d}[\boldsymbol{M}*]}{\boldsymbol{dt}} = (\boldsymbol{K_r} + \boldsymbol{K_{nr}})[\boldsymbol{M}*] \qquad \text{eq5}$$

Integration of this equation yields the time evolution of the concentration of the excited molecules [M*] (see Figure 2.1).

$$[M*] = [M*]_0 \, e^{(-t/\tau)} \qquad \text{eq6}$$

$$\text{With } \boldsymbol{\tau} = \frac{\mathbf{1}}{\boldsymbol{K_r} + \boldsymbol{K_{nr}}} \qquad \text{eq7}$$

$[M*]_0$ being the concentration of excited molecules at time 0 resulting from light excitation. The *fluorescence lifetime* τ is in the range of 10^{-9} s (0.5 - 20ns for commonly used fluorescence transitions). τ describes the average time that a molecule stays in its excited state before emitting a photon [7]. The resonance

transfer or FRET (K_T) is included in non-radiative deactivation pathways (K_{nr}). It can be defined as the difference between the rates K_{nr} of the donor only and K_{nr} of the donor in presence of the acceptor. The fluorescence intensity begins to decrease when molecules are in their excited states. This decrease depends upon the rate of electron de-excitation and it can be deduced from eq7:

$$\boldsymbol{I_t = I_0 e^{-t/\tau}} \qquad \text{eq8}$$

With $K_T(r)=1/\tau_D$, eq9

The rate of energy transfer K_T is in fact the slope of the curve measuring the fluorescence donor lifetime in a semi-logarithmic representation (Figure 4.4).

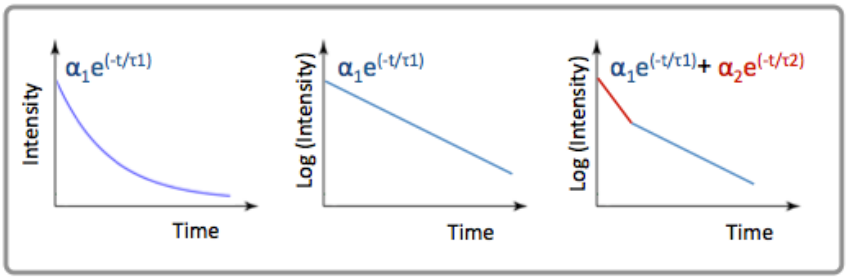

Figure 4.4 : Fluorescence lifetime decay profiles: τ2< τ1 (inspired from the Nikon website) .

The fluorescence impulse response function I(t) is often represented by a multiexponential decay model

$$I(t) = \sum_i \alpha_i e^{-t/\tau_i} \qquad \text{eq10}$$

where τi are the decay times and αi are the amplitudes of the components. The values of α_i and τ_i may have direct or indirect molecular signification. For a fluorophores mixture, if each component has a single decay time, τ_i are their decay times. The parameters α_i and τ_i cannot always be attributed to molecular features of the sample. Alternatively, the measured intensity decay can be fitted with equation (10). The values of α_i and τ_i can be used to calculate the *fractional contribution* f_i of each decay time τ_i to the steady-state intensity:

$$f_i = \frac{\alpha_i \tau_i}{\sum_i \alpha_i \tau_i} \qquad \text{eq11}$$

The resolution of multiple τ_i is increasingly difficult as they are more closely spaced. The statistically significant resolution of closely τ_i requires a high signal-to-noise ratio and a large number of photons collected. The calculation of the energy transfer efficiency from the donor fluorescence lifetime in the presence and absence of the acceptor (equation 11) assumes that in experimental conditions the donor

decays according to a single-exponential model. If the donor displays a multi-exponential decay, τ_i *values* can be used to calculate the average lifetime τ. It is defined as the average time that the fluorophore remains in the excited state and it is defined as:

$$\langle \tau \rangle = \frac{\int_0^\infty t\, I(t)dt}{\int_0^\infty I(t)dt} = \sum_i f_i \tau_i \qquad \text{eq12}$$

In order to simplify data representation, mean lifetime τ_{mean} has been largely used in FRET experiments [8-11]. It is given by

$$\tau_{mean} = \sum_i a_i \tau_i = \int I(t)dt \qquad \text{eq13}$$

3.2.3. FRET measurement

3.2.3.1. Introduction

Among the different previously described non-radiative deactivation processes (K_{nr}) the energy transfer between dipoles was first described by Förster in 1926 and Perrin in 1932. *Förster resonance energy transfer* or FRET is a physical process in which the energy of a chromophore (called Donor [D]) in its excited state, is transferred non-radiatively to a neighbouring chromophore (called Acceptor [A]) while in its ground state [5]. This physical process has been often applied experimentally for investigating molecule interactions at distances beyond the diffraction limited resolution (for review see [5, 7]). For instance, FRET measurements (generally used in spectroscopy and microscopy) allow for the investigation of the formation of protein complexes in living cells and tissues, as well as for conformational changes of single proteins such as biosensors. {For review [6], [7], [12]}.

3.2.3.2. FRET basis

FRET is one possible pathway for the relaxation of the excited state molecules. This phenomenon occurs only under appropriate conditions of proximity and orientation between two fluorophores (donor and acceptor):

1. this form of energy transfer occurs in the near field of the donor. In other words, the distance (r) between the donor and the acceptor must be less than ten nanometers (r < 10nm) in order that $K_T \neq 0$.

2. the energy transfer is achieved between molecules with resonant oscillation dipole moments (overlapping wave functions). This requires an overlap between the donor emission spectrum and the acceptor excitation spectrum.
3. the orientation of the emission dipole moment of the donor with respect to the excitation dipole moment of the acceptor must be fulfilled in order for FRET to occur.

The theoretical concept for FRET was developed following both the classical model by Perrin in 1925 and the quantum-mechanical model by Perrin in 1932 and Förster in 1946-1949. [13], [14], [15] (for review [6] and [5]).

If one considers a single donor and acceptor separated by the distance r, the rate of energy transfer $K_T(r)$ can be calculated as a probability of transfer energy quantum from donor to acceptor per time unit, given by the fundamental equation:

$$K_T(r) = \frac{\Phi_D \kappa^2}{\tau_D r^6}\left(\frac{9000\ln(10)}{128\pi^5 n^4 N_A}\right) J(\lambda) \int_0^\infty F_D(\lambda) d\lambda \qquad \text{eq14}$$

Where Φ_D is the donor quantum yield (as previously described in this chapter) in the absence of acceptor, τ_D the donor lifetime in absence of acceptor; n is the refractive index of the medium; N_A is the Avogadro's number, J(λ) is the overlap integral, F_D is the normalized fluorescence intensity of the donor; κ^2 is the dimensionless orientation factor describing the relative spatial orientation of the donor and acceptor transition moments. Note that ε_A, Φ_D and *n* are fixed by the choice of FRET pairs and medium. Therefore, $K_T(r)$ variation is mainly dependent on r and κ.

Equation 14 is not easy to use for the design of biochemical experiments ([6]). This is why the Förster distance R_0 was introduced by Förster in 1948. When the transfer rate $K_T(r)$ is equal to the decay rate of the donor in absence of acceptor, the one-half of the donor molecules decay by energy transfer process. Once the value of R_0 is known, the rate of energy transfer K_T can be easily calculated:

$$K_T = \frac{1}{\tau}\left(\frac{R_0}{r}\right)^6 \qquad \text{eq15}$$

With

$$K_T(r) = 1/\tau_D \qquad \text{eq16}$$

One obtains (from eq 14)

$$R_0^6 = \Phi_D \kappa^2 \left(\frac{9000\ln(10)}{128\pi^5 n^4 N_A}\right) \int_0^\infty F_D(\lambda)\varepsilon_A(\lambda)\lambda^4 d\lambda \qquad \text{eq17}$$

R_0 is given in $M^{-1}cm^{-1}$ and it could be simplified by:

$$R_0^6 = 8{,}79\ 10^{-5}[\Phi_D \kappa^2 J(\lambda) n^{-4}] \quad \text{eq18}$$

This expression allows Förster distance to be calculated from the spectral properties of the donor and the acceptor, and from the donor quantum yield Φ_D [13].

The FRET efficiency is dependent on the inverse sixth power of intermolecular separation (r) (discussed in the next section).

Additionally, Förster distance is usually reported for an assumed value of κ^2 of 2/3 characterizing free FRET pairs. This question of dipole-dipole orientation is discussed later.

Directly, if the transfer rate is much faster than the decay rate, then energy transfer will be efficient. Otherwise, FRET will be inefficient.

A crucial step in the practical FRET implementation is the knowledge of several major parameters:

- The quantum yield of the fluorophore donor only Φ_D
- The overlap integral J(λ) between donor and acceptor fluorophore
- The orientation factor κ^2 between two fluorophore dipole

3.2.3.3. Overlap integral J(λ)

J(λ) is the *overlap integral* between the donor emission and the acceptor absorption spectra (expressed as $M^{-1}\,cm^{-1}\,nm^4$) defined as

$$J(\lambda) = \frac{\int_0^\infty F_D(\lambda)\varepsilon_A(\lambda)\lambda^4 d\lambda}{\int_0^\infty F_D(\lambda) d\lambda} \quad \text{eq19}$$

Where $F_D(\lambda)$ is the corrected fluorescence donor (dimensionless) and ε_A is the extinction coefficient of the acceptor at λ (expressed in $M^{-1}cm^{-1}$).

3.2.3.4. Orientation factor κ^2

κ^2 can vary from 0 to 4 according to the following equation:

$$\kappa^2 = (\cos\theta_T - 3\cos\theta_D\cos\theta_A)^2 = (\sin\theta_D\sin\theta_A\cos\Phi - 2\cos\theta_D\cos\theta_A)^2 \quad \text{eq20}$$

Where θ_A, θ_D, θ_T and Φ are described in Figure 4.5:

Additionally, the fluctuation of *refractive index* n could induce errors in calculated distance r but this effect is not usually considered.

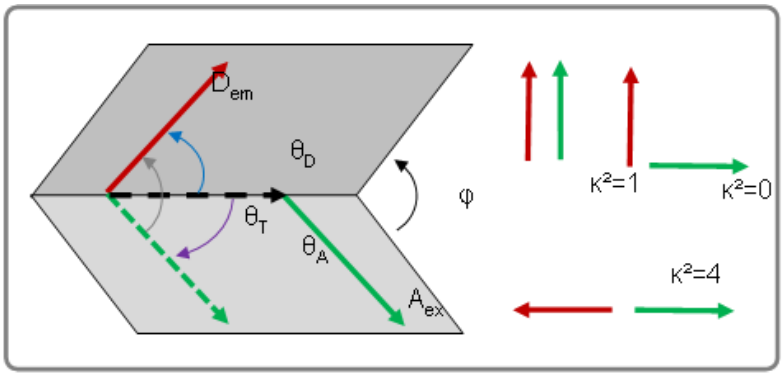

Figure 4.5: Parameters intervening in the calculation of the orientation factor κ^2.

The orientation factor (κ^2) characterizes the statistical average of the relative fluorophore orientations, which determines both how well the fluorophore dipoles are coupled and how efficiently energy is transferred (Figure 4.5). However, if the dipoles are perpendicular, κ^2 becomes 0, which would result in serious errors in the calculated distance. This question has been discussed in detail [16] [17] [18]. In general, variation of κ^2 does not induce major errors in the calculated distance, but for intramolecular FRET in biosensors this question can be discussed. In fact, in rigid molecule, (as polypeptide with 4 to 9 amino-acid residus) with isotropic orientational distribution (statistically randomly distributed) of the donor and the acceptor transition moments, but with no rotation during the lifetime of excited state (frozen), the value of κ^2=0,476 can be used. The optimal value κ^2 at room temperature is κ^2=2/3 [19]. For fluorophore bound to macromolecules (i.e. fluorescent proteins) segmental motions of the donor and acceptor tend to randomize the orientations and κ^2=2/3 is classically used [6, 20]. Computational simulations showed that κ^2 converges to 2/3 in FRET sensor where the D–A pair is presumed to be freely mobile [21] Finally, the evaluation of errors in distance (r) induce by approximation on κ^2 has been reported, but is no more than 10% [20].

3.2.3.5. Energy transfer Efficiency

The *efficiency of energy transfer* (E) can be defined as the ratio of the relaxation rate due to energy transfer divided by the sum of all relaxation rates.

$$E = \frac{K_{T(r)}}{\tau_D^{-1} + K_T(r)} \qquad \text{eq21}$$

The rate of energy transfer is often defined as a function of inverse sixth power of distance between the two molecules.

$$E = \frac{R_0^6}{R_0^6 + r^6} \qquad \text{eq22}$$

The first factor that affects the FRET signal is the distance (r) between the fluorophores. The most sensitive range of r is between 0.7–1.4 R_0, corresponding to 90–10% FRET efficiency (Figure 4.6). R_0 is usually ranging from 4 to 7 nm, hence, protein conformational change in this range is ideal for the largest FRET dynamic in biosensors.

The *transfer efficiency* (E) is typically measured using the relative fluorescence intensity of the donor, in absence (F_D) or presence (F_{DA}) of acceptor.

$$E = 1 - \frac{F_{DA}}{F_D} = 1 - \frac{\int I_{DA}(t)dt}{\int I_D(t)dt} \qquad \text{eq23}$$

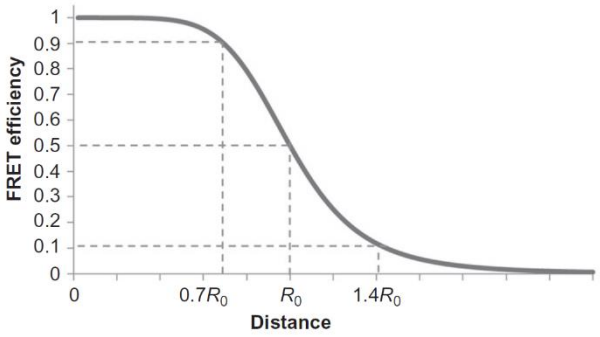

Figure 4.6: FRET efficiency as a function of the distance between the donor and the acceptor. The FRET efficiency is 50% when the distance is equal to the Förster distance (R_0). FRET efficiencies ranging from 10% to 90 % correspond to distances between fluorophores of 1,4 R_0 and 0,7 R_0 respectively.

Where F_{DA} is the intensity of donor fluorescence emission in presence of acceptor and F_D is the intensity of donor fluorescence in absence of acceptor and I_D and I_{DA} are respectively the intensity decays of the donor alone and the donor in the presence of the acceptor.

The transfer efficiency can also be calculated from the lifetimes under these respective conditions (τ_D and τ_{DA})

$$E = 1 - \frac{\tau_{DA}}{\tau_D} \qquad \text{eq24}$$

The FRET kinetic measurement can be performed by the calculation of ratio (R) between two stationary states of kinetic. This ratio (R) is classically used for measurement by FRET-based biosensors (see next section)[22].

Both equations 23 and 24 are only applicable to donor acceptor pairs that are separated by a fixed distance. However, single exponential decays are rare in biology.

The mean lifetime τ_{mean} defined by Eq. 15 has been largely used in FRET experiments [8-11]. This mean lifetime is then equivalent to the area of the fluorescence intensity decay which is related to the FRET efficiency *E*. However, the mean lifetime does not correspond to the correct average lifetime, which is defined by Eq. 12.

3.2.3.6. FRET measurements of molecular populations

In FRET analysis, particularly for biosensors, two elements must be usually considered: the interacting fluorophores population and the FRET efficiency.
The distance distribution function P(r) describes the normalized probability of finding the specific donor/acceptor pairs separation.
The *transfer efficiency (E)* can be written*:*

$$E = \int_0^\infty \frac{P(r)R_0^6}{R_0^6+r^6}dr \qquad \text{eq25}$$

Bulk measurements of FRET efficiency by intensity-based methods cannot distinguish between an increase in FRET efficiency (i.e., coupling efficiency) and an increase in FRET population (concentration of FRET species) since both parameters are not resolved. FRET measurements based on the analysis of the donor fluorescence lifetime may resolve this problem, with multi-exponential decay models ([7] and [23]). The assumption that interacting and non-interacting populations are present, allow determining both the efficiency of interaction and the fractional population of interacting molecules. In the first instance, the presence/absence of FRET is determined by fitting experimental data to a single-exponential decay [6]. Sufficient reduction in the measured lifetime indicates the existence of FRET. Additional analysis is subsequently applied to determine the source of lifetime reduction. In this case, a bi-exponential fluorescence decay model applied to data, allows the determination of the fluorescence lifetimes of non-interacting and interacting subpopulations or two distinct levels of interaction in case of many biosensors. In time domain measurement (see next section), data may be fitted by iterative convolution with:

$$I(t) = IRF(t) \otimes \left\{Offset + \sum_i \alpha_i e^{-t/\tau_i}\right\} \quad \text{eq26}$$

Where IRF(t) is the instrumental response and Offset is the baseline, τ_i are the lifetime of interacting or non interacting populations and α_i are the pre-exponential factors relating to absolute species concentration [24].

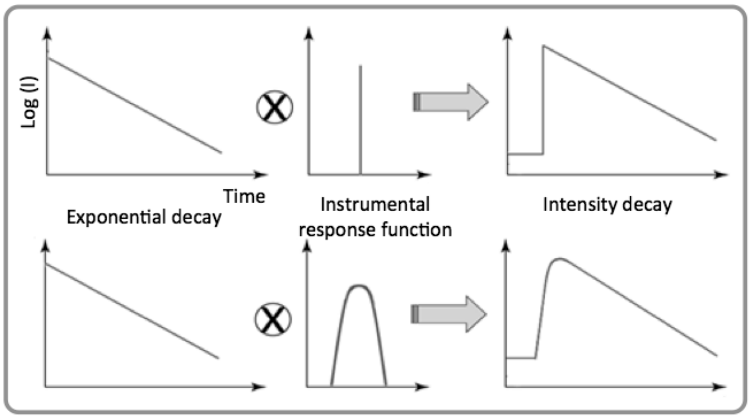

Figure 4.7: **Illustration of the convolution product.** When the instrumental response function (IRF) of the FLIM system is temporally short, the measured intensity decay is almost identical to the sample decay. If the IRF is large, the collected decay becomes well different of the sample decay and it is thus necessary to take into account this IRF to obtain correct lifetime estimations.

3.2.3.7. Conclusion on FRET principles and applications

It is difficult to obtain quantitative determination of labelled molecules which are in interaction from steady-state images. The fluorescence intensity does not only depend on the FRET efficiency but also on the unknown local concentration of dyes. Up to eight measurements at different excitation wavelengths and in different emission wavelength bands can be used to obtain calibrated FRET results from steady state data [7]. In lifetime data, however, FRET shows up as a dramatical decrease of the donor lifetime [6]. At first, qualitative FRET results can be obtained by fitting decay curves with a single exponential approximation. Quantitative measurements require multi-exponential decay analysis [6]. The proportion of donor molecules involved in energy transfer is given by the ratio of the two exponential decay amplitudes, α_2/α_1, while the average coupling efficiency of the FRET pairs is given by the lifetime ratio τ_2 / τ_1.

A major complication of many *in vivo* FRET experiments is the large and differential contribution of cellular autofluorescence to the measured donor and acceptor fluorescence. Autofluorescence contributions can be sometimes corrected

by acquiring an additional image [25], or they can be minimized by the use of spectral lifetime image microscopy [26].

When autofluorescence is substantial, determination of FRET efficiency by fluorescence lifetime measurement (FLIM) might be advantageous because autofluorescence lifetime is usually very short and can be included in the fit of lifetime data. Finally, one has to consider limitations imposed by the available instrumentation. For example, lifetime measurements require relatively sophisticated instrumentation that is not yet widely available.

3.2.3.8. Few considerations on Fluorescent Proteins

Green Fluorescence Proteins from the jellyfish *Aequorea Victoria* is well characterized and has provided a myriad of applications in cellular biology [27, 28]. GFP engineering has generated a large range of fluorescent proteins of different colors [29] enabling scientists to consider dynamic localization of several proteins of interest in living cells [1].

Properties of these fluorescent proteins (FP) reveal that they are excellent candidates for FRET based biological applications (see table 1). The choice of a particular FP as donor or acceptor is very important and is mainly based on the analysis of their respective excitation and emission spectra. FPs must meet certain criteria to form a FRET pair : (i) an effective overlap between the emission spectrum of the fluorophore donor and the excitation spectrum of the acceptor ; (ii) a large extinction coefficient at the region of excitation, (iii) a high quantum yield (ratio photons emitted / photons absorbed) ; (iv) a separation between the excitation and the emission spectra of the donor and of the acceptor; (v) good photostability ; (vi) high brightness ; (vii) minimal perturbation of environment by FPs (toxicity) ; (viii) minimum sensitivity to cellular environment (pH, chloride) and (ix) inability or at least limited capacity to dimerize and/or oligomerize. The last consideration is very important because the use of oligomerizing FPs may compromise the interpretation of the FRET signal. In 2006, Dunn *et al* [30] have elegantly demonstrated that the use of monomeric FPs significantly increased the FRET efficiency of a kinase activity reporter. However, FPs expression level must be sufficiently high to provide enough signal, but not too high otherwise it becomes cytotoxic. In contrast, some tetrameric FPs can be toxic to bacteria when produced in large quantities but this is not the

case for monomeric FPs. All these requirements need to be considered and therefore suggest compromise in the choice of a particular FP in a specific context.

Main Fluorescent Proteins

Protein	Color	Organism	Excitation peak (nm)*	Emission peak (nm)*	Brightness	Photo-stability	Oligome-rization	Reference
eCFP	Cyan	Aequorea victoria	433/445	475/503	++	+++	Weak Dimer	Cubitt et al., 1995
meCFP	Cyan	Aequorea victoria	433/452	475/505	++	+++	Monomer	Zacharias et al., 2002
Cerulean	Cyan	Aequorea victoria	433/445	475/503	+++	++	Weak Dimer	Rizzo et al., 2004
mCerulean	Cyan	Aequorea victoria	433/445	475/503	+++	++	Monomer	Rizzo et al., 2004
eGFP	Green	Aequorea victoria	488	507	+++	++++	Weak Dimer	Tsien et al., 1998
meGFP	Green	Aequorea victoria	488	507	+++	++++	Monomer	Heim et al., 1995
eYFP	Yellow	Aequorea victoria	514	527	++++	++	Weak Dimer	Miyawaki et al., 1999
Venus	Yellow	Aequorea victoria	515	528	++++	+	Weak Dimer	Nagai et al., 2002
mVenus	Yellow	Aequorea victoria	515	528	++++	+	Monomer	Nagai et al., 2002
DsRed	Red	Discosoma sp.	558	583	++++	++++	Tetramer	Matz et al., 1999
mRFP1	Red	Discosoma sp.	584	607	++	+	Monomer	Campbell et al., 2002
tdTomato	Red	Discosoma sp.	554	581	++++	+++	Tandem Dimer	Shaner et al., 2004
mCherry	Red	Discosoma sp.	587	610	++	+++	Monomer	Shaner et al., 2004

Example of FRET Pairs Fluorescent Proteins

FRET-pair	Recommended Donors	Recommended Acceptors	Donor Excitation (nm)	Acceptor Emission (nm)	Laser	R_0**	Reference
Cyan-Yellow	meCFP / mCerulean	eYFP / mVenus	433-452 / 433-445	527 / 528	Violet	4,92 ± 0,10	Allen and Zhang, 2006.
Green-Red	meGFP	mRFP1/ mCherry / tdTomato	488	607 / 610 / 581	Argon	4,73 ± 0,09	Harvey et al., 2008

** Maximal wavelengths of the excitation and emission spectra.*
*** R_0 : Förster distances r_0 for FRET-pairs of fluorescent proteins. R_0 values are given in nanometers. The number of "+" corresponds to the superiority degree of the specific parameter. The colors in the second column represent the emission fluorescence of the corresponding fluorescent protein.*

Table 1: Properties of frequently used FPs and their implementation as FRET pair for ratiometric and fluorescence lifetime imaging. (adapted from [33, 34]) [29, 33-45].

Fortunately, FPs are continually subjected to molecular engineering to improve their intrinsic properties and to increase the number of variants [31, 32]. Generally, FRET can be evaluated by ratiometric methods measuring the fluorescence emitted by the acceptor in response to the excitation of the donor fluorophore. Others approaches have emerged in recent years with fluorescent protein engineering and rely on the donor fluorescence lifetime measurements.

3.2.4. FRET measurements: methods and instrumentation.

As previously described, FRET induces modification of several properties of the emitted fluorescence. Different techniques thus arise from these modification measurements [46, 47], such as monitoring the fluorescence emission spectrum, the lifetime, the anisotropy… In the particular case of biosensor application, the most popular technique is called the **sensitized emission** which consists in acquiring the fluorescence intensity emitted by the donor only and the acceptor only. However, several other techniques are very interesting alternative for quantifying the molecular activity: i) the **spectral imaging** which consists in exciting at one wavelength and measuring the whole emission spectrum and ii) the **fluorescence lifetime imaging (FLIM)** for measuring the donor fluorescent protein lifetime changes.

Each of these techniques has its own advantages and drawbacks. Using two extreme examples, the sensitized emission is the simplest method and can be performed on nearly all conventional microscopes but it requires a great care regarding biological references while FLIM needs tricky instrumentations but can yield unambiguous measurements of FRET efficiency. In this part, we will thus describe systems needed to perform reliable biosensor imaging experiments.

3.2.4.1. Intensity based approaches

The most intuitive and easy methods to perform FRET measurements are based on fluorescence intensity. The technique that we will discuss consists in imaging the sensitized emission i.e the fraction of acceptor emission induced by the non radiative energy transfer from the donor molecule. These measurements can be achieved through either ratiometric or spectral imaging.

Ratiometric approach

FRET measurements using biosensors are usually performed by acquiring fluorescence emitted by the donor and the acceptor. Resulting data are usually represented by the ratio of these fluorescence measurements after appropriate corrections. The classical ratiometric approach, that is based on equation 14, consists in measuring at least 3 channels: i) excitation and observation of the donor (I_{donor}), ii) excitation of the donor and observation of the acceptor (I_{FRET}) ,and iii) excitation and observation of the acceptor ($I_{acceptor}$). $I_{acceptor}$ is needed to compensate for donor and acceptor concentration differences, thus accounting for bleed-through and nonspecific excitation [48]. In the case of biosensor measurements performed on living cell, the amount of donor and acceptor are identical and the last channel acquisition is useless. In this particular case, only i) and ii) are required and as we will see in the data analysis section, correction by acceptor channel will even decrease signal to noise ratio of measured ratio. This experimental condition is formally similar to the well described conditions used to image calcium with ratiometric indicators, except that calcium probes like fura-2 show a ratiometric change for two different excitation wavelength, whereas biosensors show a ratiometric change of the fluorescence emission for one excitation wavelength.

One major advantage of this technique is that it only requires 2 wide-field or confocal images allowing high speed acquisitions of fluorescence images with systems equipped with appropriate filter sets available in most imaging core facilities (table 2).

Channel	**Excitation filter**	**Excitation Dichroic**	**Emission filter**
I_{donor}	420/20	450	475/40
I_{FRET}	420/20	450	535/25

Table 2: example of adapted filter set for the CFP/YFP FRET pair [48].

Special care must however be taken about the delay between the acquisition of I_{donor} and I_{FRET} in order to avoid artifacts due to cell movement between two images (see methodology section). Traditional system needs a filter cube change and thus a delay of several hundreds of ms between images acquisitions, which is not negligible compare to cells or organelles movements. Instead of changing the fluorescence cube, which may worsen image registration, a faster solution is using a filter wheel between the microscope and the camera, which allow changes in the emission filter

in less than 100 msec. Solutions have also been developed to perform simultaneous acquisitions of both channels as described in the following scheme [49-51]

These widefield configurations allow fast acquisition of both channels but they lack of optical sectioning capability. Confocal microscopes can also be used in the same way with excitation of the donor and simultaneous collection of the fluorescence emitted by donor and acceptor molecules. This allows for three dimensional localization of biosensor response, and video-rate confocal microscopes can be used when a high spatial resolution is needed, as shown by early use of biochemical biosensors [52]. The use of confocal microscope also opens the way to more complex acquisition procedure like spectral imaging.

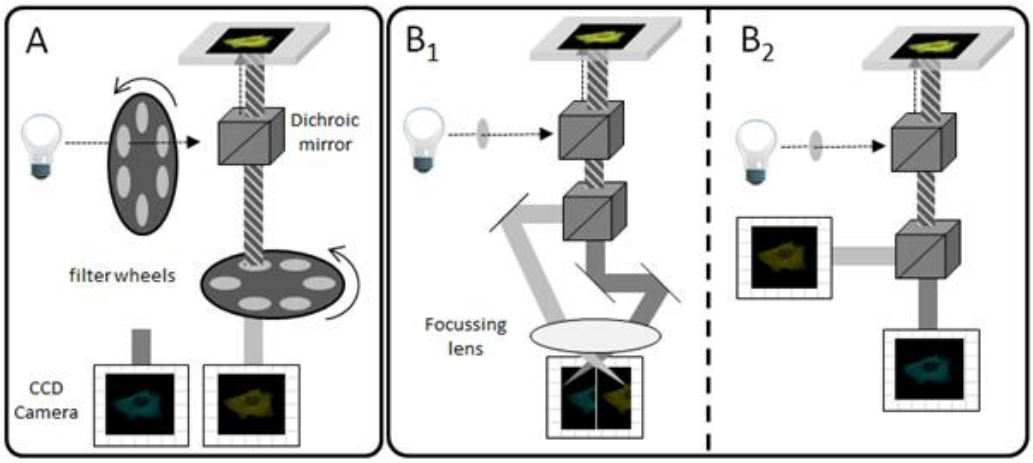

Figure 5: Examples of setup optimized for ratiometric FRET measurements. In panel A, images are acquired sequentially. Fast filter wheel allows fast switching between both acquisitions (10-30ms). In panel B, images are acquired simultaneously. A dichroic mirror is used to separate the emission from donor and acceptor molecules. A focusing lens can then be used for casting the light of both channels on each half of the same camera (B1) or two different cameras can be used for light collection (B2).

Spectral imaging

Most of the newest confocal microscopes are designed for spectral imaging either in sequential mode or most interestingly for biosensor imaging in simultaneous mode [53]. Indeed, for FRET applications, spectral imaging is a slower but more precise configuration for measuring sensitized emission. It consists in measuring for each pixel of an image the overall emission spectrum and not only limited to two bandwidth using filters (see figure 6 for more detail about the setup).

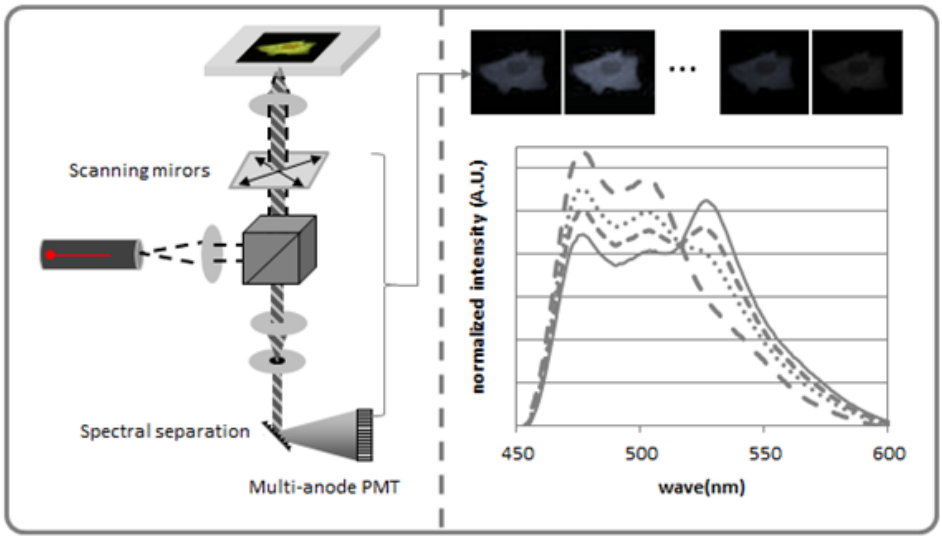

Figure 6: Simplified scheme of a confocal setup allowing spectral imaging in simultaneous mode. Briefly, lasers beam scans the specimen using scanning mirrors. The pinhole conjugated to the focal plane rejects light emitted by objects outside this focal plane and results in optical sectioning. Spectral separation is then achieved by a grating combined to recycling systems allowing minimal loss of light. The light is then collected using a multi-anode PMT. The fluorescence spectrum is recorded for each pixel .

Gathering fluorescence emission spectra then allows donor and acceptor emission spectra to be separated according to the distinct shape of both spectra after spectral unmixing. Fluorescence signal is then analyzed in the same way as with traditional ratiometric images. It however allows distinguishing the real FRET signal from other elements that may alter this measurement, such as autofluorescence or the presence of multiple fluorophores in the sample and can then be used in more complex biological environments.

Lifetime based approaches

Fluorescence lifetime is inherently quantitative and is most of the time independent on the concentration of fluorophore. Furthermore, FRET FLIM experiments only need measurements of the donor fluorescence lifetime (cf. Eqs. 16, 18 and 29), which makes it extremely valuable for simultaneous multi biosensor measurements. Lifetime measurement however requires dedicated and more sophisticated instruments than ratiometric imaging. It can be determined in either the time domain (TD FLIM) or the frequency domain (FD FLIM) (Fig. 7). In the following paragraphs, we will focus on the two most representative techniques: Time Correlated Single Photon Counting (TCSPC) for TD FLIM and phase and modulation measurements for FD FLIM.

Time domain: TCSPC

Most TCSPC systems are implemented on confocal microscope equipped with:

- A pulsed laser source. The source must produce short laser pulses (from several hundred femtoseconds to picoseconds width) with a frequency usually ranging from 10 to 80 MHz. It is interesting to note that Ti:Sa laser matches these specifications which can be of great help for deep and non-invasive biosensor imaging.
- Detectors with a fast instrumental response. Optimal instrumental response function can be obtained using multi-channel plate or latest generation of avalanche photodiodes (<50ps full width at half maximum) but they are extremely fragile and require special handling care. TCSPC manufacturers thus also provide more robust detectors i.e. optimized Photo-Multiplier Tubes, with an IRF around 250ps adapted for TCSPC experiments but which necessitates particular attention during photon decay curves analysis.
- Photon counting card. All of them rely on the same principle based on a time amplitude converter. It consists in a linear tension ramp started by the arrival of a photon and stopped by the next laser pulse. The output voltage will thus be proportional to the photon arrival time. However, the ramp is only triggered by a photon arrival followed by a laser pulse, which means that if two-photon are acquired between two laser pulses, only the first photon will be measured. This is the pulse pile up effect (Fig 8A). To avoid this statistic selection of fastest photons, one have to limit the acquisition frequency to one hundredth of the excitation frequency (giving rise to an error every 10,000 photons) which explains the longer acquisition time of this technique.

An example of such a setup [23] is presented in figure 8B.

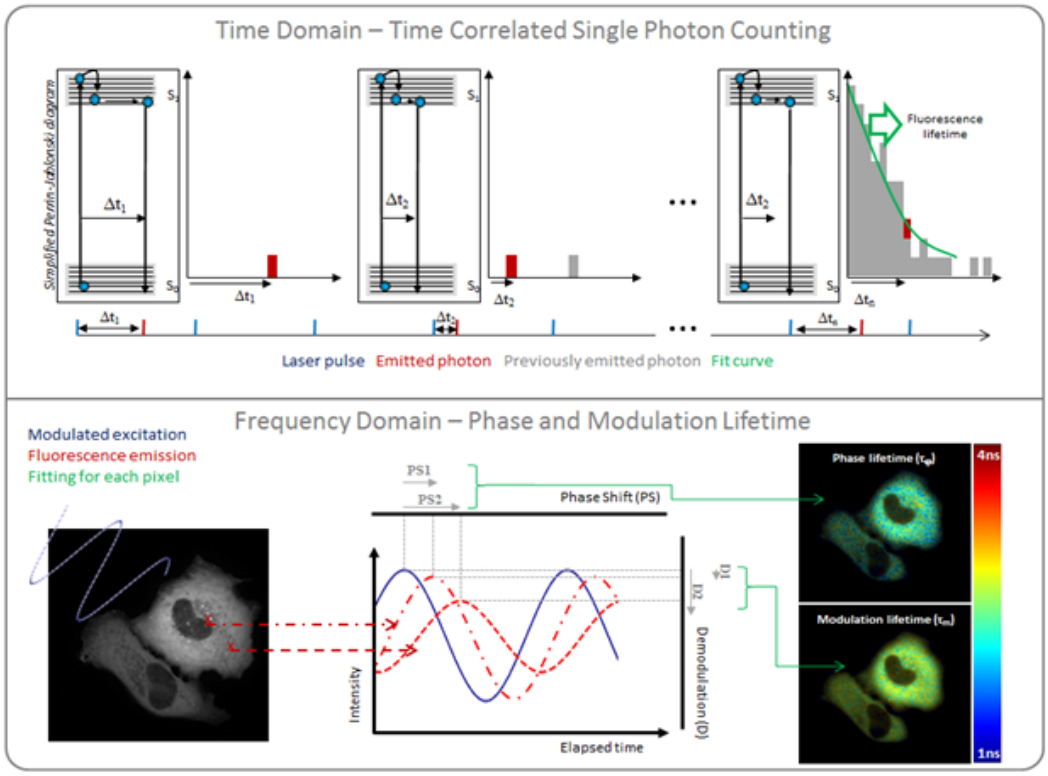

Figure 7: Principle of lifetime measurements. (**A)** In time domain, a pulsed laser is used to excite fluorophores. The time between photon excitation and emission is measured and it is accumulated to get an histogram of photon emission time. Fluorescence lifetime is then estimated from the slope of this exponential decay. (**B**) In frequency domain; a modulated excitation is used to excite the sample. Monitoring of fluorescence phase and modulation shift compared to a reference with known fluorescence lifetime is used to calculate phase and modulation lifetimes.

Frequency domain: phase and modulation

In many experimental FD FLIM systems described in the literature, the modulated excitation light source is composed of a laser (laser diodes, solid-state, gas or dye lasers) combined with an external modulator (either an acousto-optic modulator or an electro-optic modulator) [54-56]. Recently, the advent of commercially available light emitting diode (LED), which can be directly modulated, contributed to simplify the instrumentation and reduces the cost of FD FLIM systems [57-59].

Measurement of the phase and modulation quantities can be performed with two approaches: the heterodyne and the homodyne methods. The heterodyne method is the preferred approach for accurately estimating fluorescence lifetime components in cuvette experiments. It has also been successfully applied in FLIM experiments by combining it with scanning mode and single channel detector (usually with a gain modulated photomultiplier [54]). This method is thus compatible with laser scanning

microscopes (such as confocal and multiphoton microscope), which offer high three-dimensional spatial resolution, and good signal to noise ratio.

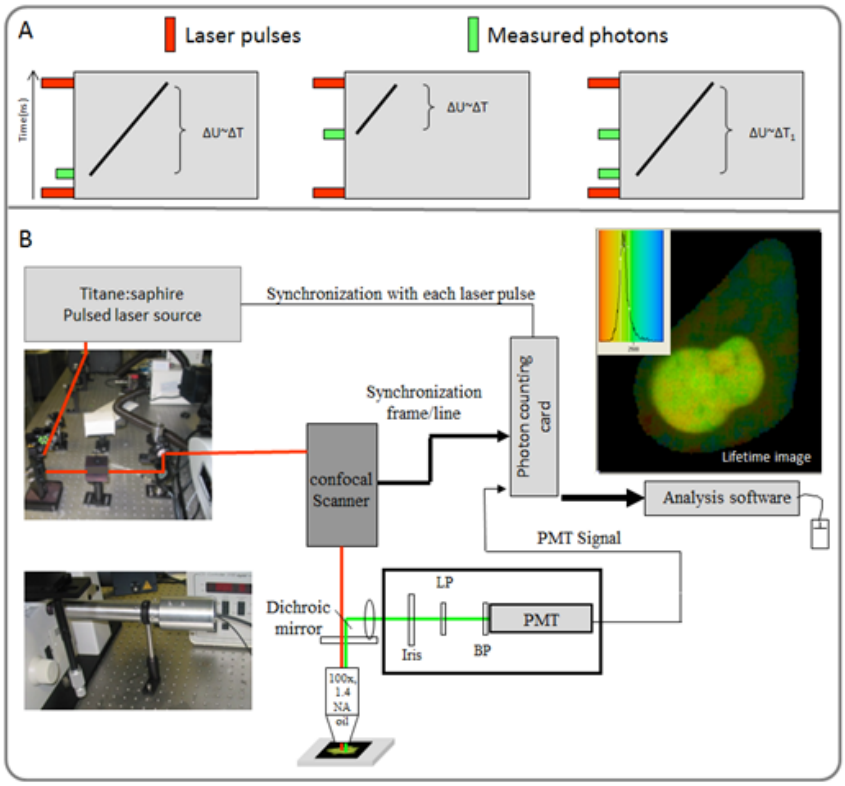

Figure 8: A: Principle of the time amplitude conversion. On the left, a fast photon is measured and starts the linear tension ramp resulting on a large ΔU corresponding to the difference in time between a photon emission and the following laser pulse. While excitation is at constant frequency, the measured ΔU is proportional to the photon emission time. The same explanation is also valid for a slow photon (middle scheme). However, if two photons are emitted between two laser pulses, only the first one is measured. This effect called "pulse pile up" induces an artifactitious decrease in the measured fluorescence lifetime. **B:** scheme of a typical TCSPC acquisition setup with a laser source allowing two-photon excitation. Pictures on the left show the injection of infrared laser in a confocal scanhead (upper panel) and the detection module adapted on the descanned position of the confocal microscope.

The homodyne method, which consists in modulating the excitation light and the detector at the same frequency, is routinely used in many biological and biophysical laboratories because it can be performed with widefield detectors (like a modulated intensified CCD camera). This approach has then been implemented in classical fluorescence widefield microscopy which enables rapid FLIM image acquisition [57-60]. However, one limitation inherent to this system is the non-confocality of the excitation, and consequently of the fluorescence emission. For improving axial discrimination of the FD FLIM system, it can be simply combined with either a single plane illumination strategy [61] or a spinning disk module [62, 63] (an example of such an implementation is presented in figure 9).

Nowadays, several companies (ISS, Intelligent Imaging Innovations, Lambert Instruments) propose commercial FD FLIM systems that can be fully integrated with all commercial multiphoton, confocal or wide-field microscopes.

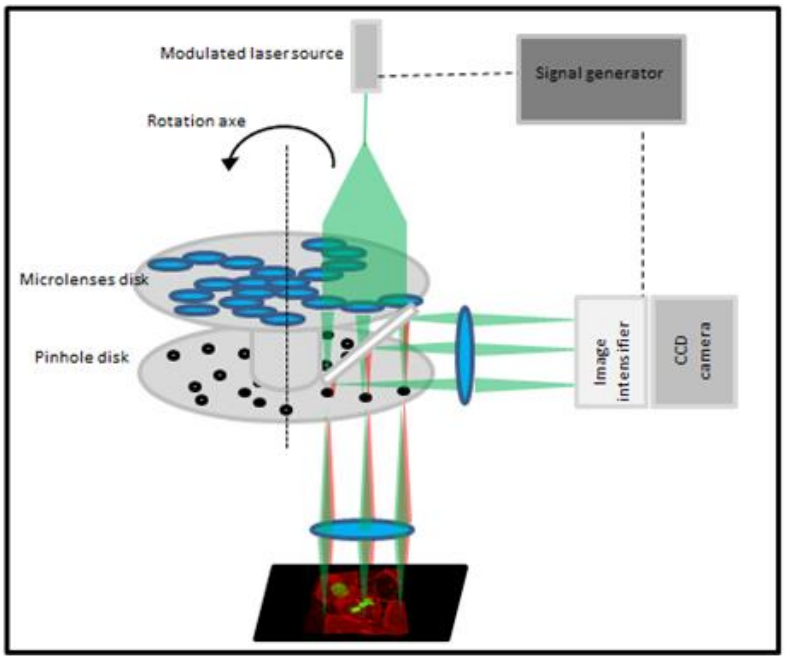

Figure 9: Scheme of a phase and modulation acquisition system adapted on a spinning disk system to ensure fast fluorescence lifetime measurement with optical sectioning capability.

3.2.5. Data analysis

3.2.5.1. Ratiometric Imaging

Data processing for reaching quantitative FRET measurements between two fluorescent molecules with ratiometric imaging has been exhaustively covered [64-66]. Briefly, in order to correct for both varying unknown concentrations of the donor and acceptor and instrumental artifacts (e.g. spectral bleed-through), a large number of methods have been proposed with different number of images and thus different level of complexity [64, 65, 67]. Among all these, the most robust and widely used requires the acquisition of three fluorescence images. In this case, the ratio *R* is defined by [68]:

$$R = \frac{I_{FRET} - \alpha \times I_{Donor} - \beta \times I_{Acceptor}}{I_{Donor}} \quad (27)$$

where $I_{Acceptor}$ is the fluorescence intensity measured with acceptor emission filter after acceptor excitation, I_{Donor} and I_{FRET} are fluorescence intensities measured

respectively with spectral bandpass of donor and acceptor after donor excitation, α and β are the correction factors for respectively the bleed-through of the donor into the acceptor emission filter after donor excitation and the bleed-through of the acceptor into the acceptor emission filter after donor excitation.

In the particular case of a single-chain biosensor, the expression (27) can be simplified. Indeed donor and acceptor concentrations are identical which implies that bleed-through correction factors α and β are linearly dependent and that fluorescence intensities $I_{Acceptor}$ and I_{Donor} are proportional. By taking into account these simplifications, a straightforward calculation leads to:

$$R = \frac{I_{FRET}}{I_{Donor}} - c \qquad (28)$$

where *c* is a constant dependent on the fluorophores properties. This constant which is just an offset modification of the ratio *R* does not give any supplementary information.

For a single-chain biosensor, the ratio *R* is then fully described by fluorescence intensities ratio I_{FRET}/I_{Donor}. Consequently the third fluorescence image $I_{Acceptor}$ (see Eq. (27)) is not useful; this additional image acquisition will just increase the complexity of instrumentation, the time of acquisition (and thus the related movements artifacts) and the noise propagation in the ratio calculation.

Even if the expression of the ratio is extremely simple, we emphasize on the fact that obtaining reliable *R* values requires a special care and numerous corrections which have been exhaustively detailed elsewhere [68, 69]. Briefly, we need to compensate for instrumental artifacts (camera offset subtraction, shading or flat-field correction for the non-uniformity of the illumination, correction for misalignments between two fluorescence images due to chromatic aberration) and for chemical and biological artifacts (photobleaching correction for taking into account that the donor and acceptor photobleach at different rates [70]), optional autofluorescence subtraction, correction for cell movement or deformation between acquisition time).

Calculation of the corrected ratio *R* from acquired fluorescence images can be performed instantaneously pixel by pixel and calculated *R* values can be displayed with pseudo-color superimposed on the fluorescence intensity image in real time enabling to follow in live the biosensor activity [71-73] (see Fig.10). Ideally for a

sensor binding to a single molecule (like fura-2), the ligand concentration [*L*] is directly related to the ratio as [74].

$$[L] \propto \frac{R - R_{\min}}{R_{\max} - R} \tag{29}$$

where R_{min} and R_{max} are respectively the minimal and maximal ratios. However, regarding single chain biosensors, it is usually not possible to have access to these ratios. In this case, the normalized ratio $\Delta R/R_{t0}$ can be used for facilitating the comparison between all cell responses (cf. Fig.10). This normalized ratio is defined by

$$\frac{\Delta R}{R_{t_0}} = \frac{\left| R - R_{t_0} \right|}{R_{t_0}} \tag{30}$$

where R_{t0} is the initial ratio (measured at time t=0).

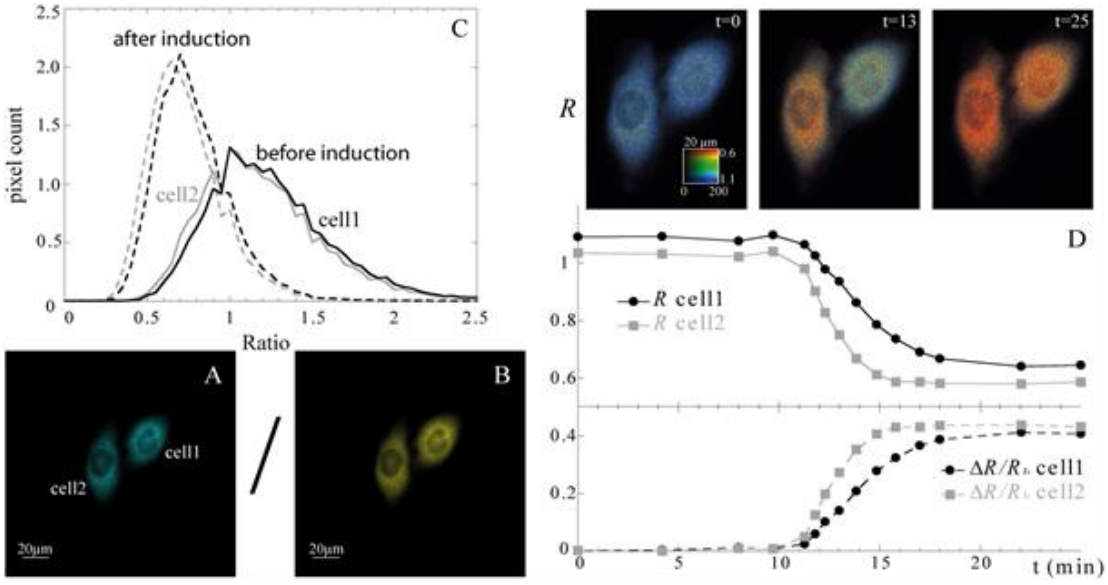

Figure 10: Data analysis for FRET imaging with a standard wide field epi-fluorescence microscope. The fluorescence intensity images of living cells transfected with $^{T}Epac^{VV}$ acquired with two distinct filters sets: donor emission and acceptor emission (after donor excitation) are shown respectively in (**A**) and (**B**). The resulting ratio *R* can be calculated pixel by pixel (after instrumental correction) and the ratio distributions of both cells are indicated in (**C**) before (t=0) and after induction (t=25min). The mean ratio is extracted from these distributions for each cell and it is plotted as a function of time in (**D**). The corresponding ratio images are also represented in the upper part of the panel. Finally, we have also indicated in (**D**) the normalized ratio $\Delta R/R_{t0}$ which simplifies the comparison between cell responses.

We emphasize on the fact that this normalized ratio (and the ratio *R*) gives just an indication on relative changes between the biosensor “on” and “off” state. In other words, determination of individual concentrations of both biosensor states with

ratiometric imaging is not feasible in the cellular environment [75], since all biosensors expressed are not optically active. In fact, the maturation and the photo-degradation (photobleaching) of the two fluorescent proteins (donor and acceptor) are processed at different rates [70, 76]. This leads to a population of biosensors whose fluorescence emission is no more related to the physiological state of the cell (unresponsive donor only and acceptor only single-chain biosensor).

3.2.5.2. Fluorescence Lifetime Imaging

Unlike ratiometric imaging which is based on fluorescence intensity directly related to the fluorophore concentration (of both the donor and the acceptor), lifetime measurements are independent of these concentrations. It allows determining quantitatively the proportion of interacting donor and the FRET efficiency in living cells.

Frequency Domain (FD) lifetime imaging

- **Recovering phase shift and modulation depth in single frequency experiments.**

The first step of FD FLIM data analysis consists in retrieving the phase and modulation values (φ and m) from fluorescent images acquired with either the heterodyne or the homodyne method (see section II: FRET measurements).

With the heterodyne method, the detector is modulated at a frequency $\omega+\Delta\omega$ (where $\Delta\omega$ is a low frequency in the kHz range) which is slightly different of the modulation frequency ω of the excitation source. The resulting signal collected by the FLIM system ($S_{\text{heterodyne}}$) is thus modulated in time at the low frequency $\Delta\omega$

$$S_{\text{heterodyne}} \propto 1+\frac{m_{ex}m_{de}m}{2}\cos(\Delta\omega t+\Delta\phi-\varphi) \qquad (31)$$

where $\Delta\varphi$ is the phase shift between the excitation and the detection, m_{ex} and m_{de} are respectively the modulation amplitude of the excitation and the detection. By recording this signal $S_{\text{heterodyne}}$ at various time-delays t and by fitting it as a function of time with a cosine function of the low cross-correlation frequency $\Delta\omega$, we can extract the phase shift φ and modulation depth m for each pixel of the FLIM image.

In the homodyne implementation (when the frequency of the excitation and detection are identical), the collected signal which is no more modulated is a DC component defined by

$$S_{\text{homodyne}} \propto 1 + \frac{m_{ex} m_{de} m}{2} \cos(\Delta\phi - \varphi) \tag{32}$$

with m_{ex} and m_{de} respectively the modulation amplitude of the excitation and the detection. The phase shift $\Delta\phi$ between the excitation and the detection varies from 0 to 360° (2π) with K equally spaced intervals. For each phase shift $\Delta\phi$, the DC collected signal is recorded for each pixel of the FLIM image. By fitting this collected signal S_{homodyne} with a cosine function of $\Delta\phi$, the resulting phase φ and modulation m are calculated pixel-by-pixel (cf. Fig.11).

- **Calculation of the fluorescence lifetime and data representation**

Once phase φ and modulation m have been determined for each pixel of the image, these m and φ values are further manipulated for evaluating the fluorescence lifetime of the sample. In order to obtain correct lifetime values with both methods (heterodyne and homodyne method), calibration of FLIM system with a reference of known fluorescence lifetime τ_{ref} is indispensable for taking into account the phase shift and modulation introduced by the electronics and optics (cf. Eqs. (31)-(32)). The fluorescence lifetime of an unknown sample is then defined by [77]

$$\tau_m = \frac{1}{\omega} \sqrt{\frac{m_{ref}^2}{m^2} \left(1 + \omega^2 \tau_{ref}^2\right) - 1} \tag{33}$$

$$\tau_\varphi = \frac{1}{\omega} \tan\left(\varphi - \varphi_{ref} + \tan^{-1}\left(\omega \tau_{ref}\right)\right) \tag{34}$$

where φ_{ref} and m_{ref} are respectively phase and modulation values estimated from the reference. We emphasize on the fact that these fluorescence lifetimes (τ_m and τ_φ) are calculated for each pixel. The resulting FLIM image, which is displayed using a color scale, is usually superimposed on the intensity image in order to highlight the brightest regions (see Fig.11).

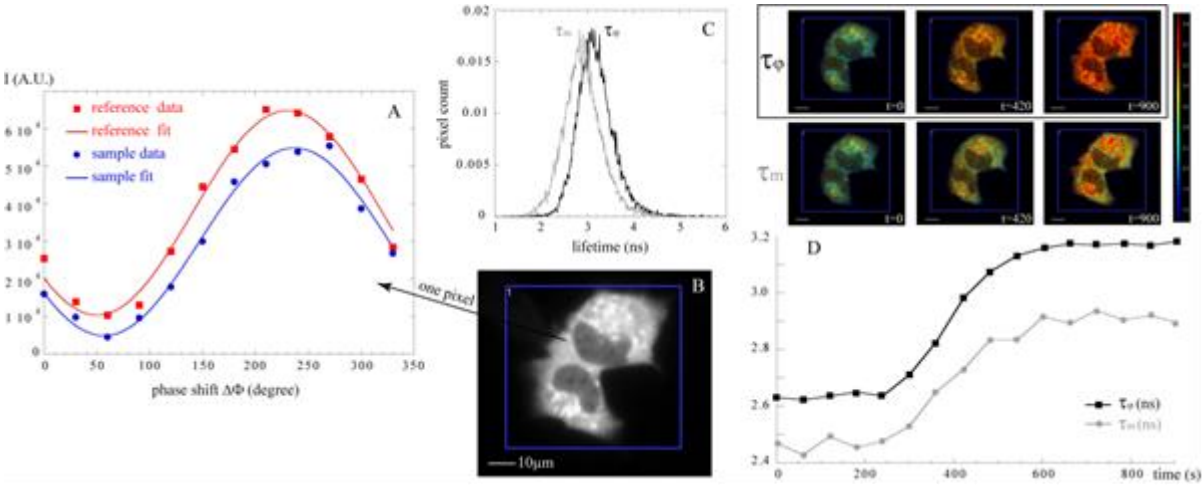

Figure 11: Data analysis of fluorescence lifetime measurements acquired with homodyne method. (**A)** Experimental reference and sample fluorescence intensities (dots) as a function of the phase shift $\Delta\phi$ between excitation and detection for one pixel; corresponding fits from which we deduced the phase φ and modulation m are indicated with lines. (**B)** Fluorescence intensity image of living cells transfected with ^{T}Epac^{VV}. Phase and modulation lifetimes (τ_m and τ_φ) distributions for the selected area is represented in (**C**). Mean values are deduced from these distributions and their evolutions in time are shown in (**D**). Corresponding phase and modulation lifetime images are also displayed for three distinct times.

When using FD FLIM system to record biosensor activity in living cells, evolutions in time of the phase and modulation lifetimes (τ_φ and τ_m) are sometimes represented [73]. However this method gives just an indication on the relative changes between the two states of the biosensor. In fact, these phase and modulation lifetimes acquired during single frequency experiment do not correspond to true lifetimes of the biosensor. To recover these true lifetime components, it is necessary to acquire multiple frequency FLIM images and to fit pixel by pixel the experimental phase φ and modulation *m* for each frequency ω with a function of ω [59]. Experimental data are usually adjusted to the theory by minimizing an error function (using a Levenberg-Marquardt algorithm) without any *a priory* on lifetime components [59, 78, 79]. If it can be assumed that the lifetime information is the same for all pixels of the FLIM image, data can be globally analyzed [80, 81]. In both cases, obtaining reliable lifetime components is time consuming and it is hardly accessible to the nonexpert.

Time Domain (TD) lifetime imaging

- **Extracting lifetime components**

In time domain methods, fluorescent samples are repeatedly excited by short pulses of light and resulting fluorescence intensity decay histograms can be recorded

for each pixel of the FLIM image with different detectors (see section II). Regardless of the technique employed, experimental lifetime components are usually deduced by adjusting experimental decay histograms with the theory. In TD FLIM, the theoretical detected intensity profile *F(t)* which is dependent of both the fluorescence sample and the instrumentation is defined by Eq. 26.

This fitting procedure is usually performed with the least square method (LSM) which consists in minimizing an error function χ^2 defined as the total squared differences between experimental data points x_i and theoretical values s_i deduced from Eq. (26) :

$$\chi^2_{LSM} = \frac{1}{N_d - p} \sum_{i=1}^{N_d} \frac{(s_i - x_i)^2}{x_i} \tag{35}$$

where N_d is the number of data points and p is the number of fitting parameters. The minimization of this error function is generally performed with the Levenberg Marquardt algorithm which has been implemented in most of the commercially available FLIM analysis software. This commonly used FLIM image analysis strategy is robust and gives reliable results when the number of photons is large [8, 11, 23, 82] (cf. Fig.12).

However, if the total number of photons is low, the LS method becomes inaccurate because its error function assumes that the noise is described with a Gaussian instead of a distribution which is incorrect. In the case of a low number of photons, one solution named adaptive Monte Carlo data inflation algorithm (AMDI) consists in inflating statistically the number of photons for being compatible with the LS method [11]. Another possibility which is called the maximum likelihood estimation (MLE) method [82, 83] is to modify the error function for taking into account the Poisson noise distribution. This error function is now defined as [83]:

$$\chi^2_{MLE} = \frac{2}{N_d - p} \sum_{i=1}^{N_d} (s_i - x_i) - \frac{2}{N_d - p} \sum_{i=1}^{N_d} x_i \ln\left(\frac{s_i}{x_i}\right) \tag{36}$$

It was demonstrated that both solutions (AMDI and MLE methods) give an accurate lifetime components estimation of multi-exponential intensity decays with a reduced number of photons, in comparison with the LS method [11, 82]. Finally, it has been recently demonstrated that an alternative method based on Bayesian analysis enables to estimate correctly the lifetime of mono-exponential decays with

few photons [84]. However this method was never applied with multi-exponential decays which prevents from envisaging it in the context of biosensor activity measurements.

- **Exploiting data**

As already mentioned, the fluorescence intensity decay of a single-chain biosensor is described with multi-exponential terms (cf. Eq. 10).

Regardless of the fitting method employed (and previously described), the final purpose of the FLIM data analysis is to correctly extract both the proportions and the lifetime components for each pixel of the image. This can be achieved preferentially without constraining any fitting parameters (cf. Fig.12). However, for sample emitted fluorescence whose intensity decay is multi-exponential, the correct estimation of all parameters with standard fitting method requires a large number of photons (N>100000 [85]). For decreasing this number and consequently the acquisition time and phototoxicity, we have already detailed in previous paragraphs two solutions based on algorithm implementation (MLE and AMDI). An alternative solution consists in reducing the number of fitting parameters by constraining one of them, for example the donor lifetime but it necessitates that the donor lifetime is mono-exponential and that it has been precisely determined in a previous experiment (which requires a modified biosensor without acceptor). Another possibility is to analyze the data globally but it is valid only if one can assume that the lifetime information is identical for all pixels of the FLIM image (or a selected area) [86, 87]. In all cases, it requires expertise and computation time for obtaining reliable lifetime values with fitting methods.

Once lifetime components have been correctly estimated, resulting lifetime images are displayed using a color scale and are usually overlaid on the intensity image for weighting the lifetime value with the fluorescence intensity (cf. Fig.12). However, due to the large number of parameters (proportion and lifetime components), it is not possible to represent the evolution of all of them. In order to simplify data representation, the mean lifetime τ_{mean} defined by Eq. 13 has been largely used in FRET experiments [8-11]. However, the mean lifetime does not correspond to the correct average lifetime which is defined by Eq. 12. This average lifetime has been recently used for biosensor activity recording [88]. However, we

should inform the reader that this quantity is not monotonous as a function of the donor lifetime in presence of the acceptor. In other words, one average lifetime value can be found with two distinct donor lifetimes in presence of the acceptor for a fixed proportion of interacting donor. Consequently the knowledge of both the average lifetime and the fraction of interacting donor are not enough to entirely characterize the fluorescent sample. Due to the non-uniqueness of the average lifetime, it is also necessary to combine them with another parameter (e.g. FRET efficiency).

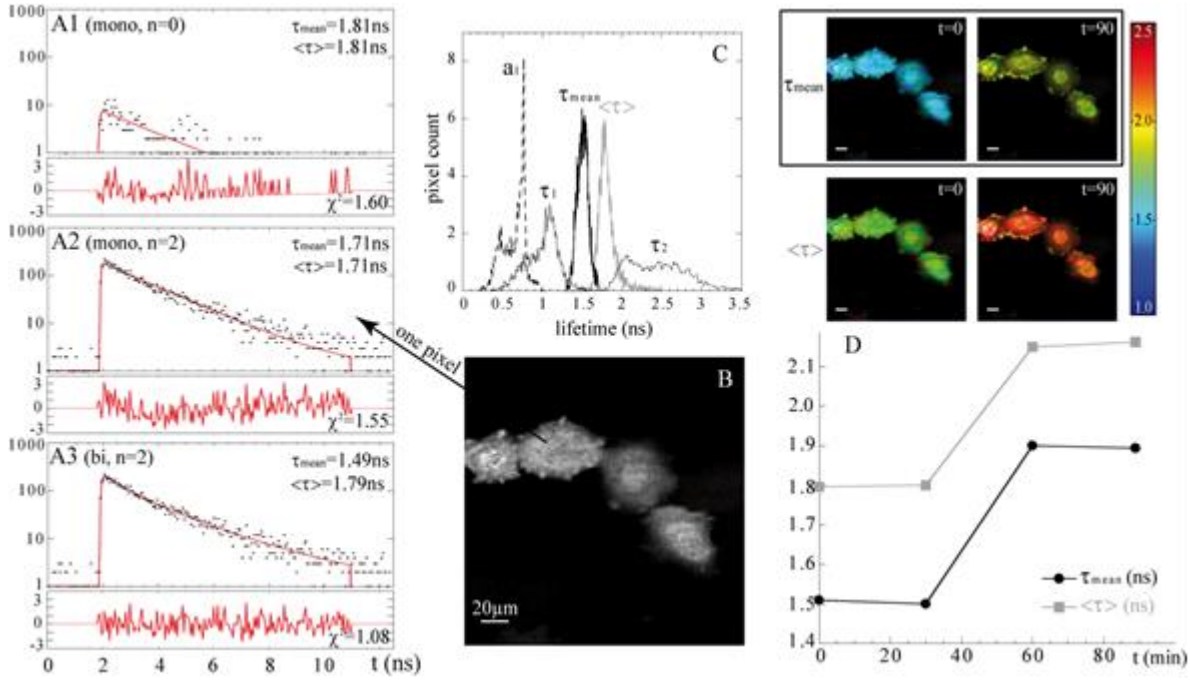

Figure 12: Data analysis of fluorescence lifetime measurements acquired with the time correlated single photon counting (TCSPC) method. **A1**: typical experimental intensity decay (dots) acquired in few ms per pixel (corresponding to an acquisition time of 300s for the complete image represented in B); the fit obtained with standard least square method (LSM) is indicated with line. Due to low number of photon count *N*, the error function (χ^2) is non flat and elevated indicating that the adjustment is not perfect. **A2**: one possibility to increase *N* consists in applying a spatial binning of factor n (sum all pixels comprised in a $(2n+1)^2$ squared region). In this case, the fit is slightly improved but χ^2 is still non flat because the monoexponential model is not adapted. **A3**: when the biexponential model is used, the fit is satisfying which means that the sample proportion and lifetime can be correctly estimated. (**B**): fluorescence intensity image of living cells transfected with $^{T}Epac^{VV}$. The distributions of all fitting parameters (α_1, τ_1 and τ_2) for the complete image are shown in (**C**). We have also represented the mean lifetime τ_m and the average lifetime $<\tau>$ distributions. Their evolutions as a function of time are plotted in (**D**). The corresponding mean and average lifetime images are also displayed in the upper part of the panel.

Non fitting based approaches

In the previous section, we mention the fact that the correct analysis of the acquired fluorescent signal with fitting methods is time consuming and necessitates a high level of expertise. In order to simplify the analysis of FLIM images and to make it accessible to the non-expert user, novel methods based on non-fitting approaches

have been developed recently [89-92]. In this section, we limit our review to two approaches which are applicable to a large range of lifetime acquisition techniques: the minimal fraction of interacting donor (mf_D) [90] and the polar approach or phasor [89, 91]. We then voluntary omit the rapid lifetime determination which is restricted on time gated FLIM images with two temporal channels [93, 94].

The minimal fraction of interacting donor mf_D which has been introduced by Padilla-Parra et al. [90] can be applied with all TD FLIM techniques (TCSPC, Time Gated,…). It is defined by

$$mf_D = \frac{1-\langle\tau\rangle/\tau_2}{\left(\langle\tau\rangle/(2\tau_2)-1\right)^2} \tag{37}$$

where τ_2 is the lifetime of the donor alone and $<\tau>$ is the mean lifetime defined by Eq. (12) (see previous section). The computation of $<\tau>$ is straightforward and it can be performed pixel by pixel and be recovered on-line during FLIM acquisition. When the lifetime of the donor alone τ_2 is mono-exponential and known (implying that it has been measured in a previous experiment which is typically not performed in biosensor experiment), we deduce from Eq. (37) that the computation of the mf_D is a simple calculation that can be performed on-line on a standard computer. This is a major advantage when following the biosensor activity during time in live cells, since the user has immediately quantitative information which is the minimal fraction of interacting donor. This indicator varies between 0 when there is no interaction and 1 when all the donors interact. It is a robust indicator however we remind the reader that it only gives information on the minimum of the interacting proportion and not on the exact quantity α_1.

The polar approach or phasor is another non-fitting method that has been successfully applied in FLIM experiments. This method was initially described by Jameson et al. [95] and then successively improved by different groups [96-98]. It consists in converting the lifetime image into a new two dimensional histogram called polar or phasor. In this polar representation, each point which is defined with [*u;v*] coordinates corresponds to one pixel of the FLIM image and vice versa. Consequently, one FLIM image is transforming into a scatter diagram whose position gives an indication on the number of exponential present in the intensity decay. For example, when the fluorescence emitted by the sample decays mono-exponentially,

the scattered diagram is localized on the semicircle centered at [0.5, 0] with a radius of 0.5 (see Fig.13). Short fluorescence lifetimes are close to the coordinates [1, 0], whereas long lifetimes approach the origin ([0, 0]). If multiple lifetime components are present in the sample, the scattered histogram is located inside the semicircle which can be helpful for identifying a mixture of several molecular species or a FRET phenomenon [89, 96]. This approach can be applied with both FD [96] and TD [89, 92] FLIM acquisition systems and it has been recently used with biosensor [75, 99].

In TD FLIM experiments, the *u* and *v* coordinates are respectively the cosine and sine transforms of the fluorescence intensity decay *I(t)* and they are defined by

$$u = \int I(t) \times \cos(\omega t) dt \Big/ \int I(t) dt \tag{38}$$

$$v = \int I(t) \times \sin(\omega t) dt \Big/ \int I(t) dt \tag{39}$$

where ω is the laser repetition angular frequency.

For FD FLIM experiments, ω is the angular frequency of light modulation and the *u* and *v* coordinates which are directly related to the phase φ and modulation *m* measured with the FD FLIM system, are given by

$$u = m\cos(\varphi) \tag{40}$$

$$v = m\sin(\varphi) \tag{41}$$

In both cases (TD and FD FLIM experiments), determination of the [*u,v*] coordinates can be performed instantaneously. However, the polar representation gives just visual information on the biosensor state but it does not allow obtaining really quantitative information on FRET parameters.

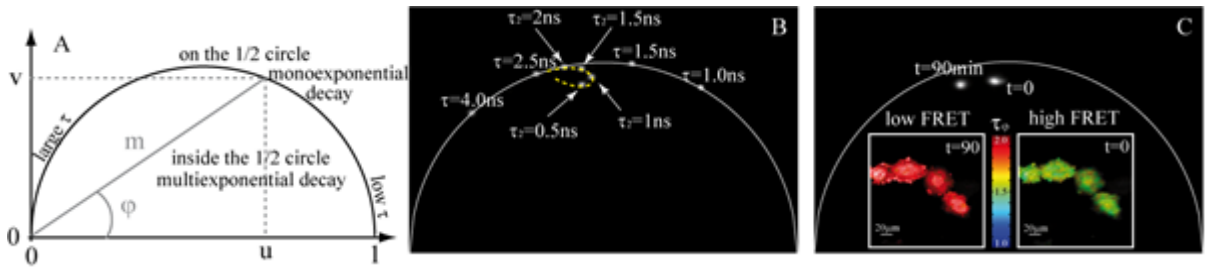

Figure 13: Data analysis of fluorescence lifetime measurements with the polar approach or phasor. **A**: illustration of the polar representation. Lifetime measurements of fluorescent sample with single exponential decay are localized on the semicircle. If multiple lifetime components are present in the sample, the FLIM acquisitions are located inside the semi-circle. **B**: example of the polar representation with simulated FLIM images. As expected, spots corresponding to FLIM images simulated with monoexponential decays are positioned on the semi circle and spots issues from

simulated data with biexponential decays are inside. We have also represented with dashed line the FRET trajectory for a proportion of interacting donor α_1=0.5. **C:** application of the polar representation to biosensor experiment realized in living cells transfected with $^{T}Epac^{VV}$. We can clearly distinguish two spots corresponding to both conformations of the biosensor (high FRET and low FRET). We have also displayed resulting phase lifetime images.

Recently, Leray and coworkers have demonstrated that it is possible to retrieve quantitatively the FRET parameters from the polar coordinates [91]. In fact, the fraction of interacting donor α_1 and the fluorescence lifetime of the donor in presence of the acceptor τ_1 can be analytically expressed with [91]

$$\tau_1 = \frac{1-u-v\tau_2\omega}{\omega\left(v-u\tau_2\omega\right)} \tag{42}$$

$$\alpha_1 = \frac{\tau_2 \times \left(1+\tau_1^2\omega^2\right)\left(1-u-u\tau_2^2\omega^2\right)}{\left(\tau_1-\tau_2\right)\left(-1+u+u\tau_1^2\omega^2+\tau_1\tau_2\omega^2+u\tau_2^2\omega^2+u\tau_1^2\tau_2^2\omega^4\right)} \tag{43}$$

If the lifetime of the donor alone τ_2 is mono-exponential and it has been measured in a previous experiment (requiring a modified biosensor without acceptor), we can easily deduce from Eqs. (42)-(43) both the lifetime of the donor in presence of the acceptor and the fraction of the interacting donor. We emphasize on the fact that these calculations can be performed during the time lapse acquisition of the biosensor activity which makes possible to follow in live the evolution of both the FRET efficiency and the proportion of interacting donor α_1.

3.2.6. Design and optimization of genetically encoded Kinase activity reporters (KARs)

Design of a FRET-biosensor for imaging biochemistry in live cells is based on the development of a single polypeptide capable of generating a conformational change which modulates FRET efficiency in response to a biochemical event such as phosphorylation in this context.

A genetically encoded kinase activity reporter is composed of the following key elements: a molecular recognition element (MRE) consisting of a substrate peptide for the kinase of interest and a phosphoamino acid binding domain to detect the target activity, and a reporting element consisting of a fluorescent protein-based FRET couple flanking the sensing element. These functional parts are pasted together with linkers whose optimization is needed as they readily affect overall biosensor dynamic range. (Fig. 14).

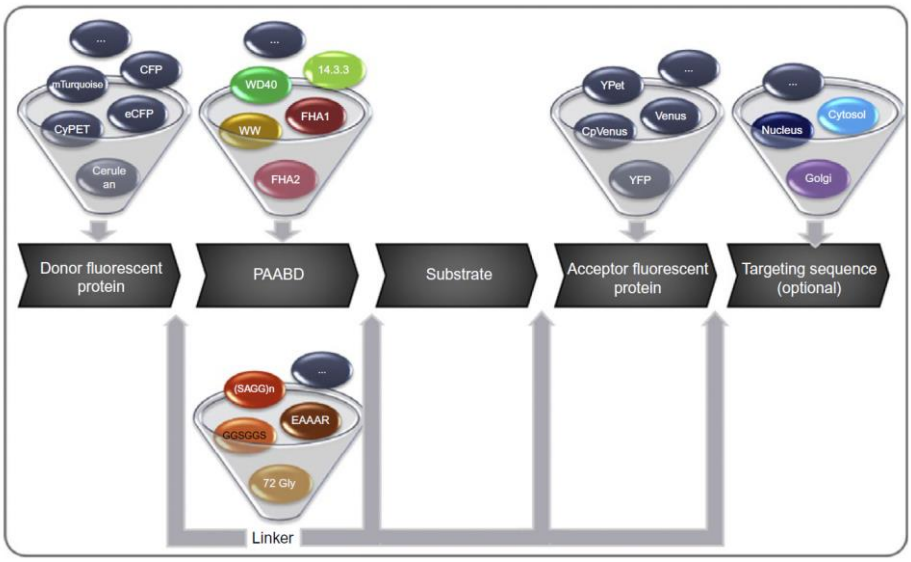

Figure 14: Necessary ingredients for making KARs.

The identification and/or optimization of the different constituents of a KAR are reviewed in this section. A range of kinase activity reporters has been designed on this model and allows activity monitoring of many tyrosine and serine/threonine kinases.

3.2.6.1. Substrate peptide identification

Many methodological approaches have proven themselves useful in order to identify and characterize that a peptide sequence acts as a specific substrate for a kinase of interest.

The first approach identifies a specific substrate *in silico* by using databases of known substrate sequences of kinases such as UniProtKB/Swiss-Prot which provide reliable protein sequences associated with a very high level of annotation and high level of integration with additional databases. However, peptides selected by some knowledge-based libraries (such as UniProt for instance) can have multiple phospho-acceptor sites. Others database such as KinasePhos can predict phosphorylation sites within given proteins and provides information on the exact positioning of phosphorylation sites with a link to the corresponding catalytic protein kinases involved [4].

Another approach relies on the use of the kinase target sequence from a protein known to be phosphorylated by the kinase of interest. Since many kinases have multiple isoforms, substrate sequence could be modified to be more specific

toward a protein kinase isoform. The protein kinase C family, with its 10 members, is a good example [100, 101]. The first genetically encoded PKC-FRET-based reporter (CKAR) is an effective reporter for all PKC isoforms [102, 103] but each isoform has its own activation signature [104]. Kajimoto *et al.* have designed a new genetically encoded reporter based on the first CKAR but with an ultra specific substrate to measure only PKCδ activity in different cell compartments. In order to make CKAR more selective for PKCδ, they selected 11 known substrates of PKCδ threonine as phospho-acceptor residue and isoleucine at the position +3 was kept to facilitate binding of the PAABD (see below, section phosphoamino acid binding domain (PAABD)). Sensors with candidate substrate sequences were characterized *in vitro* and *in cellulo* (see below, section *in vitro* and *in cellulo* characterization) for specificity and selectivity. While being time-consuming, it can provide highly specific and selective kinase activity reporter.

The last approach enables the identification of protein kinases substrates through large-scale analysis using high-density peptide microarrays from various biological samples. The use of high throughput technologies has become an essential step to create and/or optimize a kinase activity reporter especially when specific substrates of the kinase of interest are not yet known (for review[105]).

To this extent, two libraries are established for substrate identification with peptide microarray. First, knowledge-based libraries contain many small peptide sequences isolated from known proteins. The second library contains *de novo* synthesized peptides using either randomly generated peptides or a combinatorial approach. The first type of library allows the determination of phosphorylation sites using overlapping peptide scans from a known protein sequence. Furthermore, combinatorial and randomly generated peptides libraries are useful to detect specific kinase substrates. Combinatorial libraries defined one or more amino acids at fixed positions (*eg* isoleucine at +3 position after the unique phospho-acceptor residue) while other amino acids (except serine, threonine, tyrosine) are placed at randomized positions. The number of generated peptides is very high compared to knowledge-based libraries. Combinatorial libraries have successfully identified PKA [106, 107] and PKG substrates [107, 108].

In some cases, a phosphorylation site cannot solely determine substrate specificity of protein kinases. Substrate specificity is also determined by short

sequences named “docking site” which are specifically recognized by a kinase. Indeed, many studies report that docking sites dramatically increase the efficiency with which a substrate is phosphorylated by a kinase *in vitro* and *in cellulo* [109-111]. The case of the kinase MAPK/ERK is a good example because MAPK family members such as ERK, p38 and JNK have similar phosphorylation sites. Distinct docking sites for ERK, p38 and JNK have been identified. It ensures substrate targeting and can be used to design a kinase activity reporter with high sensitivity and selectivity.

Erkus was the first genetically encoded FRET biosensor of ERK activity in different compartments of single living cells [112]. Erkus has a docking site (D domain) connected to the C-terminal of the sensor. This D domain is a common docking site contained in most known endogenous substrates of ERK and increases the probability of substrate phosphorylation by ERK [113, 114]. However, Harvey *et al*. [38] developed a new genetically encoded FRET-based biosensor EKAR (EKARc and EKARn target cytoplasm and nucleus respectively). As an improvement, EKAR exhibits a new ERK-specific docking site (FQFP), adjacent to the substrate resulting in a FRET signal 3 times larger than that of Erkus, while others potential docking sites tested in this context greatly reduced FRET signal of the sensor. This shows that docking sites are very important in the design of new specific and selective kinase activity reporters, (See for review [115]), and was recently highlighted in a sensor for the M-phase promoting factor [116].

3.2.6.2. Phosphoamino acid binding domain (PAABD)

Upon specific phosphorylation, the PAABD recognizes and binds to the phosphorylated substrate resulting in a conformational change of the polypeptide that somehow alters in opposite way the fluorescence emission of the two fluorophores and the choice of a good PAABD is a key element of KAR design [117]. Protein phosphorylation may lead to the formation of molecular signaling complexes through interactions between specific phosphorylated residues and binding domains. Several binding domains named “modular domains” and “adaptors molecules” have been well characterized and are able to activate a specific pathway. Activation of transmembrane receptors triggers phosphorylation on tyrosine residues that results in the recruitment and binding of adapter molecules such as Src-homology 2 / 3 (SH2 SH3) and phosphotyrosine binding (PTB) domains. Similarly, signal transduction

involves phosphorylation on serine/threonine residues and thus constitutes consensus sequences recognized by other adapter molecules including 14.3.3 proteins, forkhead associated (FHA) domains, WW domains and WD40 domains. The phospho-acceptor residue within the substrate sequence then first guides the choice of the PAABD.

Several factors should be considered as they can affect the efficiency and the reversibility of the PAABD binding to the phosphorylated substrate. For example, in order to measure compartmentalized PKA activity in single living cells, Zhang *et al.* [118] developed a genetically encoded A-kinase activity reporter (AKAR). This first generation of PKA sensor (AKAR1) used 14-3-3 as a PAABD. Due to the high binding affinity of this PAABD towards phosphorylated substrate, once phosphorylated, the sensor was blocked in closed conformation making it weakly sensitive to cellular phosphatases activity and thus irreversible and incompatible with dynamic measurements of PKA activity. To circumvent this problem, 14-3-3 was replaced by a FHA domain in subsequent versions of AKAR [119], yielding AKAR2. When tested in cells, it showed a better dynamic response and a reversible behaviour. Similarly, a FHA domain was also used in the first Erk biosensor Erkus [112]. Shortly after, the development of EKAR [38] saw the FHA domain replaced by a WW domain. Although both sensors followed the same design principle, comparative analysis of EKAR and Erkus reveals that dynamic response of EKAR is greatly improved; the dynamic range of EKAR was higher than those of Erkus [38].

Considerations regarding FHA and WW domains can be found in [120], and [121], respectively.

3.2.6.3. Optimal linker combinations in FRET-based biosensors

Fooling around with linkers, (ie: swapping linker from one sensor to another) might prove to be an easier way, and should be considered on first instance. Making highly sensitive FRET-biosensors remains difficult and requires fine-tuning. While being dreadful and time consuming, linker optimization is a crucial step in biosensor design. In fact, FRET efficiency depends essentially on the distance and the orientation of the two fluorophores (See section I) [122], which places linkers at the heart of biosensor dynamic range. Linkers are mainly composed of amino acids such as glycine, proline, and alanine giving them full flexibility. The classical flexible linker

consists of (GGSGGS)n which keeps fluorophores at “safe” distance from one another [123], and the rigid linker is composed of (EAAAR)n where FPs are held in “fixed” distance and orientation.

In order to optimize and accelerate the development of FRET-based biosensors, Ibraheem *et al.* [124] have used a reliable high throughput method by undertaking the optimization of a methylation-sensitive H3K27 sensor- H3K27-MetBio (trimethylation of lysine 27 of Histone 3)- mainly based on change in length of linkers. They focused on the optimization of the linker between the PAABD and the substrate. Screening of biosensor variants was performed in colonies of *E.coli*, through the generation of many hundreds of different linker combinations using several screening libraries. The efficiency of H3K27-MetBio was improved with a FRET signal efficiency 2.3 times larger than the original sensor [124] .

In a recent study, Piljic *et al.* focused on the optimization of linker flanking the FPs [125]. They developed a reliable and rapid method to generate multiple genetically encoded FRET sensors variants and tested them in reversely transfected mammalian cells. Long linkers improve the flexibility of the sensor and favor orientation of donor towards acceptor fluorophore even if sometimes, certain short and rigid linkers produce a greater FRET signal [125]. Improvements of biosensors could also be achieved by varying the linker composition in amino acids using combinatorial and randomly generated linker libraries for detecting the most effective linker composition.

Finally, Komatsu *et al*. established highly sensitive FRET biosensor backbones. Their strategy completely abolished the dependence of the sensors on the orientation of the two fluorophores. Indeed, prediction of the exact orientation of the donor and the acceptor in optimized sensor is rather difficult [103, 126]. Instead, they optimized biosensor backbones relying entirely on the distance between both fluorophores by modifying the linker between the PAABD and the substrate [127]. Regular repetitions of the motif (SAGG)n (where n is the number of repetitions (13-61)) and the 72 polyglycine linker [128] were utilized and compared [127]. All generated backbones highlighted that long and flexible linkers reduce the proportion of biosensors folding in the basal state therefore improve the biosensor dynamic range.

3.2.6.4. Choosing a FRET pair

Historically, the first FRET measurements were performed with the blue fluorescent protein (BFP) and the enhanced green fluorescent protein (eGFP) as FRET pair combination [1, 129]. Although these FPs meet the requirements for FRET measurements, BFP has an unfortunate tendency to bleach much faster than eGFP. The Cyan Fluorescent Protein (CFP) and the Yellow Fluorescent Protein (YFP) FRET pair quickly replaced the BFP-eGFP FRET pair to monitor Ca^{2+} variations in individual live cells [130].

The everlasting improvement of fluorescent proteins while beneficial for biosensor optimization could become overwhelming, as the possible combination seems to be endless. Nowadays, cloning procedures are much easier, thus easing up the process. Choice for FRET pairs should be guided by 1) up to date/optimized fluorophores 2) red-shifted to minimize photo-toxicity 3) mono-exponential lifetime when considering FRET-FLIM measurement methods. The idea here is to tap into the distance (Ro) and eventually dipole-dipole orientation (κ^2) in order to maximize FRET efficiency (see section I)

Blue/Yellow FRET pairs

This “original FRET-pair” is still used in most biosensors today because of its good spectral properties. Many variants derived from these FPs have rapidly emerged and significantly increased FRET efficiency. The monomeric (m)Cerulean [43] and the mTurquoise2 [131] are the preferred variant of the CFP, while monomeric citrine and Venus [42] proved to be the most popular variant of the YFP. Cerulean has a better quantum yield, a higher extinction coefficient, a fluorescence lifetime with a single exponential decay and an increased brightness than conventional CFP (see table 1). mCitrine shows a better tolerance to pH variations and quenching by chloride ions, while Venus is characterized by a quicker maturation within cells.

Along these lines, a “sticky” FRET pairs, known as CyPET and YPet has been optimized from a cyan-yellow FRET pair by Daugherty’s lab in 2005, using quantitative evolutionary strategy [132]. The resulting FRET pairs showed a 20-fold ratiometric FRET signal change instead of the 3-fold for the parental pair, in a context where fluorophores were separated by a caspase 3 cleavable substrate. While this

FRET pair provides substantial improvement is sensitivity and dynamic range for some biosensor [132], the poor folding and expression of CyPET at 37°C limits its usefulness for live cell studies [34]. Nevertheless, YPet remains one of the brightest YFP and displays superior FRET efficiency when paired with a cyan donor fluorophore such as eCFP, alleviating from any ill effects stemming from CyPET, [127, 133].

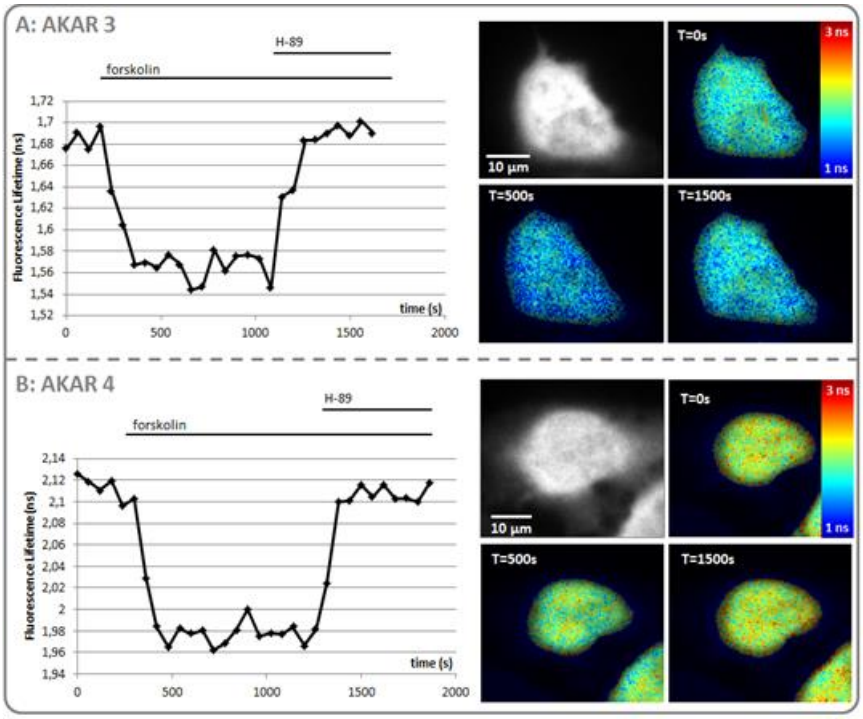

Figure 15: **U20S cells transfected with AKAR3** (**A**) or AKAR 4 (**B**). PKA was activated using an adenylate cyclase activator (forskolin) and then inhibited with H-89. Lifetime measurements were performed in frequency domain, as described in (section II).Graphs represent the average phase fluorescence lifetime measured for the entire cell as a function of time. Images represent intensity (top left) and phase lifetime (others) at specific times.

Lately circularly permuted (cp) fluorophores have appeared as a good way to enhance dynamic range of biosensor. These cp have flourish in scientific report has a solid solution for biosensor optimization [35, 71]. Technically, it consists of a fluorescent protein in which the N- and C- termini are fused together through a flexible linker. This protein engineering has allow for the emergence of other type of biosensor resting solely on the fluctuation of fluorescence properties upon binding of analyte to molecular switch positioned in the linker region [134]. Note that such fluorophores are more sensitive to their photochemical environment such as pH and temperature in this configuration/protein structure. The first biosensor successfully improved using this strategy is the Ca2+ indicator (yellow cameleon) exhibiting nearly

6 fold increase in dynamic range of FRET efficiency upon Ca^{2+} binding to the biosensor [135]. Since then, cpFPs essentially cpVenus has been implemented in other biosensors, including, AKAR3 [35], AKAR4 [71] and recently $^{t}Epac^{vv}$ [136]. The simple swapping of the CFP for the Cerulean as donor between AKAR3 and AKAR4 in combination with the cpVenus improves the dynamic range of AKAR series. Indeed AKAR4 shows a slight average difference in fluorescence lifetime in control experiments when compare to AKAR3 (Fig 15).

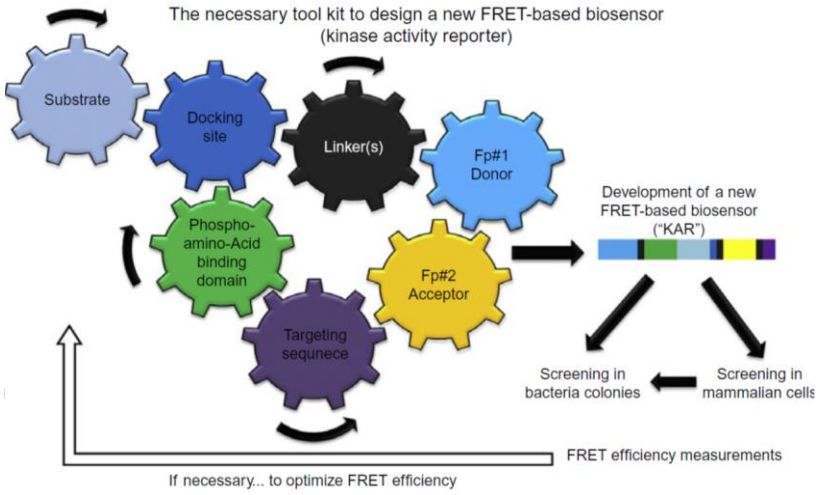

Figure 16: Overall methodology for creation and/or optimization of KAR biosensors.

Green/Red FRET pairs

In 2004, many other variants of fluorescent proteins have emerged with the discovery and characterization of a new Red Fluorescent Protein (RFP) named *Discosoma sp.* red fluorescent protein (DsRed) isolated from the coral of *Dicosoma genus* in 1999 [40]. Although red-shifted FP variants would undoubtedly result in lower phototoxicity upon biological sample illumination (less energy) they are not commonly employed for sensing application. The only example is the ERK biosensor EKAR [38] in its green-red version that did not show a large dynamic range (unpublished results). However, green-red FRET pair has proven its usefulness in detection of molecular interaction by FRET-FLIM. Besides, even in their optimized versions, intrinsic fluorescence properties of RFPs (oligomerisation, quantum yield, brighteness….) do not stand a chance when compared with their yellow counterparts. Indeed the historical FRET pair is cyan-yellow based, and has received much attention directed towards its optimization. Ongoing efforts for developing red-shifted variants will most likely yield adequate acceptor that will prove themselves useful in multi-sensing approaches.

In light of opportunities offered by newly engineered FPs, many studies suggest alternatives to conventional FRET pairs. Combining the yellow or green fluorescent proteins as a donor with orange or red fluorescent proteins as acceptor is now possible. Although these FRET pairs have mostly been used in proteins interactions studies, they have recently emerged as an alternative to CFP/YFP FRET pair in biosensor design [38].

The following figure (Fig. 16) illustrates the process necessary for the creation and/or the optimization of KAR biosensors

3.2.6.5. Targeting FRET-biosensors to subcellular compartments

Biosensors can be addressed to distinct subcellular compartments in order to gain information on the compartmentalized activity of a kinase of interest. This is achieved by adding an additional amino acid sequence fused at the N-terminal or C-terminal extremity of the sensor. Several subcellular targeting sequences have been isolated and are now well characterized (Table 3).

Subcellular targeted location	Targeting sequences	Références
Cytosol	LALKLAGLDI (at C-terminal)	Gallegos et al (2006)
Nucleus	PKKRKVEDA (at C-terminal)	Gallegos *et al.* (2006) Ananthanarayanan *et al.* (2005)
Golgi	33 amino residues of eNOS (at N-terminal)	Sasaki *et al.* (2003) Gallegos *et al.* (2006)
Endoplasmic reticulum	MLLPVLLLGLLGAAAD (at N-terminal) + KDEL (at C-terminal)	Palmer *et al.* (2004)
Plasma membrane	MGCIKSK (at N-terminal)	Violin *et al.* (2003) Kunkel *et al.* (2005) Gallegos *et al.* (2006)

Table 3: Adapted from [4] & [102, 103, 126, 137-139].

3.2.6.6. In vitro and in cellulo characterization of new FRET biosensors

Two paths can be exploited to test newly built and optimized biosensors: *in vitro* and *in cellulo*. Note that results from one approach do not imply that similar results would be obtained when using the other one. However, characterization remains the bottleneck through which every biosensor has to pass. Characterization is a crucial step as it determines the efficiency of new FRET-based biosensors and

thus requires several considerations. The results should provide evidence that the sensor generated is specific to the kinase of interest and should assess the dynamic range of the biosensor in the presence of the activator and/or inhibitor. This step usually relies on pharmacological agents, which can be limited when considering their availability and specificity.

In vitro characterization: Upon expression of biosensors, in bacterial system for instance, lysates are subjected to stringent purification procedures to retrieve only full-length protein from truncated protein due to proteolytic degradation. Now, in solution (see chapter 4, spectroscopy section) with the purified protein kinase of interest and ATP, in a 96 well plate screening format or in a spectrophotometer cuvette, properties of biosensor are evaluated. Ratiometric measurements methods (see section II for details) are then employed in different experimental conditions: before and after addition of ATP and purified kinase, and control wells for baseline ratio determination

In addition, phosphorylation levels of the biosensor expressed in mammalian cells can be estimated by immunoprecipitation and detected by PhosphoTag western. Overall amounts of expressed biosensors is then revealed by anti-GFP antibody [127].

In cellulo characterization consists of expressing the biosensor in a mammalian cell models and assessing the ratiometric signal in the presence of specific activator and inhibitors of the kinase of interest. Biosensor control constructs (earlier version or non phosphorylatable biosensor) undergoes similar experimental conditions. Transient transfection of plasmid DNA encoding biosensors is an accessible and inexpensive approach, which is sufficient to produce biosensors using cellular transcriptional machinery. Kinase activity measurement in a cellular context can also evaluate the specificity of a biosensor candidate: kinase blockers should prevent the ratiometric response to activators, demonstrating the involvement of one specific kinase family into the process being studied. This strategy is more often seen as a complementary than an alternative method to evaluate FRET efficiency of candidate sensors.

In vitro and *in cellulo* characterizations are often used to evaluate quantitatively the effect of several kinase inhibitors to determine the most effective inhibitor of the kinase of interest. Indeed, they can serve as high-throughput

screening to evaluate rapidly the effects of several pharmacological treatments on activation or extinction of a particular pathway. For such assays, it remains essential that the biosensor exhibits a robust and reproducible signal. This is generally assessed by the Z-factor, a statistical parameter that compares the dynamic range to data variation [123]. A schematic representation of such an experimental design is proposed in figure 17 (Fig. 17).

3.2.7. Considerations for KAR measurements

3.2.7.1. Controlling acquisition systems

As previously described, several techniques allow quantifying FRET for KAR imaging. Each of them requires a dedicated setup and thus adapted characterization procedures. The most advanced acquisition techniques (spectral acquisition, TD and FD FLIM…) mainly require rigorous characterization of the systems and optimized acquisition conditions as described in the literature [23, 26, 59, 140]. They can then be directly used for KAR imaging and yield unambiguous quantification of FRET efficiencies. Ratiometric imaging, despite easier acquisition procedure, can results in erroneous interpretation of FRET efficiency due to classical drawbacks of quantitative fluorescence imaging. The apparent easier acquisition procedure makes it available to researchers who are unaware of the factor that might complicate fluorescence quantification. We will thus focus here on some key elements responsible for these misinterpretations.

Fluorescence microscopy is mainly used for a qualitative imaging of proteins, lipids or nuclear acids distribution in cells. Indeed, quantifying the distribution of these molecules is strongly complicated by various optical, physical and biological parameters [141]. Many of them can be circumvented by ratiometric imaging and are not an issue in the case of KAR imaging. However several parameters remain critical. For example, the properties of the illumination sources, the optics of the microscope or the sensitivity and signal to noise ratio of the detectors can affect both fluorescence and ratio measurements. Some of these parameters can be easily optimized by an advised choice of the elements available on the acquisition systems. For instance, using apochromatic objective with corrected chromatic aberration to avoid focusing the excitation wavelength at two different positions will prevent strong border effects. Others are more difficult to avoid (Fig. 18 gives several examples) and

will strongly depend on the acquisition technique used for measuring the ratio (Sequential Ratio: SR, Dual View Ratio: DVR, Dual Channel Ratio, DCR).

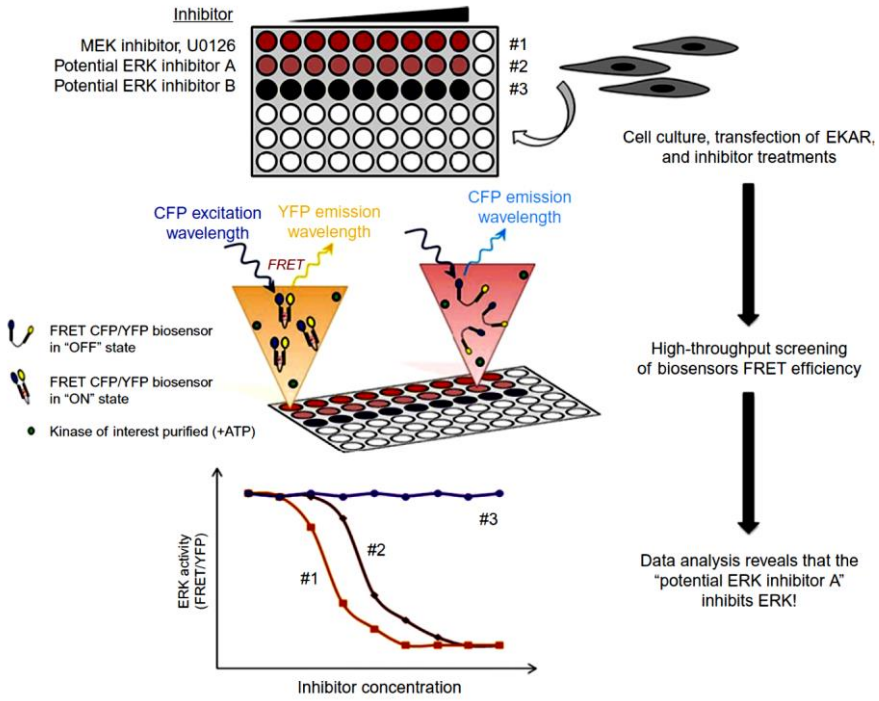

Figure 17: Schematic representation of the method for the evaluation of kinase inhibitor with FRET-based Biosensor EKAR by high throughput screening.

Field illumination

Non homogeneous field illumination and light collection is a classical problem encountered both in widefield and in confocal microscopy and can yield to significant differences in intensity measurements from the center to the border of an image. We encouraged users to verify the field homogeneity of its own system using a reference sample. In ratio imaging, this may not be a major issue if the field non-homogeneity is the same for sequential ratio (this is most of the time the case for SR, Fig.18 A). Indeed, if each pixel of the emitted I_{FRET} and I_{donor} images are multiplied by a same factor, the ratio measurements will stay accurate despite non-homogeneities in the field. On the contrary, for dual-view or dual channel ratio, this may be a major issue because both images are measured on either two distinct detector parts or two different cameras. Detector variability is thus spatially uncorrelated and may strongly impact the ratio values (Fig. 18 B and C). It is thus absolutely required to suppress this field illumination homogeneity by acquiring reference images using fluorescent solutions. When differences in field illumination persist, corrections can be carried out

by normalizing pixel intensities using reference images. This procedure is called the shading correction [142].

Besides correcting for spatial field inhomogeneities, the shading correction also intrinsically calibrates the absolute ratio value. Shading images are acquired with a uniform sample of a fluorescent chromophore, chosen to emit fluorescence at both wavelenghts of interest. In the particular case of CFP-like and YFP-like chromophores, a suitable fluorescent dye is Coumarin 343, which emits at both wavelengths. When each acquired image is divided by its corresponding shading image, by definition, the ratio of coumarin dye is equal to 1 [74, 143]. This method thus defines ratio values with respect to a reference chromophore and thus defines the "balance" between the two channels. This procedure allows easier comparison between setups, which may have different spectral sensitivities.

Image mis-registration between acquisition channels.

In the sequential ratio set-up, the images acquired at two wavelengths may not be perfectly registered. This may result from wedge effects caused by the non-parallel faces of the emission filter. This is easily corrected by a translation of one of the image by a few pixels and algorithm exist to determine the optimal sub-pixel registration correction [144]. In addition, if the objective has a chromatic aberration, sequential ratio allows for a focus correction by a fixed value which can be accurately determined using fluorescent beads. When cellular movement occurs at the time scale of the sequential acquisition, no correction can be applied and the system is just not fast enough for measuring the biological event of interest and simultaneous detection with dual view or dual channels may be needed. In these configurations, in addition to the linear translation of one image with respect to the other, non-linear deformation may occur as a result of different optical path followed by both wavelengths, and more elaborate algorithm that correct for image skewing must be applied. Misregistration effects are nonetheless a common cause of data misinterpretation and the experimenter should look carefully at the images for border effects which usually show a typical rainbow appearance (Fig 18 D).

3.2.7.2. Controlling biological samples

Parameters such as temperature or pH can directly affect chromophore properties. In addition, these physical parameters plus other biologically relevant

parameters (osmolarity, ion and metabolites concentrations…) may alter the activity of signaling cascades (including kinases) and hence the measurements obtained with KAR biosensors. Experimental conditions must therefore be controlled in order to minimize the impact of such parameters.

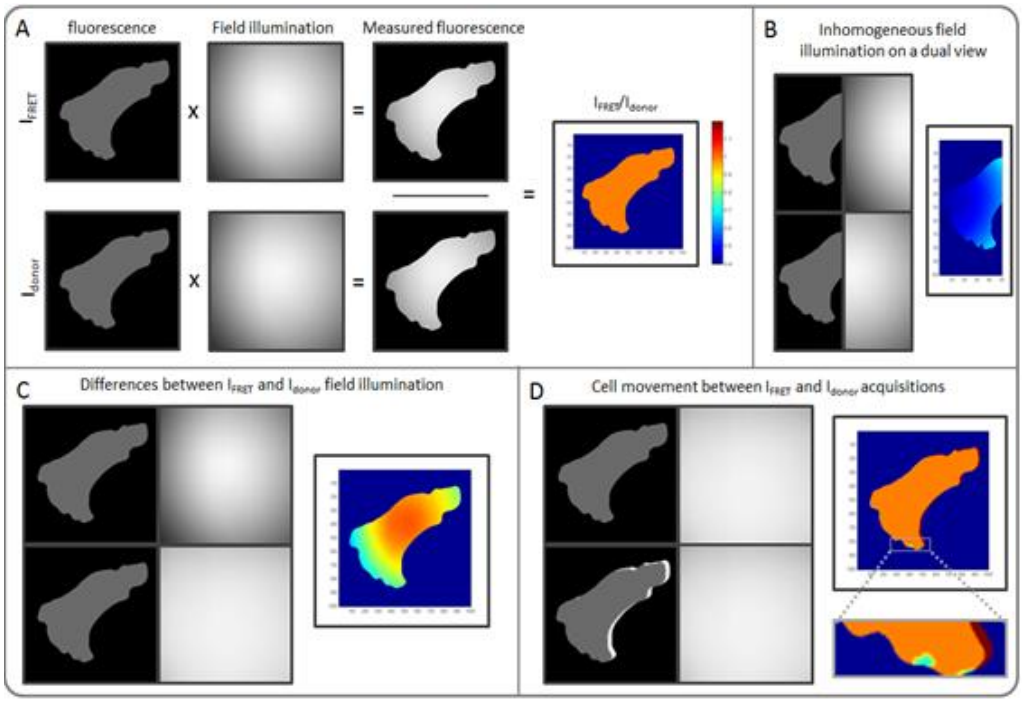

Figure 18: Field illumination and cell movement between I_{FRET} and I_{donor} acquisition channels effects on ratio imaging. For each panel, cell exhibiting an equal I_{FRET} and I_{donor} is imaged through a non-homogeneous field illumination and ratio image is calculated. Procedure is detailed in A. The expected ratio value is thus equal to one for the whole image. In B-D, we can see erroneous ratio images due to different sources of artifacts. See text for more details.

Temperature

Concerning the temperature, experiments must be carried out at a stable temperature (usually 37°C) inside thermostated space surrounding the whole microscope. These incubators require hours to warm up and reach a stable temperature and should always be turned on to ensure optimal stability. The temperature probe should be positioned as close as possible to the sample. The thermal inertia due to contact with both the objective and the microscope stage might need direct control with thermostatic controllers. While temperature probes are most of the time positioned in the air, there can be a large difference between the average enclosure and the sample temperature. Calibration of this difference must thus be performed by positioning the temperature probe in the medium [145].

Imaging media and perfusion

In long-term experiments, drying of the imaging medium modifies ionic concentrations and pH. Buffered medium can be used for short-term experiments (from two to four hours depending on cell type). For longer measurements, the use of a CO_2 incubator and a perfusion system to renew culture medium is recommended. In all cases, media containing phenol red should be avoided, as this molecule is slightly fluorescent and leads to an unwanted fluorescent signal. Phenol red free medium must be preferred. Details for the preparation of dedicated imaging media can be found in [38, 51].

Perfusion systems are very useful to add drugs into the sample. Alternatively, drugs in preheated medium can be applied manually in the dish with a Pasteur pipette. This can however lead to motion artifacts because of shear stress, and some practice is necessary.

Biosensor expression level

Transfection agents or electroporation are often chosen to transfect cells with biosensors plasmids. Viruses (for example: adenoviruses or Sinbis) can be considered for kinase activity measurement in cells resistant to classic transfection method [146], or in tissue [147]. However, the biosensor expression level can induce differences in amplitude response. Indeed, the FRET probes destabilize the reaction equilibrium between a kinase and its substrates. We therefore recommend performing measurements on cells with equivalent KAR expression level. To avoid the variations caused by the sensor expression levels, the creation of a stable cell line might be an alternative of choice.

Photo-induced effects

Photo-induced effects are other sources of artifacts. Among these effects the most obvious is cell death, easily noticeable by changes in cell morphology. Photo-stress is more tricky to observe and can result in cell auto-fluorescence. While auto-fluorescence spectra are broad and cannot be corrected by filters, and auto-fluorescence lifetime is very short and can be confused with a FRET event, both spectral and lifetime properties of auto-fluorescence can create artifacts in measurements with both intensity ratio and lifetime based techniques. The last photo-induced effect is the photo-bleaching that can also falsify measurements with

all techniques, therefore leading to unacceptable errors in data interpretation. Extensive controls of photo-induced effect on cells expressing a KAR negative reference are thus indispensable (See paragraph negative control hereafter).

These photo-induced effects depend on laser power and exposure time. Thus, it will be less critical for techniques that require a lower illumination power ($P_{average}$: measured using a powermeter). For example, ratiometric measurements will be less affected than FD-FLIM experiments and TSCPC is the most stressful method because of the time necessary to scan an entire cell. Since most biosensors are based on the CFP/YFP FRET pair (or their variants such as Cerulean, Turquoise, CyPet, Venus, circularly permutated Venus, YPet...), we will focus on these fluorophores to exemplify the acquisition time and power required for each technique (performed on our systems).

In ratiometric measurements, after exciting the donor, the exposure time is set to ~500 ms and ~200 ms ($P_{average}$< 1 mW) for CFP and YFP respectively with our microscopy system [48]. As described in the analysis section of this chapter, acquiring a channel with excitation and observation of YFP is a requisite control in intermolecular FRET. It is, however, not recommended in the case of sensor imaging, because this optional correction step will increase both photo-induced effects and noise, without improving results. Acceptors excitation can however be useful in another way. Indeed, acceptor photo-bleaching can be a good negative control to recover a basal level after activation of the kinase of interest. The photo-induced effect arising from this high energy laser excitation must however be controlled [71].

For FLIM, the acquisition time strongly depends on the technique used. For FD FLIM measurements using our set-up, the exposure time of the donor is comprised between 100 ms and 300 ms with a laser power $P_{average}$= 4mW send to a spinning disk system equipped with a 63x oil objective (NA=1.4). To achieve optimal compromise between the number of phase images and the accuracy of lifetime determination, 12 phase shifted images are chosen. Moreover achieving a good signal to noise ratio often requires averaging each images three times. From these constraints, the overall exposure time for one lifetime image is comprised between 3 to almost 10 sec. For time resolved lifetime measurements with our system, a field-scan takes about 5 minutes (still with an average laser power of a few mW) and will

require data binning to achieve precise lifetime map while the measurements per pixel only takes few tens of milliseconds.

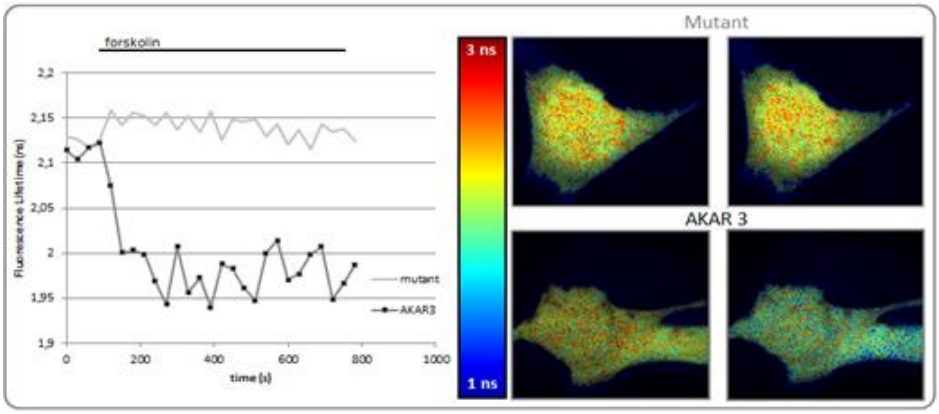

Figure 19: U20S cells transfected with AKAR3 or AKAR3 inactive mutant. PKA was activated using an adenylate cyclase activator (forskolin, 12.5 μM). Lifetime measurements were performed in frequency domain, as described in Section II. Graphs represent the average phase fluorescence lifetime measured for the entire cell as a function of time. Experiments with either biosensor were performed separately, but are represented on the same graph for clarity. Images represent phase lifetime before (left panel) and after (right panel) induction.

The choice of imaging technique thus depends on i) the time resolution ii) the number of images needed iii) the spatial resolution. For example TCSPC can be used to obtain a precise image of the subcellular localization of kinase activity before and after the activation of the biological signal, while ratiometric measurement or phase and modulation technique will be preferred to achieve precise estimate of kinase activity kinetics over time. The use of biosensor targeted to subcellular compartment measured by ratio imaging can also be a solution to achieve precise activity localization without compromising acquisition speed.

In conclusion, we suggest avoiding any unnecessary exposure of fluorophores especially the donor in FLIM experiments; moreover photo-bleaching of the CFP will occur faster than for YFP variants. For example (and if it is possible) find the focus using transmitted light rather than a mercury lamp. Due to the numerous possible photo-induced artifacts, negative controls are indispensable.

Negative Control

Sensing applications require the creation of a control biosensor. Concerning KAR the phosphorylable residue within the substrate (serine, threonine, or tyrosine) may be mutated to a non-phosphorylable amino acid such as glycine or alanine. Expressed in cells, it should not produce a FRET signal in response to the

stimulation of the kinase of interest. It will therefore serve as negative control and provide the basal level of FRET signal in living cells. An example of such an experiment is presented in figure 19 (Fig. 19). There is unfortunately no positive control for FRET measurements in living cells (all sensors in folded position), but a strong induction using activating agents can be envisaged as an alternative. Molecular strategies for such a positive control should be envisioned in the near future as both control biosensors could provide a complete sensing range.

3.2.7.3. Biosensor dynamic range and reproducibility

The dynamic range of a biosensor is a critical parameter to consider, and increasing this range is often the purpose of biosensor optimization. The dynamic range depends directly on FRET efficiency and can be increased by switching fluorophores, improving linkers, and enhancing kinase binding to the biosensor (with the insertion of a docking domain for example) as described earlier (see section IV). Possessing the appropriate pharmacology allowing maximum stimulation and inhibition is essential for estimating this dynamic range. More than just control, the amplitude revealed (as well as other criterions such as sensitivity) directs the choice of the biosensor to use.

As another example, the Extracellular regulated Kinase Activity Reporter (EKAR) [38] shows a relatively low dynamic range, both for ratiometric or lifetime based measures, compared to a cAMP biosensor ($^{T}Epac^{VV}$) recently published [136]. Indeed, cells expressing EKAR exhibit a 20% average $\Delta R/R$ and 120 ps ± 20 average $\Delta\tau$, while cells expressing $^{T}Epac^{VV}$ results in a mean $\Delta R/R$ of more than 80% and a mean $\Delta\tau$ of 700 ps ± 50 ps both after maximum stimulation/inhibition (10 cells per conditions, unpublished results). While these biosensors differ in their composition, the fluorophores of $^{T}Epac^{VV}$ were optimized to improved FRET efficiency whatever the technique employed. Indeed, the donor fluorophore of $^{T}Epac^{VV}$ (mTurquoise) is characterized by a phase lifetime of 3,7 ns [148] instead of the 2,3 of Cerulean [149] in EKAR, which improved the dynamic range in fluorescence lifetime measurements. As an acceptor, $^{T}Epac^{VV}$ use a dimer of CpVenus-Venus instead of a single Venus in EKAR, in order to improve detection of the sensitized emission (See section IV).

After all these considerations related to fluorescence, FRET measurements, data analysis, creation/optimization of biosensor and methodologies for kinase activity measurements, we would like to enlighten the reader about the way data are being employed today in system biology approaches.

3.2.8. Towards quantitative approaches in biological processes

The molecular toolkit for kinases activity reporters is called to address the role of kinases in the orchestration of signal transmission within the cells. It remains challenging to understand how a signal pattern is organized and provides accurate integration and appropriate cellular decision while mobilizing common effectors in response to different inputs. Indeed kinases like Erk, PKA, Akt are considered as common effectors and their spatiotemporal dynamics drives cellular functions. Receptors are often acting as organizer of signal integration, giving its shape to the signal: transitory, sustained, all-or-none.

Regarding Erk, MAPK/Erk network exhibits plasticity and different dynamical properties may arise from connections within this network. For instance, rewiring of Erk pathway architecture in the context of NGF or EGF stimulation in PC12 cells (model for neurone differentiation) is believed to built the dynamical response observed for these growth factors: transient or sustained MAPK/Erk cascade activation following EGF or NGF stimulation, respectively [150, 151].

Similar dynamical properties of the MAPK/Erk pathway have been suspected to affect signaling cascade involved in cell death [152]. Actually, subcellular localization of MAPK/Erk pathway components and dynamical spatiotemporal changes are believed to determine cell fate between proliferation and death [153]. Sustained Erk activation, which is sufficient to induce cell death, is often associated with cell death mediated by ROS [154] because these radicals can suppress protein-phosphatases activities of MKP (MAPK-specific Phosphatases), exerting key roles in the regulation of MAPK/Erk dynamics [155]. Inhibition of MAPK/Erk activation using inhibitors against components of the MAPK cascade has a survival effect on cells induced to die following chemicals or physicals challenges. Forced *MAPK/Erk* cytosolic localization prevents a survival or a mitogenic response, but potentiates activities of specific pro-apoptotic proteins such as DAPK [156], Bik [157] and PEA-

15 [158] *via* the activation of PI3K/Akt pathway. Depending on cell type and stimulus, compartmentalized MAPK activity will mediate either cell survival or cell death (see for review [3]). *Thus, spatial signatures for the signal propagation of the MAPK/Erk signaling pathway have started to be explored both at experimental and theoretical levels in many different cellular models, from gametes to tissues* [159-161].

Scaffolding proteins and interactions of kinases with specific components of the cell architecture also determine the spatial and temporal integration of the cAMP/PKA signal [162-164]. In addition, the simple spatial organization of the cell also determines the spatiotemporal organization of the signal leading to differential activation within the cell compartment. Indeed, in the case of the cAMP/PKA signaling cascade, modeling studies [165] and imaging experiments [166, 167] revealed the importance of cell morphology in the particular situation of neurons, where sub-membrane domains display faster and stronger responses than the bulk somatic cytosol [168]. It is therefore of great importance to address the question of intracellular signal integration bearing in mind the multi-dimensional -space and time- parameters which determine the physiological outcome of an external signal.

Kinase Activity Reporters methodologies will definitely be able to generate enough data to be considered for modeling approaches. Still, while recording dynamical pathway, which may exhibit variation from one cell to another, one needs to identify within these apparently variable responses, reliable marks or features which are common between experiments and invariant to changes in cell morphologies or behaviors. These marks may be obtained through acute stimulation / inhibition of a pathway [169] but a response hierarchy may also be obtained from constitutive fluctuations in the activity of the biosensors [170]. The latter approach is performed in a non-perturbed pathway, in conditions closer to a physiological range than the one in acute inhibition or activation. In concept, fluctuation analysis is quite scalable to a large number of components and require further developed mathematical tools to ingrate this large sets of component activities.

3.2.9. Outlook and perspective

3.2.9.1. What about multisensing?

In prospect to detect several parameters simultaneously in the same cell, the idea of using multiple probes is becoming more and more attractive. As the number

of available tools is increasing, monitoring several modulators of the same pathway provides opportunities towards the understanding of cells reaction dynamics. The principal challenge of those experiments is the combination of the well-chosen fluorophores pairs with the appropriate technique. Several parameters have to be considered and are well described and illustrated in the excellent review by Carlson and Campbell [171].

Piljic and coworkers [172] present such an example of multisensing applied to the monitoring of several effectors involved in the regulation of calcium chloride conductance. It was achieved in epithelial cell line using simultaneously 4 biosensors, including 3 FRET-based sensors. These refined experiments were performed by ratiometric imaging taking advantage of i) the spectral shift between the two FRET pairs (namely CFP/YFP and mOrange/mCherry), and ii) the subcellular targeting of some of these sensor has been used to spatially discriminate signals from each reporters.

Taking into account the complexity, dynamics and stress reactivity of cellular environment, measurements of molecular dynamics could require combination of fluorescence analysis techniques such as fluorescence lifetime, spectrum or intensity fluctuations analysis, and development of a multimodal microscopy suitable for different complexity degree of the living matter: cells, tissues and whole organism. So far biosensor recording has been achieved using mainly ratiometric techniques, however FRET-FLIM could emerge as an interesting alternative.

3.2.9.2. Kinase activity measurements in living animals.

Studying kinase activity profiles in living tissue or animals provides new insights on cells behavior in intact biological context. Few publications describe the use of FRET-based biosensor in living animals. For example ATP levels in a transgenic worm (*Caenorhabditis elegans* expressing ATeam [173]) , or cAMP levels in the fruit-flies (transgenic *Drosophilia melanogatser* expressing GFP-PKA [174, 175]) as well as Rac GTPase activity in zebrafish (pRaichu RacFRET mRNA microinjected in *Danio rerio* embryos [176]) has already been performed.

However, these first experiments have highlighted some difficulties. Indeed, biosensor overexpression can lead to abnormal embryonic development or lethality depending on promoter strength, simply because the cAMP biosensor is built on an

active PKA enzyme bearing its intact catalytic activity [174]. It is therefore strongly suggested to use biosensors which have no biological effect such as AKAR and indeed, the expression of these sensors proved to be harmless and did not affect memory processes in the living drosophila [177]. The depth at which measurements must be done, combined to the required low KAR expression levels, render measuring relevant variations more difficult [176]. The use of two photon excitation microscope which increases the imaging depth and reduce the phototoxicity must be preferred for opaque tissues or deep imaging for both ratio imaging and TD-FLIM experiments and indeed provided new insight on cAMP/PKA signaling processes in living drosophila [177].

Generation of transgenic mice expressing FRET-based biosensor remains a challenge [178], for example because of the two fluorophore's cDNAs recombination [179]. Although this has already been done, the low expression levels (probably due to gene silencing) complicate the imaging procedure [180]. Nevertheless, transgenic mice were generated for some KAR including EKAR and AKAR (with a high expression level), and successful kinase activity measurement were realized notably in auricular skin and small intestine [179]. Another line has been developed with a ubiquitous cAMP sensor expression which allowed direct cAMP measurement on a variety of primary cell preparations [181]. As a perspective, transgenic animals can be designed for ubiquitous or tissue specific KAR expression. Furthermore, the combination of animals expressing a KAR and mutated/KO/overexpressing gene involved in the regulation of the kinase of interest can increase our understanding of regulatory networks.

While being somewhat challenging in a practical way, kinase activity measurements and biosensors in general, have help scientists better their understanding of biological processes. These tools allow for the generation of data set that can be exploited by mathematician for modeling approaches of regulatory networks. Finally, since biosensors experiments are performed within an intact physiological context, new light is being shed onto the spatiotemporal dynamic of molecular effectors involved in the regulation cellular functions.

Acknowledgments

This work was encouraged and supported by two CNRS national networks the GDR2588 and the RTmFm as well as the University Lille1. The opportunity for such a chapter arose thanks to the French biosensor workgroup.
Financial contributions came from various sources for equipment, bench fees, and Ph.D student grants. This work was funded by the CNRS, the University Lille1, the GEFLUC, the Nord-Pas de Calais Région Council, the European Regional Developmental Funds, a Leica Microsystems partnership, and the French Research Agency ANR 07-PFTV-01101. We are grateful to the imaging platform BICeL (Bio Imaging Center of Lille) and the Interdisciplinary Research Institute: IRI CNRS USR3078.

References

1. Heim, R. and R.Y. Tsien, Engineering green fluorescent protein for improved brightness, longer wavelengths and fluorescence resonance energy transfer. Curr Biol, 1996. **6**(2): p. 178-82.
2. Frommer, W.B., M.W. Davidson, and R.E. Campbell, *Genetically encoded biosensors based on engineered fluorescent proteins.* Chem Soc Rev, 2009. **38**(10): p. 2833-41.
3. Riquet, F., et al., Reporting Kinase Activities: Paradigms, Tools and Perspectives. BMB JBM, 2011. **1**(2): p. 10-18.
4. Kunkel, M.T. and A.C. Newton, *Spatiotemporal Dynamics of Kinase Signaling Visualized by Targeted Reporters.* Curr Protoc Chem Biol, 2009. **1**(1): p. 17-18.
5. Valeur B., *Molecular Fluorescence: Principles and Applications.* 2001: Molecular Fluorescence: Principles and Applications.
6. Lakowicz J. R., *Principles of fluorescence spectroscopy* 1999: Kluwer Academic/Plenium Publishers.
7. Periasamy A., D.R.N., *molecular imaging FRET microscopy and spectroscopy*. 2005: Oxford university press.
8. Sun, Y., R.N. Day, and A. Periasamy, Investigating protein-protein interactions in living cells using fluorescence lifetime imaging microscopy. Nature Protocols, 2011. **6**(9): p. 1324-1340.
9. Camuzeaux B, S.C., Héliot L, Coll J, Duterque-Coquillaud M, Imaging Erg and Jun transcription factor interaction in living cells using fluorescence resonance energy transfer analyses. Biochem Biophys Res Commun, 2005. **332**(4): p. 1107-1114.
10. Yockell-Lelièvre, J., et al., Functional cooperation between Stat-1 and ets-1 to optimize icam-1 gene transcription. Biochem Cell Biol, 2009. **87**(6): p. 905-918.
11. Trinel, D., et al., Upgrading Time Domain FLIM Using an Adaptive Monte Carlo Data Inflation Algorithm. Cytometry Part A, 2011. **79A**: p. 528-537.
12. Pietraszewska-Bogiel A., G., T. W., *FRET microscopy: from principle to routine technology in cell biology.* J Microsc, 2011. **241**(2): p. 111-8.
13. Forster T., Intermolecular energy migration and fluorescence. Ann. Phys. , 1948. **2**: p. 55-57.
14. Clegg R. M., M.A.I.H., Lilley D. M. J., *THE 4-WAY DNA JUNCTION - A FLUORESCENCE RESONANCE ENERGY-TRANSFER STUDY.* Brazilian Journal of Medical and Biological Research, 1993. **26**(4): p. 405-416.
15. Clegg R. M., M.A.I.H., Lilley D. M. J., Sener, M., Govindjee,, From Forster resonance energy transfer to coherent resonance energy transfer and back, in Optical Biopsy Vii, R.R. Alfano, Editor. 2010.
16. Steinberg, I.Z., Long-range nonradiative transfer of electronic excitation energy in proteins and polypeptides. Annual review of biochemistry, 1971. **40**: p. 83-114.
17. Dale R. E., E.J., and Blumberg W. E., the oreintation freedom of molecular probes. Teh oreintation factor in inttramolecular energy transfer. Biophys. J. , 1979. **26**: p. 161-194.
18. Dale R.E., E.J., *Intramolecular energy transfer and molecular conformation.* Proc Natl Acad Sci U S A, 1976. **73**(2): p. 161-163.
19. Haas E., W.M., Katchalski-Katzir E., Steinberg I. Z., *Distribution of end-to-end distances of oligopeptides in solution as estimated by energy transfer.* Proc Natl Acad Sci U S A, 1975. **72**(5): p. 1807-1811.
20. Haas E., K.-K.E., Steinberg, I. Z.,, Effect of the orientation of donor and acceptor on the probsbility of energy transfer involving electronic transitions of mixed polarizations. Biochemistry, 1978. **17**: p. 5064-5070.
21. Pantano, S., *In silico description of fluorescent probes in vivo.* Journal of Molecular Graphics & Modelling, 2008. **27**(4): p. 563-567.
22. Campbell, R.E., Fluorescent-protein-based biosensors: modulation of energy transfer as a design principle. Anal Chem, 2009. **81**(15): p. 5972-9.
23. Waharte, F., C. Spriet, and L. Heliot, Setup and characterization of a multiphoton FLIM instrument for protein-protein interaction measurements in living cells. Cytometry A, 2006. **69**(4): p. 299-306.
24. Peter M., A.-B.S.M., Hughes M. K., Keppler M. D., Prag S., Marsh M., Vojnovic B., Ng T.,, *Multiphoton-FLIM quantification of the EGFP-mRFP1 FRET pair for localization of membrane receptor-kinase interactions.* Biophys J., 2005. **88**(2): p. 1224-1237.

25. Nagy P., B.L., Balázs M., Hyun W. C., Lockett S. J., Chiang N.Y., Waldman F., Feuerstein B.G., Damjanovich S., Szöllosi J., *EGF-induced redistribution of erbB2 on breast tumor cells: flow and image cytometric energy transfer measurements.* Cytometry., 1998. **32**(2): p. 120-131.
26. Spriet, C., et al., Correlated fluorescence lifetime and spectral measurements in living cells. Microsc Res Tech, 2007. **70**(2): p. 85-94.
27. Prasher, D.C., et al., Primary structure of the Aequorea victoria green-fluorescent protein. Gene, 1992. **111**(2): p. 229-33.
28. Shimomura, O., F.H. Johnson, and Y. Saiga, Extraction, purification and properties of aequorin, a bioluminescent protein from the luminous hydromedusan, Aequorea. J Cell Comp Physiol, 1962. **59**: p. 223-39.
29. Tsien, R.Y., *The green fluorescent protein.* Annu Rev Biochem, 1998. **67**: p. 509-44.
30. Dunn, T.A., et al., Imaging of cAMP levels and protein kinase A activity reveals that retinal waves drive oscillations in second-messenger cascades. J Neurosci, 2006. **26**(49): p. 12807-15.
31. Davidson, M.W. and R.E. Campbell, *Engineered fluorescent proteins: innovations and applications.* Nat Methods, 2009. **6**(10): p. 713-17.
32. Shaner, N.C., P.A. Steinbach, and R.Y. Tsien, *A guide to choosing fluorescent proteins.* Nat Methods, 2005. **2**(12): p. 905-9.
33. Shaner, N.C., G.H. Patterson, and M.W. Davidson, *Advances in fluorescent protein technology.* J Cell Sci, 2007. **120**(Pt 24): p. 4247-60.
34. Wang, Y., J.Y. Shyy, and S. Chien, Fluorescence proteins, live-cell imaging, and mechanobiology: seeing is believing. Annu Rev Biomed Eng, 2008. **10**: p. 1-38.
35. Allen, M.D. and J. Zhang, Subcellular dynamics of protein kinase A activity visualized by FRET-based reporters. Biochem Biophys Res Commun, 2006. **348**(2): p. 716-21.
36. Campbell, R.E., et al., *A monomeric red fluorescent protein.* Proc Natl Acad Sci U S A, 2002. **99**(12): p. 7877-82.
37. Cubitt, A.B., et al., *Understanding, improving and using green fluorescent proteins.* Trends Biochem Sci, 1995. **20**(11): p. 448-55.
38. Harvey, C.D., et al., *A genetically encoded fluorescent sensor of ERK activity.* Proc Natl Acad Sci U S A, 2008. **105**(49): p. 19264-9.
39. Heim, R., A.B. Cubitt, and R.Y. Tsien, *Improved green fluorescence.* Nature, 1995. **373**(6516): p. 663-4.
40. Matz, M.V., et al., *Fluorescent proteins from nonbioluminescent Anthozoa species.* Nat Biotechnol, 1999. **17**(10): p. 969-73.
41. Miyawaki, A., et al., *Dynamic and quantitative Ca2+ measurements using improved cameleons.* Proc Natl Acad Sci U S A, 1999. **96**(5): p. 2135-40.
42. Nagai, T., et al., A variant of yellow fluorescent protein with fast and efficient maturation for cell-biological applications. Nat Biotechnol, 2002. **20**(1): p. 87-90.
43. Rizzo, M.A., et al., *An improved cyan fluorescent protein variant useful for FRET.* Nat Biotechnol, 2004. **22**(4): p. 445-9.
44. Shaner, N.C., et al., Improved monomeric red, orange and yellow fluorescent proteins derived from Discosoma sp. red fluorescent protein. Nat Biotechnol, 2004. **22**(12): p. 1567-72.
45. Zacharias, D.A., et al., Partitioning of lipid-modified monomeric GFPs into membrane microdomains of live cells. Science, 2002. **296**(5569): p. 913-6.
46. Jares-Erijman, E.A. and T.M. Jovin, *FRET imaging.* Nat Biotechnol, 2003. **21**(11): p. 1387-95.
47. Jares-Erijman, E.A. and T.M. Jovin, *Imaging molecular interactions in living cells by FRET microscopy.* Curr Opin Chem Biol, 2006. **10**(5): p. 409-16.
48. Depry, C. and J. Zhang, *Visualization of kinase activity with FRET-based activity biosensors.* Curr Protoc Mol Biol, 2010. **Chapter 18**: p. Unit 18 15.
49. Jalink, K.R., J., FilterFRET: Quantitative imaging of sensitized emission., in Laboratory Techniques in Biochemistry and Molecular Biology, e. T. W. J. Gadella, Editor. 2009, Elsevier: burlington. p. 289-349.
50. Schechter, M.B., G., Widefield application letter: FRET Sensitized Emmission Wizard Widefield. reSOLUTION, 2009. **4**.
51. Borner, S., et al., FRET measurements of intracellular cAMP concentrations and cAMP analog permeability in intact cells. Nat Protoc, 2011. **6**(4): p. 427-38.
52. Hempel, C.M., et al., Spatio-temporal dynamics of cyclic AMP signals in an intact neural circuitm. Nature, 1996. **384**(6605): p. 166-9.
53. Garini, Y., I.T. Young, and G. McNamara, *Spectral imaging: principles and applications.* Cytometry A, 2006. **69**(8): p. 735-47.
54. Booth, M.J. and T. Wilson, *Low-cost, frequency-domain, fluorescence lifetime confocal microscopy.* Journal of Microscopy-Oxford, 2004. **214**: p. 36-42.
55. Gadella, T.W.J., T.M. Jovin, and R.M. Clegg, Fluorescence Lifetime Imaging Microscopy (Flim) - Spatial-Resolution of Microstructures on the Nanosecond Time-Scale. Biophysical Chemistry, 1993. **48**(2): p. 221-239.
56. Gratton, E., et al., Fluorescence lifetime imaging for the two-photon microscope: time-domain and frequency-domain methods. Journal of Biomedical Optics, 2003. **8**(3): p. 381-390.
57. Herman, P., et al., *Frequency-domain fluorescence microscopy with the LED as a light source.* Journal of Microscopy-Oxford, 2001. **203**: p. 176-181.

58. van Geest, L.K. and K.W.J. Stoop, *FLIM on a wide field fluorescence microscope.* Letters in Peptide Science, 2003. **10**(5-6): p. 501-510.
59. Leray, A., et al., Optimized protocol of a frequency domain fluorescence lifetime imaging microscope for FRET measurements. Microsc Res Tech, 2009. **72**(5): p. 371-9.
60. Schneider, P.C. and R.M. Clegg, Rapid acquisition, analysis, and display of fluorescence lifetime-resolved images for real-time applications. Rev. Sci. Instrum., 1997. **68**(11): p. 4107-4119.
61. Klaus Greger, 5 Manuel J. Neetz,2,5 Emmanuel G. Reynaud,1,3,* Ernst H.K. Stelzer, Three-dimensional Fluorescence Lifetime Imaging with a Single Plane Illumination Microscope provides an improved Signal to Noise Ratio. Optics express, 2011. **19**(21): p. 20743-20750.
62. van Munster, E.B., et al., Combination of a spinning disc confocal unit with frequency-domain fluorescence lifetime imaging microscopy. Cytometry Part A, 2007. **71A**(4): p. 207-214.
63. Buranachai, C., et al., Rapid Frequency-Domain FLIM Spinning Disk Confocal Microscope: Lifetime Resolution, Image Improvement and Wavelet Analysis. J. Fluoresc., 2008. **18**: p. 929-942.
64. Gordon, G.W., et al., Quantitative Fluorescence Resonance Energy Transfer Measurements Using Fluorescence Microscopy. Biophys J, 1998. **74**: p. 2702-2713.
65. Xia, Z. and Y. Liu, Reliable and Global Measurement of Fluorescence Resonance Energy Transfer Using Fluorescence Microscopes. Biophys J, 2001. **81**: p. 2395-2402.
66. Hoppe, A., K. Christensen, and J.A. Swanson, *Fluorescence Resonance Energy Transfer-Based Stoichiometry in Living Cells.* Biophys J, 2002. **83**: p. 3652-3664.
67. Jalink, K. and J. van Rheenen, *FilterFRET: Quantitative imaging of sensitized emission*, in *FRET and FLIM Techniques*, T.W.J. Gadella, Editor. 2009, Academic Press: Burlington.
68. Hodgson, L., F. Shen, and K. Hahn, *Biosensors for Characterizing the Dynamics of Rho Family GTPases in Living Cells.* Current Protocols in Cell Biology, 2010. **46**: p. 14.11.1-14.11.26.
69. Brito, M., E. Guiot, and P. Vincent, Imaging PKA activation inside neurons in brain slice preparations, in Neuromethods. 2012.
70. Hodgson, L., et al., Imaging and Photobleach Correction of Mero-CBD, Sensor of Endogenous Cdc42 Activation. Methods in Enzymology, 2006. **406**: p. 140-156.
71. Depry, C. and J. Zhang, *Visualization of Kinase Activity with FRET-Based Activity Biosensors.* Current Protocols in Molecular Biology, 2010. **18**: p. 18.15.1-18.15.9.
72. Ting, A.Y., et al., Genetically encoded fluorescent reporters of protein tyrosine kinase activities in living cells. PNAS, 2001. **98**(26): p. 15003-15008.
73. Klarenbeek, J.B., et al., A mTurquoise-Based cAMP Sensor for Both FLIM and Ratiometric Read-Out Has Improved Dynamic Range. PLOS ONE, 2011. **6**(4): p. e19170.
74. Grynkiewicz, G., M. Poenie, and R.Y. Tsien, *A new generation of Ca2+ indicators with greatly improved fluorescence properties.* J Biol Chem, 1985. **260**(6): p. 3440-50.
75. Hinde, E., et al., Biosensor Förster resonance energy transfer detection by the phasor approach to fluorescence lifetime imaging microscopy. Microsc Res Tech, 2011.
76. Llères, D., S. Swift, and A.I. Lamond, Detecting Protein-Protein Interactions In Vivo with FRET using Multiphoton Fluorescence Lifetime Imaging Microscopy (FLIM). Current Protocols in Cytometry, 2007. **12**: p. 12.10.1-12.10.19.
77. Elder, A.D., et al., Calibration of a wide-field frequency-domain fluorescence lifetime microscopy system using light emitting diodes as light sources. Journal of Microscopy-Oxford, 2006. **224**: p. 166-180.
78. Squire, A., P.J. Verveer, and P.I.H. Bastiaens, *Multiple frequency fluorescence lifetime imaging microscopy.* Journal of Microscopy, 2000. **197**: p. 136-149.
79. Lakowicz, J.R., et al., Analysis of Fluorescence Decay Kinetics From Variable-Frequency Phase Shift and Modulation Data. Biophys. J., 1984. **46**: p. 463-477.
80. Verveer, P.J. and P.I.H. Bastiaens, Evaluation of global analysis algorithms for single frequency fluorescence lifetime imaging microscopy data. J. Microsc., 2003. **209**(1): p. 1-7.
81. Esposito, A., H.C. Gerritsen, and F.S. Wouters, Fluorescence Lifetime Heterogeneity Resolution in the Frequency Domain by Lifetime Moments Analysis. Biophys. J., 2005. **89**: p. 4286-4299.
82. Maus, M., et al., An Experimental Comparison of the Maximum Likelihood Estimation and Nonlinear Least-Squares Fluorescence Lifetime Analysis of Single Molecules. Anal. Chem., 2001. **73**(9): p. 2078-2086.
83. Laurence, T.A. and B.A. Chromy, *Efficient maximum likelihood estimator fitting of histograms.* Nature Methods, 2010. **7**(5): p. 338-339.
84. Barber, P.R., et al., *A Bayesian method for single molecule, fluorescence burst analysis.* Biomedical Optics Express, 2010. **1**(4): p. 1148-1158.
85. Köllner, M. and J. Wolfrum, *How many photons are necessary for fluorescence-lifetime measurements ?* Chem. Phys. Lett., 1992. **200**: p. 199-204.
86. Barber, P.R., et al., Multiphoton time-domain fluorescence lifetime imaging microscopy: practical application to protein–protein interactions using global analysis. J. R. Soc. Interface, 2009. **6**: p. S93-S105.
87. Grecco, H.E., P. Roda-Navarro, and P.J. Verveer, *Global analysis of time correlated single photon counting FRET-FLIM data.* Optics express, 2009. **17**(8): p. 6493-6508.
88. Harvey, C.D., et al., *A genetically encoded fluorescent sensor of ERK activity.* PNAS, 2008. **105**(49): p. 19264–19269.

89. Digman, M.A., et al., The phasor approach to fluorescence lifetime imaging analysis. Biophys J, 2008. **94**(2): p. L14-6.
90. Padilla-Parra, S., et al., Quantitative FRET analysis by fast acquisition time domain FLIM at high spatial resolution in living cells. Biophys J, 2008. **95**(6): p. 2976-88.
91. Leray, A., et al., Three-dimensional polar representation for multispectral fluorescence lifetime imaging microscopy. Cytometry A, 2009. **75**(12): p. 1007-14.
92. Leray, A., et al., Quantitative comparison of polar approach versus fitting method in time domain FLIM image analysis. Cytometry Part A, 2011. **79A**(2): p. 149-158.
93. Elson, D.S., et al., Real-time time-domain fluorescence lifetime imaging including single-shot acquisition with a segmented optical image intensifier. New Journal of Physics, 2004. **6**(180).
94. Ballew, R.M. and J.N. Demas, An error analysis of the rapid lifetime determination method for the evaluation of single exponential decays. Anal. Chem., 1989. **61**: p. 30-33.
95. Jameson, D.M., E. Gratton, and R.D. Hall, The Measurement and Analysis of Heterogeneous Emissions by Multifrequency Phase and Modulation Fluorometry. Appl Spectrosc Rev, 1984. **20**(1): p. 55-106.
96. Clayton, A.H., Q.S. Hanley, and P.J. Verveer, Graphical representation and multicomponent analysis of single-frequency fluorescence lifetime imaging microscopy data. J Microsc, 2004. **213**(Pt 1): p. 1-5.
97. Redford, G.I. and R.M. Clegg, Polar plot representation for frequency-domain analysis of fluorescence lifetimes. J Fluoresc, 2005. **15**(5): p. 805-15.
98. Fereidouni, F., et al., A modified phasor approach for analyzing time-gated fluorescence lifetime images. J. Microsc., 2011. **244**(3): p. 248-258.
99. Eichorst, J.P., et al., Phase Differential Enhancement of FLIM to Distinguish FRET Components of a Biosensor for Monitoring Molecular Activity of Membrane Type 1 Matrix Metalloproteinase in Live Cells. J. Fluoresc., 2011. **21**: p. 1763-1777.
100. Kazi, J.U. and J.W. Soh, *Isoform-specific translocation of PKC isoforms in NIH3T3 cells by TPA.* Biochem Biophys Res Commun, 2007. **364**(2): p. 231-7.
101. Way, K.J., E. Chou, and G.L. King, Identification of PKC-isoform-specific biological actions using pharmacological approaches. Trends Pharmacol Sci, 2000. **21**(5): p. 181-7.
102. Gallegos, L.L., M.T. Kunkel, and A.C. Newton, Targeting protein kinase C activity reporter to discrete intracellular regions reveals spatiotemporal differences in agonist-dependent signaling. J Biol Chem, 2006. **281**(41): p. 30947-56.
103. Violin, J.D., et al., A genetically encoded fluorescent reporter reveals oscillatory phosphorylation by protein kinase C. J Cell Biol, 2003. **161**(5): p. 899-909.
104. Kajimoto, T., et al., Protein kinase C {delta}-specific activity reporter reveals agonist-evoked nuclear activity controlled by Src family of kinases. J Biol Chem, 2010. **285**(53): p. 41896-910.
105. Thiele, A., G.I. Stangl, and M. Schutkowski, *Deciphering enzyme function using peptide arrays.* Mol Biotechnol, 2011. **49**(3): p. 283-305.
106. Luo, K., P. Zhou, and H.F. Lodish, The specificity of the transforming growth factor beta receptor kinases determined by a spatially addressable peptide library. Proc Natl Acad Sci U S A, 1995. **92**(25): p. 11761-5.
107. Tegge, W.J. and R. Frank, Analysis of protein kinase substrate specificity by the use of peptide libraries on cellulose paper (SPOT-method). Methods Mol Biol, 1998. **87**: p. 99-106.
108. Dostmann, W.R., et al., Exploring the mechanisms of vascular smooth muscle tone with highly specific, membrane-permeable inhibitors of cyclic GMP-dependent protein kinase Ialpha. Pharmacol Ther, 2002. **93**(2-3): p. 203-15.
109. Bardwell, A.J., M. Abdollahi, and L. Bardwell, Docking sites on mitogen-activated protein kinase (MAPK) kinases, MAPK phosphatases and the Elk-1 transcription factor compete for MAPK binding and are crucial for enzymic activity. Biochem J, 2003. **370**(Pt 3): p. 1077-85.
110. Fernandes, N., et al., Use of docking peptides to design modular substrates with high efficiency for mitogen-activated protein kinase extracellular signal-regulated kinase. ACS Chem Biol, 2007. **2**(10): p. 665-73.
111. Jacobs, D., et al., Multiple docking sites on substrate proteins form a modular system that mediates recognition by ERK MAP kinase. Genes Dev, 1999. **13**(2): p. 163-75.
112. Sato, M., Y. Kawai, and Y. Umezawa, Genetically encoded fluorescent indicators to visualize protein phosphorylation by extracellular signal-regulated kinase in single living cells. Anal Chem, 2007. **79**(6): p. 2570-5.
113. Sharrocks, A.D., S.H. Yang, and A. Galanis, *Docking domains and substrate-specificity determination for MAP kinases.* Trends Biochem Sci, 2000. **25**(9): p. 448-53.
114. Smith, J.A., et al., Identification of an extracellular signal-regulated kinase (ERK) docking site in ribosomal S6 kinase, a sequence critical for activation by ERK in vivo. J Biol Chem, 1999. **274**(5): p. 2893-8.
115. Holland, P.M. and J.A. Cooper, *Protein modification: docking sites for kinases.* Curr Biol, 1999. **9**(9): p. R329-31.
116. Gavet, O. and J. Pines, Activation of cyclin B1-Cdk1 synchronizes events in the nucleus and the cytoplasm at mitosis. J Cell Biol, 2010. **189**(2): p. 247-59.
117. Ibraheem, A. and R.E. Campbell, *Designs and applications of fluorescent protein-based biosensors.* Curr Opin Chem Biol, 2010. **14**(1): p. 30-6.

118. Zhang, J., et al., Genetically encoded reporters of protein kinase A activity reveal impact of substrate tethering. Proc Natl Acad Sci U S A, 2001. **98**(26): p. 14997-5002.
119. Zhang, J., et al., Insulin disrupts beta-adrenergic signalling to protein kinase A in adipocytes. Nature, 2005. **437**(7058): p. 569-73.
120. Durocher, D., et al., The molecular basis of FHA domain:phosphopeptide binding specificity and implications for phospho-dependent signaling mechanisms. Mol Cell, 2000. **6**(5): p. 1169-82.
121. Lu, P.J., et al., Function of WW domains as phosphoserine- or phosphothreonine-binding modules. Science, 1999. **283**(5406): p. 1325-8.
122. Nagai, T. and A. Miyawaki, *A high-throughput method for development of FRET-based indicators for proteolysis.* Biochem Biophys Res Commun, 2004. **319**(1): p. 72-7.
123. VanEngelenburg, S.B. and A.E. Palmer, *Fluorescent biosensors of protein function.* Curr Opin Chem Biol, 2008. **12**(1): p. 60-5.
124. Ibraheem, A., et al., A bacteria colony-based screen for optimal linker combinations in genetically encoded biosensors. BMC Biotechnol, 2011. **11**: p. 105.
125. Piljic, A., et al., *Rapid development of genetically encoded FRET reporters.* ACS Chem Biol, 2011. **6**(7): p. 685-91.
126. Kunkel, M.T., et al., Spatio-temporal dynamics of protein kinase B/Akt signaling revealed by a genetically encoded fluorescent reporter. J Biol Chem, 2005. **280**(7): p. 5581-7.
127. Komatsu, N., et al., Development of an optimized backbone of FRET biosensors for kinases and GTPases. Mol Biol Cell, 2011. **22**(23): p. 4647-56.
128. Levskaya, A., et al., Spatiotemporal control of cell signalling using a light-switchable protein interaction. Nature, 2009. **461**(7266): p. 997-1001.
129. Mitra, R.D., C.M. Silva, and D.C. Youvan, Fluorescence resonance energy transfer between blue-emitting and red-shifted excitation derivatives of the green fluorescent protein. Gene, 1996. **173**(1 Spec No): p. 13-7.
130. Miyawaki, A., et al., Fluorescent indicators for Ca2+ based on green fluorescent proteins and calmodulin. Nature, 1997. **388**(6645): p. 882-7.
131. Goedhart, J., et al., Structure-guided evolution of cyan fluorescent proteins towards a quantum yield of 93%. Nat Commun. **3**: p. 751.
132. Nguyen, A.W. and P.S. Daugherty, *Evolutionary optimization of fluorescent proteins for intracellular FRET.* Nat Biotechnol, 2005. **23**(3): p. 355-60.
133. Ouyang, M., et al., Determination of hierarchical relationship of Src and Rac at subcellular locations with FRET biosensors. Proc Natl Acad Sci U S A, 2008. **105**(38): p. 14353-8.
134. Kawai, Y., M. Sato, and Y. Umezawa, Single color fluorescent indicators of protein phosphorylation for multicolor imaging of intracellular signal flow dynamics. Anal Chem, 2004. **76**(20): p. 6144-9.
135. Nagai, T., et al., Expanded dynamic range of fluorescent indicators for Ca(2+) by circularly permuted yellow fluorescent proteins. Proc Natl Acad Sci U S A, 2004. **101**(29): p. 10554-9.
136. Klarenbeek, J.B., et al., A mTurquoise-based cAMP sensor for both FLIM and ratiometric read-out has improved dynamic range. PLoS One, 2011. **6**(4): p. e19170.
137. Ananthanarayanan, B., Q. Ni, and J. Zhang, Signal propagation from membrane messengers to nuclear effectors revealed by reporters of phosphoinositide dynamics and Akt activity. Proc Natl Acad Sci U S A, 2005. **102**(42): p. 15081-6.
138. Palmer, A.E., et al., Bcl-2-mediated alterations in endoplasmic reticulum Ca2+ analyzed with an improved genetically encoded fluorescent sensor. Proc Natl Acad Sci U S A, 2004. **101**(50): p. 17404-9.
139. Sasaki, K., M. Sato, and Y. Umezawa, Fluorescent indicators for Akt/protein kinase B and dynamics of Akt activity visualized in living cells. J Biol Chem, 2003. **278**(33): p. 30945-51.
140. Spriet, C., et al., *Enhanced FRET contrast in lifetime imaging.* Cytometry A, 2008. **73**(8): p. 745-53.
141. KW Dunn, S.M., JN Myers and FR Maxfield *Applications of ratio fluorescence microscopy in the study of cell physiology.* The FASEB Journal, 1994. **8**: p. 573-583.
142. Tomazevic, D., B. Likar, and F. Pernus, *Comparative evaluation of retrospective shading correction methods.* J Microsc, 2002. **208**(Pt 3): p. 212-23.
143. Tsien, R.Y. and A.T. Harootunian, *Practical design criteria for a dynamic ratio imaging system.* Cell Calcium, 1990. **11**(2-3): p. 93-109.
144. Thevenaz, P., U.E. Ruttimann, and M. Unser, *A pyramid approach to subpixel registration based on intensity.* IEEE Trans Image Process, 1998. **7**(1): p. 27-41.
145. Dross, N., et al., *Mapping eGFP oligomer mobility in living cell nuclei.* PLoS One, 2009. **4**(4): p. e5041.
146. Liu, S., J. Zhang, and Y.K. Xiang, FRET-based direct detection of dynamic protein kinase A activity on the sarcoplasmic reticulum in cardiomyocytes. Biochem Biophys Res Commun, 2011. **404**(2): p. 581-6.
147. Castro, L.R., et al., Type 4 phosphodiesterase plays different integrating roles in different cellular domains in pyramidal cortical neurons. J Neurosci, 2010. **30**(17): p. 6143-51.
148. Goedhart, J., et al., Bright cyan fluorescent protein variants identified by fluorescence lifetime screening. Nat Methods, 2010. **7**(2): p. 137-9.
149. Kremers, G.J., et al., Cyan and yellow super fluorescent proteins with improved brightness, protein folding, and FRET Forster radius. Biochemistry, 2006. **45**(21): p. 6570-80.
150. Kriegsheim, A., C. Preisinger, and W. Kolch, *Mapping of signaling pathways by functional interaction proteomics.* Methods Mol Biol, 2008. **484**: p. 177-92.

151. Santos, S.D., P.J. Verveer, and P.I. Bastiaens, Growth factor-induced MAPK network topology shapes Erk response determining PC-12 cell fate. Nat Cell Biol, 2007. **9**(3): p. 324-30.
152. Mebratu, Y. and Y. Tesfaigzi, How ERK1/2 activation controls cell proliferation and cell death: Is subcellular localization the answer? Cell Cycle, 2009. **8**(8): p. 1168-75.
153. Ebisuya, M., K. Kondoh, and E. Nishida, The duration, magnitude and compartmentalization of ERK MAP kinase activity: mechanisms for providing signaling specificity. J Cell Sci, 2005. **118**(Pt 14): p. 2997-3002.
154. Dong, J., et al., EGFR-independent activation of p38 MAPK and EGFR-dependent activation of ERK1/2 are required for ROS-induced renal cell death. Am J Physiol Renal Physiol, 2004. **287**(5): p. F1049-58.
155. Boutros, T., E. Chevet, and P. Metrakos, Mitogen-activated protein (MAP) kinase/MAP kinase phosphatase regulation: roles in cell growth, death, and cancer. Pharmacol Rev, 2008. **60**(3): p. 261-310.
156. Chen, C.H., et al., Bidirectional signals transduced by DAPK-ERK interaction promote the apoptotic effect of DAPK. Embo J, 2005. **24**(2): p. 294-304.
157. Mebratu, Y.A., et al., The BH3-only protein Bik/Blk/Nbk inhibits nuclear translocation of activated ERK1/2 to mediate IFNgamma-induced cell death. J Cell Biol, 2008. **183**(3): p. 429-39.
158. Trencia, A., et al., Protein kinase B/Akt binds and phosphorylates PED/PEA-15, stabilizing its antiapoptotic action. Mol Cell Biol, 2003. **23**(13): p. 4511-21.
159. Maeder, C.I., et al., Spatial regulation of Fus3 MAP kinase activity through a reaction-diffusion mechanism in yeast pheromone signalling. Nat Cell Biol, 2007. **9**(11): p. 1319-26.
160. Blossey, R., et al., Signal propagation of the MAPK cascade in Xenopus oocytes: role of bistability and ultrasensitivity for a mixed problem. J Math Biol. **64**(1-2): p. 1-39.
161. Kholodenko, B.N. and M.R. Birtwistle, *Four-dimensional dynamics of MAPK information processing systems.* Wiley Interdiscip Rev Syst Biol Med, 2009. **1**(1): p. 28-44.
162. Tasken, K. and E.M. Aandahl, Localized effects of cAMP mediated by distinct routes of protein kinase A. Physiol Rev, 2004. **84**(1): p. 137-67.
163. Willoughby, D. and D.M. Cooper, *Organization and Ca2+ regulation of adenylyl cyclases in cAMP microdomains.* Physiol Rev, 2007. **87**(3): p. 965-1010.
164. Wong, W. and J.D. Scott, *AKAP signalling complexes: focal points in space and time.* Nat Rev Mol Cell Biol, 2004. **5**(12): p. 959-70.
165. Neves, S.R., et al., Cell shape and negative links in regulatory motifs together control spatial information flow in signaling networks. Cell, 2008. **133**(4): p. 666-80.
166. Gervasi, N., et al., Dynamics of protein kinase A signaling at the membrane, in the cytosol, and in the nucleus of neurons in mouse brain slices. J Neurosci, 2007. **27**(11): p. 2744-50.
167. Castro, L.R., et al., Type 4 phosphodiesterase plays different integrating roles in different cellular domains in pyramidal cortical neurons. J Neurosci. **30**(17): p. 6143-51.
168. Castro, L., et al., PDE4 control on cAMP/PKA compartmentation revealed by biosensor imaging in neurons. Hormone and Metabolic Research, 2012. **in press**.
169. Taylor, R.J., et al., Dynamic analysis of MAPK signaling using a high-throughput microfluidic single-cell imaging platform. Proc Natl Acad Sci U S A, 2009. **106**(10): p. 3758-63.
170. Machacek, M., et al., *Coordination of Rho GTPase activities during cell protrusion.* Nature, 2009. **461**(7260): p. 99-103.
171. Carlson, H.J. and R.E. Campbell, *Genetically encoded FRET-based biosensors for multiparameter fluorescence imaging.* Curr Opin Biotechnol, 2009. **20**(1): p. 19-27.
172. Piljic, A. and C. Schultz, *Simultaneous recording of multiple cellular events by FRET.* ACS Chem Biol, 2008. **3**(3): p. 156-60.
173. Kishikawa, J., et al., MRT letter: Expression of ATP sensor protein in Caenorhabditis elegans. Microsc Res Tech, 2011. **75**(1): p. 15-9.
174. Lissandron, V., et al., Transgenic fruit-flies expressing a FRET-based sensor for in vivo imaging of cAMP dynamics. Cell Signal, 2007. **19**(11): p. 2296-303.
175. Lissandron, V., et al., Improvement of a FRET-based indicator for cAMP by linker design and stabilization of donor-acceptor interaction. J Mol Biol, 2005. **354**(3): p. 546-55.
176. Kardash, E., J. Bandemer, and E. Raz, Imaging protein activity in live embryos using fluorescence resonance energy transfer biosensors. Nat Protoc, 2011. **6**(12): p. 1835-46.
177. Gervasi, N., P. Tchenio, and T. Preat, PKA dynamics in a Drosophila learning center: coincidence detection by rutabaga adenylyl cyclase and spatial regulation by dunce phosphodiesterase. Neuron. **65**(4): p. 516-29.
178. Fan-Minogue, H., et al., *Noninvasive molecular imaging of c-Myc activation in living mice.* Proceedings of the National Academy of Sciences. **107**(36): p. 15892-15897.
179. Kamioka, Y., et al., Live Imaging of Protein Kinase Activities in Transgenic Mice Expressing FRET Biosensors. Cell Struct Funct, 2012.
180. Yamaguchi, Y., et al., Live imaging of apoptosis in a novel transgenic mouse highlights its role in neural tube closure. J Cell Biol, 2011. **195**(6): p. 1047-60.
181. Calebiro, D., et al., Persistent cAMP-signals triggered by internalized G-protein-coupled receptors. PLoS Biol, 2009. **7**(8): p. e1000172.

Part 4: Results

4.1. Research article – Novel reporter for faithful monitoring of ERK2 dynamics in living cells and model organisms

François Sipieter[1,2,4,5,8], Benjamin Cappe[1,2,8], Mariano Gonzalez Pisfil[4,8], Corentin Spriet[7], Jean-François Bodart[5], Katia Cailliau-Maggio[5], Peter Vandenabeele[1,2,3], Laurent Héliot[4,8], Franck Riquet[1,2,6,8]

[1] Molecular Signaling and Cell Death Unit, Department of Biomedical Molecular Biology, Ghent University, B-9052 Ghent, Belgium

[2] Molecular Signaling and Cell Death Unit, Inflammation Research Center (IRC), a VIB-UGent department, B-9052 Ghent, Belgium

[3] Methusalem Program, Ghent University, B-9052 Ghent, Belgium

[4] Team Biophotonique Cellulaire Fonctionnelle, Laboratoire de Physique des Lasers, Atomes et Molécules (PhLAM), CNRS UMR 8523, F-59655 Villeneuve d'Ascq, France

[5] Team Régulation des Signaux de Division, Structural and Functional Glycobiology Unit (UGSF), CNRS UMR 8576, Lille 1 University, F-59655 Villeneuve d'Ascq, France

[6] Structural and Functional Glycobiology Unit (UGSF), CNRS UMR 8576, Lille 1 University, F-59655 Villeneuve d'Ascq, France

[7] TISBio, Structural and Functional Glycobiology Unit (UGSF), CNRS UMR 8576, FR3688, Lille 1 University, F-59655 Villeneuve d'Ascq, France

[8] Groupement de Recherche Microscopie Imagerie du Vivant, GDR2588-MIV CNRS, F-59655 Villeneuve d'Ascq, France

Published in Plos One, 2015

Research Article

Novel reporter for faithful monitoring of ERK2 dynamics in living cells and model organisms

François Sipieter[12458], Benjamin Cappe[128], Mariano Gonzalez Pisfil[48], Corentin Spriet[7], Jean-François Bodart[5], Katia Cailliau-Maggio[5], Peter Vandenabeele[123], Laurent Héliot[48], Franck B. Riquet[1268*]

[1]Molecular Signaling and Cell Death Unit, Department of Biomedical Molecular Biology, Ghent University, Ghent, Belgium.

[2]Molecular Signaling and Cell Death Unit, Inflammation Research Center (IRC), VIB, Ghent, Belgium.

[3]Methusalem Program, Ghent University, Ghent, Belgium.

[4]Equipe Biophotonique Cellulaire Fonctionnelle, Laboratoire de Physique des Lasers, Atomes et Molécules (PhLAM), CNRS-UMR 8523, Villeneuve d'Ascq, France.

[5]Regulation of Signal Division Team, Structural and Functional Glycobiology Unit (UGSF), CNRS-UMR 8576, Lille 1 University, Villeneuve d'Ascq, France.

[6]Structural and Functional Glycobiology Unit (UGSF), CNRS-UMR 8576, Lille 1 University, Villeneuve d'Ascq, France.

[7]TISBio, Structural and Functional Glycobiology Unit (UGSF), CNRS-UMR 8576, FR3688, Lille 1 University, Villeneuve d'Ascq, France.

[8]Groupement de Recherche Microscopie Imagerie du Vivant, GDR2588 MIV-CNRS, Villeneuve d'Ascq, France.

* Corresponding author:

Franck B. Riquet, franck.riquet@irc.vib-ugent.be (FR)

Abstract

Uncoupling of ERK1/2 phosphorylation from subcellular localization is essential towards the understanding of molecular mechanisms that control ERK1/2-mediated cell-fate decision. ERK1/2 non-catalytic functions and discoveries of new specific anchors responsible of the subcellular compartmentalization of ERK1/2 signaling pathway have been proposed as regulation mechanisms for which dynamic monitoring of ERK1/2 localization is necessary. However, studying the spatiotemporal features of ERK2, for instance, in different cellular processes in living cells and tissues requires a tool that can faithfully report on its subcellular distribution. We developed a novel molecular tool, ERK2-LOC, based on the T2A-mediated coexpression of strictly equimolar levels of eGFP-ERK2 and MEK1, to faithfully visualize ERK2 localization patterns. MEK1 and eGFP-ERK2 were expressed reliably and functionally both in vitro and in single living cells. We then assessed the subcellular distribution and mobility of ERK2-LOC using fluorescence microscopy in non-stimulated conditions and after activation/inhibition of the MAPK/ERK1/2 signaling pathway. Finally, we used our coexpression system in *Xenopus laevis* embryos during the early stages of development. This is the first report on MEK1/ERK2 T2A-mediated coexpression in living embryos, and we show that there is a strong correlation between the spatiotemporal subcellular distribution of ERK2-LOC and the phosphorylation patterns of ERK1/2. Our approach can be used to study the spatiotemporal localization of ERK2 and its dynamics in a variety of processes in living cells and embryonic tissues.

4.1.1. Introduction

Extracellular signal-Regulated protein Kinases 1 and 2 (ERK1/2) are members of the Mitogen Activated Protein Kinase (MAPK) superfamily. The ERK1/2 signaling pathway plays an important role in the cellular signaling network by regulating several cellular processes, such as cell survival, proliferation, migration, differentiation and death, depending on the cellular context [1,2]. The ERK1/2 signaling pathway displays the characteristic three-tiered core cascade MAPK architecture [3], ensuring not only signal transduction but also amplification of signals from different membrane-stimulated receptors, such as Receptor Tyrosine Kinases (RTK) and G Protein-Coupled Receptors (GPCRs) [4,5]. Activation of the pathway by

different extracellular stimuli triggers sequential phosphorylation of the protein kinases Raf, MAPK/ERK Kinase 1/2 (MEK1/2) and ERK1/2, which constitute a conserved signaling module. Compelling evidence indicates that the ERK1/2 cascade is involved in the pathogenesis, progression and oncogenic behavior of several human cancers, including lung, breast, colorectal and pancreatic cancer, as well as glioblastoma and melanoma [6,7].

Though the biochemical events of ERK1/2 signaling have been well characterized, a central question remains: How can this signaling cascade trigger different cellular outcomes? An increasing number of papers have shown that modulation of the duration, magnitude and subcellular compartmentalization of ERK1/2 activity by specific key regulators are interpreted by the cell to determine cell fate [8,9]. Moreover, preservation of the integrity of cell decisions requires control of the dynamic subcellular distribution of ERK1/2 and its ability to access ERK1/2 substrates. In resting cells, components of the ERK1/2 signaling pathway are mainly sequestered in the cytoplasm by cytoplasmic scaffold/anchoring proteins [10]. One of the positive regulators of the ERK1/2 cascade is the evolutionarily conserved Kinase Suppressor of Ras (KSR), which facilitates activation of the pathway by bringing the components of ERK1/2 signaling close to Ras at the plasma membrane [11]. MEK1 is sequestered in the cytoplasm of resting cells by its N-terminal nuclear export sequence (NES) and functions as a cytoplasmic anchor for inactive ERK2 [12]. Upon extracellular stimulation and activating phosphorylation, MEK1 and ERK2 are released from cytoplasmic anchors and rapidly translocate into the nucleus [13–16]. Besides its apparent cytoplasmic localization, 5% of MEK1 can be found in the nucleus at the peak of activation of the pathway [17]. MEK1 can rapidly transit between the cytoplasm and the nucleus much faster than ERK2 and therefore acts as a nuclear export shuttle for ERK2 and other nuclear proteins [18]. Besides differences between cells in spatiotemporal dynamics of ERK1/2 [19], it appears that ERK1/2 phosphorylation and subcellular distribution are uncoupled in several cellular models due to interaction of ERK1/2 with various anchors/scaffolds [20,21]. Upon mitogenic stimulation, ERK1/2 signaling upregulates the expression of short-lived nuclear anchors such as MAPK phosphatases (MKP), which leads to dephosphorylation of ERK1/2 and accumulation of its inactive form in the nucleus several hours after pathway activation [21,22]. Monitoring the dynamic behavior of

ERK1/2 in single cells will resolve this apparently conflictual relationship and evaluate the effects of specific regulators of ERK1/2 compartmentalization on cell fate determination.

To visualize ERK1/2 dynamics in living cells, various studies used ERK1/2 tagged with GFP-like fluorescent proteins and found that overexpressed eGFP-ERK2 is predominantly localized in the nucleus of resting cells. This unexpected localization of eGFP-ERK2 was due to the disruption of MEK/ERK balance [12,15]. This problem has been often ignored [16,23–25] or tackled by coexpression of MEK1 to restore the balance and the cytoplasmic localization of ERK2 expressed at high levels in serum-starved cultures without stimulation [26,27]. These coexpression strategies mostly suffer from the inconsistency of the coexpression patterns of ERK2 and MEK1 in different cells. Coexpression of eGFP-ERK2 and MEK1 is generally associated with an abnormally short persistence of eGFP-ERK2 in the nucleus of resting cells, in contrast to endogenous ERK2, which remains in the nucleus several hours after mitogenic stimulation [21,26,27]. To overcome this difficulty, other studies selected cells expressing low levels of eGFP-ERK2 (100–150 nM) compared to the estimated endogenous protein level (1 μM) [28] to obtain a faithful localization profile of the kinase in serum-starved conditions [29]. However, transfected cells are dimly fluorescent, which are unsuitable for long-term video imaging. As a new approach to maintain the endogenous MEK/ERK balance, an exogenous tagged version of ERK1 was re-expressed in ERK1-deficient cell lines by transient transfection of a plasmid encoding ERK1 under the control of a strong promoter [30]. Cells were selected for tagged-ERK1 expression level on the basis that the nucleus was not brighter than the cytoplasm in the starved conditions. Nevertheless, the delicate MEK/ERK balance was progressively disrupted a few hours after transfection, resulting again in aberrant nuclear accumulation of ERK1 in non-stimulated conditions. Another study used a retroviral tagging approach and introduced the full-length sequence of YFP as a new exon into one allele of the *erk2* gene [19]. The tagged ERK2 was in minority compared to the wild-type protein, which led to proper subcellular distribution of tagged-ERK2 in the starved conditions. But again the fluorescent intensity was dim due to the low expression level. All these approaches are limited by the need for severe imaging conditions (causing phototoxicity, photobleaching and decrease of

signal to noise ratio) that are not compatible with live cell video-microscopy, especially considering the stress-sensitive nature of MAPK pathways [31].

To avoid the artefacts in ERK2 localization patterns and facilitate the long-term functional imaging, we developed a novel ERK2 localization reporter named ERK2-LOC. We employed the T2A-mediated coexpression of ERK2 and MEK1 to enable faithful monitoring of eGFP-ERK2 localization dynamics in both basal and growth factor-stimulated conditions. Our procedure was characterized using standard biochemical approaches and validated by live-cell imaging in living NIH-3T3 cells. Final verification was conducted in the *Xenopus laevis* model during the early developmental stages. This is the first time that ERK2 localization is studied in living embryos. Our simple approach can be used for the reliable study of the spatiotemporal dynamic of ERK2 in living cells and in live model organisms.

4.1.2. Materials and Methods

Ethics Statement

All animal experiments were performed at Lille 1 University according to the rules of the European Community Council guidelines (86/609/EEC) for laboratory animal experimentation. The local institutional review board (*Comité d'Ethique en Expérimentation Animale Nord-Pas-De-Calais* (CEEA, 07/2010) approved all animal experimental protocols in this study.

Reagents

Recombinant mouse fibroblast growth factor 4 (FGF4, #5846-F4-025/CF) was purchased from R&D Systems and fetal bovine serum (FBS, #10082-147) from Gibco, Life Technologies. Other reagents, *e.g.*, bovine serum albumin (BSA, fraction V, #05482), dimethylsulfoxide (DMSO, #D8418) and MEK inhibitor (U0126, #U120) were from Sigma Aldrich.

Plasmid constructs

The plasmid pCS2-Myr-TdTomato-T2A-Histone2B-GFP was kindly provided by Dr. Shankar Srinivas (Department of Physiology Anatomy and Genetics, University of Oxford, United Kingdom). *Xenopus laevis* ERK2 (xERK2) plasmid was a kind gift from Dr. Lynn Heasley (Health Science Center, University of Colorado, Denver, USA).

Primer name	Oligonucleotide sequence (5'→3')	Tm(°C) / %GC
BackboneΔAgeI-F	GCTACTTGTTCTTTTTGCAACCGGTGGATCCCATCGATTCGAATTC	70 / 46
Backbone7G-F1	CCGGTGGCGCGCC GCTAGC*GGTGGCGGAGGTGGCGGAGGT*TA	84 / 76
Backbone7G-R1	CCGGTA*ACCTCCGCCACCTCCGCCACC*GCTAGC GGCGCGCCA	84 / 76
Backbone7G-F2	CTAGCGGCACCGGTGGCTGTACAAG*GGAGGCGGTGGAGGCGGTGGG*	82 / 72
Backbone7G-R2	CTAG*CCCACCGCCTCCACCGCCTCC*CTTGTACAGCCACCGGTGCCG	82 / 72
Backbone7G-F3	CC*GGAGGTGGCGGAGGTGGCGGG*ACTAGTCCAGGCGCGCCTCCGC	84 / 78
Backbone7G-R3	TCGAGCGGAGGCGCGCCTGGACTAGT*CCCGCCACCTCCGCCACC*T	84 / 73
xERK2.AgeI-BamHI-F	TACCGGT GGATCCAC**ATG**GCAGCGGCAGCGGCCTCGTC	79 / 68
xERK2.XhoI-R	GAGGCTCGAG**TCA**GTACCCTGGCTGGAATCTAGCG	71 / 60
eGFP.AscI-F	CGCCGGCGCGCCAGCCATGGTGAGCAAGGGCGAGG	81 / 77
eGFP.NheI-R	ACCGCTAGCCTTGTACAGCTCGTCCATGCC	70 / 60
T2A.AscI-F	CGCGCCGGACTAGTCCATCGAT*GGCAGTGGAGAGGGCAGAGGAAGTCTGCT AACATGCGGTGACGTCGAGGAGAATCCTGGCCCA*GGTGG	84 / 62
T2A.AscI-R	CGCGCCACC*TGGGCCAGGATTCTCCTCGACGTCACCGCATGTTAGCAGACTT CCTCTGCCCTCTCCACTGCC*ATCGATGGACTAGTCCGG	84 / 62
xMEK1.SpeI-F	GGACTAGTCCAACATGCCTAAAAAGAAGCCT	64 / 45
xMEK1.ClaI-F	CCATCGATGGCCACTCCGGCGGCATGGGTTG	74 / 68
mMEK1.SpeI-F1	GGACTAGTCCAAGATGCCCAAGAAGAAGCCG	67 / 55
mMEK1.SpeI-F2	GGACTAGTCCCAAGAAGAAGCCGACGCCCATCCAGCTG	73 / 61
mMEK1.ClaI-R	CCATCGATGGCGATGCTGG CAGCGTGGGTTG	73 / 65
mMEK1.AscI-R	AGGCGCGCC**TCA**GATGCTGGCAGCGTGGGTTGGTGTGCTGGG	81/ 69

Abbreviations: 7G, 7-glycine linker; F, forward primer; R, reverse primer. Restriction enzyme sites are underlined and start/stop codons are in bold.

Table 1. Sequence of oligonucleotide primers used in this study.

The plasmid encoding *Rattus norvegicus* ERK2 (rERK2) fused at its N-terminal to the enhanced green fluorescent protein (eGFP-rERK2) was a kind gift from Dr. Georges Baffet (UMR1085 INSERM, University of Rennes, France). All oligonucleotides are listed in Table 1. The synthetized DNA sequence encoding the *Thosea asigna* virus 2A peptide (T2A peptide) was inserted into the pCS2+ backbone in frame between untagged *Mus musculus* MEK1 (mMEK1) and eGFP-rERK2 to build the expression vector pCS2-mMEK1-2A-eGFP-rERK2 (abbreviated rERK2-LOC). We next fused a mCherry to the N-terminus of mMEK1 to generate the construct named pCS2-mCherry-mMEK1-2A-eGFP-rERK2. The full-length cDNA sequences of MEK1 and ERK2 from *Xenopus laevis* were subcloned upstream and downstream, respectively, of the T2A peptide. We fused an eGFP to the N-terminus of xERK2 to generate the construct named pCS2-xMEK1-2A-eGFP-xERK2 (abbreviated xERK2-LOC). As a control, we fused the T2A sequence to the N-

terminus of eGFP-xERK2 (pCS2-2A-eGFP-xERK2). Based on published studies, we kept a Gly-Ser-Gly (GSG) linker between MEK1 and the T2A sequences to optimize cleavage efficiency [32,33]. The cloning procedure is detailed in Supplementary Material (plasmid constructs). All PCR products were gel purified and digested with restriction endonucleases according to the cloning strategies. All resulting constructs were verified by restriction digestion followed by agarose gel electrophoresis, or by PCR colony screening (#2200210, MasterTaq Kit, 5Prime), and then validated by sequencing (Genoscreen, France). Restriction endonucleases *Pfu* and *Taq* DNA polymerase, Klenow fragment, Mung Bean Nuclease, T4 Polynucleotide kinase (PNK), T4 DNA ligase, as well as dNTPs, ATP and specific buffers were purchased from New England Biolabs. All oligonucleotides were synthesized by Eurogentech (Belgium). Each complementary oligonucleotide designed to create double-stranded cassettes was 5'-phosphorylated by T4 PNK and then purified using Bio-Gel P-6 Micro Bio-Spin chromatography columns (#732-6222, Biorad). DNA fragments were all purified on Qiagen plasmid purification columns (#28106, #28706 and # 27106, Qiagen).

Cell Culture and Transfection

NIH-3T3 cells were purchased from American Type Culture Collection (VA, USA) and maintained at 37°C under 5% CO_2 in Dulbecco's Modified Eagle Medium (DMEM, #11885-084) supplemented with 10% FBS and 100 U/mL penicillin/streptomycin (P/S, #15140-122) (Gibco, Life Technologies). For live imaging, NIH3T3 cells were plated on 35-mm dishes (#81156, ibiTreat, Ibidi) to reach 60% confluence at the time of transfection, performed using JetPrime reagent (#114-15, Polyplus) according to the manufacturer's instructions. Cells were starved by adding 1% FBS for 24 h before experiments began. One hour before cell imaging, medium was replaced with preheated Leibovitz L-15 bicarbonate-free medium (#11415-049, Gibco, Life Technologies) supplemented with 1% FBS and 100 units/mL P/S at 37°C in air.

SDS-PAGE and Immunoblotting

At specified intervals after treatment, NIH-3T3 cells were washed twice in ice-cold PBS and scraped using ice-cold RIPA lysis buffer (50 mM Tris-HCl, pH 7.5; 150 mM NaCl; 1 mM EDTA; 0.5% sodium deoxycholate; 1% Triton X-100 and 0.1% SDS)

or immunoprecipitation lysis buffer (10 mM Tris-HCl, pH 8.0; 150 mM NaCl; 2 mM EDTA; 10% glycerol and 1% NP40). Lysis buffer was freshly supplemented with 1X EDTA-free Complete protease (#05892791001, Roche) and 1X PhosStop phosphatase inhibitor cocktail (#04906845001, Roche). Extracted proteins (30 µg) were separated in 12% SDS polyacrylamide gels and then transferred onto nitrocellulose membranes (Amersham Bioscience). Protein extracts from 10 whole *Xenopus laevis* embryos were prepared as described [34] and loaded into a 12% SDS polyacrylamide gel. Membranes were blocked using TBS with 0.05% Tween20 (TBS-T) containing 5% non-fat dry milk (Biorad) or in 2% BSA for phospho-antibodies. The antibodies were anti-ERK2 (polyclonal rabbit IgG (C-14) and monoclonal mouse IgG2b (D-2) from Santa Cruz Biotechnology, 1:1000), anti-actin (polyclonal goat IgG (I-19) from Santa Cruz Biotechnology, 1:1000) and anti-GFP (monoclonal mouse IgG1κ, clones 7.1 and 13.1, from Roche (#11814460001), 1:1000). The phosphorylated forms of MAPK/ERK1/2 were detected using the anti-MAPK activated (diphosphorylated ERK1/2) antibody (monoclonal mouse IgG1, clone MAPK-YT, from Sigma Aldrich (M9692), 1:2000). HRP-conjugated secondary antibodies were anti-rabbit IgG, anti-mouse IgG or anti-goat IgG (whole antibody from Santa Cruz Biotechnology (sc-2004, sc-2005, sc-2020), 1:10000). Membranes were developed using the Luminata Classico Western HRP Chemiluminescence Detection Reagents (WBLUC0500, Millipore).

Immunoprecipitation of MAPK/ERK2 and MBP phosphorylation assay

NIH-3T3 cell lysates (300 µg of protein) were immunoprecipitated directly as described [35]. Briefly, 50 µL of protein G magnetic beads (Millipore) per condition were washed and then conjugated with 1 µg of anti-ERK2 (C-14) or anti-GFP antibodies on a rotating wheel at 4°C overnight. Note that this anti-ERK2 antibody can also detect ERK1 although to a lesser extent. Antibodies against HA (#11583816001, Roche) were used as a control. The next day, antibody-conjugated beads were added to each sample and incubated on a rotating wheel at 4°C for 2 h. Supernatant was removed and beads were washed in lysis buffer. The MBP phosphorylation assay was performed on immunoprecipitated endogenous ERK2 and eGFP-ERK2 according to the manufacturer's instructions (#2430444, Millipore). MBP proteins were subjected to SDS-PAGE (15% gel) and immunoblotted using an

anti-phospho MBP antibody (monoclonal mouse IgG, clone p12, from Millipore (#05429), 1:1000).

Immunofluorescence

NIH-3T3 cells were seeded in eight-well dishes (#80826, ibiTreat, Ibidi). At specified time intervals, cells were fixed in 4% paraformaldehyde in PBS for 10 min. Afterwards, cells were rinsed three times with PBS and permeabilized with 0.5% Triton X-100 in PBS for 5 min. Cells were then blocked in 2% FBS; 5% normal goat serum and 2% BSA in PBS) for 1 h at room temperature and with primary antibodies in blocking solution at 4°C overnight. The antibodies were anti-MAPK activated (diphosphorylated ERK1/2, 1:500), anti-ERK2 (D-2, 1:200) and anti-ERK1/2 (polyclonal rabbit IgG from Abcam (ab17942), 1:200). The next day, cells were rinsed three times with PBS and incubated in blocking solution containing anti-mouse Alexa Fluor 488 (polyclonal goat IgG from Life Technologies (A-10667), 1:500) and/or anti-rabbit Alexa Fluor 594 secondary antibodies (polyclonal goat IgG from Life Technologies (A-11012), 1:500) for 1 h at room temperature in the dark. After three more washes with PBS, slides were mounted in ProLong Gold anti-fading reagent (P36930, Life Technologies) and stored at 4°C in the dark.

Xenopus embryo manipulation, RNA microinjection and immunostaining

Hormonal stimulation of female frogs, eggs collection, fertilization and dejellying of embryos were performed as previously described [36]. *Xenopus* embryos were staged as described [37]. Plasmids encoding eGFP-xERK2, 2A-eGFP-xERK2 and xMEK1-2A-eGFP-xERK2 were linearized with *Not*I, purified and transcribed using SP6 RNA polymerase and the mMessage mMachine kit (AM1340, Ambion, Life Technologies) according to the manufacturer's instructions. Synthetic RNAs were purified with Chroma Spin column (#636073, Clontech). Embryos at the one-cell stage were microinjected with 500 pg of RNA. Embryos at different stages were collected for western blotting and immunostaining or directly processed for whole-embryo confocal microscopy. Blastula, gastrula and tailbud stage embryos were placed in an imaging chamber containing a layer of 2% agarose MP (#11388983001, Roche) and 1/10 Marc's Modified Ringers (MMR) solution (1 M NaCl; 20 mM KCl; 10 mM $MgCl_2$; 20 mM $CaCl_2$ and 50 mM Hepes, pH 7.5). *Xenopus laevis* embryos were fixed in 4% paraformaldehyde at 4°C overnight with gentle

shaking in glass vials and then processed for whole-mount immunostaining [38]. Antibodies were anti-ERK2 (D-2, 1:50) and Alexa Fluor 488 goat anti-mouse IgG secondary antibodies (1:100). Embryos were cut in half at the equator, and the animal half was mounted on a curved slide in ProLong Gold anti-fading reagent and stored at 4°C in the dark.

Fluorescence imaging and data analysis

Live-cell, immunofluorescence imaging and FRAP experiments were all performed with an inverted confocal Leica TCS SP5 X microscope (DMI6000, Leica Microsystems). For all experiments, a 63x/1.2NA water immersion objective was used, except for the result shown in Fig. 1A (40x/1.3NA oil immersion objective). Image size was 1024 x 1024 pixels and the zoom factor was 1, for a pixel size of 0.5 µm. The confocal pinhole was set to 1.0 Airy, for a 0.921 µm optical slice. Laser sources were either a white light laser (Koheras) for live-cell imaging and immunofluorescence preparations, or an argon laser (Leica Microsystems) used at a wavelength of 488 nm for FRAP experiments. All experiments were performed at 37°C.

To quantify ERK2 nuclear translocation, we measured the average fluorescence intensity in the nucleus ($Fnuc$) and in the cytoplasm ($Fcyto$) to determine a nucleo-cytoplasmic concentration index (CI) calculated as follows:

$$CI = \frac{Fnuc - BG}{Fcyto - BG}$$

where *BG* corresponds to the average fluorescence intensity background. Fluorescence intensity in fixed cells was quantified manually using ImageJ software (National Institutes of Health) by drawing specific ROIs in the nucleus and cytoplasm, and outside the cell for background. Fluorescence intensity quantification of ERK2-LOC dynamics in single cells was done automatically with Volocity image analysis software (Perkin Elmer), which required segmentation of fluorescence labeled cells throughout the entire time-lapse. This was done by incubating the cells with Hoechst before starting the experiment to discriminate nuclei from whole cells and to define a mask around each nucleus. Cytoplasm fluorescence intensity of ERK2-LOC was then measured by subtracting fluorescence intensity due to the nucleus from that of the whole cell.

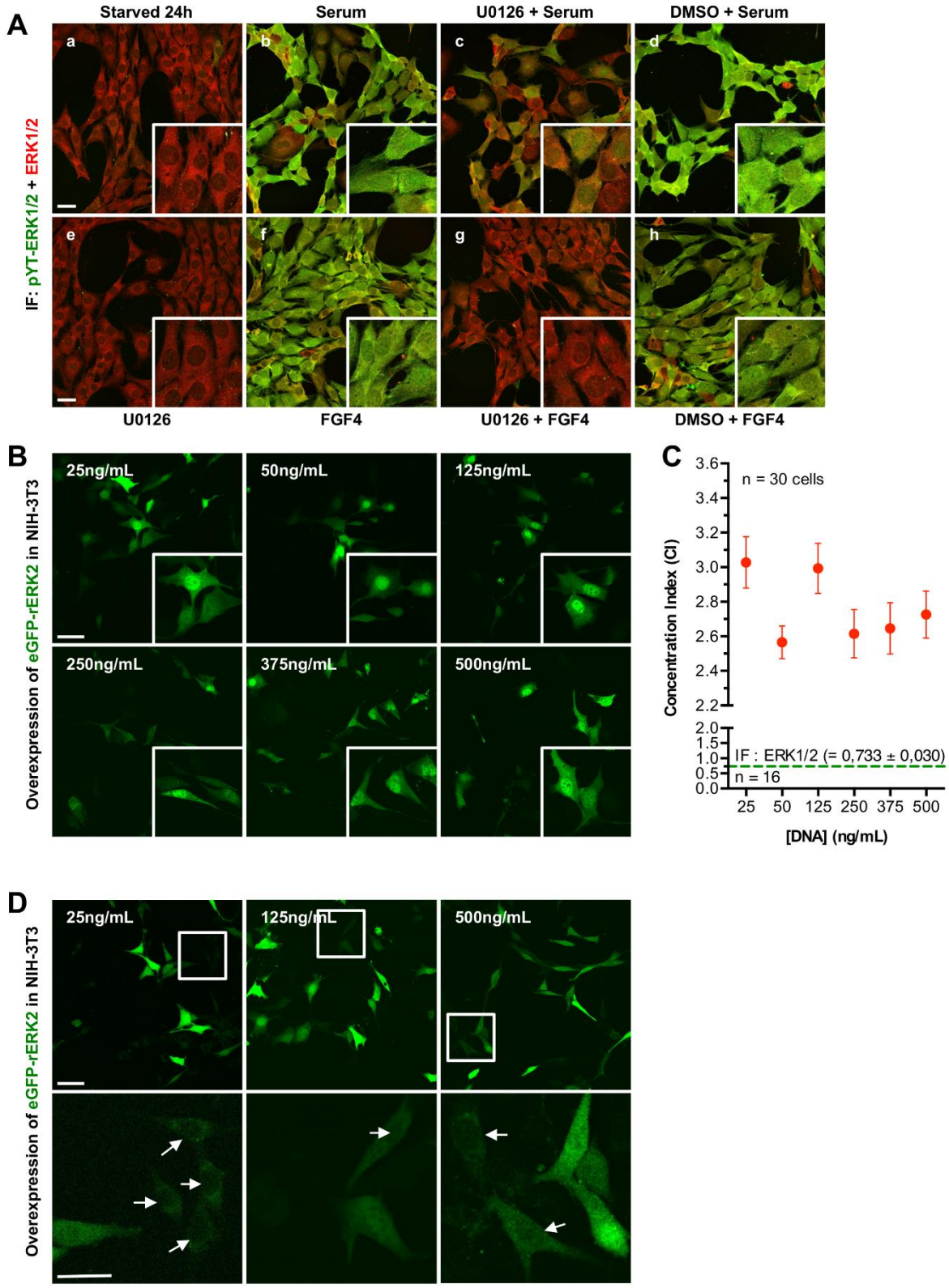

Fig. 1. Overexpression of eGFP-rERK2 induces nuclear accumulation of eGFP-rERK2. (A) NIH3T3 cells were serum-starved for 24 h (a) and then stimulated with 10% serum (b) or 100 ng/mL FGF4 (f). In other conditions, cells were pretreated with 20 µM U0126 (c, e, g) or vehicle DMSO (d, h) for 30 min before stimulation with 10% serum (c, d) or FGF4 (g, h). Cells were fixed, processed for

double immunofluorescence with antibodies against total ERK1/2 and activated di-phosphorylated YT-ERK1/2, and then imaged by confocal microscopy. A maximum-intensity projection of a 5-µm thick z-stack (step size: 0.3 µm) for each overlapping image is shown. **(B)** NIH-3T3 cells were transiently transfected with increasing amounts of eGFP-rERK2 plasmid as indicated on the top left of each image, serum-starved for 24 h, fixed, and then imaged by confocal microscopy. The total amount of DNA was kept at 500 ng/mL of medium in all conditions. Higher magnification images of representative eGFP-rERK2 localization are shown in white squares (bottom right). Scale bars: 50 µm. **(C)** Relationship between the concentration of eGFP-rERK2 plasmid and the concentration index (CI). Higher CI values reflect greater accumulation of eGFP-ERK2 in the nucleus. Average CI was determined by examination of at least 30 randomly selected cells for each of the transfected conditions from two independent experiments. Average CI value for endogenous ERK1/2 in serum-starved NIH-3T3 is also shown (green dotted line). **(D)** NIH-3T3 cells transfected with 25, 125 or 500 ng/mL of eGFP-rERK2 were observed under severe imaging conditions to visualize cells that express very low level of eGFP-rERK2 protein (upper panel, white squares). Higher magnification images of these cells exhibiting mainly cytoplasmic localization of eGFP-rERK2 are also shown (bottom panel, white arrows). Scale bars: 50 µm.

Whole *Xenopus laevis* embryos at early stages of development were imaged with an upright confocal Nikon A1 microscope (Eclipse FN1, Nikon). A 25x/1.1NA objective lens was used, and pinhole was set to 0.6 Airy for an optical slice of 1.04 µm. Image size was 1024 x 1024 pixels acquired at a speed of 0.5 frames/sec (scanning speed of 512 Hz). The zoom factor was 1 for a pixel size of 0.5 µm. 3D reconstructions of the confocal z-stack images were performed using NIS Elements 4.3 software (Nikon) and ImageJ (National Institutes of Health). *Xenopus laevis* embryos tailbud stage were imaged on an upright Nikon Eclipse 80i epifluorescence microscope equipped with a 4x/0.13NA Plan Fluor objective (Nikon) and a CoolSNAP ES CCD Photometrics camera (Roper Scientific).

Fast-FRAP experiments

In Fast-FRAP experiments, pre-bleach acquisition, bleaching and fluorescence recovery measurements were performed by repeatedly scanning one line across a targeted cell. Scanning was bidirectional at 1400 Hz. The zoom factor was 5, yielding a pixel size of 0.048 µm. Resulting X(t) images were 1024 x 14416 pixels. Pre-bleach acquisition was carried out to compensate for the loss of fluorescence due to the acquisition. A bleaching ROI was set across either the cell nucleus or the cytoplasm. Fast-FRAP acquisition was as follows: 1 sec of pre-bleach acquisition, 150 ms of bleaching, and 3 sec of fluorescence recovery measurements. Bleaching was achieved with the laser operating at 95% power with the AOTF set to 100%. For imaging, laser power was attenuated to 2% of the AOTF. Fluorescence was detected between 500 nm and 570 nm. Fluorescence recovery curves were exported and analyzed using LAS AF and MATLAB (MathWorks). Curve normalization was done using the “double normalization” formula [39]:

$$I_{FRAP\ NORM} = \frac{I_{Ref\ Pre}}{I_{Ref}\ (t)} \cdot \frac{I_{FRAP}(t)}{I_{FRAP\ Pre}}$$

with $I_{FRAP}(t)$ as the fluorescense intensity in the FRAP ROI, $I_{Ref}(t)$ as the reference fluorescence intensity along the same line scan, $I_{FRAP\ Pre}$ as the mean fluorescence intensity before bleaching in the FRAP ROI, and $I_{Ref\ Pre}$ as the reference for mean fluorescence intensity before bleaching along the same line scan. All measurements were corrected for background noise.

Statistics

Results are presented as means ± SEM. Statistical analyses were performed using PRISM 6.0 software (GraphPad). One-way and two-way ANOVA and Dunnett's test, accepting $p \leq 0.05$ as significant, as well as a two-tailed unpaired *t*-test were used to compare CI values. Curves of FRAP experiments were fitted by one-phase exponential equations. Differences between two groups for half-life recovery and percentage of immobile fraction were analyzed using a two-tailed unpaired *t*-test. The cleavage efficiency of T2A peptide, the expression level of tagged-ERK2 and the ratio of phospho/total ERK2 were quantified by densitometry using Image J (National Institutes of Health).

4.1.3. Results

4.1.3.1. Validation of endogenous ERK1/2 dynamics in NIH3T3 cells

To ensure that our cellular system behaves as described [21], the phosphorylation profile and subcellular localization of endogenous ERK1/2 in NIH-3T3 fibroblast cells were examined using specific activators and/or inhibitors of the pathway (Fig. 1A). In non-stimulated conditions, ERK1/2 displayed a basal phosphorylation and was localized mainly in the cytoplasm (a). Pretreatment of non-stimulated cells with U0126 reduced this phosphorylation (e). Phosphorylation of ERK1/2 induced by serum (10%) or FGF4 (100 ng/mL) resulted in ERK1/2 nuclear translocation and homogenous distribution of ERK1/2 throughout the cells (b and f). U0126 pretreatment dramatically decreased both serum- and FGF4- induced phosphorylation of ERK1/2 and prevented the nuclear accumulation of ERK1/2 (c and g). However, ERK1/2 phosphorylation was not completely abolished when cells

were simultaneously treated with U0126 and serum: phosphorylation signals were still detectable in the cytoplasm and the nucleus (c). In contrast, neither phosphorylation nor localization of ERK1/2 was altered when cells were treated with DMSO and either serum or FGF4 (d and h). These results are in accordance with previous reports [21] and demonstrate the proper functioning of our biological system.

4.1.3.2. Artefacts in localization of over-expressed eGFP-rEKR2 in NIH-3T3 cells

We assessed the subcellular distribution of overexpressed eGFP-ERK2 in NIH-3T3 cells in serum-starved and non-stimulated conditions. We documented ERK2 localization in NIH-3T3 cells transiently transfected with the rat ERK2 (rERK2) fused to the C-terminus of the enhanced green fluorescent protein (eGFP-rERK2). Note that the eGFP-rERK2 function was not altered as previously reported [29]. To obtain various eGFP-rERK2 expression levels within a population of NIH-3T3 cells, they were transiently transfected with eGFP-rERK2 plasmids in concentrations ranging from 25 to 1000 ng/mL to generate dim and bright fluorescence. The subcellular distribution of overexpressed eGFP-ERK2 in serum-starved and non-stimulated NIH-3T3 cells is presented in Fig. 1B. eGFP-rERK2 accumulated in the nucleus of brightly fluorescent cells but was homogenously distributed between cytoplasm and nucleus in weakly fluorescent cells. This pattern was confirmed by the nucleo-cytoplasmic concentration index (CI) results (Fig. 1C, red dots), which are different from those of endogenous ERK1/2 (CI = 0.733 ± 0.030, n = 16,) in similar experimental conditions (Fig. 1Aa and 1C, green dotted line). The differences observed in CI values among plasmid concentration (Fig. 1C) reflect important cell-to-cell variations in eGFP-rERK2 expression and thus in eGFP-rERK2 subcellular distribution. eGFP-ERK2 in serum-starved NIH-3T3 cells across the range of plasmid concentrations used was faithfully detected only in the weakly fluorescent cells (Fig. 1D) and when the previously described severe imaging conditions were used [29]. Consistent with previous studies, plasmids encoding eGFP-rERK2 and mCherry-mMEK1 (Fig. 2A, #2 and #3) were transiently co-transfected in equal amounts (final concentration of 1 µg/mL) to avoid saturation of ERK2 binding partners in the cytoplasm and subsequent nuclear accumulation of eGFP-rERK2 [26,27]. Twenty-four hours after transfection and serum starvation, confocal images of fluorescent

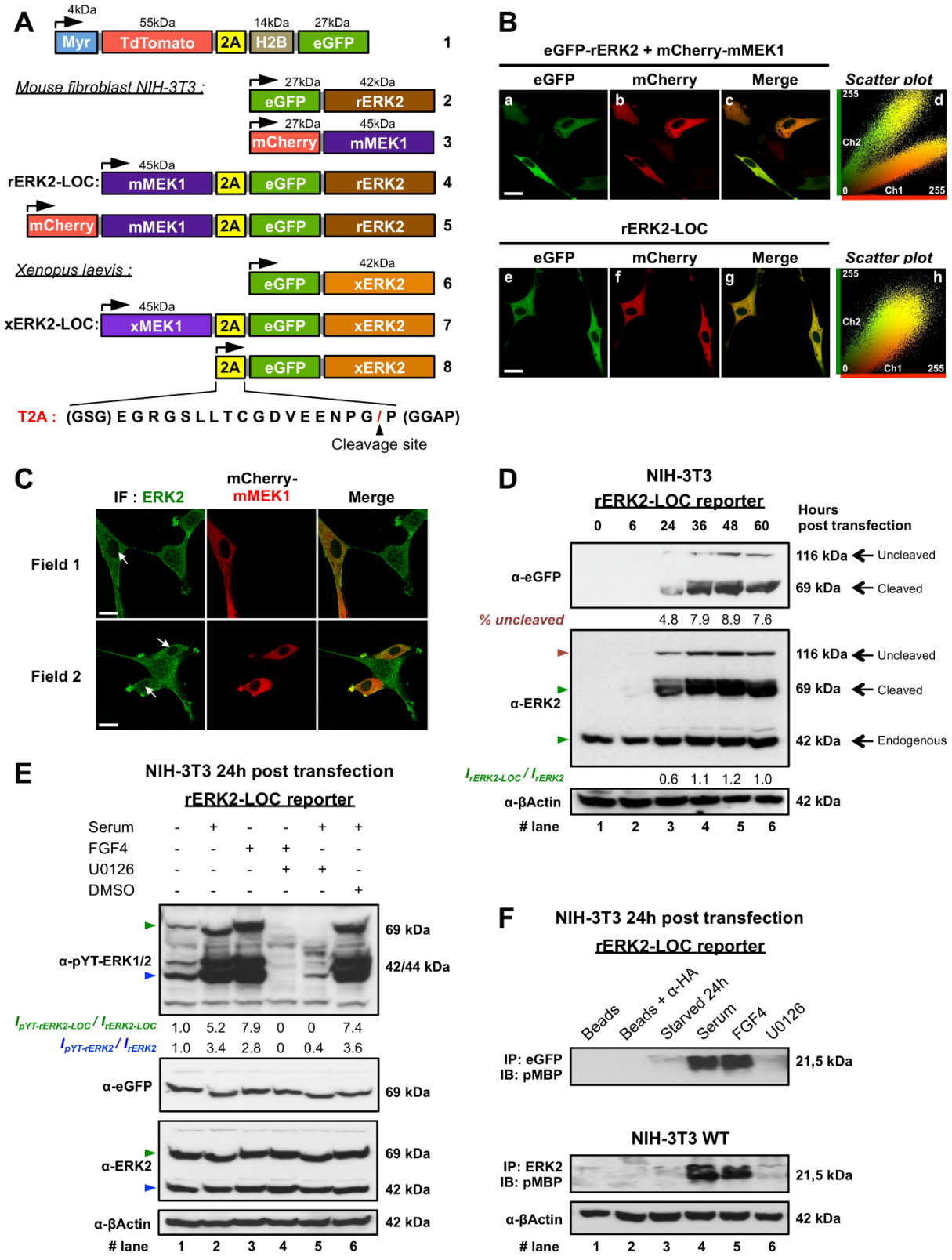

Fig. 2. Equimolar co-expression of eGFP-rERK2 and mMEK1 restores cytoplasmic localization of eGFP-rERK2. (**A**) Schematic representation of all genetically encoded molecular constructs used in this study. The corresponding amino acid sequence of 2A (yellow box) encodes a T2A peptide isolated from plasmid Myr-TdTomato-2A-H2B-eGFP (#1). Amino acids (GSG) and (GGAP) improve cleavage efficiency. The red slash symbol at the peptide C-terminal end indicates the 2A peptide cleavage site. (**B**) Fluorescence confocal imaging of NIH-3T3 cells after transfection with different

plasmids and serum starvation for 24 h: top, transfection with eGFP-rERK2 (#2) and mCherry-mMEK1 (#3) plasmids; bottom, transfection with mCherry-mMEK1-2A-eGFP-rERK2 (#5). Representative images are shown of rERK2 protein distribution (green: a, e), mMEK1 distribution (red: b, f) and the merged image (c, g). Corresponding scatter plots of green and red intensities of each pixel on the whole images are shown (d, h). Co-localized pixels are visualized in yellow. Scale bar: 20 µm. (**C**) Fluorescence confocal imaging of NIH-3T3 cells transfected with mCherry-mMEK1 (middle, red) and labeled with an anti-ERK2 antibody (left, green) after 24 h of serum starvation. Co-localization of rERK2 and mCherry-mMEK1 is shown in the merged images (right, yellow). White arrows point to nuclei of transfected cells. Scale bar: 20 µm. (**D**) Western blot analysis of NIH-3T3 cells transfected with rERK2-LOC at the indicated time-points. Cell lysates were analyzed by immunoblotting with the indicated antibodies (left of each blot). The percentage of uncleaved polypeptide (full-length mMEK1-2A-GFP-rERK2, red triangle) was quantified by densitometry. Quantitative comparison of the levels of overexpressed rERK2-LOC and endogenous ERK2 (green triangles, middle panel) is indicated below the blot as $I_{rERK2\text{-}LOC}$/ $I_{rERK2.}$ (**E**) After 24 h of serum starvation, NIH-3T3 cells transfected with rERK2-LOC were left untreated or were pretreated for 1 h with U0126 or DMSO, and then stimulated with serum or FGF4 for 15 min. Corresponding cell lysates were immunoblotted with the indicated antibodies (left of each blot). Relative phosphorylation levels of rERK2-LOC (green triangles) and endogenous ERK2 (blue triangles) were measured by densitometry. The ratios of phosphorylated protein to total proteins ($I_{pYT\text{-}rERK2\text{-}LOC}$ / $I_{rERK2\text{-}LOC}$ and $I_{pYT\text{-}ERK2}$ / I_{ERK2}) are indicated below the top blot. (**F**) rERK2-LOC–transfected NIH-3T3 cells were serum starved for 24 h and then left untreated or incubated or not with U0126 for 1 h before stimulation with serum or FGF4 for 15 min. Cells lysates were immunoprecipitated with anti-eGFP (top panel) or anti-ERK2 antibodies (middle panel), and ERK1/2 kinase activity was assayed *in vitro*. The phosphorylated form of MBP (pMBP) was detected by immunoblotting. Unconjugated beads and beads conjugated with anti-HA antibodies were used as a control in the assays. Lysate inputs for immunoprecipitation were probed with anti-β-actin antibody as a loading control. At least two independent experiments and 15 cells were measured from fixed cells. Biochemical data are representative of at least two independent experiments.

single cells in the red and green channels showed a marked heterogeneous expression of mCherry-mMEK1 and eGFP-rERK2 due to transient transfection (Fig. 2B, upper panel). In cells coexpressing eGFP-rERK2 and mCherry-mMEK1 in similar proportions, eGFP-rERK2 was localized in the cytoplasm. But cells expressing more eGFP-rERK2 in comparison to mCherry-mMEK1 showed a more prominent nuclear localization of the kinase (Fig. 2Bc-d).

4.1.3.3. Faithful eGFP-ERK2 localization restored in living NIH3T3 cells

To provide an accurate and faithful read-out of the subcellular distribution of ERK2 regardless of its expression level, and to monitor the spatiotemporal signature of ERK2 in living cells by fluorescence imaging, we constructed and validated a novel molecular tool: rERK2-LOC (Fig. 2A, #4). Based on previous reports and our own observations (Figs. 1 and 2B, a-d), we reasoned that over-expression of eGFP-rERK2 should be counter-balanced by coexpression of equal amounts of mMEK1, the main interacting partner of ERK2, in order to maintain the system's equilibrium. To that end, we used the T2A peptide, which functions as a reliable ribosomal skip mechanism to produce multiple polypeptides from a unique translation start site (Fig. 2Aa and Materials and Methods).

To assess mouse ERK2 localization in serum-starved conditions, NIH-3T3 cells transiently transfected with the mCherry-mMEK1-2A-eGFP-rERK2 plasmid (Fig. 2B, lower panel) were imaged by fluorescence confocal microscopy. eGFP-rERK2 and mCherry-mMEK1 were co-expressed in all transfected cells, as observed in the overlay image (Fig. 2Bg). Co-localization analysis based on the generation of a scatter-plot on the whole image of red intensities *versus* green intensities for each pixel confirmed co-localization and indicated comparable expression levels of ERK2 and MEK1 (Fig. 2Bh). The results show that T2A mediated the equimolar coexpression of eGFP-rERK2 and mCherry-mMEK1 and that cytoplasmic localization of eGFP-ERK2 was restored in serum-starved, non-stimulated cells regardless of the expression level (Fig. 1Aa). However, the nuclei of transfected cells appear “darker” than the nuclei of non-transfected cells harboring a more uniform distribution of endogenous ERK1/2 between the cytoplasm and the nucleus (Figs. 1Aa and 2C, ERK2 immunostaining). We hypothesized that this could be due to the disruption of the initial MEK1/ERK2 ratio in NIH-3T3 cells after T2A-mediated coexpression of eGFP-rERK2 and mCherry-mMEK1 [40]. To increase the proportion of MEK1 with respect to that of endogenous ERK2, NIH-3T3 cells were then transfected with mCherry-mMEK1, serum starved for 24 h, and then immunostained for total ERK2 (Fig. 2C). Interestingly, mCherry-mMEK1 overexpression decreased the level of endogenous ERK2 in the nucleus, consistent with our previous observations (Fig. 2Be).

4.1.3.4. Functional validation of the 2A-mediated eGFP-rERK2 and rMEK1 coexpression system

Analysis of western blot data from NIH3T3 cells transfected with the mMEK1-2A-eGFP-rERK2 plasmid and harvested 0, 6, 24, 36, 48, and 60 h later showed that eGFP-rERK2 expression was detectable 24 h after transfection and remained stable from 36 h (Fig. 2D, upper and middle panel). Interestingly, the average abundance of eGFP-rERK2 ranged from 0.6- to 1.2-fold relative to that of endogenous ERK2 (Fig. 2D, below middle panel) normalized against actin (Fig. 2D, lower panel). Average cleavage efficiency decreased slightly over time from 95.2% to a minimum of 92.1% (Fig. 2D, below upper panel). All experiments were performed 24 h after transfection, when average cleavage efficiency and relative abundance were optimal. rERK2-LOC was validated by monitoring its phosphorylation status (Fig. 2E) and kinase activity

(Fig. 2F) on NIH3T3 cells transfected with rERK2-LOC upon activation and/or inhibition of the ERK1/2 signaling pathway. Similar phosphorylation patterns were observed for rERK2-LOC and endogenous ERK1/2 (Fig. 2E, upper panel). rERK2-LOC and endogenous ERK2 were substantially phosphorylated in response to serum and FGF4 compared to absence of stimulation. However, densitometry (below the upper panel) revealed a pronounced effect of serum (between 5.2- and 7.4-fold higher, lanes 2 & 6) and FGF4 (7.9-fold higher, lane 3) relative to the basal phosphorylation of rERK2-LOC (lane 1) when compared with the phosphorylation status of endogenous ERK2 (between 3.4- to 3.6-fold higher in serum-treated conditions (lanes 2 & 6) and 2.8-fold higher in FGF4-treated condition (lane 3) relative to the basal value. Pretreatment with U0126 prevented serum- and FGF4-induced phosphorylation of both rERK2-LOC and endogenous ERK2; no phosphorylation signal was detectable in lanes 4 and 5, except for endogenous ERK2 in lane 5, which has a 0.4-fold phosphorylation signal relative to the basal value. In a complementary approach, MBP-based *in vitro* kinase assay was used to determine the kinase activities of rERK2-LOC (Fig. 2F, upper panel) and endogenous ERK2 (Fig. 2F, middle panel). Phospho-MBP (p-MBP) immunoblotting showed that rERK2-LOC and endogenous ERK2 had equivalent phosphorylation capabilities in cells treated with serum or FGF4, demonstrating the functional kinase activity of rERK2-LOC. Treatment with U0126 impaired the kinase activity of both rERK2-LOC and endogenous ERK2 alike. The results of biochemical assays show that eGFP-rERK2 was coexpressed with mMEK1 by means of the 2A system, and that it fulfills the biochemical functions of endogenous ERK2 in NIH3T3 cells.

4.1.3.5. Enhanced contrast monitoring of eGFP-ERK2 in living cells

The relevance and the faithfulness of our novel ERK2 localization reporter were further characterized. The subcellular distributions of overexpressed eGFP-rERK2 and rERK2-LOC were examined and compared to immuno-localized endogenous ERK1/2 proteins monitored by fluorescence imaging on fixed NIH-3T3

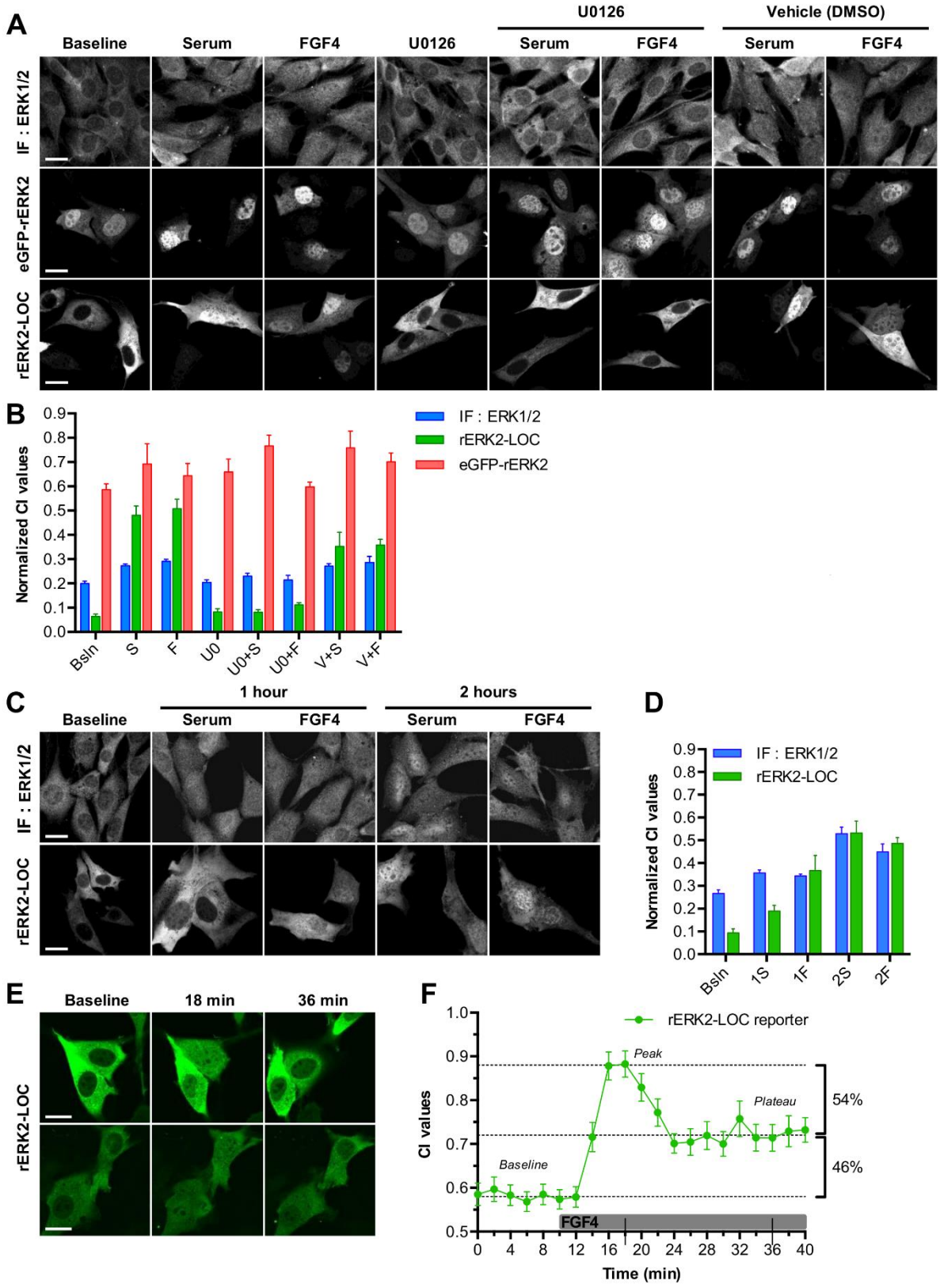

Fig. 3. rERK2-LOC expression faithfully reports localization of ERK2.(A) Non-transfected (top row) and transfected NIH-3T3 cells overexpressing either eGFP-rERK2 (middle row) or rERK2-LOC (bottom row) were serum starved for 24 h, and then were left untreated or were treated with U0126 or DMSO for 1 h. Next, they were stimulated with serum or FGF4 for 15 min, or were left unstimulated (baseline). All cells were fixed and non-transfected cells were processed for immunofluorescence using the anti-ERK1/2 antibody (top row) and all cells were imaged by confocal microscopy. Shown

are representative images of ERK2 localization under the different treatments. Scale bars: 20 µm. **(B)** Quantitative comparison of the nucleo-cytoplasmic concentration index (CI) of ERK2 between endogenous ERK1/2 (blue bars), overexpressed eGFP-rERK2 (red bars) and rERK2-LOC (green bars). CI values were normalized between 0 and 1 ($\overline{CI}$ values), where 0 and 1 are respectively the minimal and maximal CI values obtained. Bsln: baseline, S: serum, F: FGF4, U0: U0126, V: vehicle (DMSO). **(C)** Non-transfected (top row) and transfected NIH-3T3 cells overexpressing rERK2-LOC (bottom row) were serum starved for 24 h and then stimulated with serum or FGF4 for 1 or 2 h, or left untreated (baseline). All cells were fixed and non-transfected cells were processed for immunofluorescence using the anti-ERK1/2 antibody (top row) and all cells were imaged by confocal microscopy. Shown are representative images of ERK2 localization under the different treatments. Scale bar: 20 µm. **(D)** Quantitative comparison of nucleo-cytoplasmic concentration index (CI) of ERK2 at the indicated time-points between endogenous ERK1/2 (blue bars) and overexpressed rERK2-LOC (green bars). CI values were normalized between 0 (minimum obtained) and 1 (maximum obtained) ($\overline{CI}$ values). Bsln: baseline; 1S and 1F: 1 h serum and 1 h FGF4; 2S and 2F: 2 h serum and 2 h FGF4. **(E)** Monitoring of the subcellular distribution of rERK2-LOC in (24h) serum-starved NIH-3T3 cells by time-lapse confocal microscopy every 2 min for 10 min (baseline) and after FGF4 stimulation (100 ng/mL) for 30 min. **(F)** Nuclear and cytoplasmic intensities of each rERK2-LOC transfected cell were measured with Volocity software for each time-point to calculate the concentration index values (CI). Vertical error bars represent the average ± SEM. Two-way ANOVA test, accepting $p \leq 0.05$ as significant, was performed to compare $\overline{CI}$ values differences between endogenous ERK1/2, eGFP-rERK2 and rERK2-LOC for a same treatment. One-way ANOVA test, accepting $p \leq 0.05$ as significant, was performed to compare $\overline{CI}$ values among all the treatments (Table 2 and 3). At least two independent experiments were performed. The number of cells per condition (n) from fixed cells is indicated in Table 2 and Table 3 for statistical analysis; at least 80 cells were measured for time-lapse microscopy.

cells following different treatments. In accordance with our other observations (Fig. 1B), overexpressed eGFP-rERK2 accumulated heavily in the nucleus in both non-stimulated and treated cells regardless of the treatment (Fig. 3A, middle panel). By contrast, T2A-mediated MEK1/ERK2 coexpression resulted in a subcellular distribution of rERK2-LOC (Fig. 3A, lower panel) like that of endogenous ERK1/2 (Fig. 3A, upper panel). The results show that rERK2-LOC localization was strictly cytoplasmic when the ERK1/2 signaling pathway was inhibited, and that it accumulated in the nucleus when the pathway was activated.

To quantify the ERK2 subcellular distribution in different experimental conditions, CI values were normalized between 0 and 1 (abbreviated $\overline{CI}$ values) (Fig. 3B) and are listed in Table 2. We noticed no significant variations in overexpressed eGFP-rERK2 subcellular distribution regardless of the treatment used to activate or inhibit the ERK1/2 pathway, except for $\overline{CI}_{\text{U0+S}}$ and $\overline{CI}_{\text{V+S}}$ (Table 2). More importantly, incubation of the cells with U0126 in the presence or absence of serum or FGF4 failed to reestablish the cytoplasmic localization of eGFP-rERK2. Normalized CI values for eGFP-rERK2 transfected cells treated with serum ($\overline{CI}_{\text{S}}$) or U0126 and serum ($\overline{CI}_{\text{U0+S}}$) were respectively 1.1- and 1.3-fold higher than non-stimulated cells (referred as baseline condition, $\overline{CI}_{\text{Bsln}}$) (0,692 ± 0,083, n = 5 and 0.767 ± 0.043, n = 6 versus 0.586 ± 0.024, n = 10; $p \leq 0.05$), indicating that eGFP-ERK2 concentrated

much more in the nucleus in U0126 condition. These data do not agree with the effect of treatments on endogenous ERK1/2 (Table 2). Remarkably, consistent with the data in Fig. 2B-C, $\overline{CI}_{\text{BsIn}}$ as well as $\overline{CI}_{\text{U0}}$ values for cells expressing rERK2-LOC were respectively 3.1- and 2.5-fold lower than that of endogenous ERK1/2 in non-stimulated conditions (0.064 ± 0.009, n = 12 versus 0.200 ± 0.009, n = 16; $p \leq 0.001$) (Table 2). Whereas in non-stimulated cells rERK2-LOC was localized mainly in the cytoplasm, stimulation by serum or FGF4 provoked nuclear accumulation that was markedly enhanced relative to endogenous ERK1/2. $\overline{CI}$ values of rERK2-LOC in cells stimulated with serum or FGF4 were 7.5- and 7.9-fold higher than non-stimulated cells, respectively. In comparison, $\overline{CI}$ values of endogenous ERK1/2 were 1.4- and

	Treatments	$\overline{CI}$	n	S	*p* value	Fold-change	$\Delta\overline{CI}$	Ratio rERK2-LOC / IF:ERK1/2
eGFP-rERK2	Baseline	0.586 ± 0.024	10					
	Serum	0.692 ± 0.083	5	ns	0.4658	1.18		
	FGF4	0.643 ± 0.050	6	ns	0.9065	1.10		
	U0126	0.659 ± 0.054	8	ns	0.6977	1.13		
	U0126 + serum	0.767 ± 0.043	6	*	0.0355	1.31		
	U0126 + FGF4	0.598 ± 0.019	11	ns	0.9997	1.02		
	DMSO + serum	0.759 ± 0.068	7	*	0.0353	1.30		
	DMSO + FGF4	0.701 ± 0.036	10	ns	0.1933	1.20		
IF:ERK1/2	Baseline	0.200 ± 0.009	16					
	Serum	0.273 ± 0.007	9	***	0.0003	1.37	0.073 ± 0.011	
	FGF4	0.291 ± 0.008	27	****	< 0.0001	1.46	0.091 ± 0.012	
	U0126	0.204 ± 0.011	13	ns	0.9996	1.02	0.004 ± 0.014	
	U0126 + serum	0.230 ± 0.012	12	ns	0.2652	1.15	0.030 ± 0.016	
	U0126 + FGF4	0.214 ± 0.019	7	ns	0.957	1.07	0.014 ± 0.021	
	DMSO + serum	0.271 ± 0.010	18	****	< 0.0001	1.36	0.071 ± 0.013	
	DMSO + FGF4	0.287 ± 0.025	6	***	0.0002	1.44	0.087 ± 0.026	
rERK2-LOC	Baseline	0.064 ± 0.009	12					
	serum	0.480 ± 0.007	7	****	< 0.0001	7.50	0.416 ± 0.041	5.70
	FGF4	0.508 ± 0.008	16	****	< 0.0001	7.94	0.444 ± 0.040	4.88
	U0126	0.083 ± 0.011	15	ns	0.9952	1.30	0.019 ± 0.016	4.75
	U0126 + serum	0.082 ± 0.012	6	ns	0.9994	1.28	0.018 ± 0.014	0.60
	U0126 + FGF4	0.112 ± 0.019	11	ns	0.7481	1.75	0.048 ± 0.013	3.43
	DMSO + serum	0.353 ± 0.010	7	****	< 0.0001	5.52	0.289 ± 0.058	4.07
	DMSO + FGF4	0.358 ± 0.025	18	****	< 0.0001	5.60	0.294 ± 0.026	3.38

Statistical significance for differences among overexpressed eGFP-rERK2, endogenous ERK1/2 and rERK2-LOC was tested by one-way ANOVA and Dunnett's test, accepting $p \leq 0.05$ as significant. The ratio between $\Delta\overline{CI}$ of endogenous ERK1/2 and rERK2-LOC shows the differences in magnitude order in function of the treatment. Symbols: $\overline{CI}$, average of CI values ± SEM; $\Delta\overline{CI}$, difference between means compared to baseline value as reference; SEM, Standard Error of Mean; n, number of cells analyzed; S: statistically significant; ns, p > 0.05; *, p ≤ 0.05; **, p ≤ 0.01; ***, p ≤ 0.001; ****, p ≤ 0.0001.

Table 2. Statistical analysis of $\overline{CI}$ and $\Delta\overline{CI}$ values for overexpressed eGFP-ERK2, endogenous ERK1/2 and rERK2-LOC, 15 min after serum or FGF4 stimulation.

1.5-fold higher than baseline value under the same experimental conditions (Table 2). The difference of averaged $\overline{CI}$ values ($\Delta\overline{CI}$) between baseline and serum or FGF4 stimulation for rERK2-LOC was 5.7- and 4.9-fold higher than that for endogenous ERK1/2, confirming several orders of magnitude in the nuclear translocation for rERK2-LOC (Table 2). In addition, treatment with U0126 alone or combined with serum or FGF4 caused no significant change in $\overline{CI}$ for rERK2-LOC, in accordance with endogenous ERK1/2 (Table 2).

As several studies reported that simple coexpression of MEK1 with tagged-ERK2 derived from different plasmids disturbed the distribution of tagged ERK2, evidenced by its abnormally short persistence in the nucleus upon stimulation [26,27,30], we monitored the localization of rERK2-LOC and compared it with that of endogenous ERK1/2 at 1 and 2 h after serum or FGF4 stimulation (Fig. 3C). Consistent with a previous study [21], endogenous ERK1/2 was distributed relatively homogenously throughout the cells 1 h after addition of serum or FGF4 (Fig. 3C, upper panel). But 2 h after serum or FGF4 stimulation, it accumulated in the nucleus. Surprisingly, the results clearly show that rERK2-LOC mimicked endogenous ERK1/2 in response to the different treatments (Fig. 3C, bottom panel) and exhibited progressive nuclear accumulation in serum-starved NIH-3T3 cells treated with serum or FGF4 (Fig. 3D). $\overline{CI}$ values of rERK2-LOC after 2 h in serum- or FGF4-stimulated conditions were 5.7- and 5.2-fold higher than baseline, respectively. In comparison, $\overline{CI}$ values of endogenous ERK1/2 were only 2.0- and 1.7-fold higher than baseline under the same experimental conditions (Table 3). The difference of averaged $\overline{CI}$ values ($\Delta\overline{CI}$) between baseline and 2 h serum or 2 h FGF4 stimulation for rERK2-LOC was 1.7- and 2.2-fold higher than that for endogenous ERK1/2, confirming that late nuclear accumulation is also markedly enhanced using rERK2-LOC (Table 3).

To monitor rERK2-LOC dynamics at higher temporal resolution in living NIH-3T3 cells, we used automated time-lapse confocal microscopy with a temporal resolution of 2 min for 40 min. After a baseline period of 10 min (CI = 0.582 ± 0.004), rERK2-LOC entered the nucleus between 2 and 4 min after FGF4 addition and reached a maximum within 8 min after stimulation (CI = 0.880 ± 0.002) (Fig. 3E-F and S1 Movie). These results are in agreement with previous studies on ERK2 translocation kinetics following FGF4 treatment on NIH-3T3 cells [29]. Whereas a sustained ERK2 nuclear localization was reported in similar experimental conditions

[21,29], our results show a decrease of 54% from the initial peak, but sill 46% above the baseline for the remaining time of the experiment (CI = 0.719 ± 0.006). Taken together, these results show that our novel molecular reporter of ERK2 localization substantially set up the monitoring of ERK2. It provides an emphasized relocation of the coexpressed ERK2 while remaining faithful to that of the endogenous under all experimental conditions.

	Treatments	$\overline{CI}$	n	S	*p* value	Fold-change	$\Delta\overline{CI}$	Ratio rERK2-LOC / IF:ERK1/2
IF:ERK1/2	Baseline	0.267 ± 0.016	18					
	1 h - serum	0.357 ± 0.013	21	**	0.0066	1.34	0.090 ± 0.021	
	1 h - FGF4	0.343 ± 0.009	27	*	0.0172	1.29	0.077 ± 0.018	
	2 h - serum	0.529 ± 0.029	19	****	< 0.0001	1.98	0.262 ± 0.033	
	2 h – FGF4	0.449 ± 0.035	14	****	< 0.0001	1.68	0.183 ± 0.038	
rERK2-LOC	Baseline	0.093 ± 0.018	13					
	1 h - serum	0.189 ± 0.025	11	ns	0.4524	2.03	0.096 ± 0.031	1.07
	1 h - FGF4	0.367 ± 0.066	15	***	0.0003	3.95	0.274 ± 0.069	3.56
	2 h - serum	0.532 ± 0.053	16	****	< 0.0001	5.72	0.439 ± 0.055	1.68
	2 h – FGF4	0.486 ± 0.026	12	****	< 0.0001	5.23	0.393 ± 0.032	2.15

Statistical significance for differences among endogenous ERK1/2 and rERK2-LOC was tested by one-way ANOVA and Dunnett's test, accepting $p \leq 0.05$ as significant. The ratio between $\Delta\overline{CI}$ of endogenous ERK1/2 and rERK2-LOC shows the differences in magnitude orders in function of the treatment. Symbols: $\overline{CI}$, average of CI values ± SEM; $\Delta\overline{CI}$, difference between means compared to baseline value as reference; SEM, Standard Error of Mean; n, number of cells analyzed; S: statistically significant; ns, $p > 0.05$; *, $p \leq 0.05$; **, $p \leq 0.01$; ***, $p \leq 0.001$; ****, $p \leq 0.0001$.

Table 3. Statistical analysis of $\overline{CI}$ and $\Delta\overline{CI}$ values for endogenous ERK1/2 and rERK2-LOC, 1 h and 2 h after serum or FGF4 stimulation.

4.1.3.6. rERK2-LOC provides a relevant read-out for ERK2 mobility

To finalize our characterization and validation in living cells, we determined mobility of rERK2-LOC in living NIH-3T3 cells in comparison to that of overexpressed eGFP-rERK2 or eGFP alone using high-speed FRAP measurements. Fixed NIH3T3 cells expressing eGFP were used to calibrate our imaging setup (Fig. 4A). Based on rERK2-LOC dynamics in serum-starved NIH-3T3 cells after FGF4 stimulation (Fig. 3E), only serum-stimulated cells with rERK2-LOC accumulating in the nucleus were imaged and compared to cells overexpressing free eGFP or eGFP-rERK2 (Fig. 4B-C).

Comparative analysis of cumulative fluorescence recovery curves showed that nuclear free eGFP (blue curve) retained very high mobility, reflecting the passive diffusion of the fluorescent protein throughout the cell (Fig. 4D). The fluorescence

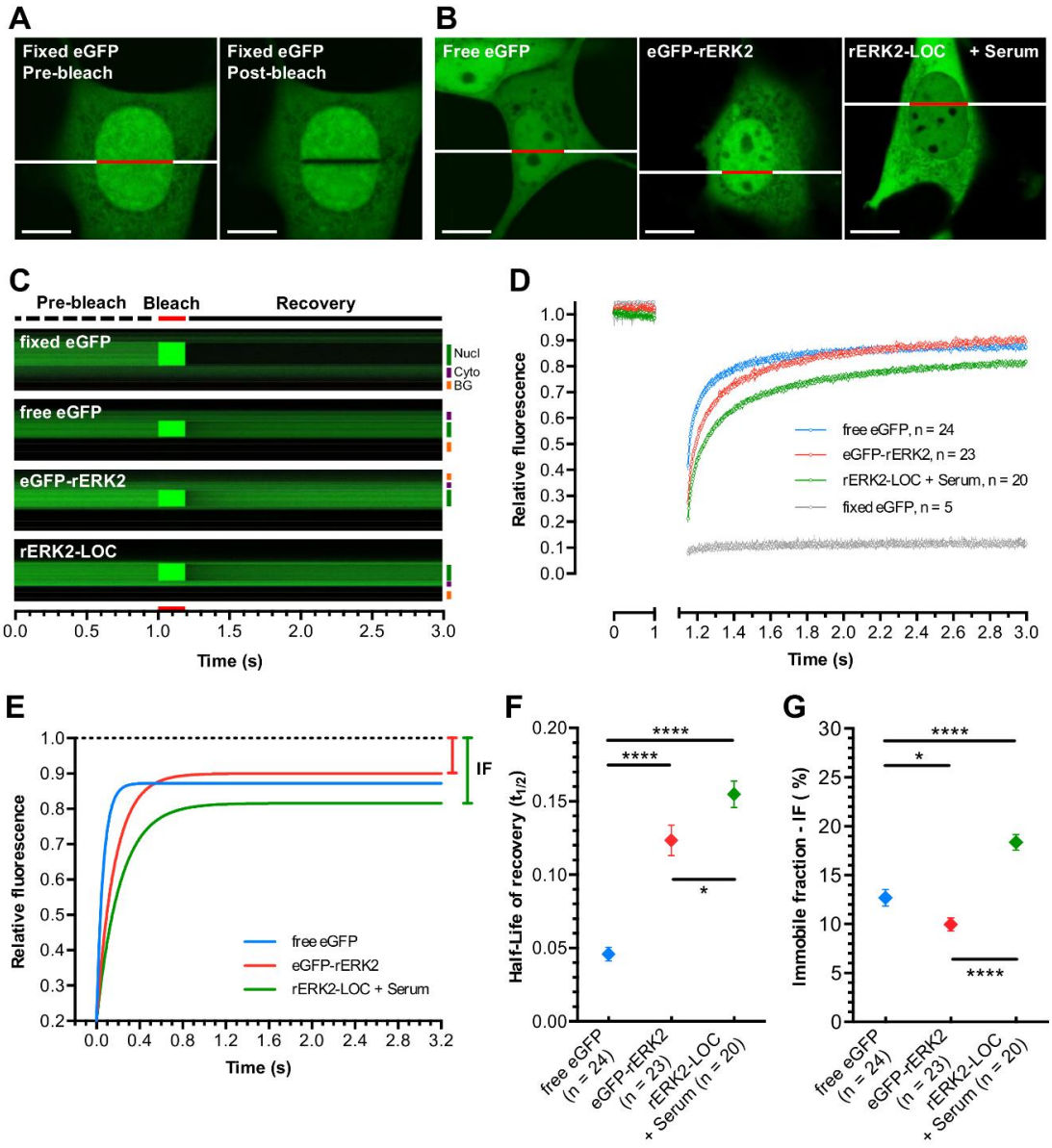

Fig. 4. Mobility of rERK2-LOC measured by high-speed FRAP. (A) eGFP-transfected NIH-3T3 cells were fixed. Individual living cells were imaged as described in the Materials and Methods section. Image sequences before (left) and after (right) photobleaching are shown. Scale bars: 10 µm. **(B)** NIH-3T3 cells were transfected with eGFP (left), eGFP-rERK2 (middle) or rERK2-LOC (right) and then serum starved for 24 h. Cells overexpressing rERK2-LOC were stimulated with serum to trigger its nuclear translocation. Bleached ROI correspond to the red lines drawn across the nuclei. Scale bars: 10 µm. **(C)** Representative kymograms (xt) of fluorescence intensity measured along the line (both red and white) across the selected cells for each experimental condition over-time are shown, indicating the FRAP measurement sequence: pre-bleach of 1 s (broken dark line), bleach of 150 ms (red lines) and post-bleach of 2 s (solid dark line). Correction for overall bleaching effects was applied. Nucl: nucleus (green line), Cyto: cytoplasm (purple line), BG: background (yellow line). **(D-E)** Curves of cumulative fluorescence recovery over time for fixed eGFP (grey curve), free eGFP (blue curve), overexpressed eGFP-rERK2 (red curve) and rERK2-LOC after serum stimulation (green curve, 8 min after serum stimulation) were normalized **(D)** and fitted **(E)**. **(F-G)** Average half-life of recovery ($t_{1/2}$) and immobile fraction (IF) calculation for cells serum-starved for 24 h and overexpressing free eGFP (blue symbol) or eGFP-rERK2 (red symbol), and serum-stimulated cells overexpressing rERK2-LOC (green symbol, 8 min after serum stimulation). At least two independent experiments were performed. The number of individual cells used for each condition is indicated above each symbol. Statistical significance was determined by a two-tailed unpaired *t*-test (ns, no significant; *, ≤ 0.05; ****, ≤ 0.0001).

recovery curve of overexpressed eGFP-rERK2 (red curve) mimicked that of free eGFP, as previously reported [29]. In contrast, after serum stimulation and accumulation of rERK2-LOC in the nucleus (t = 8 min after stimulation), fluorescence recovery of rERK2-LOC (green curve) indicated a marked reduction of mobility in the nucleus, which contrasts with a previous study reporting no difference in mobility measurements between overexpressed free eGFP and eGFP-rERK2 [26].

Next, fluorescence recovery curves were fitted to a one-phase exponential-association equation (Fig. 4E) and the recovery process was characterized by the half-life of fluorescence recovery ($t_{1/2}$) to accurately describe and compare protein mobility (Fig. 4F). In comparison with the extremely high mobility of free eGFP ($t_{1/2}$ = 0.046 s ± 0.005, n = 24), the half-life recovery of overexpressed eGFP-rERK2 *versus* rERK2-LOC were 0.123 s ± 0.010 (n = 23) and 0.155 s ± 0.009 (n = 20), respectively (p = 0.03). We did not observe a more significant difference between eGFP-rERK2 and rERK2-LOC, indicating that overexpressed eGFP-rERK2 may still bind slightly to nuclear partners. We also calculated the percentage of the immobile fraction (IF) (Fig. 4G) defined by the value between the complete fluorescence recovery asymptote and the pre-bleach value being equal to 1 (Fig. 4E, black dotted line). The corresponding values for free eGFP and overexpressed eGFP-rERK2 were 12.68% ± 0.85 (n = 24) and 9.95% ± 0.68 (n = 23), respectively ($p \leq 0.05$). This was clearly significantly different from the value obtained with rERK2-LOC (IF = 18.37% ± 0.80, n = 20, $p \leq 0.0001$). Thus, despite very rapid ERK2 shuttling to and from the nucleus, we detected, as previously reported [29], a significantly slower mobility and turnover of rERK2-LOC in the nucleus of stimulated cells compared to overexpressed eGFP-rERK2.

Additional FRAP experiments were next performed to assess changes in the mobility of rERK2-LOC between the cytoplasm and the nucleus of serum-starved NIH-3T3 cells before and after serum stimulation (S1 Fig). Following the same experimental protocol, a stripe across the nucleus and the cytoplasm of the same cell was bleached a few seconds apart (S1A Fig). As shown in S1B-D Fig., the immobile fraction of rERK2-LOC was significantly reduced in the cytoplasm of serum-stimulated cells (IF = 6.36% ± 0.99, n = 12) in comparison to that of rERK2-LOC in the cytoplasm of serum-starved cells (IF = 14.00% ± 2.70, n = 9, $p \leq 0.05$), demonstrating the dissociation of a pool of rERK2-LOC from its cytoplasmic partners

upon stimulation. Interestingly, the immobile fraction of rERK2-LOC in the nuclei of serum-stimulated cells (IF = 14.83% ± 1.26, n = 12) was significantly larger from that of rERK2-LOC in the cytoplasm of the same analyzed cells ($p \leq 0.0001$). We observed also similar immobile fractions of rERK2-LOC in the nuclei of serum-stimulated cells and the cytoplasm of serum-starved cells, suggesting that rERK2-LOC binds to nuclear and cytoplasmic scaffolds/anchors, respectively. Collectively, the data obtained with equimolar expression of eGFP-rERK2 and mMEK1 are consistent with previous studies using different strategies to report ERK1/2 dynamics in living cells [29,30]. In contrast to these studies, no stringent imaging conditions were required, making our approach compatible with long-term functional monitoring of ERK2 dynamics in living cells.

4.1.3.7. Spatiotemporal subcellular distribution of xERK2-LOC in Xenopus laevis embryo

After fully characterizing and successfully validating the faithful reporting of ERK2 dynamics by our T2A-mediated coexpression system in living cells, we tested our reporter rERK2-LOC in a relevant multicellular model organism. In *Xenopus laevis* embryos, FGF signaling plays a crucial role in the formation of mesoderm [41] and particularly in maintenance of the mesoderm through a feedback loop that involves MAPK/ERK2 cascade-mediated stabilization of Brachyury expression [42–44]. Several studies used a specific antibody against activated ERK1/2 in whole *Xenopus laevis* embryos at different stages of development. Immunohistochemical analysis showed strong activation of ERK2 in whole-mount embryos at the end of gastrulation around the dorsal lip of blastopore [45,46]. To gain insight into ERK2 localization in relation to spatiotemporal patterns of ERK2 activation at different stages of development (Fig. 5B), we further employed our 2A-mediated coexpression approach. To test whether the T2A peptide functions in *Xenopus laevis* embryos, we microinjected mRNA from the original plasmid pMyr-TdTomato-T2A-H2B-eGFP (Fig. 2A, #1) into embryos at the one-cell stage. Maximum-intensity projection showed that in stage 8 embryos H2B-eGFP and Myr-TdTomato were present exclusively in the nucleus and at the plasma membrane, respectively, as reported in other model organisms [47,48] (Fig. 5A). To determine the subcellular distribution of endogenous xERK2, we immunostained fixed, whole-mount, stage 8 embryos with anti-ERK2

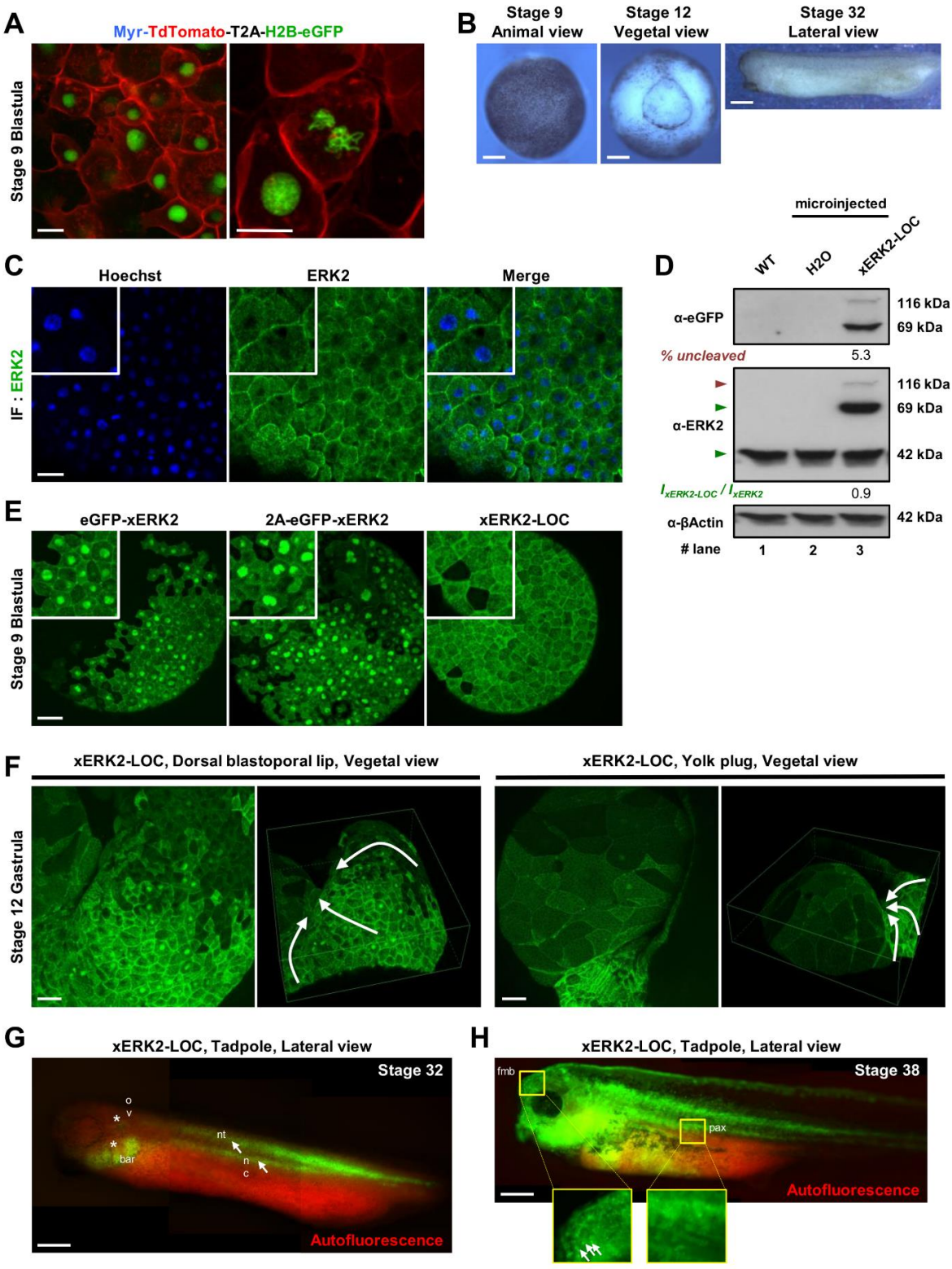

Fig. 5. Spatiotemporal subcellular distribution of xERK2-LOC in living *Xenopus laevis* embryo. **(A)** Embryos were injected with 500 ng of Myr-TdTomato-T2A-Histone2B-GFP mRNA. Maximum-intensity projection of a z-stack of 40 confocal images with a z-step of 0.59 µm is shown at 40X (left, scale bar: 10 µm) and at 63X magnification (right, scale bar: 20 µm). Pictures were merged to visualize Myr-mCherry at the plasma membrane and H2B-eGFP in the nucleus. **(B)** xERK2-LOC subcellular distribution was visualized at several stages of *Xenopus laevis* development (stage 9 blastula, stage 12 blastula and stage 32 tadpole). Scale bar: 200 µm. **(C)** Stage 9 embryos were fixed and processed for immunofluorescence with antibody against total ERK2 (green) and stained for DNA

with Hoechst (blue) as described in the Materials and Methods section. Scale bar: 100 µm. **(D)** Protein extracts were prepared from uninjected (WT, lane 1), H_2O injected (lane 2) and xERL2-LOC overexpressing embryos (lane 3) and immunoblotted with antibodies against GFP (top panel), ERK2 (middle panel) and β-actin (bottom panel). The percentage of uncleaved xERK2-LOC was measured by densitometry and is shown below the top panel in lane 3. The levels of overexpressed xERK2-LOC relative to endogenous ERK2 (green triangles, middle) are indicated below the blot as $I_{xERK2\text{-}LOC}/\ I_{xERK2}$. **(E)** Embryos were injected with 500 ng of eGFP-xERK2, 2A-eGFP-xERK2 (control) or xERK2-LOC mRNA. Projections of at least 60 confocal 0.7-µm sections of animal cells at stage 9 blastula are shown. Higher magnification images of representative subcellular distributions of xERK2 are shown in white squares (top left). Scale bar: 150 µm. **(F)** Monitoring of xERK2-LOC subcellular distribution in the cells of the dorsal blastoporal lip (left panel) and the yolk plug (right panel) in stage-12 gastrula. Projection and 3D reconstruction of z-series of 108 confocal 1.50-µm sections (left panel) and 86 confocal 1.00-µm sections (right panel) are shown. White arrows indicate the trajectories of the cells leading to a progressive internalization of the yolk plug. Scale bar: 150 µm. **(G-H**) Several images from different viewpoints were recorded and combined to create a whole image of the developing embryos expressing xERK2-LOC, head to the left, at stage 32 (**G**) and stage 38 (**H**) tadpoles. The spatiotemporal localization of xERK2-LOC (green) in the embryonic structures, enhanced by autofluorescence of embryo and yolk (red signal), corresponds to notochord (nc), neural tube (nt) (both white arrows), otic vesicle (ov) and branchial arch region (bar) (both white asterisks) **(G)**. Higher magnification of the forebrain-midbrain boundary (fmb) and para-axial structures (pax) are shown in yellow squares **(H)**. Small white arrows indicate xERK2-LOC nuclear accumulation in several cells of the forebrain-midbrain boundary. Scale bar: 500 µm. At least two independent experiments were performed from animal caps, fixed embryos, or live embryos, and at least ten embryos were imaged. Biochemical data are representative of at least two independent experiments.

antibody (Fig. 5C). Overlay of anti-ERK2 and Hoechst staining revealed that most xERK2 was localized in the cytoplasm of ectodermal cells.

To explore xERK2 dynamics in living embryos, we microinjected embryos at the one-cell stage with mRNA encoding eGFP-xERK2, 2A-eGFP-xERK2 without xMEK1 sequence as a control, or xMEK1-2A-eGFP-xERK2 (xERK2-LOC). Given that ERK2 can be activated by mechanical stress or wounding [46], live imaging of intact embryos was performed, while preserving ectodermal tissue integrity (Fig. 5E). Maximum-intensity projection revealed nuclear accumulation of eGFP-xERK2 and 2A-eGFP-xERK2. In contrast, expression of xERK2-LOC resulted in a more homogenous distribution of the kinase within blastomeres, with a slight tendency towards the cytoplasm, reminiscent of the immuno-localization of endogenous ERK2 in fixed embryos (Fig. 5C). In parallel, we assessed xERK2-LOC protein expression levels in embryos at stage 8 by western blot analysis (Fig. 5D) using both anti-GFP (upper panel) and anti-ERK2 (middle panel) antibodies. The proportion of uncleaved polypeptide was slightly lower in *Xenopus laevis* embryos (5.3%) in comparison to cultured NIH-3T3 cells (Fig. 2D, upper panel).

At the gastrula stage (stage 11), we investigated xERK2-LOC subcellular distribution in embryonic cells of the dorsal lip of the blastopore region, where FGF signaling is known to activate ERK1/2 pathway. In line with this information, we

observed a patch of ectodermal cells just above the dorsal lip of the blastopore exhibiting a strong accumulation of xERK2-LOC in the nucleus (Fig. 5F, left panel and S3 Movie). These observations are in agreement with the previously reported immuno-localization of activated di-phosphorylated ERK2 [46]. Finally, a nuclear localization of xERK2-LOC was seen in large endodermal cells of the yolk plug (Fig. 5F, right panel and S4 Movie), although no activation of ERK2 had been detected by immunohistochemistry [46].

Since no toxicity was observed and embryos developed normally, we explored the localization of xERK2-LOC at later developmental stages in living embryos. At the early tadpole stage (stage 32), GFP fluorescence was detected mainly in the neural tube, the notochord, and the somites (white arrows), as well as in the otic vesicle and the branchial arch region (white asterisks) (Fig. 5G). Red fluorescence due to known autofluorescence of *Xenopus laevis* embryos was advantageously used to achieve optimum contrast for accurate localization of xERK2-LOC in embryonic structures. At stage 38, when the *Xenopus laevis* tadpole becomes transparent, xERK2-LOC was widespread in the head region and the para-axial structures (Fig. 5H and S5 Movie). Remarkably, xERK2-LOC accumulated in the nuclei of a small patch of cells in the forebrain-midbrain boundary but not in para-axial structures (Fig. 5H and S5 Movie). Once again, our results highlighted the faithful subcellular distribution of xERK2 provided by xERK2-LOC in comparison to immuno-localized activated di-phosphorylated ERK2 in the *Xenopus laevis* embryo.

4.1.4. Discussion

The MAPK/ERK1/2 pathway plays an important role in many cellular processes: cell proliferation, migration, differentiation, and even cell death [14,49–51]. Aside from the activity of ERK1/2, its subcellular localization is instrumental in signal integration in the cell fate decision [8,52,53]. Many approaches have been used to monitor ERK1/2 dynamics in living cells, but some of them do not localize the kinase of interest correctly in non-stimulated cells [24,26]. Moreover, they are often laborious and unsuitable for long-term imaging [29], or they are time consuming because transgenic cell lines have to be generated [30]. We overcame these limitations by designing a novel molecular tool, ERK2-LOC. Characterization and

validation of the tool in living cells and tissue showed that ERK2-LOC is functional, faithful, easy to use, and biologically relevant.

Various studies used ERK2 tagged with GFP-like fluorescent proteins to monitor the spatiotemporal localization of ERK2 in individual living cells. However, these studies disregarded the predominantly nuclear localization of eGFP-rERK2 in resting cells [16,23–25] (Fig. 1). It has been known for a long time that disruption of the MEK/ERK balance disturbs ERK2 localization [12,15]. Aside from favoring conditions where a low expression level of eGFP-rERK2 was managed [29] (Fig. 1D), this problem was solved by co-expressing mMEK1, thereby restoring the proper cytoplasmic localization of overexpressed eGFP-rERK2 in serum-starved cultures without stimulation [26,27]. This results in a more controlled MEK/ERK ratio in transfected cells (Fig. 2B, upper panel). Given that expression levels of co-transfected mCherry-MEK1 and eGFP-ERK2 in the same cell cannot be controlled due to the limitations of co-transfection techniques [26] (Fig. 2B, upper panel), ERK2 subcellular distribution throughout the cell is necessarily affected. From this observation, it became obvious that proper quantification of ERK2 dynamics in response to specific stimuli requires a robust system for reliable coexpression at the single cell level. While multiple heterologous proteins can be coexpressed in living cells by different approaches, such as use of the Internal Ribosomal Entry Site (IRES) sequence and use of bidirectional or multiple promoters in the same plasmid, these systems suffer from problems related to coexpression efficiency [54,55]. A more promising approach described as a 2A-mediated coexpression system (for review [33,48,56]), was used in our study. 2A-linked proteins have been efficiently expressed *in vitro* in a wide variety of cultured eukaryotic cells and embryonic stem cells, and even *in vivo* in embryos and whole organisms [47,48] but never reported in *Xenopus laevis* model. While no protein degradation or side effects of premature termination of translation have been reported [57], previous work described variability in the 2A peptide-mediated cleavage, depending on the choice of 2A peptide and the cellular model [48]. Further support for the 2A strategy is found in previous studies demonstrating robust equimolar coexpression of this approach in studies of the molecular interactions of G-coupled proteins [55] and T-cell development in CD3-deficient mice [58]. Although we used an optimized peptide (see Materials and Methods), a slight difference in cleavage efficiencies between NIH-3T3 cells and an

embryonic cell system was noted. The efficiency ranged from 91.1% (Fig. 2D) in NIH3T3 cells to 94.7% in *Xenopus* embryos (Fig. 5D); the presence of an uncleaved MEK1/ERK2 polypeptide could affect ERK2 functions in both model systems. Actually, MEK1–ERK2 fusion polypeptide was reported to produce a constitutively active fusion ERK2 in the absence of upstream signaling [59]. In this context, a mutated form of MEK1 (nuclear export/activity region) in fusion with ERK2 was able to induce PC12 differentiation and NIH3T3 transformation. Wild type and mutated MEK1-ERK2 fusions had no effect on the activity of endogenous ERK1/2 [59]. Interestingly, immunofluorescence results showed that the subcellular localization of the mutated MEK1–ERK2 fusion protein was nuclear, while that of the wild type was essentially cytoplasmic. A more efficient 2A derived peptide, such as P2A, might be used to alleviate system perturbation linked to uncleaved MEK1–ERK2 polypeptide [48].

Recent studies quantified the MEK/ERK ratio in different cellular contexts by biochemical approaches [60,61]. Both proteins are in the micromolar range, but the reported MEK/ERK ratios in HeLa cells are considerably different: 3.1/2.1 [62], 1.4/0.96 [60] and 1/10 [61], as well as in PC12 cells, 0.6/1.25 [63] and 0.68/0.26 [64]. They also varied depending on the cell type, ranging from 1 in *Xenopus laevis* oocyte, Cos7 and Rat1 cells, to about 2 in CHO, 208F, and PC12 cells, and up to almost 13 in NIH3T3 cells [40,60,61]. Recently the role of ERK2 has been emphasized. In a murine system, $ERK2^{-/-}$ embryonic lethality was attributed to failure of placenta and trophoblastic development [65,66], while $ERK1^{-/-}$ embryos are viable and fertile but have problems in thymic development. In the same line of thought, knockdown of ERK2 in *zebrafish* model prevents epiboly and the blastula to gastrula transition, while ERK1 knockdown provokes subtle defects in the embryogenesis [67]. Moreover, the reported 4/1 ERK2/ERK1 ratio in NIH-3T3 cells in both relative and activated forms was proposed to explain the preeminent role of ERK2 in cellular functions over that of ERK1 [68]. In the *Xenopus laevis* model, the maternally inherited ERK2 isoform is important for oocyte maturation and the MEK/ERK ratio is 1:1 [60,69]. In all cellular models, ratios were determined in systems at equilibrium. In our approach, one can only assume that co-expression generated equimolar ERK2 and MEK1 concentrations, but these were not quantified in our experimental systems at equilibrium. Therefore, we settled on a consensual 1:1 co-expression ratio of

MEK1/ERK2 based on the following considerations. First, these studies quantified the pool of ERK1/2 and MEK1/2 rather than distinct isoforms. Second, various MEK/ERK ratios have been reported for the same cell type. Third, it is technically difficult to express 13 times more rERK2 than mMEK1 proteins in living NIH3T3 cells. Fourth, we intended to use our reporter in the *Xenopus laevis* model system. Indeed, our purpose here was foremost to counter-balance eGFP-rERK2 overexpression with identical amounts of its partner MEK1. We did not intend to reproduce a mammalian expression system shadowing that of the cellular model system or even a synthetic network, but rather to faithfully mimic the subcellular distribution of the endogenous ERK2 for functional monitoring purposes.

Our approach resulted in the intended disruption of the initial MEK/ERK balance by co- overexpression of ERK2 and MEK1 in equimolar proportions at the single cell level. We show that it did not disturb ERK2 dynamics in living cells (Fig. 3E) or embryos (Fig. 5G-H). Although ERK2 is the only ERK isoform expressed in *Xenopus* embryos until mid-blastula transition, a two-fold increase in the proportion of total xERK2 (Fig. 5D) and overexpression of xMEK1 *via* our xERK2-LOC reporter did not alter embryonic development (Fig. 5G-H). In addition, overexpression of eGFP-xERK2 was not toxic to *Xenopus* embryos, indicating that artefacts in eGFP-xERK2 nuclear localization were not detrimental to ongoing cellular programs at these developmental stages (data not shown). Specific GFP fluorescence signals were detected at later stages (late gastrula, tadpole), pointing to the long half-life of exogenous xERK2 protein in these embryos. We conclude that our strategy is a non-invasive method for assessing functional ERK2 dynamics in living embryos during early *Xenopus laevis* embryogenesis. We were well aware of the uncoupling functions of ERK, but we used ERK2 localization in *Xenopus* as a surrogate for ERK activation. Any disruptive effects of xERK2-LOC on the signaling network will be further characterized in the future.

In contrast to overexpressed eGFP-rERK2, the dynamics of ERK2-LOC was faithful under our experimental conditions. Visualization of rERK2-LOC was actually enhanced at the single living cell level, as shown by fluorescence microscopy (Fig. 3B,D). Depending on the treatment, ERK2-LOC nuclear translocation or cytoplasmic retention was readily visible (Fig. 3A) and faithfully matched that of the endogenous pattern. This was not the case for overexpressed eGFP-rERK2 even in U0126 pre-

treated cells (in the presence or absence of serum or FGF4). Cells accumulated overexpressed eGFP-rERK2 in the nucleus independently of MEK1-mediated TEY-phosphorylation (Fig. 3A, middle image row, U0126 treatments), pointing-out the limit of eGFP-rERK2 over-expression and questioning the consequences and relevance of MEK1 phosphorylation of the overexpressed eGFP-rERK2 in this experimental context. The marked absence of a fluorescence signal in the nuclei of rERK2-LOC transfected cells in non-stimulated conditions (Fig. 2B, lower panel and Fig. 3A, bottom row left) resembles the endogenous situation (Fig. 3A, top row left). This prompted us to assess the role of overexpressed MEK1, and we showed that the increased amount of MEK1 in the cellular system was responsible for retention of the pool of endogenous ERK2 in the cytoplasm (Fig. 2C).

Protein over-expression is bound to affect signaling networks and cellular functions. Using figure 2B as an example, FGF increases the CI for endogenous ERK1/2 by about 50% but increases it about ten-fold for the rERK2-LOC reporter. The balance of ERK2 binding to MEK1 *versus* other interacting proteins, such as anchors, scaffold, activators and effectors, is likely influenced. ERK2 activation of targets may well be increased, and overexpressed MEK1 likely also influences endogenous ERK2 and the binding of exogenous ERK2 to DNA and microtubules. To prevent over-expression from perturbing the spatio-temporal aspects of the signaling pathways, recently developed alternative approaches could be implemented. Nowadays, based on directed genome editing technology by Clustered Regularly Interspaced Short Palindromic Repeats (CRISPR) [70], endogenous proteins can be knocked in to insert fluorescent proteins. However, based on our experience, two conditions should be met to make long-term functional imaging feasible: the expression level of the protein of interest should be sufficiently high, and fluorescent proteins with a high quantum yield (brightness) should be used.

Quantitative analysis of rERK2-LOC after different treatments (Fig. 3B) also faithfully shadowed that of endogenous ERK2, with comparable kinetic in NIH3T3 cells (Fig. 3F and S1 Movie) and in HeLa cells (S2 Movie). This enhanced translocation was seen in time-lapse experiments, in which NIH3T3 cells expressing rERK2-LOC were monitored every 2 min before and after FGF4 treatment (Fig. 3F). Based on the calculated concentration index, an initial nuclear burst of rERK2-LOC was visible, peaking between 4 to 8 minutes after FGF4 induction, as expected [29].

With regards to over-expression driven perturbations of the signaling network, several explanations can be proposed for the subsequent CI decrease. Nuclear anchors saturation and the presence of exogenous MEK1 in ERK2 export from the nucleus could be responsible. However the expected sustained activation profile of ERK2 [29] has been maintained since CI did not decrease to initial baseline level.

Concerning ERK2 diffusion, the significantly slower mobility of rERK2-LOC compared to overexpressed eGFP-rERK2 in FRAP experiments (Fig. 4D) indicates the stimulus-dependent binding of ERK2 to specific nuclear targets. So, saturation of ERK2-binding sites due to overexpression of eGFP-rERK2 without sufficient amount of MEK1 around altered the shuttling and resulted in accumulation of the kinase in the nucleus, where eGFP-rERK2 behaved as a free monomer. However the slight difference in diffusion of overexpressed eGFP-rERK2 (Fig. 4D) could indicate that it might still bind slightly to nuclear partners. Our results using rERK2-LOC unambiguously showed a decrease of ERK2 mobility in the nucleus, demonstrating that equimolar coexpression of mMEK1 counterbalances the overexpression of eGFP-rERK2 and thus prevents saturation of the limited ERK2 nuclear binding sites. This result is at odds with a previous study [26] that reported no difference in mobility between overexpressed free eGFP and eGFP-rERK2, and which was attributed to the use of cells with strong overexpression [29]. Because of the high ERK2 nuclear concentration, detection of eGFP-rERK2 nuclear binding upon stimulation of the pathway was not possible in their experimental settings.

As described in previous studies, mitogenic stimulation triggers rapid entry of ERK2 into the nucleus followed by massive nuclear accumulation of ERK2 several hours after the stimulation. On the other hand, non-mitogenic signals trigger only the initial translocation of ERK2 [21,71]. The characteristic mitogenic response was observed in NIH-3T3 cells transfected with rERK2-LOC, whereas an abnormally brief nuclear localization of ERK2 was generally associated with uncontrolled coexpression of MEK1/ERK2 [26,27,30]. Indeed, rERK2-LOC subcellular distribution was identical to that of endogenous ERK1/2 [21], with progressive nuclear accumulation 1 h and 2 h after either serum or FGF4 stimulation. It was reported that the late nuclear accumulation of ERK2 requires nuclear anchors such as MKP1 and MKP2, the expression of which is induced by ERK1/2 signaling [21,22,71]. ERK2-mediated phosphorylation of MKPs triggers inactivation and nuclear retention of

ERK2 through high-affinity interactions, limiting access to activated MEK1 in the cytoplasm. Consistent with previous studies, this late accumulation of ERK2 in the nucleus is uncoupled from MEK1-dependent TEY-phosphorylation of ERK2 [20,22]. Thus, since rERK2-LOC subcellular distribution matched endogenous ERK2 localization over time, we suggest that our rERK2-LOC reporter is regulated in the same way as the endogenous ERK2 by the endogenous regulatory proteins of the ERK1/2 signaling pathway. In addition, recent findings identified a similar mechanism for uncoupling TEY-phosphorylation from ERK2 nuclear localization at the early phase of the stimulation [20]. This uncoupling mechanism is not explainable by the sole expression of specific nuclear anchors and relies on a Casein Kinase 2-dependent SPS-phosphorylation in the kinase insert domain of ERK2 that is independent of ERK2 activation [72]. In *Xenopus laevis* embryo, spatiotemporal distribution of xERK2-LOC coincided with that of phosphorylated ERK2 in the region around the blastopore at stage 12, where an increase of ERK2 activation occurs, as well as at late gastrula and tadpole stages [46] (Fig. 5E, left panel, Fig. 5G-H and S3 Movie). In addition, we also found xERK2-LOC in the nuclei of large cells of the yolk plug at stage 12 (Fig. 5F, right panel and S4 Movie), although no activation of ERK2 was previously detected by immunohistochemistry [46]. These findings shed light on the importance of closely correlating ERK1/2 activation to its subcellular localization to determine cell fate and assess the involvement of specific spatiotemporal regulators of the ERK1/2 pathway. Considering the kinase-independent functions of ERK2 that have been reported both in the cytoplasm and in the nucleus [73,74], this has become particularly relevant.

4.1.5. Conclusion

In this study, limitations in eGFP-tagged ERK2 expression were solved by using a T2A “self-cleaving” peptide in bicistronic plasmids. Previous studies have shown that the cleavage efficiency of T2A is much higher than that of other 2A sequences [47,48]. So we fused the T2A sequence in frame between MEK1 and ERK2. The 2A peptide strategy enabled equimolar coexpression of MEK1 and ERK2 and restored the localization dynamics of ERK2. More importantly, we show that the expression pattern of the coexpressed proteins was consistent among the transfected cells. We confirmed the functionality of rERK2-LOC by using several biochemical approaches. Upon stimulation, rERK2-LOC rapidly translocated into the

nucleus, but its translocation was blocked by MEK1/2 inhibition. Fast-FRAP experiments in the nucleus and in the cytoplasm revealed a differential diffusion of rERK2-LOC, depending on its activation state and its subcellular localization. Given the stability of T2A-linked protein coexpression, we coexpressed MEK1 and eGFP-xERK2 in *Xenopus laevis* embryos to monitor xERK2 localization at different embryonic developmental stages. This is the first report on the subcellular localization of xERK2 in living embryos. Our ERK2-LOC reporters could be used in conjunction with ERK1/2 activity measurements [60,75,76] in several biological systems to assess whether pharmacological inhibitors affect specifically ERK1/2 activity and/or ERK2 subcellular distribution [7]. Finally, this 2A-mediated coexpression system is versatile and makes it possible to build on existing reporters by adding coding sequences from other genes (Raf, KSR, PEA-15) that are relevant to the regulation of the ERK1/2 signaling pathway. Taken together, our study has revealed that 2A-mediated coexpression of eGFP-ERK2 and MEK1 is a reliable and user-friendly strategy to faithfully monitor ERK2 in living cells and in a whole organism.

Acknowledgements

This work was encouraged by the CNRS *Groupement de recherche* (GDR) 2588 "*Microscopie et Imagerie du Vivant*" scientific community. We thank the *Biophotonique Cellulaire Fonctionnelle* Team and the VIB Bio Imaging Core, where all microscopy experiments were performed. We thank Dr. Amin Bredan for advice and editing of this manuscript.

Fundings

FS is a joint PhD student between Lille1 University and Ghent University, and is funded by Lille 1 University, the Centre National de la Recherche Scientifique (CNRS), and Vandenabeele's group research funding: Fonds Wetenschappelijk Onderzoek (FWO G.0875.11) and Methusalem grant (Bijzonder Onderzoeksfonds, BOF09/01M00709). PV is senior full professor at Ghent University. FR is a visiting research professor at Ghent University and full associate professor at Lille 1 University. Research in the Vandenabeele group is further supported by Belgian grants (Interuniversity Attraction Poles, IAP 7/32), Flemish grants (FWO G.0973.11, FWO G.0A45.12N, FWO G.0172.12, FWO G.0787.13N, FWO G.0C31.14N), Ghent University grants (Multidisciplinary Research Platforms (MRP), Ghent Researchers On Unfolded Proteins in Inflammatory Disease (GROUP-ID) consortium), grant from the Foundation against Cancer, 2012-188) and grants from Vlaams Instituut voor Biotechnologie (VIB). This research is supported by the Agence Nationale pour la Recherche (ANR): G2Progress program (ANR-13-BSV2-0016-02). This work was funded by grants from contrat Plan Etat-Région "Campus Intelligent" and ANR "Multimodal" and DynamIC and supported by contrat with Leica Microsystems.

References

1. Raman M, Chen W, Cobb MH. Differential regulation and properties of MAPKs. Oncogene. 2007;26: 3100–12. doi:10.1038/sj.onc.1210392
2. Shaul YD, Seger R. The MEK/ERK cascade: From signaling specificity to diverse functions. Biochim Biophys Acta - Mol Cell Res. 2007;1773: 1213–1226. doi:10.1016/j.bbamcr.2006.10.005

3. English J, Pearson G, Wilsbacher J, Swantek J, Karandikar M, Xu S, et al. New insights into the control of MAP kinase pathways. Exp Cell Res. 1999;253: 255–70. doi:10.1006/excr.1999.4687
4. Naor Z, Benard O, Seger R. Activation of MAPK cascades by G-protein-coupled receptors: the case of gonadotropin-releasing hormone receptor. Trends Endocrinol Metab. 2000;11: 91–9. doi:10.1016/S1043-2760(99)00232-5
5. McKay MM, Morrison DK. Integrating signals from RTKs to ERK/MAPK. Oncogene. 2007;26: 3113–21. doi:10.1038/sj.onc.1210394
6. Davies H, Bignell GR, Cox C, Stephens P, Edkins S, Clegg S, et al. Mutations of the BRAF gene in human cancer. Nature. 2002;417: 949–54. doi:10.1038/nature00766
7. Roberts PJ, Der CJ. Targeting the Raf-MEK-ERK mitogen-activated protein kinase cascade for the treatment of cancer. Oncogene. 2007;26: 3291–3310. doi:10.1038/sj.onc.1210422
8. Ebisuya M, Kondoh K, Nishida E. The duration, magnitude and compartmentalization of ERK MAP kinase activity: mechanisms for providing signaling specificity. J Cell Sci. 2005;118: 2997–3002. doi:10.1242/jcs.02505
9. Kholodenko BN, Hancock JF, Kolch W. Signalling ballet in space and time. Nat Rev Mol Cell Biol. 2010;11: 414–26. doi:10.1038/nrm2901
10. Wortzel I, Seger R. The ERK Cascade: Distinct Functions within Various Subcellular Organelles. Genes Cancer. 2011;2: 195–209. doi:10.1177/1947601911407328
11. Morrison DK, Davis RJ. Regulation of MAP kinase signaling modules by scaffold proteins in mammals. Annu Rev Cell Dev Biol. 2003;19: 91–118. doi:10.1146/annurev.cellbio.19.111401.091942
12. Fukuda M, Gotoh Y, Nishida E. Interaction of MAP kinase with MAP kinase kinase: its possible role in the control of nucleocytoplasmic transport of MAP kinase. EMBO J. 1997;16: 1901–8. doi:10.1093/emboj/16.8.1901
13. Yao Z, Flash I, Raviv Z, Yung Y, Asscher Y, Pleban S, et al. Non-regulated and stimulated mechanisms cooperate in the nuclear accumulation of MEK1. Oncogene. 2001;20: 7588–7596. doi:10.1038/sj.onc.1204963
14. Yoon S, Seger R. The extracellular signal-regulated kinase: multiple substrates regulate diverse cellular functions. Growth Factors. 2006;24: 21–44. doi:10.1080/02699050500284218
15. Lenormand P, Sardet C, Pagès G, L'Allemain G, Brunet A, Pouysségur J. Growth factors induce nuclear translocation of MAP kinases (p42mapk and p44mapk) but not of their activator MAP kinase kinase (p45mapkk) in fibroblasts. J Cell Biol. 1993;122: 1079–88. doi:10.1083/jcb.122.5.1079
16. Ando R, Mizuno H, Miyawaki A. Regulated fast nucleocytoplasmic shuttling observed by reversible protein highlighting. Science. 2004;306: 1370–3. doi:10.1126/science.1102506
17. Furuno T, Hirashima N, Onizawa S, Sagiya N, Nakanishi M. Nuclear shuttling of mitogen-activated protein (MAP) kinase (extracellular signal-regulated kinase (ERK) 2) was dynamically controlled by MAP/ERK kinase after antigen stimulation in RBL-2H3 cells. J Immunol. 2001;166: 4416–21. doi:10.4049/jimmunol.166.7.4416
18. Adachi M, Fukuda M, Nishida E. Nuclear export of MAP kinase (ERK) involves a MAP kinase kinase (MEK)-dependent active transport mechanism. J Cell Biol. 2000;148: 849–56. doi:10.1083/jcb.148.5.849
19. Cohen-Saidon C, Cohen AA, Sigal A, Liron Y, Alon U. Dynamics and Variability of ERK2 Response to EGF in Individual Living Cells. Mol Cell. 2009;36: 885–893. doi:10.1016/j.molcel.2009.11.025
20. Caunt CJ, McArdle CA. Stimulus-induced uncoupling of extracellular signal-regulated kinase phosphorylation from nuclear localization is dependent on docking domain interactions. J Cell Sci. 2010;123: 4310–20. doi:10.1242/jcs.076349
21. Pouysségur J, Volmat V, Lenormand P. Fidelity and spatio-temporal control in MAP kinase (ERKs) signalling. Biochem Pharmacol. 2002;64: 755–763. doi:10.1016/S0006-2952(02)01135-8
22. Caunt CJ, Armstrong SP, Rivers CA, Norman MR, McArdle CA. Spatiotemporal regulation of ERK2 by dual specificity phosphatases. J Biol Chem. 2008;283: 26612–23. doi:10.1074/jbc.M801500200
23. Aoki K, Kumagai Y, Sakurai A, Komatsu N, Fujita Y, Shionyu C, et al. Stochastic ERK activation induced by noise and cell-to-cell propagation regulates cell density-dependent proliferation. Mol Cell. Elsevier; 2013;52: 529–40. doi:10.1016/j.molcel.2013.09.015
24. Shankaran H, Ippolito DL, Chrisler WB, Resat H, Bollinger N, Opresko LK, et al. Rapid and sustained nuclear-cytoplasmic ERK oscillations induced by epidermal growth factor. Mol Syst Biol. 2009;5: 332. doi:10.1038/msb.2009.90
25. Zhang K, Duan L, Ong Q, Lin Z, Varman PM, Sung K, et al. Light-mediated kinetic control reveals the temporal effect of the Raf/MEK/ERK pathway in PC12 cell neurite outgrowth. PLoS One. 2014;9: e92917. doi:10.1371/journal.pone.0092917
26. Burack WR, Shaw AS. Live Cell Imaging of ERK and MEK: simple binding equilibrium explains the regulated nucleocytoplasmic distribution of ERK. J Biol Chem. 2005;280: 3832–3837. doi:10.1074/jbc.M410031200
27. Horgan AM, Stork PJ. Examining the mechanism of Erk nuclear translocation using green fluorescent protein. Exp Cell Res. 2003;285: 208–220. doi:10.1016/S0014-4827(03)00037-5
28. Ferrell JE. Tripping the switch fantastic: how a protein kinase cascade can convert graded inputs into switch-like outputs. Trends Biochem Sci. 1996;21: 460–6. doi:10.1016/S0968-0004(96)20026-X
29. Costa M, Marchi M, Cardarelli F, Roy A, Beltram F, Maffei L, et al. Dynamic regulation of ERK2 nuclear translocation and mobility in living cells. J Cell Sci. 2006;119: 4952–4963. doi:10.1242/jcs.03272

30. Lidke DS, Huang F, Post JN, Rieger B, Wilsbacher J, Thomas JL, et al. ERK nuclear translocation is dimerization-independent but controlled by the rate of phosphorylation. J Biol Chem. 2010;285: 3092–102. doi:10.1074/jbc.M109.064972
31. Stephens DJ, Allan VJ. Light microscopy techniques for live cell imaging. Science. 2003;300: 82–6. doi:10.1126/science.1082160
32. Minskaia E, Ryan MD. Protein coexpression using FMDV 2A: effect of “linker” residues. Biomed Res Int. 2013;2013: 291730. doi:10.1155/2013/291730
33. Szymczak-Workman AL, Vignali KM, Vignali DAA. Design and construction of 2A peptide-linked multicistronic vectors. Cold Spring Harb Protoc. 2012;2012: 199–204. doi:10.1101/pdb.ip067876
34. Messenger NJ, Kabitschke C, Andrews R, Grimmer D, Núñez Miguel R, Blundell TL, et al. Functional specificity of the Xenopus T-domain protein Brachyury is conferred by its ability to interact with Smad1. Dev Cell. 2005;8: 599–610. doi:10.1016/j.devcel.2005.03.001
35. Shaul Y, Seger R. The detection of MAPK signaling. Curr Protoc Mol Biol. 2006;Chapter 18: Unit 18.12. doi:10.1002/0471142727.mb1812s73
36. Papin C, Smith JC. Gradual refinement of activin-induced thresholds requires protein synthesis. Dev Biol. 2000;217: 166–72. doi:10.1006/dbio.1999.9531
37. Nieuwkoop PD, Faber J. Normal table of Xenopus laevis (Daudin): a systematical and chronological survey of the development from the fertilized egg till the end of metamorphosis. New York: Garland Pub; 1994.
38. Dehennaut V, Slomianny M-C, Page A, Vercoutter-Edouart A-S, Jessus C, Michalski J-C, et al. Identification of structural and functional O-linked N-acetylglucosamine-bearing proteins in Xenopus laevis oocyte. Mol Cell Proteomics. 2008;7: 2229–45. doi:10.1074/mcp.M700494-MCP200
39. Phair RD, Gorski SA, Misteli T. Measurement of dynamic protein binding to chromatin in vivo, using photobleaching microscopy. Methods Enzymol. Elsevier; 2004;375: 393–414. doi:10.1016/S0076-6879(03)75025-3
40. Sturm OE, Orton R, Grindlay J, Birtwistle M, Vyshemirsky V, Gilbert D, et al. The mammalian MAPK/ERK pathway exhibits properties of a negative feedback amplifier. Sci Signal. 2010;3: ra90. doi:10.1126/scisignal.2001212
41. Yao Y, Li W, Wu J, Germann UA, Su MSS, Kuida K, et al. Extracellular signal-regulated kinase 2 is necessary for mesoderm differentiation. Proc Natl Acad Sci U S A. 2003;100: 12759–64. doi:10.1073/pnas.2134254100
42. LaBonne C, Burke B, Whitman M. Role of MAP kinase in mesoderm induction and axial patterning during Xenopus development. Development. 1995;121: 1475–86. doi:10.1016/0168-9525(96)81381-3
43. Smith JC, Armes NA, Conlon FL, Tada M, Umbhauer M, Weston KM. Upstream and downstream from Brachyury, a gene required for vertebrate mesoderm formation. Cold Spring Harb Symp Quant Biol. 1997;62: 337–46. doi:10.1101/SQB.1997.062.01.040
44. Gotoh Y, Masuyama N, Suzuki A, Ueno N, Nishida E. Involvement of the MAP kinase cascade in Xenopus mesoderm induction. EMBO J. 1995;14: 2491–8. doi:10.1016/0168-9525(96)81382-5
45. LaBonne C, Whitman M. Localization of MAP kinase activity in early Xenopus embryos: implications for endogenous FGF signaling. Dev Biol. 1997;183: 9–20. doi:10.1006/dbio.1996.8497
46. Christen B, Slack JM. Spatial response to fibroblast growth factor signalling in Xenopus embryos. Development. 1999;126: 119–25. Available: http://www.ncbi.nlm.nih.gov/pubmed/9834191
47. Trichas G, Begbie J, Srinivas S. Use of the viral 2A peptide for bicistronic expression in transgenic mice. BMC Biol. 2008;6: 40. doi:10.1186/1741-7007-6-40
48. Kim JH, Lee S-R, Li L-H, Park H-J, Park J-H, Lee KY, et al. High cleavage efficiency of a 2A peptide derived from porcine teschovirus-1 in human cell lines, zebrafish and mice. PLoS One. 2011;6: e18556. doi:10.1371/journal.pone.0018556
49. Cross TG, Scheel-Toellner D, Henriquez N V., Deacon E, Salmon M, Lord JM. Serine/threonine protein kinases and apoptosis. Exp Cell Res. 2000;256: 34–41. doi:10.1006/excr.2000.4836
50. Whitmarsh a J, Davis RJ. A central control for cell growth. Nature. 2000;403: 255–6. doi:10.1038/35002220
51. Cagnol S, Chambard J-C. ERK and cell death: mechanisms of ERK-induced cell death--apoptosis, autophagy and senescence. FEBS J. 2010;277: 2–21. doi:10.1111/j.1742-4658.2009.07366.x
52. Tomida T, Oda S, Takekawa M, Iino Y, Saito H. The temporal pattern of stimulation determines the extent and duration of MAPK activation in a Caenorhabditis elegans sensory neuron. Sci Signal. 2012;5: ra76. doi:10.1126/scisignal.2002983
53. Tomida T. Visualization of the spatial and temporal dynamics of MAPK signaling using fluorescence imaging techniques. J Physiol Sci. 2015;65: 37–49. doi:10.1007/s12576-014-0332-9
54. Hennecke M, Kwissa M, Metzger K, Oumard A, Kröger A, Schirmbeck R, et al. Composition and arrangement of genes define the strength of IRES-driven translation in bicistronic mRNAs. Nucleic Acids Res. 2001;29: 3327–34. doi:10.1093/nar/29.16.3327
55. Goedhart J, van Weeren L, Adjobo-Hermans MJW, Elzenaar I, Hink MA, Gadella TWJ. Quantitative co-expression of proteins at the single cell level--application to a multimeric FRET sensor. PLoS One. 2011;6: e27321. doi:10.1371/journal.pone.0027321
56. Tang W, Ehrlich I, Wolff SBE, Michalski A-M, Wölfl S, Hasan MT, et al. Faithful expression of multiple proteins via 2A-peptide self-processing: a versatile and reliable method for manipulating brain circuits. J Neurosci. 2009;29: 8621–9. doi:10.1523/JNEUROSCI.0359-09.2009

57. Fang J, Qian J-J, Yi S, Harding TC, Tu GH, VanRoey M, et al. Stable antibody expression at therapeutic levels using the 2A peptide. Nat Biotechnol. 2005;23: 584–90. doi:10.1038/nbt1087
58. Szymczak AL, Workman CJ, Wang Y, Vignali KM, Dilioglou S, Vanin EF, et al. Correction of multi-gene deficiency in vivo using a single “self-cleaving” 2A peptide-based retroviral vector. Nat Biotechnol. 2004;22: 589–94. doi:10.1038/nbt957
59. Robinson MJ, Stippec S a, Goldsmith E, White M a, Cobb MH. A constitutively active and nuclear form of the MAP kinase ERK2 is sufficient for neurite outgrowth and cell transformation. Curr Biol. 1998;8: 1141–50. doi:10.1016/S0960-9822(07)00485-X
60. Fujioka A, Terai K, Itoh RE, Aoki K, Nakamura T, Kuroda S, et al. Dynamics of the Ras/ERK MAPK cascade as monitored by fluorescent probes. J Biol Chem. 2006;281: 8917–26. doi:10.1074/jbc.M509344200
61. Legewie S, Schoeberl B, Blüthgen N, Herzel H. Competing docking interactions can bring about bistability in the MAPK cascade. Biophys J. 2007;93: 2279–88. doi:10.1529/biophysj.107.109132
62. Schoeberl B, Eichler-Jonsson C, Gilles ED, Müller G. Computational modeling of the dynamics of the MAP kinase cascade activated by surface and internalized EGF receptors. Nat Biotechnol. 2002;20: 370–5. doi:10.1038/nbt0402-370
63. Brightman F a., Fell D a. Differential feedback regulation of the MAPK cascade underlies the quantitative differences in EGF and NGF signalling in PC12 cells. FEBS Lett. 2000;482: 169–74. doi:10.1016/S0014-5793(00)02037-8
64. Sasagawa S, Ozaki Y, Fujita K, Kuroda S. Prediction and validation of the distinct dynamics of transient and sustained ERK activation. Nat Cell Biol. 2005;7: 365–73. doi:10.1038/ncb1233
65. Hatano N, Mori Y, Oh-hora M, Kosugi A, Fujikawa T, Nakai N, et al. Essential role for ERK2 mitogen-activated protein kinase in placental development. Genes Cells. 2003;8: 847–56. doi:10.1046/j.1365-2443.2003.00680.x
66. Saba-El-Leil MK, Vella FDJ, Vernay B, Voisin L, Chen L, Labrecque N, et al. An essential function of the mitogen-activated protein kinase Erk2 in mouse trophoblast development. EMBO Rep. 2003;4: 964–8. doi:10.1038/sj.embor.embor939
67. Krens SFG, He S, Lamers GEM, Meijer AH, Bakkers J, Schmidt T, et al. Distinct functions for ERK1 and ERK2 in cell migration processes during zebrafish gastrulation. Dev Biol. 2008;319: 370–83. doi:10.1016/j.ydbio.2008.04.032
68. Lefloch R, Pouysségur J, Lenormand P. Single and combined silencing of ERK1 and ERK2 reveals their positive contribution to growth signaling depending on their expression levels. Mol Cell Biol. 2008;28: 511–27. doi:10.1128/MCB.00800-07
69. Huang CY, Ferrell JE. Ultrasensitivity in the mitogen-activated protein kinase cascade. Proc Natl Acad Sci U S A. 1996;93: 10078–83. doi:10.1073/pnas.93.19.10078
70. Sander JD, Joung JK. CRISPR-Cas systems for editing, regulating and targeting genomes. Nat Biotechnol. Nature Publishing Group; 2014;32: 347–55. doi:10.1038/nbt.2842
71. Volmat V, Camps M, Arkinstall S, Pouysségur J, Lenormand P. The nucleus, a site for signal termination by sequestration and inactivation of p42/p44 MAP kinases. J Cell Sci. 2001;114: 3433–3443.
72. Zehorai E, Yao Z, Plotnikov A, Seger R. The subcellular localization of MEK and ERK--a novel nuclear translocation signal (NTS) paves a way to the nucleus. Mol Cell Endocrinol. 2010;314: 213–20. doi:10.1016/j.mce.2009.04.008
73. Rauch J, Volinsky N, Romano D, Kolch W. The secret life of kinases: functions beyond catalysis. Cell Commun Signal. BioMed Central Ltd; 2011;9: 23. doi:10.1186/1478-811X-9-23
74. Hong S-K, Yoon S, Moelling C, Arthan D, Park J-I. Noncatalytic function of ERK1/2 can promote Raf/MEK/ERK-mediated growth arrest signaling. J Biol Chem. 2009;284: 33006–18. doi:10.1074/jbc.M109.012591
75. Sipieter F, Vandame P, Spriet C, Leray A, Vincent P, Trinel D, et al. From FRET imaging to practical methodology for kinase activity sensing in living cells. Prog Mol Biol Transl Sci. 2013;113: 145–216. doi:10.1016/B978-0-12-386932-6.00005-3
76. Ahmed S, Grant KG, Edwards LE, Rahman A, Cirit M, Goshe MB, et al. Data-driven modeling reconciles kinetics of ERK phosphorylation, localization, and activity states. Mol Syst Biol. 2014;10: 718. doi:10.1002/msb.134708
77. Yu KK, Aguilar K, Tsai J, Galimidi R, Gnanapragasam P, Yang L, et al. Use of mutated self-cleaving 2A peptides as a molecular rheostat to direct simultaneous formation of membrane and secreted anti-HIV immunoglobulins. PLoS One. 2012;7: e50438. doi:10.1371/journal.pone.0050438

Supporting Information

Plasmid Constructs

pCS2-xMEK1-2A-GFP-xERK2

The *Xenopus laevis* ERK2 sequence (xERK2) was amplified by polymerase chain reaction (PCR) using the forward primer xERK2.AgeI-BamHI-F (*Age*I and *Bam*HI sites underlined; start codon in bold), and the reverse primer xERK2.XhoI-R, (*Xho*I site underlined; stop codon in bold). To amplify eGFP from pEGFP-N1 (Clontech, USA), forward primer eGFP.AscI-F (*Asc*I site underlined) and reverse primer eGFP.NheI-R (*Nhe*I site underlined) without stop codon were then designed. xERK2 and eGFP PCR products were purified, digested and ligated sequentially into the pCS2-7G backbone at the *Age*I–*Xho*I and *Asc*I–*Nhe*I sites, respectively, to create the intermediary vector pCS2-eGFP-7G-xERK2. We adopted a cassette-cloning strategy using the complementary oligonucleotides T2A.AscI-F and T2A.AscI-R to generate a double-stranded cassette containing the 2A peptide sequence derived from the *Thosea asigna* virus (italic) and two unique restriction sites, *Spe*I and *Cla*I (underlined). The resulting cassette flanked by *Asc*I overhangs was then ligated into the pCS2-eGFP-7G-xERK2 vector at the *Asc*I site to create the control vector pCS2-2A-eGFP-7G-xERK2. The *Xenopus laevis* MEK1 sequence (xMEK1) was then obtained by two-step PCR from five stage-8 blastula embryos. Poly(A)+ RNA was reverse transcribed into cDNA, and after first-strand synthesis, the cDNA was used as a template for the PCR step. xMEK1 was amplified by PCR using the forward primer xMEK1.SpeI-F and the reverse primer xMEK1.ClaI-R, containing *Spe*I and *Cla*I sites, respectively (underlined). The PCR product was ligated into the *Spe*I and *Cla*I sites in the T2A cassette to produce the final expression vector pCS2-xMEK1-2A-eGFP-7G-xERK2. Note that the Gly-Ser-Gly (GSG) linker between MEK1 and the T2A sequences was maintained to optimize cleavage efficiency [32,77].

pCS2-mMEK1-2A-GFP-rERK2

The eGFP-rERK2 sequence from peGFP-C1-rERK2 was obtained by digestion with *Nhe*I and *Bam*HI restriction enzymes. eGFP-rERK2 was then purified and ligated into the *Nhe*I and *Bam*HI sites in the pCS2-7G backbone to create the expression vector pCS2-eGFP-rERK2. The *Mus musculus* MEK1 (mMEK1) sequence was obtained using the procedure described above for xMEK1, using 100

ng of total RNA extracted from NIH-3T3 cells. mMEK1 was amplified by PCR using the forward primer mMEK1.SpeI-F and the reverse primer mMEK1.ClaI-R, containing *Spe*I and *Cla*I sites, respectively (underlined). The PCR product was ligated into the *Spe*I and *Cla*I sites in the previously constructed pCS2-2A-eGFP-7G-xERK2 to produce the intermediary vector pCS2-mMEK1-2A-eGFP-7G-xERK2. The mMEK1-2A fragment was excised from the intermediary vector using *Asc*I, purified, and ligated in frame to the corresponding restriction site in linearized pCS2-eGFP-rERK2 to create the final expression vector pCS2-mMEK1-2A-eGFP-rERK2.

pCS2-mCherry-mMEK1-2A-GFP-rERK2

The peGFP-N1 vector was digested with *Age*I and *Not*I to remove the eGFP sequence, and then filled in with Klenow and re-ligated. The resulting vector was cut with *Nhe*I and a cassette containing a 7-glycine linker (italic) and two unique restriction sites, *Age*I and *Bsr*GI (underlined), were inserted in the *Nhe*I site, producing pClontech-N1-7G. The forward and reverse complementary oligonucleotides used to create the cassette were Backbone-7G-F2 and Backbone-7G-R2. The mCherry sequence from pmCherry-N1 vector was then subcloned into the *Age*I and *Bsr*GI restriction sites of pClontech-N1-7G to generate the pClontech-7G-mCherry intermediary vector. pClontech-N1-7G-mCherry and pCS2-mMEK1-2A-eGFP-rERK2 were digested with *Nhe*I and *Spe*I, respectively, and incubated with Mung Bean Nuclease to create blunt-ends extremities. The resulting 7G-mCherry fragment was ligated into pCS2-mMEK1-2A-eGFP-rERK2, producing the final expression vector pCS2-mCherry-mMEK1-2A-eGFP-rERK2.

pmCherry-7G-mMEK1

The pmCherry-C1 vector was cut with *Bsp*EI and *Xho*I. Complementary oligonucleotides Backbone-7G-F3 and Backbone-7G-R3 were annealed to each other to generate a double-stranded cassette containing a 7-glycine linker (italic) and two unique restriction sites, *Spe*I and *Asc*I (underlined). The cassette flanked by *Bsp*EI and *Xho*I overhangs was then ligated into the pmCherry-C1 at *Bsp*EI and *Xho*I sites to create the pmCherry-C1-7G intermediary vector. mMEK1 was amplified by PCR using the forward primer mMEK1.SpeI-F2, incorporating a *Spe*I site (underlined) and a stop codon (bold), and the reverse primer mMEK1.AscI-R (*Asc*I site underlined). The PCR product was ligated into pmCherry-C1-7G at the *Spe*I and *Asc*I sites, producing the final expression vector pmCherry-C1-7G-mMEK1.

Supplementary Figure

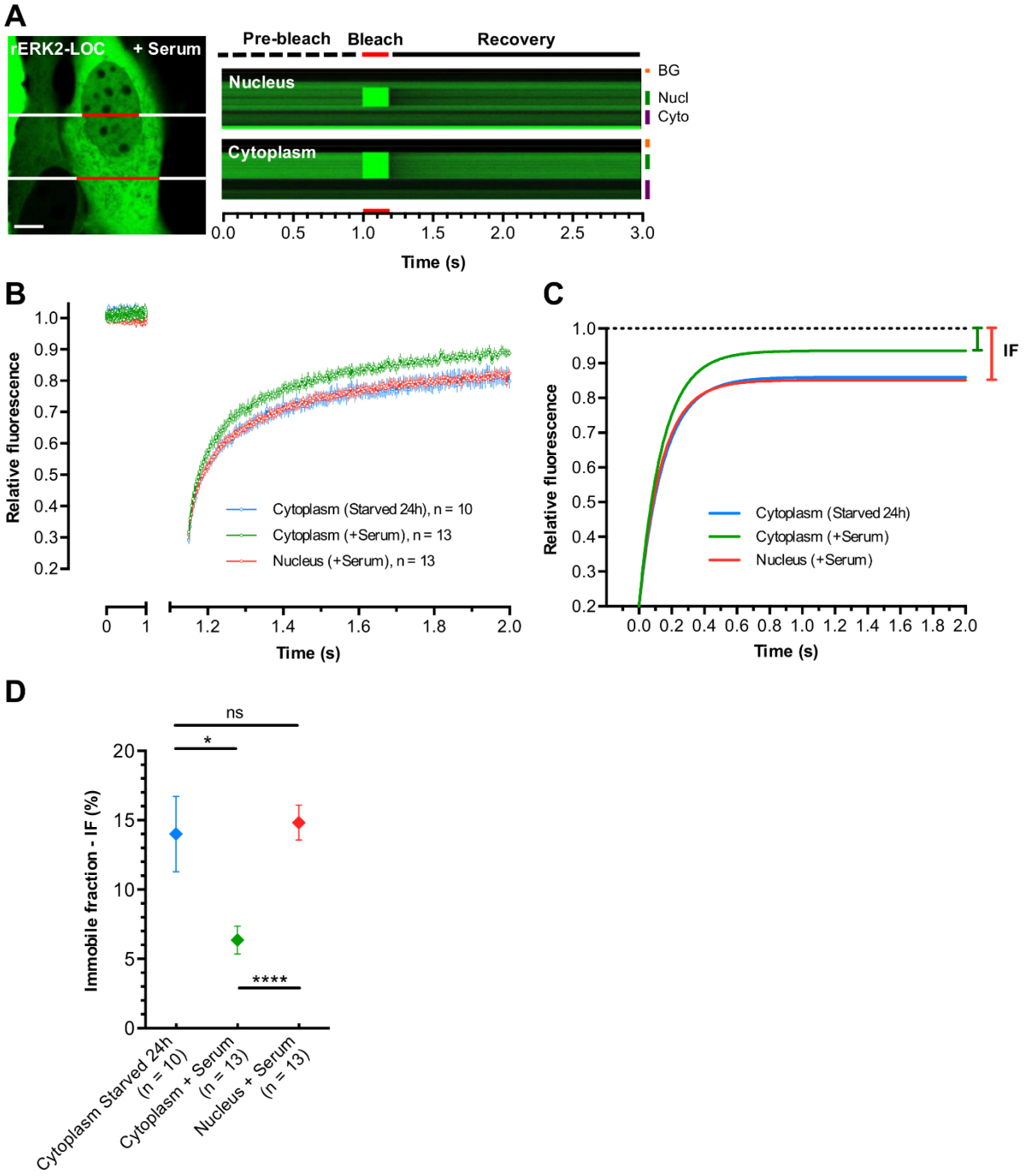

S1 Fig. Comparison of rERK2-LOC mobility in the nucleus and cytoplasm of NIH-3T3 by high-speed FRAP measurements. (A) NIH-3T3 cells were transfected with rERK2-LOC and serum-starved for 24 h. Bleaching was first performed in the cytoplasm of non-stimulated cells, and in both the nucleus and the cytoplasm of the same cell after serum stimulation along the red lines drawn (left panel). Representative kymograms (xt) of fluorescence intensity measured along the lines (both red and white) across the selected cells for each experimental condition over time are shown (right panel). Scale bar: 10 µm. **(B-C)** Curves of cumulative fluorescence recovery over time for rERK2-LOC in resting cell cytoplasm (blue curve), and in cytoplasm (green curve) and nucleus (red curve) 8 min after serum stimulation were normalized **(B)** and fitted **(C)**. **(D)** Immobile fractions (IF) were calculated for all conditions (corresponding color symbols). The number of photobleached cells is indicated above each symbol. Statistical significance was determined by a two-tailed unpaired *t*-test (ns, no significant; *, ≤ 0.05; ****, ≤ 0.0001).

Movie Captions

S1 Movie. rERK2-LOC spatiotemporal localization in serum-starved NIH-3T3 cells after FGF4 stimulation.

S2 Movie. rERK2-LOC spatiotemporal localization in serum-starved HeLa cells after hEGF stimulation.

S3 Movie. xERK2-LOC subcellular distribution in a living Xenopus laevis embryo at the dorsal lip of the blastopore.

The movie shows a vegetal view of the embryo (stage 12, late gastrula) and is made from 108 confocal z-planes using a 1.50-µm step size between sections. The confocal z-series 3D reconstruction of the dorsal lip of blastopore shows the accumulation of rERK2-LOC in the nuclei of blastoporal cells located in the push inward area.

S4 Movie. xERK2-LOC subcellular distribution in a living Xenopus laevis embryo at the yolk plug.

The movie shows a vegetal view of the embryo (stage 12, late gastrula) overexpressing xERK2-LOC and is made from 86 confocal z-planes using a 1.00-µm step size between sections. The confocal z-series 3D reconstruction of the yolk plug shows the accumulation of rERK2-LOC in the nuclei of large endodermal cells.

S5 Movie. Imaging of xERK2-LOC in a whole living Xenopus laevis stage 38 tadpole.

The embryo, head to the left, shows substantial nuclear accumulation of xERK2-LOC in the cells of the forebrain-midbrain boundary.

4.2. Research article – A novel approach for rapid development of optimized FRET-based biosensors for signaling network interrogation in living cells

François Sipieter[1,2,3,4,*], Benjamin Cappe[1,2,*], Olivier Gavet[5], Laurent Héliot[4], Pierre Vincent[6] and Franck B. Riquet[1,2,3]

*These authors contributed equally to this work

[1] Molecular Signaling and Cell Death Unit, Department of Biomedical Molecular Biology, Ghent University, B-9052 Ghent, Belgium.

[2] Molecular Signaling and Cell Death Unit, Inflammation Research Center (IRC), a VIB-UGent department, B-9052 Ghent, Belgium.

[3] Structural and Functional Glycobiology Unit (UGSF), CNRS UMR 8576, Lille 1 University, F-59655 Villeneuve d'Ascq, France.

[4] Team Biophotonique Cellulaire Fonctionnelle, Laboratoire de Physique des Lasers, Atomes et Molécules (PhLAM), CNRS UMR 8523, F-59655 Villeneuve d'Ascq, France.

[5] Institut Gustave Roussy (IGR), CNRS-UMR 8200, Paris-Sud University, F-94805 Villejuif, France.

[6] Neurobiologie des processus adaptatifs (NPA), CNRS UMR 7102, UMPC, F-75005, Paris, France.

Article in preparation

Research Article

A novel approach for rapid development of optimized FRET-based biosensors for signaling network interrogation in living cells

François Sipieter[1,2,3,4,*], Benjamin Cappe[1,2,*], Olivier Gavet[5], Laurent Héliot[4], Pierre Vincent[6] and Franck B. Riquet[1,2,3]

*These authors contributed equally to this work

[1] *Molecular Signaling and Cell Death Unit, Department of Biomedical Molecular Biology, Ghent University, B-9052 Ghent, Belgium.*

[2] *Molecular Signaling and Cell Death Unit, Inflammation Research Center (IRC), a VIB-UGent department, B-9052 Ghent, Belgium.*

[3] *Structural and Functional Glycobiology Unit (UGSF), CNRS UMR 8576, Lille 1 University, F-59655 Villeneuve d'Ascq, France.*

[4] *Team Biophotonique Cellulaire Fonctionnelle, Laboratoire de Physique des Lasers, Atomes et Molécules (PhLAM), CNRS UMR 8523, F-59655 Villeneuve d'Ascq, France.*

[5] *Institut Gustave Roussy (IGR), CNRS-UMR 8200, Paris-Sud University, F-94805 Villejuif, France.*

[6] *Neurobiologie des processus adaptatifs (NPA), CNRS UMR 7102, UMPC, F-75005, Paris, France.*

4.2.1. Introduction

Real-time cellular network interrogation provides spatio-temporal information necessary to study intricate signal transduction in dynamic cellular processes leading to cell fate decision [1–3]. Fluorogenic approaches relying on fluorescent indicators are considered nowadays as instrumental towards this goal. Description of promising prospect of Förster Resonance Energy Transfer (FRET) [4] applied to biology has enhanced experimental strategy designs to study biochemical events in their native context. In this repertoire, genetically encoded intramolecular biosensors based on FRET (hereafter called FRET biosensors) have enriched the scientist toolbox. The archetypal structure of such reporters comprised a molecular recognition element (MRE) serving as bioreceptor usually flanked by two fluorescent proteins (FPs) acting as transducer (for review, [5]). Using rather simple ratiometric measurements, recordings of ionic species [6,7] and second messengers concentration fluctuation [8,9] as well as post-translational modifications [10–13] and protease activities [14,15] in conjunction with dedicated cellular events are within our reach. Kinase activity reporter is one of such subtype of FRET biosensors. A Kinase Activity Reporter (AKAR), the first of its kind, was engineered to report specifically on protein kinase A (PKA) activity [16]. However, to provide meaningful and detailed spatiotemporal kinase activity signature in living cells, several rounds of optimization and additional refining were necessary to yield a specific and sensitive FRET biosensor. The case of AKAR is a clear example and much was learnt along the way considering substrate specificity, biosensor reversibility and sensing domain topology as well as recognition domain optimization for adequate pairing with the sensitized substrate [17].

Genetically encoded FRET biosensors present several advantages in comparison with other fluorogenic probes including high signal-to-noise ratio, easy to transfect into cell lines and simple ratiometric imaging [18,19]. The dark side of FRET biosensors concerns their sensitivity in particular for *in vivo* applications. To be efficient such a FRET biosensor must allow spatio-temporal functional imaging at high frequency sampling [20,21], harbor no innate localization and behave in an inert fashion so as to avoid buffering effect [17] onto the evaluated signaling molecule. In addition, a few biosensors' key requirements [17,20,22–26] should be considered. To fit to this tender, the developer is facing additional challenges. While specific

structural requirements/constraints favorable for FRET to occur between fluorescent proteins are known [4], concerning intramolecular FRET biosensor, orientation of fluorescent proteins is not foreseeable, and no 3D structure prediction is possible so far. In an attempt to establish some ground rules for biosensor engineering, biophysical modeling of biosensor based on small-angle X-ray scattering (SAXS) experimental data was reported. But data were gathered from already validated biosensors [7,27]. Mathematical modeling was also employed to infer fluorescent proteins dimerization and linker length on distance dependent FRET in the context of intramolecular biosensor [26]. The current consensus in the field is that, biosensor engineering remains a time consuming empirical optimization process by trials and errors.

To produce sensitive FRET biosensors, several research groups focused on the engineering of fluorescent proteins to provide GFP variants with improved fluorescent properties dedicated for FRET applications [24,28,29]. But these new optimized variants, were not sufficient for generating highly sensitive FRET biosensors. Other parameters could affect biosensor efficiency such as the orientation and the distance between fluorescent proteins [4]. The emergence of circularly permutated (cp) fluorescent protein variants [9,30] as well as the design of rigid or flexible linkers with various lengths [26] led to the generation of new FRET biosensors with increased dynamic range. Several positional combinations of key molecular elements comprised in these FRET biosensors were investigated to generate a suitable arrangement for dynamic range improvement [20]. For example, structural evidences support that CFP should be preferentially positioned at the C-terminal of the biosensor and not at the N-terminal as usually found [26]. In light of the diversity of potential combinations to produce an optimized FRET biosensor, a ready-to-use plasmid library with various FRET pairs was made available [25], a generic backbone with enhanced performance was validated [26] and a versatile toolkit [31] was reported. However, the time-consuming constraint remains since the aforementioned strategies rely on classical molecular cloning method to produce a vast number of potential successful combinations.

Driven by flexibility and versatility to produce tailor-made biosensor without hampering the dynamic range and therefore the sensitivity, we have developed a method for accelerating the development and optimization of FRET biosensors.

Considering the number of potential kinase substrates, the existence of several different Phospho Amino Acid Binding Domain (PAABD) and fluorescent protein variants available, four libraries based on the Gateway technology [32] were built: a library of flanking N-terminal and C-terminal fluorescent proteins, a substrate domain library and a recognition domain library. In this context the Gateway *att r*ecombination sequences are acting as short linkers flanking each functional element of the biosensor. This methodology was applied on both PKA and ERK1/2 biosensors. While characterization and validation conducted in different cellular models showed no detrimental effect on AKAR performance, the sensitivity and dynamic range of EKAR (ERK-ACT) were much improved. ERK-ACT was then utilized for the spatio-temporal monitoring of ERK1/2 activity throughout the cell cycle in single living cells, revealing particular signatures of ERK1/2 activity that were not recorded before with previous ERK biosensors [23,26].

4.2.2. Material and Methods

All steps used for generating FRET biosensors were rigorously described and detailed in a patent application. *Application nr GB 1400997.1. Riquet F et al. Priority date: 2014.06.20*.

Cell culture and transfection

HeLa cells (ECACC 93021013) and HEK 293T (ATCC CRL-11268) were maintained at 37 °C under 5% CO_2 in Dulbecco's Modified Eagle Medium (DMEM, #11885-084) supplemented with 10% Fetal Bovine Serum (FBS, qualified, heat inactivated, EU-approved, South America Origin) and 100 U/mL Penicillin/Streptomycin (P/S, #15140-122) (Gibco, Thermo Fisher Scientific, Waltham, MA, USA). For live imaging, cells were resuspended in Fluorobrite DMEM (A18967, Life Technologies) after trypsinization and seeded on 8-well dishes ibiTreat (#80826, Ibidi, Martinsried, Germany) at a density of 40.000 cells/mL to reach 60% confluence at the time of transfection. Transfection was performed using JetPrime reagent (#114-15, Polyplus, Illkirch, France) according to the manufacturer's instructions. Media were changed with fresh medium 4h after transfection to reduce cytotoxicity. HeLa cells were starved by adding 1% FBS for 24 h before experiments began. The cells were placed directly inside a microscope stage chamber controlling temperature, CO2 and humidity (top stage incubator, Okolab, Burlingame, CA, USA)

1h before cell imaging to avoid aberrant cellular responses due to cell stress (e.g. temperature changes, cell manipulation, etc.).

Ratiometric imaging

Wide-field images were captured with a Nikon TiE inverted microscope with a 20x 0.5NA objective and a DS-Qi2 CMOS camera (Nikon, Japan). Images were acquired at intervals of 2 min with the Nikon NIS-Elements acquisition software using JOBS module (Nikon). A Lumencor Spectra X LED Light Engine (Lumencor, Beaverton, OR, USA) provided the excitation light source. Ratio imaging used a 440/30 excitation filter, a t440/510/575rpc multi-band dichroic mirror, and two emission filters (ET480/40M (CFP) and AT545/30M (FRET)). Excitation filters were provided by Lumencor and all dichroic mirrors and emission filters were obtained from Chroma Technology (Brattleboro, VT, USA). An automated emission filter wheel Lambda 10-B Smart Shutter (Sutter Instrument, Novato, CA, USA) was used. Analysis of EKAR and AKAR FRET biosensors was performed with custom routines written in IGOR Pro environment (Wavemetrics, Lake Oswego, OR, USA). FRET intensity was calculated as a ratio of the CFP/YFP signal for each pixel on background subtracted images. Pseudocolor images represent both the ratio and the fluorescence intensity values, where warmer colors denote high FRET and cooler colors low FRET efficiency. The calibration bar shows the fluorescence intensity values at the bottom and the ratio values on the right. The micron-scale of the images corresponds to the size of the calibration bar.

4.2.3. Results

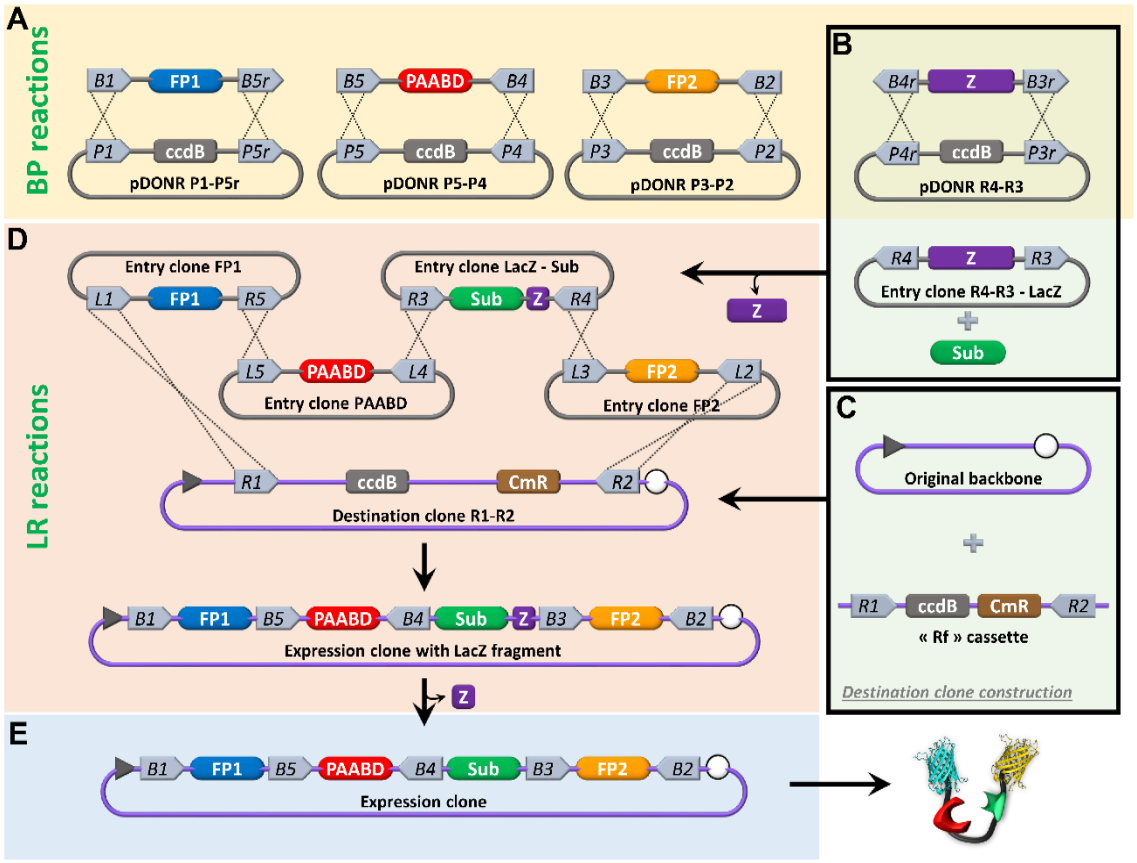

Figure 1: Overview of the Gateway cloning process adapted to Kinase Activity Reporter development. (**A**) The fluorescent proteins (FP1 and FP2) and the Phospho-Amino Acid Binding Domain (PAABD) were PCR amplified using the appropriate *att* sequences. PCR products were recombined with the corresponding pDONR vector creating Entry clones. (**B**) Due to the small length of the substrate, recombination reactions were inefficient, so an intermediate vector was especially designed to alleviate this problem. To this effect, the LacZ operon was PCR amplified with appropriate *att* sequences and the product was recombined with the corresponding pDONR. The substrate was cloned in the LacZ generated Entry clone using classical molecular cloning strategy, so to produce an Entry clone which length was also amendable for subsequent steps. (**C**) The destination vector was constructed from an original biosensor backbone, in which a "Rf" cassette was inserted using classical molecular strategy. (**D**) Intermediate expression clone was made by LR reaction with the four entry clones containing FP1, FP2, PAABD or the substrate, with the appropriate Destination vector. (**E**) Excision of the LacZ fragment by classical molecular cloning yielded the final expression clone coding for the desired kinase activity reporter.

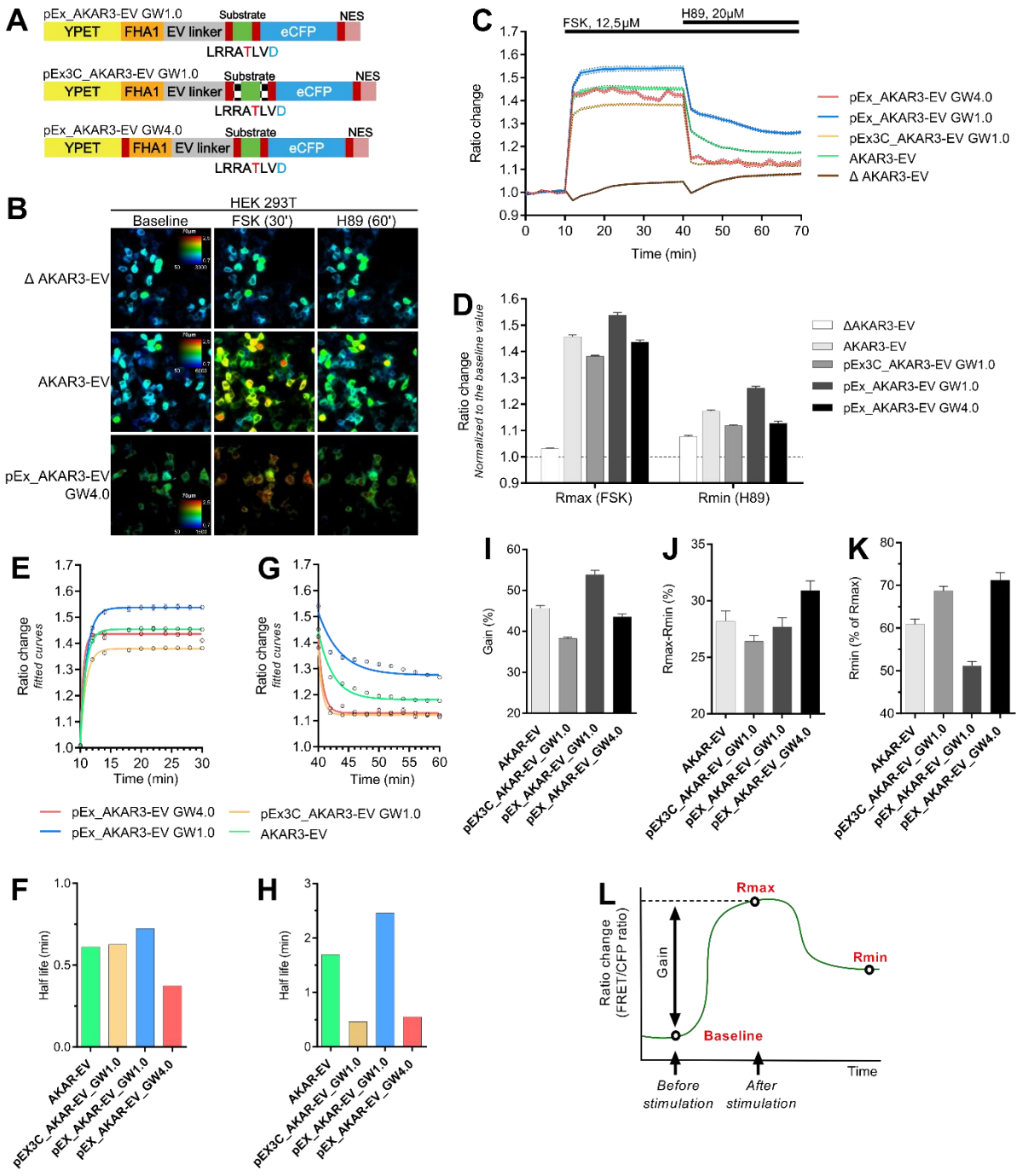

Figure 2: Optimization of AKAR3-EV biosensor by recombination cloning method. (**A**) Structure of the biosensors generated using the Gateway system. Top panel shows the structure of the biosensor for which the cloning system was used only for the substrate. Middle panel depicts a similar structure, but by inserting the substrate in an intermediate commercial vector resulting in the presence of additional sequences on either side of the substrate. Bottom panel shows the structure where the construction was achieved using multisite gateway. Red rectangles represent *att* sequences; black and white rectangles show additional sequences from the intermediate vector (pENTR3C). (**B**) Representative FRET/CFP ratio images before and after stimulation with FSK and after inhibition with H89, with AKAR3-EV mutant (upper), AKAR3-EV (middle), and pEX-AKAR3-EV GW4.0 (bottom) are shown in the intensity-modulated display mode. HEK293T cells were imaged 24h after transient transfection with a time resolution of 2min. A baseline was acquired during 10min before being stimulated with 12,5µM Forskolin (FSK) for 30min, follow by inhibition with 20µM H89. (**C**) Representation of the FRET/CFP ratio. The ratio of each cell was normalized by dividing by the

average of the FRET/CFP ratio before stimulation (baseline). (**D**) Maximal ratio after FSK activation (Rmax) and minimal ratio after H89 inhibition (Rmin) are plotted for each biosensor. Explanation concerning the graphical representation of Rmax and Rmin is shown in panel (L). (**E-G**) Fit curves of the FRET/CFP ratio for the activation and the inhibition respectively. (**F-H**) Average half-life ($t_{1/2}$) of the activation and the inhibition dynamic are plotted. (**I-K**) Ratiometric gains, differences between Rmax and Rmin, and Rmin proportions based to the Rmax, respectively, are plotted for each biosensor. (**L**) Graphical representation of the different measured parameters. The mean and SEM from at least 35 cells, from at least two independent experiments, are plotted.

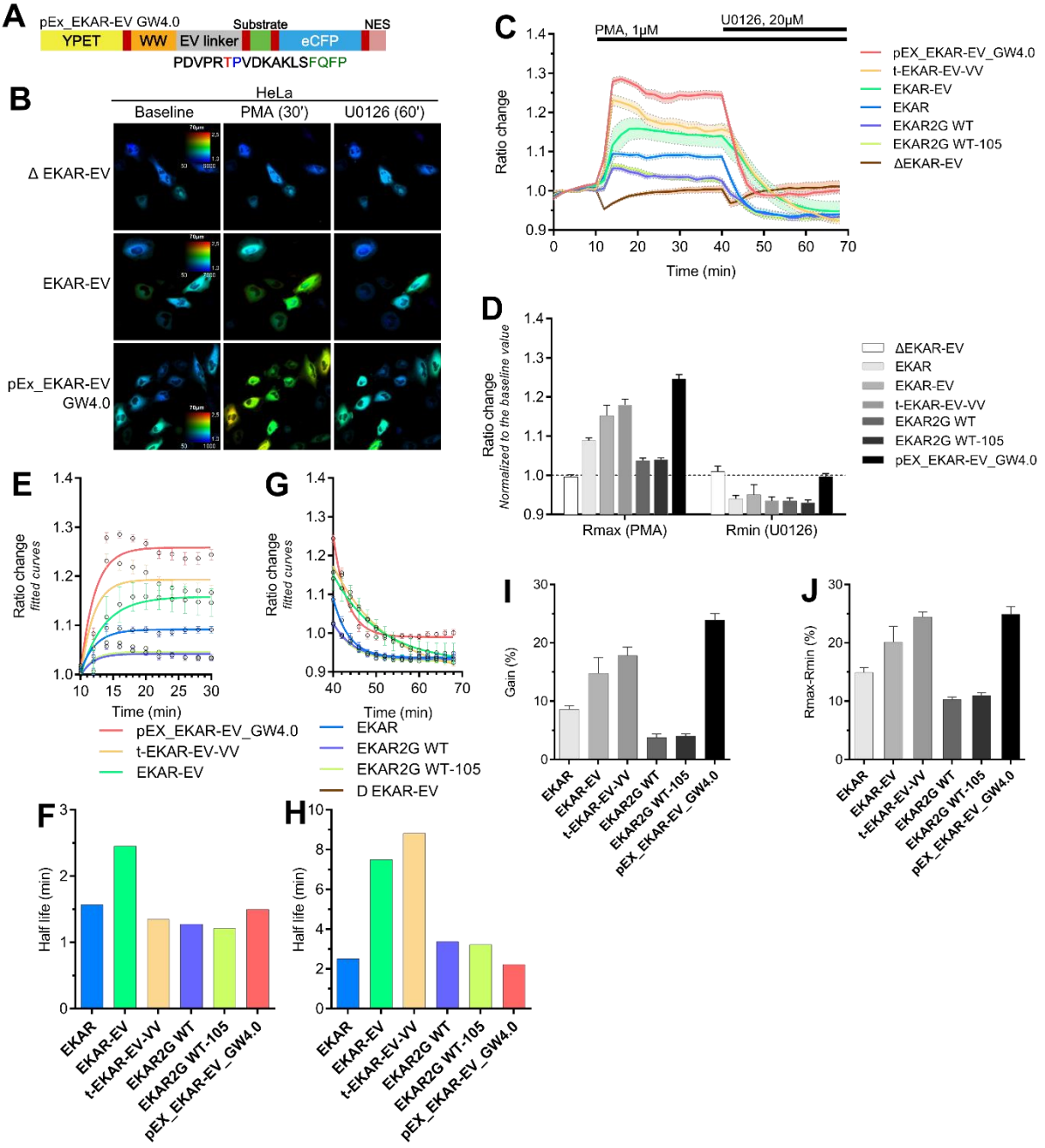

Figure 3: Marked optimization of EKAR-EV biosensor through Gateway cloning system. (**A**) Structure of the EKAR-EV GW4.0 biosensors generated using the multisite Gateway system. Red rectangles represent *att* sequences. (**B**) Representative FRET/CFP ratio images of HeLa transfected with EKAR-EV mutant (upper), EKAR-EV (middle), and pEX-EKAR-EV GW4.0 (bottom) are shown in the intensity-modulated display mode before and after stimulation with PMA and after inhibition with U0126. HeLa cells were imaged 24h after transient transfection with a time resolution of 2min. A baseline was acquired during 10min before being stimulated with 1µM Phorbol Myristate Acetate (PMA) for 30min, followed by inhibition with 20µM U0126. (**C**) Representation of the FRET/CFP ratio. The ratio of each cell was normalized by dividing by the average of the FRET/CFP ratio before stimulation (baseline). (**D**) Maximal ratio after PMA activation (Rmax) and minimal ratio after U0126 inhibition (Rmin) are plotted for each biosensor. Explanation concerning the graphical representation of Rmax and Rmin is shown in Fig.2 panel (L). (**E-G**) Fit curves of the FRET/CFP ratio for the activation and the inhibition respectively. (**F-H**) Average half-life ($t_{1/2}$) of the activation and the inhibition dynamic are plotted. (**I-J**) Ratiometric gains, and differences between Rmax and Rmin, respectively, are plotted for each biosensor. The mean and SEM from at least 35 cells, from at least two independent experiments, are plotted.

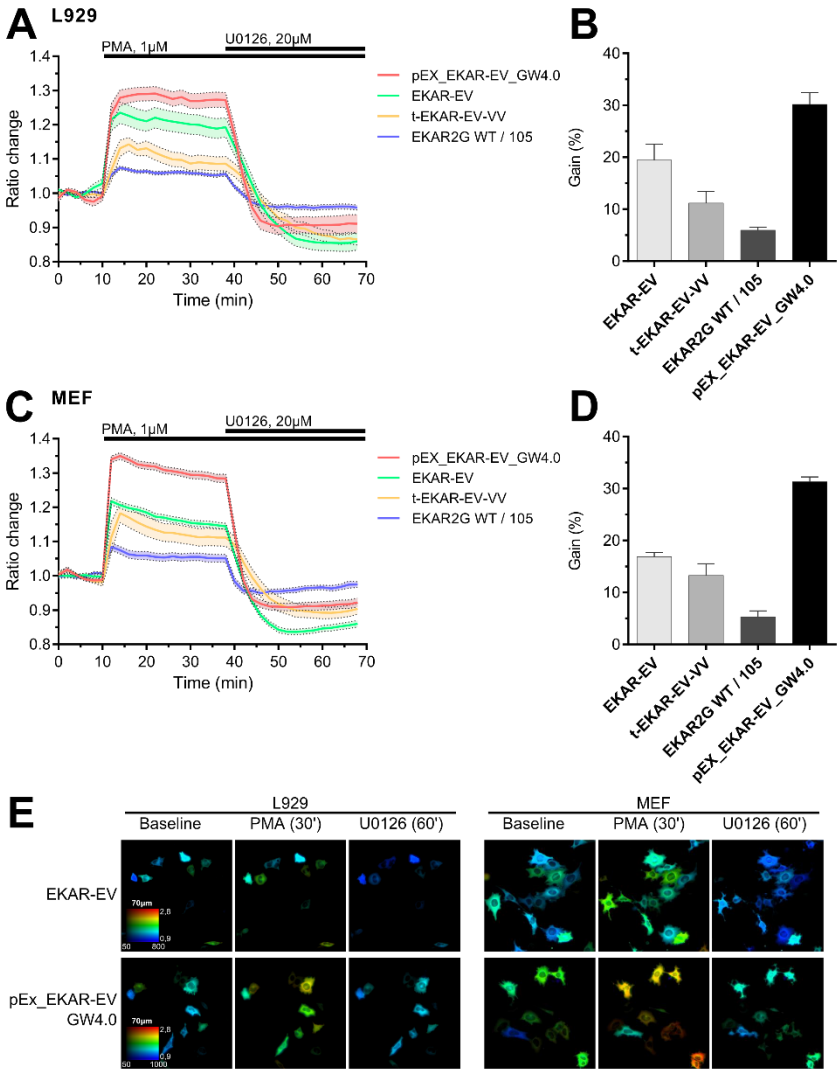

Figure 4: Comparative analysis of ERK biosensor performance in MEF and L929. Two mouse fibroblast cellular models relevant for necroptosis studies were transfected with the above-mentioned ERK biosensors. Both cell lines were imaged 24h after transient transfection with a time resolution of 2min. A baseline was acquired during 10min before stimulation of the MAPK/ERK1/2 pathway with 1µM PMA for 30min, followed by inhibition with 20µM U0126. (**A**) and (**C**) Representation of the FRET/CFP ratio. The ratio of each cell was normalized by dividing by the average of the FRET/CFP ratio before stimulation (baseline). (**B**) and (**D**) Ratiometric gains are plotted for each biosensor. Explanation concerning the graphical representation of Rmax, Rmin and gain is shown in Fig.2 panel (L). (**E**) Representative FRET/CFP ratio images of L929 (left) and MEF (right) transfected with EKAR-EV (upper), or pEX-EKAR-EV GW4.0 (bottom) are shown in the intensity-modulated display mode before and after stimulation with PMA and after inhibition with U0126.

4.2.4. Conclusion

We have developed a method for accelerating the development of FRET biosensors through the generation of biosensor libraries with multiple potential combinations based on Gateway cloning technologies. Application of this approach facilitated efforts for the construction of both PKA and ERK1/2 biosensors as a proof of feasibility and led to the identification of *att* recombination sequences as efficient linkers to upgrade biosensor's dynamic range. Newly generated PKA (AKAR3-EV-GW) and ERK1/2 (EKAR-EV-GW) biosensors exhibited an improved emission ratio change in comparison with previous constructs in single cells measurements. In addition, the reversibility of these biosensors was also upgraded hence rendering biosensors more accessible to specific phosphatases. Our methodology should be therefore applicable to the optimization and the development of further FRET biosensors.

References

1. Newman RH, Fosbrink MD, Zhang J. Genetically encodable fluorescent biosensors for tracking signaling dynamics in living cells. Chem Rev. 2011;111: 3614–66. doi:10.1021/cr100002u
2. Ebisuya M, Kondoh K, Nishida E. The duration, magnitude and compartmentalization of ERK MAP kinase activity: mechanisms for providing signaling specificity. J Cell Sci. 2005;118: 2997–3002. doi:10.1242/jcs.02505
3. Kamioka Y, Sumiyama K, Mizuno R, Sakai Y, Hirata E, Kiyokawa E, et al. Live imaging of protein kinase activities in transgenic mice expressing FRET biosensors. Cell Struct Funct. 2012;37: 65–73. Available: http://www.ncbi.nlm.nih.gov/pubmed/22277578
4. Jares-Erijman E a, Jovin TM. FRET imaging. Nat Biotechnol. 2003;21: 1387–1395. doi:10.1038/nbt896
5. Sipieter F, Vandame P, Spriet C, Leray A, Vincent P, Trinel D, et al. From FRET imaging to practical methodology for Kinase activity sensing in living cells. Prog Mol Biol Transl Sci. 2013;113: 145–216. doi:10.1016/B978-0-12-386932-6.00005-3
6. Tantama M, Hung YP, Yellen G. Imaging intracellular pH in live cells with a genetically encoded red fluorescent protein sensor. J Am Chem Soc. 2011;133: 10034–7. doi:10.1021/ja202902d
7. Thestrup T, Litzlbauer J, Bartholomäus I, Mues M, Russo L, Dana H, et al. Optimized ratiometric calcium sensors for functional in vivo imaging of neurons and T lymphocytes. Nat Methods. 2014;11: 175–82. doi:10.1038/nmeth.2773
8. Berg J, Hung YP, Yellen G. A genetically encoded fluorescent reporter of ATP:ADP ratio. Nat Methods. 2009;6: 161–6. doi:10.1038/nmeth.1288
9. Van der Krogt GNM, Ogink J, Ponsioen B, Jalink K. A comparison of donor-acceptor pairs for genetically encoded FRET sensors: application to the Epac cAMP sensor as an example. Koch K-W, editor. PLoS One. 2008;3: e1916. doi:10.1371/journal.pone.0001916
10. Herbst KJ, Allen MD, Zhang J. Spatiotemporally regulated protein kinase A activity is a critical regulator of growth factor-stimulated extracellular signal-regulated kinase signaling in PC12 cells. Mol Cell Biol. 2011;31: 4063–75. doi:10.1128/MCB.05459-11
11. Aoki K, Kumagai Y, Sakurai A, Komatsu N, Fujita Y, Shionyu C, et al. Stochastic ERK activation induced by noise and cell-to-cell propagation regulates cell density-dependent proliferation. Mol Cell. Elsevier; 2013;52: 529–40. doi:10.1016/j.molcel.2013.09.015
12. Albeck JG, Mills GB, Brugge JS. Frequency-modulated pulses of ERK activity transmit quantitative proliferation signals. Mol Cell. Elsevier Inc.; 2013;49: 249–61. doi:10.1016/j.molcel.2012.11.002
13. Carrillo LD, Krishnamoorthy L, Mahal LK. A cellular FRET-based sensor for beta-O-GlcNAc, a dynamic carbohydrate modification involved in signaling. J Am Chem Soc. 2006;128: 14768–9. doi:10.1021/ja065835+
14. Wu X, Simone J, Hewgill D, Siegel R, Lipsky PE, He L. Measurement of two caspase activities simultaneously in living cells by a novel dual FRET fluorescent indicator probe. Cytom Part A J Int Soc Anal Cytol. 2006;69: 477–486. doi:10.1002/cyto.a.20300

15. Ai H, Hazelwood KL, Davidson MW, Campbell RE. Fluorescent protein FRET pairs for ratiometric imaging of dual biosensors. Nat Methods. 2008;5: 401–3. doi:10.1038/nmeth.1207
16. Zhang J, Ma Y, Taylor SS, Tsien RY. Genetically encoded reporters of protein kinase A activity reveal impact of substrate tethering. Proc Natl Acad Sci U S A. 2001;98: 14997–15002. doi:10.1073/pnas.211566798
17. Aye-Han N-N, Ni Q, Zhang J. Fluorescent biosensors for real-time tracking of post-translational modification dynamics. Curr Opin Chem Biol. 2009;13: 392–7. doi:10.1016/j.cbpa.2009.07.009
18. Miyawaki A. Visualization of the spatial and temporal dynamics of intracellular signaling. Dev Cell. 2003;4: 295–305. Available: http://www.ncbi.nlm.nih.gov/pubmed/12636912
19. Aoki K, Kiyokawa E, Nakamura T, Matsuda M. Visualization of growth signal transduction cascades in living cells with genetically encoded probes based on Förster resonance energy transfer. Philos Trans R Soc Lond B Biol Sci. 2008;363: 2143–2151. doi:10.1098/rstb.2008.2267
20. Fritz RD, Letzelter M, Reimann A, Martin K, Fusco L, Ritsma L, et al. A Versatile Toolkit to Produce Sensitive FRET Biosensors to Visualize Signaling in Time and Space. Sci Signal. 2013;6: rs12–rs12. doi:10.1126/scisignal.2004135
21. Doupé DP, Perrimon N. Visualizing and manipulating temporal signaling dynamics with fluorescence-based tools. Sci Signal. 2014;7: re1. doi:10.1126/scisignal.2005077
22. Depry C, Zhang J. Visualization of kinase activity with FRET-based activity biosensors. Ausubel FM, Brent R, Kingston RE, Moore DD, Seidman JG, Smith JA, et al., editors. Curr Protoc Mol Biol. Hoboken, NJ, USA: John Wiley & Sons, Inc.; 2010;Chapter 18: Unit 18.15. doi:10.1002/0471142727.mb1815s91
23. Harvey CD, Ehrhardt AG, Cellurale C, Zhong H, Yasuda R, Davis RJ, et al. A genetically encoded fluorescent sensor of ERK activity. Proc Natl Acad Sci U S A. 2008;105: 19264–9. doi:10.1073/pnas.0804598105
24. Frommer WB, Davidson MW, Campbell RE. Genetically encoded biosensors based on engineered fluorescent proteins. Chem Soc Rev. 2009;38: 2833–41. doi:10.1039/b907749a
25. Piljić A, de Diego I, Wilmanns M, Schultz C. Rapid development of genetically encoded FRET reporters. ACS Chem Biol. 2011;6: 685–91. doi:10.1021/cb100402n
26. Komatsu N, Aoki K, Yamada M, Yukinaga H, Fujita Y, Kamioka Y, et al. Development of an optimized backbone of FRET biosensors for kinases and GTPases. Mol Biol Cell. 2011;22: 4647–56. doi:10.1091/mbc.E11-01-0072
27. Mertens HDT, Piljić A, Schultz C, Svergun DI. Conformational analysis of a genetically encoded FRET biosensor by SAXS. Biophys J. 2012;102: 2866–75. doi:10.1016/j.bpj.2012.05.009
28. Karasawa S, Araki T, Nagai T, Mizuno H, Miyawaki A. Cyan-emitting and orange-emitting fluorescent proteins as a donor/acceptor pair for fluorescence resonance energy transfer. Biochem J. 2004;381: 307–12. doi:10.1042/BJ20040321
29. Nguyen AW, Daugherty PS. Evolutionary optimization of fluorescent proteins for intracellular FRET. Nat Biotechnol. 2005;23: 355–360. doi:10.1038/nbt1066
30. Nagai T, Yamada S, Tominaga T, Ichikawa M, Miyawaki A. Expanded dynamic range of fluorescent indicators for Ca(2+) by circularly permuted yellow fluorescent proteins. Proc Natl Acad Sci U S A. 2004;101: 10554–10559. doi:10.1073/pnas.0400417101
31. Fritz RD, Letzelter M, Reimann A, Martin K, Fusco L, Ritsma L, et al. A versatile toolkit to produce sensitive FRET biosensors to visualize signaling in time and space. Sci Signal. 2013;6: rs12. doi:10.1126/scisignal.2004135
32. Walhout a J, Temple GF, Brasch M a, Hartley JL, Lorson M a, van den Heuvel S, et al. GATEWAY recombinational cloning: application to the cloning of large numbers of open reading frames or ORFeomes. Methods Enzymol. 2000;328: 575–592. doi:10.1016/S0076-6879(00)28419-X

4.3. Research article – Spatio-temporal characterization of ERK activity in survival, apoptosis and necroptosis

François Sipieter[1,2,4,5,7], Benjamin Cappe[1,2,7], Pierre Vincent[6,7], Peter Vandenabeele[1,2,3] and Franck B. Riquet[1,2,4,7]

[1] Molecular Signaling and Cell Death Unit, Department of Biomedical Molecular Biology, Ghent University, B-9052 Ghent, Belgium

[2] Molecular Signaling and Cell Death Unit, Inflammation Research Center (IRC), a VIB-UGent department, B-9052 Ghent, Belgium

[3] Methusalem Program, Ghent University, B-9052 Ghent, Belgium

[4] Structural and Functional Glycobiology Unit (UGSF), CNRS UMR 8576, Lille 1 University, F-59655 Villeneuve d'Ascq, France

[5] Team Biophotonique Cellulaire Fonctionnelle, Laboratoire de Physique des Lasers, Atomes et Molécules (PhLAM), CNRS UMR 8523, F-59655 Villeneuve d'Ascq, France

[6] Neurobiologie des processus adaptatifs (NPA), CNRS UMR 7102, UMPC, F-75005, Paris, France.

[7] Groupement de Recherche Microscopie Imagerie du Vivant, GDR2588- CNRS, F-59655 Villeneuve d'Ascq, France

Article in preparation

Research Article

Spatio-temporal characterization of ERK activity in survival, apoptosis and necroptosis

François Sipieter[1,2,4,5,7], Benjamin Cappe[1,2,7], Pierre Vincent[6,7], Peter Vandenabeele[1,2,3] and Franck B. Riquet[1,2,4,7]

[1] Molecular Signaling and Cell Death Unit, Department of Biomedical Molecular Biology, Ghent University, B-9052 Ghent, Belgium

[2] Molecular Signaling and Cell Death Unit, Inflammation Research Center (IRC), a VIB-UGent department, B-9052 Ghent, Belgium

[3] Methusalem Program, Ghent University, B-9052 Ghent, Belgium

[4] Structural and Functional Glycobiology Unit (UGSF), CNRS UMR 8576, Lille 1 University, F-59655 Villeneuve d'Ascq, France

[5] Team Biophotonique Cellulaire Fonctionnelle, Laboratoire de Physique des Lasers, Atomes et Molécules (PhLAM), CNRS UMR 8523, F-59655 Villeneuve d'Ascq, France

[6] Neurobiologie des processus adaptatifs (NPA), CNRS UMR 7102, UMPC, F-75005, Paris, France.

[7] Groupement de Recherche Microscopie Imagerie du Vivant, GDR2588- CNRS, F-59655 Villeneuve d'Ascq, France

4.3.1. Introduction

For a long time, necrosis has been considered as an uncontrolled and unregulated form of cell death, but accumulating evidence suggests that its occurrence is tightly regulated and involves signaling pathways [1]. This contributed to the characterization of a new form of programmed necrosis referred to as “necroptosis” [2–6]. Tumor Necrosis Factor alpha (TNFα)-induced necroptosis relies on a signaling pathway involving mainly two serine-threonine kinases: Receptor-Interacting Protein Kinase 1 and 3 (RIPK1 and RIPK3) [5]. Recently, the pseudo-kinase Mixed-Lineage Kinase Like (MLKL) was identified as the crucial executioner of necroptosis downstream of RIPK3 [7,8].

TNF signaling occurs through a complex multi-step pathway based on cell death checkpoints directing the cell to a specific cellular response [9]. The first checkpoint is organized by the kinase RIPK1 that is positioned at the crossroads of cell death and survival [2]. RIPK1 ubiquitination state is crucial as it determines whether RIPK1 functions as a molecular platform allowing the recruitment of molecular adapters with the ability to elicit a pro-survival response or as a kinase that promotes cell death. The second checkpoint decides on cell death type depending on the pro-death complex that binds RIPK1 [3,9]. Upon phosphorylation by RIPK3 and a conformational change, MLKL appears to form oligomers that localize at the plasma membrane and compromise its ability to preserve ionic homeostasis leading to its permeabilization [8,10–12]. However, regulatory mechanisms of necroptosis remain poorly understood. This is even more complex because molecules mobilized to activate a specific cell death pathway are mostly common to other programmed cell death. The identification of molecules or processes that are specifically required for necroptosis induction and regulation would upgrade necroptosis from a signaling cascade to a specific cellular function.

Extracellular signal-regulated protein kinases 1 and 2 (ERK1/2) which are members of the mitogen activated protein kinase (MAPK) superfamily are able to engage cell proliferation, survival and cell death depending on the cellular context [13,14]. Interestingly, activation of ERK1/2 was reported to be involved in different modes of programmed cell death such as apoptosis, autophagy and ferroptosis in various cellular models [15–20]. It is now accepted that the regulation of the duration, magnitude and subcellular compartmentalization of ERK1/2 activity by specific

spatio-temporal regulators is interpreted by the cell towards cell fate determination [21]. Sustained cytoplasmic ERK1/2 activity, besides inhibiting survival and proliferative signals in the nucleus, is rather implicated in senescence and autophagy by potentiating activity of cytoplasmic pro-death proteins. In contrast, sustained nuclear compartmentalization of ERK1/2 activity might promote apoptosis [18]. However, Devin and colleagues investigated the molecular mechanism between RIPK1 and MAPKs by using both RIPK1$^{-/-}$ and TRAF2$^{-/-}$ mouse embryonic fibroblasts (MEF) [22]. They provided strong evidences of the implication of both RIPK1 and TRAF2 in TNFα-induced JNK, p38 and ERK1/2 activation as a drop of 70% in ERK1/2 activity was observed in RIPK1$^{-/-}$ cells. Interestingly, by using a kinase-dead form of RIPK1, RIPK1 (K45A), in RIPK1$^{-/-}$ cells, they revealed that RIPK1 kinase activity is only required for ERK1/2 but not for p38 and JNK activation. Moreover, in accordance with previous studies, a RIPK1 kinase-dependent ERK1/2 phosphorylation upon TNFα stimulation was reported in L929 cells [23]. Recently, Zhang and colleagues revealed that ERK1/2 might play a prominent role in glutamate-induced necroptosis in HT-22 cells [24]. However, in the context of ischemia-reperfusion (IR) injury in rat retinas, Gao and colleagues uncovered a link between ERK1/2 activation and RIPK1/3 pathway [25].

Owing to the importance of ERK1/2 spatio-temporal dynamics in determining cellular responses [26,27] and compelling evidences of ERK1/2 involvement in necroptosis, we investigated the ERK1/2 spatio-temporal code in TNFα-induced necroptosis using fluorescence-based reporters of both ERK1/2 activity and localization in single living cells. In combination with chemical inhibition strategies targeting specific effectors of necroptosis we report on the complex relationships between ERK1/2 and RIPK signaling pathways.

4.3.2. Materials and methods

Antibodies, Cytokines and Reagents

Recombinant human TNFα, produced in our laboratory, has a specific biological activity of $3x10^7$ IU/mg and was used at 600 IU/ml to stimulate L929 and MEF cells. MEK1/2 inhibitor U0126 and propidium iodide (PI) (Sigma Aldrich, Steinheim, Germany) was used at 20µM and 3µM respectively. RIPK1 inhibitor, necrostatin-1 (Nec-1) (Calbiochem, Merck KGaA, Darmstadt, Germany) was used at

10mM. The caspase peptide inhibitor, zVAD-fmk (Bachem, Bubendorf, Switzerland) was used at 10µM. IAP antagonist BV6 was used at 1µM (Genentech Inc., South San Francisco, CA, USA). SytoxGreen (Thermo Fisher Scientific, Waltham, MA, USA) was used at 5µM. The following antibodies were used for western blot: anti-ERK1/2 (Abcam, Cambridge, UK, ab17942, 1:1000), anti-β-actin (Santa Cruz Biotechnology, Santa Cruz, CA, USA, I-19, 1:1000), anti-ERK2 (Santa Cruz Biotechnology, Santa Cruz, CA, USA, C-14, 1:1000), anti-RIPK1 (BD Biosciences, Franklin Lakes, NJ, USA, 610459, 1:1000), anti-β tubulin (Abcam, Cambridge, UK, ab6046, 1:1000) and anti-activated MAPK/ERK1&2 (diphosphorylated ERK1/2) antibody (clone MAPK-YT, Sigma Aldrich, M9692, 1:2000). HRP-conjugated secondary antibodies were anti-rabbit IgG, anti-mouse IgG or anti-goat IgG (Santa Cruz Biotechnology, sc-2004, sc-2005, sc-2020 respectively, 1:10000).

Plasmids

The plasmid encoding eGFP-ERK2 and MEK1 in equimolar proportion has been used for spatio-temporal localization of ERK2 (ERK2-LOC) and has been described by Riquet and colleagues (in press). The plasmid encoding an optimized version of the previous FRET biosensor EKAR-EV [28] has been used to monitor ERK1/2 activity in single cells measurements (ERK1/2-ACT) (Sipieter et al., in preparation).

Cell culture

L929 and MEF cells were cultured at 37 °C under 5% CO_2 in Dulbecco's Modified Eagle Medium (DMEM) supplemented with 10% Fetal Bovine Serum (FBS, qualified, heat inactivated, EU-approved, South America Origin) and 100 U/mL Penicillin/Streptomycin (Gibco, Thermo Fisher Scientific). For live imaging, cells were resuspended in Fluorobrite DMEM (Gibco, Thermo Fisher Scientific) after trypsinization and seeded on 8-well dishes ibiTreat (Ibidi, Martinsried, Germany) at a density of 15.000 cells/mL to reach 60% confluence at the time of transfection. Transfections were performed using JetPrime reagent Polyplus, Illkirch, France) according to the manufacturer's instructions. The medium was changed with fresh medium 4h after transfection to reduce cytotoxicity. Cells were starved by adding 1% FBS for 12 h before experiments began. For microscopy experiments, cells were placed directly inside a microscope stage chamber under controlled temperature,

CO2 and humidity (top stage incubator, Okolab, Burlingame, CA, USA) 1h before cell imaging.

Western blotting

At specified time intervals after TNFα addition, L929 cells were washed twice in ice-cold PBS and scraped using ice-cold RIPA lysis buffer (50 mM Tris-HCl, pH 7.5; 150 mM NaCl; 1 mM EDTA; 0.5% sodium deoxycholate; 1% Triton X-100 and 0.1% SDS) freshly supplemented with EDTA-free Complete protease inhibitor cocktail tablets (no. 11873580001) and phosphatase inhibitor cocktail tablets (PhosSTOP, no. 04906837001) (Roche Diagnostics Belgium N.V., Vilvoorde, Belgium). Extracted proteins (30 µg) were separated on 12% SDS polyacrylamide gels and then transferred onto nitrocellulose membranes (Amersham Bioscience, UK). Membranes were blocked using TBS with 0.05% Tween20 (TBS-T) containing 5% non-fat dry milk (Biorad, CA, USA) or in 2% BSA for phospho-antibodies. Luminata Classico Western HRP Chemiluminescence Detection Reagents (Millipore, Molsheim, France) was used for antibodies detection.

Immunostaining

At specified time intervals upon TNFα addition, L929 cells were fixed with 4% paraformaldehyde in PBS for 10 min. Afterwards, cells were rinsed three times with PBS and permeabilized with 0.5% Triton X-100 in PBS for 5 min. Cells were incubated with a blocking solution composed of 2% FBS; 5% normal goat serum and 2% BSA in PBS for 1 h at room temperature and then further incubated with primary antibodies in blocking solution at 4°C overnight. The antibodies were anti-MAPK activated (Sigma Aldrich, 1:500). After washing steps, cells were incubated in blocking solution containing anti-mouse Alexa Fluor 488 (Thermo Fisher Scientific, A-10667, 1:500) for 1 h at room temperature in the dark. Finally, cells were incubated for 10 min in Hoechst 33258 (10µg/mL) and then slides were mounted in ProLong Gold anti-fading reagent (Thermo Fisher Scientific, P36930).

In situ proximity ligation assay (PLA)

PLA was performed on fixed cells following a standard immunostaining protocol according to the manufacturer's instructions. At the time of incubation of secondary antibodies, we used anti-mouse MINUS and anti-rabbit PLUS PLA probes for the recognition of RIPK1 and ERK1/2 respectively.

Analysis of cell death

Cell death was determined by measuring Sytox Green intensity using a FLUOstar Omega fluorescence plate reader (BMG Labtech, USA) with excitation/emission filters of 485/520nm (Gain set at 1100, 20 flashes per well, orbital averaging with a diameter of 3 mm). Triton X-100 at a final concentration of 0.1% was added at the end of time-lapse experiments during 1h to obtain the maximal fluorescence intensity. Cell death was also detected by monitoring Hoechst and PI fluorescence intensity using video-microscopy with excitation filters 395/25 & 575/25, and emission filters 440/40 & 632/60, respectively; and quantified using Image J.

Fluorescence and Ratiometric imaging

Wide-field images were captured with a Nikon TiE inverted microscope with a 20x 0.5NA objective and a DS-Qi2 CMOS camera (Nikon, Japan). Images were acquired at intervals of 4 min with the Nikon NIS-Elements acquisition software using JOBS module (Nikon). A Lumencor Spectra X LED Light Engine (Lumencor, Beaverton, OR, USA) provided the excitation light source. Ratio imaging used a 440/30 excitation filter, a t440/510/575rpc multi-band dichroic mirror, and two emission filters (ET480/40M (CFP) and AT545/30M (FRET)). For ERK2 distribution imaging a 395/25 (Hoechst), 470/24 (GFP), and 555/25 (mCherry and PI) excitation filters, a t390/475/515/630rpc multi-band dichroic mirror, and three emission filters (ET480/40m (Hoechst), ET525/50m (GFP) and ET632/60m (mCherry and PI)) were used. Excitation filters were provided by Lumencor and all dichroic mirrors and emission filters were obtained from Chroma Technology (Brattleboro, VT, USA). An automated emission filter wheel Lambda 10-B Smart Shutter (Sutter Instrument, Novato, CA, USA) was used. Analysis of ERK1/2-ACT biosensor was performed with custom routines written in IGOR Pro environment (Wavemetrics, Lake Oswego, OR, USA). FRET intensity was calculated as a ratio of the CFP/YFP signal for each pixel on background subtracted images. Pseudocolor images represent both the ratio and the fluorescence intensity values, where warmer colors denote high FRET and cooler colors low FRET efficiency. The calibration bar shows the fluorescence intensity values at the bottom and the ratio values on the right. The micron-scale of the images corresponds to the size of the calibration bar. A kymographic FRET image measured among the selected cells was performed on ImageJ. Analysis of subcellular distribution of ERK2 in individual live cells for time-lapse of 16 h was

performed manually using Image J to avoid errors due to automated tracking. The results are represented as kymographic images as well.

4.3.3. Results and discussion

4.3.3.1. ERK1/2 is a pro-necrotic molecule

To investigate the involvement of ERK1/2 activity in TNFα-induced necroptosis, L929sAhFas were treated with increasing concentrations of MEK inhibitor U0126 (Fig. 1A and 1B) and then monitored by video-microscopy in the presence of PI and Hoechst stains. Results show that ERK1/2 signaling pathway inhibition reduced necroptosis in a dose dependent manner (Fig. 1B). More interestingly, necroptosis was not abolished by ERK1/2 inhibition but only delayed. Similarly, data collected with an alternative cell death assay (Sytox Green), under the same experimental conditions, showed the same trend: the number of dead cell is decreased by almost 50% with U0126 (Fig. 1A), suggesting that ERK1/2 is a pro-necroptotic molecule in this cellular context. These results are in agreement with a previous study reporting that ERK1/2 inhibition protects L929 from TNFα-induced necroptosis but to a lesser extent compared to Nec-1 that specifically inhibits RIPK1 kinase activity [29]. However, Cho and colleagues also observed a decrease of TNFα-induced necroptosis by U0126 in Jurkat cells. In contrast, another study did not observed inhibition of TNFα+BV6-induced necroptosis after ERK1/2 signaling pathway inhibition in L929 cells [23].

4.3.3.2. Biphasic phosphorylation of ERK1/2 during TNFα induced necroptosis in L929

Most studies advocating a predominant role of ERK1/2 pathway in cell death processes indicate a sustained and compartmentalized ERK1/2 phosphorylation between 6 and 72h (for review, [18]). In L929 cells, phosphorylation patterns of ERK1/2 during TNFα-induced necroptosis recorded by western blot showed a biphasic phosphorylation of ERK1/2. Indeed, TNFα provoked a rapid and transient phosphorylation of ERK1/2 between 5 and 15min after TNFα treatment followed by sustained phosphorylation starting 2h after TNFα stimulation (Fig. 1C). Surprisingly, combined treatment with TNFα and Nec-1 decreased the duration of transient phosphorylation of ERK1/2 and markedly reduced the late sustained phosphorylation

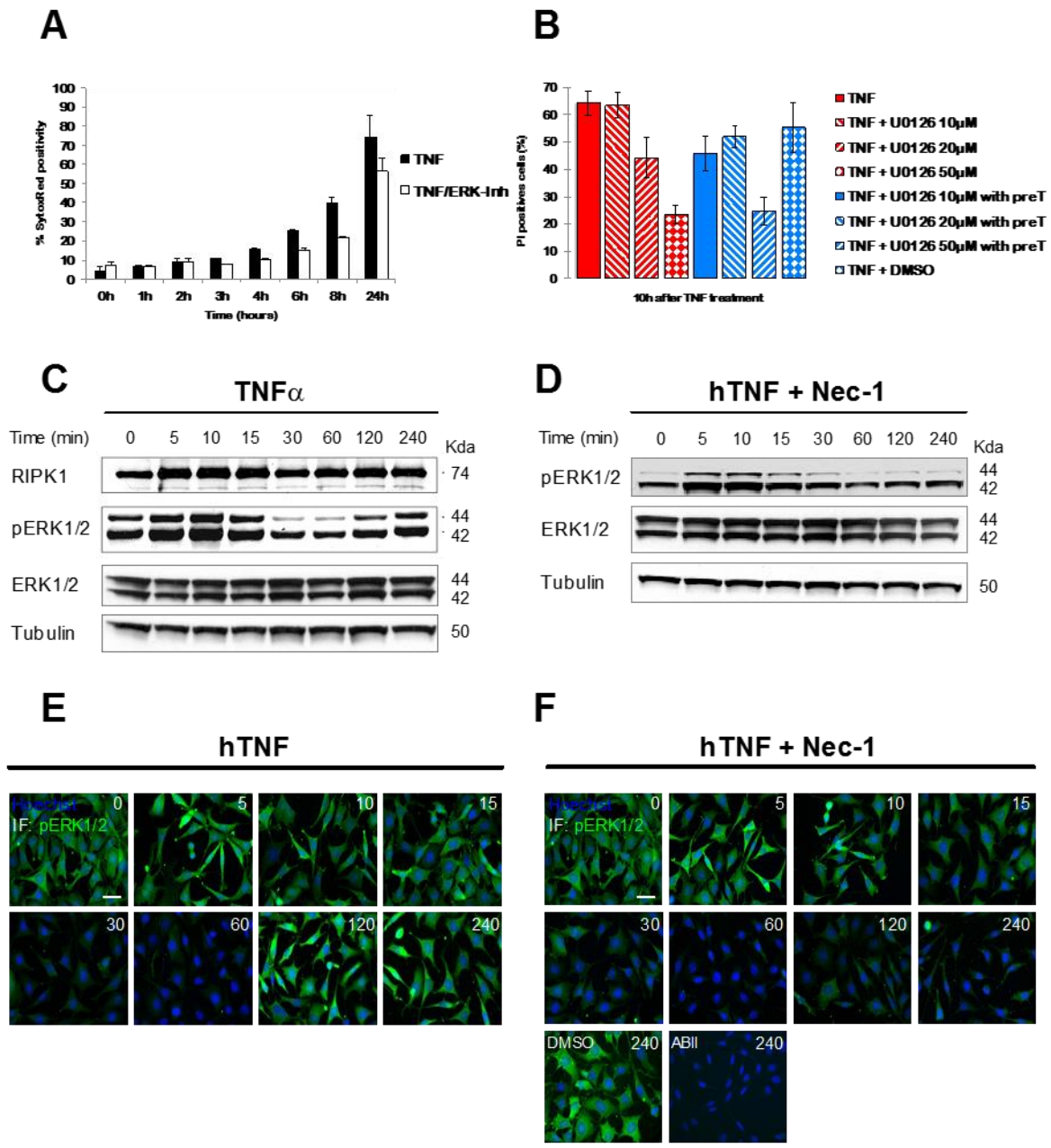

Figure 1: ERK1/2 is affected during TNFα-induced necroptosis in L929 cells. (**A**) L929 cells were pretreated for 30 min with 20µM of the MEK1/2 inhibitor U0126 and then stimulated with TNFα. Cell death was analyzed by Sytox Green staining at different time points using Fluostar fluorometer. (**B**) L929 cells were pretreated or not for 30 min with U0126 at 10µM, 20µM or 50µM and subsequently stimulated by TNFα. DMSO was added as a control at a volume equivalent to 50µM treatment condition. Cell death was monitored by Hoechst staining and PI uptake by video-microscopy for 10 h after TNFα stimulation and analyzed. preT: pretreatment with U0126. (**C-D**) L929 cells were serum-starved for 12h and then pretreated (**D**) or not (**C**) for 30 min with Nec-1 and subsequently stimulated with TNFα at the indicated time points. Cells were then lysed and immunoblotted as indicated on the left of each blot. Corresponding molecular weights are also indicated on the right of each blot. (**E-F**) L929 cells were serum-starved for 12h and then pretreated (**F**) or not (**E**) with 10µM Nec-1 and subsequently stimulated with TNFα at the indicated time points. Cells were fixed and processed for immunofluorescence with antibody against di-phosphorylated activated ERK1/2 (green) and stained for DNA with Hoechst (blue). DMSO was added as a control at a volume equivalent to 10µM treatment condition. ABII corresponds to a control with the secondary antibodies but without primary antibodies. Scale bar: 40µm.

of ERK1/2 (Fig. 1D). These observations could suggest that RIPK1 kinase activity is involved in the phosphorylation of ERK1/2 in accordance with previous studies [22,23]. To definitively determine the effect of RIPK1 on ERK1/2 phosphorylation, we evaluated the effect of Nec-1 in serum-induced ERK1/2 phosphorylation in L929 cells. We found that Nec-1 did not alter ERK1/2 phosphorylation under these experimental conditions, suggesting thereby a RIPK1-mediated phosphorylation of ERK1/2 upon TNFα stimulation [29] (Fig. 2A). However, combined treatment with TNFα and U0126 (30min before 2h and 30min before 4h TNFα stimulation) abolished the late sustained phosphorylation of ERK1/2 (Fig. 2B). These observations suggest that the late sustained ERK1/2 phosphorylation is conducted by ERK1/2 signaling and not by an alternative inhibition of ERK1/2 specific phosphatases due to ROS production [18,30,31] occurring in the late phase of necroptosis [6,32].

4.3.3.3. ERK1/2 phosphorylation is mainly cytoplasmic during TNFα-induced necroptosis in L929

Together with a sustained activity, ERK1/2 sequestration is also considered as hallmarks of ERK1/2-mediated cell death [18]. Assessment of phosphorylated-ERK1/2 localization during TNFα-induced necroptosis in L929 by immunofluorescence confirmed the biphasic phosphorylation of ERK1/2 and its inhibition by Nec-1 (Fig. 1E and 1F). Upon TNFα stimulation, phospho-ERK1/2 is mainly localized in the cytoplasm in both the early and late stages of ERK1/2 phosphorylation. However, it remains unclear whether the kinase is sequestered or not. While immunostaining provide a snapshot of compartmentalized ERK1/2 activity at different time points, live imaging of ERK1/2 is required to uncover unexpected dynamics of ERK1/2 in correlation with TNFα-induced necroptosis. For example, in response to TNFα, RIPK1 is rapidly modified with ubiquitin chains (between 5 and 15 min after TNFα treatment), which is associated with a pro-survival response [9,33] and could therefore provoke a transient translocation of ERK1/2 to the nucleus [34], undetectable by immunofluorescence.

4.3.3.4. ERK2 and RIPK1 interacts

Due to the toxicity of over-expression of RIPK1/3 in living cells, it was critical to over-express tagged-RIPK proteins in MEF or L929 cells. Therefore, we used *in situ* proximity ligation assay (PLA) [35] to examine whether ERK2 and RIPK1 interact. Interestingly, upon TNFα stimulation of L929 cells, results show a strong interaction

of ERK2 and RIPK1 at the time-point of 30min visualized by an increasing number of red spots compare to the control condition without TNFα stimulation (Fig. 3). Recently, a study showed that RIPK1 could interact constitutively with ERK1/2 and transiently with MEK2 upon eleostearic acid (ESA)-induced atypical RIPK1-dependent apoptotic cell death [36]. However, regarding the kinetic of ERK1/2 phosphorylation and the detection of interaction between RIPK1 and ERK2 in L929 cells, the functional interaction between ERK2 and RIPK1 in this cellular context should be further studied.

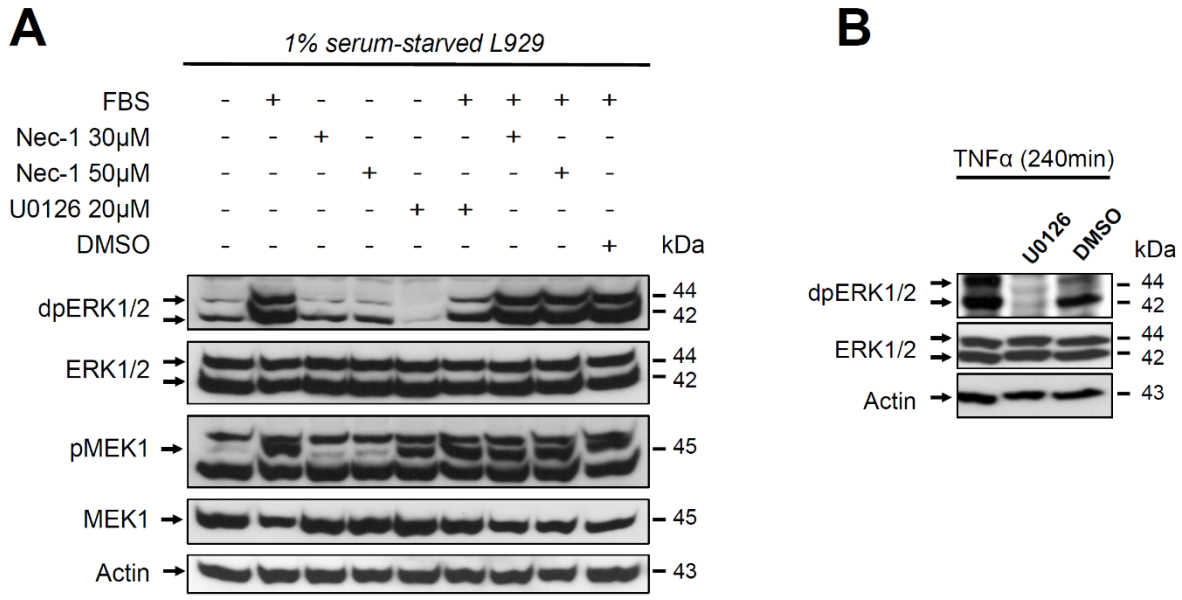

Figure 2: Nec-1 does not alter ERK1/2 phosphorylation upon serum stimulation in L929. (**A**) L929 cells were serum-starved for 12h and then pretreated or not for 30 min with either Nec-1 at 30μM and 50μM or U0126 at 20μM or DMSO at a volume equivalent to 50μM treatment condition. Cells were subsequently stimulated with 10% serum (fetal bovine serum, FBS). Cells were lysed and immunoblotted as indicated on the left of the blot. (**B**) L929 cells were serum-starved for 12h and stimulated with TNFα for 4 hours. 30 min before the time point, cells were treated with U0126 at 20μM for 30min and then lysed and immunoblotted as indicated on the left on the blot.

4.3.3.5. Spatio-temporal activity of ERK1/2 in necroptosis

We investigated ERK1/2 activity dynamics following necroptosis stimulation. We first used a genetically encoded FRET biosensor for ERK1/2 (EKAR-EV) [28]. However, this reporter failed to reveal any changes in ERK1/2 activity upon TNFα-induced necroptosis in L929 cells, which was inconsistent with our biochemical data. We estimated the phosphorylation level of ERK1/2 upon TNFα stimulation of serum-starved L929 cells compared with those upon serum stimulation. We found ERK1/2 phosphorylation was increased 1,5-fold in L929 cells stimulated with serum relative to TNFα stimulation, explaining thereby in part why the biosensor used did not detect

any changes in ERK1/2 activity level in TNFα-induced necroptosis. Recently, we developed a method to build and/or optimize genetically encoded FRET biosensor (Sipieter et al., in preparation) leading to the optimization of ERK1/2 FRET biosensor (ERK1/2-ACT). We characterized the biosensor dynamic range in our cellular models (L929 and MEF) by activating and inhibiting ERK1/2 signaling pathway with phorbol myristate acetate (PMA) and U0126 respectively. The results showed an emission ratio change that was almost improved by 2-fold relative to the initially construct in these cellular models (Sipieter et al., in preparation). Our newly optimized biosensor has facilitated our efforts to monitor the spatio-temporal dynamics of ERK1/2 over a long period.

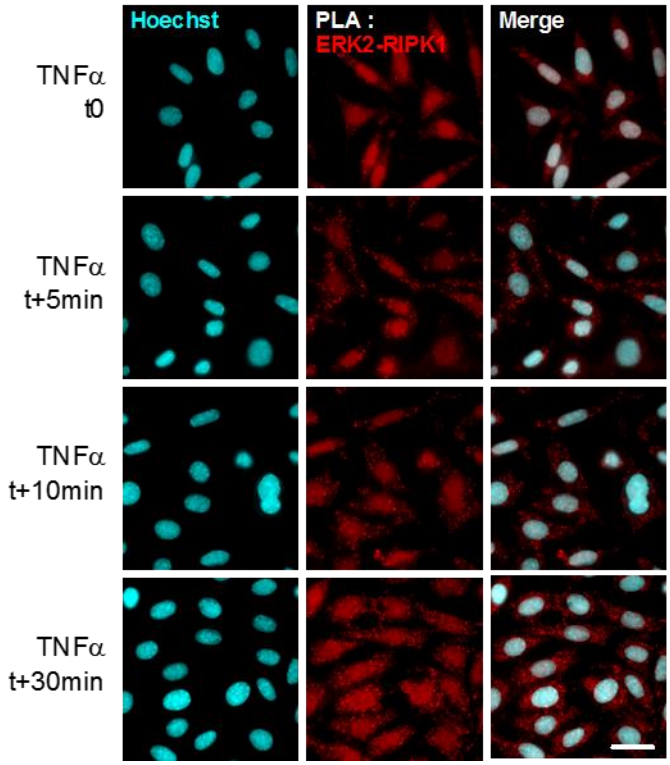

Figure 3: ERK2 and RIPK1 interact upon TNFα-induced necroptosis in L929. L929 cells were serum-starved for 12h and subsequently stimulated with TNFα for the indicated time. Cells were fixed and processed for immunofluorescence with antibodies against ERK2 and RIPK1. ERK2 and RIPK1 association was visualized by a PLA. Red spots correspond to detected interactions between ERK1 and RIPK1. Scale bar: 50μm.

Time-lapse FRET imaging of ERK1/2-ACT in MEF cells revealed a stochastic ERK1/2 activity pulses in the control condition in accordance with previous reports [37] (Fig. 4A-C). This stochastic ERK1/2 activation can be observed in a wide range of cellular models without stimulation during a time-lapse acquisition [37]. We further investigated the effect of a necroptotic and an apoptotic trigger on ERK1/2 activity. Kymographic FRET images revealed that the frequency of ERK1/2 activity pulses

markedly increased upon TNFα+BV6+zVAD-induced necroptosis in the signaling phase of necroptosis (Fig. 4G-I). Notably, we also observed a higher basal ERK1/2 activity in the last phase of cell death. In contrast, a gradual increase of ERK1/2 activity was detected upon TNFα+BV6-induced apoptosis (Fig. 4J-L). However, BV6 + zVAD condition show a basal increase of ERK1/2 activity consistent with previous studies [23] (Fig. 4D-F). These findings argue for a specific spatio-temporal signature of ERK1/2 depending on the programmed cell death. In order to uncover the molecular mechanisms underlying the spatio-temporal activity of ERK1/2, we used different chemical inhibitor of ERK1/2 signaling. For example, ERK1/2 activity pulses were suppressed with Raf inhibitor AZ628 (data not shown), reflecting a Raf-dependent phosphorylation of ERK1/2 upon necroptosis and apoptosis stimulation. Our next efforts will include inhibitors of RIPK pathway such as Nec-1 and RIPK3 inhibitors to elucidate crosstalk between RIPK and ERK1/2 signaling pathways through potential feedback loops.

4.3.3.6. Spatio-temporal distribution of ERK2 in necroptosis

Cytoplasmic or nuclear ERK1/2 sequestration is considered as hallmark of ERK1/2-mediated cell death. We further monitored subcellular ERK1/2 distribution following cell death stimulation in MEF cells by time-lapse microscopy. Using ERK2-LOC reporter, we observed brief transient translocations of ERK1/2 in the nucleus in the control condition but also in stimulated conditions, which might reflect stochastic ERK1/2 activation over a long time-lapse (Fig. 5). But interestingly, our results revealed a progressive accumulation of ERK1/2 in the nucleus starting between 1 to 2 hours before cell death upon both TNFα+BV6-induced apoptosis (Fig. 5B and 5C) and TNFα+BV6+zVAD-induced necroptosis (Fig. 5D and 5E). We want to further elucidate the molecular mechanism underlying this ERK2 nuclear accumulation

4.3.3.7. Development of kinase activity reporters for RIPK1 and RIPK3

Read-outs / hallmarks to correlate the spatio-temporal ERK1/2 code with necroptosis occurrence [38] are scarce. Since the kinase activity of RIPK1 and/or RIPK3 are crucial in the initiation step of necroptosis, we set out to develop new FRET-based kinase biosensors to specifically report on RIPK1 and RIPK3 kinase activities [39]. Based on our innovative methodology for the generation of new FRET biosensors, several biosensors have been efficiently generated for RIPK1 and RIPK3. Numerous

substrate peptides included sequences containing auto-phosphorylation sites of RIPK1 and RIPK3, RIPK3 substrates such as MLKL, as well as phosphorylation peptides derived from non-published RIPK1 substrates, phosphopeptides identified during phosphoproteomics experiments and from CelluSpots™ peptide arrays containing phosphoserine and/or phosphothreonine. The generated RIPK1 and RIPK3 biosensors and their negative controls have been transiently introduced in L929 and MEF cells to check their efficiency upon the appropriate necroptosis triggers to induce the kinase activity of RIPK1 and RIPK3. Our first results in TNFα-induced necroptosis in L929 cells show a response for several biosensors (emission ratio of 10-15%) leading to a first generation of FRET biosensors for RIPK1 and RIPK3. We still need to determine the specificity and selectivity of these biosensors by using a chemical inhibitory approach of RIPK signaling before optimization of their dynamic range.

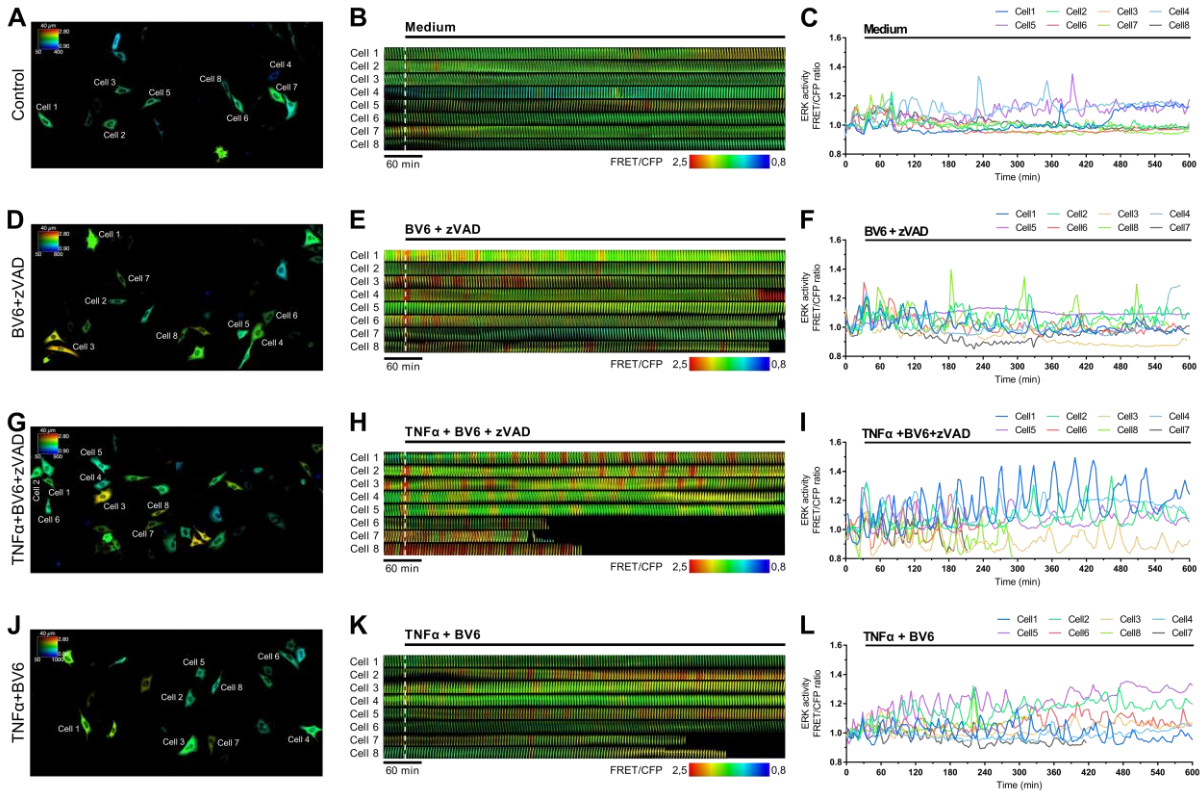

Figure 4: ERK1/2 activity profiles upon cell death stimulation in MEF. MEF cells were transiently transfected with the FRET biosensor ERK1/2-ACT and serum starved for 12h. After 24h, cells were pretreated or not with 10µM BV6 and/or 10µM zVAD for 1h and then stimulated or not with 600IU TNFα for 15h. (**A**), (**D**), (**G**), and (**J**) Representative FRET/CFP ratio images before TNFα stimulation are shown. Each panel combines two different fields and selected cells are shown. (**B**), (**E**), (**H**), and (**K**) Kymographic FRET images of indicated cells 10 h after the beginning of the experiment are shown. Images were acquired every 4 min. The dashed line corresponds to the induction. (**C**), (**F**), (**I**), and (**L**) FRET/CFP ratio of indicated cells are plotted against time.

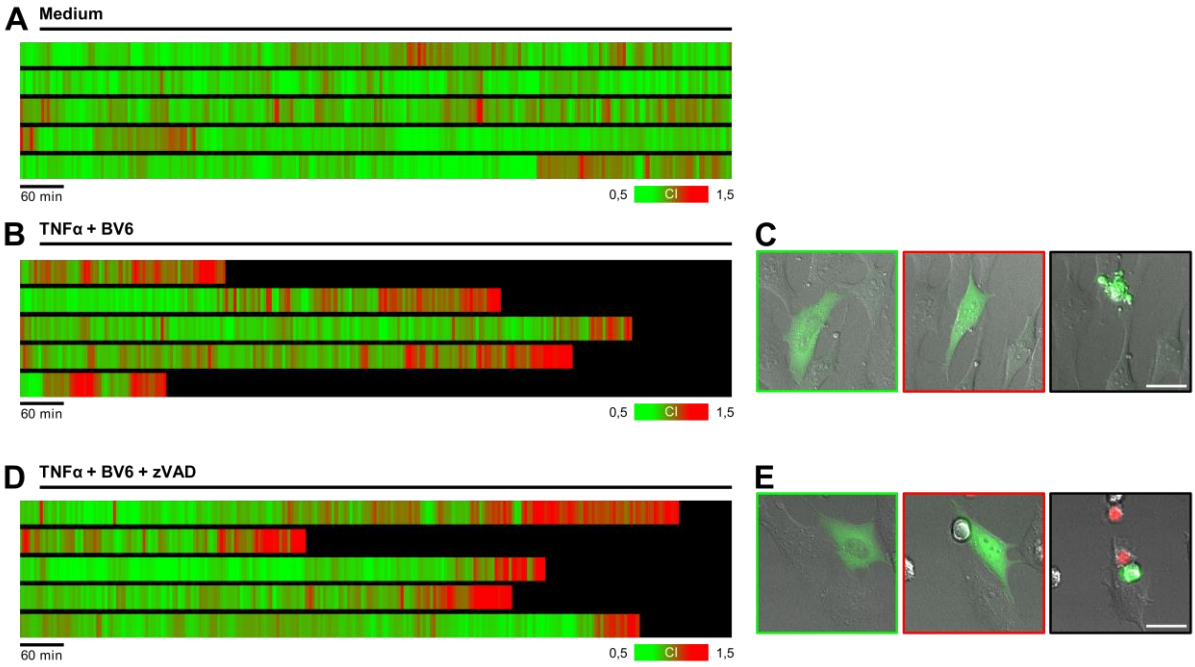

Figure 5: ERK1/2 subcellular distribution upon cell death stimulation in MEF. MEF cells were transiently transfected with the ERK2 localization reporter, ERK2-LOC, and serum starved for 12h. After 24h, cells were pretreated or not with 10µM BV6 and/or 10µM zVAD for 1h and then stimulated or not with 600IU TNFα for 15h. (**A**), (**B**) and (**D**) Kymographic images of ERK2 concentration index (CI) 10 h after the beginning of the experiment are shown. Each line corresponds to one cell. Images were acquired every 4 minutes. CI is representative of ERK2 subcellular distribution and is calculated as (F nucleus – F background) / (F cytoplasm – F background), where F corresponds to the fluorescence intensity. Green colors reflect a localization of ERK2 mostly cytoplasmic whereas red colors denote rather an accumulation of ERK2 into the nucleus. The CI scale bar is defined between 0,5 and 1,5 CI values. (**C**) and (**E**) Representative images of ERK2 localization during apoptosis (**C**) and necroptosis (**E**). Line color is representative of the CI values. Dark color indicates dead cells. Scale bar: 50µm.

4.3.4. Conclusion

Here, we provide evidences for the involvement of ERK1/2 in TNFα-induced necroptosis in L929 cells as ERK1/2 inhibition markedly delays necroptosis in a dose-dependent manner. We revealed a biphasic phosphorylation of ERK1/2 and a RIPK1-mediated phosphorylation of ERK1/2 depending on the cellular context. Owing to the importance of ERK1/2 spatio-temporal dynamics in determining cellular responses, we used FRET biosensors to determine relationships between ERK1/2 and RIPK. We found a differential spatio-temporal signature of ERK1/2 activation depending on the type of cell death in MEF cells. Regarding the oscillations of ERK1/2 activities in necroptosis observed for the first time, it is crucial to emphasize the importance of single-cell measurements because stochastic and growth factors-induced oscillatory kinase activation as well as heterogeneity in cellular responses are obscured in averaged cell population [26]. Although there is a lack of tools or

markers for detection of necroptosis, further studies using ERK biosensor and RIPK biosensors will provide new insights into the molecular mechanisms underlying necroptosis. A very exciting challenge would be to monitor several kinase activities at the same time in the same sample [40] to correlate several kinase activities and hence determining the precise crosstalk between each signaling node (Demeautis et al., to be submitted).

Acknowledgements

We are grateful to Dr. RA Toillon, M Guilbert and L Aubert for their helpful support and the optimization protocol for the *In situ* proximity ligation assay (PLA).

References

1. Golstein P, Kroemer G. Cell death by necrosis: towards a molecular definition. Trends Biochem Sci. 2007;32: 37–43. doi:10.1016/j.tibs.2006.11.001
2. Declercq W, Vanden Berghe T, Vandenabeele P. RIP kinases at the crossroads of cell death and survival. Cell. 2009;138: 229–32. doi:10.1016/j.cell.2009.07.006
3. Vandenabeele P, Galluzzi L, Vanden Berghe T, Kroemer G. Molecular mechanisms of necroptosis: an ordered cellular explosion. Nat Rev Mol Cell Biol. 2010;11: 700–714. doi:10.1038/nrm2970
4. Vandenabeele P, Declercq W, Berghe T Vanden. Necrotic cell death and “necrostatins”: now we can control cellular explosion. Trends Biochem Sci. 2008;33: 352–355. doi:10.1016/j.tibs.2008.05.007
5. Vandenabeele P, Declercq W, Van Herreweghe F, Vanden Berghe T. The role of the kinases RIP1 and RIP3 in TNF-induced necrosis. Sci Signal. 2010;3: re4. doi:10.1126/scisignal.3115re4
6. Berghe T Vanden, Vanlangenakker N, Parthoens E, Deckers W, Devos M, Festjens N, et al. Necroptosis, necrosis and secondary necrosis converge on similar cellular disintegration features. Cell Death Differ. Nature Publishing Group; 2010;17: 922–30. doi:10.1038/cdd.2009.184
7. Sun L, Wang H, Wang Z, He S, Chen S, Liao D, et al. Mixed lineage kinase domain-like protein mediates necrosis signaling downstream of RIP3 kinase. Cell. Elsevier Inc.; 2012;148: 213–27. doi:10.1016/j.cell.2011.11.031
8. Dondelinger Y, Declercq W, Montessuit S, Roelandt R, Goncalves A, Bruggeman I, et al. MLKL compromises plasma membrane integrity by binding to phosphatidylinositol phosphates. Cell Rep. Elsevier; 2014;7: 971–81. doi:10.1016/j.celrep.2014.04.026
9. O’Donnell MA, Ting AT. Chronicles of a death foretold: dual sequential cell death checkpoints in TNF signaling. Cell Cycle. 2010;9: 1065–71. Available: http://www.ncbi.nlm.nih.gov/pubmed/20237426
10. Galluzzi L, Kepp O, Kroemer G. MLKL regulates necrotic plasma membrane permeabilization. Cell Res. Nature Publishing Group; 2014;24: 139–40. doi:10.1038/cr.2014.8
11. Wang H, Sun L, Su L, Rizo J, Liu L, Wang L-F, et al. Mixed Lineage Kinase Domain-like Protein MLKL Causes Necrotic Membrane Disruption upon Phosphorylation by RIP3. Mol Cell. Elsevier Inc.; 2014;54: 133–146. doi:10.1016/j.molcel.2014.03.003
12. Chen X, Li W, Ren J, Huang D, He W, Song Y, et al. Translocation of mixed lineage kinase domain-like protein to plasma membrane leads to necrotic cell death. Cell Res. Nature Publishing Group; 2014;24: 105–21. doi:10.1038/cr.2013.171
13. Shaul YD, Seger R. The MEK/ERK cascade: from signaling specificity to diverse functions. Biochim Biophys Acta. 2007;1773: 1213–1226. doi:10.1016/j.bbamcr.2006.10.005
14. Raman M, Chen W, Cobb MH. Differential regulation and properties of MAPKs. Oncogene. 2007;26: 3100–12. doi:10.1038/sj.onc.1210392
15. Martin P, Pognonec P. ERK and cell death: cadmium toxicity, sustained ERK activation and cell death. FEBS J. 2010;277: 39–46. doi:10.1111/j.1742-4658.2009.07369.x
16. Zhuang S, Schnellmann RG. A Death-Promoting Role for Extracellular Signal-Regulated Kinase. J Pharmacol Exp Ther. 2006;319: 991–997. doi:10.1124/jpet.106.107367
17. Cagnol S, Van Obberghen-Schilling E, Chambard J-C. Prolonged activation of ERK1,2 induces FADD-independent caspase 8 activation and cell death. Apoptosis. 2006;11: 337–46. doi:10.1007/s10495-006-4065-y
18. Cagnol S, Chambard J-C. ERK and cell death: mechanisms of ERK-induced cell death--apoptosis, autophagy and senescence. FEBS J. 2010;277: 2–21. doi:10.1111/j.1742-4658.2009.07366.x
19. Yagoda N, von Rechenberg M, Zaganjor E, Bauer AJ, Yang WS, Fridman DJ, et al. RAS-RAF-MEK-dependent oxidative cell death involving voltage-dependent anion channels. Nature. 2007;447: 864–8. doi:10.1038/nature05859

20. Carr EL, Kelman A, Wu GS, Gopaul R, Senkevitch E, Aghvanyan A, et al. Glutamine uptake and metabolism are coordinately regulated by ERK/MAPK during T lymphocyte activation. J Immunol. 2010;185: 1037–44. doi:10.4049/jimmunol.0903586
21. Ebisuya M, Kondoh K, Nishida E. The duration, magnitude and compartmentalization of ERK MAP kinase activity: mechanisms for providing signaling specificity. J Cell Sci. 2005;118: 2997–3002. doi:10.1242/jcs.02505
22. Devin A, Lin Y, Liu Z. The role of the death-domain kinase RIP in tumour-necrosis-factor-induced activation of mitogen-activated protein kinases. EMBO Rep. 2003;4: 623–7. doi:10.1038/sj.embor.embor854
23. Vanlangenakker N, Vanden Berghe T, Bogaert P, Laukens B, Zobel K, Deshayes K, et al. cIAP1 and TAK1 protect cells from TNF-induced necrosis by preventing RIP1/RIP3-dependent reactive oxygen species production. Cell Death Differ. Nature Publishing Group; 2011;18: 656–65. doi:10.1038/cdd.2010.138
24. Zhang M, Li J, Geng R, Ge W, Zhou Y, Zhang C, et al. The inhibition of ERK activation mediates the protection of necrostatin-1 on glutamate toxicity in HT-22 cells. Neurotox Res. 2013;24: 64–70. doi:10.1007/s12640-012-9361-4
25. Gao S, Andreeva K, Cooper NGF. Ischemia-reperfusion injury of the retina is linked to necroptosis via the ERK1/2-RIP3 pathway. Mol Vis. 2014;20: 1374–87. doi:20:1374-1387 <http://www.molvis.org/molvis/v20/1374>
26. Doupé DP, Perrimon N. Visualizing and manipulating temporal signaling dynamics with fluorescence-based tools. Sci Signal. 2014;7: re1. doi:10.1126/scisignal.2005077
27. Tomida T. Visualization of the spatial and temporal dynamics of MAPK signaling using fluorescence imaging techniques. J Physiol Sci. 2015;65: 37–49. doi:10.1007/s12576-014-0332-9
28. Komatsu N, Aoki K, Yamada M, Yukinaga H, Fujita Y, Kamioka Y, et al. Development of an optimized backbone of FRET biosensors for kinases and GTPases. Mol Biol Cell. 2011;22: 4647–56. doi:10.1091/mbc.E11-01-0072
29. Cho Y, McQuade T, Zhang H, Zhang J, Chan FK-M. RIP1-dependent and independent effects of necrostatin-1 in necrosis and T cell activation. Alberola-Ila J, editor. PLoS One. 2011;6: e23209. doi:10.1371/journal.pone.0023209
30. Sánchez-Perez I, Murguía JR, Perona R. Cisplatin induces a persistent activation of JNK that is related to cell death. Oncogene. 1998;16: 533–40. doi:10.1038/sj.onc.1201578
31. Kim HS, Song M-C, Kwak IH, Park TJ, Lim IK. Constitutive induction of p-Erk1/2 accompanied by reduced activities of protein phosphatases 1 and 2A and MKP3 due to reactive oxygen species during cellular senescence. J Biol Chem. 2003;278: 37497–510. doi:10.1074/jbc.M211739200
32. Goossens V, Grooten J, De Vos K, Fiers W. Direct evidence for tumor necrosis factor-induced mitochondrial reactive oxygen intermediates and their involvement in cytotoxicity. Proc Natl Acad Sci U S A. 1995;92: 8115–8119. Available: http://www.ncbi.nlm.nih.gov/pubmed/7667254
33. Li H, Kobayashi M, Blonska M, You Y, Lin X. Ubiquitination of RIP Is Required for Tumor Necrosis Factor -induced NF- B Activation. J Biol Chem. 2006;281: 13636–13643. doi:10.1074/jbc.M600620200
34. Pouysségur J, Volmat V, Lenormand P. Fidelity and spatio-temporal control in MAP kinase (ERKs) signalling. Biochem Pharmacol. 2002;64: 755–63. Available: http://www.ncbi.nlm.nih.gov/pubmed/12213567
35. Söderberg O, Leuchowius KJ, Gullberg M, Jarvius M, Weibrecht I, Larsson LG, et al. Characterizing proteins and their interactions in cells and tissues using the in situ proximity ligation assay. Methods. 2008;45: 227–232. doi:10.1016/j.ymeth.2008.06.014
36. Obitsu S, Sakata K, Teshima R, Kondo K. Eleostearic acid induces RIP1-mediated atypical apoptosis in a kinase-independent manner via ERK phosphorylation, ROS generation and mitochondrial dysfunction. Cell Death Dis. 2013;4: e674. doi:10.1038/cddis.2013.188
37. Aoki K, Kumagai Y, Sakurai A, Komatsu N, Fujita Y, Shionyu C, et al. Stochastic ERK activation induced by noise and cell-to-cell propagation regulates cell density-dependent proliferation. Mol Cell. Elsevier; 2013;52: 529–40. doi:10.1016/j.molcel.2013.09.015
38. Kepp O, Galluzzi L, Lipinski M, Yuan J, Kroemer G. Cell death assays for drug discovery. Nat Rev Drug Discov. 2011;10: 221–237. doi:10.1038/nrd3373
39. Sipieter F, Ladik M, Vandenabeele P, Riquet F. Shining light on cell death processes - a novel biosensor for necroptosis, a newly described cell death program. Biotechnol J. 2014;9: 224–240. doi:10.1002/biot.201300200
40. Carlson HJ, Campbell RE. Genetically encoded FRET-based biosensors for multiparameter fluorescence imaging. Curr Opin Biotechnol. 2009;20: 19–27. doi:10.1016/j.copbio.2009.01.003

4.4. Research Article – Single wavelength excitation dual color FLIM for multiplexing genetically encoded FRET biosensors

Claire Déméautis[1,2], François Sipieter[3,4,5], Julien Roul[1,2], Catherine Chapuis[1,2], Sergi Padilla-Parra[6], Franck B. Riquet[3,5] and Marc Tramier[1,2]

[1] CNRS UMR 6290, F-35000 Rennes, France

[2] Institut Génétique et Développement de Rennes (IGDR), Université de Rennes 1, F-35000 Rennes, France

[3] Molecular Signaling and Cell Death Unit (UMSCD), Department of Biomedical Molecular Biology, Inflammation Research Center (IRC), a VIB-UGent department, B-9052 Ghent, Belgium

[4] Team Biophotonique Cellulaire Fonctionnelle, Laboratoire de Physique des Lasers, Atomes et Molécules (PhLAM), CNRS UMR 8523, F-59655 Villeneuve d'Ascq, France

[5] Structural and Functional Glycobiology Unit (UGSF), CNRS UMR 8576, Lille 1 University, F-59655 Villeneuve d'Ascq, France.

[6] Division of Structural Biology, University of Oxford, The Henry Wellcome Building for Genomic Medicine, Headington, Oxford OX3 7BN, United Kingdom.

Manuscript to be submitted in 2015 in Biophysical Journal

Research Article

Single wavelength excitation dual color FLIM for multiplexing genetically encoded FRET biosensors

Claire Déméautis[1,2], François Sipieter[3,4,5], Julien Roul[1,2], Catherine Chapuis[1,2], Sergi Padilla-Parra[6], Franck B. Riquet[3,5] and Marc Tramier[1,2]

[1] CNRS UMR 6290, F-35000 Rennes, France

[2] Institut Génétique et Développement de Rennes (IGDR), Université de Rennes 1, F-35000 Rennes, France

[3] Molecular Signaling and Cell Death Unit (UMSCD), Department of Biomedical Molecular Biology, Inflammation Research Center (IRC), a VIB-UGent department, B-9052 Ghent, Belgium

[4] Team Biophotonique Cellulaire Fonctionnelle, Laboratoire de Physique des Lasers, Atomes et Molécules (PhLAM), CNRS UMR 8523, F-59655 Villeneuve d'Ascq, France

[5] Structural and Functional Glycobiology Unit (UGSF), CNRS UMR 8576, Lille 1 University, F-59655 Villeneuve d'Ascq, France.

[6] Division of Structural Biology, University of Oxford, The Henry Wellcome Building for Genomic Medicine, Headington, Oxford OX3 7BN, United Kingdom.

Corresponding authors:
Marc Tramier, marc.tramier@univ-rennes1.fr
and Franck Riquet, franck.riquet@irc.vib-UGent.be

Running title:
Multiplex FRET by dual color FLIM

Key words: mTFP1, sREACh, LSSmOrange, mKate2, PKA, ERK

Abstract

Genetically encoded Förster Resonance Energy Transfert (FRET) biosensors are powerful tools for monitoring spatiotemporal biochemical activities in living samples. A very exciting challenge is to follow two FRET biosensors at the same time in the same sample and in the same cellular compartment. But the multiplex approach suffers from two limitations: (i) a spectral bleed-through of the first acceptor in the second donor emission band that depends on the concentration of the two biosensors and (ii) the multiple excitation wavelengths which necessitates sequential acquisition that is not adequate to follow fast signal changes in highly dynamic biochemical activities.

Taking advantage of the long stoke shift of LSSmOrange, we have used 440 nm single excitation wavelength of the two donor mTFP1 and LSSmOrange and a dual color FLIM to simultaneously measure two genetically encoded FRET biosensors. Moreover, thanks to the non-fluorescent acceptor sREACh for mTFP1 and of red-shifted mKate2 for LSSmOrange, we were able to avoid any spectral bleed-trough. With a dual spectral FLIM system we were able to detect fluorescence lifetime images of mTFP1 and LSSmOrange simultaneously and in the same cellular localization. We validated our approach by applying this methodology to simultaneously determine ERK and PKA activation in the same Hela cell using EKAR2G and AKAR4 biosensors respectively modified with mTFP1/sREACh and LSSmOrange/mKate2 fluorescent protein pairs. The activation of PKA signaling pathway with forskolin, had no effect on ERK1/2 activity. However, activating ERK1/2 signaling pathway with EGF, led to the identification of two distinct HeLa cell subpopulations, highlighting a cross talk between these two signaling pathways poorly understood in this cellular model.

4.4.1. Introduction

Genetically encoded Förster Resonance Energy Transfert (FRET) biosensors are powerful tools for monitoring spatiotemporal biochemical activities in living samples. Since the cameleon [1], the first biosensor using fluorescent proteins developed to measure calcium concentration, several families of genetically encoded biosensors were engineered such as: RhoGTPase activities reporters for cytoskeleton dynamics studies [2,3], cAMP and cGMP towards functional imaging of signaling pathways in neuroscience [4,5], quite a few specific kinase activities [6–9] and tension sensor across proteins [10,11]. The main advantage of these tools is to monitor the amplitude, the duration and the location of a biochemical activity during time-lapse fluorescence microscopy acquisition in intact living samples. Such methodology is already widely used, particularly in cell biology where spatio-temporal regulation is a key parameter. Owing to complex crosstalk between signaling pathways, multi-parameter biosensing experiments have become essential to correlate biochemical activities without lag time during a dedicated cellular process. A very exciting challenge has thus been to follow several FRET biosensors on the same sample at the same time and in the same location [12].

Commonly, FRET is measured by the fluorescence intensity ratio of the acceptor to the donor (ref). In that case, whatever the two fluorescent protein FRET pairs chosen, CFP/YFP and mOrange/mCherry [13], mTFP1/mCitrine and mAmetrine/tdTomato [14,15], mTagBFP/sfGFP and mVenus/mKok [16], the multiplex approach suffers from two limitations: (i) a spectral bleed-through of the first acceptor in the second donor emission band that depends directly from the respective quantities of the two biosensors and (ii) the multiple excitation wavelength which requires sequential acquisition that is not adequate to follow fast signal dynamics or signal changes in highly motile sample. To overcome the first limitation, a meroCBD biosensor modified with a far red organic fluorophore (Alexa750) was used for probing Cdc42 simultaneously with a genetically encoded CFP/YFP FRET-based biosensor for Rho A [17]. This approach prevents spectral bleed-through but cannot be generalized to all genetically encoded FRET biosensors where organic fluorophores are not easily usable to replace fluorescent proteins. Very recently, an elegant method based on linear unmixing of 3D excitation/emission fingerprints applied to three biosensors simultaneously was published [18]. This type of approach

based on image calculation is often limited by the different biosensors expression level and a poor signal to noise ratio after complex image corrections. To overcome the second limitation, the two FRET pairs CFP/YFP and Sapphire/RFP in combination with a single violet excitation were used [19] resulting in no lag time in biochemical activity recording. But again in this case the spectral bleed-through and excitation crosstalk necessitates linear unmixing. Another interesting approach for multiplexing two FRET activities simultaneously was developed by Schervakova and co-workers (2012) by using a large stokes shift orange fluorescent protein (LSSmOrange). The authors used a CFP-YFP together with LSSmOrange-mKate2 biosensors enabling imaging of apoptotic activity and calcium fluctuations in real time [20] using intensity-based methods.Other studies were carried out utilizing Fluorescence Lifetime Imaging Microscopy (FLIM) instead of ratio imaging to measure FRET. When FRET occurs, donor fluorescence lifetime decreases. This method requires measurement of the donor fluorescence only and is independent of emission from the acceptor. By using CFP and YFP as donor and the same red acceptor (tHcRed), FLIM of CFP and YFP donor allows distinguishing the two different FRET signals [21]. Combination of FLIM-FRET of a red-shifted TagRFP/mPlum pair with ratio imaging of a CFP/Venus pair allows maximizing the spectral separation while at the same time overcoming the low quantum yield of the far-red acceptor mPlum [22]. The two last examples alleviated the spectral bleed-through but not the limitation associated to the multiple excitations.

Here, we report a method dealing with the different limitations presented above. Taking advantage of the long stoke shift of LSSmOrange [20], we have used 440 nm single excitation wavelength of the two donor mTFP1 and LSSmOrange and a dual color FLIM to measure simultaneously signals from two genetically encoded FRET biosensors. Moreover, we have used the non-fluorescent acceptor sREACh [23] for mTFP1 and of red-shifted mKate2 [24] for LSSmOrange, avoiding the spectral bleed-trough between the two biosensors. We validated our approach by applying this methodology to monitor, for the first time, simultaneously two kinase activities with no lag time or spatial distribution discrimination using three different FLIM setups. ERK and PKA interplay in living HeLa cells was re-examined using EKAR2G [25] and AKAR4 [26] biosensors respectively modified with mTFP1/sREACh and LSSmOrange/mKate2 fluorescent protein pairs. By activating

PKA with forskolin, the ERK pathway is not activated as expected. But surprisingly, by activating ERK with EGF, PKA is also activated for a subpopulation of cells denoting a cross talk between these two signaling pathways in Hela cell line.

4.4.2. Materials and methods

Reagents

Human epithelial growth factor (EGF, #E9644) was purchased from Sigma Aldrich and Forskoline (Fsk, #1099) from Tocris. PKA inhibitor (H89 dihydrochloride, #2910) and phosphodiesterase inhibitor (IBMX, #2845) were purchased from Tocris and MEK inhibitor (U0126, #U120) and dimethylsulfoxide (DMSO, #D8418) from Sigma Aldrich.

Plasmids

FRET biosensor plasmid EKAR2G (mTFP1/Venus, Addgene plasmid #39813) was a gift from Pr. Olivier Pertz (Department of Biomedicine, University of Basel, Switzerland). AKAR4 plasmid was kindly provided by Dr. Jin Zhang (Department of Pharmacology and Molecular Sciences, Johns Hopkins University School of Medicine, Baltimore, USA). EKAR2G (mTFP1/Venus) vector was digested with *Not*I and *Kpn*I to release the Venus insert generating the EKAR2G (mTFP1/-) vector. sREACh was amplified from the pmTFP1-10-sREACh plasmid using the forward primer sREACh.NotI-F (*Not*I site underlined) and the reverse primer sREACh.KpnI (*Kpn*I site underlined). sREACh PCR product was then inserted into the corresponding restriction sites in the EKAR2G (mTFP1/-) backbone in frame with EKAR2G Molecular Recognition Element (MRE) and the upstream mTFP1 fluorescent protein to create the new expression vector EKAR2G (mTFP1/sREACh) AKAR4 (Cerulean/cpVenus) vector was digested to remove sequentially Cerulean (*BamH*I and *Sph*I) and cpVenus (*Sac*I and *EcoR*I) inserts. LSSmOrange and mKate2 fluorescent proteins were then amplified from pLSSmOrange-C1 and pmKate2-N1 respectively using the following primers pairs (forward/reverse): LSSmOrange.BamHI-F/ LSSmOrange.SphI-R and LSS-mKate2.SacI-F/mKate2.EcoRI-R. LSSmOrange and mKate2 PCR products were subsequently sub-cloned into the corresponding restriction sites in the AKAR4 (-/cpVenus) and AKAR4 (LSSmOrange/-) backbones respectively in frame with the AKAR4 MRE to create the new expression vector AKAR4 (LSSmOrange/mKate2). All resulting

constructs were verified by restriction digestion followed by agarose gel electrophoresis and then validated by sequencing (VIB). All enzymes and buffers were purchased from New England Biolabs. All oligonucleotides were synthesized by Integrated DNA Technologies (Belgium). DNA fragments were all purified on Qiagen plasmid purification columns (#28106, #28706 and # 27106, Qiagen).

Cell Culture and Transfection

HeLa cells were purchased from the European Collection of Cell Cultures (UK). Hela and U2OS cells are maintained at 37°C under 5% CO_2 in Dulbecco's Modified Eagle Medium (DMEM, #E15-009, PAA) supplemented with 10% fetal bovine serum (FBS, #A15-101, PAA), 1% penicillin/streptomycin (P/S, #15140-122, Gibco, Life Technologies) and 1% L-Glutamine (Glu, #25030024, Gibco, Life Technologies). For live imaging, HeLa cells were plated on Lab-Tek 4 wells (#055078, Dominique Dutscher). Transfections were performed using JetPrime reagent (#114-15, Polyplus) according to the manufacturer's instructions. One well on 4 of the Lab-Tek received 1 µg of total DNA per mL of medium. Four hours following transfection, medium was replaced with normal medium.

Imaging for biosensing experiments

Twelve hours before the acquisitions, normal medium was replaced with FluoroBrite phenol red-free medium (#A18967-01, Life Technologies) containing 0.1% FBS at 37°C in air (400µl in each well). For cell induction under microscope, the activators or inhibitors were diluted in pre-heated FluoroBrite medium (qsp 100µl) and were carefully added to avoid full activation of ERK1/2 signaling pathway.

Single wavelength excitation dual color FLIM systems

To achieve our methodology, a FLIM system with particular features is needed. The scheme in Figure 1 describes these characteristics: single wavelength excitation at 440 nm of a pulsed laser coupled to a live cell fluorescence microscope and dual color detection coupled to a FLIM detection. For this study, we have used three different systems:

Time gated FLIM system

The fastFLIM is a time-gated FLIM prototype developed for its capability of very fast time-lapse acquisition [27]. Briefly, a picosecond pulsed supercontinuum

laser at 80 MHz frequency was used for excitation. After wavelength selection of the supercontinuum at 440 nm (with about 10 nm narrow band of excitation), the laser is coupled to a multifocal spinning disk CSU10 (Yokogawa, Japan) and cells are imaged using a 63x or 20x oil immersion objective (NA = 1.4 or 0.70 respectively). At the emission side, an identical dual view system (480/30 nm and 579/34 nm channels) is used in front of a High Rate Intensifier coupled to a CCD camera (Picostar, LaVision, Germany). Five time-gated images of 2 ns gate width are sequentially acquired (from 100 to 300 ms exposure time depending on the intensity of the sample) with different delays from 0 to 8 ns. The stack of images is then used for direct calculation of mean fluorescence lifetime in a pixel by pixel basis [28].

TCSPC confocal system

This system is a confocal microscope Leica SP8 (Manheim, Germany) with SMD module based on Picoquant hardware (Berlin, Germany). Briefly, a 440 nm diode pulsed laser at 40MHz repetition rate is fiber-coupled to the confocal head of an inverted microscope with a 63x or 40x oil immersion objective (NA = 1.4 or 1.30 respectively) and the fluorescence emission after passing through pinhole set at 1 Airy unit is directed to the external port connected to a two color coupling module with a dicroic mirror of 505 nm splits the fluorescence in two channels with 480/30 nm and 579/34 nm band pass filters. Two optical fibers are used to couple two SPAD detectors (MPD for the cyan channel and TauSPAD for the orange channel) used as Single Photon Counting detectors. A Picoharp 300 is used for Time-Correlation and for image reconstruction using scanning signals to recover FLIM images (TTTR method). Lifetime determination from cell to cell was determined by fitting the fluorescence decay of the whole cell Region Of Interest with a single exponential model.

Frequency Domain FLIM system

This microscope is a LIFA system from Lambert Instrument (Groningen, Netherlands) in a widefield mode. The system was used during MiFoBio 2014 a thematic school supported by CNRS with the support of Photonlines (Saint-Germain-en-Laye, France). Briefly, a 440 nm modulated laser diode at 40 MHz frequency was directed to a liquid fiber connected to an Olympus inverted microscope for Khoeler illumination using a 60x oil immersion objective (NA = 1.4). At the emission side, a dual view is used to split the field of view of the camera in two color with a dicroic

mirror of 505 nm spliting the fluorescence in two channels with 480/30 nm and 579/34 nm band pass filters. The intensified CCD camera is modulated in a homodyne mode at 40 MHz frequency and 12 images at different phase shift are acquired. Phase lifetime are then calculated by fitting the sinusoidal response of the fluorescence emission and by comparing it with a calibration measurement on fluorescein (4 ns lifetime).

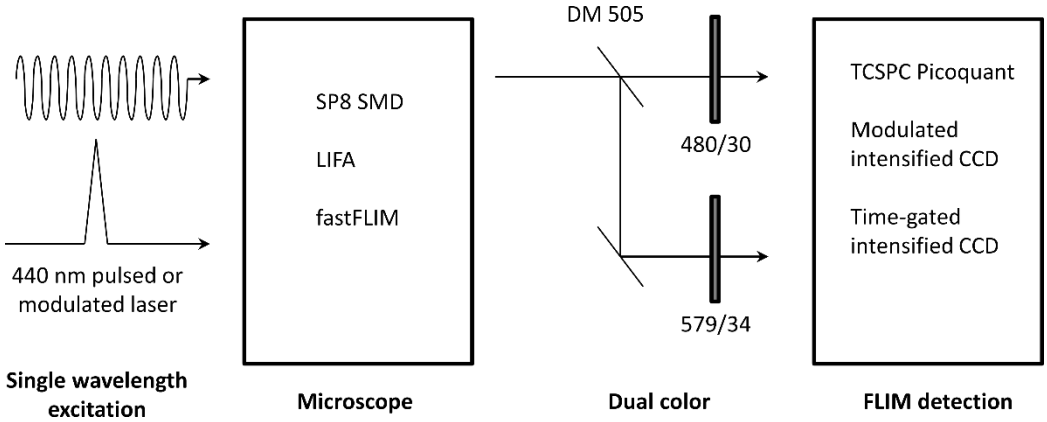

Figure 1: General scheme of single wavelength excitation dual color FLIM systems. Sample illumination is performed by either a pulsed or a modulated laser source at 440 nm that is injected into the microscope. The microscope, a SP8 SMD, a Lifa or fastFLIM, is coupled to a dicroic mirror of 505 nm splitting the fluorescence in two channels with 480/30 nm (blue channel) and 579/34 nm (orange channel) band pass filter to achieve dual color imaging. Fluorescence lifetimes are measured using a TCSPC Picoquant module for the SP8 SMD, a modulated intensified CCD for the Lifa or a time-gated intensified CCD for the fastFLIM.

Data analysis

The fastFLIM system gives us an intensity image from the first time-gated image and a lifetime image from the calculation of the direct first order temporal mean of the recorded decay ($<\tau> = \Sigma\ t_i\ I_i\ /\ \Sigma\ I_i$ where t_i and I_i correspond to the correlated time and the intensity of the time-gated channel I, respectively). Segmentation of the different cells was carried out to recover the mean lifetime at different time points of the experiments.

For the TCSPC analysis, Symphotime software (Picoquant, Berlin, Germany) was used to analyze our acquisitions. The channel 1 (blue channel) or 2 (orange channel) was selected. The Region of Interest on the different cells were fitted using a single exponential decay.

For frequency domain FLIM, we used the calculated phase image done by the LiFA software, the modulation image being noisier. Segmentation of the different

cells was carried out to recover the mean phase lifetime at different time points of the experiments.

4.4.3. Results and discussion

LSSmOrange is an appropriate FRET donor for mKate2 and can be simultaneously used with mTFP1 in single wavelength excitation dual color FLIM

Here, we propose an original methodology based on single wavelength excitation associated to FRET-FLIM. To complement a cyan donor for FRET excited at 440 nm, we looked for a second donor with the capabilities to be excited at the same wavelength but with a red-shifted emission. Large Stoke Shift mOrange (LSSmOrange) has the property to be excited at 440 nm and to emit in the orange at 572 nm [20]. First of all, we verified that this fluorescent protein harbors appropriate fluorescent properties for FRET by FLIM. By acquiring its fluorescence decay using TCSPC method, we showed that LSSmOrange exhibits a mono-exponential fluorescence decay, with a lifetime of 2.75+/-0.07 ns (n=11) (Fig. 2A). Then we verified that mKate2 is an appropriate acceptor for LSSmOrange by constructing an LSSmOrange-mKate2 tandem (the donor and the acceptor being joined by a short peptide linker YSDLELKLRILQSTVPRARDPPVAT). LSSmOrange alone and LSSmOrange-mKate2 tandem were transfected in U2OS cells. We have acquired FLIM with both systems (TCSPC using Leica SP8 with SMD module and time gated FLIM using the fastFLIM prototype [27]). By comparing the fluorescence decays acquired by TCSPC, we observed a faster decay for LSSmOrange-mKate2 tandem compare to LSSmOrange alone directly related to FRET process between LSSmOrange and mKate2 (Fig. 2A). This difference in the decay indicates that mKate2 is an appropriate acceptor for LSSmOrange as previously seen [20] for intensity based measurements. Images acquired using the fastFLIM system are presented in Fig 2B. The system is equipped with a dual view system and, as expected, the fluorescence emission is only recorded in the orange channel. When LSSmOrange was expressed alone, we recovered a lifetime of 2.76 +/-0.03 ns (n = 34) but when we expressed LSSmOrange-mKate2 tandem we have measured a decreased lifetime of 2.32 +/- 0.08 ns (n = 56) corresponding to a mean FRET efficiency (pseudoE = 1 - $<\tau>$ / $<\tau>_D$ where $<\tau>_D$ relates to the lifetime of the donor alone) of 0.16 (Fig. 2B). For the comparison, by using an equivalent FLIM system,

the donor lifetime for the EGFP/mCherry pair decreases from 2.45 ns alone to 2.23 ns in tandem (mean FRET efficiency of 0.09) and the donor lifetime for the mTFP1/EYFP pair decreases from 2.71 ns alone to 2.08 ns in tandem (mean FRET efficiency of 0.23) [29]. It indicated that LSSmOrange/mKate2 FRET pair presents an interesting potential with a higher FRET efficiency in tandem compared to EGFP/mCherry pair, the mTFP1/EYFP pair remaining the best pair compared to the two others.

mTFP1 is a monomeric Teal Fluorescent Protein [30] which is excited at 440 nm In this study and is an appropriate cyan donor for FRET by FLIM [29]. Since LSSmOrange can also be excited at 440 nm, is this fluorescent protein compatible with mTFP1 in our dual color FLIM approach when using single wavelength excitation? To answer this question, by using 440 nm single wavelength excitation and cyan / orange channels for dual color FLIM, we have verified that mTFP1 and LSSmOrange co-expressed in the same cell harbored the same lifetime compared to what was found for the both fluorescent proteins alone (Fig. S1). These results demonstrate that these two donors can be simultaneously used as FRET donors using single wavelength excitation FLIM.

4.4.4. sREACh is a good non-fluorescent FRET acceptor for mTFP1 to avoid spectral bleed-through in LSSmOrange channel when using dual color FLIM

Next, we co-expressed mTFP1-YFP and LSSmOrange-mKate2 tandems in U2OS cell to determine whether both FRET acceptors, YFP and mkate2, were also compatible with single wavelength excitation dual color FLIM approach. As shown in Fig. 3A, the recovered lifetime in the orange channel was not -comparable to the lifetime recover in cells expressing only LSSmOrange-mKate2. The recovered lifetime in the orange channel depends of the mTFP1-YFP expression. When the mTFP1-YFP contribution increased (monitored by the fluorescence intensity ratio between cyan channel and orange channel), the lifetime of LSSmOrange-mKate2 also increased from 2.3 ns to 2.9 ns. It has to be noted that the lifetime of 2.9 ns corresponds to the YFP lifetime. In fact, the orange filter is a 579/34 nm band pass allowing the end of YFP spectrum to pass through. Thus, the increased lifetime of

LSSmOrange-mKate2 tandem corresponds to a spectral bleed-through of YFP in the LSSmOrange donor channel.

To avoid this problem, we replaced the YFP acceptor by sREACh (super Resonance Energy Accepting Chromoprotein). This protein, which is a YFP variant, is also excited at 514nm (same excitation spectrum as YFP) but emits one hundred times less than YFP [23]. Using a purposefully developed mTFP1-sREACh tandem, we compared acceptor efficiency of sREACh to that of YFP in an attempt to resolve the spectral bleed-through artifact caused by yellow acceptor in orange channel (Fig. S2).

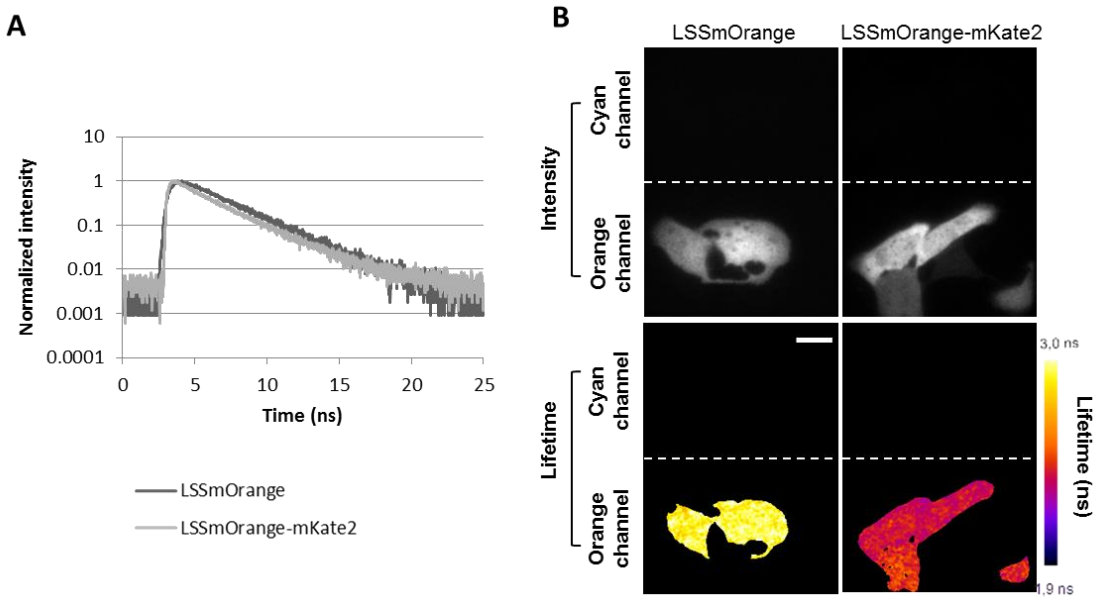

Figure 2: Mono-exponential decay (A) and lifetime (B) of LSSmOrange and LSSmOrange-mKate2 tandem. (**A**) Graphical representation of fluorescence lifetime decay profiles acquired on U2OS cells expressing either LSSmOrange or LSSmOrange-mKate2 tandem. LSSmOrange shows a mono-exponential decay while LSSmOrange-mKate2 tandem harbors a bi-exponential decay The LSSmOrange-mKate2 decay has a shorter slope than the LSSmOrange decay corresponding to a shorter lifetime (**B**). Intensity and Fluorescence lifetime measurements of LSSmOrange or LSSmOrange-mKate2 expressed in U2OS cells using the fastFLIM system. The orange channel provides either intensity or fluorescence lifetimes for LSSmOrange alone or for LSSmOrange-mKate2 tandem. Difference in LSSmOrange fluorescence lifetimes between both conditions is visible. mKate2 is a good acceptor for LSSmOrange and this two fluorescent proteins is a good FRET pairs.

Next, we wanted to verify that both FRET pairs mTFP1/sREACh and LSSmOrange/mkate2 were adapted for single wavelength excitation dual color approach. To record potential LSSmOrange-mKate2 lifetime differences correlated to mTFP1-Yellow acceptor expression levels, U2OS cells were co-transfected with a fixed concentration of LSSmOrange-mKate2 plasmid (0.5µg/µl) while varying mTFP1, mTFP1-YFP or mTFP1-sREACh plasmids concentration (0.25µg/µl up to

1µg/µl). We then measured the corresponding lifetime of LSSmOrange-mKate2 (and potential spectral bleed-through signals) in the orange channel. Results are plotted versus the intensity ratio of cyan channel to orange channel in Fig. 3B. In the presence of mTFP1 alone, the measured LSSmOrange-mKate2 lifetime slightly increased from 2.42 to 2.6 ns (only 7.4 % increase) occurring between an intensity ratio of 0.71 to 2.66. The increase corresponds to the lifetime contribution of mTFP1 (2.6 ns) in the orange channel. In presence of mTFP1-sREACh, the measured LSSmOrange-mKate2 lifetime decreased from 2.29 to 2.15 ns (only 6.1 % decrease). This slight decrease occurred between an intensity ratio of 0.78 up to 2.28 and corresponds to the lifetime contribution of sREACh (short lifetime) in the orange channel. Finally, in the presence of mTFP1-YFP, the LSSmOrange-mKate2 lifetime measured ranged from 2.49 to 2.83ns (up to 13.7% increase) as already seen in Fig. 4.

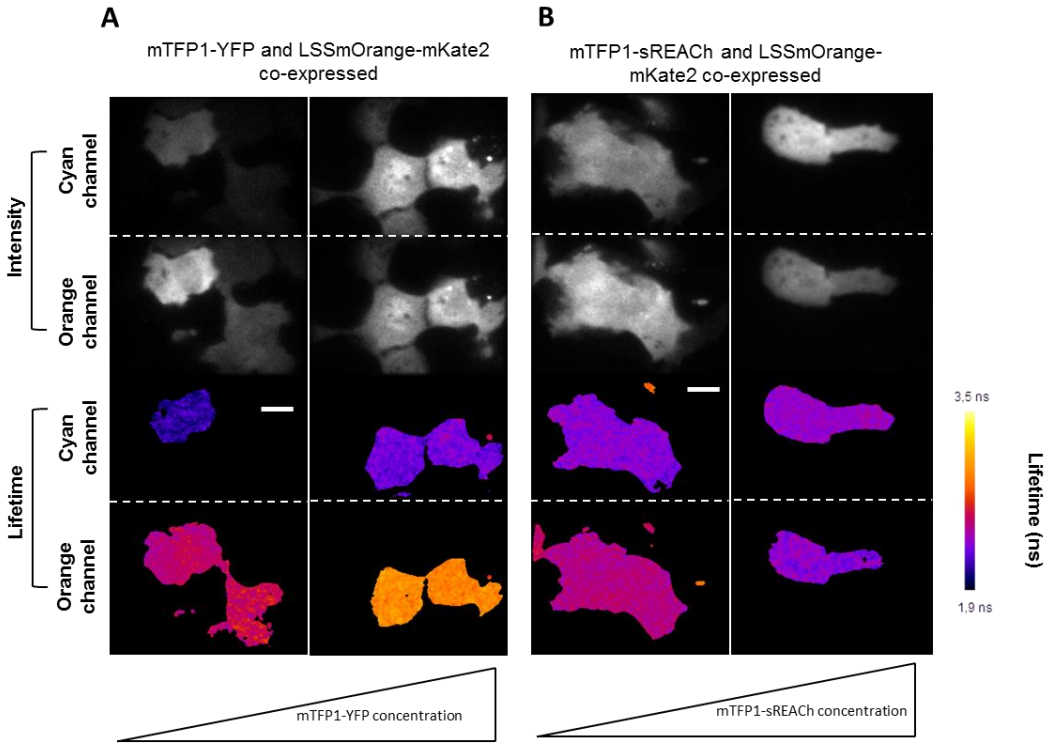

Figure 3: co-expression of mTFP1-YFP and LSSmOrange-mKate2 with a mTFP1-YFP or mTFP1-sREACh concentration gradient. Fluorescence intensity or lifetime images of U2OS cells expressing either mTFP1-YFP (**A**) or mTFP1-sREACh (**B**) with LSSmOrange-mKate2 acquired using fastFLIM system. (**A**) The higher fluorescence intensity of mTFP1-YFP in presence of LSSmOrannge-mKate2 correlated with the measurement of a higher LSSmOrange fluorescence lifetime in the orange channel. A striking 600ps (2,3ns to 2,9ns) increase between LSSmOrange fluorescence lifetimes was calculated depending on mTFP1-YFP intensity measurements. mTFP1 fluorescence lifetimes was measured for each condition and remained steady at 2,1ns. (**B**) The high expression level of mTFP1-sREACh, in presence of LSSmOrange-mKate2, only amounted to a negligible fluorescence lifetime decrease in the orange channel when compare to the fluorescence lifetime measured in the orange channel when mTFP1-sREACh was weakly expressed.

This steep increase began when the cyan to orange intensity ratio reached 0.29 and continued until 1.20. This difference of intensity ratio range is coherent with the potential spectral bleed-through of the YFP acceptor in the orange channel since the intensity bleed-through in the orange channel coming from cyan expression increases the orange intensity and then decreases the ratio. Then, the spectral bleed-through lifetime contribution in the orange channel is definitely less important when using sREACh compared to YFP. In the standard condition of equivalent expression of cyan pair and orange pair (about 1.5 ratio in our experimental conditions), we can conclude that when using LSSmOrange-mKate2 and mTFP1-sREACh pairs, the spectral bleed-through contribution gives about 3% variation in the orange channel lifetime which is negligible.

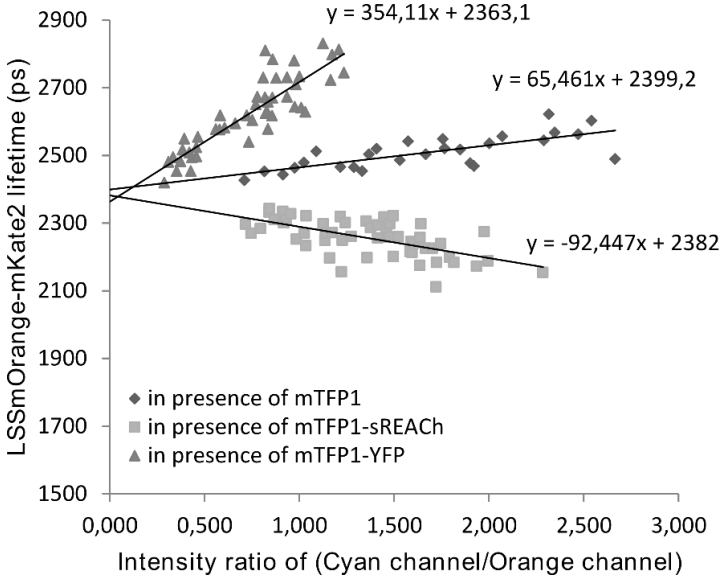

Figure 4: mTFP1-sREACh avoids spectral bleed-through when used in combination with LSSmOrange-mKate2 with dual color FLIM. Graphical representation of LSSmOrange-mKate2 lifetimes in presence of mTFP1, mTFP1-YFP and mTFP1-sREACh plotted as a function of cyan channel over orange channel intensity ratio. In the presence of mTFP1, LSSmOrange-mKate2 lifetime was slightly increased (2,42ns to 2,6ns), while it was markedly increased in the presence of mTFP1-YFP (2,49ns to 2,83ns). In presence of mTFP1-sREACh, LSSmOrange-mKate2 lifetime was decreased from 2,29ns to 2,15ns. The spectral bleed-through lifetime contribution in the orange channel is less important when using sREACh versus YFP as an acceptor for mTFP1.

4.4.5. Single wavelength excitation dual color FLIM methodology can be used to simultaneously monitor ERK and PKA kinase activities in a single cell

As a proof of concept/feasibility we decided apply our approach to the simultaneous monitoring of two major proteins kinases, Protein Kinase A (PKA) and Extracellular Regulated Kinase 1/2 (ERK1/2). Two main reasons motivated our

choice. The interplay between cAMP/PKA and ERK1/2 signaling pathways has been well established and documented (for review [31]). Compelling evidences demonstrated that the ERK1/2 cascade is regulated by cAMP/PKA pathway (for review [32]). This crosstalk was reported to modulate the duration and the strength of ERK1/2 activity [33]. Kinase Activity Reporters for both PKA [26,34,35] and ERK1/2 [25,36–38] have already pass few rounds of optimization, so we reasoned that the effect of FRET pairs swapping on biosensors performances would not preempted kinase activity monitoring in living cells.

To this end, we generated new versions of AKAR4 and EKAR2G, that we named AKAR^{dual} and EKAR^{dual} harboring the following FRET pairs LSSmOrange/mKate2 and mTFP1/sREACh, respectively. To characterize of our optimized biosensors for dual color-FLiM, standard biosensing reference experiments were carried out on HeLa cells co-epxressing AKAR^{dual} and EKAR^{dual} and single kinase activity recordings were performed using fast-FLIM system. Biosensor sensitivity was assessed upon dedicated activation and subsequent inhibition of either cAMP/PKA or ERK1/2 signaling pathways (Fig. S3). AKAR^{dual} and EKAR^{dual} both show the typical and expected response.

To validate and evaluate the transferability of our approach we simultaneously monitored PKA and ERK1/2 activities by single wavelength excitation dual color FLIM (Fig. 5) using fastFLIM (A), Lifa (B), and TCSPC (C) systems. These experiments were performed in HeLa expressing AKAR^{dual} and EKAR^{dual}, upon co activation and co inhibition of both signaling pathways. Although three different systems were used a readily visible trend was observed, showing characteristic biosensors responses. Pathway activations resulted in a lifetime decrease consistent with biosensors conformational changes after their respective phosphorylation by PKA for AKAR^{dual} and ERK1/2 for EKAR^{dual}. Upon dual pathway inhibitions increased lifetime values were recorded as a consequence of biosensor relaxation due to the shift in the equilibrium of the kinase/phosphatase balance. These results show that the applicability of our methodology is independent on the system employed and can be easily transposed to any FLIM microscope. It is noteworthy to indicate that, differences in the amplitude of measured lifetime and in terms of temporal resolution across imaging systems. First, results on the LiFa system presents a clear delay in ERK1/2 activation. But this does not come from the FLIM method used and can be

attributed to the temperature since frequency domain FLIM time-gated experiments carried out at 37°C using a microscope incubator. Second, the lifetime decrease after activation for both biosensors appears slower when using TCSPC. It corresponds typically on the result of a long acquisition time for this method (here 1 minute each 6 minutes) for TCSPC compared to fastFLIM or LiFA (here few seconds each 2 minutes). In fact, the first time point in TCSPC is the measurement of the mean activation of the two biosensors between 0 to 1 minute after activation which corresponds an intermediate lifetime. For fastFLIM and LIFA, there is no intermediate lifetime. The first time point was measured between 0 to few seconds after activation (high lifetime), the two biosensors having no time to be activated. The second one was measured 2 minutes after activation (low lifetime) when the two biosensors are already completely activated. FLIM methods such as fastFLIM or LiFA take benefit to non-fitting approaches where the number of detected photons for reliable lifetime measurement is low [39]. Our work validates the use of these methods having fast acquisition to reveal fast cellular processes (such as kinase activation pathway). Finally, as expected, the lifetime difference between non-activated to activated biosensor is not in favor of the fastFLIM approach where the 2ns temporal gate promotes a less precise lifetime than for TCSPC but still sufficient. For LiFA comparison, it is more difficult to conclude since the nature of the measurements are different (phase lifetime vs mean lifetime).

In order to further control that spectral bleed-through add to no effect on kinase activity measurements, we performed the following crosscheck experiments. HeLa cells transfected with both AKAR^{dual} and EKAR^{dual} were subjected to either forskolin/H89 or to EGF/U0126 treatment and monitored by fastFLIM system along time (Fig. 6). As expected, the forskolin-mediated increase in intracellular levels of cAMP resulted in an activation of PKA and so a decrease in AKAR^{dual} fluorescence lifetime while amounting to no effect on EKR1/2 activity. H89-mediated PKA inhibition counteracted the recorded PKA activation by an increase in AKAR^{dual} fluorescence lifetime back to the basal activity level. Interestingly, EKAR^{dual} fluorescence lifetime did increase upon H89 treatment. This come to no surprise with respect to the known multifaceted pharmacology of H89 that has also been reported to inhibit other kinases including mitogen activated protein kinase kinas- 1 (MEK1) [40] (Fig. 6A).

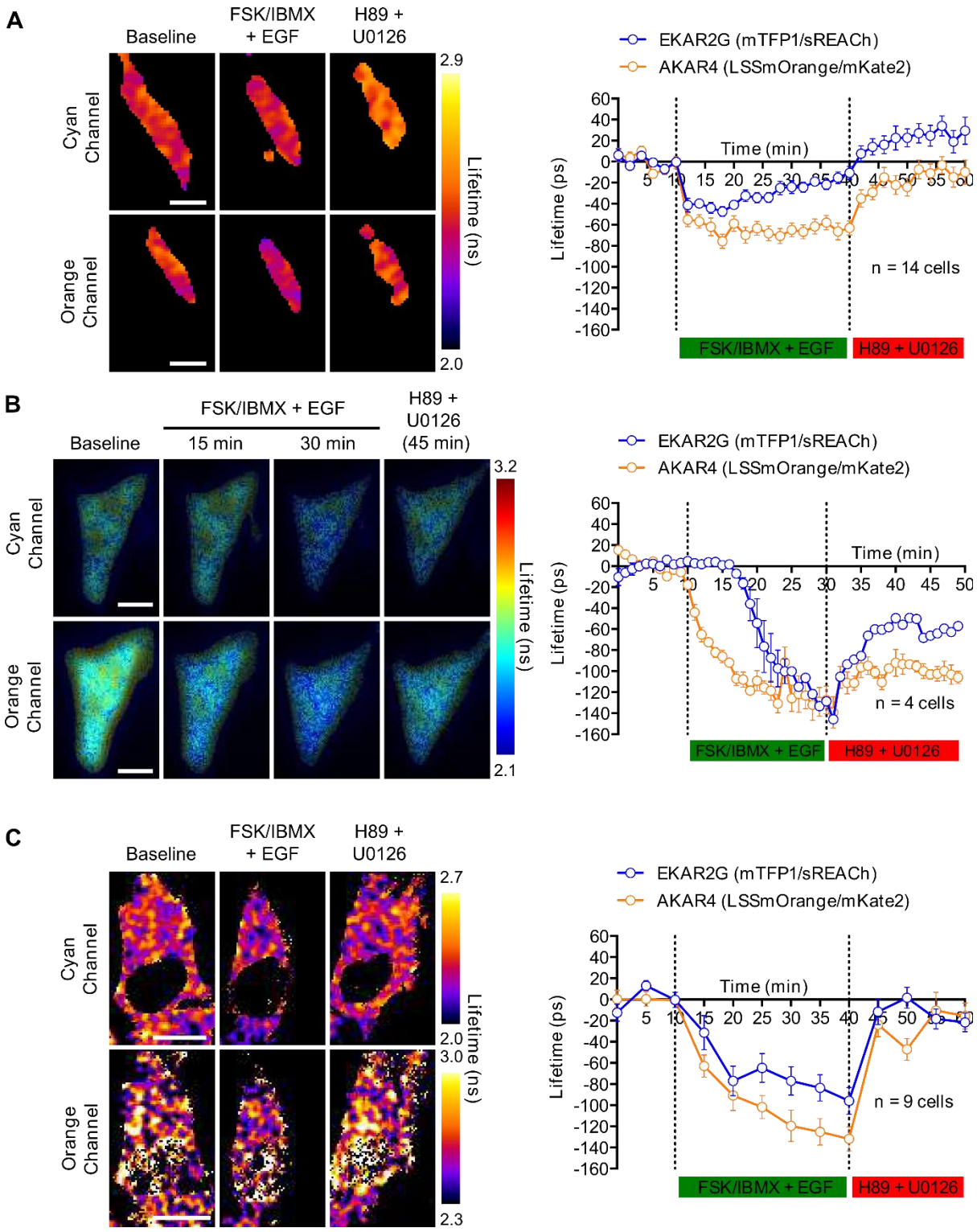

Figure 5: Simultaneous spatio-temporal monitoring of ERK and PKA kinase activities using fastFLIM, Lifa and TCSPC. Fluorescence lifetime measurements of AKAR^{dual} and EKAR^{dual} on the fastFLIM (**A**), Lifa (B) and TCSPC (**C**) system. Graphs represent AKAR^{dual} (orange) and EKAR^{dual} (blue) fluorescence lifetime measurements during the baseline, activation and inhibition phases. For the three systems, fluorescence lifetimes during the baseline phase remained stable, PKA and ERK pathway stimulations (Forskolin and EGF) resulted in a decrease in fluorescence lifetime for both biosensors. The subsequent addition of inhibitors (H89 and U0126) caused a fluorescence lifetime increase of both biosensors.

When monitoring ERK and PKA kinase activities upon EGF/U0126 treatment (Fig. 6B), EKAR^{dual} presented its characteristic behavior. First a decrease and then an increase of EKAR^{dual} fluorescence lifetime were measured upon EGF and subsequent U0126 treatment, respectively. Surprisingly, an increase of PKA activity when also recorded in response to EGF, as witness by the marked decrease of fluorescence lifetime for AKAR^{dual}, which was barely affected by U0126 treatment in these experimental conditions. The intricate relationship between PKA and ERK signal transduction pathways has been amply studied. It is usually presented from the following perspective: how cAMP/PKA modulates ERK1/2 activity [31] where Raf isoforms expression levels were shown to be implicated in the various responses exerted by cAMP/PKA on MAPKs signaling. Recently a specific position (Y330) on the PKA catalytic subunit was identified and shown to be directly regulated by RTK [41]. This confirmed earlier report showing an EGF-stimulated PKA activity increase in mammalian cells [42].

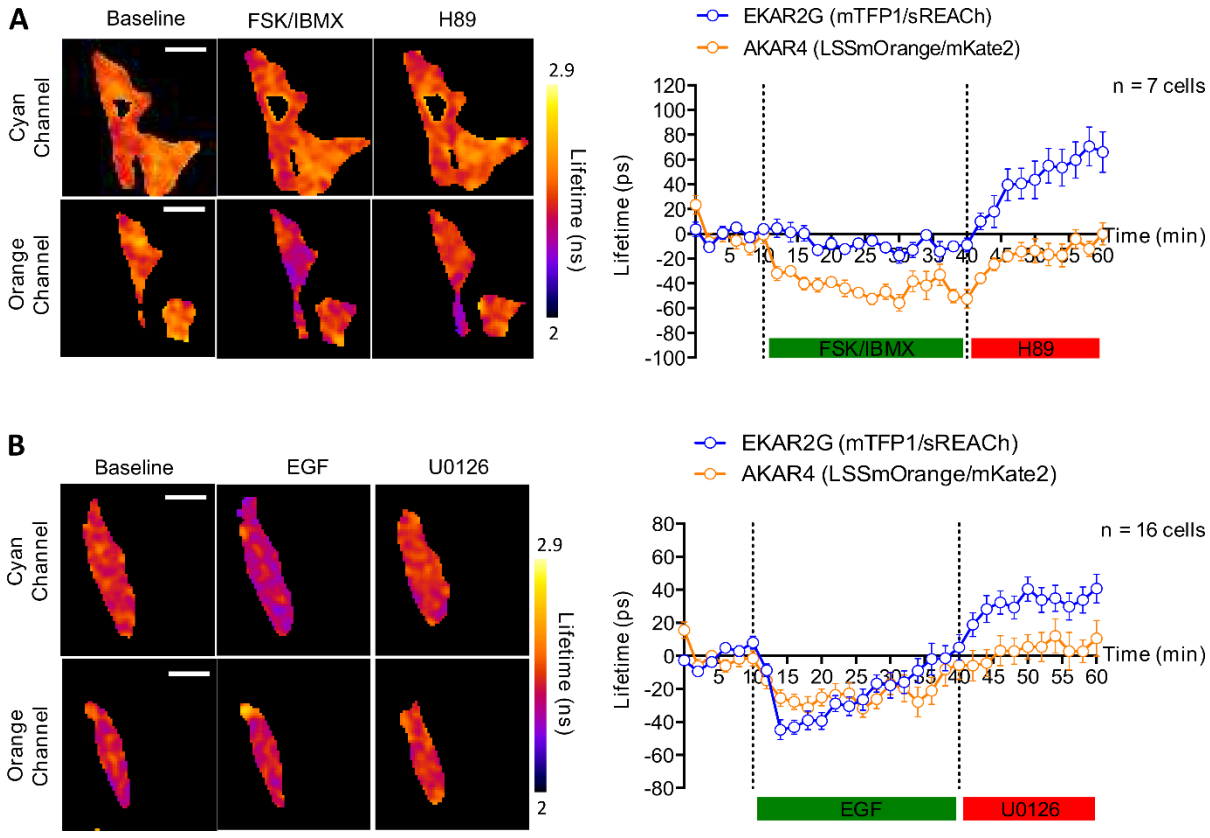

Figure 6: activation and inhibition of one biosensor: activation and inhibition of AKAR (A) or EKAR (B) when both biosensors are expressed on the fastFLIM system. Fluorescence lifetime measurement of AKAR^{dual} and EKAR^{dual} on the fastFLIM system. The graphs plot the AKAR^{dual} (orange) and EKAR^{dual} (blue) lifetime during the baseline, AKAR^{dual} (**A**) or EKAR^{dual} (**B**) activation and inhibition. During the baseline phase, the lifetimes remained stable. Forskolin addition (**A**) caused a lifetime decrease corresponding to the biosensor conformational changes after the phosphorylation by PKA for AKAR^{dual}. The EKAR^{dual} lifetime remained stable so EKAR^{dual} was not activated. The H89

addition (**A**) provoked a lifetime increase related to biosensor inhibitions. (**B**) EGF stimulation caused a lifetime decrease of both biosensors. U0126 addition prompted a marked lifetime increase for EKAR^{dual}; and the AKAR^{dual} lifetime slightly increased upon U0126.

In light of this result, we went on to closely examine the EGF-mediated effect on PKA activity in HeLa cells transfected with AKAR^{dual} (Fig. 7). Representation of the average fluorescence lifetime along time reflected the already observed response, a decrease of AKAR^{dual} fluorescence lifetime symptomatic of an increase of PKA activity which was unaffected by U0126 treatment (Fig. 7A). Conversely, when fluorescence lifetimes for each single cell were plotted, it clearly highlighted the presence of two distinct cell populations showing a difference in PKA activity upon EGF treatment (Fig. 7B), for which average responses were plotted (Fig. 7C).

The heterogeneous nature of all cultured cell lines and HeLa cells in particular, could be a starting point towards the explanation of cellular subtype responses. In a ultimate experimental conditions, we set out to untangle potential the crosstalk between PKA and ERK1/2 signaling pathway on HeLa cells co-transfected with AKAR^{dual} and EKAR^{dual} and analyzed on the basis of the sub-population differential response (Fig. 7D). Interestingly, cells in which PKA activity was moderately affected were the ones that showed a poor increase in ERK activity upon EGF treatment. By opposition, cells harboring an increased PKA activity showed also an augmented ERK activity. This last data set clearly exemplified the relevance of our multiparametric kinase activity measurements in these experimental settings and how it can further our understanding of signal transduction pathways involving protein kinases.

4.4.6. Conclusion

Here we report on the validation of a multiplexing approach to follow two genetically encoded FRET-based kinase activity reporters at the same time in the same sample and in the same cellular compartment. We have applied this approach to study simultaneously ERK1/2 and PKA kinases activities in Hela cells. A surprising behavior of two cellular subpopulations upon EGF stimulation was uncovered in these cells. Conventional biochemical approaches provide an averaged cell population response and thus forbid subpopulation behavior analysis. Conversely, immunofluorescence could allow this kind of evaluation but definitely not with the same temporal resolution.

Since FLIM is adequate for quantitative intermolecular FRET [43], our approach is easily transposable to study protein-protein interactions. It opens open new perspectives to multiplex interactions studies. Based on continuous fluorescent proteins engineering, the possibility to expand our method to three biosensors is near; for example by using a non-fluorescent acceptor for LSSmOrange, and third large stoke shift donor such as LSSmKate [44] in combination with an infra-red acceptor such as IRFP670 [45].

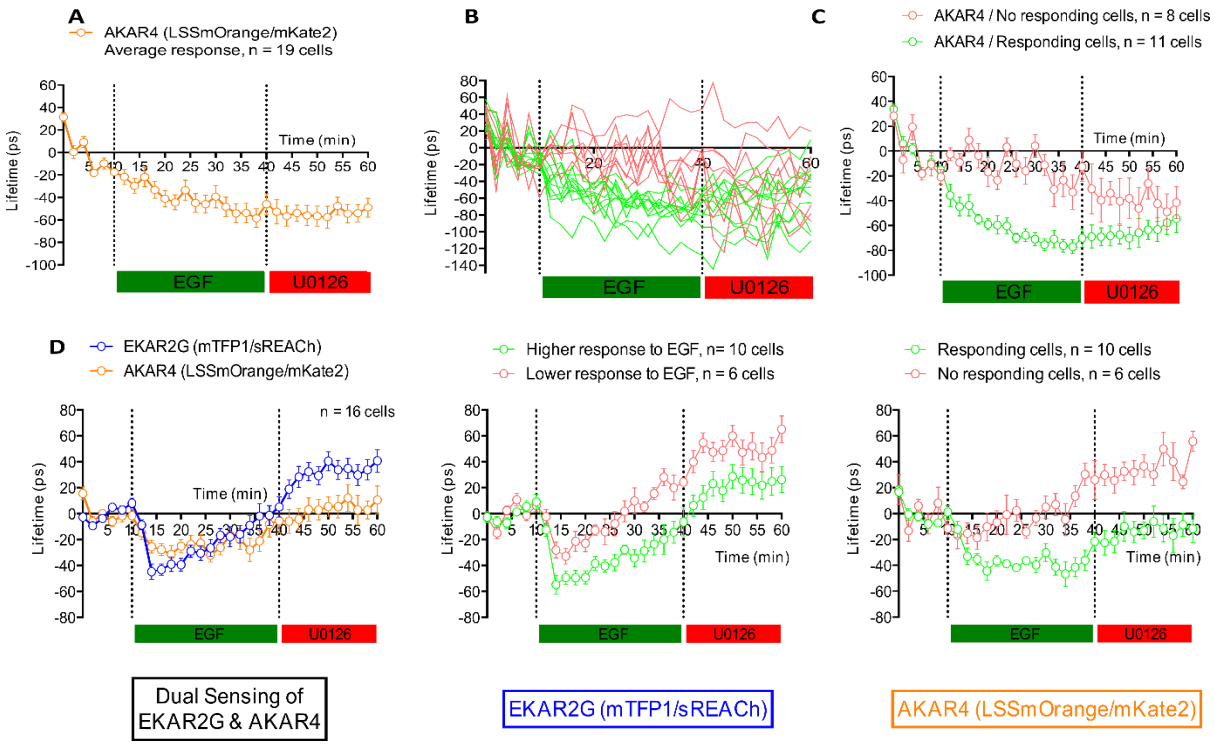

Figure 7: activation and inhibition by EGF and U0126 of AKAR^{dual} alone (A, B and C) or co-expressed (D) with EKAR^{dual} on the fastflim system. The graph plots the AKAR^{dual} lifetime during the baseline, activation by EGF and inhibition by U0126. The average of the lifetime measurement of all cells was plotted in **A**. The graph **B** represents AKAR^{dual} lifetime measurements cell by cell during the 3 phases. (**C**). Two distinct patterns can be discriminated. The red line corresponds to the cells not responding to the activation and the green line corresponds to the cells responding to the activation by EGF. (**D**) The AKAR^{dual} and EKAR^{dual} fluorescence lifetime during the baseline, activation by EGF and inhibition by U0126 are represented. Now data were plotted for each biosensor taking the aforementioned patterns into consideration; for EKAR^{dual} (middle plot), two responses were identified, cells responding weakly (red line) or strongly (green line) to the EGF. For AKAR^{dual}, two responses were also identified, cells not responding (red line) and cells responding (green line) to EGF stimulation.

Acknowledgment

We thank the Microscopy Rennes Imaging Centre (MRic) imaging facilities. We also thank Photonlines to provide a LiFA system during MiFoBio 2014 CNRS thematic school. We thank Jin Zhang (The Johns Hopkins University School of Medicine, Baltimore, MD, USA) for AKAR4 plasmid and Olivier Pertz (University of Basel, Basel, CH) for EKAR2G biosensor plasmid. This work was encouraged by the CNRS *Groupement de recherche* (GDR) 2588 "*Microscopie et Imagerie du Vivant*" scientific community.

Fundings

CD PhD fellowship is partly funded by Region Bretagne. The development of the fastFLIM prototype to MT is supported by IBiSA, Region Bretagne and Rennes Metropole. Research in the MT group is further supported by CNRS and UR1. FS is a joint PhD student between Lille1 University and Ghent University, and is funded by Lille 1 University, the *Centre National de la Recherche Scientifique* (CNRS), and Vandenabeele's group research funding: *Fonds Wetenschappelijk Onderzoek* (FWO G.0875.11) and Methusalem grant (*Bijzonder Onderzoeksfonds*, BOF09/01M00709). FR is a visiting research professor at Ghent University and full associate professor at Lille 1 University. Research in the Vandenabeele group is further supported by Belgian grants (Interuniversity Attraction Poles, IAP 7/32), Flemish grants (FWO G.0973.11, FWO G.0A45.12N, FWO G.0172.12, FWO G.0787.13N, FWO G.0C31.14N), Ghent University grants (Multidisciplinary Research Platforms (MRP), Ghent Researchers On Unfolded Proteins in Inflammatory Disease (GROUP-ID) consortium), grant from the Foundation against Cancer, 2012-188) and grants from *Vlaams Instituut voor Biotechnologie* (VIB). This research is supported by the *Agence Nationale pour la Recherche* (ANR): KinBioFRET program (ANR- 11-BSV5-0023) and G2Progress program (ANR-13-BSV2-0016-02).

Conflict of interest: Authors declare no conflict of interest.

References

1. Miyawaki A, Llopis J, Heim R, McCaffery JM, Adams J a, Ikura M, et al. Fluorescent indicators for Ca2+ based on green fluorescent proteins and calmodulin. Nature. 1997;388: 882–887. doi:10.1038/42264
2. Itoh RE, Kurokawa K, Ohba Y, Yoshizaki H, Mochizuki N, Matsuda M. Activation of rac and cdc42 video imaged by fluorescent resonance energy transfer-based single-molecule probes in the membrane of living cells. Mol Cell Biol. 2002;22: 6582–91. doi:10.1128/MCB.22.18.6582-6591.2002
3. Hinde E, Digman M a., Hahn KM, Gratton E. Millisecond spatiotemporal dynamics of FRET biosensors by the pair correlation function and the phasor approach to FLIM. Proc Natl Acad Sci U S A. 2013;110: 135–40. doi:10.1073/pnas.1211882110
4. Gervasi N, Hepp R, Tricoire L, Zhang J, Lambolez B, Paupardin-Tritsch D, et al. Dynamics of Protein Kinase A Signaling at the Membrane, in the Cytosol, and in the Nucleus of Neurons in Mouse Brain Slices. J Neurosci. 2007;27: 2744–2750. doi:10.1523/JNEUROSCI.5352-06.2007
5. Violin JD, Zhang J, Tsien RY, Newton AC. A genetically encoded fluorescent reporter reveals oscillatory phosphorylation by protein kinase C. J Cell Biol. 2003;161: 899–909. doi:10.1083/jcb.200302125
6. Fuller BG, Lampson M a, Foley E a, Rosasco-Nitcher S, Le K V., Tobelmann P, et al. Midzone activation of aurora B in anaphase produces an intracellular phosphorylation gradient. Nature. 2008;453: 1132–1136. doi:10.1038/nature06923
7. Macůrek L, Lindqvist A, Lim D, Lampson M a, Klompmaker R, Freire R, et al. Polo-like kinase-1 is activated by aurora A to promote checkpoint recovery. Nature. 2008;455: 119–123. doi:10.1038/nature07185
8. Verbeek DS, Goedhart J, Bruinsma L, Sinke RJ, Reits E a. PKC gamma mutations in spinocerebellar ataxia type 14 affect C1 domain accessibility and kinase activity leading to aberrant MAPK signaling. J Cell Sci. 2008;121: 2339–49. doi:10.1242/jcs.027698
9. Sipieter F, Vandame P, Spriet C, Leray A, Vincent P, Trinel D, et al. From FRET imaging to practical methodology for Kinase activity sensing in living cells. Prog Mol Biol Transl Sci. 2013;113: 145–216. doi:10.1016/B978-0-12-386932-6.00005-3
10. Borghi N, Sorokina M, Shcherbakova OG, Weis WI, Pruitt BL, Nelson WJ, et al. E-cadherin is under constitutive actomyosin-generated tension that is increased at cell-cell contacts upon externally applied stretch. Proc Natl Acad Sci U S A. 2012;109: 12568–73. doi:10.1073/pnas.1204390109
11. Grashoff C, Hoffman BD, Brenner MD, Zhou R, Parsons M, Yang MT, et al. Measuring mechanical tension across vinculin reveals regulation of focal adhesion dynamics. Nature. Nature Publishing Group; 2010;466: 263–266. doi:10.1038/nature09198
12. Carlson HJ, Campbell RE. Genetically encoded FRET-based biosensors for multiparameter fluorescence imaging. Curr Opin Biotechnol. 2009;20: 19–27. doi:10.1016/j.copbio.2009.01.003
13. Piljic A, Schultz C. Simultaneous Recording of Multiple Cellular Events by FRET. ACS Chem Biol. 2008;3: 156–160. doi:10.1021/cb700247q
14. Ai H, Hazelwood KL, Davidson MW, Campbell RE. Fluorescent protein FRET pairs for ratiometric imaging of dual biosensors. Nat Methods. 2008;5: 401–3. doi:10.1038/nmeth.1207
15. Ding Y, Ai H, Hoi H, Campbell RE. Förster resonance energy transfer-based biosensors for multiparameter ratiometric imaging of Ca2+ dynamics and caspase-3 activity in single cells. Anal Chem. 2011;83: 9687–93. doi:10.1021/ac202595g
16. Su T, Pan S, Luo Q, Zhang Z. Monitoring of dual bio-molecular events using FRET biosensors based on mTagBFP/sfGFP and mVenus/mKOκ fluorescent protein pairs. Biosens Bioelectron. Elsevier; 2013;46: 97–101. doi:10.1016/j.bios.2013.02.024

17. Machacek M, Hodgson L, Welch C, Elliott H, Pertz O, Nalbant P, et al. Coordination of Rho GTPase activities during cell protrusion. Nature. 2009;461: 99–103. doi:10.1038/nature08242
18. Woehler A. Simultaneous quantitative live cell imaging of multiple FRET-based biosensors. PLoS One. 2013;8: e61096. doi:10.1371/journal.pone.0061096
19. Niino Y, Hotta K, Oka K. Simultaneous live cell imaging using dual FRET sensors with a single excitation light. Koch K-W, editor. PLoS One. 2009;4: e6036. doi:10.1371/journal.pone.0006036
20. Shcherbakova DM, Hink MA, Joosen L, Gadella TWJ, Verkhusha V V. An orange fluorescent protein with a large Stokes shift for single-excitation multicolor FCCS and FRET imaging. J Am Chem Soc. 2012;134: 7913–23. doi:10.1021/ja3018972
21. Peyker A, Rocks O, Bastiaens PIH. Imaging activation of two Ras isoforms simultaneously in a single cell. Chembiochem. 2005;6: 78–85. doi:10.1002/cbic.200400280
22. Grant DM, Zhang W, McGhee EJ, Bunney TD, Talbot CB, Kumar S, et al. Multiplexed FRET to image multiple signaling events in live cells. Biophys J. 2008;95: L69–71. doi:10.1529/biophysj.108.139204
23. Ganesan S, Ameer-Beg SM, Ng TTC, Vojnovic B, Wouters FS. A dark yellow fluorescent protein (YFP)-based Resonance Energy-Accepting Chromoprotein (REACh) for Förster resonance energy transfer with GFP. Proc Natl Acad Sci U S A. 2006;103: 4089–94. doi:10.1073/pnas.0509922103
24. Shcherbo D, Murphy CS, Ermakova G V, Solovieva EA, Chepurnykh T V, Shcheglov AS, et al. Far-red fluorescent tags for protein imaging in living tissues. Biochem J. 2009;418: 567–74. doi:10.1042/BJ20081949
25. Fritz RD, Letzelter M, Reimann A, Martin K, Fusco L, Ritsma L, et al. A versatile toolkit to produce sensitive FRET biosensors to visualize signaling in time and space. Sci Signal. 2013;6: rs12. doi:10.1126/scisignal.2004135
26. Depry C, Allen MD, Zhang J. Visualization of PKA activity in plasma membrane microdomains. Mol Biosyst. 2011;7: 52–8. doi:10.1039/c0mb00079e
27. Leray A, Padilla-Parra S, Roul J, Héliot L, Tramier M. Spatio-Temporal Quantification of FRET in living cells by fast time-domain FLIM: a comparative study of non-fitting methods [corrected]. PLoS One. 2013;8: e69335. doi:10.1371/journal.pone.0069335
28. Padilla-Parra S, Audugé N, Coppey-Moisan M, Tramier M. Quantitative FRET analysis by fast acquisition time domain FLIM at high spatial resolution in living cells. Biophys J. 2008;95: 2976–2988. doi:10.1529/biophysj.108.131276
29. Padilla-Parra S, Audugé N, Lalucque H, Mevel JC, Coppey-Moisan M, Tramier M. Quantitative comparison of different fluorescent protein couples for fast FRET-FLIM acquisition. Biophys J. 2009;97: 2368–2376. doi:10.1016/j.bpj.2009.07.044
30. Ai H, Henderson JN, Remington SJ, Campbell RE. Directed evolution of a monomeric, bright and photostable version of Clavularia cyan fluorescent protein: structural characterization and applications in fluorescence imaging. Biochem J. 2006;400: 531–540. doi:10.1042/BJ20060874
31. Gerits N, Kostenko S, Shiryaev A, Johannessen M, Moens U. Relations between the mitogen-activated protein kinase and the cAMP-dependent protein kinase pathways: comradeship and hostility. Cell Signal. 2008;20: 1592–607. doi:10.1016/j.cellsig.2008.02.022
32. Stork PJS, Schmitt JM. Crosstalk between cAMP and MAP kinase signaling in the regulation of cell proliferation. Trends Cell Biol. 2002;12: 258–66. doi:10.1016/S0962-8924(02)02294-8
33. Herbst KJ, Allen MD, Zhang J. Spatiotemporally regulated protein kinase A activity is a critical regulator of growth factor-stimulated extracellular signal-regulated kinase signaling in PC12 cells. Mol Cell Biol. 2011;31: 4063–75. doi:10.1128/MCB.05459-11
34. Allen MD, Zhang J. Subcellular dynamics of protein kinase A activity visualized by FRET-based reporters. Biochem Biophys Res Commun. 2006;348: 716–21. doi:10.1016/j.bbrc.2006.07.136
35. Zhang J, Ma Y, Taylor SS, Tsien RY. Genetically encoded reporters of protein kinase A activity reveal impact of substrate tethering. Proc Natl Acad Sci U S A. 2001;98: 14997–15002. doi:10.1073/pnas.211566798
36. Harvey CD, Ehrhardt AG, Cellurale C, Zhong H, Yasuda R, Davis RJ, et al. A genetically encoded fluorescent sensor of ERK activity. Proc Natl Acad Sci U S A. 2008;105: 19264–9. doi:10.1073/pnas.0804598105
37. Komatsu N, Aoki K, Yamada M, Yukinaga H, Fujita Y, Kamioka Y, et al. Development of an optimized backbone of FRET biosensors for kinases and GTPases. Mol Biol Cell. 2011;22: 4647–56. doi:10.1091/mbc.E11-01-0072
38. Vandame P, Spriet C, Riquet F, Trinel D, Cailliau-Maggio K, Bodart J-F. Optimization of ERK Activity Biosensors for both Ratiometric and Lifetime FRET Measurements. Sensors. 2014;14: 1140–1154. doi:10.3390/s140101140
39. Padilla-Parra S, Auduge N, Coppey-Moisan M, Tramier M. Non fitting based FRET–FLIM analysis approaches applied to quantify protein–protein interactions in live cells. Biophys Rev. 2011;3: 63–70. doi:10.1007/s12551-011-0047-6
40. Murray AJ. Pharmacological PKA inhibition: all may not be what it seems. Sci Signal. 2008;1: re4. doi:10.1126/scisignal.122re4
41. Caldwell GB, Howe AK, Nickl CK, Dostmann WR, Ballif BA, Deming PB. Direct modulation of the protein kinase a catalytic subunit α by growth factor receptor tyrosine kinases. J Cell Biochem. 2012;113: 39–48. doi:10.1002/jcb.23325

42. Fishman D, Galitzki L, Priel E, Segal S. Epidermal growth factor regulates protein kinase A activity in murine fibrosarcoma cells: differences between metastatic and nonmetastatic tumor cell variants. Cancer Res. 1997;57: 5410–5. Available: http://www.ncbi.nlm.nih.gov/pubmed/9393768
43. Padilla-Parra S, Tramier M. FRET microscopy in the living cell: different approaches, strengths and weaknesses. Bioessays. 2012;34: 369–76. doi:10.1002/bies.201100086
44. Piatkevich KD, Hulit J, Subach OM, Wu B, Abdulla A, Segall JE, et al. Monomeric red fluorescent proteins with a large Stokes shift. Proc Natl Acad Sci U S A. 2010;107: 5369–74. doi:10.1073/pnas.0914365107
45. Shcherbakova DM, Verkhusha V V. Near-infrared fluorescent proteins for multicolor in vivo imaging. Nat Methods. 2013;10: 751–4. doi:10.1038/nmeth.2521

Supplementary Material

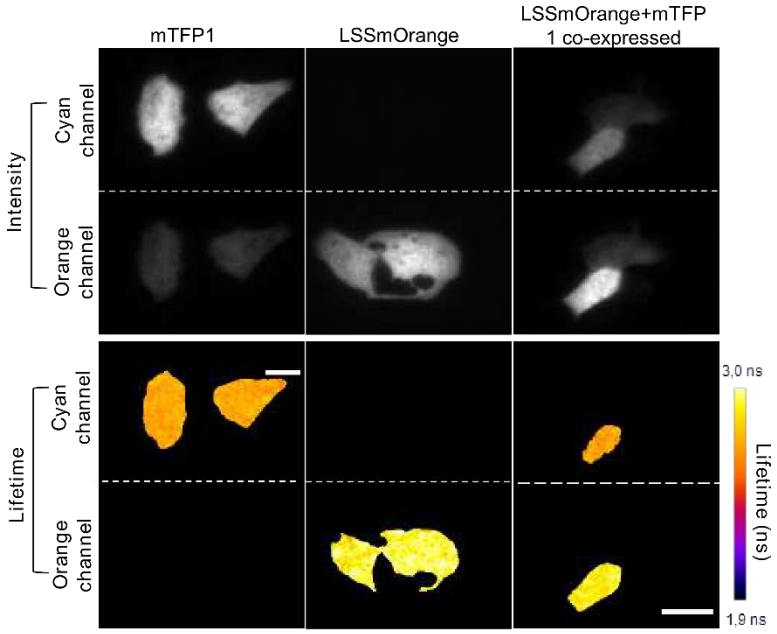

Supplementary Figure 1: mTFP1 and LSSmOrange simultaneously used as FRET donors with single wavelength excitation FLIM. Dual color FLIM images were acquired simultaneously in the cyan (480/30 nm) and in the orange (579/34 nm) channels at 440 nm single wavelength excitation on U2OS cells expressing mTFP1 alone, LSSmOrange alone and both fluorescent proteins. These acquisitions were carried out using the fastFLIM prototype with the dual view. The lifetimes are measured distinctly for each channel. When mTFP1 was expressed alone we observed a major part of the fluorescence emission in cyan channel. But, due to the large emission spectrum of mTFP1, spectral bleed-through was detectable in the orange channel. However, this intensity was insufficient to determine a fluorescence lifetime in this channel. For the cyan channel, we found a lifetime of 2.62 +/- 0.03 ns (n=28). When LSSmOrange was expressed alone, as expected no signal was detectable in cyan channel and the lifetime measured in the orange channel was of 2.76 +/- 0.03 ns (n=34). Interestingly, when both fluorescent proteins were co-expressed in U2OS cells, lifetimes identical to those previously recovered in cells expressing donors alone with 2.62 +/- 0.03 ns (n=23) for mTFP1 and 2.76 +/- 0.04 (n=23) for LSSmOrange in the two distinct channels. The small mTFP1 spectral bleed-through was not sufficient to corrupt LSSmOrange lifetime measurements.

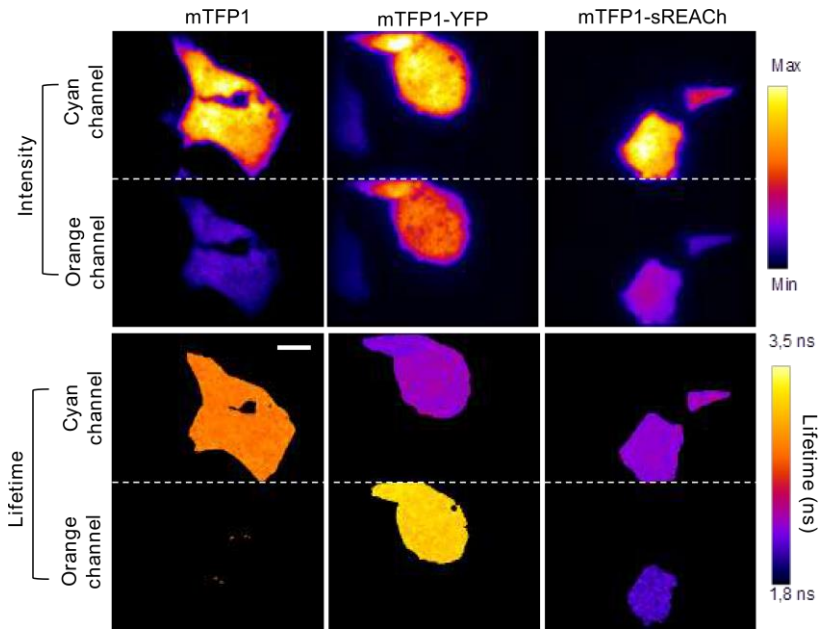

Supplementary Figure 2: Spectral bleed through of mTFP1, mTFP1-YFP and mTFP1-sREACh in the orange channel. Acquisitions of U2OS cells expressing mTFP1, mTFP1-YFP and mTFP1-sREACh alone were carried out on the fastFLIM system. For each condition, the lifetime in the cyan channel is measured. For mTFP1-YFP, the high lifetime is measured on the orange channel corresponding at the YFP lifetime. For the mTFP1-sREACh, the short lifetime is measured on the orange channel corresponding at the mix of the little mTFP1 spectral bleed through and the sREACh lifetime. By comparing mTFP1, mTFP1-YFP and mTFP1-sREACh on U2OS cell line; we noted that for a equivalent intensity in the cyan channel corresponding to a similar mTFP1 expression, we recovered more intensity in orange channel when mTFP1-YFP was expressed compare to mTFP1-sREACh. So sREACh significantly decreases the spectral bleed-through in the orange channel. Moreover, mTFP1-sREACh tandem exhibited a lifetime of 2.1 +/- 0.06 ns (n=56). This lifetime is equivalent to the mTFP1-YFP lifetime (2.1 +/- 0.03 ns, n=40) showing that YFP can be replaced by sREACh as acceptor for mTFP1. mTFP1-YFP and mFP1-sREACh lifetime are similar (2,1ns). sREACh is a good acceptor for mTFP1 and decrease the spectral bleed through on the orange channel.

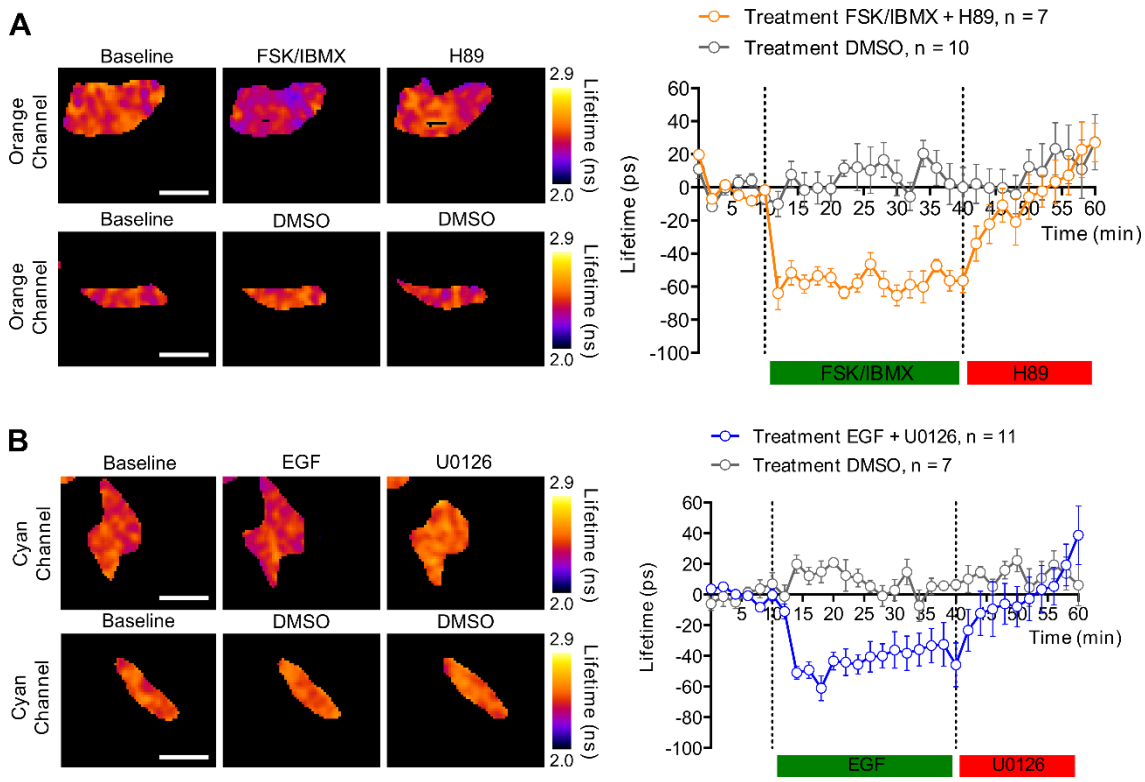

Supplementary Figure 3: AKAR^{dual} and EKAR^{dual} characterization by FLIM. Acquisitions of HeLa cells co-expressing AKAR^{dual} (**A**) or EKAR^{dual} (**B**) were carried out on the fastFLIM system. The graphs plot the AKAR^{dual} (orange) and EKAR^{dual} (blue) lifetime during the baseline, activation, and inhibition phases. Treatment of HeLa cells with either forskolin and IBMX or EGF resulted in a lifetime decrease characteristic of PKA and ERK1/2 pathway activation. Subsequent treatment of cells with either H89 or U0126 produced a lifetime increase consistent with PKA or ERK1/2 signaling pathway inhibition. For AKAR^{dual} and EKAR^{dual}, the biosensor activation involves a lifetime decreases (≈60ps) and the biosensor inhibition imply a lifetime increases (≈80ps). Note that in both cases, control experiments performed in the presence of DMSO amounted to no sensible variation in lifetime measurements confirming that biosensor specificity was unaffected and that recorded responses were symptomatic of the signaling pathway being examined.

Part 5: Summary and discussion

ERK1/2 signaling pathway plays an important role in cellular signaling network by regulating several cellular processes including survival, proliferation, differentiation, cell migration, neuronal plasticity and cell death depending on cellular context and the type of stimulation [57,59,264]. ERK1/2 was reported to mediate different programmed cell death such as apoptosis and autophagy in various cellular models (for review, [372]). This involvement of ERK1/2 in different cell death forms translates into its sustained and sequestered activity. This is considered as hallmarks of ERK-mediated cell death and is often linked to the presence of ROS [372]. Sustained cytoplasmic ERK1/2 activity, besides inhibiting survival and proliferative signals in the nucleus, triggers autophagy [376]. In contrast, sustained nuclear compartmentalization of ERK1/2 activity might rather promote apoptosis [346,392]. Sequestration of ERK1/2 depends also on expression of ERK1/2 specific subcellular anchors such as MKP1, MKP2 and MKP3 phosphatases [400,401]. The first report of ERK1/2 involvement in TNFα-induced necroptosis came from Devin and colleagues who investigated the molecular mechanism between RIPK1 and MAPKs by using both $RIPK1^{-/-}$ and $TRAF2^{-/-}$ MEF [430]. It was shown that TRAF2 and the kinase activity of RIPK1 are required for ERK1/2 phosphorylation but not for p38 and JNK activation upon TNFα stimulation [430,431]. The identity of downstream substrates of TRAF2/RIPK1 remains to be investigated because depletion of specific MAP3K does not alter TNFα-mediated ERK1/2 phosphorylation probably due to redundancy mechanisms. Nevertheless, multiple cell models using other stimuli than TNFα and both genetic and chemical approaches to inhibit ERK1/2 strongly suggest a prominent role of ERK1/2 in the execution of necroptosis [409,410].

In order to study the role of ERK1/2 in TNFα-induced necroptosis in L929 cells, we first used MEK1/2 inhibitor U0126. We could reduce necroptosis in a dose dependent manner. Interestingly, necroptosis was not blocked by ERK1/2 inhibition but only delayed. In agreement, similar results were obtained with an alternative cell death assay suggesting that ERK1/2 is a pro-necroptotic molecule. One study has revealed a similar effect of ERK1/2 inhibition on TNFα-induced necroptosis in L929 cells [471] but to a lesser extent compared to Nec-1 inhibitory effect of necroptosis. In this same study, a decrease of TNFα-induced necroptosis in Jurkat cells by U0126 was observed, supporting once more the idea that ERK1/2 could protect and act as a modulator of necroptosis. In contrast, another study in L929 cells did not observe

inhibition of TNFα+BV6-induced necroptosis by U0126 [439]. However, it was shown that neither p38, JNK and ERK were required for TNFα-induced necroptosis in MEF cells [440]. These conflicting observations could indicate that ERK1/2 involvement in TNFα-induced necroptosis is cell type dependent. Note that in this last study, cell death was quantified only 24 h after treatment of MEF cells with TNFα and U0126, which can hamper evaluation and interpretation of ERK1/2 inhibitory effect on cell death. Indeed, our results show that the number of dead cells is decreased by almost 50% with U0126 at the time point of 8h after TNFα stimulation, whereas the number of dead cells is quite similar at 24h, hence emphasizing the importance to consider effect of ERK1/2 inhibition on the cell death kinetic. In a next step the specific contribution of ERK1/2 in necroptosis could be examine by knockdown or other chemical inhibitors of the pathway.

Using L929 model, we then assessed phosphorylation patterns of ERK1/2 upon TNFα stimulation. Interestingly, we observed a biphasic phosphorylation: an initial rapid and transient phosphorylation followed by a sustained phosphorylation starting 2 h after TNFα stimulation and lasting several hours. In agreement, similar results were obtained for JNK and p38 in L929 cells upon TNFα stimulation. Transient activation could promote a cell survival and abrogate cell cytotoxicity, whereas sustained activation may trigger the cell death machinery [443,444]. Therefore we tested whether RIPK1 inhibition could impact ERK1/2 phosphorylation. Combined treatment with TNFα and Nec-1 decreased the duration of transient phosphorylation of ERK1/2 and strongly reduced the late sustained phosphorylation, in accordance with previous studies [430,439]. To definitively determine the effect of RIPK1 on ERK1/2 phosphorylation, we evaluated the effect of Nec-1 in serum-induced ERK1/2 phosphorylation in L929 cells. We found that Nec-1 did not alter ERK1/2 phosphorylation under these experimental conditions, suggesting thereby a RIPK1-dependent phosphorylation of ERK1/2 upon TNFα stimulation. However, it is not clear whether ERK1/2 sustained phosphorylation is directly attributable to RIPK1 or represent secondary effects. To assess whether ROS production could be responsible for the sustained phosphorylation of ERK1/2 due to the inhibition of phosphatases as previously reported for JNK [472,473], a late inhibition of MEK1/2 by U0126 was performed 4 hours after TNFα stimulation. This led to a strong decrease of ERK1/2 phosphorylation. So, our data suggest that the late sustained

ERK1/2 phosphorylation is conducted by ERK1/2 signaling pathway and not by an alternative inhibition of phosphatases due to ROS production [97,372,400] occurring in the late phase of necroptosis [474,475]. Together with a sustained activity, ERK1/2 sequestration is also considered as hallmarks of ERK1/2-mediated cell death [372]. Immunofluorescence study performed on L929 upon TNFα stimulation revealed that phosphorylated-ERK1/2 is mainly localized in the cytoplasm in both the early and late stages of ERK1/2 phosphorylation. It remains unclear whether the kinase is sequestered or transiently translocated into the nucleus in response to TNFα. While the exact mechanism of RIPK1-dependent ERK1/2 phosphorylation is not clearly established, we wondered if ERK1/2 could interact with RIPK1 or RIPK3. Interestingly, our results showed a strong interaction of ERK2 and RIPK1 at the time-point of 30min after TNFα stimulation of L929 cells. In agreement, a recent study reported that RIPK1 could interact constitutively with ERK1/2 and transiently with MEK2 upon eleostearic acid (ESA)-induced atypical RIPK1-dependent apoptotic cell death [438]. However, regarding the kinetic of ERK1/2 phosphorylation and the detection of interaction between RIPK1 and ERK2 in L929 cells, the functional interaction between ERK2 and RIPK1 in this cellular context should be further studied. In a next step, it would be interesting to reduce the time scale during the signaling phase of necroptosis and to evaluate the ability of RIPK1 and ERK2 inhibition to suppress this interaction.

Although biochemical data, snapshot acquisitions or time-points measurement can provide very valuable information, dissecting and manipulating signaling pathways require high spatio-temporal resolution that can be achieve *via* functional imaging. Study of ERK1/2 dynamics in subcellular compartments has already uncovered unexpected functions of ERK1/2 for determining cell fate. Shankaran and colleagues found that EGF-induced ERK1/2 activation in HMEC cells elicits oscillatory translocation of ERK1/2 between the cytoplasm and the nucleus [476]. More recently, oscillatory activation of JNK and ERK1/2 in 3T3 cells have been detected with TNFα or IL-1β using specific translocation reporters [445]. Owing to the importance of ERK1/2 spatio-temporal dynamics in determining cellular responses [413,477] and compelling evidences of ERK1/2 involvement in necroptosis, it became crucial to investigate the spatio-temporal dynamic of ERK1/2 in TNFα-induced necroptosis. To that effect, we developed, optimized and used fluorescence-based

reporters of both ERK1/2 activity and ERK2 localization in single living cells in real time.

To visualize ERK1/2 dynamics in living cells, various studies used ERK1/2 tagged with GFP-like fluorescent proteins and found that overexpressed eGFP-ERK2 is predominantly localized in the nucleus of resting cells. This unexpected localization of eGFP-ERK2 was due to the disruption of MEK/ERK balance [234]. This problem has been often ignored [449] and several studies selected cells expressing low levels of eGFP-ERK2 compared to the endogenous to obtain a faithful localization profile of the kinase in serum-starved conditions [446]. However, transfected cells were dimly fluorescent, which is unsuitable for long-term video imaging. To avoid artefacts in ERK2 localization patterns and facilitate long-term functional imaging, we developed a novel ERK2 localization reporter named ERK2-LOC. We employed the T2A-mediated equimolar coexpression of ERK2 and MEK1 [461,462,478] to enable faithful monitoring of eGFP-ERK2 localization in both basal and growth factor-stimulated conditions. ERK2-LOC was characterized using standard biochemical approaches and validated by live-cell imaging in living NIH-3T3 cells and ultimately in the *Xenopus laevis* model during early developmental stages.

To monitor ERK1/2 activity following cell death induction, we first used a genetically encoded FRET biosensor for ERK1/2 (EKAR-EV) [451]. However, this reporter failed to reveal any changes in ERK1/2 activity upon TNFα-induced necroptosis in L929 cells. We developed a method to build and/or optimize genetically encoded FRET biosensor (Sipieter *et al.*, in preparation) that led to the optimization of ERK1/2 FRET biosensor (ERK1/2-ACT). We characterized the dynamic range of this newly optimized ERK biosensor in our cellular models (L929 and MEF) by activating and inhibiting ERK1/2 signaling pathway with PMA and U0126 respectively. Results showed an emission ratio change that was almost improved by 2-fold relative to the initially construct (Sipieter *et al.*, in preparation). In addition, the reversibility of these biosensors was also upgraded hence rendering biosensors more accessible to specific phosphatases.

The newly optimized fluorescent-based reporters have facilitated our efforts to monitor the spatio-temporal dynamics of ERK1/2 over long period in our cellular context. Time-lapse FRET imaging of ERK1/2-ACT in MEF cells revealed a stochastic ERK1/2 activation in basal condition without stimulation in accordance with

previous reports [479]. This stochastic activation was observed in a wide range of cellular models [479]. We further investigated the effect of a necroptotic and an apoptotic trigger in MEF cells on ERK1/2 activity. Upon TNFα + BV6 + zVAD-induced necroptosis, we observed that the frequency of ERK1/2 activity pulses markedly increased in the signaling phase of necroptosis followed by a higher basal ERK1/2 activity in the last phase of cell death. In contrast, a gradual increase of ERK1/2 activity was detected upon TNFα + BV6-induced apoptosis. These results argue for a specific spatio-temporal signature of ERK1/2 depending on the programmed cell death at least in MEF cells. Therefore it would be interesting to extend the spatio-temporal study of ERK1/2 activity in other cellular models such as L929 and Jurkat cells. Indeed, TNFα + zVAD-induced necroptosis in Jurkat cells was inhibited by Nec-1 and by U0126 as well [471]. In the same line, the use of different triggers leading to a same cell death program could be performed to determine if these spatio-temporal signatures of ERK1/2 activities can be considered as markers of a particular cell death process or not. TNFα-, TNFα + zVAD-, IFNβ/dsRNA- and FasL + zVAD-induced necroptosis could be used. However, we could observed a basal increase of ERK1/2 activity upon BV6 + zVAD stimulation consistent with previous studies [439]. ERK1/2 was reported to have elevated phosphorylation levels under cIAP1 inhibition by using BV6 [480] accompanied by increased RIPK1 kinase activity upon TNFα stimulation, hence emphasizing a protecting role of cIAP1 from TNFα-induced necroptosis [439]. In a next step, the specific contribution of cIAP1 in ERK1/2 activity could be examined. For instance, it has already been shown that a differential spatio-temporal signature of ERK1/2 activity depending on the type of cell death. It would therefore be interesting to use different chemical inhibitor of ERK1/2 signaling to uncover the molecular mechanisms underlying the spatio-temporal activity of ERK1/2.

Our next efforts will include inhibitors of RIPK1/3 pathway such as Nec-1 and RIPK3 inhibitors to elucidate crosstalk between RIPK1/3 and ERK1/2 signaling pathways through potential feedback loops [219]. Subcellular ERK1/2 distribution following cell death stimulation in MEF cells was also monitored. Using ERK2-LOC reporter, we observed brief transient translocations of ERK1/2 in the nucleus in the control condition but also in stimulated conditions, which might reflect stochastic ERK1/2 activation over a long time-lapse [479]. Interestingly enough, our results

revealed a progressive accumulation of ERK1/2 in the nucleus starting between 1 to 2 hours before cell death upon both TNFα+BV6-induced apoptosis and TNFα+BV6+zVAD-induced necroptosis. It remains therefore to elucidate the molecular mechanism underlying this ERK2 nuclear accumulation. Likely, ROS production and subsequent inhibition of ERK1/2 phosphatases could be responsible at that timing [372]. However, it would be interesting to inquire whether mere impairment of ERK1/2 nuclear translocation through PEA-15 overexpression [241,481] could affect cell death progression.

Regarding ERK1/2 activity oscillations upon necroptosis stimulation, it appears essential to emphasize the importance of single-cell measurements because stochastic activation, TNFα-induced oscillatory kinase activation and the heterogeneity in cellular responses would have been impossible to monitor using averaged cell population assays. In addition, our efforts to improve the ERK1/2 FRET biosensor have contributed greatly to these findings because the optimization led to increase both its dynamic range and its reversibility. It would have been quite difficult to easily detect oscillations in ERK1/2 activity in our cellular models with previous versions of EKAR harboring a poor reversibility, thereby hampering the monitoring of fast ERK1/2 activity variation. Similarly, Regot *et al.* developed a new approach to monitor oscillations in JNK activity, as the previous JNK FRET biosensor was too slow in reporting JNK inhibition [445]. This emphasizes once more the importance of biosensors/tools engineering to avoid data misinterpretation even if the time-consuming constraint remains. This led us to create a new methodology for accelerating the development and optimization of sensitive FRET biosensors. Although MAPKs pathways have been extensively studied over the last decade (for review [62]), we believe that major findings about regulatory mechanisms of ERK1/2 signaling for cell fate determination remain to be elucidated using these FRET biosensors. Recently, live imaging of ERK1/2 activities in subcellular compartments has uncovered unexpected dynamics of ERK1/2. Albeck and colleagues showed that ERK1/2 is activated in asynchronous pulses at the basal state and that components at different levels of the pathway can modulate amplitude or frequency of EGF-induced ERK1/2 activity and hence regulate cellular proliferation [416]. In addition, Aoki and colleagues found that Raf induces stochastic ERK1/2 activation pulses under normal cell culture conditions and that different cell densities regulate the

frequency but not amplitude of ERK1/2 oscillations and hence cell proliferation [479]. They also elegantly demonstrated the propagation of these ERK1/2 oscillations to other adjacent cells.

Read-outs / hallmarks to correlate the spatio-temporal signature of ERK1/2 activity with necroptosis occurrence are scarce [38]. Since the kinase activity of RIPK1 and/or RIPK3 are crucial in the initiation step of necroptosis, we set out to develop new FRET-based kinase biosensors to specifically report on RIPK1 and RIPK3 kinase activities [454]. Based on our innovative methodology for the generation of new FRET biosensors, several biosensors have been efficiently generated for RIPK1 and RIPK3. Our first results in TNFα-induced necroptosis in L929 cells show a response for several biosensors (emission ratio of 10-15%) leading to a first generation of FRET biosensors for RIPK1 and RIPK3. We still need to determine the specificity and selectivity of these biosensors by using a chemical inhibitory approach of RIPK signaling before optimization of their dynamic range.

A very exciting challenge would be to monitor several kinase activities at the same time in the same sample [455] to correlate RIPK1 and RIPK3 as well as ERK1/2 activities hence determining the precise crosstalk between each signaling node. To this aim, we recently contribute to the development of a multiplex FRET biosensor approach based on new mTFP1/sREACh and LSSmOrange/mKate2 FRET pairs (Demeautis *et al.*, to be submitted).

Altogether, based on compelling evidences of ERK1/2 involvement in TNFα-induced necroptosis, we hypothesized that ERK1/2 spatio-temporal dynamics could be modulated. Results gathered though functional imaging approaches revealed oscillations in ERK1/2 activity that so far has not been reported in this particular context, which reinforce the idea that ERK1/2 is implicated in TNFα-induced necroptosis.

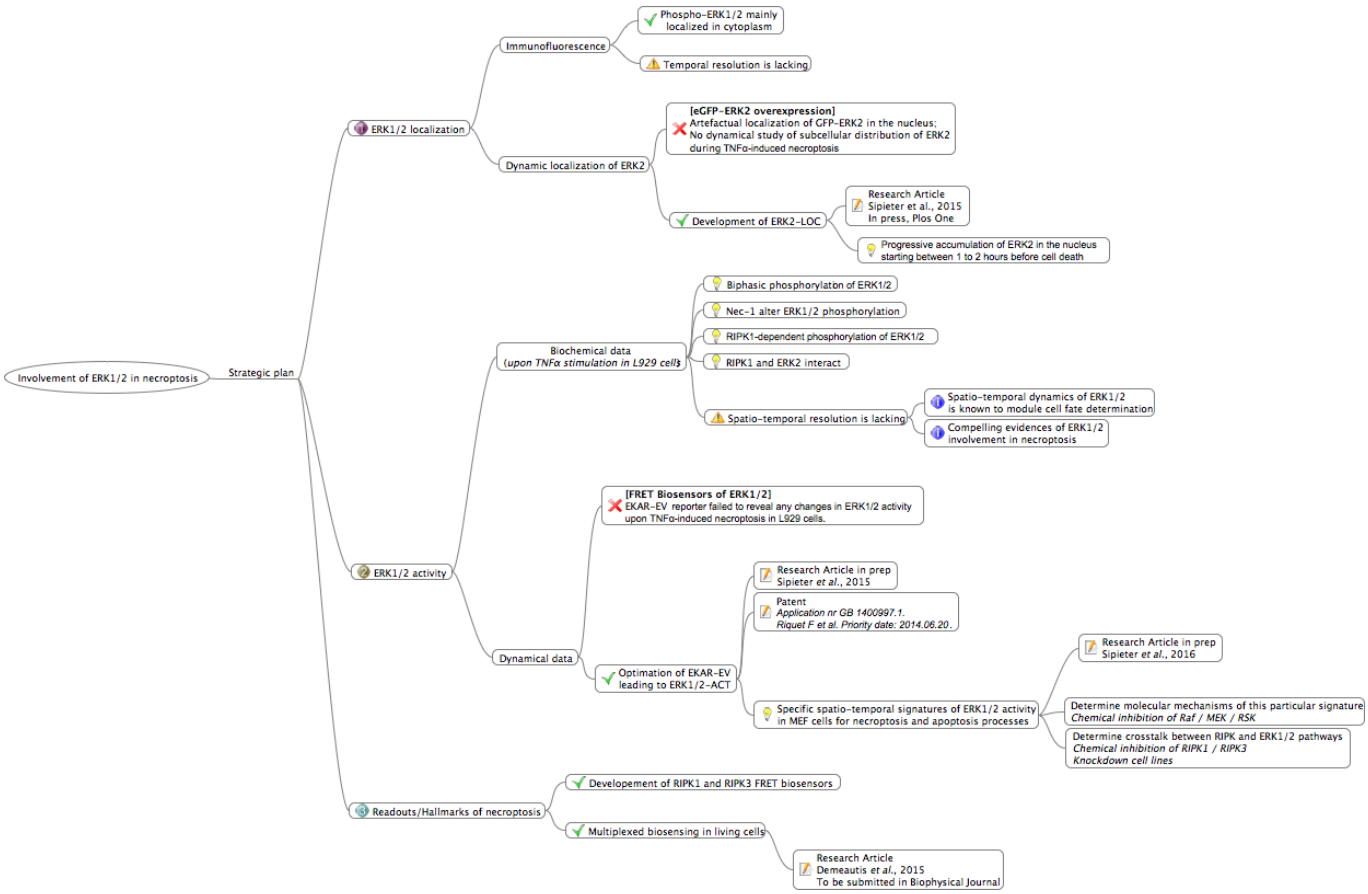

Figure 16: Schematic overview summarizing the strategy established for this research project. This project brain map, in a sort of decision tree shape, has helped throughout the guidance of this thesis. Outputs at both the scientific and biotechnological levels have also been indicated for reviewing purposes.

Résumé de la thèse

1. Introduction

1.1. Les morts cellulaires programmées

La nécroptose est aujourd'hui définie comme une mort programmée caspase indépendante. Elle présente un rôle physiopathologique et montre une implication dans certains mécanismes antiviraux, des maladies neuro-dégénératives ou encore les phénomènes d'ischémie–reperfusion. Cependant, notre compréhension des mécanismes moléculaires de la nécroptose commence tout juste à voir le jour. La nécroptose induite par le TNFα fait intervenir une voie de signalisation spécifique impliquant deux kinases, RIPK1 et RIPK3 et la pseudo-kinase MLKL, identifiée en 2012 comme étant l'exécuteur crucial de la nécroptose en aval de RIPK3.

***Sipieter F**, Ladik M, Vandenabeele P, Riquet F. Shining light on cell death processes - a novel biosensor for necroptosis, a newly described cell death program. Biotechnol J. 2014;9: 224–40. doi:10.1002/biot.201300200*

Résumé

La mort cellulaire contribue au maintien de l'homéostasie, mais de nouvelles preuves confirment l'implication de la mort cellulaire programmée dans certaines maladies. Le concept de mort cellulaire programmée, qui a été proposé il y a plusieurs décennies concernant l'apoptose, englobe désormais la nécroptose, un programme de mort cellulaire nouvellement caractérisé. Les recherches sur la mort cellulaire programmée sont devenues essentielles pour le développement de nouvelles thérapies. Pour étudier les signalisations de mort cellulaire et leurs mécanismes moléculaires, de nouvelles approches biochimiques et fluorogéniques ont été conçues. Ici, nous apportons d'abord un aperçu des différents types de morts cellulaires programmées puis l'importance des études de la mort cellulaire d'un point de vue plus dynamique. Ensuite, nous nous focalisons à la fois sur les signalisations, apoptotique et nécroptotique ainsi que sur leurs mécanismes moléculaires en fournissant pour chacune une revue

systématique de toutes les méthodes et approches qui ont été utilisées. Nous soulignons ensuite la contribution des approches avancées d'imagerie basées sur les sondes fluorescentes, les rapporteurs et les biosenseurs FRET pour l'étude de la mort cellulaire programmée. Parce que les voies de signalisation apoptotique et nécrotique partagent plusieurs effecteurs moléculaires, nous discutons comment ces nouveaux outils pourraient être utilisés pour discriminer l'apoptose de la nécroptose. Nous décrivons aussi notre stratégie expérimentale vers le développement des biosenseurs FRET pour la détection de la nécroptose en cellules vivantes. Enfin, nous ouvrons sur la façon dont la mesure dynamique des biomolécules dans des modèles vivants jouera un rôle dans le pronostic et le traitement personnalisé des patients.

1.2. Les voies de signalisation ERK1/2

La cascade de signalisation ERK1/2 est une voie de signalisation très conservée chez les eucaryotes. Elle intègre de nombreux signaux afin de moduler la réponse de la cellule. Les protéines ERK1 et ERK2 sont des sérines/thréonines kinases. Elles ont 83% d'identité et sont exprimées de façon ubiquitaire. Les MAPKs régulent divers programmes cellulaires comme l'embryogenèse, la prolifération, la différenciation et l'apoptose selon le type de stimulation, l'état d'activation et l'environnement de la cellule. La cascade ERK1/2 est constituée de trois niveaux, chacun étant composé d'une kinase. La kinase la plus proche de la source du signal est appelée MAP3K (isoformes de Raf) qui est activée par une protéine en amont (fixation de petites protéines G de la famille Ras sur la partie C terminale et phosphorylation). Elle phosphoryle et active ensuite une MAP2K (MEK1/2) qui à son tour phosphoryle et active une MAPK (ERK1/2). Ces enzymes sont finement régulées afin d'engager une réponse cellulaire spécifique. Ces réponses sont dépendantes de nombreux paramètres tels que la durée d'activation, la localisation subcellulaire des kinases ou encore l'interaction avec d'autres protéines. La modulation des fonctions des acteurs de la cascade est réalisée par des mécanismes de type déphosphorylation/phosphorylation et des interactions protéine-protéine. Les phosphatases influencent ainsi la cascade ERK1/2 de façon soit positive soit négative dépendamment de leur position dans la cascade.

Les kinases ERK1/2 sont des protéines nucléocytoplasmiques dont la localisation subcellulaire est dépendante du type et de l'intensité du signal. Afin de mettre en évidence et de mesurer les mécanismes régulant la localisation subcellulaire d'ERK1/2, l'imagerie en cellules vivantes a été utilisée. Des études utilisant le phénomène biophysique de FRET ont montré que MEK1 et ERK2 interagissaient et que cette interaction est en grande partie responsable de la rétention cytoplasmique de ERK2. La distribution subcellulaire de ERK1/2 est ainsi contrôlée par le nombre et l'affinité des partenaires de ERK1/2 dans chacun des compartiments cellulaires. L'activation des protéines ERK1/2 induit leur translocation nucléaire permettant à ERK1/2 l'accès aux facteurs de transcription qui sont alors phosphorylés et/ou stabilisés dans le but de modifier l'expression de gènes cibles. La forme active de ERK1/2 transite dans le noyau grâce à un transport actif impliquant la phosphorylation d'un motif SPS par la CK2 et l'interaction avec l'importine 7.

1.3. Implication de ERK1/2 dans les processus de mort cellulaire

Bien que l'activation de différentes MAPKs ait été impliquée dans de nombreux processus cellulaires, l'activation des kinases ERK1/2 a également été rapportée dans plusieurs types de morts cellulaires programmées telles que l'apoptose, l'autophagie ou encore récemment la ferroptose. Par ailleurs, la régulation de l'activité de ERK1/2 en termes d'amplitude, de durée et de localisation *via* des régulateurs spatio-temporels spécifiques est interprétée par la cellule pour la détermination du destin cellulaire.

1.4. Pourquoi utiliser des approches dynamiques pour la compréhension des fonctions de ERK1/2 ?

Les techniques d'analyse classiques ont déjà permis d'identifier et de caractériser de nombreux mécanismes de régulation liés à l'activité des protéines kinases. Cependant, ces techniques, telles que l'immunoblot ou l'immunocytochimie utilisant des anticorps reconnaissant les résidus phosphorylés, génèrent des résultats moyennés à l'échelle d'une population cellulaire et ne représentent qu'un cliché à un instant donné du processus cellulaire étudié. Le développement d'approches d'imagerie est donc nécessaire pour s'affranchir des inconvénients des

méthodes expérimentales traditionnelles. Les biosenseurs FRET codés génétiquement permettent de révéler et de suivre la dynamique de protéines kinases en cellules vivantes avec une résolution spatiale et temporelle élevée, tout en préservant l'intégrité et l'environnement cellulaire (contexte physiologique). Dans le contexte de la voie de signalisation ERK1/2, cette approche permettrait sans doute de répondre à certaines interrogations : comment l'activation d'une seule protéine kinase (ERK1/2) est-elle capable d'engager des réponses cellulaires aussi variées ? Le type cellulaire, le type de stimulation mais également la modulation de la dynamique spatio-temporelle de ERK1/2 seraient à l'origine de la diversité des réponses cellulaires engagées.

1.5. Article de revue – Reporting kinase activities: paradigms, tools and perspectives

Riquet F, Vandame P, **Sipieter F**, Cailliau-Maggio K, Spriet C, Héliot L and Bodart J-F. Reporting Kinase activities: paradigms, tools and perspectives. Journal of Biological Medicine 2011:1(2) 10-18.

Résumé

Etudier la complexité des réseaux de signalisation impliquant la phosphorylation est devenu une nécessité vers une meilleure compréhension des fonctions cellulaires tant au niveau physiologique que pathologique, ainsi que dans une perspective thérapeutique. Nous choisissons ici d'illustrer le propos en prenant à titre d'exemple les protéines kinases MAPKs, Akt et PKA, pour lesquelles la régulation spatio-temporelle de leurs activités respectives est cruciale pour l'accomplissement de fonctions cellulaires spécifiques. Afin de dépasser les limites des approches traditionnelles, des nouvelles méthodes d'imagerie basées sur la fluorescence (FRET) et la bioluminescence ont été développées. Elles génèrent des données avec une résolution spatiale et temporelle augmentée en cellule unique et à l'échelle du tissu. Nous discutons également des propriétés des rapporteurs d'activité kinase basés sur le FRET ou la bioluminescence.

2. Buts et objectifs

2.1 Objectifs scientifiques

L'activation du TNFR1 par le TNF constitue le modèle d'étude de la nécroptose le plus utilisé à ce jour. Selon le contexte cellulaire, l'activation du TNFR1 est à l'origine de 3 voies de signalisation distinctes, comprenant chacun des points de contrôle spécifiques.

Le premier point de contrôle est déterminé par RIPK1, qui selon son état d'ubiquitination, engagera soit une voie de survie, soit la mort cellulaire. Dans le cas d'un engagement vers la mort cellulaire (*e.g.* déubiquitination de RIPK1, inhibition de la voie de survie), un second point de contrôle détermine le type de mort cellulaire qui sera engagée, et cela en fonction de la nature des complexes pro-morts interagissant avec RIPK1. Au sein du complexe I assemblé après stimulation par le TNFα, RIPK1 contribue à l'activation des MAPKs, telles que p38, JNK et ERK1/2. Bien que plusieurs études aient rapporté ce phénomène en réponse au TNFα, le rôle de RIPK1 et les mécanismes moléculaires concourant à l'activation des MAPKs restent encore indéterminées. TRAF2 est une molécule adaptatrice recrutée à la membrane suite à l'activation du TNFR1 par le TNFα. Des études ont mis en évidence l'implication de TRAF2 dans l'activation des kinases JNK et IKK. De plus, la surexpression de TRAF2 engendre l'activation de p38 et ERK1/2. Devin et collaborateurs ont examiné les mécanismes moléculaires impliqués entre RIPK1 et les MAPKs dans des fibroblastes embryonnaires de souris (MEF) déficients pour RIPK1 ou TRAF2. Leurs résultats mettent en évidence l'implication de RIPK1 et de TRAF2 pour l'activation de JNK, p38 et ERK1/2 en réponse à la stimulation par TNFα. En effet, une diminution de 70% de l'activation de ERK1/2 a été observée dans les cellules RIPK1$^{-/-}$. De plus, l'expression dans cette lignée d'une forme mutée de RIPK1 pour son activité kinase (K45A) a permis de mettre en évidence la nécessité de l'activité de RIPK1 pour l'activation de ERK1/2, contrairement à p38 et JNK. L'identification des effecteurs moléculaires en amont de l'activation de ERK1/2 reste à déterminer puisque ni MEKK1 ni MEKK3 ni même A-Raf et B-Raf semblent nécessaires à l'activation de JNK, p38 et ERK1/2 en réponse au TNFα. Des mécanismes de redondances suite à la présence de nombreuses isoformes de MAP3K pourrait expliquer ce résultat. A ce jour, la séquence d'évènements

conduisant à l'activation de ERK1/2 par le TNFα, dépendante de l'activité de RIPK1, n'est pas élucidée et le rôle de ERK1/2 dans ce contexte cellulaire reste à déterminer.

Seulement quelques publications suggèrent un rôle de ERK1/2 dans la nécroptose stimulée par le TNFα. Zhang et collaborateurs ont mis en évidence le rôle primordial de ERK1/2 dans la nécroptose induite par le glutamate dans les cellules HT-22. Leur étude a révélée des niveaux d'activation de ERK1/2 élevés dans ces conditions et un blocage de la nécroptose suite à l'inhibition de ERK1/2. Il a été rapporté que l'inhibition de RIPK1 par Nec-1 empêche la nécroptose provoquée par le glutamate dans les cellules HT-22 *via* l'inhibition de la phosphorylation de ERK1/2. Cependant, l'inhibition de RIPK1 ne présente aucune conséquence sur p38 et JNK, soulignant ainsi le rôle de ERK1/2 dans cette mort nécrotique induite par le glutamate. De manière contradictoire, une autre étude a montré que l'apoptose induite par la shikonine dans les cellules leucémiques HL60 et K562 était amplifiée par l'inhibition de RIPK1 *via* l'inactivation de ERK1/2, suggérant ici un rôle pro-survie de ERK1/2 dans ce contexte. Par ailleurs, un lien entre l'activation de ERK1/2 et la voie de signalisation RIPK1/3 a été mis en évidence par Gao et collaborateurs dans un contexte d'ischémie–reperfusion de rétines de rat. 12h après le traumatisme, il a été observé dans des cellules ganglionnaires rétiniennes de rat des niveaux de phosphorylation élevés de ERK1/2 ainsi qu'une accumulation de RIPK3, mais aucun effet sur RIPK1. L'injection intravitréenne d'U0126 a permis d'inhiber ERK1/2 et d'empêcher l'accumulation de RIPK3 ce qui a conduit à une diminution de la nécroptose. Ces résultats soulignent de nouveau le rôle de ERK1/2 dans l'exécution de la nécroptose. Cependant, cette étude indique un rôle de ERK1/2 en amont de RIPK3, ce qui est en contradiction avec le modèle actuel préconisant un rôle pour ERK1/2 en aval du complexe pro-nécrotique.

Les mécanismes moléculaires sous-jacents à l'activation de ERK1/2 par RIPK1 sont mal connus. Récemment, une étude a mis en évidence une nouvelle forme de mort cellulaire apoptotique RIPK1-dependante induite par l'acide éléostéarique (ESA) au niveau de laquelle la voie de signalisation ERK1/2 est impliquée. Dans ce contexte il a été montré que ERK1/2 interagissait de façon constitutive avec RIPK1, et de manière transitoire avec MEK2. Les auteurs ont également montré que l'apoptose ESA-induite nécessitait la déphosphorylation de

RIPK1, puis la phosphorylation de ERK1/2 via MEK2, ainsi qu'une diminution de la phosphorylation des protéines AIF. AIF, tout comme ERK1/2, se trouvent alors relocalisés dans le noyau. Ce processus s'accompagne d'une production de ROS et de dysfonctionnements mitochondriaux, aboutissant à la mort cellulaire. Cependant, dans le cadre de la nécroptose RIPK1-dependante induite par le TNFα, les phosphorylations croisées entre RIPK1 et RIPK3 contribuent à la stabilisation du ripoptosome ce qui entraine une production progressive de ROS. De plus, étant donné que l'élévation des niveaux intracellulaires de ROS contribue à inhiber les phosphatases spécifiques de ERK1/2, l'activation de ERK1/2 au cours de la nécroptose pourrait être davantage une conséquence qu'une cause de la production de ROS. Par ailleurs, en accord avec de précédentes études, la phosphorylation de ERK1/2 RIPK1-dépendante a été observée dans le contexte des cellules L929 stimulées par le TNFα. Dans ce même contexte cellulaire, l'inhibition de cIAP1 par le BV6 a entrainé une augmentation significative des niveaux de phosphorylation de ERK1/2 ainsi que de l'activité de RIPK1, accompagnés par une élévation de la production de ROS. Ces résultats soulignent ici le rôle protecteur de cIAP1 dans la nécroptose induite par le TNFα, ainsi que l'implication de cIAP1 dans la régulation de la phosphorylation de ERK1/2.

En lien avec l'activation des MAPKs induite par le TNFα, il a été rapporté que le TNFα entrainait une activation biphasique de JNK, constitué d'une première activation transitoire, suivie d'une activité soutenue sur plusieurs heures. Dans les cellules L929, la stimulation par le TNFα entraine également une activité transitoire de JNK et p38, puis seule une activation soutenue de p38 a été détectée. L'activation soutenue de JNK a pu être mise en évidence suite à l'inhibition des phosphatases de JNK par les ROS consécutive à la stimulation par le TNFα.

La mesure des variations d'activité kinase, telle que ERK1/2, en cellules vivantes est nécessaire tant elles participent à la détermination de l'engagement dans un processus cellulaire spécifique. En effet, alors qu'une activation transitoire est promotrice de la survie cellulaire et permet de contrecarrer les signaux de mort, une activation soutenue constitue quant à elle un marqueur de l'engagement d'un processus de mort cellulaire. Récemment, une étude a décrit des comportements oscillatoires de l'activation de JNK et ERK1/2 dans les cellules 3T3 stimulées par le TNFα ou l'IL-1β, par le biais de rapporteurs de localisation. De plus, il a aussi été

montré que d'autres voies de signalisation, telle que p38/MAPK, pouvaient moduler la fréquence sans pour autant affecter l'amplitude des oscillations de l'activité ERK1/2. Au regard des profils oscillatoires d'activité de ERK1/2, il est important ici de souligner l'apport des mesures d'activité en cellules uniques permettant d'isoler ce type de profil d'activité provenant de la stochasticité du système ou de l'action de facteurs de croissance et cytokines. Ces mesures peuvent ainsi contribuer à la mise en évidence de l'hétérogénéité des réponses cellulaires. Cependant, l'utilisation d'approches plus globales telles que des approches biochimiques ne permettent pas de mettre en évidence ce type de signature individuelle tant elles contribuent à moyenner la réponse d'une population cellulaire à un temps donné.

Au vu de l'importance de la dynamique spatio-temporelle des MAPKs dans l'orientation de la réponse cellulaire et des faisceaux d'indices de l'implication de ERK1/2 dans la nécroptose stimulée par le TNFα, nous avons entrepris l'étude de la dynamique de ERK1/2 dans le contexte de la nécroptose induite par le TNFα *via* l'utilisation de rapporteurs fluorescents de la localisation et de l'activité de ERK1/2 en cellules vivantes. En combinaison avec l'utilisation d'inhibiteurs chimiques spécifiques de la nécroptose et de la voie de signalisation ERK1/2, nous avons commencé à clarifier le lien entre les voies de signalisation ERK1/2 et RIPK1/3.

Les objectifs scientifiques de cette thèse sont les suivants:

- Etudier l'implication de ERK1/2 dans la nécroptose induite par le TNFα dans les cellules L929 et MEF, deux modèles murins d'étude de la nécroptose TNFR1 dépendante
- Déterminer la dynamique spatio-temporelle de ERK1/2 dans ce processus de nécroptose
- Identifier les effecteurs moléculaires impliqués dans la phosphorylation TNFα-induite de ERK1/2 et l'interrelation entre les cascades de signalisation RIPK1/3 et ERK1/2
- Corréler la signature spatio-temporelle de ERK1/2 avec des marqueurs de l'initiation et de l'exécution de la nécroptose

2.2. Objectifs biotechnologiques:

Plusieurs études ont rapporté la localisation spatio-temporelle de ERK2 en cellules uniques par la surexpression de ERK2 étiquetée avec un variant de la GFP. L'expression de la GFP-ERK2 dans les cellules L929 et MEF a entrainé une accumulation nucléaire anormale de la GFP-ERK2 en condition de privation sérum et en l'absence de stimulation de la voie de signalisation ERK1/2. En effet, de manière indépendante de la phosphorylation, les cellules surexprimant la GFP-ERK2 présentaient une accumulation nucléaire lorsque l'intensité de fluorescence était élevée, alors que la protéine surexprimée était distribuée de manière homogène entre le cytoplasme et le noyau dans les cellules présentant un faible niveau de fluorescence. Sur la base de cette observation et de nos ambitions, il est donc apparu nécessaire de développer un outil moléculaire permettant un suivi fidèle et dynamique de la distribution subcellulaire de ERK2 en cellules vivantes par imagerie de fluorescence.

En parallèle de la localisation, nous avons entrepris la mesure de l'activité spatio-temporelle de ERK1/2. Afin d'établir les profils d'activité de ERK1/2 dans le contexte de la nécroptose induite par le TNFα, nous avons utilisé un rapporteur d'activité kinase génétiquement codé reposant sur le FRET (EKAR-EV). Cependant ce rapporteur n'a pas permis l'enregistrement de variation d'activité de ERK1/2 lors de la nécroptose stimulée par le TNFα dans les cellules L929, ce qui était en désaccord avec nos données biochimiques préalables. Nous avons donc avancé deux hypothèses: (i) la phosphorylation de ERK1/2 ne s'accompagne pas systématiquement de variation d'activité, ou (ii) le rapporteur fait défaut n'étant pas suffisamment sensible pour détecter les variations d'activité dans le contexte de la signalisation du TNFα. Après avoir écarté la première hypothèse dans notre contexte d'étude, nous avons développé une méthode rapide pour la construction et/ou l'optimisation de biosenseurs FRET génétiquement codés. Enfin, dans le but de corréler l'activité de deux kinases, le développement d'une approche permettant la mesure simultanée d'activités kinase dans un même échantillon biologique semble aussi être requis.

Les objectifs technologiques de cette thèse sont les suivants:

- Résoudre les problèmes liés à la surexpression de la GFP-ERK2, source de la distribution artéfactuelle de la kinase
- Optimiser le rapporteur d'activité kinase de ERK1/2 (EKAR-EV) afin de réaliser les mesures spatio-temporelles d'activité de ERK1/2 dans le contexte de la nécroptose TNFα-induite
- Développer des rapporteurs d'activité kinase pour RIPK1 et RIPK3 pour le suivi de l'initiation et de l'exécution de la nécroptose
- Développer une approche d'imagerie fonctionnelle pour la mesure simultanée de deux activités kinase dans un même échantillon biologique

3. Approches Expérimentales

3.1. Co-expression équimolaire des kinases GFP-ERK2 et MEK1 pour le suivi dynamique de GFP-ERK2 en cellules vivantes

Dans cette section, nous présentons la stratégie de co-expression des kinases GFP-ERK2 et MEK1 utilisant un peptide viral « 2A » de la famille des *Picornaviridae* qui permet la génération de deux polypeptides distincts issus d'un seul polypeptide par un mécanisme traductionnel de « skipping » ribosomal ou CHYSEL. Ce mécanisme permet ainsi une production équimolaire fixe des protéines co-exprimées. De nombreuses versions de la séquence 2A ont été développées et optimisées. Plus petites et plus fiables qu'une séquence IRES, les séquences 2A sont de plus en plus utilisées en biotechnologie et en biomédecine.

3.2. Chapitre d'ouvrage – From FRET imaging to practical methodology for kinase activity sensing in living cell.

Sipieter F, Vandame P, Spriet C, Leray A, Vincent P, Trinel D, Bodart J-F, Riquet FB, Héliot L. From FRET imaging to practical methodology for kinase activity sensing in living cells. Prog Mol Biol Transl Sci. 2013;113: 145–216. doi:10.1016/B978-0-12-386932-6.00005

Résumé:

Les processus biologiques sont intrinsèquement dynamiques. Bien que les méthodes traditionnelles apportent des indications précieuses pour la compréhension de nombreux phénomènes biologiques, la possibilité de mesurer, quantifier et de localiser des protéines dans une cellule, un tissu, et même un embryon a révolutionné notre façon de pensée et a encouragé les scientifiques à développer des outils moléculaires pour mesurer/évaluer la dynamique des protéines ou de complexes protéiques dans leur contexte physiologique. Ces efforts actuels reposent sur l'émergence de techniques de biophotonique et l'amélioration de sondes fluorescentes, permettant des mesures précises et fiables des fonctions cellulaires. La

marche de la «biochimie *in vivo* » a commencé, apportant déjà des résultats impressionnants.

4. Résultats

4.1. Article de recherche – Novel reporter for faithful monitoring of ERK2 dynamics in living cells and model organisms.

Sipieter F, Cappe B, Gonzalez Pisfil M, Spriet C, Bodart J-F, Cailliau-Maggio K, Vandenabeele P, Héliot L, Riquet FB. Novel reporter for faithful monitoring of ERK2 dynamics in living cells and model organisms. PlosOne 2015. *In press*.

Résumé:

Le découplage entre la phosphorylation et la localisation de ERK1/2 est essentiel à la compréhension des mécanismes moléculaires contrôlés par ERK1/2. De plus, les fonctions non catalytiques de ERK1/2 et la découverte de nouvelles ancres spécifiques responsables de la compartimentation subcellulaire de la voie de signalisation ERK1/2 ont été proposés comme des mécanismes de régulation pour lesquels la mesure et le suivi dynamique de la localisation de ERK1/2 est nécessaire. Cependant, l'étude des caractéristiques spatio-temporelles de ERK2, par exemple, dans différents processus cellulaires dans les cellules et tissus vivants nécessite un outil qui puisse rapporter sa distribution subcellulaire le plus fidèlement possible à l'endogène. Nous avons développé un tel outil moléculaire nommé ERK2-LOC, basé sur la co-expression équimolaire de MEK1 et de eGFP-ERK2 grâce à la séquence virale T2A. MEK1 et eGFP-ERK2 ont été co-exprimés de manière fiable et fonctionnelle à la fois *in vitro* et en cellules vivantes. Nous avons ensuite évalué la distribution subcellulaire et la mobilité d'ERK2-LOC par microscopie de fluorescence en condition basale et également après activation et inhibition de la voie de signalisation ERK1/2. Enfin, nous avons utilisé notre système de co-expression dans l'embryon de Xénope pendant les premiers stades du développement embryonnaire.

C'est la première fois que ERK2 et MEK1 sont co-exprimés dans des embryons vivants et les résultats révèlent une forte corrélation entre la distribution spatio-temporelle d'ERK2-LOC et les profils de phosphorylation de ERK1/2. Enfin, notre approche peut être utilisée pour étudier la localisation spatio-temporelle d'ERK2 dans une variété de processus cellulaires à la fois en cellules vivantes et dans les tissus embryonnaires.

4.2. Article de recherche en préparation – A novel approach for rapid development of optimized FRET-based biosensors for signaling network interrogation in living cells

Sipieter F, Cappe B, Gavet O, Héliot L, Vincent P and Riquet FB. A novel approach for rapid development of optimized FRET-based biosensors for signaling network interrogation in living cells. 2015. *In preparation*.

La dynamique des protéines kinases est déterminante dans de nombreux processus cellulaires. Dans ce contexte, il est donc devenu nécessaire de disposer d'outils permettant l'analyse de la dynamique de ces protéines kinases. De nombreux résultats ont été obtenus grâce à l'utilisation de biosenseurs FRET rapporteur d'activité kinase. Toutefois, leur répertoire est très loin de couvrir l'ensemble des kinases du vivant. A l'heure actuelle, environ 518 kinases ont été identifiées et environ 26 biosenseurs kinasiques ont été obtenus.

Le faible nombre de biosenseurs de kinase disponibles s'explique en grande partie par la complexité de ces outils moléculaires. En effet, la construction des biosenseurs FRET codés génétiquement nécessite l'insertion précise d'éléments spécifiques dans une séquence nucléotidique selon un enchaînement donné. Aussi, compte tenu de la complexité structurale de ces outils moléculaires, il est impossible de prédire quel enchainement adéquat produira un biosenseur performant. A l'heure actuelle, l'unique façon de procéder repose sur la construction empirique des biosenseurs issus de la combinaison multiple d'éléments spécifiques.

Le processus de construction des biosenseurs repose ainsi exclusivement sur des techniques classiques de clonage moléculaire. Cependant, ces techniques de

clonage requièrent un investissement extrêmement important en termes de temps et de coûts pour réaliser chacune des constructions envisagées avant même de connaître si ces dernières se révéleront efficaces ou non.

Il existe par conséquent un réel besoin de nouveaux biosenseurs de kinase, et d'une technologie qui facilite leur construction.

Patent: « *Biosenseurs de kinase et leur procédé de fabrication*. » Application nr GB 1400997.1. Riquet F et al. (including **Sipieter F**): Priority date: 2014.06.20.

Résumé:

La présente invention concerne des acides nucléiques codant des biosenseurs de kinase construits à partir d'éléments modulables, leur procédé de fabrication, ainsi que les biosenseurs de kinase codés par lesdits acides nucléiques.

4.3. Article de recherche en préparation – Spatio-temporal characterization of ERK activity in survival, apoptosis and necroptosis.

Sipieter F, Cappe B, Grootjans S, Ladik M, Vincent P, Vandenabeele P and Riquet FB. Spatio-temporal characterization of ERK activity in survival, apoptosis and necroptosis. 2016. *In preparation*.

Afin d'étudier l'implication de ERK1/2 dans la nécroptose TNFα-induite dans les L929, nous avons testé l'effet d'inhibiteurs chimiques de la cascade de signalisation ERK1/2. Nos résultats mettent en évidence un retard significatif de la nécroptose de manière dose-dépendante, sans pour autant la bloquer. Nos données sont en accord avec les études antérieures suggérant ainsi un rôle pro-nécrotique de ERK1/2 dans ce contexte cellulaire.

Les profils de phosphorylation de ERK1/2 révèlent une activité biphasique et compartimentée dans ces conditions expérimentales. Par ailleurs, l'inhibition de l'activité de RIPK1 par la nécrostatine-1 dans les L929 stimulées préalablement par le TNFα perturbe les profils de phosphorylation de ERK1/2, suggérant ainsi que RIPK1 soit impliquée dans l'activation de ERK1/2 induite par le TNFα.

La régulation spatio-temporelle de l'activité de ERK1/2 étant déterminante dans l'orientation de la réponse cellulaire, nous avons étudié le code d'activation spatio-temporel de ERK1/2 au cours de la nécroptose *via* l'utilisation en cellules vivantes de rapporteurs fluorescents de l'activité et de la localisation de ERK1/2. Afin d'assurer un suivi fidèle de la distribution subcellulaire de ERK2, nous avons développé un nouveau rapporteur génétiquement codé, appelé ERK2-LOC. Cet outil nous a permis d'observer une translocation transitoire de ERK2 suite à la stimulation des L929 par le TNFα, suivi d'une accumulation nucléaire progressive de ERK2. Cette signature est considérée comme caractéristique de l'implication de ERK1/2 dans les processus de mort cellulaire.

L'examen des profils d'activité de ERK1/2 au cours de la nécroptose a été initialement réalisé grâce à l'utilisation d'un rapporteur FRET d'activité kinase (EKAR-EV). Ce biosenseur n'a pas permis l'enregistrement de variations d'activité, contrairement aux résultats obtenus par biochimie. L'optimisation de EKAR-EV, par une approche nouvellement développée, a amélioré substantiellement sa gamme dynamique (ERK1/2-ACT). L'utilisation de ERK1/2-ACT a permis de mettre en évidence pour la première fois une signature spatio-temporelle spécifique de l'activité de ERK1/2 au cours de la nécroptose.

Dans la perspective de corréler les signatures d'activité de ERK1/2 avec celles des kinases RIPK1 et RIPK3, nous avons également développé une première génération de biosenseurs FRET pour ces kinases initiatrices de la nécroptose.

4.4. Article de recherche en préparation – Single wavelength excitation dual color FLIM for multiplexing genetically encoded FRET biosensors.

Déméautis C, **Sipieter F**, Roul J, Chapuis C, Padilla-Parra S, Riquet FB and Tramier M. Single wavelength excitation dual color FLIM for multiplexing genetically encoded FRET biosensors (*to be submitted in Biophysical Journal, 2015*).

Résumé:

Les biosenseurs codés génétiquement basés sur *le Förster Resonance Energy Transfert* (FRET) sont des outils performants pour la mesure spatio-temporelle d'activités biochimiques dans des

échantillons biologiques vivants. A l'heure actuelle une des nécessités consiste en la mesure simultanée de deux activités kinase en cellules vivantes et dans un même compartiment subcellulaire. Cependant l'approche multiplex souffre de certaines limitations : (i) une fuite spectrale du premier donneur dans le canal d'émission du deuxième donneur, et ceci en lien avec la concentration relative entre les deux biosenseurs, (ii) de multiple longueurs d'onde d'excitation nécessitant une acquisition séquentielle incompatible avec le suivi de variations rapides d'activités biochimiques. Sur la base du long déplacement de Stoke de la LSSmOrange, nous avons utilisé une longueur d'onde unique d'excitation pour les donneurs mTFP1 et LSSmOrange sur notre microscope « dual color FLIM » permettant ainsi la mesure simultanée d'activités kinase *via* deux biosenseurs FRET indépendants. De plus la combinaison d'un accepteur non-fluorescent sREACh avec mTFP1 et un accepteur rouge-lointain mKate2 avec LSSmOrange a résolu les problèmes liés à la fuite spectrale. L'utilisation d'un système « dual color FLIM » a permis de réaliser la mesure simultanée des durées de vie de fluorescence de mTFP1 et LSSmOrange dans un même compartiment cellulaire. Par la suite, l'approche a été validée dans un contexte biologique spécifique visant à mesurer simultanément les variations d'activités de ERK1/2 et PKA en cellules HeLa. Dans cette perspective, les biosenseurs EKAR2G et AKAR4 ont été respectivement modifiés avec les couples de protéines fluorescentes mTFP1/sREACh et LSSmOrange/mKate2, puis validés. L'activation de la voie de signalisation PKA par la forskoline a été sans effet sur l'activité de ERK1/2. En revanche, l'activation de la voie de signalisation ERK1/2 par l'EGF a conduit à l'identification de deux sous-populations distinctes de cellules HeLa tout en mettant en évidence une interrelation entre ces deux voies de signalisation.

5. Discussion générale et conclusion

Sur la base d'un faisceau d'indices concernant l'implication de ERK1/2 dans la nécroptose, nous avons fait l'hypothèse d'un rôle possible de ERK1/2 dans la régulation de la nécroptose TNFα-induite. Les premiers résultats ont rapidement confirmés que l'inhibition de la voie signalisation ERK1/2 entrainait un retard prononcé de la nécroptose stimulée par le TNFα. A la vue de récentes études rapportant la pertinence de la dynamique spatio-temporelle dans l'orientation de la réponse cellulaire vers un processus cellulaire spécifique, nous nous sommes naturellement dirigé vers une approche expérimentale permettant d'accéder à ce niveau d'information. Nos efforts concentrés dans le développement et l'optimisation de rapporteurs fluorescents génétiquement codés ont permis de révéler un comportement encore jamais détecté de ERK1/2 dans la nécroptose TNFα-induite dans des lignées de fibroblastes murins. Une accumulation nucléaire progressive de ERK1/2 a été mise en évidence entre une à deux heures avant la mort de la cellule par apoptose et par nécroptose. De plus, une augmentation de la fréquence des pics d'activité de ERK1/2 lors de la phase de signalisation de la nécroptose a été observée et se distingue de la dynamique spatio-temporelle de l'activité de ERK1/2 dans l'apoptose médiée par le TNFα dans le même modèle cellulaire. Ces résultats renforcent l'idée de l'implication de ERK1/2 dans la nécroptose TNFα-induite RIPK1 dépendante.

Par ailleurs, considérant le manque de marqueurs pour la détection et la visualisation de la nécroptose en cellules vivantes, nous avons entrepris le développement de biosenseurs FRET rapporteurs d'activité kinase pour RIPK1 et RIPK3. Puis, dans l'optique de pouvoir réaliser la mesure simultanée de l'activité de ces deux kinases, nous avons participé au développement et à la validation d'une méthode d'imagerie dédiée. Enfin, les approches développées et utilisées dans ce travail de thèse sont en adéquation avec l'étude dynamique des processus biologiques et nous encourage à poursuivre nos efforts concernant les kinases RIPK1, RIPK3 et ERK1/2 tant dans la nécroptose que dans d'autres processus cellulaires dans lesquelles ces kinases sont impliquées.

References

1. Sun L, Wang H, Wang Z, He S, Chen S, Liao D, et al. Mixed lineage kinase domain-like protein mediates necrosis signaling downstream of RIP3 kinase. Cell. Elsevier Inc.; 2012;148: 213–27. doi:10.1016/j.cell.2011.11.031
2. Wu J, Huang Z, Ren J, Zhang Z, He P, Li Y, et al. Mlkl knockout mice demonstrate the indispensable role of Mlkl in necroptosis. Cell Res. Nature Publishing Group; 2013;23: 994–1006. doi:10.1038/cr.2013.91
3. Murphy JMMM, Czabotar PEEE, Hildebrand JMMM, Lucet ISSS, Zhang JG, Alvarez-Diaz S, et al. The pseudokinase MLKL mediates necroptosis via a molecular switch mechanism. Immunity. Elsevier Inc.; 2013;39: 443–453. doi:10.1016/j.immuni.2013.06.018
4. Sun L, Wang X. A new kind of cell suicide: mechanisms and functions of programmed necrosis. Trends Biochem Sci. Elsevier Ltd; 2014;39: 587–593. doi:10.1016/j.tibs.2014.10.003
5. Zhao J, Jitkaew S, Cai Z, Choksi S, Li Q, Luo J, et al. Mixed lineage kinase domain-like is a key receptor interacting protein 3 downstream component of TNF-induced necrosis. Proc Natl Acad Sci. 2012;109: 5322–5327. doi:10.1073/pnas.1200012109
6. Cai Z, Jitkaew S, Zhao J, Chiang H-C, Choksi S, Liu J, et al. Plasma membrane translocation of trimerized MLKL protein is required for TNF-induced necroptosis. Nat Cell Biol. Nature Publishing Group; 2013;16: 55–65. doi:10.1038/ncb2883
7. Chen X, Li WW, Ren J, Huang D, He W, Song Y, et al. Translocation of mixed lineage kinase domain-like protein to plasma membrane leads to necrotic cell death. Cell Res. Nature Publishing Group; 2014;24: 105–121. doi:10.1038/cr.2013.171
8. Cho Y, Challa S, Moquin D, Genga R, Ray TD, Guildford M, et al. Phosphorylation-Driven Assembly of the RIP1-RIP3 Complex Regulates Programmed Necrosis and Virus-Induced Inflammation. Cell. Elsevier Ltd; 2009;137: 1112–1123. doi:10.1016/j.cell.2009.05.037
9. He S, Wang L, Miao L, Wang T, Du F, Zhao L, et al. Receptor interacting protein kinase-3 determines cellular necrotic response to TNF-alpha. Cell. Elsevier Ltd; 2009;137: 1100–1111. doi:10.1016/j.cell.2009.05.021
10. Li J, McQuade T, Siemer AB, Napetschnig J, Moriwaki K, Hsiao YS, et al. The RIP1/RIP3 necrosome forms a functional amyloid signaling complex required for programmed necrosis. Cell. 2012;150: 339–350. doi:10.1016/j.cell.2012.06.019
11. Xie T, Peng W, Yan C, Wu J, Gong X, Shi Y. Structural insights into RIP3-mediated necroptotic signaling. Cell Rep. The Authors; 2013;5: 70–8. doi:10.1016/j.celrep.2013.08.044
12. Hildebrand JM, Tanzer MC, Lucet IS, Young SN, Spall SK, Sharma P, et al. Activation of the pseudokinase MLKL unleashes the four-helix bundle domain to induce membrane localization and necroptotic cell death. Proc Natl Acad Sci U S A. 2014; doi:10.1073/pnas.1408987111
13. Dondelinger Y, Declercq W, Montessuit S, Roelandt R, Goncalves A, Bruggeman I, et al. MLKL compromises plasma membrane integrity by binding to phosphatidylinositol phosphates. Cell Rep. The Authors; 2014;7: 971–81. doi:10.1016/j.celrep.2014.04.026
14. Wang H, Sun L, Su L, Rizo J, Liu L, Wang L-FF, et al. Mixed Lineage Kinase Domain-like Protein MLKL Causes Necrotic Membrane Disruption upon Phosphorylation by RIP3. Mol Cell. Elsevier Inc.; 2014;54: 133–146. doi:10.1016/j.molcel.2014.03.003
15. Murphy JM, Lucet IS, Hildebrand JM, Tanzer MC, Young SN, Sharma P, et al. Insights into the evolution of divergent nucleotide-binding mechanisms among pseudokinases revealed by crystal structures of human and mouse MLKL. Biochem J. 2014;457: 369–77. doi:10.1042/BJ20131270
16. Su L, Quade B, Wang H, Sun L, Wang X, Rizo J. A Plug Release Mechanism for Membrane Permeation by MLKL. Structure. Elsevier Ltd; 2014; 1–12. doi:10.1016/j.str.2014.07.014
17. Galluzzi L, Kepp O, Kroemer G. MLKL regulates necrotic plasma membrane permeabilization. Cell Res. Nature Publishing Group; 2014;24: 139–40. doi:10.1038/cr.2014.8
18. Yoon S, Bogdanov K, Kovalenko A, Wallach D. Necroptosis is preceded by nuclear translocation of the signaling proteins that induce it. Cell Death Differ. Nature Publishing Group; 2015; 1–8. doi:10.1038/cdd.2015.92
19. Levine B, Klionsky DJ. Development by Self-DigestionMolecular Mechanisms and Biological Functions of Autophagy. Dev Cell. 2004;6: 463–477. doi:10.1016/S1534-5807(04)00099-1
20. Van Der Vaart A, Mari M, Reggiori F. A picky eater: Exploring the mechanisms of selective autophagy in Human Pathologies. Traffic. 2008;9: 281–289. doi:10.1111/j.1600-0854.2007.00674.x
21. Lorin S, Hamaï A, Mehrpour M, Codogno P. Autophagy regulation and its role in cancer. Semin Cancer Biol. 2013;23: 361–379. doi:10.1016/j.semcancer.2013.06.007
22. Choi AMK, Ryter SW, Levine B. Autophagy in human health and disease. N Engl J Med. 2013;368: 651–662. doi:10.1056/NEJMra1205406
23. Yang J, Carra S, Zhu W-G, Kampinga HH. The Regulation of the Autophagic Network and Its Implications for Human Disease. Int J Biol Sci. 2013;9: 1121–1133. doi:10.7150/ijbs.6666
24. He C, Klionsky DJ. Regulation mechanisms and signaling pathways of autophagy. Annu Rev Genet. 2009;43: 67–93. doi:10.1146/annurev-genet-102808-114910

25. Kawamata T, Kamada Y, Kabeya Y, Sekito T, Ohsumi Y. Organization of the pre-autophagosomal structure responsible for autophagosome formation. Mol Biol Cell. 2008;19: 2039–50. doi:10.1091/mbc.E07-10-1048
26. Chan EY, Tooze S a. Evolution of Atg1 function and regulation. Autophagy. 2009;5: 758–765. doi:8709 [pii]
27. Kroemer G, Mariño G, Levine B. Autophagy and the Integrated Stress Response. Mol Cell. 2010;40: 280–293. doi:10.1016/j.molcel.2010.09.023
28. Levine B, Yuan J. Autophagy in cell death: An innocent convict? J Clin Invest. 2005;115: 2679–2688. doi:10.1172/JCI26390
29. Galluzzi L, Aaronson S a, Abrams J, Alnemri ES, Andrews DW, Baehrecke EH, et al. Guidelines for the use and interpretation of assays for monitoring cell death in higher eukaryotes. Cell Death Differ. 2009;16: 1093–1107. doi:10.1038/cdd.2009.44
30. Maiuri MC, Zalckvar E, Kimchi A, Kroemer G. Self-eating and self-killing: crosstalk between autophagy and apoptosis. Nat Rev Mol Cell Biol. 2007;8: 741–752. doi:10.1038/nrm2239
31. Pattingre S, Tassa A, Qu X, Garuti R, Liang XH, Mizushima N, et al. Bcl-2 antiapoptotic proteins inhibit Beclin 1-dependent autophagy. Cell. 2005;122: 927–939. doi:S0092-8674(05)00692-6 [pii]\r10.1016/j.cell.2005.07.002
32. White E. Autophagic cell death unraveled: Pharmacological inhibition of apoptosis and autophagy enables necrosis. Autophagy. 2008. pp. 399–401.
33. Jin S. Autophagy, mitochondrial quality control, and oncogenesis. Autophagy. 2: 80–4.
34. White E, DiPaola RS. The double-edged sword of autophagy modulation in cancer. Clin Cancer Res. 2009;15: 5308–16. doi:10.1158/1078-0432.CCR-07-5023
35. Sperandio S, de Belle I, Bredesen DE. An alternative, nonapoptotic form of programmed cell death. Proc Natl Acad Sci U S A. 2000;97: 14376–14381. doi:10.1073/pnas.97.26.14376
36. Sperandio S, Poksay K, de Belle I, Lafuente MJ, Liu B, Nasir J, et al. Paraptosis: mediation by MAP kinases and inhibition by AIP-1/Alix. Cell Death Differ. 2004;11: 1066–75. doi:10.1038/sj.cdd.4401465
37. Wang Y, Li X, Wang L, Ding P, Zhang Y, Han W, et al. An alternative form of paraptosis-like cell death, triggered by TAJ/TROY and enhanced by PDCD5 overexpression. J Cell Sci. 2004;117: 1525–32. doi:10.1242/jcs.00994
38. Kepp O, Galluzzi L, Lipinski M, Yuan J, Kroemer G. Cell death assays for drug discovery. Nat Rev Drug Discov. 2011;10: 221–37. doi:10.1038/nrd3373
39. Dixon SJ, Lemberg KM, Lamprecht MR, Skouta R, Zaitsev EM, Gleason CE, et al. Ferroptosis: An Iron-Dependent Form of Nonapoptotic Cell Death. Cell. 2012;149: 1060–1072. doi:10.1016/j.cell.2012.03.042
40. Yang WS, Sriramaratnam R, Welsch ME, Shimada K, Skouta R, Viswanathan VS, et al. Regulation of ferroptotic cancer cell death by GPX4. Cell. 2014;156: 317–331. doi:10.1016/j.cell.2013.12.010
41. Dixon SJ, Patel D, Welsch M, Skouta R, Lee E, Hayano M, et al. Pharmacological inhibition of cystine-glutamate exchange induces endoplasmic reticulum stress and ferroptosis. Elife. 2014;2014: 1–25. doi:10.7554/eLife.02523
42. Vanden Berghe T, Linkermann A, Jouan-Lanhouet S, Walczak H, Vandenabeele P. Regulated necrosis: the expanding network of non-apoptotic cell death pathways. Nat Rev Mol Cell Biol. Nature Publishing Group; 2014;15: 135–47. doi:10.1038/nrm3737
43. Kurz T, Gustafsson B, Brunk UT. Intralysosomal iron chelation protects against oxidative stress-induced cellular damage. FEBS J. 2006;273: 3106–3117. doi:10.1111/j.1742-4658.2006.05321.x
44. Gao M, Monian P, Quadri N, Ramasamy R, Jiang X. Glutaminolysis and Transferrin Regulate Ferroptosis. Mol Cell. Elsevier Inc.; 2015;59: 298–308. doi:10.1016/j.molcel.2015.06.011
45. Dixon SJ, Stockwell BR. The role of iron and reactive oxygen species in cell death. Nat Chem Biol. 2013;10: 9–17. doi:10.1038/nchembio.1416
46. Linkermann A, Skouta R, Himmerkus N, Mulay SR, Dewitz C, De Zen F, et al. Synchronized renal tubular cell death involves ferroptosis. Proc Natl Acad Sci. 2014;111: 16836–16841. doi:10.1073/pnas.1415518111
47. Sun X, Ou Z, Xie M, Kang R, Fan Y, Niu X, et al. HSPB1 as a novel regulator of ferroptotic cancer cell death. Oncogene. 2015; 1–9. doi:10.1038/onc.2015.32
48. Lonskaya I, Potaman VN, Shlyakhtenko LS, Oussatcheva E a., Lyubchenko YL, Soldatenkov V a. Regulation of poly(ADP-ribose) polymerase-1 by DNA structure-specific binding. J Biol Chem. 2005;280: 17076–17083. doi:10.1074/jbc.M413483200
49. Chiu LY, Ho FM, Shiah SG, Chang Y, Lin WW. Oxidative stress initiates DNA damager MNNG-induced poly(ADP-ribose) polymerase-1-dependent parthanatos cell death. Biochem Pharmacol. 2011;81: 459–470. doi:10.1016/j.bcp.2010.10.016
50. Fatokun AA, Dawson VL, Dawson TM. Parthanatos: mitochondrial-linked mechanisms and therapeutic opportunities. Br J Pharmacol. 2014;171: 2000–2016. doi:10.1111/bph.12416
51. Wang Y, Dawson VL, Dawson TM. Poly(ADP-ribose) signals to mitochondrial AIF: A key event in parthanatos. Exp Neurol. 2009;218: 193–202. doi:10.1016/j.expneurol.2009.03.020
52. Wang Y, Kim NS, Haince J-F, Kang HC, David KK, Andrabi S a, et al. Poly(ADP-ribose) (PAR) binding to apoptosis-inducing factor is critical for PAR polymerase-1-dependent cell death (parthanatos). Sci Signal. 2011;4: ra20. doi:10.1126/scisignal.2000902
53. Gerö D, Szabó C. Poly(ADP-ribose) polymerase: a new therapeutic target? Curr Opin Anaesthesiol. 2008;21: 111–21. doi:10.1097/ACO.0b013e3282f63c15

54. Cuevas BD, Abell a N, Johnson GL. Role of mitogen-activated protein kinase kinase kinases in signal integration. Oncogene. 2007;26: 3159–71. doi:10.1038/sj.onc.1210409
55. Morrison DK. MAP Kinase Pathways. Cold Spring Harb Perspect Biol. 2012;4: a011254–a011254. doi:10.1101/cshperspect.a011254
56. Qi M. MAP kinase pathways. J Cell Sci. 2005;118: 3569–3572. doi:10.1242/jcs.02470
57. Raman M, Chen W, Cobb MH. Differential regulation and properties of MAPKs. Oncogene. 2007;26: 3100–12. doi:10.1038/sj.onc.1210392
58. Wortzel I, Seger R. The ERK Cascade: Distinct Functions within Various Subcellular Organelles. Genes Cancer. 2011;2: 195–209. doi:10.1177/1947601911407328
59. Shaul YD, Seger R. The MEK/ERK cascade: From signaling specificity to diverse functions. Biochim Biophys Acta - Mol Cell Res. 2007;1773: 1213–1226. doi:10.1016/j.bbamcr.2006.10.005
60. Tanoue T, Nishida E. Molecular recognitions in the MAP kinase cascades. Cell Signal. 2003;15: 455–62. doi:10.1016/S0898-6568(02)00112-2
61. Bardwell L, Thorner J. A conserved motif at the amino termini of MEKs might mediate high-affinity interaction with the cognate MAPKs. Trends Biochem Sci. 1996;21: 373–4. doi:10.1016/0968-0004(96)30032-7
62. Cargnello M, Roux PP. Activation and function of the MAPKs and their substrates, the MAPK-activated protein kinases. Microbiol Mol Biol Rev. 2011;75: 50–83. doi:10.1128/MMBR.00031-10
63. Dérijard B, Hibi M, Wu IH, Barrett T, Su B, Deng T, et al. JNK1: a protein kinase stimulated by UV light and Ha-Ras that binds and phosphorylates the c-Jun activation domain. Cell. 1994;76: 1025–37. doi:10.1016/0092-8674(94)90380-8
64. Johnson GL, Nakamura K. The c-jun kinase/stress-activated pathway: regulation, function and role in human disease. Biochim Biophys Acta. 2007;1773: 1341–1348. doi:10.1016/j.bbamcr.2006.12.009
65. Kyriakis JM, Banerjee P, Nikolakaki E, Dai T, Rubie EA, Ahmad MF, et al. The stress-activated protein kinase subfamily of c-Jun kinases. Nature. 1994;369: 156–60. doi:10.1038/369156a0
66. Gupta S, Barrett T, Whitmarsh AJ, Cavanagh J, Sluss HK, Dérijard B, et al. Selective interaction of JNK protein kinase isoforms with transcription factors. EMBO J. 1996;15: 2760–70.
67. Bode AM, Dong Z. The functional contrariety of JNK. Mol Carcinog. 2007;46: 591–598. doi:10.1002/mc.20348
68. Bogoyevitch MA, Ngoei KRW, Zhao TT, Yeap YYC, Ng DCH. c-Jun N-terminal kinase (JNK) signaling: Recent advances and challenges. Biochim Biophys Acta - Proteins Proteomics. Elsevier B.V.; 2010;1804: 463–475. doi:10.1016/j.bbapap.2009.11.002
69. Lawler S, Fleming Y, Goedert M, Cohen P. Synergistic activation of SAPK1/JNK1 by two MAP kinase kinases in vitro. Curr Biol. 1996;8: 1387–90.
70. Kyriakis JM, Avruch J. Mammalian MAPK Signal Transduction Pathways Activated by Stress and Inflammation: A 10-Year Update. Physiol Rev. 2012;92: 689–737. doi:10.1152/physrev.00028.2011
71. Mizukami Y, Yoshioka K, Morimoto S, Yoshida K i. A novel mechanism of JNK1 activation. Nuclear translocation and activation of JNK1 during ischemia and reperfusion. J Biol Chem. 1997;272: 16657–62.
72. Davis RJ. Signal transduction by the JNK group of MAP kinases. Cell. 2000;103: 239–252. doi:10.1016/S0092-8674(00)00116-1
73. Chang L, Karin M. Mammalian MAP kinase signalling cascades. Nature. 2001;410: 37–40. doi:10.1038/35065000
74. Dhanasekaran DN, Johnson GL. MAPKs: function, regulation, role in cancer and therapeutic targeting. Oncogene. 2007;26: 3097–9. doi:10.1038/sj.onc.1210395
75. Huang G, Shi LZ, Chi H. Regulation of JNK and p38 MAPK in the immune system: Signal integration, propagation and termination. Cytokine. 2009;48: 161–169. doi:10.1016/j.cyto.2009.08.002
76. Rincón M, Davis RJ. Regulation of the immune response by stress-activated protein kinases. Immunol Rev. 2009;228: 212–24. doi:10.1111/j.1600-065X.2008.00744.x
77. Jaeschke A, Karasarides M, Ventura J, Ehrhardt A, Zhang C, Flavell RA, et al. JNK2 Is a Positive Regulator of the cJun Transcription Factor. Mol Cell. 2006;23: 899–911. doi:10.1016/j.molcel.2006.07.028
78. Sabapathy K, Hochedlinger K, Nam SY, Bauer A, Karin M, Wagner EF. Distinct roles for JNK1 and JNK2 in regulating JNK activity and c-Jun-dependent cell proliferation. Mol Cell. 2004;15: 713–25. doi:10.1016/j.molcel.2004.08.028
79. Turjanski AG, Vaqué JP, Gutkind JS. MAP kinases and the control of nuclear events. Oncogene. 2007;26: 3240–3253. doi:10.1038/sj.onc.1210415
80. Chen CY, Gherzi R, Andersen JS, Gaietta G, Jürchott K, Royer HD, et al. Nucleolin and YB-1 are required for JNK-mediated interleukin-2 mRNA stabilization during T-cell activation. Genes Dev. 2000;14: 1236–48.
81. Chen CY, Del Gatto-Konczak F, Wu Z, Karin M. Stabilization of interleukin-2 mRNA by the c-Jun NH2-terminal kinase pathway. Science. 1998;280: 1945–9. doi:10.1126/science.280.5371.1945
82. Ming XF, Kaiser M, Moroni C. c-jun N-terminal kinase is involved in AUUUA-mediated interleukin-3 mRNA turnover in mast cells. EMBO J. 1998;17: 6039–48. doi:10.1093/emboj/17.20.6039
83. Dhanasekaran DN, Reddy EP. JNK signaling in apoptosis. Oncogene. 2008;27: 6245–6251. doi:10.1038/onc.2008.301

84. Liu J, Lin A. Role of JNK activation in apoptosis: a double-edged sword. Cell Res. 2005;15: 36–42. doi:10.1038/sj.cr.7290262
85. Tournier C, Hess P, Yang DD, Xu J, Turner TK, Nimnual A, et al. Requirement of JNK for stress-induced activation of the cytochrome c-mediated death pathway. Science. 2000;288: 870–4. doi:10.1126/science.288.5467.870
86. Behrens A, Sibilia M, Wagner EF. Amino-terminal phosphorylation of c-Jun regulates stress-induced apoptosis and cellular proliferation. Nat Genet. 1999;21: 326–9. doi:10.1038/6854
87. Yang DD, Kuan CY, Whitmarsh AJ, Rincón M, Zheng TS, Davis RJ, et al. Absence of excitotoxicity-induced apoptosis in the hippocampus of mice lacking the Jnk3 gene. Nature. 1997;389: 865–70. doi:10.1038/39899
88. Verheij M, Bose R, Lin XH, Yao B, Jarvis WD, Grant S, et al. Requirement for ceramide-initiated SAPK/JNK signalling in stress-induced apoptosis. Nature. 1996;380: 75–9. doi:10.1038/380075a0
89. Wilson DJ, Fortner K a, Lynch DH, Mattingly RR, Macara IG, Posada J a, et al. JNK, but not MAPK, activation is associated with Fas-mediated apoptosis in human T cells. Eur J Immunol. 1996;26: 989–94. doi:10.1002/eji.1830260505
90. Zanke BW, Boudreau K, Rubie E, Winnett E, Tibbles L a, Zon L, et al. The stress-activated protein kinase pathway mediates cell death following injury induced by cis-platinum, UV irradiation or heat. Curr Biol. 1996;6: 606–13.
91. Fan M, Chambers TC. Role of mitogen-activated protein kinases in the response of tumor cells to chemotherapy. Drug Resist Updat. 2001;4: 253–267. doi:10.1054/drup.2001.0214
92. Fuchs SY, Fried VA, Ronai Z. Stress-activated kinases regulate protein stability. Oncogene. 1998;17: 1483–90. doi:10.1038/sj.onc.1202184
93. Oleinik N V, Krupenko NI, Krupenko SA. Cooperation between JNK1 and JNK2 in activation of p53 apoptotic pathway. Oncogene. 2007;26: 7222–7230. doi:10.1038/sj.onc.1210526
94. Lei K, Davis RJ. JNK phosphorylation of Bim-related members of the Bcl2 family induces Bax-dependent apoptosis. Proc Natl Acad Sci U S A. 2003;100: 2432–7. doi:10.1073/pnas.0438011100
95. Yamamoto K, Ichijo H, Korsmeyer SJ. BCL-2 is phosphorylated and inactivated by an ASK1/Jun N-terminal protein kinase pathway normally activated at G(2)/M. Mol Cell Biol. 1999;19: 8469–78.
96. Srivastava RK, Mi QS, Hardwick JM, Longo DL. Deletion of the loop region of Bcl-2 completely blocks paclitaxel-induced apoptosis. Proc Natl Acad Sci U S A. 1999;96: 3775–80. doi:10.1073/pnas.96.7.3775
97. Sánchez-Perez I, Murguía JR, Perona R. Cisplatin induces a persistent activation of JNK that is related to cell death. Oncogene. 1998;16: 533–40. doi:10.1038/sj.onc.1201578
98. Ebisuya M, Kondoh K, Nishida E. The duration, magnitude and compartmentalization of ERK MAP kinase activity: mechanisms for providing signaling specificity. J Cell Sci. 2005;118: 2997–3002. doi:10.1242/jcs.02505
99. Han J, Lee JD, Bibbs L, Ulevitch RJ. A MAP kinase targeted by endotoxin and hyperosmolarity in mammalian cells. Science. 1994;265: 808–11. doi:10.1126/science.7914033
100. Cuadrado A, Nebreda AR. Mechanisms and functions of p38 MAPK signalling. Biochem J. 2010;429: 403–17. doi:10.1042/BJ20100323
101. Jiang Y, Chen C, Li Z, Guo W, Gegner J a, Lin S, et al. Characterization of the structure and function of a new mitogen-activated protein kinase (p38beta). J Biol Chem. 1996;271: 17920–6. doi:10.1074/jbc.271.30.17920
102. Cuenda a, Cohen P. Stress-activated protein kinase-2/p38 and a rapamycin-sensitive pathway are required for C2C12 myogenesis. J Biol Chem. 1999;274: 4341–6. doi:10.1074/jbc.274.7.4341
103. Raingeaud J, Gupta S, Rogers JS, Dickens M, Han J, Ulevitch RJ, et al. Pro-inflammatory cytokines and environmental stress cause p38 mitogen-activated protein kinase activation by dual phosphorylation on tyrosine and threonine. J Biol Chem. 1995;270: 7420–6. doi:10.1074/jbc.270.13.7420
104. Goldsmith ZG, Dhanasekaran DN. G protein regulation of MAPK networks. Oncogene. 2007;26: 3122–3142. doi:10.1038/sj.onc.1210407
105. Bagrodia S, Dérijard B, Davis RJ, Cerione R a. Cdc42 and PAK-mediated signaling leads to Jun kinase and p38 mitogen-activated protein kinase activation. J Biol Chem. 1995;270: 27995–8.
106. Bradley JR, Pober JS. Tumor necrosis factor receptor-associated factors (TRAFs). Oncogene. 2001;20: 6482–91. doi:10.1038/sj.onc.1204788
107. Zarubin T, Han J. Activation and signaling of the p38 MAP kinase pathway. Cell Res. 2005;15: 11–18. doi:10.1038/sj.cr.7290257
108. Stein B, Brady H, Yang MX, Young DB, Barbosa MS. Cloning and characterization of MEK6, a novel member of the mitogen-activated protein kinase kinase cascade. J Biol Chem. 1996;271: 11427–33.
109. Brancho D, Tanaka N, Jaeschke A, Ventura J-J, Kelkar N, Tanaka Y, et al. Mechanism of p38 MAP kinase activation in vivo. Genes Dev. 2003;17: 1969–78. doi:10.1101/gad.1107303
110. Tanaka N, Kamanaka M, Enslen H, Dong C, Wysk M, Davis RJ, et al. Differential involvement of p38 mitogen-activated protein kinase kinases MKK3 and MKK6 in T-cell apoptosis. EMBO Rep. 2002;3: 785–91. doi:10.1093/embo-reports/kvf153
111. Wang L, Ma R, Flavell R a, Choi ME. Requirement of mitogen-activated protein kinase kinase 3 (MKK3) for activation of p38alpha and p38delta MAPK isoforms by TGF-beta 1 in murine mesangial cells. J Biol Chem. 2002;277: 47257–62. doi:10.1074/jbc.M208573200

112. Bellon S, Fitzgibbon MJ, Fox T, Hsiao HM, Wilson KP. The structure of phosphorylated p38gamma is monomeric and reveals a conserved activation-loop conformation. Structure. 1999;7: 1057–65. doi:10.1016/S0969-2126(99)80173-7
113. Dérijard B, Raingeaud J, Barrett T, Wu IH, Han J, Ulevitch RJ, et al. Independent human MAP-kinase signal transduction pathways defined by MEK and MKK isoforms. Science. 1995;267: 682–5. doi:10.1126/science.7839144
114. Wagner EF, Nebreda ÁR. Signal integration by JNK and p38 MAPK pathways in cancer development. Nat Rev Cancer. Nature Publishing Group; 2009;9: 537–549. doi:10.1038/nrc2694
115. Ben-Levy R, Hooper S, Wilson R, Paterson HF, Marshall CJ. Nuclear export of the stress-activated protein kinase p38 mediated by its substrate MAPKAP kinase-2. Curr Biol. 1998;8: 1049–57. doi:10.1016/S0960-9822(98)70442-7
116. Gaestel M. MAPKAP kinases - MKs - two's company, three's a crowd. Nat Rev Mol Cell Biol. 2006;7: 120–30. doi:10.1038/nrm1834
117. Morrison DK, Davis RJ. Regulation of MAP kinase signaling modules by scaffold proteins in mammals. Annu Rev Cell Dev Biol. 2003;19: 91–118. doi:10.1146/annurev.cellbio.19.111401.091942
118. Cuenda A, Cohen P, Buée-Scherrer V, Goedert M. Activation of stress-activated protein kinase-3 (SAPK3) by cytokines and cellular stresses is mediated via SAPKK3 (MKK6); comparison of the specificities of SAPK3 and SAPK2 (RK/p38). EMBO J. 1997;16: 295–305. doi:10.1093/emboj/16.2.295
119. Goedert M, Cuenda A, Craxton M, Jakes R, Cohen P. Activation of the novel stress-activated protein kinase SAPK4 by cytokines and cellular stresses is mediated by SKK3 (MKK6); comparison of its substrate specificity with that of other SAP kinases. EMBO J. 1997;16: 3563–71. doi:10.1093/emboj/16.12.3563
120. Kim C, Sano Y, Todorova K, Carlson B a, Arpa L, Celada A, et al. The kinase p38 alpha serves cell type-specific inflammatory functions in skin injury and coordinates pro- and anti-inflammatory gene expression. Nat Immunol. 2008;9: 1019–27. doi:10.1038/ni.1640
121. Lee JC, Laydon JT, McDonnell PC, Gallagher TF, Kumar S, Green D, et al. A protein kinase involved in the regulation of inflammatory cytokine biosynthesis. Nature. 1994. pp. 739–7346. doi:10.1038/372739a0
122. Kuma Y, Campbell DG, Cuenda A. Identification of glycogen synthase as a new substrate for stress-activated protein kinase 2b/p38beta. Biochem J. 2004;379: 133–9. doi:10.1042/BJ20031559
123. Roux PP, Blenis J. ERK and p38 MAPK-Activated Protein Kinases: a Family of Protein Kinases with Diverse Biological Functions. Microbiol Mol Biol Rev. 2004;68: 320–344. doi:10.1128/MMBR.68.2.320-344.2004
124. Adams RH, Porras A, Alonso G, Jones M, Vintersten K, Panelli S, et al. Essential role of p38alpha MAP kinase in placental but not embryonic cardiovascular development. Mol Cell. 2000;6: 109–116. doi:10.1016/S1097-2765(05)00014-6
125. Engel FB, Schebesta M, Duong MT, Lu G, Ren S, Madwed JB, et al. p38 MAP kinase inhibition enables proliferation of adult mammalian cardiomyocytes. Genes Dev. 2005;19: 1175–87. doi:10.1101/gad.1306705
126. Nishida K, Yamaguchi O, Hirotani S, Hikoso S, Higuchi Y, Watanabe T, et al. p38 Mitogen-Activated Protein Kinase Plays a Critical Role in Cardiomyocyte Survival but Not in Cardiac Hypertrophic Growth in Response to Pressure Overload. Mol Cell Biol. 2004;24: 10611–10620. doi:10.1128/MCB.24.24.10611-10620.2004
127. Thornton TM, Rincon M. Non-classical p38 map kinase functions: cell cycle checkpoints and survival. Int J Biol Sci. 2009;5: 44–51. doi:10.7150/ijbs.5.44
128. Todd DE, Densham RM, Molton S a, Balmanno K, Newson C, Weston CR, et al. ERK1/2 and p38 cooperate to induce a p21CIP1-dependent G1 cell cycle arrest. Oncogene. 2004;23: 3284–95. doi:10.1038/sj.onc.1207467
129. Bulavin D V, Higashimoto Y, Popoff IJ, Gaarde W a, Basrur V, Potapova O, et al. Initiation of a G2/M checkpoint after ultraviolet radiation requires p38 kinase. Nature. 2001;411: 102–7. doi:10.1038/35075107
130. Puri PL, Wu Z, Zhang P, Wood LD, Bhakta KS, Han J, et al. Induction of terminal differentiation by constitutive activation of p38 MAP kinase in human rhabdomyosarcoma cells. Genes Dev. 2000;14: 574–84.
131. Lemke LE, Bloem LJ, Fouts R, Esterman M, Sandusky G, Vlahos CJ. Decreased p38 MAPK activity in end-stage failing human myocardium: p38 MAPK alpha is the predominant isoform expressed in human heart. J Mol Cell Cardiol. 2001;33: 1527–40. doi:10.1006/jmcc.2001.1415
132. Perdiguero E, Ruiz-Bonilla V, Gresh L, Hui L, Ballestar E, Sousa-Victor P, et al. Genetic analysis of p38 MAP kinases in myogenesis: fundamental role of p38α in abrogating myoblast proliferation. EMBO J. 2007;26: 1245–1256. doi:10.1038/sj.emboj.7601587
133. Eckert RL, Efimova T, Balasubramanian S, Crish JF, Bone F, Dashti S. p38 Mitogen-activated protein kinases on the body surface--a function for p38 delta. J Invest Dermatol. 2003;120: 823–8. doi:10.1046/j.1523-1747.2003.12120.x
134. Bogoyevitch MA, Gillespie-Brown J, Ketterman AJ, Fuller SJ, Ben-Levy R, Ashworth A, et al. Stimulation of the Stress-Activated Mitogen-Activated Protein Kinase Subfamilies in Perfused Heart: p38/RK Mitogen-Activated Protein Kinases and c-Jun N-Terminal Kinases Are Activated by Ischemia/Reperfusion. Circ Res. 1996;79: 162–173. doi:10.1161/01.RES.79.2.162

135. Cook S a, Sugden PH, Clerk A. Activation of c-Jun N-terminal kinases and p38-mitogen-activated protein kinases in human heart failure secondary to ischaemic heart disease. J Mol Cell Cardiol. 1999;31: 1429–34. doi:10.1006/jmcc.1999.0979
136. Kim JK, Pedram A, Razandi M, Levin ER. Estrogen prevents cardiomyocyte apoptosis through inhibition of reactive oxygen species and differential regulation of p38 kinase isoforms. J Biol Chem. 2006;281: 6760–7. doi:10.1074/jbc.M511024200
137. Capano M, Crompton M. Bax translocates to mitochondria of heart cells during simulated ischaemia: involvement of AMP-activated and p38 mitogen-activated protein kinases. Biochem J. 2006;395: 57–64. doi:10.1042/BJ20051654
138. Cuenda A, Rousseau S. p38 MAP-kinases pathway regulation, function and role in human diseases. Biochim Biophys Acta. 2007;1773: 1358–75. doi:10.1016/j.bbamcr.2007.03.010
139. Guay J, Lambert H, Gingras-Breton G, Lavoie JN, Huot J, Landry J. Regulation of actin filament dynamics by p38 map kinase-mediated phosphorylation of heat shock protein 27. J Cell Sci. 1997;110 (Pt 3: 357–68.
140. Hoover HE, Thuerauf DJ, Martindale JJ, Glembotski CC. alpha B-crystallin gene induction and phosphorylation by MKK6-activated p38. A potential role for alpha B-crystallin as a target of the p38 branch of the cardiac stress response. J Biol Chem. 2000;275: 23825–33. doi:10.1074/jbc.M003864200
141. Sumida T. Temporary blockade of contractility during reperfusion elicits a cardioprotective effect of the p38 MAP kinase inhibitor SB-203580. AJP Hear Circ Physiol. 2005;288: H2726–H2734. doi:10.1152/ajpheart.01183.2004
142. Xia Z, Dickens M, Raingeaud J, Davis RJ, Greenberg ME. Opposing effects of ERK and JNK-p38 MAP kinases on apoptosis. Science. 1995;270: 1326–31. doi:10.1126/science.270.5240.1326
143. English J, Pearson G, Wilsbacher J, Swantek J, Karandikar M, Xu S, et al. New insights into the control of MAP kinase pathways. Exp Cell Res. 1999;253: 255–70. doi:10.1006/excr.1999.4687
144. Wellbrock C, Karasarides M, Marais R. The RAF proteins take centre stage. Nat Rev Mol Cell Biol. 2004;5: 875–885. doi:10.1038/nrm1498
145. Chong H, Vikis HG, Guan K-L. Mechanisms of regulating the Raf kinase family. Cell Signal. 2003;15: 463–469. doi:10.1016/S0898-6568(02)00139-0
146. O'Neill E, Kolch W. Conferring specificity on the ubiquitous Raf/MEK signalling pathway. Br J Cancer. 2004;90: 283–8. doi:10.1038/sj.bjc.6601488
147. Kolch W. Meaningful relationships: the regulation of the Ras/Raf/MEK/ERK pathway by protein interactions. Biochem J. 2000;351 Pt 2: 289–305.
148. Provot S, Nachtrab G, Paruch J, Chen AP, Silva A, Kronenberg HM. A-raf and B-raf are dispensable for normal endochondral bone development, and parathyroid hormone-related peptide suppresses extracellular signal-regulated kinase activation in hypertrophic chondrocytes. Mol Cell Biol. 2008;28: 344–357. doi:10.1128/MCB.00617-07
149. Gotoh Y, Nishida E. Activation mechanism and function of the MAP kinase cascade. Mol Reprod Dev. 1995;42: 486–492. doi:10.1002/mrd.1080420417
150. Papin C, Denouel-Galy A, Laugier D, Calothy G, Eychène A. Modulation of kinase activity and oncogenic properties by alternative splicing reveals a novel regulatory mechanism for B-Raf. J Biol Chem. 1998;273: 24939–47.
151. Lange-Carter C a, Pleiman CM, Gardner a M, Blumer KJ, Johnson GL. A divergence in the MAP kinase regulatory network defined by MEK kinase and Raf. Science. 1993;260: 315–9. doi:10.1126/science.8385802
152. Zheng CF, Guan KL. Properties of MEKs, the kinases that phosphorylate and activate the extracellular signal-regulated kinases. J Biol Chem. 1993;268: 23933–9.
153. Chen Z, Gibson TB, Robinson F, Silvestro L, Pearson G, Xu BE, et al. MAP Kinases. Chem Rev. 2001;101: 2449–2476. doi:10.1021/cr000241p
154. Alessandrini A, Brott BK, Erikson RL. Differential expression of MEK1 and MEK2 during mouse development. Cell Growth Differ. 1997;8: 505–11.
155. Shaul YD, Gibor G, Plotnikov A, Seger R. Specific phosphorylation and activation of ERK1c by MEK1b: a unique route in the ERK cascade. Genes Dev. 2009;23: 1779–90. doi:10.1101/gad.523909
156. Barnier J V, Papin C, Eychène A, Lecoq O, Calothy G. The mouse B-raf gene encodes multiple protein isoforms with tissue-specific expression. J Biol Chem. 1995;270: 23381–9.
157. Papin C, Denouel-Galy A, Laugier D, Calothy G, Eychène A. Modulation of kinase activity and oncogenic properties by alternative splicing reveals a novel regulatory mechanism for B-Raf. J Biol Chem. 1998;273: 24939–24947. doi:10.1074/jbc.273.38.24939
158. Seger R, Seger D, Lozeman FJ, Ahn NG, Graves LM, Campbell JS, et al. Human T-cell mitogen-activated protein kinase kinases are related to yeast signal transduction kinases. J Biol Chem. 1992;267: 25628–31.
159. Shaul YD, Gibor G, Plotnikov A, Seger R. Specific phosphorylation and activation of ERK1c by MEK1b: A unique route in the ERK cascade. Genes Dev. 2009;23: 1779–1790. doi:10.1101/gad.523909
160. Yung Y, Yao Z, Hanoch T, Seger R. ERK1b, a 46-kDa ERK isoform that is differentially regulated by MEK. J Biol Chem. 2000;275: 15799–808. doi:10.1074/jbc.M910060199
161. Aebersold DM, Shaul YD, Yung Y, Yarom N, Yao Z, Hanoch T, et al. Extracellular signal-regulated kinase 1c (ERK1c), a novel 42-kilodalton ERK, demonstrates unique modes of regulation, localization, and function. Mol Cell Biol. 2004;24: 10000–15. doi:10.1128/MCB.24.22.10000-10015.2004

162. Gonzalez F a, Raden DL, Rigby MR, Davis RJ. Heterogeneous expression of four MAP kinase isoforms in human tissues. FEBS Lett. 1992;304: 170–8. doi:0014-5793(92)80612-K [pii]
163. Naor Z, Benard O, Seger R. Activation of MAPK cascades by G-protein-coupled receptors: the case of gonadotropin-releasing hormone receptor. Trends Endocrinol Metab. 2000;11: 91–9. doi:10.1016/S1043-2760(99)00232-5
164. Pierce KL, Luttrell LM, Lefkowitz RJ. New mechanisms in heptahelical receptor signaling to mitogen activated protein kinase cascades. Oncogene. 2001;20: 1532–1539. doi:10.1038/sj.onc.1204184
165. Marmor MD, Skaria KB, Yarden Y. Signal transduction and oncogenesis by ErbB/HER receptors. Int J Radiat Oncol Biol Phys. 2004;58: 903–913. doi:10.1016/j.ijrobp.2003.06.002
166. McKay MM, Morrison DK. Integrating signals from RTKs to ERK/MAPK. Oncogene. 2007;26: 3113–21. doi:10.1038/sj.onc.1210394
167. Downward J. Control of ras activation. Cancer Surv. 1996;27: 87–100.
168. Lynch SJ, Snitkin H, Gumper I, Philips MR, Sabatini D, Pellicer A. The differential palmitoylation states of N-Ras and H-Ras determine their distinct Golgi subcompartment localizations. J Cell Physiol. 2015;230: 610–9. doi:10.1002/jcp.24779
169. Wright LP, Philips MR. CAAX modification and membrane targeting of Ras. J Lipid Res. 2006;47: 883–91. doi:10.1194/jlr.R600004-JLR200
170. Salaun C, Greaves J, Chamberlain LH. The intracellular dynamic of protein palmitoylation. J Cell Biol. 2010;191: 1229–38. doi:10.1083/jcb.201008160
171. Philips MR. Compartmentalized signalling of Ras. Biochem Soc Trans. 2005;33: 657–61. doi:10.1042/BST0330657
172. Chiu VK, Bivona T, Hach A, Sajous JB, Silletti J, Wiener H, et al. Ras signalling on the endoplasmic reticulum and the Golgi. Nat Cell Biol. 2002;4: 343–350. doi:10.1038/ncb783
173. Zimmermann S. Phosphorylation and Regulation of Raf by Akt (Protein Kinase B). Science (80-). 1999;286: 1741–1744. doi:10.1126/science.286.5445.1741
174. Leevers SJ, Paterson HF, Marshall CJ. Requirement for Ras in Raf activation is overcome by targeting Raf to the plasma membrane. Nature. 1994;369: 411–414. doi:10.1038/369411a0
175. Dhillon AS, Meikle S, Yazici Z, Eulitz M, Kolch W. Regulation of Raf-1 activation and signalling by dephosphorylation. EMBO J. 2002;21: 64–71.
176. Diaz B, Barnard D, Filson A, MacDonald S, King A, Marshall M. Phosphorylation of Raf-1 serine 338-serine 339 is an essential regulatory event for Ras-dependent activation and biological signaling. Mol Cell Biol. 1997;17: 4509–16.
177. King a J, Sun H, Diaz B, Barnard D, Miao W, Bagrodia S, et al. The protein kinase Pak3 positively regulates Raf-1 activity through phosphorylation of serine 338. Nature. 1998;396: 180–183. doi:10.1038/35019122
178. Fabian JR, Daar IO, Morrison DK. Critical tyrosine residues regulate the enzymatic and biological activity of Raf-1 kinase. Mol Cell Biol. 1993;13: 7170–9. doi:10.1128/MCB.13.11.7170.Updated
179. Zheng CF, Guan KL. Activation of MEK family kinases requires phosphorylation of two conserved Ser/Thr residues. EMBO J. 1994;13: 1123–1131.
180. Alessi DR, Saito Y, Campbell DG, Cohen P, Sithanandam G, Rapp U, et al. Identification of the sites in MAP kinase kinase-1 phosphorylated by p74raf-1. EMBO J. 1994;13: 1610–9.
181. Eblen ST, Slack-Davis JK, Tarcsafalvi A, Parsons JT, Weber MJ, Catling AD. Mitogen-activated protein kinase feedback phosphorylation regulates MEK1 complex formation and activation during cellular adhesion. Mol Cell Biol. 2004;24: 2308–2317. doi:10.1128/MCB.24.6.2308-2317.2004
182. Slack-Davis JK, Eblen ST, Zecevic M, Boerner SA, Tarcsafalvi A, Diaz HB, et al. PAK1 phosphorylation of MEK1 regulates fibronectin-stimulated MAPK activation. J Cell Biol. 2003;162: 281–91. doi:10.1083/jcb.200212141
183. Cobb MH, Goldsmith EJ. How MAP kinases are regulated. J Biol Chem. 1995;270: 14843–14846. doi:10.1074/jbc.270.25.14843
184. Payne DM, Rossomando a J, Martino P, Erickson a K, Her JH, Shabanowitz J, et al. Identification of the regulatory phosphorylation sites in pp42/mitogen-activated protein kinase (MAP kinase). EMBO J. 1991;10: 885–892.
185. Yoon S, Seger R. The extracellular signal-regulated kinase: multiple substrates regulate diverse cellular functions. Growth Factors. 2006;24: 21–44. doi:10.1080/02699050500284218
186. Lenormand P, Sardet C, Pagès G, L'Allemain G, Brunet A, Pouysségur J. Growth factors induce nuclear translocation of MAP kinases (p42mapk and p44mapk) but not of their activator MAP kinase kinase (p45mapkk) in fibroblasts. J Cell Biol. 1993;122: 1079–88. doi:10.1083/jcb.122.5.1079
187. Chen RH, Sarnecki C, Blenis J. Nuclear localization and regulation of erk- and rsk-encoded protein kinases. Mol Cell Biol. 1992;12: 915–927. doi:10.1128/MCB.12.3.915
188. Yao Z, Flash I, Raviv Z, Yung Y, Asscher Y, Pleban S, et al. Non-regulated and stimulated mechanisms cooperate in the nuclear accumulation of MEK1. Oncogene. 2001;20: 7588–7596. doi:10.1038/sj.onc.1204963
189. Gonzalez F a., Raden DL, Davis RJ. Identification of substrate recognition determinants for human ERK1 and ERK2 protein kinases. J Biol Chem. 1991;266: 22159–22163.
190. von Kriegsheim A, Baiocchi D, Birtwistle M, Sumpton D, Bienvenut W, Morrice N, et al. Cell fate decisions are specified by the dynamic ERK interactome. Nat Cell Biol. Nature Publishing Group; 2009;11: 1458–64. doi:10.1038/ncb1994

191. Marchetti S, Gimond C, Chambard J-C, Touboul T, Roux D, Pouysségur J, et al. Extracellular signal-regulated kinases phosphorylate mitogen-activated protein kinase phosphatase 3/DUSP6 at serines 159 and 197, two sites critical for its proteasomal degradation. Mol Cell Biol. 2005;25: 854–64. doi:10.1128/MCB.25.2.854-864.2005
192. Okazaki K, Sagata N. The Mos/MAP kinase pathway stabilizes c-Fos by phosphorylation and augments its transforming activity in NIH 3T3 cells. EMBO J. 1995;14: 5048–59.
193. Plotnikov A, Zehorai E, Procaccia S, Seger R. The MAPK cascades: signaling components, nuclear roles and mechanisms of nuclear translocation. Biochim Biophys Acta. Elsevier B.V.; 2011;1813: 1619–33. doi:10.1016/j.bbamcr.2010.12.012
194. Bononi A, Agnoletto C, De Marchi E, Marchi S, Patergnani S, Bonora M, et al. Protein kinases and phosphatases in the control of cell fate. Enzym Res. 2011;2011: 329098. doi:10.4061/2011/329098
195. Fey D, Croucher DR, Kolch W, Kholodenko BN. Crosstalk and signaling switches in mitogen-activated protein kinase cascades. Front Physiol. 2012;3: 355. doi:10.3389/fphys.2012.00355
196. Chuderland D, Konson A, Seger R. Identification and characterization of a general nuclear translocation signal in signaling proteins. Mol Cell. 2008;31: 850–61. doi:10.1016/j.molcel.2008.08.007
197. Bendetz-Nezer S, Seger R. Role of non-phosphorylated activation loop residues in determining ERK2 dephosphorylation, activity, and subcellular localization. J Biol Chem. 2007;282: 25114–25122. doi:10.1074/jbc.M703120200
198. Marshall CJ. Specificity of receptor tyrosine kinase signaling: transient versus sustained extracellular signal-regulated kinase activation. Cell. 1995;80: 179–185. doi:10.1016/0092-8674(95)90401-8
199. Alessi DR, Gomez N, Moorhead G, Lewis T, Keyse SM, Cohen P. Inactivation of p42 MAP kinase by protein phosphatase 2A and a protein tyrosine phosphatase, but not CL100, in various cell lines. Curr Biol. 1995;5: 283–295. doi:S0960-9822(95)00059-5 [pii]
200. Tárrega C, Blanco-Aparicio C, Muñoz JJ, Pulido R, Tarrega C, Munoz JJ. Two clusters of residues at the docking groove of mitogen-activated protein kinases differentially mediate their functional interaction with the tyrosine phosphatases PTP-SL and STEP. J Biol Chem. 2002;277: 2629–2636. doi:10.1074/jbc.M108874200
201. Muñoz JJ, Tárrega C, Blanco-Aparicio C, Pulido R. Differential interaction of the tyrosine phosphatases PTP-SL, STEP and HePTP with the mitogen-activated protein kinases ERK1/2 and p38alpha is determined by a kinase specificity sequence and influenced by reducing agents. Biochem J. 2003;372: 193–201. doi:10.1042/BJ20021941
202. Pettiford SM, Herbst R. The MAP-kinase ERK2 is a specific substrate of the protein tyrosine phosphatase HePTP. Oncogene. 2000;19: 858–69. doi:10.1038/sj.onc.1203408
203. Camps M, Nichols A, Arkinstall S. Dual specificity phosphatases: a gene family for control of MAP kinase function. FASEB J. 2000;14: 6–16.
204. Karlsson M, Mandl M, Keyse SM. Spatio-temporal regulation of mitogen-activated protein kinase (MAPK) signalling by protein phosphatases. Biochem Soc Trans. 2006;34: 842–845. doi:BST0340842 [pii]\n10.1042/BST0340842
205. Caunt CJ, Keyse SM. Dual-specificity MAP kinase phosphatases (MKPs): Shaping the outcome of MAP kinase signalling. FEBS J. 2013;280: 489–504. doi:10.1111/j.1742-4658.2012.08716.x
206. Brondello JM, Brunet A, Pouysségur J, McKenzie FR. The dual specificity mitogen-activated protein kinase phosphatase-1 and -2 are induced by the p42/p44(MAPK) cascade. J Biol Chem. 1997;272: 1368–1376. doi:10.1074/jbc.272.2.1368
207. Brondello JM, Pouysségur J, McKenzie FR. Reduced MAP kinase phosphatase-1 degradation after p42/p44MAPK-dependent phosphorylation. Science (80-). 1999;286: 2514–2517. doi:8131 [pii]
208. Volmat V, Camps M, Arkinstall S, Pouysségur J, Lenormand P. The nucleus, a site for signal termination by sequestration and inactivation of p42/p44 MAP kinases. J Cell Sci. 2001;114: 3433–3443.
209. Stork PJS, Schmitt JM. Crosstalk between cAMP and MAP kinase signaling in the regulation of cell proliferation. Trends Cell Biol. 2002;12: 258–66. doi:10.1016/S0962-8924(02)02294-8
210. Gerits N, Kostenko S, Shiryaev A, Johannessen M, Moens U. Relations between the mitogen-activated protein kinase and the cAMP-dependent protein kinase pathways: comradeship and hostility. Cell Signal. 2008;20: 1592–607. doi:10.1016/j.cellsig.2008.02.022
211. Kao S, Jaiswal RK, Kolch W, Landreth GE. Identification of the mechanisms regulating the differential activation of the mapk cascade by epidermal growth factor and nerve growth factor in PC12 cells. J Biol Chem. 2001;276: 18169–77. doi:10.1074/jbc.M008870200
212. Vaudry D, Stork PJS, Lazarovici P, Eiden LE. Signaling pathways for PC12 cell differentiation: making the right connections. Science. 2002;296: 1648–9. doi:10.1126/science.1071552
213. Santos SDM, Verveer PJ, Bastiaens PIH. Growth factor-induced MAPK network topology shapes Erk response determining PC-12 cell fate. Nat Cell Biol. 2007;9: 324–330. doi:10.1038/ncb1543
214. Enserink JM, Christensen AE, de Rooij J, van Triest M, Schwede F, Genieser HG, et al. A novel Epac-specific cAMP analogue demonstrates independent regulation of Rap1 and ERK. Nat Cell Biol. 2002;4: 901–906. doi:10.1038/ncb874
215. Smith FD, Langeberg LK, Cellurale C, Pawson T, Morrison DK, Davis RJ, et al. AKAP-Lbc enhances cyclic AMP control of the ERK1/2 cascade. Nat Cell Biol. 2010;12: 1242–9. doi:10.1038/ncb2130
216. Qi Y, Ge H. Modularity and dynamics of cellular networks. PLoS Computational Biology. 2006. pp. 1502–1510. doi:10.1371/journal.pcbi.0020174

217. Alexander RP, Kim PM, Emonet T, Gerstein MB. Understanding modularity in molecular networks requires dynamics. Sci Signal. 2009;2: pe44. doi:10.1126/scisignal.281pe44
218. Shin S-YS-Y, Rath O, Choo S-MS-M, Fee F, McFerran B, Kolch W, et al. Positive- and negative-feedback regulations coordinate the dynamic behavior of the Ras-Raf-MEK-ERK signal transduction pathway. J Cell Sci. 2009;122: 425–435. doi:10.1242/jcs.036319
219. Fujita Y, Komatsu N, Matsuda M, Aoki K. Fluorescence resonance energy transfer based quantitative analysis of feedforward and feedback loops in epidermal growth factor receptor signaling and the sensitivity to molecular targeting drugs. 2014;281: 3177–3192. doi:10.1111/febs.12852
220. Sasagawa S, Ozaki Y, Fujita K, Kuroda S. Prediction and validation of the distinct dynamics of transient and sustained ERK activation. Nat Cell Biol. 2005;7: 365–73. doi:10.1038/ncb1233
221. Purvis JE, Lahav G. Encoding and decoding cellular information through signaling dynamics. Cell. 2013;152: 945–956. doi:10.1016/j.cell.2013.02.005
222. Kholodenko BN, Hancock JF, Kolch W. Signalling ballet in space and time. Nat Rev Mol Cell Biol. 2010;11: 414–26. doi:10.1038/nrm2901
223. Sapkota GP, Cummings L, Newell FS, Armstrong C, Bain J, Frodin M, et al. BI-D1870 is a specific inhibitor of the p90 RSK (ribosomal S6 kinase) isoforms in vitro and in vivo. Biochem J. 2007;401: 29–38. doi:10.1042/BJ20061088
224. Roux PP, Ballif B a, Anjum R, Gygi SP, Blenis J. Tumor-promoting phorbol esters and activated Ras inactivate the tuberous sclerosis tumor suppressor complex via p90 ribosomal S6 kinase. Proc Natl Acad Sci U S A. 2004;101: 13489–13494. doi:10.1073/pnas.0405659101
225. Karbowniczek M, Robertson GP, Henske EP. Rheb inhibits C-raf activity and B-raf/C-raf heterodimerization. J Biol Chem. 2006;281: 25447–56. doi:10.1074/jbc.M605273200
226. Aksamitiene E, Achanta S, Kolch W, Kholodenko BN, Hoek JB, Kiyatkin A. Prolactin-stimulated activation of ERK1/2 mitogen-activated protein kinases is controlled by PI3-kinase/Rac/PAK signaling pathway in breast cancer cells. Cell Signal. 2011;23: 1794–805. doi:10.1016/j.cellsig.2011.06.014
227. Yang HW, Shin M-G, Lee S, Kim J-R, Park WS, Cho K-H, et al. Cooperative activation of PI3K by Ras and Rho family small GTPases. Mol Cell. 2012;47: 281–90. doi:10.1016/j.molcel.2012.05.007
228. Sato K, Shin M-S, Sakimura A, Zhou Y, Tanaka T, Kawanishi M, et al. Inverse correlation between Thr-669 and constitutive tyrosine phosphorylation in the asymmetric epidermal growth factor receptor dimer conformation. Cancer Sci. 2013;104: 1315–22. doi:10.1111/cas.12225
229. Dougherty MK, Müller J, Ritt D a., Zhou M, Zhou XZ, Copeland TD, et al. Regulation of Raf-1 by direct feedback phosphorylation. Mol Cell. 2005;17: 215–224. doi:10.1016/j.molcel.2004.11.055
230. Brunet A, Pagès G, Pouysségur J. Growth factor-stimulated MAP kinase induces rapid retrophosphorylation and inhibition of MAP kinase kinase (MEK1). FEBS Lett. 1994;346: 299–303. doi:10.1016/0014-5793(94)00475-7
231. Ma L, Chen Z, Erdjument-Bromage H, Tempst P, Pandolfi PP. Phosphorylation and functional inactivation of TSC2 by Erk implications for tuberous sclerosis and cancer pathogenesis. Cell. 2005;121: 179–93. doi:10.1016/j.cell.2005.02.031
232. Gureasko J, Galush WJ, Boykevisch S, Sondermann H, Bar-Sagi D, Groves JT, et al. Membrane-dependent signal integration by the Ras activator Son of sevenless. Nat Struct Mol Biol. 2008;15: 452–461. doi:10.1038/nsmb0608-651a
233. Yu W, Fantl WJ, Harrowe G, Williams LT. Regulation of the MAP kinase pathway by mammalian Ksr through direct interaction with MEK and ERK. Curr Biol. 1998;8: 56–64. doi:10.1016/S0960-9822(98)70020-X
234. Fukuda M, Gotoh Y, Nishida E. Interaction of MAP kinase with MAP kinase kinase: its possible role in the control of nucleocytoplasmic transport of MAP kinase. EMBO J. 1997;16: 1901–8. doi:10.1093/emboj/16.8.1901
235. Fukuda M, Gotoh I, Gotoh Y, Nishida E. Cytoplasmic Localization of Mitogen-activated Protein Kinase Kinase Directed by Its NH 2 -terminal, Leucine-rich Short Amino Acid Sequence, Which Acts as a Nuclear Export Signal*. Biochemistry. 1996;271: 20024 –20028. doi:10.1074/jbc.271.33.20024
236. Furuno T, Hirashima N, Onizawa S, Sagiya N, Nakanishi M. Nuclear shuttling of mitogen-activated protein (MAP) kinase (extracellular signal-regulated kinase (ERK) 2) was dynamically controlled by MAP/ERK kinase after antigen stimulation in RBL-2H3 cells. J Immunol. 2001;166: 4416–21. doi:10.4049/jimmunol.166.7.4416
237. Adachi M, Fukuda M, Nishida E. Nuclear export of MAP kinase (ERK) involves a MAP kinase kinase (MEK)-dependent active transport mechanism. J Cell Biol. 2000;148: 849–56. doi:10.1083/jcb.148.5.849
238. Pouysségur J, Volmat V, Lenormand P. Fidelity and spatio-temporal control in MAP kinase (ERKs) signalling. Biochem Pharmacol. 2002;64: 755–763. doi:10.1016/S0006-2952(02)01135-8
239. Fujioka A, Terai K, Itoh RE, Aoki K, Nakamura T, Kuroda S, et al. Dynamics of the Ras/ERK MAPK cascade as monitored by fluorescent probes. J Biol Chem. 2006;281: 8917–26. doi:10.1074/jbc.M509344200
240. Sturm OE, Orton R, Grindlay J, Birtwistle M, Vyshemirsky V, Gilbert D, et al. The mammalian MAPK/ERK pathway exhibits properties of a negative feedback amplifier. Sci Signal. 2010;3: ra90. doi:10.1126/scisignal.2001212
241. Formstecher E, Ramos JW, Fauquet M, Calderwood D a., Hsieh JC, Canton B, et al. PEA-15 Mediates Cytoplasmic Sequestration of ERK MAP Kinase. Dev Cell. 2001;1: 239–250. doi:10.1016/S1534-5807(01)00035-1

242. Schaeffer HJ, Catling a D, Eblen ST, Collier LS, Krauss a, Weber MJ. MP1: a MEK binding partner that enhances enzymatic activation of the MAP kinase cascade. Science. 1998;281: 1668–1671. doi:10.1126/science.281.5383.1668
243. Galli S, Jahn O, Hitt R, Hesse D, Opitz L, Plessmann U, et al. A new paradigm for MAPK: Structural interactions of hERK1 with mitochondria in HeLa cells. PLoS One. 2009;4. doi:10.1371/journal.pone.0007541
244. Torii S, Kusakabe M, Yamamoto T, Maekawa M, Nishida E. Sef Is a Spatial Regulator for Ras / MAP Kinase Signaling. Dev Cell. 2004;7: 33–44.
245. Chuderland D, Seger R. Protein-protein interactions in the regulation of the extracellular signal-regulated kinase. Mol Biotechnol. 2005;29: 57–74. doi:10.1385/MB:29:1:57
246. Burkhard KA, Chen F, Shapiro P. Quantitative analysis of ERK2 interactions with substrate proteins: roles for kinase docking domains and activity in determining binding affinity. J Biol Chem. 2011;286: 2477–85. doi:10.1074/jbc.M110.177899
247. Sharrocks AD, Yang SH, Galanis A. Docking domains and substrate-specificity determination for MAP kinases. Trends in Biochemical Sciences. 2000. pp. 448–453. doi:10.1016/S0968-0004(00)01627-3
248. Tanoue T, Adachi M, Moriguchi T, Nishida E. A conserved docking motif in MAP kinases common to substrates, activators and regulators. Nat Cell Biol. 2000;2: 110–116. doi:10.1038/35000065
249. Lee T, Hoofnagle AN, Kabuyama Y, Stroud J, Min X, Goldsmith EJ, et al. Docking motif interactions in Map kinases revealed by hydrogen exchange mass spectrometry. Mol Cell. 2004;14: 43–55. doi:10.1016/S1097-2765(04)00161-3
250. Rubinfeld H, Hanoch T, Seger R. Identification of a Cytoplasmic- Retention Sequence in ERK2 *. 1999; 30349–30352. doi:10.1074/jbc.274.43.30349
251. Wolf I, Rubinfeld H, Yoon S, Marmor G, Hanoch T, Seger R. Involvement of the Activation Loop of ERK in the Detachment from Cytosolic Anchoring. J Biol Chem. 2001;276: 24490–24497. doi:10.1074/jbc.M103352200
252. Reszka a a, Bulinski JC, Krebs EG, Fischer EH. Mitogen-activated protein kinase/extracellular signal-regulated kinase 2 regulates cytoskeletal organization and chemotaxis via catalytic and microtubule-specific interactions. Mol Biol Cell. 1997;8: 1219–1232.
253. Adachi M, Fukuda M, Nishida E. Two co-existing mechanisms for nuclear import of MAP kinase: passive diffusion of a monomer and active transport of a dimer. EMBO J. 1999;18: 5347–58. doi:10.1093/emboj/18.19.5347
254. Khokhlatchev A V., Canagarajah B, Wilsbacher J, Robinson M, Atkinson M, Goldsmith E, et al. Phosphorylation of the MAP kinase ERK2 promotes its homodimerization and nuclear translocation. Cell. 1998;93: 605–615. doi:10.1016/S0092-8674(00)81189-7
255. Yazicioglu MN, Goad DL, Ranganathan A, Whitehurst AW, Goldsmith EJ, Cobb MH. Mutations in ERK2 binding sites affect nuclear entry. J Biol Chem. 2007;282: 28759–28767. doi:10.1074/jbc.M703460200
256. Plotnikov A, Chuderland D, Karamansha Y, Livnah O, Seger R. Nuclear extracellular signal-regulated kinase 1 and 2 translocation is mediated by casein kinase 2 and accelerated by autophosphorylation. Mol Cell Biol. 2011;31: 3515–30. doi:10.1128/MCB.05424-11
257. Whitmarsh AJ. Casein kinase 2 sends extracellular signal-regulated kinase nuclear. Mol Cell Biol. 2011;31: 3512–3514. doi:10.1128/MCB.05916-11
258. Zehorai E, Yao Z, Plotnikov A, Seger R. The subcellular localization of MEK and ERK--a novel nuclear translocation signal (NTS) paves a way to the nucleus. Mol Cell Endocrinol. 2010;314: 213–20. doi:10.1016/j.mce.2009.04.008
259. Caunt CJ, McArdle CA. Stimulus-induced uncoupling of extracellular signal-regulated kinase phosphorylation from nuclear localization is dependent on docking domain interactions. J Cell Sci. 2010;123: 4310–20. doi:10.1242/jcs.076349
260. Caunt CJ, Rivers C a, Conway-Campbell BL, Norman MR, McArdle C a. Epidermal growth factor receptor and protein kinase C signaling to ERK2: spatiotemporal regulation of ERK2 by dual specificity phosphatases. 2008;283: 6241–6252. doi:10.1074/jbc.M706624200
261. Rodríguez J, Crespo P, Rodriguez J, Crespo P. Working Without Kinase Activity: Phosphotransfer-Independent Functions of Extracellular Signal-Regulated Kinases. Sci Signal. 2011;4: re3–re3. doi:10.1126/scisignal.2002324
262. Ahmed S, Grant KG, Edwards LE, Rahman A, Cirit M, Goshe MB, et al. Data-driven modeling reconciles kinetics of ERK phosphorylation, localization, and activity states. Mol Syst Biol. 2014;10: 718. doi:10.1002/msb.134708
263. Aoki K, Kamioka Y, Matsuda M. Fluorescence resonance energy transfer imaging of cell signaling from in vitro to in vivo: basis of biosensor construction, live imaging, and image processing. Dev Growth Differ. 2013;55: 515–22. doi:10.1111/dgd.12039
264. Nishida E, Gotoh Y. The MAP kinase cascade is essential for diverse signal transduction pathways. Trends Biochem Sci. 1993;18: 128–131.
265. Chambard J-C, Lefloch R, Pouysségur J, Lenormand P. ERK implication in cell cycle regulation. Biochim Biophys Acta - Mol Cell Res. 2007;1773: 1299–1310. doi:10.1016/j.bbamcr.2006.11.010
266. Graves LM, Guy HI, Kozlowski P, Huang M, Lazarowski E, Pope RM, et al. Regulation of carbamoyl phosphate synthetase by MAP kinase. Nature. 2000;403: 328–332. doi:10.1038/35002111

267. Soloaga A, Thomson S, Wiggin GR, Rampersaud N, Dyson MH, Hazzalin CA, et al. MSK2 and MSK1 mediate the mitogen- and stress-induced phosphorylation of histone H3 and HMG-14. EMBO J. 2003;22: 2788–97. doi:10.1093/emboj/cdg273
268. Yu S, Huang H, Iliuk A, Wang W-H, Jayasundera KB, Tao WA, et al. Syk Inhibits the Activity of Protein Kinase A by Phosphorylating Tyrosine 330 of the Catalytic Subunit. J Biol Chem. 2013;288: 10870–10881. doi:10.1074/jbc.M112.426130
269. Inoki K, Ouyang H, Li Y, Guan K-L. Signaling by target of rapamycin proteins in cell growth control. Microbiol Mol Biol Rev. 2005;69: 79–100. doi:10.1128/MMBR.69.1.79-100.2005
270. Gille H, Kortenjann M, Thomae O, Moomaw C, Slaughter C, Cobb MH, et al. ERK phosphorylation potentiates Elk-1-mediated ternary complex formation and transactivation. EMBO J. 1995;14: 951–962.
271. Burch PM, Yuan Z, Loonen A, Heintz NH. An extracellular signal-regulated kinase 1- and 2-dependent program of chromatin trafficking of c-Fos and Fra-1 is required for cyclin D1 expression during cell cycle reentry. Mol Cell Biol. 2004;24: 4696–709. doi:10.1128/MCB.24.11.4696-4709.2004
272. Seth A, Alvarez E, Gupta S, Davis RJ. A phosphorylation site located in the NH2-terminal domain of c-Myc increases transactivation of gene expression. J Biol Chem. 1991;266: 23521–23524.
273. Yamamoto T, Ebisuya M, Ashida F, Okamoto K, Yonehara S, Nishida E. Continuous ERK Activation Downregulates Antiproliferative Genes throughout G1 Phase to Allow Cell-Cycle Progression. Curr Biol. 2006;16: 1171–1182. doi:10.1016/j.cub.2006.04.044
274. Baert F, Bodart J-F, Bocquet-Muchembled B, Lescuyer-Rousseau A, Vilain J-P. Xp42(Mpk1) activation is not required for germinal vesicle breakdown but for Raf complete phosphorylation in insulin-stimulated Xenopus oocytes. J Biol Chem. 2003;278: 49714–20. doi:10.1074/jbc.M308067200
275. Russo C, Beaujois R, Bodart J-F, Blossey R. Kicked by Mos and tuned by MPF-the initiation of the MAPK cascade in Xenopus oocytes. HFSP J. 2009;3: 428–40. doi:10.2976/1.3265771
276. Knauf J a., Ouyang B, Knudsen ES, Fukasawa K, Babcock G, Fagin J a. Oncogenic RAS induces accelerated transition through G2/M and promotes defects in the G2 DNA damage and mitotic spindle checkpoints. J Biol Chem. 2006;281: 3800–3809. doi:10.1074/jbc.M511690200
277. Roberts EC, Shapiro PS, Nahreini TS, Pages G, Pouyssegur J, Ahn NG. Distinct cell cycle timing requirements for extracellular signal-regulated kinase and phosphoinositide 3-kinase signaling pathways in somatic cell mitosis. Mol Cell Biol. 2002;22: 7226–41.
278. Wright JH, Munar E, Jameson DR, Andreassen PR, Margolis RL, Seger R, et al. Mitogen-activated protein kinase kinase activity is required for the G(2)/M transition of the cell cycle in mammalian fibroblasts. Proc Natl Acad Sci U S A. 1999;96: 11335–11340.
279. Shinohara M, Mikhailov A V., Aguirre-Ghiso JA, Rieder CL. Extracellular signal-regulated kinase 1/2 activity is not required in mammalian cells during late G2 for timely entry into or exit from mitosis. Mol Biol Cell. 2006;17: 5227–5240. doi:10.1091/mbc.E06-04-0284
280. Dumesic P a., Scholl F a., Barragan DI, Khavari P a. Erk1/2 MAP kinases are required for epidermal G2/M progression. J Cell Biol. 2009;185: 409–422. doi:10.1083/jcb.200804038
281. Grill C, Gheyas F, Dayananth P, Jin W, Ding W, Qiu P, et al. Analysis of the ERK1,2 transcriptome in mammary epithelial cells. Biochem J. 2004;381: 635–644. doi:10.1042/BJ20031688
282. Hatano N, Mori Y, Oh-hora M, Kosugi A, Fujikawa T, Nakai N, et al. Essential role for ERK2 mitogen-activated protein kinase in placental development. Genes Cells. 2003;8: 847–56. doi:10.1046/j.1365-2443.2003.00680.x
283. Selcher JC, Nekrasova T, Paylor R, Landreth GE, Sweatt JD. Mice lacking the ERK1 isoform of MAP kinase are unimpaired in emotional learning. Learn Mem. 2001;8: 11–9. doi:10.1101/lm.37001
284. Pagès G, Guérin S, Grall D, Bonino F, Smith A, Anjuere F, et al. Defective thymocyte maturation in p44 MAP kinase (Erk 1) knockout mice. Science. 1999;286: 1374–7. doi:10.1126/science.286.5443.1374
285. Saba-El-Leil MK, Vella FDJ, Vernay B, Voisin L, Chen L, Labrecque N, et al. An essential function of the mitogen-activated protein kinase Erk2 in mouse trophoblast development. EMBO Rep. 2003;4: 964–8. doi:10.1038/sj.embor.embor939
286. Fischer AM, Katayama CD, Pagès G, Pouysségur J, Hedrick SM. The Role of Erk1 and Erk2 in Multiple Stages of T Cell Development. Immunity. 2005;23: 431–443. doi:10.1016/j.immuni.2005.08.013
287. Krens SFG, He S, Lamers GEM, Meijer AH, Bakkers J, Schmidt T, et al. Distinct functions for ERK1 and ERK2 in cell migration processes during zebrafish gastrulation. Dev Biol. 2008;319: 370–83. doi:10.1016/j.ydbio.2008.04.032
288. Michailovici I, Harrington H a, Azogui HH, Yahalom-Ronen Y, Plotnikov A, Ching S, et al. Nuclear to cytoplasmic shuttling of ERK promotes differentiation of muscle stem/progenitor cells. Development. 2014;141: 2611–20. doi:10.1242/dev.107078
289. Webb DJ, Donais K, Whitmore L a, Thomas SM, Turner CE, Parsons JT, et al. FAK-Src signalling through paxillin, ERK and MLCK regulates adhesion disassembly. Nat Cell Biol. 2004;6: 154–161. doi:10.1038/ncb1094
290. Huang C, Jacobson K, Schaller MD. MAP kinases and cell migration. J Cell Sci. 2004;117: 4619–28. doi:10.1242/jcs.01481
291. Fang JY, Richardson BC. The MAPK signalling pathways and colorectal cancer. Lancet Oncol. 2005;6: 322–327. doi:10.1016/S1470-2045(05)70168-6
292. Santen RJ, Song RX, McPherson R, Kumar R, Adam L, Jeng M-H, et al. The role of mitogen-activated protein (MAP) kinase in breast cancer. J Steroid Biochem Mol Biol. 2002;80: 239–256. doi:10.1016/S0960-0760(01)00189-3

293. Davies H, Bignell GR, Cox C, Stephens P, Edkins S, Clegg S, et al. Mutations of the BRAF gene in human cancer. Nature. 2002;417: 949–54. doi:10.1038/nature00766
294. Wan PTC, Garnett MJ, Roe SM, Lee S, Niculescu-Duvaz D, Good VM, et al. Mechanism of activation of the RAF-ERK signaling pathway by oncogenic mutations of B-RAF. Cell. 2004;116: 855–867. doi:10.1016/S0092-8674(04)00215-6
295. Roberts PJ, Der CJ. Targeting the Raf-MEK-ERK mitogen-activated protein kinase cascade for the treatment of cancer. Oncogene. 2007;26: 3291–3310. doi:10.1038/sj.onc.1210422
296. Millington GWM. Mutations of the BRAF gene in human cancer, by Davies et al. (Nature 2002; 417: 949-54). Clin Exp Dermatol. 2013;38: 222–3. doi:10.1111/ced.12015
297. Barras D. BRAF Mutation in Colorectal Cancer: An Update. Biomark Cancer. 2015;7: 9–12. doi:10.4137/BIC.S25248
298. Kim EK, Choi E-J. Pathological roles of MAPK signaling pathways in human diseases. Biochim Biophys Acta. Elsevier B.V.; 2010;1802: 396–405. doi:10.1016/j.bbadis.2009.12.009
299. Muslin AJ. MAPK signalling in cardiovascular health and disease: molecular mechanisms and therapeutic targets. Clin Sci (Lond). 2008;115: 203–218. doi:10.1042/CS20070430
300. French AR, Sudlow GP, Wiley HS, Lauffenburger DA. Postendocytic trafficking of epidermal growth factor-receptor complexes is mediated through saturable and specific endosomal interactions. J Biol Chem. 1994;269: 15749–55.
301. Traverse S, Seedorf K, Paterson H, Marshall CJ, Cohen P, Ullrich A. EGF triggers neuronal differentiation of PC12 cells that overexpress the EGF receptor. Curr Biol. 1994;4: 694–701. doi:10.1016/S0960-9822(00)00154-8
302. Balmanno K, Cook SJ. Tumour cell survival signalling by the ERK1/2 pathway. Cell Death Differ. 2009;16: 368–77. doi:10.1038/cdd.2008.148
303. Blagosklonny M V, Schulte T, Nguyen P, Trepel J, Neckers LM. Taxol-induced apoptosis and phosphorylation of Bcl-2 protein involves c-Raf-1 and represents a novel c-Raf-1 signal transduction pathway. Cancer Res. 1996;56: 1851–4.
304. Watabe M, Masuda Y, Nakajo S, Yoshida T, Kuroiwa Y, Nakaya K. The cooperative interaction of two different signaling pathways in response to bufalin induces apoptosis in human leukemia U937 cells. J Biol Chem. 1996;271: 14067–72.
305. Favata MF, Horiuchi KY, Manos EJ, Daulerio a J, Stradley D a, Feeser WS, et al. Identification of a Novel Inhibitor of Mitogen-activated Protein Kinase Kinase. J Biol Chem. 1998;273: 18623–18632. doi:10.1074/jbc.273.29.18623
306. Alessi DR, Cuenda A, Cohen P, Dudley DT, Saltiel AR. PD 098059 is a specific inhibitor of the activation of mitogen-activated protein kinase kinase in vitro and in vivo. J Biol Chem. 1995;270: 27489–94.
307. Goillot E, Raingeaud J, Ranger A, Tepper RI, Davis RJ, Harlow E, et al. Mitogen-activated protein kinase-mediated Fas apoptotic signaling pathway. Proc Natl Acad Sci U S A. 1997;94: 3302–7. doi:10.1073/pnas.94.7.3302
308. Kim YKK, Kim HJJ, Kwon CHH, Kim JHJMJHJM, Woo JSS, Jung JSS, et al. Role of ERK activation in cisplatin-induced apoptosis in OK renal epithelial cells. J Appl Toxicol. 25: 374–82. doi:10.1002/jat.1081
309. Bacus SSS, Gudkov a V V, Lowe M, Lyass L, Yung Y, Komarov a PP, et al. Taxol-induced apoptosis depends on MAP kinase pathways (ERK and p38) and is independent of p53. Oncogene. 2001;20: 147–55. doi:10.1038/sj.onc.1204062
310. Wu Z, Wu L, Tashiro S, Onodera S, Ikejima T. Phosphorylated extracellular signal-regulated kinase up-regulated p53 expression in shikonin-induced HeLa cell apoptosis. Chin Med J (Engl). 2005;118: 671–7.
311. Stefanelli C, Tantini B, Fattori M, Stanic' I, Pignatti C, Clo C, et al. Caspase activation in etoposide-treated fibroblasts is correlated to ERK phosphorylation and both events are blocked by polyamine depletion. FEBS Lett. 2002;527: 223–28. doi:10.1016/S0014-5793(02)03242-8
312. Tang D, Wu D, Hirao A, Lahti JM, Liu L, Mazza B, et al. ERK activation mediates cell cycle arrest and apoptosis after DNA damage independently of p53. J Biol Chem. 2002;277: 12710–7. doi:10.1074/jbc.M111598200
313. Lee E-R, Kang Y-J, Kim J-H, Lee HT, Cho S-G. Modulation of apoptosis in HaCaT keratinocytes via differential regulation of ERK signaling pathway by flavonoids. J Biol Chem. 2005;280: 31498–507. doi:10.1074/jbc.M505537200
314. Stevens C, Lin Y, Sanchez M, Amin E, Copson E, White H, et al. A germ line mutation in the death domain of DAPK-1 inactivates ERK-induced apoptosis. J Biol Chem. 2007;282: 13791–803. doi:10.1074/jbc.M605649200
315. Cheng Y, Qiu F, Tashiro SI, Onodera S, Ikejima T. ERK and JNK mediate TNFalpha-induced p53 activation in apoptotic and autophagic L929 cell death. Biochem Biophys Res Commun. Elsevier Inc.; 2008;376: 483–8. doi:10.1016/j.bbrc.2008.09.018
316. Sivaprasad U, Basu A. Inhibition of ERK attenuates autophagy and potentiates tumour necrosis factor-alpha-induced cell death in MCF-7 cells. J Cell Mol Med. 2008;12: 1265–71. doi:10.1111/j.1582-4934.2008.00282.x
317. Ulisse S, Cinque B, Silvano G, Rucci N, Biordi L, Cifone MG, et al. Erk-dependent cytosolic phospholipase A2 activity is induced by CD95 ligand cross-linking in the mouse derived Sertoli cell line TM4 and is required to trigger apoptosis in CD95 bearing cells. Cell Death Differ. 2000;7: 916–24. doi:10.1038/sj.cdd.4400716

318. Kim Y-H, Lee D-H, Jeong J-H, Guo ZS, Lee YJ. Quercetin augments TRAIL-induced apoptotic death: involvement of the ERK signal transduction pathway. Biochem Pharmacol. 2008;75: 1946–58. doi:10.1016/j.bcp.2008.02.016
319. Nesterov A, Nikrad M, Johnson T, Kraft AS. Oncogenic Ras sensitizes normal human cells to tumor necrosis factor-alpha-related apoptosis-inducing ligand-induced apoptosis. Cancer Res. 2004;64: 3922–7. doi:10.1158/0008-5472.CAN-03-2219
320. Wang Y, Quon KC, Knee DA, Nesterov A, Kraft AS. RAS, MYC, and sensitivity to tumor necrosis factor-alpha-related apoptosis-inducing ligand-induced apoptosis. Cancer Res. 2005;65: 1615–6; author reply 1616–7. doi:10.1158/0008-5472.CAN-04-2757
321. Drosopoulos KG, Roberts ML, Cermak L, Sasazuki T, Shirasawa S, Andera L, et al. Transformation by oncogenic RAS sensitizes human colon cells to TRAIL-induced apoptosis by up-regulating death receptor 4 and death receptor 5 through a MEK-dependent pathway. J Biol Chem. 2005;280: 22856–67. doi:10.1074/jbc.M412483200
322. Shenoy K, Wu Y, Pervaiz S. LY303511 enhances TRAIL sensitivity of SHEP-1 neuroblastoma cells via hydrogen peroxide-mediated mitogen-activated protein kinase activation and up-regulation of death receptors. Cancer Res. 2009;69: 1941–50. doi:10.1158/0008-5472.CAN-08-1996
323. Glotin A-L, Calipel A, Brossas J-Y, Faussat A-M, Tréton J, Mascarelli F. Sustained versus transient ERK1/2 signaling underlies the anti- and proapoptotic effects of oxidative stress in human RPE cells. Invest Ophthalmol Vis Sci. 2006;47: 4614–23. doi:10.1167/iovs.06-0297
324. Zhang X, Shan P, Sasidhar M, Chupp GL, Flavell RA, Choi AMK, et al. Reactive oxygen species and extracellular signal-regulated kinase 1/2 mitogen-activated protein kinase mediate hyperoxia-induced cell death in lung epithelium. Am J Respir Cell Mol Biol. 2003;28: 305–15. doi:10.1165/rcmb.2002-0156OC
325. Zhang P, Wang YZ, Kagan E, Bonner JC. Peroxynitrite targets the epidermal growth factor receptor, Raf-1, and MEK independently to activate MAPK. J Biol Chem. 2000;275: 22479–86. doi:10.1074/jbc.M910425199
326. Zhuang S, Kinsey GR, Yan Y, Han J, Schnellmann RG. Extracellular signal-regulated kinase activation mediates mitochondrial dysfunction and necrosis induced by hydrogen peroxide in renal proximal tubular cells. J Pharmacol Exp Ther. 2008;325: 732–40. doi:10.1124/jpet.108.136358
327. Martin P, Poggi MC, Chambard JC, Boulukos KE, Pognonec P. Low dose cadmium poisoning results in sustained ERK phosphorylation and caspase activation. Biochem Biophys Res Commun. 2006;350: 803–7. doi:10.1016/j.bbrc.2006.09.126
328. Wang SH, Shih YL, Ko WC, Wei YH, Shih CM. Cadmium-induced autophagy and apoptosis are mediated by a calcium signaling pathway. Cell Mol Life Sci. 2008;65: 3640–52. doi:10.1007/s00018-008-8383-9
329. Pei B, Wang S, Guo X, Wang J, Yang G, Hang H, et al. Arsenite-induced germline apoptosis through a MAPK-dependent, p53-independent pathway in Caenorhabditis elegans. Chem Res Toxicol. 2008;21: 1530–5. doi:10.1021/tx800074e
330. Sinha D, Bannergee S, Schwartz JH, Lieberthal W, Levine JS. Inhibition of ligand-independent ERK1/2 activity in kidney proximal tubular cells deprived of soluble survival factors up-regulates Akt and prevents apoptosis. J Biol Chem. 2004;279: 10962–72. doi:10.1074/jbc.M312048200
331. Panaretakis T, Hjortsberg L, Tamm KP, Björklund A-C, Joseph B, Grandér D. Interferon alpha induces nucleus-independent apoptosis by activating extracellular signal-regulated kinase 1/2 and c-Jun NH2-terminal kinase downstream of phosphatidylinositol 3-kinase and mammalian target of rapamycin. Mol Biol Cell. 2008;19: 41–50. doi:10.1091/mbc.E07-04-0358
332. Brown L, Benchimol S. The involvement of MAPK signaling pathways in determining the cellular response to p53 activation: cell cycle arrest or apoptosis. J Biol Chem. 2006;281: 3832–40. doi:10.1074/jbc.M507951200
333. Kauffmann-Zeh A, Rodriguez-Viciana P, Ulrich E, Gilbert C, Coffer P, Downward J, et al. Suppression of c-Myc-induced apoptosis by Ras signalling through PI(3)K and PKB. Nature. 1997;385: 544–8. doi:10.1038/385544a0
334. Cagnol S, Van Obberghen-Schilling E, Chambard J-C. Prolonged activation of ERK1,2 induces FADD-independent caspase 8 activation and cell death. Apoptosis. 2006;11: 337–46. doi:10.1007/s10495-006-4065-y
335. Zhuang S, Schnellmann RG. A death-promoting role for extracellular signal-regulated kinase. J Pharmacol Exp Ther. 2006;319: 991–7. doi:10.1124/jpet.106.107367
336. Jo S-K, Cho WY, Sung SA, Kim HK, Won NH. MEK inhibitor, U0126, attenuates cisplatin-induced renal injury by decreasing inflammation and apoptosis. Kidney Int. 2005;67: 458–66. doi:10.1111/j.1523-1755.2005.67102.x
337. Wang Z, Chen X, Yang G, Zhou L. U0126 prevents ERK pathway phosphorylation and interleukin-1beta mRNA production after cerebral ischemia. Chin Med Sci J. 2004;19: 270–5. Available: http://www.ncbi.nlm.nih.gov/pubmed/15669185
338. Tewari R, Sharma V, Koul N, Sen E. Involvement of miltefosine-mediated ERK activation in glioma cell apoptosis through Fas regulation. J Neurochem. 2008;107: 616–27. doi:10.1111/j.1471-4159.2008.05625.x
339. Hill JM, Vaidyanathan H, Ramos JW, Ginsberg MH, Werner MH. Recognition of ERK MAP kinase by PEA-15 reveals a common docking site within the death domain and death effector domain. EMBO J. 2002;21: 6494–504. Available: http://www.ncbi.nlm.nih.gov/pubmed/12456656

340. Renganathan H, Vaidyanathan H, Knapinska A, Ramos JW. Phosphorylation of PEA-15 switches its binding specificity from ERK/MAPK to FADD. Biochem J. 2005;390: 729–35. doi:10.1042/BJ20050378
341. Nowak G. Protein kinase C-alpha and ERK1/2 mediate mitochondrial dysfunction, decreases in active Na+ transport, and cisplatin-induced apoptosis in renal cells. J Biol Chem. 2002;277: 43377–88. doi:10.1074/jbc.M206373200
342. Nowak G, Clifton GL, Godwin ML, Bakajsova D. Activation of ERK1/2 pathway mediates oxidant-induced decreases in mitochondrial function in renal cells. Am J Physiol Renal Physiol. 2006;291: F840–55. doi:10.1152/ajprenal.00219.2005
343. Zhuang S, Yan Y, Daubert RA, Han J, Schnellmann RG. ERK promotes hydrogen peroxide-induced apoptosis through caspase-3 activation and inhibition of Akt in renal epithelial cells. Am J Physiol Renal Physiol. 2007;292: F440–7. doi:10.1152/ajprenal.00170.2006
344. Wang X, Martindale JL, Holbrook NJ. Requirement for ERK activation in cisplatin-induced apoptosis. J Biol Chem. 2000;275: 39435–43. doi:10.1074/jbc.M004583200
345. Zhang C-L, Wu L-J, Zuo H-J, Tashiro S, Onodera S, Ikejima T. Cytochrome c release from oridonin-treated apoptotic A375-S2 cells is dependent on p53 and extracellular signal-regulated kinase activation. J Pharmacol Sci. 2004;96: 155–63. Available: http://www.ncbi.nlm.nih.gov/pubmed/15492467
346. Liu J, Mao W, Ding B, Liang C. ERKs/p53 signal transduction pathway is involved in doxorubicin-induced apoptosis in H9c2 cells and cardiomyocytes. Am J Physiol Heart Circ Physiol. 2008;295: H1956–65. doi:10.1152/ajpheart.00407.2008
347. Park BG, Yoo C Il, Kim HT, Kwon CH, Kim YK. Role of mitogen-activated protein kinases in hydrogen peroxide-induced cell death in osteoblastic cells. Toxicology. 2005;215: 115–25. doi:10.1016/j.tox.2005.07.003
348. Yeh PY, Chuang S-E, Yeh K-H, Song YC, Chang LL-Y, Cheng A-L. Phosphorylation of p53 on Thr55 by ERK2 is necessary for doxorubicin-induced p53 activation and cell death. Oncogene. 2004;23: 3580–8. doi:10.1038/sj.onc.1207426
349. Li H, Wang X, Li N, Qiu J, Zhang Y, Cao X. hPEBP4 resists TRAIL-induced apoptosis of human prostate cancer cells by activating Akt and deactivating ERK1/2 pathways. J Biol Chem. 2007;282: 4943–50. doi:10.1074/jbc.M609494200
350. Degli Esposti M, Dive C. Mitochondrial membrane permeabilisation by Bax/Bak. Biochem Biophys Res Commun. 2003;304: 455–61. Available: http://www.ncbi.nlm.nih.gov/pubmed/12729579
351. Shih A, Davis FB, Lin H-Y, Davis PJ. Resveratrol induces apoptosis in thyroid cancer cell lines via a MAPK- and p53-dependent mechanism. J Clin Endocrinol Metab. 2002;87: 1223–32. doi:10.1210/jcem.87.3.8345
352. Persons DL, Yazlovitskaya EM, Pelling JC. Effect of extracellular signal-regulated kinase on p53 accumulation in response to cisplatin. J Biol Chem. 2000;275: 35778–85. doi:10.1074/jbc.M004267200
353. Petros AM, Gunasekera A, Xu N, Olejniczak ET, Fesik SW. Defining the p53 DNA-binding domain/Bcl-x(L)-binding interface using NMR. FEBS Lett. 2004;559: 171–4. doi:10.1016/S0014-5793(04)00059-6
354. Mihara M, Erster S, Zaika A, Petrenko O, Chittenden T, Pancoska P, et al. p53 has a direct apoptogenic role at the mitochondria. Mol Cell. 2003;11: 577–90. Available: http://www.ncbi.nlm.nih.gov/pubmed/12667443
355. Leu JI-J, Dumont P, Hafey M, Murphy ME, George DL. Mitochondrial p53 activates Bak and causes disruption of a Bak-Mcl1 complex. Nat Cell Biol. 2004;6: 443–50. doi:10.1038/ncb1123
356. Woessmann W, Chen X, Borkhardt A. Ras-mediated activation of ERK by cisplatin induces cell death independently of p53 in osteosarcoma and neuroblastoma cell lines. Cancer Chemother Pharmacol. 2002;50: 397–404. doi:10.1007/s00280-002-0502-y
357. Lin LL, Wartmann M, Lin AY, Knopf JL, Seth A, Davis RJ. cPLA2 is phosphorylated and activated by MAP kinase. Cell. 1993;72: 269–78. Available: http://www.ncbi.nlm.nih.gov/pubmed/8381049
358. Kim GS, Hong JS, Kim SW, Koh J-M, An CS, Choi J-Y, et al. Leptin induces apoptosis via ERK/cPLA2/cytochrome c pathway in human bone marrow stromal cells. J Biol Chem. 2003;278: 21920–9. doi:10.1074/jbc.M204598200
359. Deiss LP, Feinstein E, Berissi H, Cohen O, Kimchi A. Identification of a novel serine/threonine kinase and a novel 15-kD protein as potential mediators of the gamma interferon-induced cell death. Genes Dev. 1995;9: 15–30. Available: http://www.ncbi.nlm.nih.gov/pubmed/7828849
360. Levy-Strumpf N, Deiss LP, Berissi H, Kimchi A. DAP-5, a novel homolog of eukaryotic translation initiation factor 4G isolated as a putative modulator of gamma interferon-induced programmed cell death. Mol Cell Biol. 1997;17: 1615–25. Available: http://www.ncbi.nlm.nih.gov/pubmed/9032289
361. Chen C-H, Wang W-J, Kuo J-C, Tsai H-C, Lin J-R, Chang Z-F, et al. Bidirectional signals transduced by DAPK-ERK interaction promote the apoptotic effect of DAPK. EMBO J. 2005;24: 294–304. doi:10.1038/sj.emboj.7600510
362. Mebratu YA, Dickey BF, Evans C, Tesfaigzi Y. The BH3-only protein Bik/Blk/Nbk inhibits nuclear translocation of activated ERK1/2 to mediate IFNgamma-induced cell death. J Cell Biol. 2008;183: 429–39. doi:10.1083/jcb.200801186
363. Panta GR, Kaur S, Cavin LG, Cortés ML, Mercurio F, Lothstein L, et al. ATM and the catalytic subunit of DNA-dependent protein kinase activate NF-kappaB through a common MEK/extracellular signal-regulated kinase/p90(rsk) signaling pathway in response to distinct forms of DNA damage. Mol Cell Biol. 2004;24: 1823–35. Available: http://www.ncbi.nlm.nih.gov/pubmed/14966265

364. Golding SE, Rosenberg E, Neill S, Dent P, Povirk LF, Valerie K. Extracellular signal-related kinase positively regulates ataxia telangiectasia mutated, homologous recombination repair, and the DNA damage response. Cancer Res. 2007;67: 1046–53. doi:10.1158/0008-5472.CAN-06-2371
365. Amaravadi R, Thompson CB. The survival kinases Akt and Pim as potential pharmacological targets. J Clin Invest. 2005;115: 2618–24. doi:10.1172/JCI26273
366. Trencia A, Perfetti A, Cassese A, Vigliotta G, Miele C, Oriente F, et al. Protein kinase B/Akt binds and phosphorylates PED/PEA-15, stabilizing its antiapoptotic action. Mol Cell Biol. 2003;23: 4511–21. Available: http://www.ncbi.nlm.nih.gov/pubmed/12808093
367. Gervais M, Dugourd C, Muller L, Ardidie C, Canton B, Loviconi L, et al. Akt down-regulates ERK1/2 nuclear localization and angiotensin II-induced cell proliferation through PEA-15. Mol Biol Cell. 2006;17: 3940–51. doi:10.1091/mbc.E06-06-0501
368. Galetic I, Maira S-M, Andjelkovic M, Hemmings BA. Negative regulation of ERK and Elk by protein kinase B modulates c-Fos transcription. J Biol Chem. 2003;278: 4416–23. doi:10.1074/jbc.M210578200
369. Dong J, Ramachandiran S, Tikoo K, Jia Z, Lau SS, Monks TJ. EGFR-independent activation of p38 MAPK and EGFR-dependent activation of ERK1/2 are required for ROS-induced renal cell death. Am J Physiol Renal Physiol. 2004;287: F1049–58. doi:10.1152/ajprenal.00132.2004
370. Burney S, Niles JC, Dedon PC, Tannenbaum SR. DNA damage in deoxynucleosides and oligonucleotides treated with peroxynitrite. Chem Res Toxicol. 1999;12: 513–20. doi:10.1021/tx980254m
371. Sasada T, Iwata S, Sato N, Kitaoka Y, Hirota K, Nakamura K, et al. Redox control of resistance to cis-diamminedichloroplatinum (II) (CDDP): protective effect of human thioredoxin against CDDP-induced cytotoxicity. J Clin Invest. 1996;97: 2268–76. doi:10.1172/JCI118668
372. Cagnol S, Chambard J-C. ERK and cell death: mechanisms of ERK-induced cell death--apoptosis, autophagy and senescence. FEBS J. 2010;277: 2–21. doi:10.1111/j.1742-4658.2009.07366.x
373. Ogier-Denis E, Pattingre S, El Benna J, Codogno P. Erk1/2-dependent phosphorylation of Galpha-interacting protein stimulates its GTPase accelerating activity and autophagy in human colon cancer cells. J Biol Chem. 2000;275: 39090–5. doi:10.1074/jbc.M006198200
374. Yang L-Y, Wu K-H, Chiu W-T, Wang S-H, Shih C-M. The cadmium-induced death of mesangial cells results in nephrotoxicity. Autophagy. 2009;5: 571–2. Available: http://www.ncbi.nlm.nih.gov/pubmed/19333000
375. Corcelle E, Nebout M, Bekri S, Gauthier N, Hofman P, Poujeol P, et al. Disruption of autophagy at the maturation step by the carcinogen lindane is associated with the sustained mitogen-activated protein kinase/extracellular signal-regulated kinase activity. Cancer Res. 2006;66: 6861–70. doi:10.1158/0008-5472.CAN-05-3557
376. Bartholomeusz C, Rosen D, Wei C, Kazansky A, Yamasaki F, Takahashi T, et al. PEA-15 induces autophagy in human ovarian cancer cells and is associated with prolonged overall survival. Cancer Res. 2008;68: 9302–10. doi:10.1158/0008-5472.CAN-08-2592
377. Subramaniam S, Unsicker K. ERK and cell death: ERK1/2 in neuronal death. FEBS J. 2010;277: 22–9. doi:10.1111/j.1742-4658.2009.07367.x
378. Subramaniam S, Unsicker K. Extracellular signal-regulated kinase as an inducer of non-apoptotic neuronal death. Neuroscience. 2006;138: 1055–65. doi:10.1016/j.neuroscience.2005.12.013
379. Nakano S, Shinde A, Kawashima S, Nakamura S, Akiguchi I, Kimura J. Inclusion body myositis: expression of extracellular signal-regulated kinase and its substrate. Neurology. 2001;56: 87–93. Available: http://www.ncbi.nlm.nih.gov/pubmed/11148241
380. Martinez-Lopez N, Athonvarangkul D, Mishall P, Sahu S, Singh R. Autophagy proteins regulate ERK phosphorylation. Nat Commun. 2013;4: 2799. doi:10.1038/ncomms3799
381. Wang J, Whiteman MW, Lian H, Wang G, Singh A, Huang D, et al. A non-canonical MEK/ERK signaling pathway regulates autophagy via regulating Beclin 1. J Biol Chem. 2009;284: 21412–24. doi:10.1074/jbc.M109.026013
382. Yumnam S, Park HS, Kim MK, Nagappan A, Hong GE, Lee HJ, et al. Hesperidin induces paraptosis like cell death in hepatoblatoma, HepG2 cells: involvement of ERK1/2 MAPK. PLoS One. 2014;9: e101321. doi:10.1371/journal.pone.0101321
383. Zhang F-J, Yang J-Y, Mou Y-H, Sun B-S, Wang J-M, Wu C-F. Oligomer procyanidins from grape seeds induce a paraptosis-like programmed cell death in human glioblastoma U-87 cells. Pharm Biol. 2010;48: 883–90. doi:10.3109/13880200903311102
384. Yagoda N, von Rechenberg M, Zaganjor E, Bauer AJ, Yang WS, Fridman DJ, et al. RAS-RAF-MEK-dependent oxidative cell death involving voltage-dependent anion channels. Nature. 2007;447: 864–8. doi:10.1038/nature05859
385. Carr EL, Kelman A, Wu GS, Gopaul R, Senkevitch E, Aghvanyan A, et al. Glutamine uptake and metabolism are coordinately regulated by ERK/MAPK during T lymphocyte activation. J Immunol. 2010;185: 1037–44. doi:10.4049/jimmunol.0903586
386. Matsushita M, Freigang S, Schneider C, Conrad M, Bornkamm GW, Kopf M. T cell lipid peroxidation induces ferroptosis and prevents immunity to infection. J Exp Med. 2015;212: 555–68. doi:10.1084/jem.20140857
387. Akhiani AA, Werlenius O, Aurelius J, Movitz C, Martner A, Hellstrand K, et al. Role of the ERK pathway for oxidant-induced parthanatos in human lymphocytes. PLoS One. 2014;9: e89646. doi:10.1371/journal.pone.0089646

388. Jin Jung K, Hyun Kim D, Kyeong Lee E, Woo Song C, Pal Yu B, Young Chung H. Oxidative stress induces inactivation of protein phosphatase 2A, promoting proinflammatory NF-κB in aged rat kidney. Free Radic Biol Med. 2013;61: 206–17. doi:10.1016/j.freeradbiomed.2013.04.005
389. Krejsa CM, Schieven GL. Impact of oxidative stress on signal transduction control by phosphotyrosine phosphatases. Environ Health Perspect. 1998;106 Suppl: 1179–84. Available: http://www.ncbi.nlm.nih.gov/pubmed/9788895
390. Ramachandiran S, Huang Q, Dong J, Lau SS, Monks TJ. Mitogen-activated protein kinases contribute to reactive oxygen species-induced cell death in renal proximal tubule epithelial cells. Chem Res Toxicol. 2002;15: 1635–42. Available: http://www.ncbi.nlm.nih.gov/pubmed/12482247
391. Lee Y-JY-S, Cho H-N, Soh J-W, Jhon GJ, Cho C-K, Chung H-Y, et al. Oxidative stress-induced apoptosis is mediated by ERK1/2 phosphorylation. Exp Cell Res. 2003;291: 251–66. Available: http://www.ncbi.nlm.nih.gov/pubmed/14597424
392. Kohda Y, Hiramatsu J, Gemba M. Involvement of MEK/ERK pathway in cephaloridine-induced injury in rat renal cortical slices. Toxicol Lett. 2003;143: 185–94. Available: http://www.ncbi.nlm.nih.gov/pubmed/12749822
393. Matsunaga Y, Kawai Y, Kohda Y, Gemba M. Involvement of activation of NADPH oxidase and extracellular signal-regulated kinase (ERK) in renal cell injury induced by zinc. J Toxicol Sci. 2005;30: 135–44. Available: http://www.ncbi.nlm.nih.gov/pubmed/15928461
394. Ozben T. Oxidative stress and apoptosis: impact on cancer therapy. J Pharm Sci. 2007;96: 2181–96. doi:10.1002/jps.20874
395. Arany I, Megyesi JK, Kaneto H, Price PM, Safirstein RL. Cisplatin-induced cell death is EGFR/src/ERK signaling dependent in mouse proximal tubule cells. Am J Physiol Renal Physiol. 2004;287: F543–9. doi:10.1152/ajprenal.00112.2004
396. Vindis C, Séguélas MH, Lanier S, Parini A, Cambon C. Dopamine induces ERK activation in renal epithelial cells through H2O2 produced by monoamine oxidase. Kidney Int. 2001;59: 76–86. doi:10.1046/j.1523-1755.2001.00468.x
397. Deora AA, Hajjar DP, Lander HM. Recruitment and activation of Raf-1 kinase by nitric oxide-activated Ras. Biochemistry. 2000;39: 9901–8. Available: http://www.ncbi.nlm.nih.gov/pubmed/10933809
398. Hoyos B, Imam A, Korichneva I, Levi E, Chua R, Hammerling U. Activation of c-Raf kinase by ultraviolet light. Regulation by retinoids. J Biol Chem. 2002;277: 23949–57. doi:10.1074/jbc.M110750200
399. Owens DM, Keyse SM. Differential regulation of MAP kinase signalling by dual-specificity protein phosphatases. Oncogene. 2007;26: 3203–13. doi:10.1038/sj.onc.1210412
400. Kim HS, Song M-C, Kwak IH, Park TJ, Lim IK. Constitutive induction of p-Erk1/2 accompanied by reduced activities of protein phosphatases 1 and 2A and MKP3 due to reactive oxygen species during cellular senescence. J Biol Chem. 2003;278: 37497–510. doi:10.1074/jbc.M211739200
401. Kamata H, Honda SI, Maeda S, Chang L, Hirata H, Karin M. Reactive oxygen species promote TNFalpha-induced death and sustained JNK activation by inhibiting MAP kinase phosphatases. Cell. 2005;120: 649–61. doi:10.1016/j.cell.2004.12.041
402. Mebratu Y, Tesfaigzi Y. How ERK1/2 activation controls cell proliferation and cell death: Is subcellular localization the answer? Cell Cycle. 2009;8: 1168–75. doi:10.1146/annurev.biophys.37.032807
403. Guise S, Braguer D, Carles G, Delacourte A, Briand C. Hyperphosphorylation of tau is mediated by ERK activation during anticancer drug-induced apoptosis in neuroblastoma cells. J Neurosci Res. 2001;63: 257–67. Available: http://www.ncbi.nlm.nih.gov/pubmed/11170175
404. Murphy LO, Blenis J. MAPK signal specificity: the right place at the right time. Trends Biochem Sci. 2006;31: 268–275. doi:10.1016/j.tibs.2006.03.009
405. Chen P, Hutter D, Yang X, Gorospe M, Davis RJ, Liu Y. Discordance between the binding affinity of mitogen-activated protein kinase subfamily members for MAP kinase phosphatase-2 and their ability to activate the phosphatase catalytically. J Biol Chem. 2001;276: 29440–9. doi:10.1074/jbc.M103463200
406. Torres C, Francis MK, Lorenzini A, Tresini M, Cristofalo VJ. Metabolic stabilization of MAP kinase phosphatase-2 in senescence of human fibroblasts. Exp Cell Res. 2003;290: 195–206. Available: http://www.ncbi.nlm.nih.gov/pubmed/14567979
407. Wu W, Pew T, Zou M, Pang D, Conzen SD. Glucocorticoid receptor-induced MAPK phosphatase-1 (MPK-1) expression inhibits paclitaxel-associated MAPK activation and contributes to breast cancer cell survival. J Biol Chem. 2005;280: 4117–24. doi:10.1074/jbc.M411200200
408. Zheng A, Kallio A, Härkönen P. Tamoxifen-induced rapid death of MCF-7 breast cancer cells is mediated via extracellularly signal-regulated kinase signaling and can be abrogated by estrogen. Endocrinology. 2007;148: 2764–77. doi:10.1210/en.2006-1269
409. Zhang M, Li J, Geng R, Ge W, Zhou Y, Zhang C, et al. The inhibition of ERK activation mediates the protection of necrostatin-1 on glutamate toxicity in HT-22 cells. Neurotox Res. 2013;24: 64–70. doi:10.1007/s12640-012-9361-4
410. Gao S, Andreeva K, Cooper NGF. Ischemia-reperfusion injury of the retina is linked to necroptosis via the ERK1/2-RIP3 pathway. Mol Vis. 2014;20: 1374–87. Available: http://www.ncbi.nlm.nih.gov/pubmed/25352744
411. Neves SR, Tsokas P, Sarkar A, Grace E a, Rangamani P, Taubenfeld SM, et al. Cell Shape and Negative Links in Regulatory Motifs Together Control Spatial Information Flow in Signaling Networks. Cell. 2008;133: 666–680. doi:10.1016/j.cell.2008.04.025

412. Avraham R, Yarden Y. Feedback regulation of EGFR signalling: decision making by early and delayed loops. Nat Rev Mol Cell Biol. Nature Publishing Group; 2011;12: 104–17. doi:10.1038/nrm3048
413. Doupé DP, Perrimon N. Visualizing and manipulating temporal signaling dynamics with fluorescence-based tools. Sci Signal. 2014;7: re1. doi:10.1126/scisignal.2005077
414. Behar M, Hoffmann A. Understanding the temporal codes of intra-cellular signals. Curr Opin Genet Dev. Elsevier Ltd; 2010;20: 684–93. doi:10.1016/j.gde.2010.09.007
415. Nakayama K, Satoh T, Igari A, Kageyama R, Nishida E. FGF induces oscillations of Hes1 expression and Ras/ERK activation. Curr Biol. 2008;18: R332–4. doi:10.1016/j.cub.2008.03.013
416. Albeck JG, Mills GB, Brugge JS. Frequency-modulated pulses of ERK activity transmit quantitative proliferation signals. Mol Cell. Elsevier Inc.; 2013;49: 249–61. doi:10.1016/j.molcel.2012.11.002
417. McBride KM, Banninger G, McDonald C, Reich NC. Regulated nuclear import of the STAT1 transcription factor by direct binding of importin-alpha. EMBO J. 2002;21: 1754–63. doi:10.1093/emboj/21.7.1754
418. Chen H-C, Reich NC. Live Cell Imaging Reveals Continuous STAT6 Nuclear Trafficking. J Immunol. 2010;185: 64–70. doi:10.4049/jimmunol.0903323
419. Nelson DE, Ihekwaba AEC, Elliott M, Johnson JR, Gibney CA, Foreman BE, et al. Oscillations in NF-kappaB signaling control the dynamics of gene expression. Science. 2004;306: 704–8. doi:10.1126/science.1099962
420. Tay S, Hughey JJ, Lee TK, Lipniacki T, Quake SR, Covert MW. Single-cell NF-kappaB dynamics reveal digital activation and analogue information processing. Nature. 2010;466: 267–71. doi:10.1038/nature09145
421. Novák B, Tyson JJ. Design principles of biochemical oscillators. Nat Rev Mol Cell Biol. 2008;9: 981–991. doi:10.1038/nrm2530
422. O'Donnell MA, Ting AT. Chronicles of a death foretold: dual sequential cell death checkpoints in TNF signaling. Cell Cycle. 2010;9: 1065–71.
423. Declercq W, Vanden Berghe T, Vandenabeele P. RIP kinases at the crossroads of cell death and survival. Cell. 2009;138: 229–32. doi:10.1016/j.cell.2009.07.006
424. Liu ZG, Han J. Cellular responses to tumor necrosis factor. Curr Issues Mol Biol. 2001;3: 79–90. Available: http://www.ncbi.nlm.nih.gov/entrez/query.fcgi?cmd=Retrieve&db=PubMed&dopt=Citation&list_uids=11719971
425. Karin M. Mitogen-activated protein kinase cascades as regulators of stress responses. Ann N Y Acad Sci. 1998;851: 139–46.
426. Davis RJ. Signal transduction by the c-Jun N-terminal kinase. Biochem Soc Symp. 1999;64: 1–12.
427. Wada T, Penninger JM. Mitogen-activated protein kinases in apoptosis regulation. Oncogene. 2004;23: 2838–49. doi:10.1038/sj.onc.1207556
428. Blackwell K, Zhang L, Thomas GS, Sun S, Nakano H, Habelhah H. TRAF2 phosphorylation modulates tumor necrosis factor alpha-induced gene expression and cell resistance to apoptosis. Mol Cell Biol. 2009;29: 303–314. doi:10.1128/MCB.00699-08
429. Reinhard C, Shamoon B, Shyamala V, Williams LT. Tumor necrosis factor alpha-induced activation of c-jun N-terminal kinase is mediated by TRAF2. EMBO J. 1997;16: 1080–92. doi:10.1093/emboj/16.5.1080
430. Devin A, Lin Y, Liu Z. The role of the death-domain kinase RIP in tumour-necrosis-factor-induced activation of mitogen-activated protein kinases. EMBO Rep. 2003;4: 623–7. doi:10.1038/sj.embor.embor854
431. Festjens N, Vanden Berghe T, Cornelis S, Vandenabeele P. RIP1, a kinase on the crossroads of a cell's decision to live or die. Cell Death Differ. 2007;14: 400–10. doi:10.1038/sj.cdd.4402085
432. Vandenabeele P, Declercq W, Van Herreweghe F, Vanden Berghe T. The role of the kinases RIP1 and RIP3 in TNF-induced necrosis. Sci Signal. 2010;3: re4. doi:10.1126/scisignal.3115re4
433. Luo Y, DeFranco DB. Opposing roles for ERK1/2 in neuronal oxidative toxicity: distinct mechanisms of ERK1/2 action at early versus late phases of oxidative stress. J Biol Chem. 2006;281: 16436–42. doi:10.1074/jbc.M512430200
434. Suh H-W, Kang S, Kwon K-S. Curcumin attenuates glutamate-induced HT22 cell death by suppressing MAP kinase signaling. Mol Cell Biochem. 2007;298: 187–94. doi:10.1007/s11010-006-9365-6
435. Han W, Xie J, Fang Y, Wang Z, Pan H. Nec-1 Enhances Shikonin-Induced Apoptosis in Leukemia Cells by Inhibition of RIP-1 and ERK1/2. Int J Mol Sci. 2012;13: 7212–7225. doi:10.3390/ijms13067212
436. Yokota H, Narayanan SP, Zhang W, Liu H, Rojas M, Xu Z, et al. Neuroprotection from retinal ischemia/reperfusion injury by NOX2 NADPH oxidase deletion. Invest Ophthalmol Vis Sci. 2011;52: 8123–31. doi:10.1167/iovs.11-8318
437. Gesslein B, Håkansson G, Carpio R, Gustafsson L, Perez M-T, Malmsjö M. Mitogen-activated protein kinases in the porcine retinal arteries and neuroretina following retinal ischemia-reperfusion. Mol Vis. 2010;16: 392–407.
438. Obitsu S, Sakata K, Teshima R, Kondo K. Eleostearic acid induces RIP1-mediated atypical apoptosis in a kinase-independent manner via ERK phosphorylation, ROS generation and mitochondrial dysfunction. Cell Death Dis. Nature Publishing Group; 2013;4: e674. doi:10.1038/cddis.2013.188
439. Vanlangenakker N, Vanden Berghe T, Bogaert P, Laukens B, Zobel K, Deshayes K, et al. cIAP1 and TAK1 protect cells from TNF-induced necrosis by preventing RIP1/RIP3-dependent reactive oxygen species production. Cell Death Differ. Nature Publishing Group; 2010;18: 656–665. doi:10.1038/cdd.2010.138

440. Lin Y, Choksi S, Shen H-M, Yang Q-F, Hur GM, Kim YS, et al. Tumor necrosis factor-induced nonapoptotic cell death requires receptor-interacting protein-mediated cellular reactive oxygen species accumulation. J Biol Chem. 2004;279: 10822–8. doi:10.1074/jbc.M313141200
441. Ventura J-J, Hübner A, Zhang C, Flavell RA, Shokat KM, Davis RJ. Chemical genetic analysis of the time course of signal transduction by JNK. Mol Cell. Elsevier Inc.; 2006;21: 701–10. doi:10.1016/j.molcel.2006.01.018
442. Festjens N, Vanden Berghe T, Vandenabeele P. Necrosis, a well-orchestrated form of cell demise: signalling cascades, important mediators and concomitant immune response. Biochim Biophys Acta. 2006;1757: 1371–87. doi:10.1016/j.bbabio.2006.06.014
443. Nagata Y, Todokoro K. Requirement of activation of JNK and p38 for environmental stress-induced erythroid differentiation and apoptosis and of inhibition of ERK for apoptosis. Blood. 1999;94: 853–63.
444. Roulston A, Reinhard C, Amiri P, Williams LT. Early activation of c-Jun N-terminal kinase and p38 kinase regulate cell survival in response to tumor necrosis factor alpha. J Biol Chem. 1998;273: 10232–9.
445. Regot S, Hughey JJ, Bajar BT, Carrasco S, Covert MW. High-sensitivity measurements of multiple kinase activities in live single cells. Cell. Elsevier Inc.; 2014;157: 1724–34. doi:10.1016/j.cell.2014.04.039
446. Costa M, Marchi M, Cardarelli F, Roy A, Beltram F, Maffei L, et al. Dynamic regulation of ERK2 nuclear translocation and mobility in living cells. J Cell Sci. 2006;119: 4952–4963. doi:10.1242/jcs.03272
447. Lidke DS, Huang F, Post JN, Rieger B, Wilsbacher J, Thomas JL, et al. ERK Nuclear Translocation Is Dimerization-independent but Controlled by the Rate of Phosphorylation. J Biol Chem. 2010;285: 3092–3102. doi:10.1074/jbc.M109.064972
448. Caunt CJ, McArdle CA. ERK phosphorylation and nuclear accumulation: insights from single-cell imaging. Biochem Soc Trans. 2012;40: 224–9. doi:10.1042/BST20110662
449. Ando R, Mizuno H, Miyawaki A. Regulated fast nucleocytoplasmic shuttling observed by reversible protein highlighting. Science. 2004;306: 1370–3. doi:10.1126/science.1102506
450. Cohen-Saidon C, Cohen AA, Sigal A, Liron Y, Alon U. Dynamics and Variability of ERK2 Response to EGF in Individual Living Cells. Mol Cell. 2009;36: 885–893. doi:10.1016/j.molcel.2009.11.025
451. Komatsu N, Aoki K, Yamada M, Yukinaga H, Fujita Y, Kamioka Y, et al. Development of an optimized backbone of FRET biosensors for kinases and GTPases. Mol Biol Cell. 2011;22: 4647–56. doi:10.1091/mbc.E11-01-0072
452. Rauch J, Volinsky N, Romano D, Kolch W. The secret life of kinases: functions beyond catalysis. Cell Commun Signal. BioMed Central Ltd; 2011;9: 23. doi:10.1186/1478-811X-9-23
453. Rodríguez J, Crespo P. Working without kinase activity: phosphotransfer-independent functions of extracellular signal-regulated kinases. Sci Signal. 2011;4: re3. doi:10.1126/scisignal.2002324
454. Sipieter F, Ladik M, Vandenabeele P, Riquet F. Shining light on cell death processes - a novel biosensor for necroptosis, a newly described cell death program. Biotechnol J. 2014;9: 224–40. doi:10.1002/biot.201300200
455. Carlson HJ, Campbell RE. Genetically encoded FRET-based biosensors for multiparameter fluorescence imaging. Curr Opin Biotechnol. 2009;20: 19–27. doi:10.1016/j.copbio.2009.01.003
456. Douin V, Bornes S, Creancier L, Rochaix P, Favre G, Prats A-C, et al. Use and comparison of different internal ribosomal entry sites (IRES) in tricistronic retroviral vectors. BMC Biotechnol. 2004;4: 16. doi:10.1186/1472-6750-4-16
457. Hellen CUT, Sarnow P. Internal ribosome entry sites in eukaryotic mRNA molecules. Genes and Development. 2001. pp. 1593–1612. doi:10.1101/gad.891101
458. Baron U, Freundlieb S, Gossen M, Bujard H. Co-regulation of two gene activities by tetracycline via a bidirectional promoter. Nucleic Acids Res. 1995;23: 3605–3606. doi:10.1093/nar/23.17.3605
459. Hennecke M, Kwissa M, Metzger K, Oumard A, Kröger A, Schirmbeck R, et al. Composition and arrangement of genes define the strength of IRES-driven translation in bicistronic mRNAs. Nucleic Acids Res. 2001;29: 3327–34. doi:10.1093/nar/29.16.3327
460. Ryan MD, King a. MQ, Thomas GP. Cleavage of foot-and-mouth disease virus polyprotein is mediated by residues located within a 19 amino acid sequence. J Gen Virol. 1991;72: 2727–2732. doi:10.1099/0022-1317-72-11-2727
461. Kim JH, Lee SR, Li LH, Park HJ, Park JH, Lee KY, et al. High cleavage efficiency of a 2A peptide derived from porcine teschovirus-1 in human cell lines, zebrafish and mice. PLoS One. 2011;6: 1–8. doi:10.1371/journal.pone.0018556
462. de Felipe P. Skipping the co-expression problem: the new 2A “CHYSEL” technology. Genet Vaccines Ther. 2004;2: 13. doi:10.1186/1479-0556-2-13
463. de Felipe P, Luke G a, Hughes LE, Gani D, Halpin C, Ryan MD. E unum pluribus: multiple proteins from a self-processing polyprotein. Trends Biotechnol. 2006;24: 68–75. doi:10.1016/j.tibtech.2005.12.006
464. Donnelly MLL, Hughes LE, Luke G, Mendoza H, Ten Dam E, Gani D, et al. The “cleavage” activities of foot-and-mouth disease virus 2A site-directed mutants and naturally occurring “2A-like” sequences. J Gen Virol. 2001;82: 1027–1041.
465. Lengler J, Holzmüller H, Salmons B, Günzburg WH, Renner M. FMDV-2A sequence and protein arrangement contribute to functionality of CYP2B1-reporter fusion protein. Anal Biochem. 2005;343: 116–124. doi:10.1016/j.ab.2005.05.004
466. Hasegawa K, Cowan AB, Nakatsuji N, Suemori H. Efficient multicistronic expression of a transgene in human embryonic stem cells. Stem Cells. 2007;25: 1707–1712. doi:10.1634/stemcells.2006-0813

467. Trichas G, Begbie J, Srinivas S. Use of the viral 2A peptide for bicistronic expression in transgenic mice. BMC Biol. 2008;6: 40. doi:10.1186/1741-7007-6-40
468. Fang J, Qian J-J, Yi S, Harding TC, Tu GH, VanRoey M, et al. Stable antibody expression at therapeutic levels using the 2A peptide. Nat Biotechnol. 2005;23: 584–90. doi:10.1038/nbt1087
469. Goedhart J, van Weeren L, Adjobo-Hermans MJW, Elzenaar I, Hink M a., Gadella TWJ. Quantitative Co-expression of proteins at the single cell level - application to a multimeric FRET sensor. PLoS One. 2011;6: 1–8. doi:10.1371/journal.pone.0027321
470. Szymczak AL, Workman CJ, Wang Y, Vignali KM, Dilioglou S, Vanin EF, et al. Correction of multi-gene deficiency in vivo using a single “self-cleaving” 2A peptide-based retroviral vector. Nat Biotechnol. 2004;22: 589–94. doi:10.1038/nbt957
471. Cho Y, McQuade T, Zhang H, Zhang J, Chan FK-M. RIP1-dependent and independent effects of necrostatin-1 in necrosis and T cell activation. Alberola-Ila J, editor. PLoS One. 2011;6: e23209. doi:10.1371/journal.pone.0023209
472. Sakon S, Xue X, Takekawa M, Sasazuki T, Okazaki T, Kojima Y, et al. NF-kappaB inhibits TNF-induced accumulation of ROS that mediate prolonged MAPK activation and necrotic cell death. EMBO J. 2003;22: 3898–3909. doi:10.1093/emboj/cdg379
473. Kamata H, Honda SI, Maeda S, Chang L, Hirata H, Karin M. Reactive Oxygen Species Promote TNFα-Induced Death and Sustained JNK Activation by Inhibiting MAP Kinase Phosphatases. Cell. 2005;120: 649–661. doi:10.1016/j.cell.2004.12.041
474. Berghe TV, Vanlangenakker N, Parthoens E, Deckers W, Devos M, Festjens N, et al. Necroptosis, necrosis and secondary necrosis converge on similar cellular disintegration features. Cell Death Differ. Nature Publishing Group; 2010;17: 922–930. doi:10.1038/cdd.2009.184
475. Goossens V, Grooten J, De Vos K, Fiers W. Direct evidence for tumor necrosis factor-induced mitochondrial reactive oxygen intermediates and their involvement in cytotoxicity. Proc Natl Acad Sci U S A. 1995;92: 8115–8119.
476. Shankaran H, Ippolito DL, Chrisler WB, Resat H, Bollinger N, Opresko LK, et al. Rapid and sustained nuclear-cytoplasmic ERK oscillations induced by epidermal growth factor. Mol Syst Biol. 2009;5: 332. doi:10.1038/msb.2009.90
477. Tomida T. Visualization of the spatial and temporal dynamics of MAPK signaling using fluorescence imaging techniques. J Physiol Sci. 2015;65: 37–49. doi:10.1007/s12576-014-0332-9
478. Sharma P, Yan F, Doronina V a, Escuin-Ordinas H, Ryan MD, Brown JD. 2A peptides provide distinct solutions to driving stop-carry on translational recoding. Nucleic Acids Res. 2012;40: 3143–51. doi:10.1093/nar/gkr1176
479. Aoki K, Kumagai Y, Sakurai A, Komatsu N, Fujita Y, Shionyu C, et al. Stochastic ERK activation induced by noise and cell-to-cell propagation regulates cell density-dependent proliferation. Mol Cell. Elsevier; 2013;52: 529–40. doi:10.1016/j.molcel.2013.09.015
480. Oberoi-Khanuja TK, Rajalingam K. IAPs as E3 ligases of Rac1. Small GTPases. 2012;3: 131–136. doi:10.4161/sgtp.19988
481. Whitehurst AW, Robinson FL, Moore MS, Cobb MH. The death effector domain protein PEA-15 prevents nuclear entry of ERK2 by inhibiting required interactions. J Biol Chem. 2004;279: 12840–7. doi:10.1074/jbc.M310031200

Curriculum Vitae

Personal

Name: François Leon Robert Sipieter
Nationality: French
Date of birth: 07.10.1986
Place of birth: Malo-les-Bains, France
Languages: French (native)
English (professional skills)
German (basics)
Address: Kortrijksesteenweg 1008
B-9000 Gent

Actual laboratory:
Unit Molecular Signaling & Cell Death
Inflammation Research Center (IRC),
a VIB-UGent Department,
Technologiepark 927,
B-9052 Gent-Zwijnaarde, Belgium

e-mail address:
francois.sipieter@irc.vib-ugent.be

Phone: +32 479 54 05 55

Education

PhD student in Molecular and Cellular Biology and Biotechnology jointly supervised by Lille 1 University / CNRS (France) and Ghent University / VIB (Belgium) (2011)
Master in Biomedical Sciences, University of Lille 1, France (2010)
Bachelor in Biomedical Sciences, University of Lille 1, France (2008)

Positions and Employment

2008 (jun to aug) **Graduate Trainee Biologist** (BSc student)
Introduction to molecular biology and microscopy
Biophotonics Team (L. Héliot), IRI-CNRS USR3078, Villeneuve d'Ascq, France.

2009 (jun to aug) **Graduate Trainee Biologist** (MSc student)
Study of molecular interactions (Cadherins) in Xenopus laevis embryos
Multicellular Dynamics Team (Y. Saka), IRI-CNRS USR3078, Villeneuve d'Ascq, France.

2009 – 2010 **Graduate Trainee Biologist** (MSc student)
Dynamical study of MAPK/ERK2 and OGT proteins during cell cycle in oocytes and Xenopus laevis embryos.
Régulation des Signaux de Division laboratory (J.F. Bodart), EA4479 / University of Lille1, Villeneuve d'Ascq, France.

2010 (sept to nov) **Contractual Engineer**
Biophotonics Team (L. Héliot), IRI-CNRS USR3078, Villeneuve d'Ascq, France.

2011 – Present **Joint PhD student**
Régulation des Signaux de Division laboratory (J.F. Bodart), EA4479, University of Lille1, Villeneuve d'Ascq, France.
Biophotonics Team (L. Héliot), IRI-CNRS USR3078, Villeneuve d'Ascq, France.
Unit of Molecular Signaling and Cell Death (P. Vandenabeele), Inflammation Research center, a VIB-UGent Department, Ghent University / VIB, Gent-Zwijnaarde, Belgium.

Participation at National and International Conferences

2010 Thematic Interdisciplinary School, "MiFoBio 2010" (CNRS), Seignosse, France [Poster].
2011 Biosensor workgroup of GDR2588 (CNRS), Lille, France [Poster].
2012 Biosensor workgroup of GDR2588 (CNRS), Montpellier, France [Poster].
2012 France BioImaging Advanced Training, FBI-AT 2012, Lille, France [Poster].
2012 Thematic Interdisciplinary School, "MiFoBio 2012" (CNRS), Talmont-St-Hilaire, France [Poster + Oral communication].
2012 *Imagerie-vivant: Nouvelles méthodologies en imagerie du vivant* (CNRS), Lyon, France [Poster].
2012 *Journée André Verbert*, Meeting of PhD students, Lille 1 University, Lille, France [Poster].
2013 Focus on Microscopy (FOM), Maastricht, Netherlands [Poster].
2013 Biosensor workgroup of GDR2588 (CNRS), Marseille, France [Poster].
2013 France BioImaging Advanced Training, FBI-AT 2013, Gif-sur-Yvette, France [Poster].
2014 Biosensor workgroup of GDR2588 (CNRS), Bordeaux, France [Poster].
2014 ICDI Symposium "Mechanisms of Innate Immunity, Cell Death and Inflammation", Ghent, Belgium.
2014 VIB Science Club Imaging@VIB, Leuven, Belgium.
2014 Thematic Interdisciplinary School, "MiFoBio 2014" (CNRS), Seignosse, France [Poster].
2015 Symposium: **"**Past, Present and Future Confocal Microscopy", Ghent, Belgium.
2015 VIB Seminar, Blankenberge, Belgium [Poster].

Grants and Prices

2010 Thematic Interdisciplinary School, "MiFoBio 2010" (CNRS), Seignosse, France [CNRS GDR2588 student grant].
2012 Thematic Interdisciplinary School, "MiFoBio 2012" (CNRS), Talmont-St-Hilaire, France [CNRS GDR2588 student grant].
2014 Thematic Interdisciplinary School, "MiFoBio 2014" (CNRS), Seignosse, France [CNRS GDR2588 student grant + Price for best Poster presentation].

Teaching and Workshop

2009

[Teaching] Master 1 students in Biology and Biotechnology, Lille 1 University, UE MO3. Teaching in French. Title: "*Etudes des mouvements morphogénétiques des calottes animales d'embryons de Xénope en réponse à un traitement à* l'activine", 2 hours.

2010

[Teaching] Master 1 students in Biology and Biotechnology, Lille 1 University.

[Teaching] Advanced Confocal Imaging Training, IRI-CNRS

Teaching in French. Title: "*Outils moléculaires pour la microscopie fonctionnelle de fluorescence en cellules vivantes*", 2 hours.

2012

[Workshops coordinator] Thematic Interdisciplinary School, "MiFoBio 2012" (CNRS), Talmont-St-Hilaire, France. Titles: (1) FRET/FLIM imaging for kinase activity sensing in living cells. (2) Monitoring of early amphibian embryogenesis phases by Optical Coherence Tomography (OCT).

2014

[Workshop coordinator] Thematic Interdisciplinary School, "MiFoBio 2014" (CNRS), Seignosse, France. Title: Dual FRET/FLIM and ratiometric FRET imaging for kinase activity sensing in living cells.

Training and Guidance Students

Pauline Vandame, Master 1 in Biology and Biotechnology (2011) and Master 2 Research in Biomedical Science ("*Biologie-Santé*") (2012), Lille 1 University, France.

Sonia Pajet, 3rd Bachelor in Biology and Biotechnology (2012), Lille 1 University, France.

Benjamin Cappe, 3rd Bachelor (2012) and Master 1 in Biology and Biotechnology (2013) and Master 2 Research in Biomedical Science ("*Biologie-Santé*") (2014), Lille 1 University, France.

Sarah Druwe, 3rd Bachelor in *Biomedische Laboratoriumtechnologie* (2014), Ghent University, Belgium.

Scientific Skills

Several standard techniques in molecular biology and biochemistry including molecular cloning, site-directed mutagenesis, construction of fusion proteins, PCR, RT-PCR, DNA and protein extraction, RNA *in vitro* transcription and purification, immunoprecipitation, Western blot, Southern blot, ELISA.

Standard techniques in cellular biology including cell culture, transfection in a range of cellular models, GFP-like based reporter assays and immunofluorescence.

A thorough practical knowledge of *Xenopus laevis* model and handling techniques including intramuscular and intraperitoneal injections, euthanization and surgical extraction of testes of male frogs, oocyte and embryo manipulation, *in vitro*

fecundation, oocyte and embryo RNA and DNA microinjection, animal cap micro-dissection, explant culture of dissected animal caps and immunohistochemistry.

A strong knowledge and practical experience in confocal and widefield fluorescence microscopy (confocal inverted Leica SP5, confocal upright Nikon A1R, Spinning disk, widefield inverted Nikon Eclipse TiE), FRAP and FRET live cell imaging applications including protein interaction, kinase activities and ionic species fluctuations monitoring in living cells. Strong experience with genetically encoded FRET-based biosensors to determine spatio-temporal signatures of protein kinases: design, construction, optimization, expression in living cells, ratiometric FRET as well as fluorescence lifetime imaging in the frequency domain (FRET/FLIM, LIFA). Experience with FRET/FLIM imaging in the time domain (TCSPC).

Experience with image analysis and especially FRET image analysis (Image J, Fiji, Volocity, Igor, NIS Element, LI-FLIM).

Patent and Publications

Riquet F, Vandame P, **Sipieter F**, Cailliau-Maggio K, Spriet C, Héliot L and Bodart J-F. Reporting Kinase activities: paradigms, tools and perspectives. Journal of Biological Medicine 2011:1(2) 10-18.

Sipieter F, Vandame P, Spriet C, Leray A, Vincent P, Trinel D, Bodart J-F, Riquet FB, Héliot L. From FRET imaging to practical methodology for kinase activity sensing in living cells. Prog Mol Biol Transl Sci. 2013;113: 145–216. doi:10.1016/B978-0-12-386932-6.00005

Sipieter F, Ladik M, Vandenabeele P, Riquet FB. Shining light on cell death processes - a novel biosensor for necroptosis, a newly described cell death program. Biotechnol J. 2014;9: 224–40. doi:10.1002/biot.201300200

Sipieter F, Cappe B, Gonzalez Pisfil M, Spriet C, Bodart J-F, Cailliau-Maggio K, Vandenabeele P, Héliot L, Riquet FB. Novel reporter for faithful monitoring of ERK2 dynamics in living cells and model organisms. PlosOne 2015 in press.

Déméautis C, **Sipieter F**, Roul J, Chapuis C, Padilla-Parra S, Riquet FB and Tramier M. Single wavelength excitation dual color FLIM with mTFP1/sREACh and LSSmOrange/mKate2 pairs for multiplexing genetically encoded FRET biosensors. Biophys. J. 2015. To be submitted.

Sipieter F, Cappe B, Gavet O, Vincent P and Riquet FB. A novel gateway-based system for rapid development and optimization of FRET biosensors in living cells. 2015. In preparation.

Sipieter F, Cappe B, Vincent P, Vandenabeele P, Riquet FB. Spatio-temporal characterization of ERK activity in survival, apoptosis and necroptosis. 2016. In Preparation.

Patent: « *Biosenseurs de kinase et leur procédé de fabrication*. » Application nr GB 1400997.1. Riquet F et al. (including **Sipieter F**): Priority date: 2014.06.20.

Acknowledgements

I would like to acknowledge all the people who contributed directly an indirectly in the development of this research project. First, I would like to thank the CNRS, Lille 1 University, the VIB and Ghent University for providing me a valuable administrative guidance to make this project possible and for their financial support throughout this interdisciplinary and international research. I especially would like to express my gratitude to my academic supervisors Franck Riquet (for Lille 1 University), Peter Vandenabeele (for Ghent University) and Laurent Héliot (for the CNRS) for offering me an unfailing support and encouragement in all situations and continuous positive reinforcement throughout these five years of study.

I would like to thank my committee members for assessing the quality and relevance of this research project and for their valuable comments: Prof. Dr. Xuefen Le Bourhis, Prof. Dr. Kris Vleminckx, Prof. Dr. Patrizia Agostinis, Prof. Dr. Georges Baffet, Dr. Saskia Lippens, Dr. Olivier Gavet and Dr. Katia Cailliau-Maggio.

I would like to sincerely thank Peter Vandenabeele for providing me with the opportunity to work into his laboratory and for his valuable supervision and guidance throughout my research. I was fortunate to benefit from this reliable source of scientific knowledge and I hope to have the possibility to continue working in his lab.

I would like to thank Franck Riquet for receiving continuous support, advices, and valuable guidance throughout all my university cursus. I do not find words to express my sincere sympathy and my deep appreciation. It was and it is a real pleasure to work in an innovative and creative environment in which teamwork is practiced with mutual support and mutual trust to prevent errors and improve the quality of the work. I gained a lot from his scientific and communicative skills and share now his scientific method of thinking providing me with a dynamic vision of biological processes.

Nowadays, biochemistry in living cells in real time has revolutionized our train of thoughts and has encouraged scientists to develop molecular tools for the assessment of protein dynamics within their physiological context. New approaches based on microscopy techniques are major challenges and are often limited by technological obstacles. Exceeding these technological barriers requires the association of skills of scientists from different backgrounds. In this context, I would like to thank Laurent Héliot offering me a reliable source of practical knowledge and guidance. I benefited from scientific insights of his team for solving complex situations with a friendly interdisciplinary working atmosphere where everyone brings complementary skills creating a synergistic and non-competitive teamwork. I would also like to thank the GDR2588-MIV CNRS for their financial support to attend at several conferences (MifoBio, FBI-AT, FOM, etc.). These participations to various workshops allowed me to build connections and develop fruitful collaborations with scientists from different disciplines to gain a better understanding on data that I have collected.

Benjamin Cappe jointed the team when I was beginning the second moiety of my thesis. He successfully completed his master 2 research. I was and I am fortunate to work with him on my project and I gained a lot from his scientific curiosity, scientific attitude of mind, patience and accuracy in his work. In the same way, I would also like to thank Maria Ladik for her helpful suggestions. Thank you both for this synergistic relationship generating insightful comments on our respective work and leading to bring out the best in us to produce the best work.

I am also very grateful to Veronique Vandevoorde for providing us very helpful guidance for administrative procedures assuring the coordination between the university administrations and without whom this joint PhD would not have been possible. Thanks a lot Veronique!

I would also to thank all of our collaborators who have contributed in some way to the project's progress. Dr. Pierre Vincent became an indispensable interlocutor. He developed a powerful and accurate dedicated image analysis interface for ratiometric FRET imaging. Without his helpful guidance and his efforts for solving intractable difficulties, my work would have been more difficult. My thanks also go to Drs May Morris, Marc Tramier, Olivier Gavet and Nadine Peyrieras for their constructive discussions, valuable suggestions, encouragement and also their kindness and availability. This thesis would not have been possible without them!

My thanks go to all members of the Laurent Héliot and Peter Vandenabeele labs and members of the Bio Imaging Core for their enthusiasm, their friendly working environment, their numerous conversations (over a coffee/drink) and of course their help in every situations that I have faced. I hope sincerely to have the possibility to continue working with them!

Finally, I would like to gratefully and deeply thank my family and friends who supported me during this time. Thank you so much!

Additionally, to those who opposed me and generously provided negative reinforcement throughout my work, I also thank as it gave me the opportunity to grow and adapt in order to turn the situation around!

"*That which does not kill us makes us stronger*"

(Friedrich Nietzsche)

It is now time to go ahead and turn the page to a new chapter….